



OpenAIR@RGU

The Open Access Institutional Repository at Robert Gordon University

<http://openair.rgu.ac.uk>

Citation Details

Citation for the version of the work held in 'OpenAIR@RGU':

CHOUDHURY, A. H., 2014. Structure, strength and defect characterisation of cement based materials. Available from *OpenAIR@RGU*. [online]. Available from: <http://openair.rgu.ac.uk>

Copyright

Items in 'OpenAIR@RGU', Robert Gordon University Open Access Institutional Repository, are protected by copyright and intellectual property law. If you believe that any material held in 'OpenAIR@RGU' infringes copyright, please contact openair-help@rgu.ac.uk with details. The item will be removed from the repository while the claim is investigated.

Structure, Strength and Defect Characterisation of Cement based Materials

A thesis presented for the Degree of PhD at the Robert Gordon
University, Aberdeen.

By

Ajmol H Choudhury

PhD Thesis

2014

Dedicated to my Parents

ABSTRACT

In cement based systems, the residual stresses are created by internal expansion. This provides toughening by the release of the residual stresses as the macro-crack propagates. While circumstantial evidence of the residual stresses exist (e.g. micro-crack formation leading to permanent deformation in flexural tests), it is very difficult to observe the mechanism in action. The quantitative estimate of the changes occurring in such cement-based systems is challenging due to the anisotropy and complexity of the material. Non-Destructive Testing (NDT) techniques were used in this research to observe the mechanism in action. An ultrasound technique is used to examine strength development and an acoustic emission (AE) technique is used to examine micro-structural changes, micro-cracks, crack initiation, crack propagation, crack arrests and crack bridging in plain concrete samples including samples containing admixtures and waste materials.

The NDT techniques were found to be accurate in being able to measure compressive strength, with good correlation between both standard mechanical testing and NDT techniques. It was shown that admixtures could be effectively used to alter the properties of a curing cement mortar. This work has also demonstrated that ultrasound can be successfully used to determine the compressive strength of concrete from an early age. The ability to pre-determine the strength of concrete through correlation with NDT test parameters may reduce the time spent waiting on concrete to set and to obtain results using standard mechanical testing methods.

The findings in this research present the effect admixtures had on the curing process of the cement based material. The introduction of certain additives into mortars have demonstrated an increase in both the rate of initial hardening and the magnitude of the compressive strength attained over the curing period depending on the mixture specification. The additives considered have been shown to actively alter and enhance the chemical process of curing from the start of hydration. Some additives that accelerate the curing process (accelerators) were found to lower the compressive strength of concrete using

the ultrasound technique. Additives that caused an increase in the final strength of mortar also increased its toughness.

The significant contributions in this research enabled observation of micro-structural changes and failure behaviour under compressive and flexural loading conditions on an on-line basis. The results obtained are encouraging and lead to increased understanding of cracking mechanisms in concrete containing various types of additives and aggregates. The application of the AE technique allowed the failure of interfacial bonding to be observed. The variation of the aggregate size and its effect on the monitored waveforms was established and the parameters in the AE signals are directly related to crack propagation (grain bridging/micro-mechanism) and strength of interfacial bonding. These findings have greatly contributed to the understanding of the concrete behaviour under complex conditions where no other technique could provide such valuable information on an online basis.

ACKNOWLEDGEMENTS

I wish to thank my supervisor Professor Iain Steel, Head of the School of Engineering, for his continuous help, support and guidance, which were a source of inspiration and encouragement while preparing this thesis.

I would like to express my sincere gratitude to my late supervisor Dr A. Siddiqui for his relentless guidance, motivation, dedicated research direction and inspiring ideas. May God almighty bless his soul in heaven.

My sincere gratitude to Dr Sha Jihan for his challenging questions that helped me to prepare for the onslaughts at the PhD viva.

I wish to thank Mr Martin Simpson, Research Degrees Officer for his continuous support and advice, especially during the difficult times I faced.

I would also like to thank Mrs Petrena Morrison, Secretary of the School of Engineering for her continuous help and assistance during my correspondence and visit to Aberdeen.

I would also like to thank the following for their help and support in the workshop and laboratory:

Mr Graeme Budge - Technician, School of Engineering

Mr Ian Tough - Technician, School of Life Sciences

DECLARATION

This thesis is presented in accordance with the regulations for the degree of Doctor of Philosophy. It has been composed by myself and has not been submitted in any previous application for a higher degree. The work of which it is a record has been done by myself. All sources of information are specifically acknowledged.

Ajmol Hussain Choudhury

Robert Gordon University

PRESENTATIONS

During the research work carried out for this thesis, the following papers and poster were presented at conferences:

1. Strength characterisation of cement based materials using NDT techniques
A.H.Choudhury, A.M.Siddiqui, I.J.Merchant, British Institute of Non-Destructive Testing Conference, Southport, 2002.
2. Acoustic Emission monitoring of cracks in cement based materials
A.H.Choudhury, A.M.Siddiqui, I.J.Merchant, British Institute of Non-Destructive Testing Conference, Southport, 2002.
3. Acoustic Emission monitoring of the Fracture Behaviour of Concrete containing various size and shape of glass aggregates, A.H.Choudhury, A.M.Siddiqui, I.J.Merchant, 26th European Conference on Acoustic Emission Testing, Berlin, 2004.
4. A comparative study of corrosion in an aluminium alloy and mild steel using Acoustic Emission and microscopic techniques, A.H.Choudhury, A.M.Siddiqui, A. Abdu, A. Mahen, 26th European Conference on Acoustic Emission Testing, Berlin, 2004.
5. Monitoring Compressive Behaviour of Concrete Containing Waste Materials as Aggregates Using Acoustic Emission, A. H. Choudhury, A. M. Siddiqui, D. Johnstone, 28th Annual conference on Acoustic Emission Testing, Krakow, 2008.
6. Compressive strength measurement of cement based materials using ultrasound waves, British Institute of Non-Destructive Testing, Conference Proceedings, Southport, 2002.

LIST OF FIGURES

Figure 1.1: Factors influencing concrete strength	7
Figure 1.2: Cracking pattern in normal strength concrete	13
Figure 1.3: Use of repeated loading tests to provide a measure of damage caused to concrete the first time it is loaded.	18
Figure 1.4: Comparison of methods for detecting damage in concrete specimens	19
Figure 1.5: The relation between concrete performance and extent of cracking	22
Figure 1.6: Fracture process zone in concrete	23
Figure 1.7: Toughening mechanisms of fracture process zone in concrete	24
Figure 1.8: (a) The coordinate system used and (b) the stress as a function of r	25
Figure 1.9: A single edge notched beam specimen for the determination of K_{Ic}	26
Figure 1.10: Relationship between number of AE hits and the applied load	35
Figure 1.11: Loading curves during three-point bending test	36
Figure 1.12: Amplitude and displacement histories	38
Figure 1.13: Relationships between AE hits and the applied load for the specimens with different deteriorated levels	38
Figure 1.14a: Apparatus for applying load and measuring deflections	39
Figure 1.14b: Results of the moment tensor analysis	39
Figure 1.15: Relationship between number of loading cycles and crack density	40
Figure 1.16: Histories of AE hit rate, amplitude and the maximum load	41
Figure 1.17: Relationship between loading phase and AE activity from stage IV to the final failure	41

Figure 2.1: A typical AE system set up	69
Figure 2.2: Transient (burst) signal and Continuous signal	70
Figure 2.3: Features of transient signals	71
Figure 3.1: Hydration of cement	75
Figure 3.2: Relationship between compressive strength of the hardened cement and water/cement ratio	76
Figure 3.3: Rebound Value vs. Strength of cube	95
Figure 3.4: Arrangement for 3-point bend test	96
Figure 3.5: Central roller in an eccentric position with respect to the notch	97
Figure 4.1: Ultrasound Measurement Experimental Set-up	99
Figure 4.2: Ultrasonic measurement image of a plain mortar	101
Figure 4.3: Ultrasonic display data of a standard mortar	102
Figure 4.4: Schematic diagram of a compressive test set-up	104
Figure 4.5: (a) Compressive test machine; (b) Digital display meter powered by hydraulic pump	104
Figure 4.6: The Acoustic Emission (AET) AMSY4 AE Vallen System	106
Figure 4.7a: The AE signal with the threshold setting	109
Figure 4.7b: The AE signal with the automatic setting	109
Figure 4.8: A plot of calibration for a plain mortar sample	111
Figure 4.9 (a): A wooden mould sample	112
Figure 4.9 (b): An un-notched sample specimen	112
Figure 4.10: Broken glass from car windows	115
Figure 4.11 (a): Sieve set-up	116
Figure 4.11 (b): A Sieve sample	116

Figure 4.12 (a): Sample mounting on a Flexural Machine	117
Figure 4.12 (b): Experimental set-up of 3-point flexural bend test	118
Figure 4.13: A.E. Vallen set up	119
Figure 4.14: An example of a typical AE Multi-plots	120
Figure 4.15: A 3-dimensional plot for sample BG1, a plain mortar	121
Figure 4.16: AE listing and Waveform for sample BG1, plain mortar	121
Figure 5.1: A comparison of compressive strength and affect of additives on strength of concrete obtained using mechanical and ultrasound tests	123
Figure 5.2: Percentage difference in compressive strength measurements of using two (US and crush test) techniques	124
Figure 5.2a: Summary of the compressive strength over 21 day for different sizes of samples	127
Figure 5.3: The change in compressive strength (measured using ultrasound) of a standard mortar (without additives) with respect to time	128
Figure 5.4: Typical changes in compressive strength of a mortar sample with addition of calcium chloride with respect to time	130
Figure 5.5: Percentage variation in compressive strength due to the addition of calcium chloride as compare to standard model	131
Figure 5.6: The change in compressive strength of a mortar with additions of potassium chloride with respect to time	132
Figure 5.7: Percentage variation in final compressive strength due to the additions of potassium chloride as compared to standard model	132
Figure 5.8: Typical change in compressive strength of a mortar sample with addition of sodium silicate with respect to time	133
Figure 5.9: Percentage variation in final compressive strength due to addition of sodium silicate as compared to standard model	134
Figure 5.10: The change in compressive strength of a mortar with addition of sodium sulphate with respect to time	135

Figure 5.11: Percentage variation in final compressive strength due to addition of sodium sulphate as compared to standard model	135
Figure 5.12: The change in compressive strength of a mortar with additions of sodium chloride with respect to time	136
Figure 5.13: Percentage variation in final compressive strength due to addition of sodium chloride as compared to standard model	137
Figure 5.14: Sodium Sulphate, 500 times magnification	138
Figure 5.15: Sodium Sulphate, 2000 times magnification	139
Figure 5.16: Elemental composition of sodium sulphate – percentage content by weight	139
Figure 5.17: Sodium silicate structure, 500 times magnification	140
Figure 5.18: Sodium silicate structure, 2000 times magnification	140
Figure 5.19: Elemental composition of sodium silicate – percentage content by weight	141
Figure 5.20: Calcium chloride, 500 times magnification	142
Figure 5.21: Calcium chloride- 2000 times magnification	142
Figure 5.22: Elemental composition of calcium chloride – percentage content by weight	143
Figure 5.23: A comparison of compressive strength obtained between actual mechanical and ultrasound tests due to the introduction of different sized glass aggregates in concrete	145
Figure 5.24: Percentage error variation between samples introduced from the ultrasonic measurement techniques	146
Figure 5.25: The best fit line of compressive strength obtained by ultrasound and mechanical methods for glass aggregates	147
Figure 5.26: A comparison of compressive strength obtained between mechanical and ultrasound tests due to the introduction of rubber aggregates in concrete	148

Figure 5.27: Percentage difference variation between samples introduced from the ultrasonic measurement techniques for rubber aggregates	149
Figure 5.28: The best fit line of compressive strength obtained by ultrasound and mechanical methods for rubber aggregates	150
Figure 5.29: The modulus of elasticity to the aggregate size ratio in terms of compressive strength	151
Figure 5.30: The best fit line of mechanical strength and modulus of elasticity obtained by ultrasound and mechanical methods for glass aggregates	152
Figure 5.31: The modulus of elasticity of concrete with rubber aggregates to the ratio of rubber in terms of compressive strength	153
Figure 5.32: The best fit line of mechanical strength and modulus of elasticity for rubber aggregates	154
Figure 6.1: AE Plots for Plain Mortar under Compressive Load	160
Figure 6.2: AE Plots for Mortar with Glass Aggregates under Compressive Load	162
Figure 6.3: AE Plots for Mortar with Rubber Aggregates under Compressive Load	164
Figure 6.4: AE plots for sample BD1 (plain concrete)	171
Figure 6.5: AE plots for sample BA2 (containing powdered glass)	173
Figure 6.6: AE plots for sample BC1 (with 40g 2-1mm aggregates)	175
Figure 6.7: AE plots for sample BE1 (with 40g 4-2mm aggregates)	177
Figure 6.8: AE plots for sample BB2 (with 80g 4-2mm aggregates)	179
Figure 6.9: AE plots for sample BG1 (plain concrete)	181
Figure 6.10: AE plots for sample BI1 (with powdered glass)	183
Figure 6.11: AE plots for sample BF1 (with 60g 2-1mm aggregates)	185
Figure 6.12: AE plots for sample BH1 (with 60g 4-2mm aggregates)	187
Figure 6.13: AE plots for sample BJ1 (with 120g 4-2mm aggregates)	189
Figure 6.14: Variations of AE Hits captured by different smaller sized un-notched mortars under flexural load test	191

Figure 6.15: Percentage of Hits variation in each of the smaller sized un-notched mortars under flexural load test	192
Figure 6.16: Variations of AE Hits captured by different larger sized un-notched mortars under flexural load test	193
Figure 6.17: Percentage of Hits variation in each of the larger sized un-notched mortars under flexural load test	193
Figure 6.18 (a-e): Distribution of AE amplitude (dB) against Location for different size of glass aggregates	196
Figure 6.19 (a-d): Optical Micro-graphs of the Fractured Surfaces of the concrete samples	197
Figures 6.20 (a), (b), (c), and (d): AE waveforms for different samples	199
Figures 6.21: AE plots and fractured specimen for Plain Mortar	202
Figures 6.22: AE plots and photo of fractured sample of Mortar with <1mm glass aggregates	204
Figures 6.23: AE plots and photographs of fractured Mortar with 1-1.7mm glass aggregates	206
Figures 6.24: AE plots and photographs of fractured Mortar with 1.7-2.36mm aggregates	208
Figures 6.25: AE plots and photographs of fractured Mortar with 2.36-3.35 mm glass aggregates	210
Figures 6.26: AE plots and photographs of fractured Mortar with 3.35 mm-4 mm Glass Aggregates	212
Figure 6.27: Variation of AE hits cascade captured by different samples	214
Figure 6.28: Relationship between modulus of rupture (MOR) versus fracture toughness (Kc) and AE hits.	216
Figure 6.29: AE Plots and Optical photographs of fractured sample and surface for plain mortar	219
Figure 6.30: AE Plots and Optical photographs of fractured sample and surface for mortar with glass slide	221
Figure 6.31: AE Plots and Optical photographs of fractured sample and surface for plain mortar with glass aggregates and glass plate	223
Figure 6.32: Number of AE hits captured by different samples under applied flexural load	224

Figure 6.33: Pie chart showing percentage of AE Hits for each sample	224
Figure 6.34: Crack growth paths of mortars	226
Figure 6.35: Crack propagation in a mortar	227
Figure 6.36: AE plots and AE listing for Sample Kolar2b (with 100g rubber)	229
Figure 6.37: AE plots and AE listing for sample Kolar3b (Mortar containing 150g rubber)	231
Figure 6.38: AE plots and AE listing for sample Kolar4b (Mortar with 200g rubber)	232
Figure 6.39: AE plots and AE listing for sample Kolar5b (Mortar containing 250g rubber)	234
Figure 6.40: Number of AE hits captured by samples with different quantities of rubber aggregates under applied flexural load	235
Figure 6.41: Pie chart showing percentage of AE Hits under applied flexural load	235
Figure 6.42: interfacial bonding of rubber with mortar	236
Figure 7.1: AE plots of plain mortar under compression	240
Figure 7.2: AE plots of mortar (15g Calcium Chloride) under compression	241
Figure 7.3: AE plots of mortar (10g Sodium Sulphate) under compression	243
Figure 7.4: AE plots of mortar (15g Sodium Sulphate) under compression	243
Figure 7.5: AE plots of mortar (25g Sodium Sulphate) under compression	244
Figure 7.6: AE plots of mortar (15g Sodium Silicate) under compression	245
Figure 7.7: AE hits produced in samples with admixtures under compressive load	249
Figure 7.8: Percentage AE hits produced by mortars with admixtures under compressive load	249
Figure 7.9: AE Plots and fractured surface for Expansive cement mortars with glass beads (3mm)	252
Figures 7.10: AE plots and optical graph for Expansive cement mortars with pebbles (3mm)	254
Figures 7.11: AE plots and optical graph for Expansive cement mortars with rough glass aggregates (3mm)	256

Figure 7.12: AE hits produced by expansive cement based mortars with aggregates under flexural load	258
Figure 7.13: Percentage of AE hits produced by expansive cement based mortars with aggregates under flexural load	258
Figure 7.14: AE plots of different mortars	261
Figure 7.15: AE Plots of different samples	263
Figure 7.16: AE Plots and listing of different samples	265
Figure 7.17: AE hits produced by different mortars with glass slide, glass aggregates and admixture under flexural load	266
Figure 7.18: Percentage of AE hits produced by different mortars with glass slide, glass aggregates and admixture under flexural load	266
Figure 7.19: Fractured Surfaces of specimens containing glass slide, admixtures and glass aggregates	268
Figure 8.1: AE plots and listing of sample Brglcam (mortar with glass plate)	270
Figure 8.2: AE plots and listing of sample Brglcam1 (mortar with glass aggregates)	271
Figure 8.3: AE plots and listing for sample NAS (Mortar with Sodium Sulphate + Glass Slide)	273
Figure 8.4 a: Crack path through a notched concrete specimen with the inclusion of a reinforcing glass plate and glass aggregate in to the matrix	275
Figure 8.4 b: Fracture surface of the concrete specimen	275
Figure 8.5: AE plots of Brgl2	276
Figure 8.6: A comparison of cascaded energy of different samples under load with aggregates and additive	278
Figure 8.7: Relationship between flexural strength/fracture toughness and AE energy of different samples	280
Figure 8.8: AE plots for sample Final2: Plain Mortar	282
Figure 8.9: AE plots for sample Conflex: Mortar containing sodium sulphate	283
Figure 8.10: AE plots for sample Cara4: Mortar containing calcium carbonate	283
Figure 8.11: Comparison of AE hits produced by typical mortar and mortars containing admixture under flexural load	284

Figure 8.12: Percentage of AE hits produced by typical mortar and mortars containing admixture under flexural load	285
Figure 8.13: Differences in AE activities under compression and flexural conditions	286
Figure 8.14: Distribution of 'located events' under compression and flexural condition	286
Figure 8.15: Amplitude signal pattern under compression and flexural condition	287
Figure 8.16: Amplitude Distribution against number of hits under compression and flexural conditions	288
Figure 8.17: TR Waveforms at failure point under compression and flexural load	288
Figure 8.18 Optical Figures: Optical micrographs of bonding between the cement paste and the aggregates	290
Figure 8.19: AE and micro-cracks related toughened matrix	294

LIST OF TABLES

Table 1.1: Fracture Energy (G_c) and fracture toughness (K_{Ic}) for common construction materials	21
Table 2.1: Non-Destructive Testing Method Categories	60
Table 2.2: AE Signal Parameters and Representations	72
Table 2.3: AE Source Classification for Composite Based Materials on Peak amplitude	73
Table 2.4: Micro-crack and Macro-crack Phases	73
Table 4.1: Ultrasonic measurement carried out on plain mortar over a 28 day period	102
Table 4.2: Cement-Sand-Water preparation for sample report	113
Table 5.1 (a): Ultrasound parameters results for small sized samples	126
Table 5.1 (b): Ultrasound parameters results for medium sized samples	126
Table 5.1 (c): Ultrasound parameters results for large sized samples	126
Table 5.2: Values of the hydration period, compressive strength and curing rate for various additives	129
Table 5.3: Modulus of Elasticity for samples with different sizes of glass aggregates	151
Table 5.4: Modulus of Elasticity for samples with different quantities of rubber aggregates	152
Table 6.1: Type of mechanism contribution made by aggregates under compressive load	166
Table 6.2: Load results at breaking point of three point bend test	169
Table 6.3: A.E. monitoring results summary of un-notched mortars containing glass aggregates	190
Table 6.4: Percentage of hits in each Sample	191
Table 6.5: Percentage of AE hits in the bigger sized un-notched samples	193
Table 6.6: Flexural strength and Fracture Toughness for each sample containing incremental aggregate sizes	215
Table 7.1: AE response of concrete with different additives under compressive loading	248

Table 8.1: Tabulated results of flexural strength, fracture toughness, and A.E. energy of different specimens	279
Table 8.2: AE Parameters under compression and flexural condition	285
Table 8.3: Role of admixtures and aggregates towards toughening and AE signals	291
Table 8.4: Establishing of toughening modes through research at RGU with the aid of AE	296

NOMENCLATURE

a	one-half of the crack length
AU	Aberdeen University
AE	Acoustic Emission
ASR	Alkali Silica Reaction
AR	Alkali-resistant
Al	Aluminium
ASNT	American Society for Non-destructive Testing
+	and
/	And/Or
b	breadth
BS	British Standards
Ca	Calcium
CaCl	Calcium Chloride
CO ₂	Carbon dioxide
Cl	Chlorine
CSIRO	Commonwealth Scientific and Industrial Research Organisation
CMOD	Crack-mouth opening displacement
d	depth
dB	decibel
$d\sigma$	compressive strength attained after the initial curing period
dt	time of the initial curing period (hr)
E	modulus of elasticity
ε	Strain
E	constant Young's Modulus
EDXA	Energy Dispersive x-ray Analysis
EN	European Standard

e.g.	For Example
F	Force
f_c	Compressive strength
Fe	Iron
FPZ	Fracture Process Zone
FRC	Fibre Reinforced Concrete
G _c	Fracture Energy
G _F	fracture energy
G_{Ic}	the critical energy strain rate per crack tip
G _{IC}	critical fracture energy release rate G _{IC}
GFRP	Glass fibre reinforced plastic
GRC	Glass-reinforced cements
GPa	Giga Pascals
<i>I</i>	moment of area
i.e.	That is
IWB	Institution of Construction Materials
J	Joules
K_c	fracture toughness/stress intensity factor
K_{Ic}	Critical stress intensity factor
kHz	Kilo-Hertz
kN	Kilo-Newton
K and k	predetermined constants depending on the mix proportions
L	Length
<i>L, B, W</i>	Length, breadth and width
LMP	Liquid Metal Porosimetry
LSAFT	Linear Synthetic Aperture Focusing Technique
<i>M</i>	bending moment

MHz	Mega Hertz
MPa	Mega-Pascals
MN	Mega Newton
m	metres
m ²	metres squared
Mg	Magnesium
mm	milli-meter
mV	milli-volts
MR	Modulus of Rupture
MRF	Material Recycling Facilities
<i>N</i>	Correction factor
N	number of cycles
Na	Sodium
NaCl	Sodium Chloride
Na ₂ SO ₄	Sodium Sulphate
NaSi	Sodium Silicate
NDE	Non-destructive evaluation
NDT	Non-Destructive testing
NMLAB	National Materials Laboratory Advisory Board
OPC	Ordinary Portland Cement
P	applied load
Param	Parametric
ρ	Density
<i>r, θ</i>	angular coordinates
<i>r_p</i>	fracture process zone size
RC	reinforced concrete
RGU	Robert Gordon University

R	Rebound value
R	average rate of curing
RMS	Root Mean Square
R^2	Coefficient of Variation
Si	Silicon
S	Sulphur
SEM	Scanning Electron Microscope
SENB	Single-edge notch bend
T.D.	Time domain
TZ	Transition Zone
US	Ultrasound
U.K.	United Kingdom
vs	Versus
V	Ultrasonic Pulse Velocity
V_{UT}	ultrasonic pulse velocity
ν	Poisson's ratio
WRF	Wave reflection factor
WRAP	Waste and Resource Action Programme
XRD	X-ray diffraction
Y	a function of a/W (a : area; W : width)
Y	Surface Energy
3D/2D	Three/Two Dimensional
σ	Stress
σ_c	Compressive stress of concrete
σ_f	Griffith fracture stress ($\sigma_f = (\frac{2YE}{\pi a})^{1/2}$)
σ_{yy}	tensile stress in y direction
σ_{xx}	tensile stress in x direction

τ_{xy}	shear stress in xy direction
μ	Poisson's ratio of concrete
/hr	per hour
μs	micro-seconds
<	Less than
>	Greater than
%	Percentage

TABLE OF CONTENTS

ABSTRACT	i
ACKNOWLEDGEMENT	iii
DECLARATION	iv
PRESENTATIONS	v
LIST OF FIGURES	vi
LIST OF TABLES	xv
NOMENCLATURE	xvii
CHAPTER 1	
INTRODUCTION	1
1.1 Introduction to Concrete	3
1.2 Brief Review of Concrete Properties	5
1.2.1 Mechanical Properties of Concrete: Strength of Concrete	6
1.2.2 Compressive Strength and the Need for Compressive Test	7
1.2.3 Flexural Test	8
1.2.4 Fracture of Concrete	8
1.3 Microstructure of Concrete	9
1.3.1 Microstructure of the Hydrated Cement Paste	11
1.3.2 Microstructure of the Aggregate	11
1.3.3 Interfacial Transition Zone	12
1.4 Toughening Mechanism in Concrete	14
1.4.1 Residual Stresses Measurement Techniques in Concrete	15
1.5 Failure and Strength of Concrete	16
1.5.1 Fracture Mechanics of Concrete	19
1.6 Non-destructive Evaluation of Concrete Using Acoustic Emission (AE) and Ultrasound (US): A Detailed Literature Review	30
1.6.1 AE in Concrete	32
1.6.2 Ultrasound (US) in Concrete	45
1.6.3 Limitations of Existing Investigation on Concrete	53
1.7 Research Objectives and Methods	54
1.7.1 Previous Collaborative Investigation	54
1.7.2 Aim of This Research	55
1.7.3 Rationale of Research Methodology	55
1.7.4 Specific Objectives Undertaken in this Research	57

CHAPTER 2	
NON DESTRUCTIVE TESTING (NDT) TECHNIQUES	59
2.1 Introduction to Non-Destructive Testing	59
2.2 Introduction to Ultrasonic Technique	61
2.2.1 Ultrasonic Theory	63
2.2.2 The Rebound Value	65
2.3 Acoustic Emission (AE) as a Non-Destructive Technique	66
2.3.1 AE Background	68
2.3.2 AE Theory	70
2.3.3 AE Signal Parameters and Representation	71
CHAPTER 3	
MATERIALS AND EXPERIMENTAL METHODS	74
3.1 Components of Modern Concrete	74
3.2 Cement and Concrete: Ordinary Portland Cement	74
3.2.1 Additives	77
3.2.2 Accelerators: Needs and Types	77
3.2.3 Chemical Effects on Concrete	79
3.2.4 Calcium Carbonate in Concrete	79
3.2.5 Sodium Sulphate in Concrete	80
3.2.6 Other Additives in Concrete	80
3.3 Expansive Cement (Modified Portland cement)	81
3.4 Aggregates in Concrete	82
3.5 Waste Materials	83
3.5.1 Glass Aggregates as Waste Materials	84
3.5.2 Rubber Aggregates	88
3.6. Concrete Reinforcements	90
3.6.1 Fibres in Concrete	90
3.6.2 Glass Fibre Reinforced Concrete	92
3.6.3 Carbon Fibre-Reinforced Concrete	93
3.7 Non-Destructive Characterisation of Concrete	94
3.7.1 Ultrasound Testing	94
3.8 Flexural Strength of Concrete	96
3.8.1 Bend Tests	96
3.8.2 Flexural / Three Point Bend Test	97

CHAPTER 4

EXPERIMENTAL METHOD	99
4.1 Ultrasonic Examination	99
4.1.1 Test Procedure	100
4.1.2 Compressive Testing	103
4.2 Acoustic Emission Monitoring System	106
4.2.1 Sensors	107
4.2.2 Pre-Amplifiers	107
4.2.3 Personal Computer and Software	107
4.3 Acoustic Emission Parameter Set-up	108
4.3.1 Threshold Selection	108
4.3.2 Test Method (Sensor Coupling Test (Auto-calibration))	110
4.4 Equipments Used	111
4.5 Sample Moulds	112
4.5.1 Sample Preparation	113
4.6 Couplant in US and AE measurement	113
4.7 Manufacturing of Specimens Measurement of Flexural Tests	114
4.8 Preparation of Waste Aggregate: Glass	115
4.8.1 Rubber	117
4.9 Flexural 3-point bend test set-up: Instron flexural testing machine	117
4.10 Acoustic Emission Set-up	118

CHAPTER 5

5.0 RESULTS AND DISCUSSIONS	122
5.1 The Development of a Model Based on Ultrasound to Monitor the Compressive Strength in Mortar over a 28 days Curing Period	123
5.2 The Size Effect of Sample Geometry	125
5.3 Effect of various additives on 28 day initial hydration time and strength	129
5.4 The Effect of Additives on the Micro-structure of Concrete	137
5.4.1 Sodium Sulphate	138
5.4.2 Sodium Silicate	140
5.4.3 Calcium Chloride	141
5.5 Compressive Strength of Concrete Containing Waste Materials as Aggregates	145

5.5.1 Calculation of the Modulus of Elasticity of Concrete Containing Waste Materials	151
5.6 Brief Summary of Ultrasound and Microscopic Results	154
CHAPTER 6	
6.1 AE Monitoring of Concrete Blocks Containing waste materials as aggregates under Compressive Load	158
6.2 Summary	165
6.3 Interfacial Bonding between Glass Aggregates and Cement	167
6.4 Three-points Tests on Smaller Blocks	169
6.4.1 Sample BD1: Plain Concrete	170
6.4.2 Sample BA2: Powdered Glass	172
6.4.3 Sample BC1: 40 g 2-1 mm Glass Aggregates	174
6.4.4 Sample BE1: 40g 4-2 mm Glass Aggregates	176
6.4.5 Sample BB2: 80 g 4-2 mm Glass Aggregates	178
6.5 Three-points Tests on Larger Blocks (210×70×70 mm)	180
6.5.1 Sample BG1: Plain Concrete (BG1)	180
6.5.2 Sample BI1: 60g Powdered Glass	182
6.5.3 Sample BF1: 60g 2-1mm Glass Aggregates	184
6.5.4 Sample BH1: 60g 4-2mm Glass Aggregates	186
6.5.5 Sample BJ1: 120g 4-2mm Glass Aggregates	188
6.5.6 Comparison and Discussion on the AE Test Results	190
6.5.7 AE Waveforms: AE Frequency Domain Analysis	198
6.6 AE Monitoring of cracks in concrete with the increment of Glass Aggregate Sizes under flexural condition	200
6.6.1 Plain Mortar: Sample KOLA0B	201
6.6.2 Mortar with < 1mm Glass aggregates: Sample KOLA2B	203
6.6.3 Mortar with 1 – 1.7 mm Glass aggregates: Sample KOLA 5B	205
6.6.4 Mortar with 1.7 – 2.36 mm Glass aggregates: Sample KOLA4B	207
6.6.5 Mortar with 2.36 – 3.35 mm Glass Aggregates: KOLA1B	209
6.6.6 Mortar with 3.35 – 4 mm Glass Aggregates: Sample KOLA 3B	211
6.6.7 Discussion	213
6.6.8 Flexural Strength Measurements	215
6.6.9 Summary	217

6.7	Monitoring Toughening Behaviour due to Addition of Various Additives and Aggregates	218
6.7.1	Crack Bridging and Grain Bridging: Plain Mortar, Mortar with Glass Plate, Mortar with Glass Aggregates and Glass Plate	218
6.7.2	Plain Mortar	218
6.7.3	Mortar with Glass Plate	220
6.7.4	Mortar with Glass Plate and Glass Aggregates	222
6.7.5	A Summary	225
6.8	AE monitoring of cracks in concrete containing Rubber Aggregates under flexural load condition	228
6.8.1	Mortar with 100 g rubber aggregates: Sample Kolar 2b	228
6.8.2	Mortar with 150 g rubber aggregates; Sample Kolar 3b	230
6.8.3	Mortar with 200g rubber aggregates: Sample Kolar4b	232
6.8.4	Mortar with 250g rubber aggregates; Sample Kolar5b	233
6.8.5	Summary	236
CHAPTER 7		
7.1	Toughness Monitoring of Concrete with Altered Properties under Compression	238
7.1.2	Plain Concrete Mortar (No additive)	239
7.1.3	Mortar with Calcium Chloride	240
7.1.4	Mortar with Sodium Sulphate (10 g, 15 g and 25 g)	241
7.1.5	Mortar with Sodium Silicate	244
7.1.6	Summary	245
7.2	AE Monitoring of Concrete Blocks Containing Smooth and Rough aggregates under Flexural Load	250
7.2.1	Expansive cement with mixed size 3mm glass beads: Exglbds3	251
7.2.2	Expansive cement with 3 mm Pebbles Sample: Expeb3	253
7.2.3	Expansive Cement Mortars with 3mm rough glass aggregates (Sample a2e)	255
7.2.4	Summary	257
7.3	AE Monitoring of Ordinary Portland Cement matrix with admixtures and glass plate	259
7.3.1	Summary	267

CHAPTER 8	
8.0	Comparison of AE Signal Parameters Emitted from Mortars Containing Admixtures and Waste Aggregates of Mixed Sizes 269
8.1	AE Monitoring of Mortars samples (14 days curing) under Flexural Load 269
8.1.1	Sample Brglcam: Mortar with Glass Plate 269
8.1.2	Sample Brglcam1: Mortar with Glass Aggregates 270
8.1.3	Mortar with Sodium Sulphate and Glass Plate (14 days curing) 272
8.1.4	AE Monitoring of Glass Plate and Glass Aggregates (28 Days Curing) Under Flexural Load 274
8.1.5	Discussion and Summary 277
8.2	Further AE Monitoring of Mortars with Admixtures under Flexural Load 281
8.2.1	Summary 284
8.3	Comparative study of AE characteristics between compression and flexural condition 285
8.4	Optical Micrographs of the Fractured Sections 290
8.5	Summary of Fracture Toughening Mechanism due to Different Inclusions 291
8.6	Summary of Research Investigations 293
CHAPTER 9	
	Conclusion 297
CHAPTER 10	
	Recommendations and Suggestions for Future Research 301
REFERENCES 304	
APPENDIX A 327	
APPENDIX B1 348	
APPENDIX B2 353	

INTRODUCTION

Concrete is one of the more sustainable building materials when both the energy consumed during its manufacture and its inherent properties in use are taken into account. The cement and concrete sector is making a concerted, coordinated effort to continually reduce its negative impact on the environment.

Cement based composite (concrete) has a wide range of applications and has been investigated over centuries to enhance its physical/mechanical properties, durability, resistance to environment, manufacturing processes etc. The research field is still active across the globe in particular to enhance its workability, performance, manufacturing process, addition of ingredients as accelerators and retarders to suit a specific application and use of waste materials to produce a healthy impact on the environment.

A mechanism for the toughening of coarse-grained ceramic has been successfully developed in the refractory industry using residual stresses at micro-structural level [115]. This was extended to concrete by the research group in Aberdeen University (AU) [56, 115-118]. They reported that toughening in concrete can be achieved by the release of the residual stresses as the macro-crack propagates. Circumstantial evidence of the creation of favourable residual stress using additives exists, but the mechanism in action has not been understood. This research work was carried out at Robert Gordon University (RGU) by using Non-Destructive Technique (NDT) to monitor and understand the role of micro-residual stress in providing toughening to cement based material.

Therefore this research concentrated on the study of concrete materials applying:

- Ultrasound (US) to examine the long term stability and development of the micro-structure.
- Acoustic Emission (A.E.) in relation to cracking mechanism, expansive matrix and interfacial bonding.

- The investigation therefore focussed on the development and application of NDT to characterise concrete and study changes under applied load in the materials at micro-structural level.

CHAPTER 1

INTRODUCTION

1.1 Introduction to Concrete

Portland cement based concrete is at present the most widely used manufactured material in the construction industry. It is not easy to identify another building material which is as flexible as concrete. It is a well chosen material where strength, permeance, durability, abrasion resistance, impermeability, and fire resistance are essential requirements [1].

Although our knowledge and understanding of the material is far from complete, and research is being continued apace, concrete has been effectively used in many cultures and in many societies. It is not just a modern material; various forms of it have been used for several millennium.

It is essential to have a proper awareness of the appropriate properties of any material if an acceptable end product is to be obtained and concrete, in this respect, is same with other materials. Concrete is the most extensively used engineering material. The reasons for this are [2]:

- Concrete is resistive to water penetration;
- Structural concrete components can be produced into wide range of shapes and sizes;
- The main ingredients for making concrete – Portland cement and aggregates are reasonably cheap and are usually obtainable on a worldwide basis;
- In contrast to the majority of other engineering materials, much less energy input is required for the manufacture of concrete. A vast amount of numerous industrial wastes can be recycled as a replacement for the cementitious material or aggregates in concrete. Concrete as a structural material therefore becomes more appealing due to the considerations of energy and resource conservations.

Although globally regarded as a very popular material, the proliferation of concrete has been a mixed blessing. If its mixture or placement is not carried out accurately or its maintenance is performed in a poor manner, then concrete structures are prone to premature deterioration. More significantly, the escalation of global concern about environmental issues and the requirement to alter our way of life for the sake of sustainable development has led to the recognition of the concrete industry as a leading user and abuser of natural resources contributing to the release of greenhouse gases [2].

These concerns have created difficult challenges for the concrete industry for present and future generations. The construction personnel and the public in general will insist on environmentally friendly high-performance building materials at a reasonable cost. This requires outstanding mechanical properties and durability [2].

On the basis of methodical analysis of the micro-mechanical behaviour of the cement-paste and its interaction with aggregate particles and other mix components, adjustment can be carried out of specific material properties without having adverse affect on the others. Additionally, modelling methods are being continuously developed that can enable us to simulate such interactions and analytically make a prediction of the outcome [3].

The chemistry of concrete and its mechanical properties [4] have been well investigated and a lot of development is being made in understanding various characteristics of its behaviour. Developments in chemical admixtures help in controlling production techniques and, in attaining the desired properties in concrete. However, there are behavioural characteristics of this famous material that are still not fully understood. The main reason for this is that the internal mechanisms that control the mechanical behaviour of concrete have not been observed directly.

There has been considerable work on the strength of concrete [5], which has mainly been connected to the overall porosity of the cement paste matrix and the quantity and nature of the aggregates. Mechanical strength is dependent on defects and not on any overall average property, e.g. mechanical/property and so it is very difficult to relate to micro-structure.

Concrete is an object for preservation of natural resources, since concrete is globally the most extensively used material. Recycled materials are being increasingly used in application of concrete manufacture. Recycled concrete for instance is being used effectively in various projects; and because the problems of alkali-silica reaction have been solved, crushed waste glass is now obtainable as a precious source of aggregate [6].

One of the major global environmental concerns is to dispose waste material safely. To investigate the suitability of waste materials such as rubber tyres, glass, etc in the manufacturing of concrete, continuous work is being carried out in various parts of the world [7].

Various attempts are in progress to considerably enhance the microstructure, and therefore the durability properties of concrete, which are not easy to attain by the use of pure Portland cement. The purpose is to make the cements and concrete cheaper, and to offer a mixture of modified properties of waste materials and Portland cements suitable for a particular application [8]. There is a growing demand for better insight into material properties, and improved control of the micro-structure developing in the construction material, to increase durability.

1.2 Brief Review of Concrete Properties

Concrete quality is dependent on the properties of the materials used, the methods of batching and mixing, and manufacturing. The essential elements of concrete are cement, mineral aggregate, and water. To enhance certain desired properties, some admixtures and agents can also be added to the concrete mix, but they are not properly regarded as concrete elements [9].

Once water is added, cement transforms into a rock hard mass. This is because the chemical reactions generate an arrangement of interlocking crystals that connect the material together. The binding agent in concrete is the mixture of cement and water and not the cement itself. The cement compounds react with water in various manners and for convenience sake all reactions with water are known as hydration. Hydration results in the creation of a gel around each of the cement particles and in time these layers of gel develop to the point that they come into contact with each other. The

commencement of conspicuous stiffening in the cement paste is termed as the *initial set*. Additional stiffening take place as the volume of gel increases and the stage at which this is complete and the final hardening process, responsible for its strength, commences is known as the *final set*. The time from the addition of the water to the initial and final set are known as the *setting times* as reported in BS 4550 [10], [11].

1.2.1 Mechanical Properties of Concrete: Strength of Concrete

In structural design the first consideration is for the structural elements to be able to carry the loads imposed; therefore strength is considered to be the most important single mechanical property of concrete. Strength is also an essential property because it is related to several other essential properties which are more difficult to measure directly, and a simple strength test can give an indication of these properties, for example increase in compressive strength of concrete gives an increase in modulus of elasticity [12]. The strength of concrete has to be qualified with terms such as tensile strength, flexural strength or compressive strength [13].

The compressive strength of the material is generally specified because the working stress theory for concrete design considers concrete as generally appropriate for sustaining compressive load. The tensile and flexural strengths of concrete are typically of the order of 10 and 15 percent, respectively, of the compressive strength [14]. Such a large difference between the tensile and compressive strength is attributed to lack of elasticity, heterogeneousness and complexity of the micro-structure of concrete [14].

Strength of concrete may be measured in a number of ways, such as, strength in compression, in tension, in shear or in flexure. All these indicate strength with resistance to a particular method of testing. The mechanics of failure is a complex phenomenon [1].

1.2.2 Compressive Strength and the Need for Compressive Test

Strength is the property normally specified in concrete design and quality control. This is because other properties of concrete, such as elastic modulus, water tightness or impermeability, and resistance to weathering agents including aggressive waters, are understood to be reliant on strength and may therefore be deduced from the strength data. The compressive strength of concrete is several times higher than other types of strength; therefore a majority of concrete elements are designed to take advantage of the greater compressive strength of the material. The variables that have an effect on the strength of concrete are shown in figure 1.1.

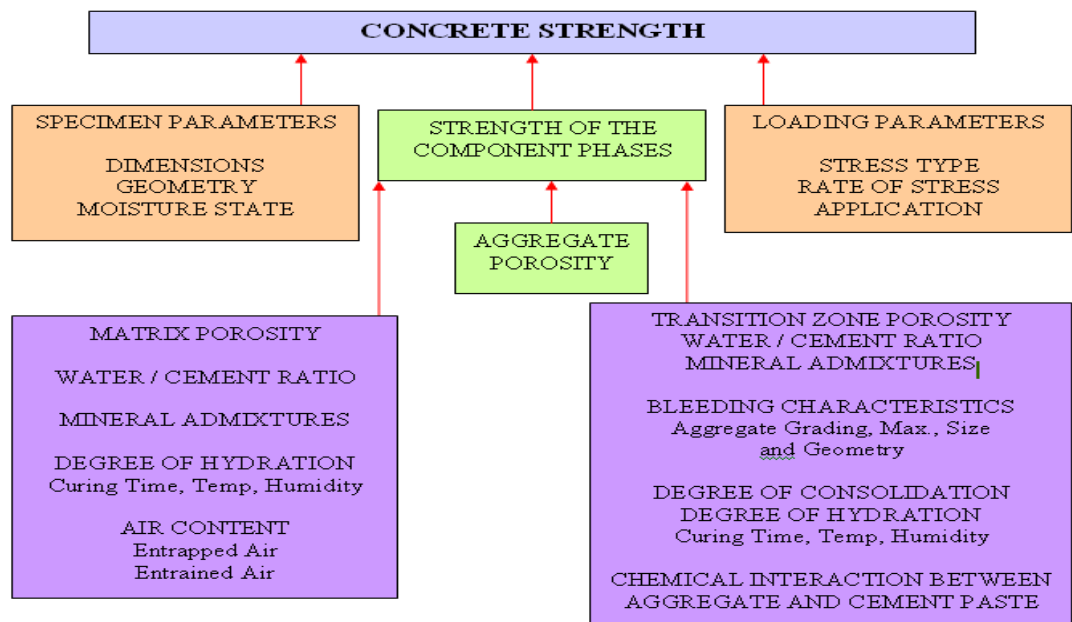


Figure 1.1: Factors influencing concrete strength [adopted from 14].

Compressive strength is usually defined as the measured maximum resistance of a concrete or mortar specimen to axial loading. It is normally expressed in Mega-Pascals (MPa) at an age of 28 days and is usually specified by the symbol f_c [15].

Compressive strength can be used as an index to judge flexural strength, once the relationship has been established for the particular mix design and size of the unit [16].

1.2.3 Flexural Test

Direct testing of concrete under tension is not possible because of its brittleness since it is difficult to grip and align. Eccentric loading and failure at or in the grips is very hard to avoid [12]. Therefore, the flexural test is preferred. This provides a way of measuring the materials behaviour subjected to beam loading.

Flexural Strength is the ability of a beam or slab to resist failure in bending. The flexural strength is usually expressed as Modulus of Rupture (MR) in MPa. Hence, laboratory mix design based on flexure may be necessary, or cement content may be chosen from past experience to yield the required design of MR. MR can be employed for field control and in the acceptance of pavements. Very few flexural testing is used for structural concrete [17]. The tensile strength of concrete is important in the design of concrete roads and runways [17].

1.2.4 Fracture of Concrete

Even though concrete is a primitive and most commonly used material, a lot of properties and characteristics of concrete is neither easily nor accurately understood, and research is still being continued using various techniques to acquire a better knowledge of the characteristics of concrete. Due to its main uses in building and construction works, as well as a selection of other heavily used applications (e.g. roadwork), understanding of its mechanical behaviour is receiving most attention from engineers and scientists using a variety of testing methods, but owing to its complex nature, there are issues of concern to both the manufacturers and users.

Concrete behaves like a structure of two dissimilar materials (aggregate and cement paste) which becomes more complex by the various quantities of materials that either make up the cement paste or function as the aggregate. The interface between the aggregate and cement is usually considered as the weakest link [19] in concrete which consequently has a major effect on the mechanical behaviour of concrete.

The interfacial bonding between the cement and aggregate performs a crucial function in the strength of concrete. With the hardening of fresh concrete, loss of moisture starts occurring in the cement paste causing shrinkage. Shrinkage does not occur in the aggregate material; the boundary conditions of the structure or the object during casting resist the shrinkage of the cement paste. The boundary conditions, non-uniform distribution of shrinkage strain and the restraints from the aggregates cause increase to tensile stresses. These tensile stresses give rise to internal flaws and cracks within the concrete before the application of any external load [19]. The mechanical behaviour of concrete is controlled by the existence and propagation of these internal cracks during loading.

It is difficult to observe the fracture nature of concrete because of its complexity. This makes the crack propagation in concrete complex and it chooses a path based on the structure and constituents of the material, hence it's behaviour is not predictable. According to Shah S.P. [13], for the design of concrete structures, it is becoming increasingly necessary to look at crack growth and propagation to avoid catastrophic failure. Failure in concrete is usually due to crack propagation. Understanding the reasons and the circumstances under which concrete fails are important for design of concrete structures, as well as developing new cement based materials.

When it is difficult for cracks to grow, a material is said to be tough and when crack propagation is easy, it is known as a brittle material. It would therefore clearly be useful to have a technique that is able to detect a crack and its propagation [18]. A number of techniques exist that are categorised as non-destructive testing techniques, which are designed to detect, and usually size, stationary cracks without damaging serviceability of the component. However one technique exists and is readily available which can detect a growing crack but not an inactive crack; this passive technique is called acoustic emission (AE). It is the application of this AE technique which is considered in this work.

1.3 Microstructure of Concrete

Many characteristics of concrete do not abide by the laws of mixture even though it is a composite material. For example, if both the aggregate and the hydrated cement paste under compressive loading are separately tested, it

would fail elastically, whereas concrete itself exhibits inelastic behaviour prior to fracture. In addition, the strength of concrete is normally much lower than the individual strength of the two components. These irregularities in the behaviour of concrete can be justified on the basis of its microstructure, particularly the vital function of the interfacial transition zone between coarse aggregate and cement paste [14].

It is essential to understand the microstructure of concrete to understand the crack propagation in concrete. It is very difficult to establish a clear pattern of the microstructure of concrete from which an opinion of the material's behaviour can be formed with confidence since concrete has a highly heterogeneous and complex microstructure. The developments in the area of materials have resulted mainly from recognition of the principle that the properties originate from the internal microstructure, i.e. modification can be made to the properties of materials by making appropriate alteration in the microstructure of a material.

The distinctive features of the concrete microstructure are [14]:

- i) Interfacial Transition Zone, which represents a small region next to the particles of coarse aggregate. It exercises a far greater influence on the mechanical behaviour of concrete than is reflected by its size;
- ii) Each of the three phases is itself a multiphase in character. For example, each aggregate particle may contain several minerals in addition to micro-cracks and voids;
- iii) The microstructure of concrete is not an intrinsic characteristic of the material, because the two components of the microstructure (interfacial transition zone and hydrated cement paste) are subject to change with time, environmental humidity and temperature.

The theoretical microstructure-property relation models are not much helpful for predicting the behaviour of concrete mainly because of the highly heterogeneous and dynamic natures of the microstructure of concrete. To understand and control the composite material such as concrete, a broad

knowledge of the important features of the microstructure of each of the three phases of concrete is nevertheless important [14].

1.3.1 Microstructure of the Hydrated Cement Paste

The various phases of hydrated cement paste are neither uniformly distributed nor uniform in size and morphology. Micro-structural inhomogeneities in solids can lead to severe effects on strength and other mechanical properties that are associated with it, because they are controlled by the micro-structural extremes, not by the average microstructures. The desirable engineering properties of hardened concrete: strength, dimensional stability, and durability are influenced by the proportion as well as the properties of the hydrated cement paste, which in turn depend on the micro-structural features, i.e. the type, amount, and distribution of solids and voids. The main source of strength in the solid products of the hydrated cement paste is the presence of the Van der Waals forces of attraction. Adhesion between two solid surfaces can be attributed to these physical forces, the degree of the adhesive action being dependent on the extent and the nature of the surfaces involved, [32] and [33].

1.3.2 Microstructure of the Aggregate

The aggregate phase is primarily responsible for the unit weight, elastic modulus, and dimensional stability of concrete. These properties of concrete "depend to large extent on the bulk density and strength of the aggregate which, in turn, are determined by physical rather than chemical characteristics of the aggregate" [14]. The properties of concrete are also affected by the shape and texture of the coarse aggregate. The aggregates, which are flat or contain elongated particles, may have adverse affect on the properties of concrete [14].

The aggregate phase is stronger than the other two phases of concrete but has no direct influence on the strength of concrete except in the case of some highly porous and weak aggregates, such as pumice. The strength of concrete however can be affected in an indirect way by the size and the shape of the coarse aggregate. The larger size of aggregate in concrete and higher the proportion of elongated and flat particles, the greater will be the tendency for

water films to accumulate next to the aggregate surface that leads to the weakening of the interfacial transition zone is known as *bleeding* in concrete technology. This bleeding tends to accumulate in the vicinity of elongated, flat, and large pieces of aggregate. In these locations, the aggregate-cement paste interfacial transition zone tends to be weak and easily prone to micro cracking. This phenomenon is responsible for the shear-bond failure at the surface of the aggregate particle [14].

1.3.3 Interfacial Transition Zone

Concrete is usually regarded as a two phase materials i.e., cement paste and aggregate phase. At macro level it can be observed that aggregate particles are scattered in a matrix cement paste. At the microscopic level, the complexities of the concrete starts showing up, especially in the vicinity of large aggregate particles. This area known as the transition zone ‘represents the interfacial region between the particles of coarse aggregate and the hardened cement paste’. Transition zone is usually a plane of weakness and therefore, has far greater influence on the mechanical behaviour of concrete [30].

The transition zone develops micro-cracks even before a structure is loaded due to drying shrinkage or temperature variation. Under the loading conditions of the structure at high stress levels, these micro-cracks propagate and bigger cracks are formed resulting in failure of bond, thus transition zone is regarded as strength limiting region in concrete [30].

The interfacial transition zone is normally regarded as the strength-limiting phase in concrete. It is the weakness of this zone that concrete fails at a significantly lower stress level than the strength of either of the two components. Since it does not require very high energy levels to expand the cracks that already exist in the interfacial transition zone, even at 50 percent of the ultimate strength, higher incremental strains may be obtained per unit of applied stress. The stress concentrations at large voids in the mortar matrix become sufficiently large to initiate cracking at stress levels that are higher than approximately 70 percent of the ultimate strength. As the stress increases, the matrix cracks steadily spread until they join the cracks originating at the interfacial transition zone. The material ruptures once the

crack system becomes continuous. Substantial energy is required for the formation and extension of matrix cracks under a compressive load. Under tensile loading on the other hand, cracks propagate quickly and at a much lower stress level. This is the reason for the failure of concrete in a brittle manner under tension but is comparatively tough under compression. This is also the reason for the tensile strength being significantly lower than the compressive strength of concrete [31].

The microstructure of the interfacial transition zone, especially the volume of voids and micro-cracks present, has an enormous effect on the stiffness or the elastic modulus of concrete. The interfacial transition zone acts as a bridge between the two components: the mortar matrix and the coarse (rough) aggregate particles (fragments) in the composite material. The composite stiffness is reduced because of the presence of the voids and micro-cracks in the interfacial transition zone, which do not allow stress transfer, even when the specific individual components are of high stiffness. Concrete is more permeable (porous) than the corresponding hydrated cement paste or mortar mainly due to the presence of micro-cracks in the interfacial transition zone at the interface coarse aggregate. An area of active research interest currently is the 'transition zone' between cement paste and the aggregate [31].

The paste nearer to the aggregate surface is considerably different to that of the bulk paste, and crucially this transition or interface zone is much weaker than the rest of the paste. Cracking will start in this zone as the load on the concrete is raised, and subsequently propagate into the hardened cement paste until crack paths are formed through the concrete, as shown in figure 1.2, which when extensively large enough will lead to complete breakdown or failure [12].

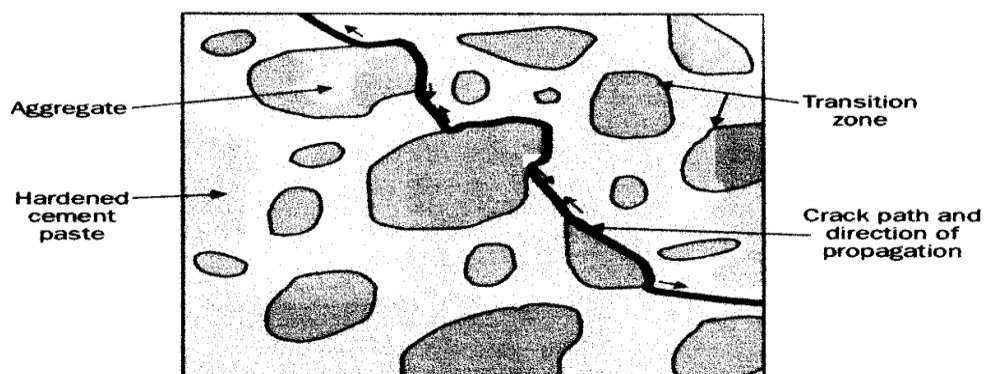


Figure 1.2: Cracking pattern in normal strength concrete [Adopted from 12].

1.4 Toughening Mechanism in Concrete

The toughness is a measure of energy while the strength is a measure of the stress required to fracture the material. Thus two materials may have very similar value of strength but different toughness values. With the propagation of cracks in concrete, many toughening mechanisms start taking place. The inelastic zone around a crack tip is expressed as the fracture process zone and is the location of these toughening mechanisms. Crack shielding, crack deflection, aggregate bridging, crack tip blunting and crack branching are some of the most common toughening mechanisms known until the present moment [34].

Crack shielding takes place when the major crack propagates into a zone that consists of a high density of flaws, such as water-filled pores, air voids attained during casting process and shrinkage cracks. Part of the energy being introduced by the applied load is consumed by the high-density flawed region. Compared to the main crack, the flawed region has a random orientation and therefore does not make contribution to the propagation of the main crack. When the main crack must alter its direction of propagation due to a strong particle, such as an aggregate lying in its path, crack deflection occurs. If the main crack path is altered more, then the greater amount of energy must be introduced into the material to cause fracture. When a crack has advanced beyond and through a particle, such as an aggregate, which is capable of distributing stresses from one side to the other (of the main crack), bridging occurs. This transfer of stress is continued until the particle ruptures or is pulled out. Bridging is at times purposely introduced (glass slide in this investigation) into concrete by adding small fibres to serve as bridges across the surface of the cracks. Some of the commonly used fibres are steel, polypropylene, aramide and glass fibres [19].

The propagation of the main crack is occasionally terminated by a large internal void; this toughening mechanism is termed as crack tip blunting. When a crack tip propagates into a void, the tip of the crack becomes blunt and an extra amount of energy is needed to propagate the crack with a blunt tip. When the main crack splits into two cracks, the toughening mechanism of crack branching is introduced into the specimen. More energy is needed to propagate two cracks through concrete than it does to propagate one crack.

These toughening mechanisms take place amongst one another and absorb a part of the energy being introduced into a concrete specimen by an external force or movement [34].

The fracture mode of a cementitious material relates very closely to the nature of fracture process that take place in that material, based on understanding of the conditions under which a number of toughening mechanisms can occur in a given material, it may be possible to control the fracture mode by tailoring the material microstructure [35].

1.4.1 Residual Stresses Measurement Techniques in Concrete

Based on the type of stresses to which a structural component is exposed and by the interactions between the defects within the component the durability of a structural component is generally determined. These stresses are an amalgamation of those applied in service and those which develop under manufacturing and processing condition, namely the 'residual stresses'. These stresses can be either beneficial and or detrimental to the service performance. For instance, they may be purposely introduced (e.g. shot peening) to improve fatigue performance. Whilst applied stresses can be taken into account during the design of a component, it is more difficult with 'residual stresses' because they are not easy to predict and measure reliably. There is an increasing emphasis on understanding the role of residual stress with the continuous effort to optimise material performance and minimize component weight. There is a requirement for improved measurement techniques and greater confidence in the results of existing techniques. The latest Department of Trade and Industry (U.K.) programme that supports research on materials measurement technology aims to go forward towards meeting both of these objectives [20].

It is doubtful that any component will not be completely inducing any residual stresses during manufacturing and processing. Residual stresses may exist in engineered components, multiphase materials and composites. Based on the type of material and the component, fundamentally, the levels of residual stress may not be significant depending on the manufacturing process. A number of mechanical techniques such as hole drilling, curvature measurements, and crack compliance are usually employed to measure

residual stress by changes in component distortion. Diffraction techniques like Electron, X-ray and neutron diffraction methods are also used. Non-Destructive Testing (NDT) methods such as magnetic effects, e.g. Barkhausen effect or magnetostrictive effect, ultrasonic piezo-spectroscopy are also being developed [20].

Eric Landis used quantitative acoustic emission [21] techniques to measure micro-fracture properties in a range of cement-based materials of varying microstructure, and concluded that materials with lower bulk fracture toughness had fewer numbers of tensile mode micro-cracks while materials with higher bulk fracture toughness had greater numbers of sliding mode micro-cracks [21].

To monitor fracture process [22] an experimental tool such as acoustic emission is well suited. Fracture processes in concrete are being examined for the past 20 years using a range of different Acoustic Emission (AE) methods with varying degrees of sophistication.

Recent investigation has focused on relating acoustic emission characteristics to properties of the fracture process zone [23], [24] and applying AE source location analysis to evaluate damage localization, [25], [26]. More advanced moment tensor analysis [27] is used to examine mixed mode fracture [28] and fracture properties of reinforced concrete structures [29]. It has therefore become obvious that the strength of AE measurement techniques is the ability to monitor microscopic damage taking place inside the material.

1.5 Failure and Strength of Concrete

According to American Standards International, fracture mechanics has enabled scientists and engineers to grasp an understanding of brittle fracture and to establish the conditions that cause a crack to grow in a brittle manner and lead to failure of the structure. Fracture mechanics offers a method to determine the measure of toughness, the limitation to which a material can sustain deformation without fracture taking place.

Concrete is described as a quasi-brittle, and only recently research has led to the development of fracture mechanics tests which are suitable for such quasi-

brittle materials. Fracture toughness provides a lot of information regarding concrete over and above what can be understood from strength [36].

In concrete, the hardened cement pastes, especially those of high compressive strength and low porosity, are brittle and cracks propagations are usually in an unstable mode. The inclusion of dense aggregates entirely changes the fracture pattern. Materials scientists have developed various techniques [37] to help them understand the mechanics of failure and to relate this knowledge to the prediction of the performance of concretes in practice.

One of the methods that have been used includes coating the surface of a concrete with a reflective photo-elastic layer. The high stress concentrations adjacent to aggregate particles may be identified when the concrete is put under load. However this only deals with the surface of the concrete and failure perhaps will occur within the body of the material [37].

Brown and Pomeroy [38] developed fracture toughness tests to see if a study of the propagation of cracks in cement paste and mortar beams would assist in resolving more general queries relating to fracture. It was observed that for hardened cement pastes, K_{IC} , the critical stress intensity factor for crack growth was constant but with mortars the value apparently increased as the cracks extended. This in effect is a blunting of the crack so that the possibility of catastrophic crack propagation is lowered. One of the reasons given is that when a crack encounters a hard aggregate particle, crack branching can take place so that instead of a single crack development a whole family of cracks could gradually be formed and this necessitate the use of larger forces and extra energy [38].

Spooner and Dougill [39] took this argument a stage further and used a range of techniques in an attempt to detect at what stage of compressive loading cracks were first formed. The photo-elastic studies suggested that high stress concentrations could be present in concrete even in an unloaded (no external loads) state so that small cracks are likely to be formed before the concrete is stressed.

Suggestion made by personnel earlier was that the measurable load-induced cracks were not formed by compressive loadings until a stress approaching

70% of the ultimate strength had been attained. This suggestion was based on the observations of the transmission of ultrasonic pulses through the loaded concrete and on the shape shown by the volumetric strain-load curves [37].

Further complicated tests were used, including the detection of acoustic emission when cracks develop, the direct measurement of volumetric strain and the measurement of a change in the initial elastic modulus as a result of a previous loading cycle. The most sensitive technique, however, was based on an analysis of the loading and unloading stress-strain curves for specimens subjected to a series of loading cycles to progressively higher strains. The entire area under the stress-strain curve up to point A is the work done during the first loading; to the same point the area is smaller by the shaded amount on the second loading [37], as shown in figure 1.3.

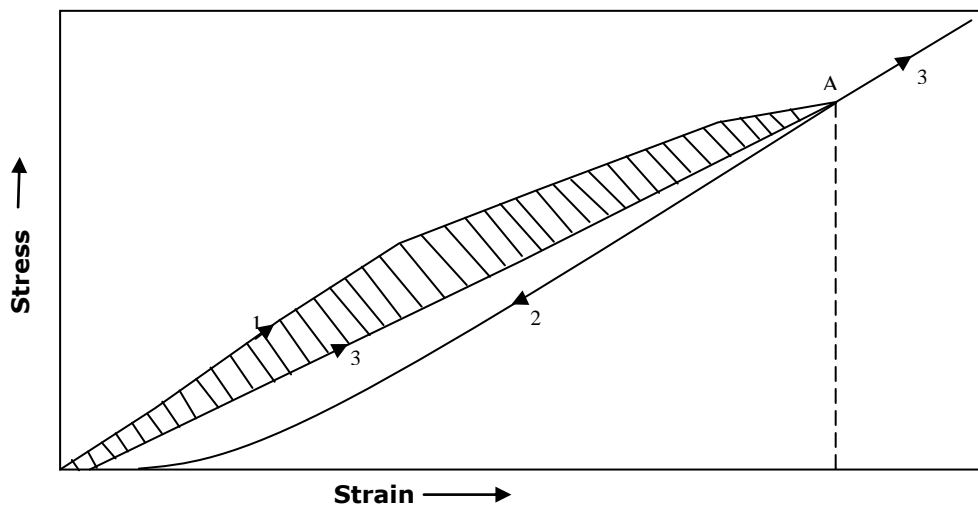


Figure 1.3: Use of repeated loading tests to provide a measure of damage caused to concrete the first time it is loaded. Shaded area represents work unrecovered between first and second loading cycles [Adopted from 37].

This irrecoverable energy was used and it's attribution is made to the internal disruption i.e. damage, or the development of cracks of the concrete. The lower loop was found to be largely reproducible and represents the typical damping capacity of the material [37]. A summary of the results from several of these techniques are shown in figure 1.4, from which it can be seen that some cracks are formed when concrete is loaded.

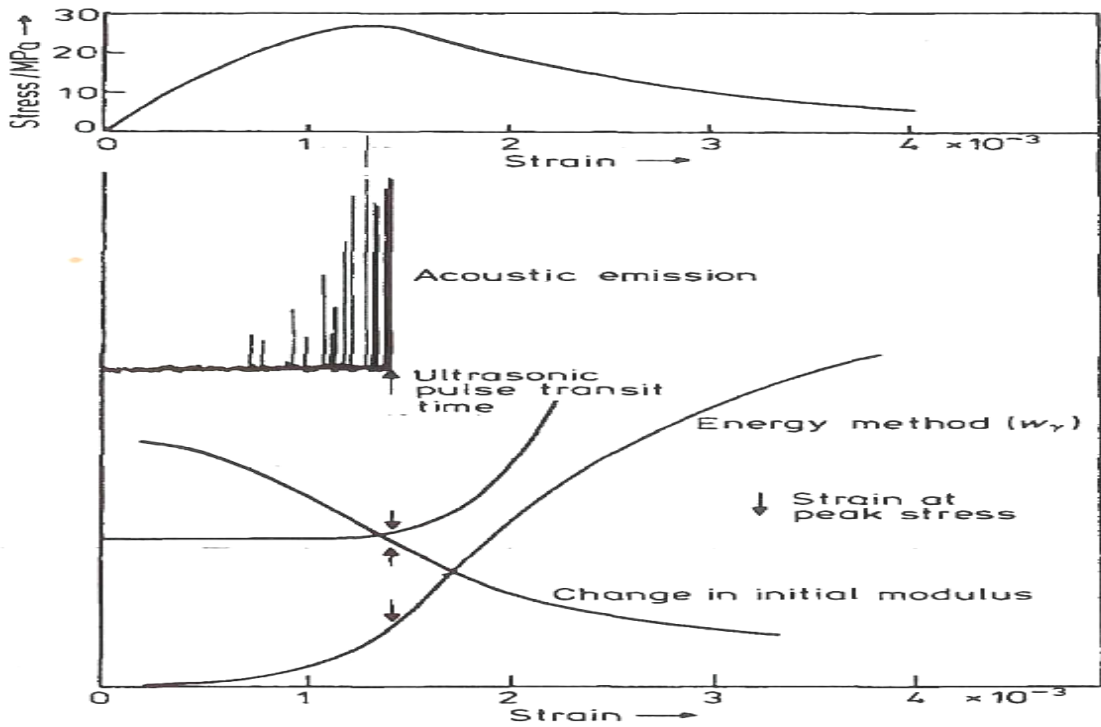


Figure 1.4: Comparison of methods for detecting damage in concrete specimens [Adopted from 37].

If cracks develop so easily in concrete then it would be possible to consider that it may not be a very stable material [37]. Far from it, as C.D. Pomeroy states that "for the cracks normally form only on the very first loading cycle to a given stress, any high stress concentrations are relieved and the stress throughout the concrete becomes more uniform. Subsequent loading to previously achieved stress levels result in no further measurable damage" [37], hence no further acoustic emission was recorded.

1.5.1 Fracture Mechanics of Concrete

The study of fracture mechanics began in about 1920, with the work of Griffith A. A. The principal aim was to understand and describe what happened during fracture in very brittle materials like glass. Later on, the subject developed rapidly, and in the last thirty years fracture mechanics has been utilized in research into concrete. A powerful means for the prediction of crack propagation is provided by fracture mechanics. For example, considering a case where it was required to determine if a given crack in a large structure, such as a concrete dam, will propagate catastrophically under certain loading conditions. The strength criteria can be adopted to predict a crack that will propagate when the stresses reach the ultimate tensile strength of the

material. For sharp cracks, however, the theory of linear elasticity predicts that the stresses at the tip of the crack approach infinity, therefore, this theory predicts that the crack will propagate regardless of how small the applied stress; which is not likely [31] and [33].

Fracture mechanics for concrete can be a helpful tool for the designer because of the insight it provides on size effects, that is, how the size of a structural element will affect the ultimate load capacity and also provides powerful criteria for the prediction of crack propagation [31] and [33].

Griffith's theory for the fracture of materials and its consequent development into fracture mechanics was described by the phenomenon that brittle materials fracture at stresses well below the theoretical failure stress because of the presence of micro-cracks within the material. The Griffith fracture stress, σ_f , is given by the relationship

$$\sigma_f = \left(\frac{2YE}{\pi a} \right)^{1/2} \quad (1.1)$$

where Y and E are the surface energy and modulus of elasticity respectively, and a is one-half of the crack length [40].

There have been a number of studies attempting to apply linear fracture mechanics to concrete, with variable results. According to J. M. Illston and P.L.J. Domone [12] three main reasons for the difficulties encountered have been suggested by the American Concrete Institute 1980:

1. Failure in compression, and to lesser extent in tension, is controlled by the interaction of many cracks
2. Cracks in cement paste or concrete do not propagate in straight lines, but follow tortuous paths around cement grains, aggregate particles, etc., which distort and blunt the cracks, as was shown in figure 1.2;
3. Concrete is a mixture of cement paste, the transition zone and the aggregate, and each has its own fracture toughness (K_{IC}), in themselves difficult to measure.

Despite these difficulties, fracture toughness (K_C), values for cement have been estimated as lying in the range 0.1 to 0.5 $\text{MN/m}^{3/2}$, and for concrete between about 0.45 and 1.40 $\text{MN/m}^{3/2}$ [41]. K_C for the transition zone seems to be smaller, about 0.1 $\text{MN/m}^{3/2}$, confirming the critical nature of this zone. Comparison of these values with those for other materials given in table 1.1 shows the brittle nature of concrete.

Table 1.1: Fracture Energy (G_C) and fracture toughness (K_C) for common construction materials [Adopted from 12].

<i>Materials</i>	G_C (J/m^2)	K_C ($\text{MN/m}^{3/2}$)
Concrete	0.03	0.2
Glass	0.01	0.8
Reinforced concrete	0.2-4.0	10-15
Pure, ductile metals	100-1000	100-350
High-strength Steels	15-120	50-150

For a heterogeneous material such as concrete, evaluation of crack propagation is impossible since (a) many cracks of different sizes, shapes and orientations either pre-exist or are formed under load and (b) the solid particles of aggregates etc. act both as crack arrestors and stress intensifiers. Nevertheless, the theory is useful as an aid to understanding the fracture and failure process [42].

Concrete behaves in an inelastic manner (non-linearly) under stress, the reason for this is that concrete is a three phase heterogeneous material: the cement, the aggregate and the transition zone (TZ). The TZ around the aggregate particles is weaker than other phases, so the presence of its high porosity and low strength allows micro-cracks to easily propagate in the transition zone only. Therefore the concrete behaves in a non-linear behaviour [43].

The existence of the transition zone and its effect on concrete behaviour is widely accepted, Kotsovos suggests that the non-linearity is due to the increase in an internal equivalent compressive stress state, but there is no experimental evidence to verify such opinion [44].

According to Hsu, and his team of investigators, the micro-crack development and propagation controls the shape of the stress-strain curve of concrete during uni-axial compression tests. His other findings are that the total amount of mortar cracking was significantly less than transition zone cracking (i.e. bond cracking) in all stages of loading. He also reported that a number of cracks are initiated at cement paste voids and cracks away from the transition zone. Shrive and El-Rahman and Shrive also support this theory of failure in compression stress state [45] and [46].

It is well known and an established fact that micro-cracks exist in the transition zone due to thermal stresses even before the application of external stresses [43] and [46].

Mehta et. al. report [43], that there are four stages of cracking (as shown in figure 1.5) that can be identified in concrete under uni-axial compression.

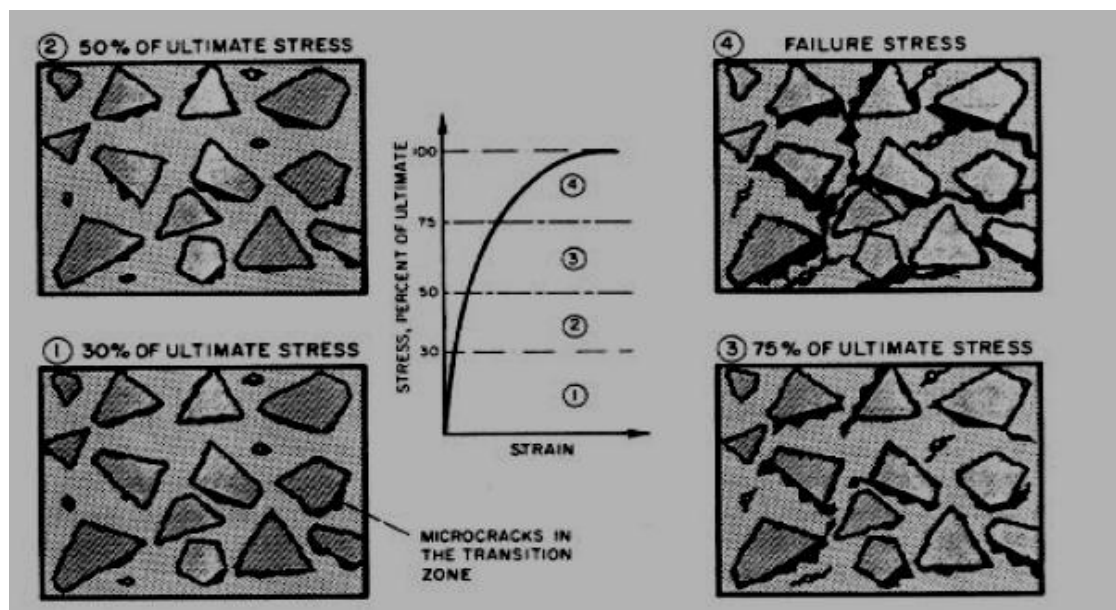


Figure 1.5: The relation between concrete performance and extent of cracking [43]

The non-linear stress-strain behaviour of concrete in compression is largely due to the increasing contribution of micro-cracking to the strain with increasing load. The four stages of cracking in concrete under uni-axial compression is illustrated in figure 1.5. In stage 1 (below 30 percent of the final load) the transition zone cracks remains steady, therefore the stress-strain curve remains approximately linear. As the stress increases beyond 30

percent of ultimate, the cracks begin to increase in length, width and number, causing non-linearity but are still stable and confined to the transition zone (stage 2). At loads above 50 percent ultimate (stage 3), the cracks start to spread into the matrix and become unstable at loads approaching 75 percent ultimate, resulting in further deviation from linearity. Above 75 percent ultimate (stage 4), spontaneous and unstable crack growth becomes increasingly frequent, leading to very high strains.

Two well-established basic criteria governing fracture of materials in either compression or tension are the stress and the energy criteria [47]. The stress principle is based on the fact that the local tensile stress developed in the vicinity of a flaw needs to be large enough to overcome the cohesive strength of the material. The energy principle recognises the fact that extension of a crack needs a certain amount of energy which is difficult to determine.

In the case of quasi-brittle materials like concrete, a large fracture process zone (FPZ), which consumes a large quantity of energy prior to failure, is normally formed ahead of the crack tip as shown in figure 1.6. This fracture process zone provides concrete with its quasi-brittle response [48].

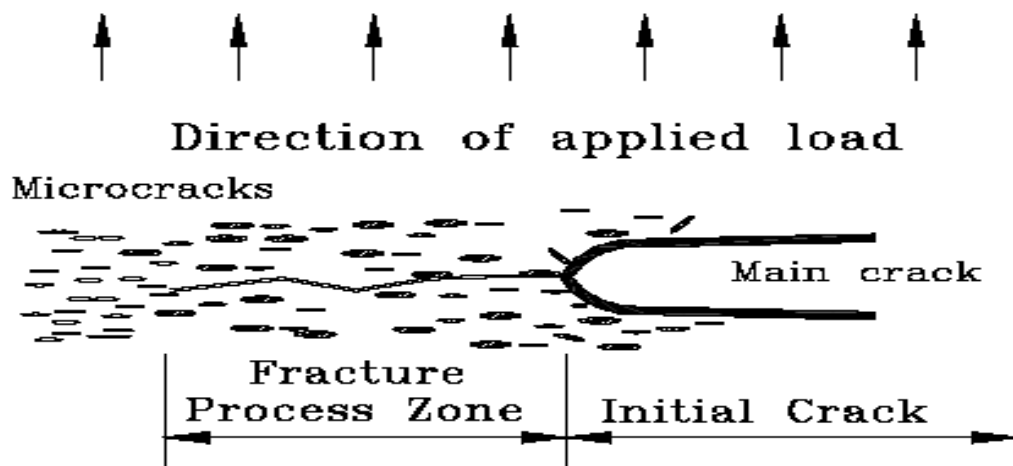


Figure 1.6: Fracture process zone in concrete [Adopted from 48 and 34].

Investigations have established the role of the fracture process zone in consuming energy in concrete during crack growth. The reason for the problems faced in the application of fracture mechanics to concrete comes from the various toughening mechanisms taking place in the fracture process

zone of concrete. These toughening mechanisms are those shown in figure 1.7. [48], [49] and [34].

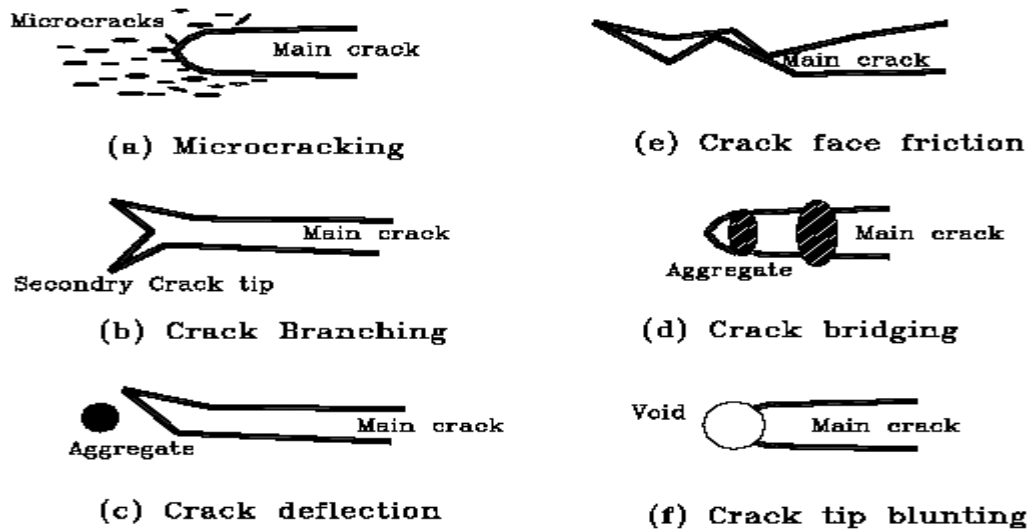


Figure 1.7: Toughening mechanisms of fracture process zone in concrete [48 and 34]

Enhancement of the concrete fracture toughness can be accomplished either by adding other energy consuming (i.e. toughening) mechanisms to concrete or by changing an existing toughening mechanism to consume more energy than it generally consumes. For instance, the significant increase of the fracture toughness of fibre reinforced concrete (FRC) compared to normal concrete is because fibres are able to consume a large quantity of energy through fibre crack bridging, fibre bending and fibre pull-out and/or fibre debonding [50] and [51].

Fracture mechanics is a broad field and that is the focus of much active research; one of the most useful single parameters from fracture mechanics that can be used in quantifying concrete fracture toughness, which is represented by K_{Ic} is named as Critical Stress Intensity Factor. The introduction of a crack into a material causes a redistribution of stress with the greatest stress being at the crack tip [52].

For brittle materials like concrete the Griffith crack model is applicable to understand/characterise/calculate it's cracking mechanism/fracture toughness.

It is possible to use elasticity theory to calculate the stresses at any point (r , θ , where r and θ are the angular coordinates of the point) in the vicinity of the crack tip as shown in figure 1.8.

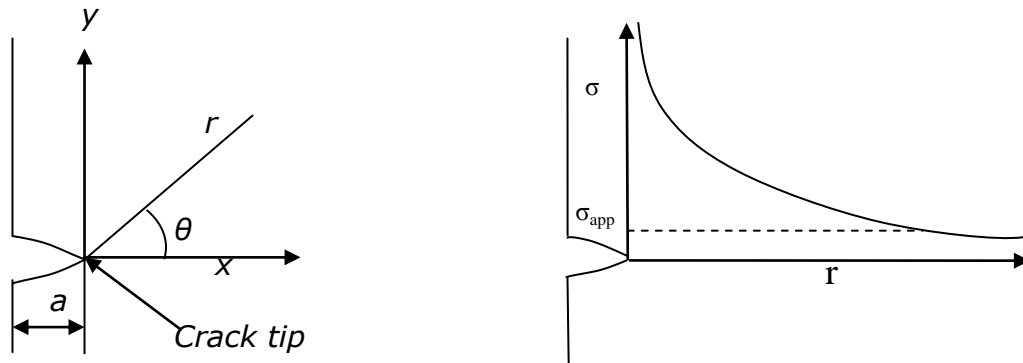


Figure 1.8: (a) The coordinate system used and (b) the stress as a function of r (σ_{app} is the applied stress).

The results of such an analysis are:

$$\sigma_{yy} \text{ (tensile stress in } y \text{ direction)} = \frac{Kc}{\sqrt{(2\pi r)}} \cos \frac{1}{2}\theta \left(1 + \sin \frac{1}{2}\theta \sin \frac{3}{2}\theta \right) \quad (1.2)$$

$$\sigma_{xx} \text{ (tensile stress in } x \text{ direction)} = \frac{Kc}{\sqrt{(2\pi r)}} \cos \frac{1}{2}\theta \left(1 - \sin \frac{1}{2}\theta \sin \frac{3}{2}\theta \right) \quad (1.3)$$

$$\tau_{xy} \text{ (shear stress in } xy \text{ direction)} = \frac{Kc}{\sqrt{(2\pi r)}} \left(\cos \frac{1}{2}\theta \sin \frac{1}{2}\theta \cos \frac{3}{2}\theta \right) \quad (1.4)$$

where Kc is known as the stress intensity factor. It should be noted that all crack tip stresses are directly proportional to Kc . In turn Kc depends on the applied load, P , and specimen geometry, e.g., for the single-edge notch bend (SENB) specimen as shown in figure 1.9, Kc is given by:

$$K_c = \frac{3PLYa^{1/2}}{2BW^2} \quad (1.5)$$

where L , B , W , and a are defined in the figure 1.9, and Y is a function of a/W .

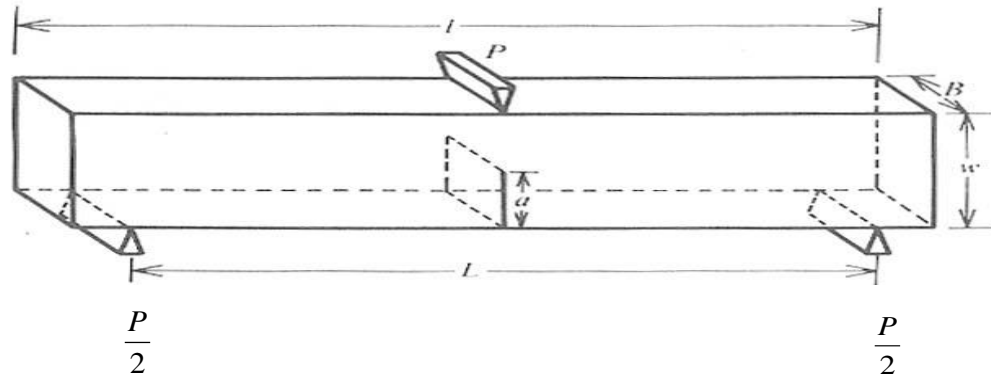


Figure 1.9: A single edge notched beam specimen for the determination of K_{IC} [adopted from 52].

As the load is increased on a single edge notched beam (SENB) specimen during testing K_c will increase in accordance with the equation (1.5) and the crack will propagate when K_c reaches the critical value K_{IC} . K_{IC} is a materials parameter and has dimensions of $MN/m^{3/2}$ and, as for G_{Ic} (the critical energy strain rate per crack tip), the lower the value the less tough the material.

K_{IC} and G_{Ic} must be related as they are both measures of the fracture toughness of a material, and the following equations show the simple relationships that exist between these parameters [52]:

$$G_{Ic} = K_{IC}^2 \div E \quad (\text{plane stress}) \quad (1.6)$$

$$G_{Ic} = (K_{IC}^2 \div E) \times (1 - \nu^2) \quad (\text{plane strain}) \quad (1.7)$$

Where E = is the Young's Modulus and ν is the Poisson's ratio.

As reported by Antoine Naaman of the Centre for Advanced Cement Based Materials, University of Michigan, the most detrimental property of cement-based materials like concrete is it's brittleness as characterised by it's poor tensile strength, and correspondingly inferior toughness. There are a number of strategies which have been utilized to improve the toughness of concrete, namely tailor the matrix composition and particle size, i.e. cement, water, mineral admixtures, aggregates, fillers, etc; add in fibres; and employ alternative processing techniques (extrusion, pultrusion, etc). Although each of these strategies depends on a number of parameters, they have at least one highly imperative common variable, which is the interface between the

cement paste and other phases in the system, such as aggregate, particulate filler or a fibre. The interfacial zone influences both the strength and toughness of the material, therefore it is essential for composite action in fibre and non-fibre reinforced systems. Therefore a number of fundamental research projects have been concentrating towards ‘‘understanding the importance of the interfacial zone in fracture’’, and the results have been integrated into micro-mechanical models and subsequently into macroscopic continuum models [53].

Mortars are made from essentially brittle components, i.e. sand grains and hardened (solidified) cement paste. Under usual conditions [53], cracks will propagate rapidly through the cement matrix, sidestepping the strong sand grains but fracturing some of the weakest. According to Antoine Naaman [53], several approaches have been made ‘‘to alter (modify) the internal microstructure of the cement paste to create residual stresses to give a tougher mortar’’. This is achieved by designing the mix so that the cement matrix expands by the growth of ettringite ($\text{Ca}_6\text{Al}_2(\text{SO}_4)_3(\text{OH})_{12}\cdot 26\text{H}_2\text{O}$), thus generating tensile residual stress between the matrix and the aggregate. The applied tensile stress subsequently increases this tension producing the micro cracking around the sand grains. Such micro cracking would discharge compensating compressive stresses in the matrix leading to a small expansion. The micro crackings coupled with the expansion provide a non-linear stress-strain curve in tension that, at least under some circumstances, promotes a tougher mortar.

Yu-Cheng Kan, K.C.Pei and Chien-Lung Chang [54] carried out experimental studies on the mechanical properties and fracture toughness of heavy concrete with various iron aggregate inclusions. They reported that the inclusion of heavy aggregates in concrete does not significantly increase the concrete strength; crack propagates along, instead of through the aggregate paste. The wave velocity of heavy concrete decreased as iron ore content increases, which implies that more iron ore introduces more voids. In comparison to regular concrete, the critical stress intensity factor, K_{IC} is different (lower) to regular mortar, in fracture mode I, based on the formula proposed (i.e. $K_{IC}=0.0597(f_c)^{0.75}$) by John and Shah [55].

Toughening of cement based materials was demonstrated using different admixtures: sodium sulphate and lime at both Robert Gordon University and Aberdeen University. Spherical and angular aggregate were used in order to give added insight into the toughening mechanism, thus establish the effect of micro cracking and grain-bridging. It was demonstrated that "the sulphate addition produced the best combination of stress-strain and toughness results, but the lime addition showed a steeper toughness curve, indicating that the lime admixture offered a better route to improving toughness, and also the expansion over 28 days was less with lime added than the sulphate" [56]. This can possibly lead to greater stability in the long term, which can be understood using ultrasound.

According to the initial collaborative work with Aberdeen University [56, 115-118] that led to this research, it was seen that there was no direct relationship between having a rising toughness curve and showing non-linear stress-strain behaviour. This led to the observation that both angular grain and non-linear stress-strain behaviour are needed to give the highest toughness. This was an indication that understanding the method of toughening cement-bonded mortars with the release of residual stress needs refinement. Steel aggregates were used to expose the mechanism for toughness increases brought about by the expansive matrix. This collaborative work demonstrated that the acoustic emissions from the samples containing steel aggregate did not exhibit micro-cracks. Instead, away from the path of samples containing sulphate produced higher number of emissions at the onset of crack propagation. On the other hand batch using steel balls generated small number of micro-cracks due to residual stress. In the case of a brittle material, the point of crack propagation resulted in one main peak of emissions [56]. It was also seen that the toughness curves with steel aggregates (angular grain) displayed increasing toughness curves even in the absence of sulphates. However, addition of sulphate to the steel grit further enhanced the toughening effect. Nevertheless, "when spherical grain was used instead there was little improvement in toughness. This was an indication that even after the release of the residual stress there was no enhancement in toughness, which indicates

the critical importance of grain-bridging to the toughening of these cement-bonded systems” [56].

Ansari F. [57] investigated deformations of concrete in a zone of micro-cracking before unstable propagation of cracks. The comparison of concrete and mortar has shown that the grains of large aggregate cause higher stress concentration which is believed to be related to existence of cracks on the surface of a cement-aggregate bond.

The investigation made by Hubbard F.H. and Dhir K. [58] on the micro-destructions of aggregate and concrete reported that on the cement-aggregate bond the greatest quantity of cracks were observed and a small number of cracks in cement matrix was also observed. With the exception of concrete with marble aggregate, the cracks on cement-aggregate bond were found to be open and continuous.

Detriche Ch. H. and Ramoda S.A. [59] reported that the resistance to propagation of cracks in mortar largely depends on dispersity and grain composition of aggregate. According to their findings, the mortar with aggregate containing large grains and smaller dispersity exhibit higher strength and resistance to cracking.

Pantazopoulo S.J. [60] reported that the volumetric expansion that develops in mechanically loaded concrete due to progressive micro-cracking is an essential measure of the degree of damage in the material microstructure, and can be employed to assess the changes effected on the resistance of concrete as damage builds up.

Mohammed E. Haque and Farhad Ansari [61] have developed a new model for the determination of fracture-mechanics parameters in concrete which require knowledge of peak load and peak crack-mouth opening displacement (CMOD) values. With this method they reported that it is possible to determine a number of important fracture parameters from the knowledge of peak load and CMOD at peak load alone. Amongst these parameters are fracture process zone size (r_p), critical fracture energy release rate (G_{IC}), fracture toughness (K_C), and fracture energy (G_F).

Nemati K.M., Monteiro P.J.M., and Cook N.G.W. [62] used Liquid Metal Porosimetry (LMP) technique to observe the compressive stress-induced micro-cracks in concrete as they exist under applied loads. They reported that the results obtained by this method can be used to better understand and evaluate the general relationship between stress level and crack development, along with the behaviour of crack due to the effect of confinement.

E. Denarie, V.E. Saouma, A. Locco, and D. Varelas [63] studied through optical fibre technology the characterisation of the fracture zone inside a cracked concrete specimen. The results from their findings indicated that there was a narrow zone on each wall (side) of the crack front with inelastic residual strains, and another where strains increased only in the presence of a neighbouring crack tip. The width of the process zone was found by the authors to be approximately three times the maximum size of aggregate.

Berthelot J.M. and Robert J.L. [64] demonstrated how acoustic emission processing is adapted to the evaluation of the actual pattern of concrete damage. They reported that the damage can be located by measuring the difference in arrival time of the acoustic emission signals, created from a single damage mechanism and detected by an arrangement of a number of transducers around the zone to be evaluated. The extent of damage is then estimated by carrying out a selective location in accordance with signal amplitude, and three damage zones are differentiated, i.e. a micro-cracked area, a macro-cracked area, and an area that may be considered as an open crack.

1.6 NONDESTRUCTIVE EVALUATION OF CONCRETE USING Acoustic Emission (AE) and Ultrasound (US): A Detailed Literature Review

NON DESTRUCTIVE EVALUATION: Research in concrete technology is a relatively young technique, and until recently has been primarily of an empirical nature. Even to this day, development efforts typically involve laborious and time-consuming trial mixes. Concrete materials technology /science has started to change this situation. By studying the micro-mechanical behaviour of the cement paste and its interaction with aggregate and particles and other mix components systematically [3], specific material properties can be modified without adversely affecting others.

Concrete is regarded as one of the simple materials but in fact is a complex material. A lot of its complex behaviours are still to be identified to utilize this material advantageously and cost-effectively. The behaviour of concrete with respect to morphology of gel structure, bond, fracture mechanism, fibrous concrete [1] are some of the areas of active research in order to have deeper understanding of the complex behaviour of these materials.

A number of laboratory non-destructive evaluation techniques have been carried out by researchers that have been very beneficial in studying fracture mechanism in concrete, damage in other composite based materials, and in the condition monitoring of ground anchorages, bridges and other structures. Andrew Starkey et. al. carried out work [65] in the condition monitoring on rock bolts used in ground anchorage systems. Their work included computer modelling, laboratory simulation and field applications leading to the development of a unique method of non-destructive evaluation on the static and dynamic response of rock bolt anchorages. The work undertaken demonstrated the effectiveness of the artificial intelligence techniques in the application of the actual behaviour of rock bolts in the field. John Steele et. al. investigated acoustic emission (AE) [66] generation during fatigue tests on glass fibre reinforced plastic (GFRP) composite column and reported that AE results can be applied as a diagnostic technique for modelling cumulative composite damage in critical composite structures such as pressure vessels and machine structures. Quite a few NDE techniques including acoustic emission (AE), were used to examine the fracture behaviour of concrete in tension and compression and other materials.

Shah SP and Choi S used different NDT methods including AE [67] to study the fracture behaviour of concrete under tension and compression. They reported that computer vision and enhanced image understanding is a very suitable technique to quantify crack openings for multiple crack displacement.

According to Eric Landis et al., Non-destructive evaluation (NDE) of concrete is a relatively immature discipline [68]. There are two main areas where concrete inspection lags behind homogeneous materials (metallic based materials). These are: (i) the heterogeneous nature of concrete which makes detection of defects difficult to separate from naturally occurring inclusions

and (ii) the second reason for the immature nature of concrete NDE is the fact that universal failure criteria do not exist for concrete structures. They carried out a study of the developments in NDE of concrete and broadly classified the deterioration of concrete into two stages. The first is the distributed micro-cracking and the accompanying increase in porosity which precedes major cracking, and the second is the major cracking which leads to de-lamination, spalling, and other larger scale, visible damage. They concluded that there is a tremendous need for effective NDE tools to evaluate concrete elements in civil engineering structures [68].

1.6.1 AE in Concrete

Acoustic Emission is surrounded by an industry that is fairly new with a variety of tasks being undertaken and exploited in the market place. A great deal of research into basic technology is being conducted alongside with the industrial development and application. Structures are being tested by companies throughout the world and valuable information is being gained about the internal health and integrity of large structures.

There are a number of papers that involve the use of acoustic emission in the analysis of concrete samples. Landis, E [21] in his work has demonstrated that AE can allow an insight into fracturing materials; showed the link between the acoustic emission technique and micro-macro cracking that occurred in a fracture test. He reported that the micro-mechanical phenomena affect the bulk mechanical properties and used Acoustic Emission techniques to monitor test pieces that are different in their make-up. The AE technique enabled the study of the effect of changes in aggregate size which resulted in variation in the AE parameters considered. Landis also suggested that in the un-notched specimens micro-cracks occurred and were found localised into a narrow band. This band finally becomes the critical crack area. The AE showed that the initial signal is evenly spread throughout the sample, an increase in AE activities occur. This narrow band is the focal point and the stress in this area increase thus causing an increase in the number of events as the load is redistributed between the new load areas. Landis [21] also pointed out that the initial AE hits are believed to be due to the rapid propagation of cracks in areas that are weak in the sample.

Wu, K. Chen, B. et Yao, W. (2001) [69] reported on the changing of aggregate size and the effect this has on the mechanical properties of concrete using AE technique. They demonstrated the possibility for AE to give an insight into the failure mechanism. Their research demonstrated that the increase of aggregate size increases fracture strength to a point. The maximum size was approximately fifteen millimetres and when this size was exceeded the specimen strength began to decline. This increase in strength of the sample can be explained by the aggregate's effect of creating a skeleton within the concrete, increasing the sample rigidity. They also reported that the increase in the total AE hits can be explained by the increase in defects with a larger aggregate [69].

Soulioti, D. et. al. [69a] had used steel wavy fibres in different volume contents in order to estimate their input into fracture toughness. They reported that the total acoustic emission activity is proportional to the fibre content, with plain concrete exhibiting 126 hits in average and reinforced concrete with 1.5% fibres producing 3143 hits throughout the bending experiment.

In the work of Wu, K. Chen, B. et Yao, W. (2001) [69], the initial period of bending test, AE is referred to as stage one and takes place in all AE tests. It is considered to be the settling in stage, when the specimen grounds itself on the roller device. The next stage is the commencement of relevant acoustic emission and in majority of the samples this increases in the number of hits as the experiment reaches final fracture. This is a very stable time in the experimental phase. Towards the end of second stage, they reported in their investigation that, the sample reaches its ultimate strength level and cracking within the sample becomes chaotic, the AE activities increase rapidly in this phase. These stages are important to all AE analysis as the key areas of the AE signal to study.

It is reported by Lysak, M.V. [70] that the AE technique helps in the study of crack initiation and sub-critical growth of cracks in quasi-brittle materials. He clearly states there is a need for further work to be carried out using the acoustic emission technique.

Dimittrios G. Aggelis et. al. [70a] studied AE behaviour of concrete under four-point bend with different contents of steel fibres to see their influence on load bearing capacity and fracture mechanism. They also reported that the total AE activity was proportional to the fibre content.

An investigation was carried out by Tasong. W. A., Lynsdale C.J. and J.C. Cripps [71] into the interfacial bonding between an aggregate and cement paste. They stated that the interfacial bond strength cannot be predicted from aggregate surface roughness alone and demonstrated the insight gained into aggregates that can be understood by the AE technique. This ability allows tailor made aggregates to be developed and used to gain certain concrete that have specific uses as they are aided by their aggregates, therefore it has become quite clear that the AE technique has a functional purpose in the development of concrete.

Labuz J.F. Cattaneo S and Chen L [72] investigated specifically towards the final stage of fracture and what can be learnt from this stage. They gained insight specifically at an area in the fractured specimen; this localised area of micro-cracking can be further understood by AE analysis.

The acoustic emission technique was applied by Eric N. Landis and B. Whittaker to examine crack growth along the grain in clear wood specimens loaded for mode I (tensile opening mode) fracture [73]. A new technique was used to estimate the energy released by an AE event, comparisons were made between AE energy and bulk mode I fracture energy. These comparisons give an idea of how much fracture energy is converted to measurable acoustic energy. Results of the energy comparison indicate a clear correlation between the fracture energy and the AE energy.

Acoustic Emission was used by H. Hadjab, J.-Fr.Thimus and M. Chabbat to investigate the characteristic of the Fracture Process Zone (length, width and how macro crack propagation) in a concrete specimen subjected to four point bending specimen relying to probability and statistics methods [74]. They carried out the analysis of the load-CMOD (crack mouth opening displacement) and AE curves, which implied that the macro-cracks extends slightly before the load reaches the peak, creating in this way the fracture process zone (FPZ). This zone results in steady crack growth before the peak load and is

also the most important key responsible for the quasi brittle fracture response of concrete beyond the ultimate (peak) load. Then the behaviour of concrete is greatly influenced by the existing fracture process zone.

Eric N. Landis and Laucie Baillon carried out experiments to relate acoustic emission energy to fracture energy of concrete [75]. They reported a 'good correlation between fracture energy and AE energy for mortar specimens, but a relatively poor one for concrete specimens. Such poor correlation is attributed to the escalating contribution of additional toughening mechanisms in the coarse-grained materials. Based on the AE discharged between the peak load and 40% post-peak, it emerges that crack forming processes do scale with AE energy release" [75]. As the coarse-grained materials exhibit a larger variety of non-crack forming energy dissipation methods than the fine-grained material, they do not present as good a fracture energy-AE energy correlation [75].

S. Yuyama and M. Ohtsu [76] had carried out an extensive amount of studies on Acoustic emission behaviour of concrete to demonstrate the effectiveness of AE techniques for evaluation of structural integrity. They reported that high AE activity is observed during un-loadings after serious damage (slips between the concrete and the reinforcement) has occurred. The relationships between the AE signals and the applied load were observed as shown figure 1.10.

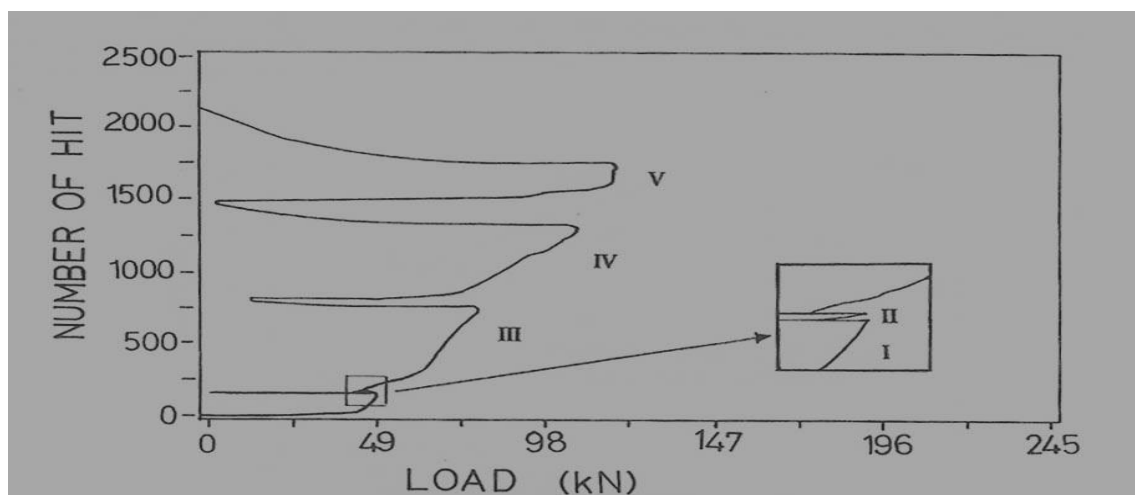


Figure 1.10: Relationship between number of AE hits and the applied load [Adopted from 76].

AE signals seen in figure 1.10 are detected at a lower load than the maximum prior load (49 kN) during the second loading. Load levels that were previously applied on a material did not generate AE activity, i.e. discontinuities created in a material do not expand or move until that former stress is exceeded. This phenomenon is known as the Kaiser Effect. Accordingly, the Kaiser effect breaks down during the second loading. It was shown that the effect starts to break down when the crack width exceeds 0.12 mm. The breakdown of the effect becomes clearer as the cracking progresses in the third, fourth and fifth loadings. High AE activities are observed during the third, fourth and fifth unloading. From the moment tensor analysis they found that the contribution of shear cracks increases as the breakdown of the Kaiser effect becomes clearer with the progress of the fracture and high AE activity is observed during the third, fourth and fifth unloading. The moment tensor analysis also found that the shear cracks generated near the reinforcing bar is responsible for this activity. The origin of these emissions was attributed to rubbings between the faces of the existing cracks or friction between the reinforcement and concrete.

Li, Z. W., Yuyama S., Osawa I., Kimpara I., Yamaguchi K. and Kageyama K., [77] studied AE behaviour of centre notched concrete beams reinforced with carbon fibre and glass fibre plastic sheets. The load curves observed during the tests is shown in figure 1.11. The three stages are explicitly visible in the case of the reinforced specimens.

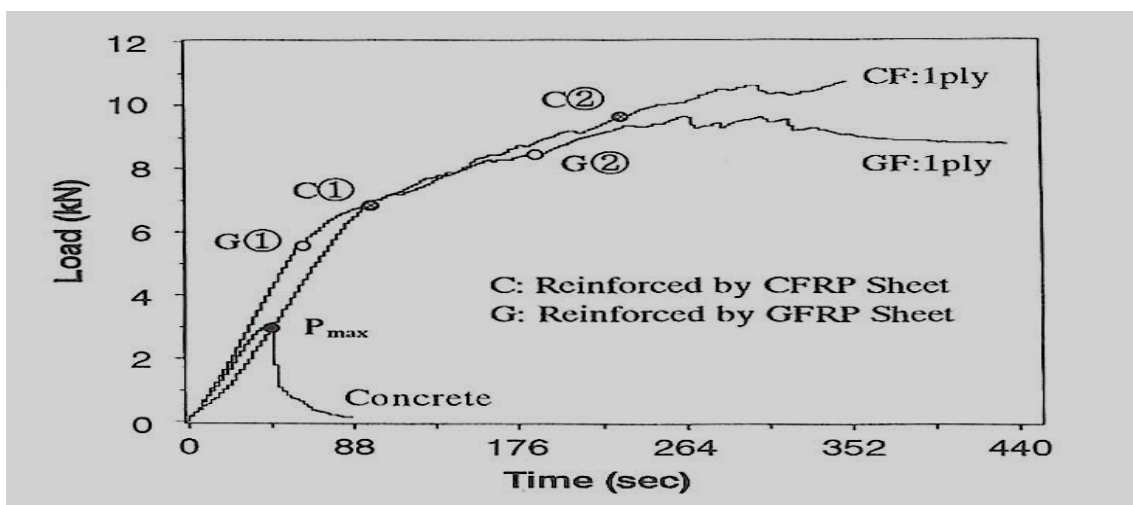


Figure 1.11: Loading curves during three-point bending test [Adopted from 77].

Stage I corresponds to the region from 0 to the point ①, where the load increases almost linearly. Stage II corresponds to the region between the points ① and ②, where the load increases still linearly though the increasing rate is smaller than that of stage I. The load becomes almost stable in stage III after the point ② till the final failure. In contrast, the load curve is very simple in the case of the specimen without reinforcement. The load increases linearly to the maximum value and decreases very rapidly due to the final failure [76]. The results of the moments of tensor analysis of cracks [77] obtained were in good agreement with visual observations of the surface cracks, thus indicating that the moment tensor analysis is very effective for quantitative evaluation of fracture processes and mechanisms.

Yuyama S., Okamoto, T. and Ngataki, S. tested and repaired reinforced concrete beams which were subjected to repeated four point bending loadings by a strain-control type machine [78]. During each loading, measurements of AE, crack width, slip length between the repaired part and the original part, and strain of concrete and reinforcement were made by using AE sensors and two different types of displacement transducers.

The measurements they made indicated that the initiation of the early tensile micro-cracks, main tensile cracks, local slips, and large-scale slips are clearly detected by AE hit measurement. When large scale slips occur at the interface between the original concrete and the repaired part, AE starts to emanate at much lower load than the previous maximum load, that is, the Kaiser effect no longer holds for the next loading and high AE activity is visible even during unloading. Thus, the breakdown of the Kaiser effect and the high activity during unloading is a good indicator for the occurrence of large-scale slips in repaired RC beam [78].

The initiation of the early tensile micro-cracks or the local slips and the mechanical rubbings of the interlocked faces due to large-scale slips show amplitude levels between 40 and 60 dB, while the initiation of the main tensile crack at 38.2 kN produces very high amplitudes that reaches nearly 80 dB, as shown in figure 1.12. Therefore, the different AE sources are distinguishable by comparing the amplitude data with the results of the visual observation and the measurement by displacement transducers.

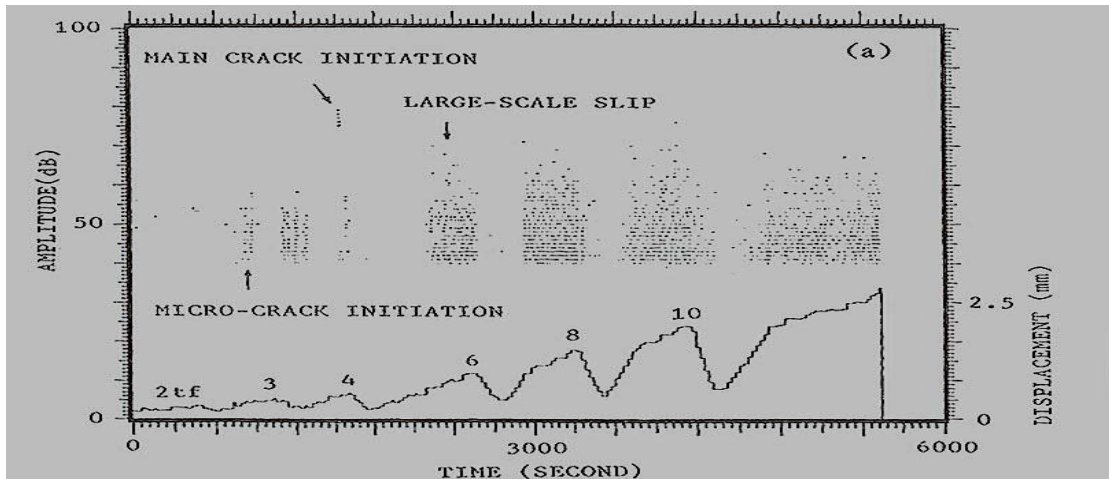


Figure 1.12: Amplitude and displacement histories [Adopted from 78].

An investigation was also carried out by Murakami, Y. and Yuyama, S. [79] on RC beams deteriorated to corrosion of reinforcement. They used three different types of specimens which were subjected to repeated four-point bending loadings, which show relationships between AE hits and the applied load for the specimens with the different deteriorated levels, as shown in figure 1.13.

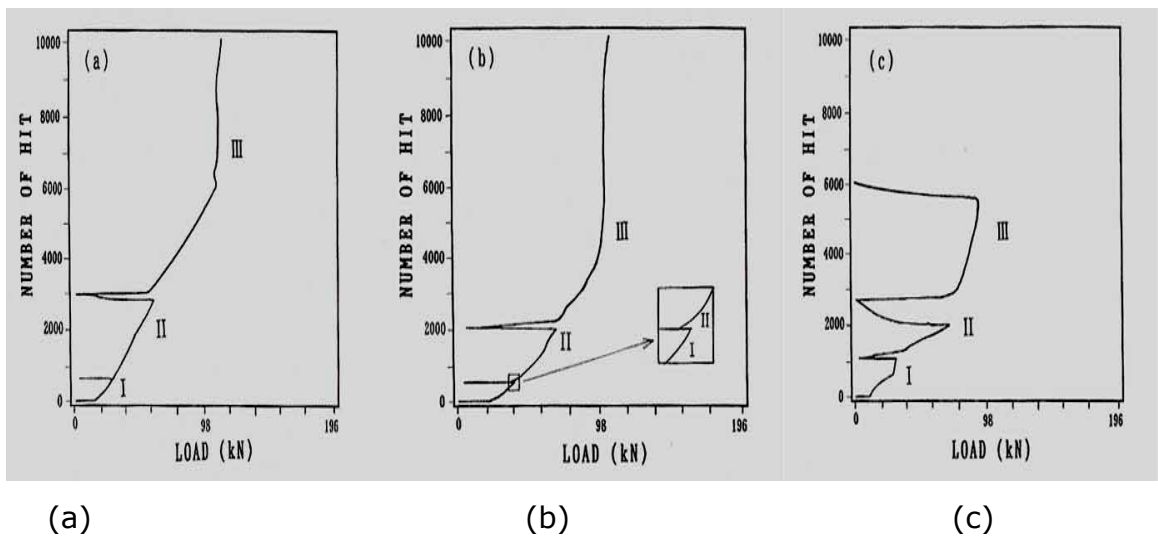


Figure 1.13 (a), (b) and (c): Relationships between AE hits and the applied load for the specimens with different deteriorated levels: (a) specimen with no corrosion damage, (b) deteriorated specimen (crack width 1 mm), (c) deteriorated specimen (crack width 4 mm) [Adopted from 79].

It can be seen that the Kaiser effect starts to break down during the third loading in the case of the specimen with no corrosion damage. However, it tends to break down during the second loading in the case of the deteriorated specimen (crack width 1 mm) and the break down is very clear during the

second loading in the heavily deteriorated one (crack width 4 mm). Different levels of AE activity are detected during unloading, depending on the different damage levels. In the specimen with no corrosion damage, relatively high AE activity is first observed during the 2nd unloading, as shown in figure 1.13 (a). However, some AE activity is already detected during the 1st unloading in the case of the deteriorated specimen (crack width 1mm). High activity is seen during the 2nd unloading in figure 1.13 (b). Quite high AE activity is observed during the 1st and the 2nd unloading in the heavily deteriorated specimen (crack width 1mm), as shown in figure 1.13 (c). The levels of AE activity during unloading reflect the damage levels induced in the specimens. Since high AE activity corresponds to the occurrence of serious damage, it can be an effective index to estimate the level of deterioration [79].

The investigators Yuyama, S., Okamoto, T., Shigeishi, M. and Ohtsu, M. [80] observed the growth of tensile cracks, shear cracks and bond failure of the reinforcement in an 'L' shaped RC rigid frame with the aid of AE monitoring, as shown in figures 1.14a and 1.14b.

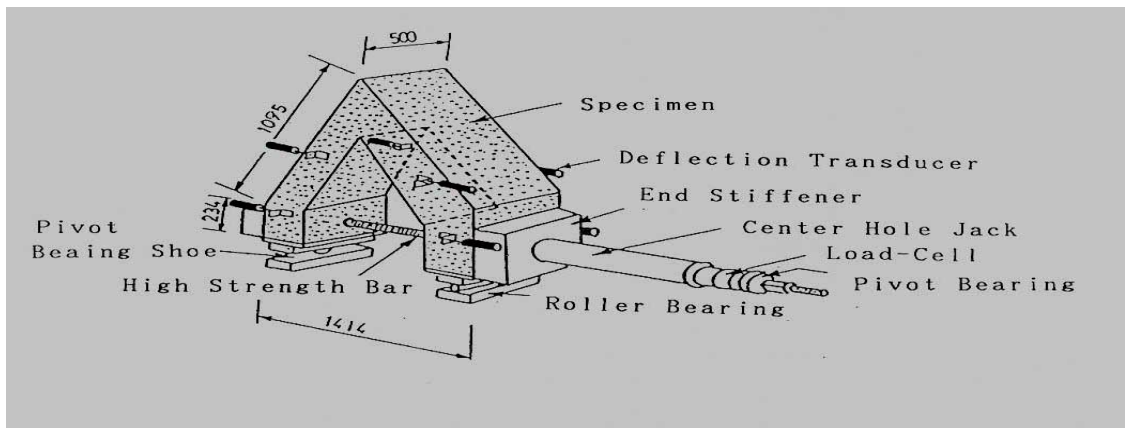


Figure 1.14a: Apparatus for applying load and measuring deflections, [adopted from 80].

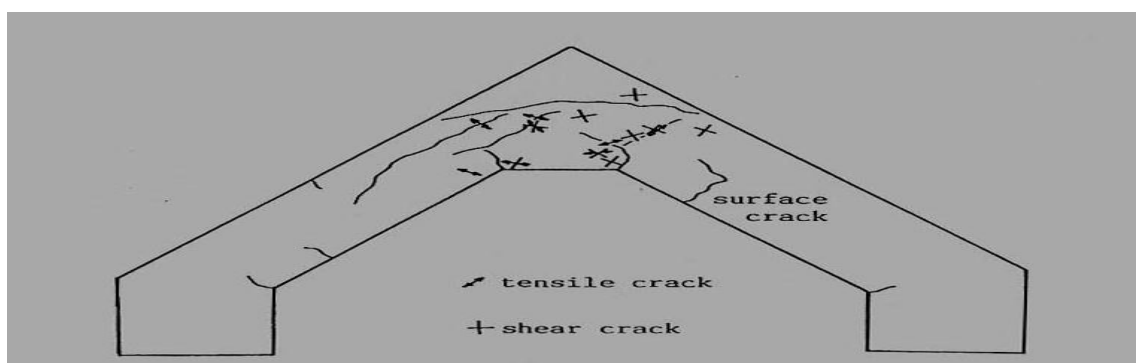


Figure 1.14b: Results of the moment tensor analysis [adopted from 80].

In this investigation, it is reported that different AE sources could be clearly distinguished by comparing the AE parameter data with the results of visual observation and crack width measurement. Moment tensor analysis was applied to classify crack types and to determine crack orientations in the fracture process, the results of which are shown in figure 1.14b. These investigators [80] showed that crack orientations were reported to be in good agreement with the visual observation of the surface cracks.

The researchers Yuyama S. et.al. [81] also carried out investigations on the applicability of AE techniques for evaluation of fatigue damage in an RC slab under laboratory conditions. They monitored AE from the initial loading to the final failure under fatigue loadings in a model RC slab of a highway bridge. In figure 1.15, a relationship between number of loading cycles and crack density defined as crack length per 1 square metre is indicated. In the cracking process four stages can clearly be observed.

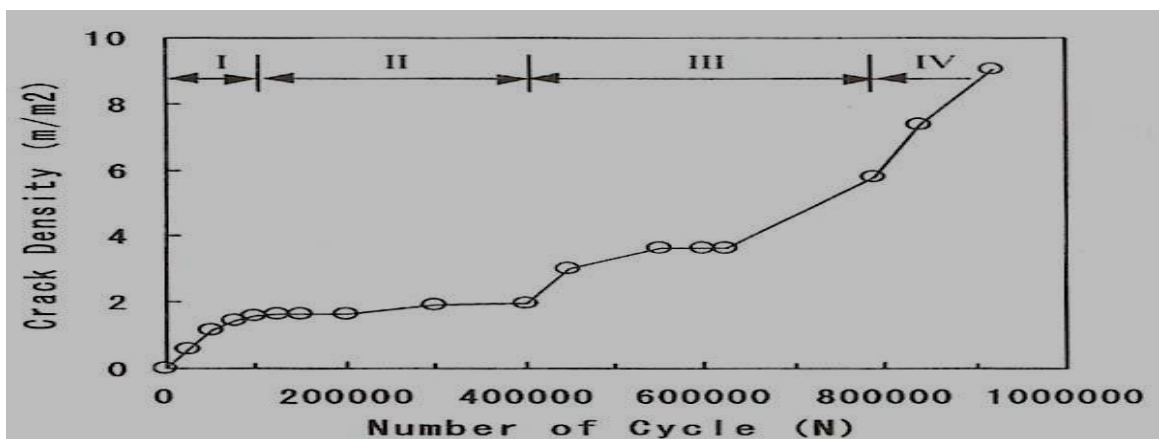


Figure 1.15: Relationship between number of loading cycles and crack density [Adopted from 81]

In stage I high AE activity is seen due to the initiation of early cracks, this is shown in figure 1.16, where it diminishes quickly and then rises again as the crack density increases the maximum load as a function of number of loading cycles, AE hit rate, amplitude and the records (histories) are also shown in figure 1.16. In stage II, the activity gradually increases exhibiting some instability, while it starts becoming stable in stage III. In stage IV, it starts increasing quickly from number of cycles (N) = 8.8×10^5 , i.e. just prior to the final failure (N = 9.17×10^5). It is therefore evident that under fatigue loadings the process of the final failure (the transition from stage III to stage IV) can be predicted and evaluated by monitoring AE signals. The

commencement of the final failure corresponds to the time when the AE activity increases considerably in stage IV [81]. Hence this investigation indicates that Acoustic emission technique is a useful tool in predicting fatigue damage in RC concrete slab.

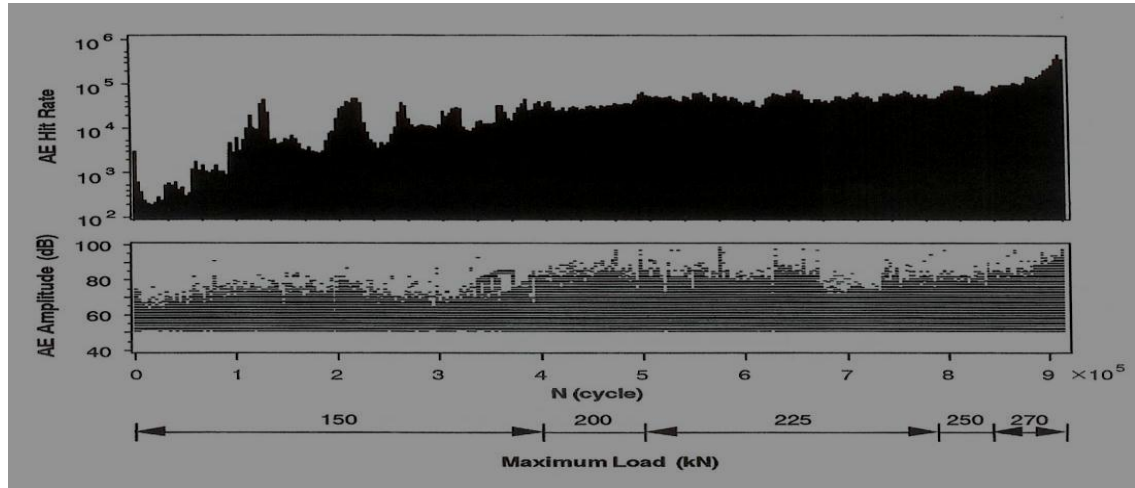


Figure 1.16: Histories of AE hit rate, amplitude and the maximum load, [adopted from 81].

It is reported by Yuyama S. et. al [82] that AE activity under loadings strongly depends on the loadings phase. An AE signal detected near the maximum load is mainly due to main crack extension called Peak Load AE. Meanwhile the AE activities observed during unloading and re-loading are considered to be from mechanical sources such as frictions due to closure and opening of the crack faces and called Closure and Opening AE respectively [82]. The correlation between the loading phase and AE activity in terms of hit rate from stage IV to the ultimate failure is shown in figure 1.17.

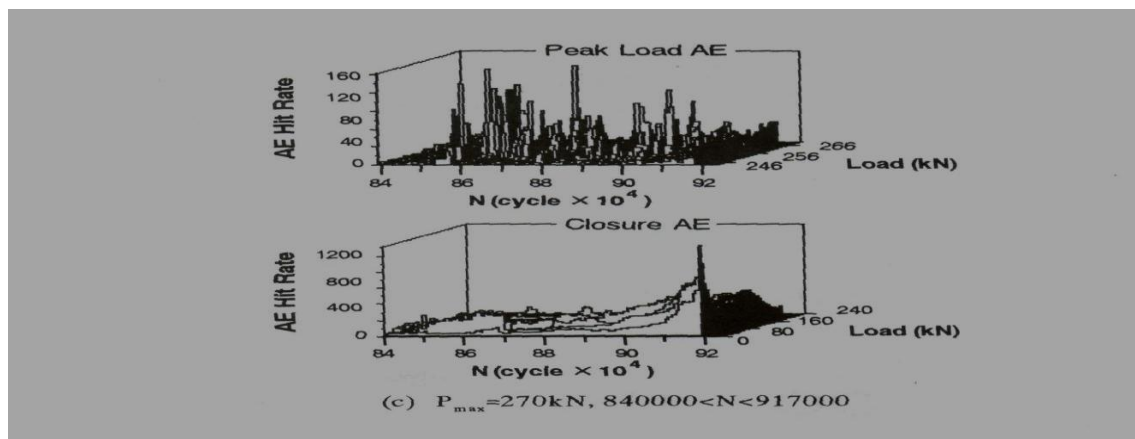


Figure 1.17: Relationship between loading phase and AE activity from stage IV to the final failure, [adopted from 81].

The most distinctive fact seen here is that the activity of closure AE increases speedily at low load levels as the cracking process approaches the final failure. This is because numerous AE signals due to mechanical causes are detected since many cracks have already existed in the specimen at this stage. This result indicates that the process of the final failure can be monitored practically by detecting the closure AE observed near the minimum load. Therefore precise analysis of relationship between the loading phase and AE activity makes it possible to evaluate fracture processes under fatigue loading [82].

After carrying out a fairly good number of investigations, Yuyama, Kishi and Ohtsu [83] concluded that the development of reliable NDT methods (including AE) to study materials characteristics and cracking processes in concrete specimens and structures are recommended.

Dunja MIKULIC et. al. [83a] carried out compressive and bending strength test on plain concrete samples and investigated the relationship between load and AE activities under different loading conditions. They reported that when the maximum amplitude was reached a major crack occurred in the concrete. It was concluded that the AE method can be employed as a reliable technique for detection of cracking in concrete.

Chengsheng Ouyang, Eric Landis and Surendra Shah applied quantitative AE techniques [84] to a laboratory study of plain concrete beams under four point loading. They loaded centre-notched and off-centre-notched beams in order to produce mode I and mixed mode failure respectively. Micro-cracking was characterised as mode I, mode II, or mixed mode using AE seismic moment tensor representation. A comparison was made between the mode of micro-cracking and the mode of the visible crack. Majority of the micro-crack planes were in a direction normal to the tensile stress for a mode I macro-crack (centre-notched), while micro-crack planes were relatively uniformly distributed for a mixed-mode macro-crack (off-centre notched). Mixed-mode micro-cracks were observed a large number even for the centre-notched beam indicating that fracture mechanisms of micro-cracks may differ from the main macro-mechanical crack. They concluded that AE measurements can provide a potentially powerful means of assessing damage.

Landis EN and Shah SP [85] applied quantitative acoustic emission techniques to basic problems of micro-fracture in cement based materials. They carried out research to characterise micro-cracking in various cement based materials, to track the growth of damage in those materials, and to examine the relationships to overall mechanical behaviour. Characterisations of the micro-cracks exhibited a dependence on the amount of inhomogeneity in the material. Fine grained materials exhibited distinct micro-fracture characteristics than coarse-grained materials. Micro-cracks were characterised in accordance with their fracture mode. The fine-grained materials tested exhibited primarily mixed-mode micro-fracture, but the coarse-grained materials demonstrated mode II (shear) micro-fracture. It was shown by them experimentally that a relationship exists between the micro-crack characteristics verified through quantitative acoustic emission analysis and the overall fracture toughness of the material [85].

Bernd Weiler, Shilang Xu, Utz Mayer [86] investigated acoustic emission analysis applied to concrete under loading conditions. They first carried out three-point bending tests on fibre-reinforced beams, (ductile steel fibre reinforcement), at constant rail speed; axial tension tests on reinforced concrete columns, and compressional tests on plain concrete specimens. They concluded that the adaptation of apparatus and evaluation methods were rather good although the complex nature of the material is a major problem. One vital factor for the quality of the measurements emerged to be the placement of the transducers with respect to the expected event locations. According to them, "AE analysis on concrete are far away from a routine application, but it has proved to be a valuable tool for laboratory tests and scientific investigations". Its applicability and acceptance will increase significantly with the progressive automation of the technique [86].

Shohei Momoki et. al. [86a] employed AE to assess the behaviour of concrete beams (plain mortars specimens and vinyl fibre reinforced layer as composite) by putting them under four point bending load. They reported that in terms of fracture development, the composite specimens with vinyl fibre reinforced mortar layer displayed higher strength than that of plain mortar. They reported that no de-bonding took place in composite specimens and the AE event locations coincided well with the observed crack locations.

A quantitative analysis of the relationship between concrete crack parameters and acoustic emission energy released during failure was carried out by Beck P., Bradshaw T.P., Lark R. J. and Holdford K.M. [87] at Cardiff School of Engineering. A study was performed by them to correlate AE energy produced during the failure of mortar specimens to either crack area or crack depth. They found no significant relationship between AE energy and fracture energy, but suggestion was made that the amount of AE energy produced by the failure of the mortar specimens could be related to crack depth, which was probably related to fracture velocity.

An investigation on the AE characteristics of fracture process of mortar, concrete and steel-fibre reinforced concrete beams was conducted by Keru Wu, Bing Chen and Wu Yao [88]. They concluded that: i) for studying the failure mechanism of concrete, AE is an effective method; ii) AE duration is the primary filter parameter. Various filters were set on the AE duration and the plots of counts versus amplitude and hits versus counts were plotted to confirm that a single failure mechanism was present in the separated amplitude distribution, and the distinctive failure mechanism can be isolated, respectively; iii) Experimental results indicated that there existed five, seven, and nine different failure mechanisms for mortar, concrete and steel-fibre-reinforced concrete, respectively, during the entire fracture process; iv) On the basis of the experiments, the AE signal parameters for different failure mechanisms involved in steel-fibre-reinforced concrete, concrete and mortar were obtained [88].

The application of acoustic emission has been extended to monitoring of steel fibre reinforced concrete which is being widely utilised for structural applications on an extensive scale. According to Stahli and Mier [88a] fibres in concrete evaded the brittle failure of the matrix thus convalescing its weak tensile properties. The prospect of crack growth will be deferred by the fibre action with increasing fibre volume content, therefore the material toughness is enhanced [88b].

According to RILEM TC212-ACD, the benefit of applying acoustic emission in a material like concrete is that the source of the AE activity is strongly linked to the mode of fracture [88c]. If the principal mode is established by analysis of

AE signals then the structure can be reinforced using appropriate design or materials with increased resistance against the precise cracking mode [88c].

According to Vogel T. [88d], analysing acoustic emission signals provide valuable information concerning the source and significance of a discontinuity in a material. AE differs from most other NDT methods on two aspects: i) the energy detected is released from the interior of the tested object rather than from some external source; ii) acoustic emission is able to detect the dynamic process connected with the degradation of structural integrity.

After analysing the application of AE on concrete and structural engineering in its entirety, Ohtsu and Landis considered 'AE to be a highly effectual method', [89], [90] and [91].

1.6.2 Ultrasound (US) in Concrete

Non-destructive testing methods can avoid most of the disadvantage of destructive testing, and especially ultrasonic testing has shown vast amount of developments as a result of computer technology, software development and applying the advanced methods of medical diagnosis to the material structure in the last few years [92].

Researchers at the Institute of Construction Materials, University of Stuttgart, Germany, [93] carried out research on Ultrasound Technique for Quality Control of Cementitious Materials and reported that the Ultrasound method they used is able to extract automatically certain parameters of Ultrasound waves recorded continuously during the setting and hardening of mortar materials.

Georgios Astyrakakis, Turgay Ozturk and Peter Grubl had investigated the spatial variation of the Young's Modulus within a large specimen and its comparability to specimen different in size but of the same concrete mix using ultrasound technique [94]. They reported that the concrete properties found by non-destructive investigations have a well defined relationship to destructively achieved results.

The techniques used for monitoring in-situ at the concreting site are lacking in various ways nowadays, therefore the needs relating to the quality control of fresh concrete are growing. Demand is growing for a new kind of quality management that may be based on ultrasound; this is due to the systematic investigations as well as the increasing number of damages at the concreting site. Fresh Concrete was monitored using a method based on ultrasound by Christian U. Grosse, Hans-Wolf Reinhardt [95]. They reported that this method "is able to analyse the setting and hardening of cementitious materials in a comprehensive manner and can be used for numerous applications, where reliable data are required. At the concreting spot, where efficiency and a low financial cost are limiting conditions, the application of this new technique can assist in enhancing the stability during construction or the progress of the construction work" [95].

Thomas Voigt, Yilmaz Akkaya and Surendra Shah [96] used Ultrasonic Wave Reflections to determine the strength of early age concrete and mortar. They compared wave reflection measurements on mortar and concrete to strength and showed that at early ages loss of reflection is linearly related to the strength gain of concrete and mortar.

Concrete complexity makes the behaviour of ultrasonic waves in concrete highly irregular, which in turn hinders non-destructive testing. Considering the complexities of the problem it would appear to be overly optimistic to attempt to devise an ultrasonic test method for the determination of concrete strength. However, considering the importance of the infrastructure problem and the magnitude of the cost of rehabilitation, major advancement is badly needed to improve the current situation [97].

An investigation into the possible use of ultrasound measurements of the influence of various accelerating admixtures and cement types for shotcrete on setting and hardening behaviour was carried out by De Belie N, C.U. Grosse, J. Kurz, and H.W. Reinhardt [98] They reported that the ultrasound measurements were visibly sensitive to the effect of the types of cement, accelerator and dosage on the setting behaviour of mortar.

C.U. Grosse and H.W. Reinhardt carried out experiments on the setting and hardening of concrete monitoring continuously by elastic waves [99]. They measured three features: the propagation velocity of the compressional wave, the transmitted energy, and the frequency spectrum and reported that all these features were sensitive to concrete age and to the concrete composition of the mixture and the deviations of the dose of retarder, of the water-cement ratio can be detected [99].

An extensive study was carried out by I. N. Prassianakis and P. Giokas to examine the mechanical properties of concrete of 28 years of age using destructive and non-destructive testing methods [100]. The results they obtained were that the compressive strength of concrete increases continuously by 39% for the cylindrical and 28% for the cubic specimens from the age of 28 days to the age of 28 years. They confirmed that higher concrete strengths are usually associated with higher ultrasonic velocity.

An investigation was carried out by Yitching Lin et. al. [101] to establish mathematical models for predicting concrete pulse velocity; experimental studies were carried out to evaluate the models. The results of their studies showed that the pulse velocity of hardened concrete can be predicted with less than 2.5% errors.

Hisham Y. Qasrawi [102] carried out combined methods of non-destructive testing to estimate concrete strength. He used both the traditional well-known rebound hammer and ultrasonic pulse velocity test methods. As a result of his study, he concluded that the i) 'use of rebound hammer alone is not suitable to estimate and predict the strength of concrete. ii) when compared to the rebound hammer, the ultrasonic pulse velocity method was found to be more efficient in predicting the concrete strength under the conditions of the work, but the use of such method is not good enough for reliable prediction of the concrete strength; iii) the use of the combined methods produced results that lie close to the true values when compared with other methods; iv) the lower strengths of concrete had shown higher prediction intervals and hence, less predictable strength by the combined methods; v) the use of the combined methods yields more consistent, reliable and closer results to the actual strength, the 95% prediction interval is quite narrow, which enhances

engineering judgement; vi) better results of prediction of strength was obtainable for estimated crushing cube strengths exceeding 20 MPa; and vii) the method can be extended to test existing structures by obtaining direct measurements on concrete elements" [102].

Comparison of DIN/ISO 8047 (Entwurf) to a number of standards on determination of ultrasonic pulse velocity in concrete were carried out by S. Popovics, K. Komlos and J. Popovics [103] including i) BS 1881 : Part 203: 1986 'Testing concrete – Recommendations for measurements of velocity of ultrasonic pulses in concrete, ii) RILEM/NDT 1 1972 'Testing of Concrete by the Ultrasonic Pulse Method, iii) GOST 17624-87 'Concrete – Ultrasonic method for strength determination'. They confirmed that these standards and specifications analysed showed significant similarities for the measurement of transit period (time) of ultrasonic longitudinal pulses in concrete, but there were also differences visible. A few standards provide extra details about the applications of the pulse velocity, such as defect detection, strength assessment, etc, but they established that the accuracy of most of these applications, including strength assessment, is inadequately low. They therefore suggested that forthcoming standards rate the reliability of the applications.

A. Van Hauwert, J.F.Thimus and F. Delannay employed ultrasonics [104] to follow crack growth. They reported that "the propagation of ultrasonic compression waves through the specimens was recorded at regular time intervals during the tests. The interpretations of the signals was in this case complicated due to the facts that occurrence of micro-cracking, that the macro-crack was a lot thinner than a saw-cut and that it was moreover bridged by fibres. It emerged that in this case both peak amplitude and energy dropped before the onset of a visible micro-crack, because of extensive micro-cracking, while the velocity only changed after substantial crack growth".

The U.S. National Bureau of Standards (NBS) [105] invented Impact-Echo Method which is an acoustic method for non-destructive evaluation of concrete and masonry, which can be used to evaluate the thickness or to identify the

crack locations, voids, and other defects in masonry structures where the block or brick units are bonded together with mortar.

M. Krause et. al [106] had made a comparative study of different pulse-echo methods such as : (a) Radar; b) Impact-Echo; c) Ultrasonic Pulse-Echo, A-scan, d) Ultrasonic Pulse Array; e) Ultrasonic Pulse-Echo, B-scan; f) Ultrasonic Pulse-Echo, B-scan, Linear Synthetic Aperture Focussing Technique (LSAFT); g) Ultrasonic Pulse-Echo: 2D-Synthetic Aperture and; the outcome of their investigations using these different techniques were that all methods applied (with one exception from both sides) could be employed to measure the thickness and the location of the tendon duct in the test samples with 8 mm aggregate size.

Thomas et al [107] used the ultrasound method for monitoring the setting and hardening of concrete using a transverse wave reflection method. They demonstrated that the method can reliably be used to monitor the hydration process of concrete; proved the strong dependency between the wave reflection measurements and the initial setting time i.e. the compressive strength development and the change of attenuation are linearly related for concrete at early ages, and also that the method can be employed as a technique to measure the compressive strength of concrete.

Researchers at the Institution of Construction Materials (IWB) [108] carried out investigations on quality control of cementitious materials using an ultrasound technique, which was able to extract automatically certain parameters of ultrasonic waves recorded continuously during the setting and hardening of mortar materials. Their analyzing techniques including the evaluation of waveform parameters like energy, frequency or velocity, describe the material behaviour and are related closely to the hydration process of the mortar.

Abid Shah [108a] utilised ultrasonic attenuation changes method to assess concrete (with different water-cement ratio) damages. He reported that attenuation increased with the escalation of damage and were greater for low water-cement ratio than high water-cement content of concrete. His

conclusion was that wave attenuation was an easy measure of assessing concrete damages.

H. K. Chai [108b] et al reported that wave attenuation based on non-linear ultrasonic testing is extremely useful in identifying and evaluating damage in in-situ concrete at its early stages. It plays a very important role in the non-linear ultrasonic response of concrete.

A. Rosch, B. Hillemeier, E. Porzig, M. Krause, C. Maierhofer [109] employed pulse velocity measurements to locate defects in highly loaded concrete columns. They used ultrasound measurements to identify areas of low quality concrete by correlating pulse velocity with the compressive strength of sample cores drilled from the unit under investigation, and showed that grid measurements and 3D-visualisation are essential tools to obtain an easy-to-read picture of the interior of the columns.

P. Ferreira Almir [110] carried out research to analyse the effect of crushed coarse aggregate on NDT relationship to compressive strength of concrete. The approach he adopted to see that effect was the introduction of aggregate crushed strength as an independent variable to the correlation models. His test results of various NDT test results confirmed that a "crushed strength effect is present, i.e. crushed coarse aggregate strength make an influence on NDT – concrete strength relationship and test results" [110].

After carrying out tests on Forensic Engineering Investigation of Reinforced Concrete Buildings, Hobbs and K. Tchoketch [110a] reported the followings: a) the main benefit of NDT method is to avert the concrete damage on the performance of building structural components; b) their usage is fast and straightforward; c) test results are accessible on site; d) concrete testing in structures is challenging in which the cores cannot be drilled, where employing less expensive equipment is required.

D. Breyse [110b] reported the combination of several methods of NDT examination applied empirically, combining two methods frequently used to

extend the reliability of the estimated compressive strength of concrete. The principle is based on relationship between observed measurements and the desired property [110b].

Various investigations were also conducted on the relationships between ultrasonic pulse velocity and strength, and elastic properties of natural and artificial stones [110c, 110d], in particular those of cement-binder concrete and mortars as well as wooden materials [110e].

The potential ability of an ultrasonic indicator to control concrete damage by non-destructive testing method were put forward by Garnier Vincent and Corneloup Gilles [111]. They reported that the non-destructive testing of the damaging of concrete is as complex as the material itself. The velocity measurement allowed obtaining overall information on the state of the material.

Research at the NSF Centre for Advanced Cement Based Materials [112] has led to the development of non-destructive test methods for evaluating the in-service performance of materials, since there is a requirement for in-service monitoring of the concrete infrastructure and assessment of existing damage in structures is necessary to target the critical damaged portions owing to surface breaking cracks and initiate repair. The method employed was based on measuring the ultrasonic wave reflection factor (WRF) between a steel mould and the hardening concrete. The methods were found to be robust and it was found that the WRF technique is applicable in the field to reliably monitor the setting and hardening of concrete.

P. Pewel Smolarkiewicz et.al. [113] demonstrated the significance of the finite element model-based simulation for studying the effects of heterogeneities on ultrasonic wave velocities and comparisons with ultrasonic test data illustrated the accuracy of their approach for modelling a highly coarse concrete specimen under increasing axial compression.

Analysis of the setting and hardening of cementitious materials using the ultrasound technique became very popular over the years. Christian U. Grosse

et. al. [114] worked on this aspect extensively, and developed an ultrasonic device which when applied to mortar materials, is capable of documenting and analysing the setting and hardening process continuously in a manner that could not be achieved by conventional techniques such as the vicat-needle test, or rheological testing methods. They reported that their method "is able to extract automatically specific parameters of US waves recorded continuously during the setting and hardening of mortar materials" [114].

D. Breysse also reported that compressive strength of concrete is the property most widely sought after, which involves the development of a technique combining index rebound and the ultrasonic pulse velocity [114a].

Ultrasound has been applied extensively to understand the mechanical properties, setting and hardening, of concrete mortars containing a variety of additives and aggregates. A variety of ultrasound strategies are being employed e.g. direct transmission method, pulse echo technique, scanning techniques, to determine the concrete strength, to detect the defects in concrete. Many investigators tried to determine the strength of the hardened concrete by velocity measurements. But the manufactured parameters of concrete such as its compactions, water cement ratio, type and content of cement in the mix and the nature, quantity and grading of the aggregates affect the compressive strength and the velocity in different ways, e.g. air voids, poor compaction, areas of low concrete strength etc. There have been a lot of efforts to develop the ultrasound measurement system as a tool to monitor the concrete properties, but more effort is needed to look at concrete with different altered properties using non-destructive methods and verify the validity of these results with destructive methods, so that a contribution can be made towards the property enhancement.

1.6.3 Appraisals and Limitations of Existing Investigation on Concrete

As revealed in section 1.6.2, numerous methods were employed using ultrasound techniques to observe concrete properties. However, no reported work has been carried out to examine the changes that took place at micro-structural level by altering the micro-structure of the component and relate this to the results obtained from destructive and non-destructive methods.

The purpose of employing ultrasound in this research is to determine the mechanical parameter of concrete i.e. velocity and thus the compressive strength, of concrete blocks with altered properties in a non-invasive way. These properties were altered using additives as accelerators and retarders; waste materials as aggregates during manufacture. The main reason for this alteration is that a contribution can be made towards the enhancement of the properties of concrete, so it can be produced economically and in an environmentally friendly manner.

According to Mitsuhiro Shigeishi [114b], AE is expected as an effective method in maintenance and management of the structure, but currently application case of AE method to actual concrete structure is hard to say being sufficiently abounding, and it has not cleared on criterion of the soundness evaluation either.

As mentioned above, very little attention has been given to the application of AE to understand the failure mechanism of concrete blocks with different aggregates, and in particular the waste materials and optimise the quality of manufactured blocks. Studies have been carried out with regards to increment of energy, i.e. fracture energy with an increase in the size of aggregate in the form of sand. However no significant work has been reported on the micro-behaviour of concrete in relation to toughening mechanism using admixtures and waste materials such as glass and rubber in the form of aggregates, and the mechanism of crack bridging in concrete using AE, which this research programme is aiming for. Although a lot of work was carried out on concrete using ultrasound and acoustic emission, field applications of AE techniques to concrete has been somewhat limited due to the highly attenuative nature of

concrete. Although concrete can be considered a fairly active material from an AE standpoint, practical applications are somewhat limited since the AE event may not generate enough energy to propagate to the structure surface.

1.7 Research Objectives and Methods

1.7.1 Previous Collaborative Investigation

A mechanism for the toughening of coarse-grained ceramic materials has been developed successfully in the refractory industry using residual stresses at the micro structural level [115]. This technology has been transferred to cement-based systems, where the residual stresses are created by internal expansion (formation of ettringite $\text{Ca}_6\text{Al}_2(\text{SO}_4)_3(\text{OH})_3 \cdot 26\text{H}_2\text{O}$) of the matrix phase, as reported by Chandler et.al [116]. This method provides toughening by the release of the residual stresses as the macro-crack propagates. While circumstantial evidence of the release of the residual stress exist (micro-crack formation leading to permanent deformation in flexural tests) it is very difficult to observe the mechanism in action. A few simple experiments [117] were conducted with conventional cement mortars and it was seen that residual stresses can be manipulated in hydraulically bonded systems and the mechanical properties (tensile) significantly enhanced. Therefore by suitable mix design, products with enhanced toughness can be manipulated without the use of reinforcing fibres [117].

Investigators at Aberdeen University (AU) in collaboration with Robert Gordon University (RGU) proposed and tested a method of engineering the microstructure of brittle composites that improves the effectiveness of non-fibrous inclusions to bridge cracks in the matrix. A number of experiments were carried out with model cement systems including aggregates such as: sand (coated and uncoated); spherical and angular glass; and expanded polystyrene balls. The results demonstrated that the interfacial bonding between the inclusions and the matrix dictates i.e. controls the path of the crack through the composite and determines whether an inclusion will act as a bridge and provide a toughening effect. In the presence of a moderately strong bond, the crack path is such as to reduce the number of bridge inclusions. In the absence of bond in the matrix, crack follows a flatter path, and more inclusions bridge the crack, but bridging is only effective with non-spherical particles [118]. It was also reported that although the initial

toughness is reduced by very weak interfaces, such composites are very likely to show rise in toughness behaviour.

As a summary, the following were found:-

- Existence of distantly spaced holes in hardened cement paste gives a flat fracture surface as condensed cement;
- Making the particles un-bonded results in a flatter fracture path compared with bonded particles;
- Use of spherical particles does not increase toughness with crack growth even if a flat fracture through the cement exists;
- Use of non-spherical particles results in an increase in toughness with crack growth so long as the crack follows a flat path [118].

1.7.2 Aim of This Research

It has become evident from the previous investigations above that the inclusions of non-spherical particles into a brittle matrix, that are bonded to the matrix, results in escalation to a flat-fracture path that elevate crack-pinning and follows a rising toughness curve. However there was no certainty of showing that the method employed increased the toughness and hence the enhancement of the mechanical properties of the tested materials.

The aim of this research is to advance the above investigation by using acoustic emission as an on-line tool, to compliment and enhance the model developed at Aberdeen University [117].

1.7.3 Rationale of Research Methodology

The quantitative estimate of the changes occurring in the cement-based systems is challenging due to the anisotropy and complexity of the material. This investigation will concentrate on the development and application of Non-Destructive Techniques to characterise the granular material. The results

obtained will be related to the theoretical work carried out at Aberdeen University [117] to understand the fracture mechanics of granular materials. Interaction of ultrasound with concrete material provides a tool to characterise its mechanical properties non-destructively. The two important ultrasound parameters measured are wave velocity and attenuation of ultrasound. Scattering and absorption of the energy cause attenuation of ultrasound. Scattering depends on the ultrasound wave frequency and the grain size. The wave velocity of ultrasound relates to the elastic properties and density of the material. The presence of internal/residual stress in a material can be determined by measuring a change in the velocity of ultrasound provided all other factors (e.g. Density) remain constant.

Currently the cement-based systems are removed from the moulds and left for twenty-eight days to set in a humid or damp environment. Measurement of ultrasound velocity and attenuation during this period may provide useful mechanical properties data on the changes occurring in the system.

Crack initiation and propagation that are directly related to the fracture toughness of the concrete can be studied using acoustic emission. The AE activity is uniquely related to the fracture toughness and for the crack initiation and propagation. AE has several advantages over the conventional NDT techniques. It is very sensitive and provides time history of micro-cracking and damage propagation in the material.

Acoustic emission is the stress wave energy in a structure, which results from crack formation or other dynamic sources within a material. These stress waves propagate to the surface of the structure, where they are detected and analysed to evaluate properties of the source (cracks) that generated the AE event. AE can be considered as a passive NDT technique since the measured ultrasonic waves are generated by the structure itself, as opposed to being interrogated by some external source (active NDE).

Initial acoustic emission monitoring has shown differences in the AE activity between toughened and non-toughened cement-bonded mortars, but further investigation is required to determine whether the mechanism relies on micro-crack formation or grain bridging.

In this research, the following additives and aggregates/bridging techniques were selected for the 3-point flexural test/compressive test:

- Plain mortar with additive: sodium sulphate/calcium carbonate/calcium chloride/sodium silicate
- Expansive cement mortar with glass beads/pebbles/glass aggregates
- Plain mortar with glass aggregates/glass slide
- Plain mortar with rubber aggregates

1.7.4 Specific Objectives Undertaken in this Research

To investigate the acoustic emission in relation to:-

- (1) The crack mechanism (grain-bridging/micro-cracking)
- (2) The expansive matrix (sulphate, lime and K-type cement additions)
- (3) Interfacial bonding

To use ultrasonic testing for:

- (1) Examination of the microstructure and long term development of the micro-structure
- (2) Long term stability of the toughening mechanism

The above investigations would allow the following objectives to be met:

- a. To establish a correlation between mechanical compressive tests and ultrasonic testing
- b. To observe the strengthening mechanism (grain bridging/micro-cracking) using AE technique; thus allowing to characterise the damage mechanisms such as micro-crack- formation during flexure tests.
- c. To observe macro-cracking and residual stress relaxation under flexural tests using AE technique; enabling to study the behaviour of mortars containing various admixtures under applied load.
- d. To understand cracking mechanism in concrete (which is only possible with the aid of AE) containing various types of aggregates, in particular, utilisation of waste materials to manufacture environmentally friendly concrete.

- e. To investigate interfacial bonding and understand what happens with the samples by loading them to fracture and studying these fractured surfaces; thus see the effect of size and mass of glass aggregates on the strength of mortars which can be explained by interfacial bonding between them and their role in the toughening mechanism.

CHAPTER 2

NON DESTRUCTIVE TESTING (NDT) TECHNIQUES

2.1 Introduction to Non-Destructive Testing

Non-destructive testing (NDT) is the name given to the various techniques which allow inspection of materials and mechanism to detect the presence, location and size of defects without impairing the ability of the tested component or equipment to function. Destructive tests are those such as tensile testing or impact tests in which samples of material are damaged, so destroying its ability to function. Non-Destructive methods have been in use for about half a century [1]. In this period, the development has taken place to such an extent that it is now considered as a powerful method for evaluating existing concrete structures with regard to their strength and durability as well as assessment and control of quality of hardened concrete. In certain cases, the investigation of crack depth, micro-cracks, and progressive deterioration are also studied by this method.

Defects such as cracks, inclusions and porosity may be introduced during the manufacture of components or as a result of degradation during service. NDT methods are chosen by manufacturers or sometimes by the end users to ensure the product integrity and reliability, avoid failures, prevent accidents, and maintain uniform quality level and sometimes to lower manufacturing costs. Different authors and organisations have categorised NDT methods into various categories. According to W. Philip and M. Bolton, for example, Non-destructive tests include [119]:

- Visual Inspection
- Dye Penetrant
- Magnetic Penetrant Inspection
- Eddy Current Systems
- Ultrasonic
- Acoustic Emission

The NDT methods have been categorised into six major categories. The table 2.1 below shows the NDT classification system adopted by The National Materials Laboratory Advisory Board (NMAB) Ad Hoc Committee on Non-destructive Evaluation of The American Society for Non-destructive Testing,

2005 (ASNT) [120]. They are (i) Visual, (ii) Penetrating radiation, (iii) Magnetic-electrical, (iv) Mechanical Vibration, (v) Thermal and (vi) Chemical-electro-chemical. Table 2.1 below shows the NDT classification system adopted by the ASNT. The first six categories (basic categories) involve basic physical processes that require transfer of matter or energy to the object being tested. The other two categories (auxiliary categories) describe processes that provide for transfer and accumulation of information and evaluation of the raw signals and images common to non-destructive testing methods.

Table 2.1: Non-Destructive Testing Method Categories (Adopted from ASNT, 2005) [120]

<u>Basic Categories</u>	<u>Objectives</u>
Mechanical and Optical	Colour, dimensions, film thickness, gauging, reflectivity, strain distribution and magnitude, surface finish, surface flaws,
Penetrating radiation	Density and chemistry variations, elemental distribution, foreign objects, inclusions, micro-porosity, misalignment, missing parts, segregation, service degradation, shrinkage,
Electromagnetic and Electronic	Alloy content, anisotropy, cavities, cold work, local strain, Hardness, thickness
Sonic and Ultrasonic	Crack initiation and propagation, cracks, voids, damping factor, de-laminations, misalignment, surface stress, tensile, shear and compressive strength, disbands, grain size, structure composites, dis-bonds, inclusions, segregations,
Thermal and Infrared	Emissivity, heat contours, thermal conductivity, voids
Chemical and Analytical	Alloy identification, elemental analysis and distribution, surface anomalies, segregation,
<u>Auxiliary Categories</u>	<u>Objectives</u>
Image Generation	Dimensional variations, dynamic performance, Magnetic field configurations,
Signal Image Analysis	Data selection, processing and display, Image enhancement

It is frequently needed to test concrete structures once the concrete has hardened to check whether the structure is appropriate for its intended application. Such tests should ideally be carried out without causing damage to the concrete. The tests that are available for examination of concrete range from the entirely non-destructive, where there is no damage to the concrete, (or those where the concrete surface is slightly damaged), to partially destructive tests, such as core tests and pull-out/pull-off tests, where the surface needs to be repaired after the test.

The range of properties that can be assessed by employing non-destructive tests and destructive tests (partially) is quite large and consist of such fundamental parameters as density, strength and elastic modulus as well as surface hardness and surface absorption, and reinforcement location, size and distance from the surface [121]. In some instances it is also possible to check the quality of workmanship and structural integrity by the capability to detect voids, cracking and de-laminations.

A good knowledge of each particular NDT method is required to ensure that a selected method is appropriate for the specific application. The method that can be used also depends on the physical properties of the material. The Ultrasonic and the Acoustic Emission techniques are used here because both techniques are commonly used to investigate flaws, material characterisation, and to correlate the strength in concrete.

2.2 Introduction to Ultrasonic Technique

The term ultrasonic is described as audio sound waves with a frequency which is greater than the human hearing range i.e. 20 Hz - 20 kHz, even though for the evaluation of materials, frequency in the range of 1 to 50 MHz is often used. The ultrasonic is referred to as acoustic vibration frequency greater than about 18,000 Hz [122]. Ultrasonic waves are also described as mechanical vibrations with low amplitude, inaudible sonic waves.

The ultrasonic technique is commonly used for flaw detection such as discontinuity detection (voids, cracks, inclusions, segregations, laminations, bursts, flakes, anomalies), detection of elastic anomalies and physical

properties such as porosity, structure and elastic constants and is also used in thickness measurement.

Ultrasonic measurements can be used as an additional technique to the destructive testing methods to determine material strength properties and also used for characterisation of material properties. The parameters that are usually used in ultrasonic testing technique are velocity, frequency, material thickness and material noise. In the ultrasonic field, several test methods are available depending on the type of material, type of tests, and the requirements of each method. Different types of transducers and coupling wedges are available to generate ultrasonic waves of several types, including longitudinal (compression), shear and surface waves according to the requirements of the personnel.

The advantages of using the ultrasonic testing technique are [123]:

- The material to be examined is not damaged as a result of the test
- No hazard or danger is faced by the user or in his/her surroundings
- The cost of material testing can be reduced
- The instrumentations are electronics and indications can be obtained in real time
- Accelerated testing of new materials as no large specialised instruments and large or explosive test specimens are required
- The method is very versatile and allows testing of a wide range of sizes and geometries
- Can be used to test the uniformity of the material (i.e. radioactive material, radium)
- The use of a high frequency, well defined sound beam permits detection and location of the smallest critical discontinuities/flaws
- Very useful in predicting the material's micro-structural property and material characterisation
- Can be used to monitor fatigue tests, tensile tests, and also used for discontinuity detection and thickness measurement
- Used to determine yield strength and fracture toughness (linked with ultrasonic wave propagation properties of the polycrystalline materials)
- Reduces maintenance costs and increases equipment reliability through online monitoring, inspection and evaluation, preventive maintenance and risk based inspections

However, there are some limitations involved with ultrasonic technique which relates to such as scanning, economy of examination, size and shape of the component and discontinuity detectability and experient knowledge. The detectability of a flaw or defect is related to sensitivity, resolution and noise discrimination. In brief, sensitivity refers to the ability of the instrument to detect a minute amount of sound energy reflected from a discontinuity. The other major problem associated with the ultrasonic technique is the scanning of very rough surfaces, abnormal shapes, very thin and inhomogeneous material which may prevent effective sound coupling and inspection. The recent development in the field of computer technology and improved software availability of 3 dimensional, 4 dimensional scanning technique has overcome some of these problems.

2.2.1 Ultrasonic Theory

There are several modes of propagation of ultrasonic waves in solids [124], the most important being

- Lamb Waves which are elastic waves whose particle motion lies in the plane defined by the plate normal along with direction of wave propagation
- Compressional or Longitudinal waves where particle motion is parallel to the direction of propagation;
- Shear or Transverse Waves, where particle motion is at right angles to the direction of propagation; and
- Surface waves of which there are a number of different forms, the most common being Rayleigh waves where particle motion is elliptical and restricted to a depth of about one wavelength from the surface.

As the stress waves travel through a material they are modified by the material itself, by the defects and by encountering boundaries including the boundary between the component and the surrounding environment.

Ultrasonic testing in composite materials such as cement or concrete are normally carried out using the through transmission technique. According to Nelligan T.J. [125], ultrasonic techniques are used in situations involving highly attenuating or scattering materials, separate transmitting and

receiving transducers on both (opposite) sides of a component are used (through transmission mode). The signal received is then amplified and analysed.

The compressive strength of concrete can be measured through the destructive testing of samples. This is not always practical and can prove time consuming. Concrete is a dense multiphase material and due to the wide variety of possible composition, proves to be a very difficult material to monitor and characterise using non-destructive techniques, *'.....there is unanimous agreement among engineers that the test methods presently available for non-destructive determination of concrete are, without exception, inadequate'* [126]. Of all non-destructive testing methods, ultrasonic examination techniques have proved to be most accurate, where a clear relationship has been developed between the ultrasonic pulse and the compressive strength of concrete.

The method by which the compressive strength of concrete can be determined using ultrasound is explained in BS 8047 Entwurf (8047) [127]. This standard describes how an ultrasonic pulse of frequencies ranging from 10-200 kHz is passed between two transducers; transmitters and receiver, positioned at either side of the concrete sample. The ultrasonic pulse velocity through the concrete specimen can be determined using the simple speed/distance/time relationship. The ultrasonic pulse velocity is linked with the compressive strength of concrete via the modulus of elasticity as given below:

$$\text{Modulus of Elasticity: } E = \frac{V^2 \rho (1 + \mu)(1 - 2\mu)}{(1 - \mu)} = \frac{\sigma}{\varepsilon} \quad (2.1)$$

where:

V = Ultrasonic Pulse Velocity (m/s)

ρ = Density (kg/m³)

σ = Stress (N/m²)

ε = Strain (Dimensionless quality)

μ = Poisson's ratio – Taken as 0.15 for concrete [128]

The ultrasonic pulse velocity (V_{UT}) is related to the compressive stress (σ_C) of concrete by the following relationship:

$$V_{UT} \propto \frac{\sqrt{\alpha c}}{\rho} \quad (2.2)$$

$$V_{UT} = \frac{N\sqrt{\alpha c}}{\rho} \quad (2.3)$$

Where ' N ' is a correction factor.

The compressive strength of concrete is however greatly influenced by its composition. Therefore it is found that the strength of a certain concrete specimen, is related to the ultrasonic pulse velocity by means of a correlation curve described by the equation, $K \cdot e^{kv}$ [129] where K and k are predetermined constants depending on the mix proportions and type of concrete aggregate. This is however the main disadvantage of this method. The correlation curve derived to relate the ultrasonic pulse velocity to the compressive strength is not the same for any two concrete mixtures. This curve is dependent on the variables k and K , which require additional data that may not always be available. For the purposes of this research, the compressive strength is derived using the relationship between the ultrasonic pulse velocity and the 'rebound value'.

2.2.2 The Rebound Value

The rebound value is an experimentally derived constant specific to concrete, related to compressive strength. The experimental procedure used to derive this value is described in BS EN 12504-2 [130]. The Schmitt hammer is the instrument commonly used for this experiment. Schmitt hammer is a appliance to measure the elastic properties of concrete. The appliance is consisted of a spring-loaded steel mass that is automatically released against a plunger once the hammer is pushed against concrete's surface. The rebound of the hammer on a graduated scale is indicated by a small sliding pointer. The test principle is based on the absorption of part of the energy i.e. spring-released energy, through plastic deformation of the concrete surface, while the remaining elastic energy trigger off the actual rebound of the hammer. The length travelled by the mass (expressed as a percentage of the initial extension of the spring) is called the Rebound number. The rebound number is

dependent on the hardness of the concrete. One end is positioned on top of the concrete sample while a spring loaded mass is dropped on the other. The spring mass will rebound vertically from the plunger. The vertical displacement of the mass is measured on a graduated scale denoting the rebound value. The rebound of the mass is proportional to the compressive strength of the concrete; hence the stronger the sample, the greater the rebound value.

This rebound value relates specifically to the compressive strength of concrete and is completely independent of the effects of commodities such as the mix proportions and aggregate type. The figure 3.5 in chapter 3 illustrates a correlation that has been drawn between the ultrasonic pulse velocity, rebound value and the compressive strength. This graph is specific to Portland cement. Provided by the manufacturer of the ultrasonic testing equipment (Proceq Testing Equipment, Canada), this graph was experimentally derived from research of over 700 concrete samples. The procedure by which the compressive strengths of the concrete samples were determined using the ultrasonic pulse measurement and the rebound value is described in section 4.

2.3 Acoustic Emission (AE) as a Non-Destructive Technique

Acoustic Emission (AE) is a practical technique that relates source of emission directly to onset of defect and its propagation in a material. Therefore AE has been applied in a wide range of non-destructive testing (NDT) techniques.

However, during the 1980's there was a decline in the number of heavy machinery and nuclear reactors due to the ending of the Cold War, this in turn caused a drop in the AE research funding. Also during the 1980's there was some distrust of AE method due to doubtful measurements of vessels. The practical AE applications exhibited a number of limitations and restrictions of the existing AE methods and equipment that lead to several wrong conclusions about the possibilities of AE as NDT instrumentation. According to CAPGO, [131a], "the most important difficulty was associated with the reliability of acoustic emission results", because:

- i) commercial AE systems can only estimate qualitatively how much damage is in the material and approximate estimate of the component's life;

ii) AE signals are very weak therefore signal discrimination were very difficult. The recognition of AE for the testing of materials was lengthy and complex.

When discussing history of AE by T. Holroyd [131b], he stated that its early utilisation was hindered by:

- i) the inherent philosophy of AE compared with all other NDT technologies and;
- ii) the complexities and cost of digital signal processing.

The Federal Highway Administration of the USA in a note about the use of AE as a NDT technique of highway bridges wrote " work has been completed on characterisation of AE in modern steels. This has shown that 90% of signals recorded are not true AE events." This historical retrospective is presented to persuade new researchers to go "back to basics" looking for subsequent "boom" in the field of the AE development and application [136].

The "Great AE Boom" occurred due to efforts of a group of researchers from industry and universities, hence leading to the appearance of AE publications. They drew great interest from the NDT community to this area of research with a promise of various applications in the future [130] and [131]. Commercialisation of the AE NDT applications was observed in Europe, USA and Japan at the same period of time [132] and [133]. The NDT market had to keep up with the theoretical research and the fast-growing AE application [134]. Due to the significant need to increase the AE publications during this period, the commercial resources generated avenues to develop high-level AE equipment and software. This led to improvement in previous limitations in data interpretation and helped deduce effective conclusions of AE results [135].

Also developments in computer technology greatly increased these capabilities in acquisition and analysis of data. Hence, recent advanced developments in AE instrumentation and signal processing capabilities had seen increased application of acoustic emission technique and interpretation of the results in a wide range of fields including civil engineering. Nowadays AE is a well-established tool; its usage is widespread and ranges from

fundamental studies focussing on clarifying the mechanism of AE generation, correlating AE signals to physical or mechanical processes and extending the knowledge of material behaviour to NDT. This generated great interest to apply the AE technique in this research work involving strength and defect characterisation of cement based materials.

2.3.1 AE Background

Acoustic emissions (AE's) are the stress waves produced as a result of the sudden internal stress redistribution in a material caused by changes in the internal structure. The likely reasons of the internal-structure changes are crack opening and closure, crack initiation and crack growth, dislocation movement, twinning, and phase transformation in monolithic materials and fibre rupture (breakage) and fibre-matrix de-bonding in composites. Most of the sources of AE's are related to damage; therefore, the detection and monitoring of these emissions are normally used to predict early failure. Besides the applications of AE in research endeavours, AE has also been used in industries, including for the detection of faults or leakage in pressure vessels, tanks, piping systems, and also used to monitor the welding and corrosion progress [117].

The difference between the AE technique and other non-destructive evaluation (NDE) methods is that AE detects the activities inside the materials, while other NDE methods attempt to examine the internal structures of the material. Additionally, AE only requires the input of one or more fairly small sensors on the surface of the structure or sample being examined so that the structure or sample can be subjected to the in-service or laboratory operation while the AE system continuously monitors the progressive damage. Other NDE techniques, such as ultrasound and x-ray, have to access the whole structure or specimen, and therefore, the structure or sample often needs to be disassembled and taken to the laboratory to be examined [137]. The AE technique is different from most other NDT methods in two key aspects. They are: (i) the signal has its origin in the material itself; and (ii) AE detects the degradation process; whilst most other techniques detect symptoms of existing geometrical discontinuities.

A large number of mechanisms can give rise to AE. Some of them are: crack formation and crack growth, phase transformation, moving dislocations, grain boundary sliding, fibre failure and de-bonding in composites etc. AE can be distinguished from other methods of investigating deformation processes in that it utilises information supplied by the deformation, as the event (deformation) occurs. AE techniques are passive and only receiving transducers are required (no energy input into a structure is required).

The discussion above also is supported by the British Institute of Non-Destructive Testing, which describes AE as the stress-wave which results from the rapid release of strain energy when micro-structural changes occur in a material [123].

Crack growth and plastic deformation are major sources of AE [138]. The AE technique is purely based on the detection and conversion of the stress or elastic waves to electrical signals. The high sensitivity technique detects the released energy from the changes in a material without having to focus in on the exact location of the source to detect it, thus making it a passive monitoring technique and a more sensitive technique compared to the other techniques such as radiography, ultrasonic and eddy current technique. A typical AE system set up is shown in figure 2.1.

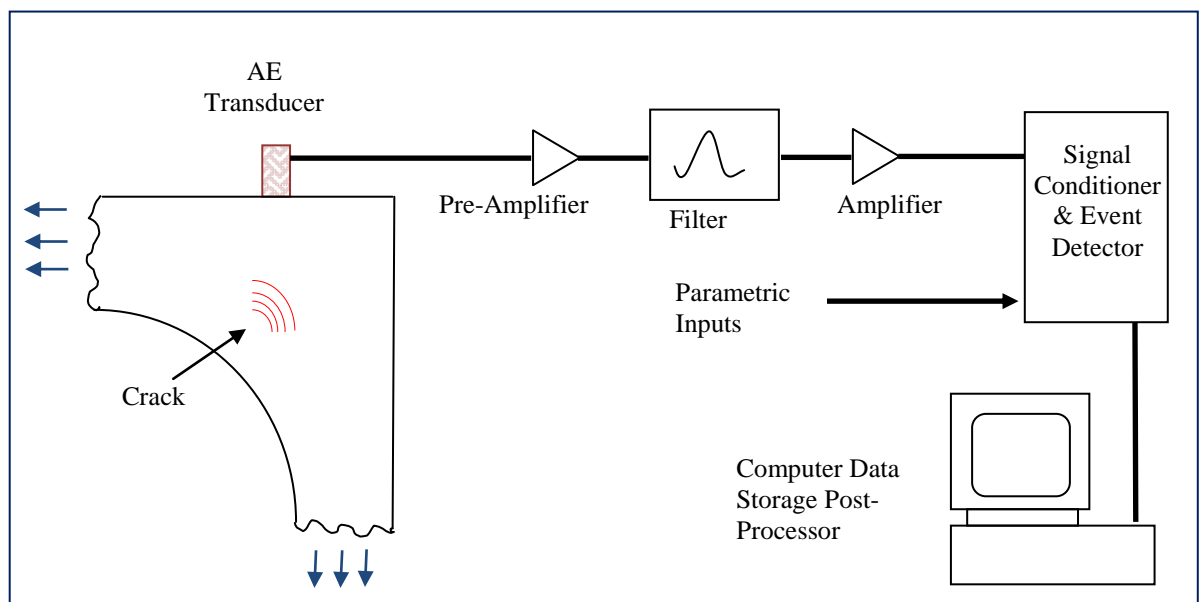


Figure 2.1: A typical AE system set up, adopted from [123].

2.3.2 AE Theory

When a material is subjected to stress by applying force (compressional, tensile or flexural) to the matrix structure of a sample, stress or elastic waves are generated, thus causing micro-structural changes. When enough force is applied to cause micro-structural changes or deformation in the material, rapid acoustic energy or sound is emitted from the atomic structure of the material in the form of discrete acoustic pulses. Each growth of defect or micro-structural changes is an unique event and cannot be reproduced [139]. These acoustic pulses then propagate or travel through the material and to the surface of the material under stress. The emitted acoustic pulses are then picked up by sensors that are coupled directly on the surface of the material under load. The waves are then converted into electrical signals in the system. Majority of the acoustic pulses emitted are broad-band in nature, extending into megahertz (MHz) region. The acoustic pulses are represented by waveform which is represented in time domain. There are two types of AE signal (as shown in figure 2.2), which are: a) Transient (burst) and b) Continuous signals. Transient signals can be separated in time, i.e. the beginning of the signals can be identified. They result from acoustic events due to local defects. Continuous signals cannot be separated in time. They are produced by various unwanted phenomena, e.g. plastic deformation or friction. These signals often include background noise which can include both mechanical and electrical disturbances.

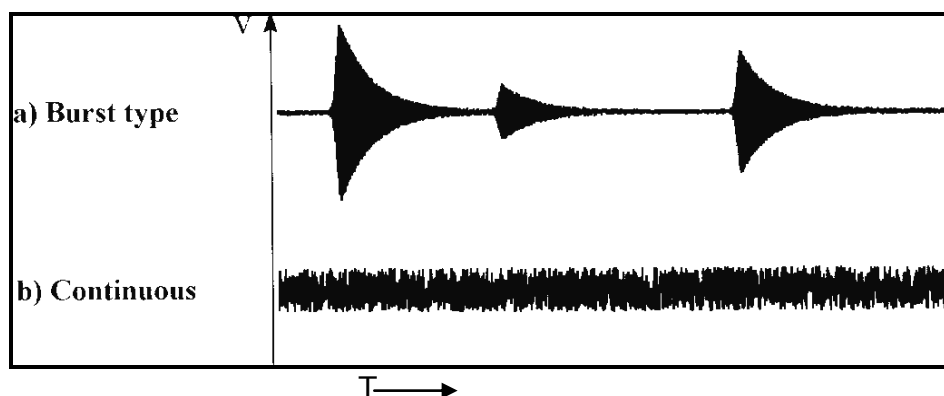


Figure 2.2: a) Transient (burst) signal and b) Continuous signal;
V: voltage (mv), T: time (μ s)

The AE system then processes the AE signal, converts the bursts detected into feature data sets, determines the source locations, calculates statistics and displays the results graphically and numerically in real time. The converted

electrical signals which represent the transmitted acoustic waves are normally presented in waveform for easier interpretation [140]. Figure 2.3 illustrates the typical waveform representation and its parameters in AE signals.

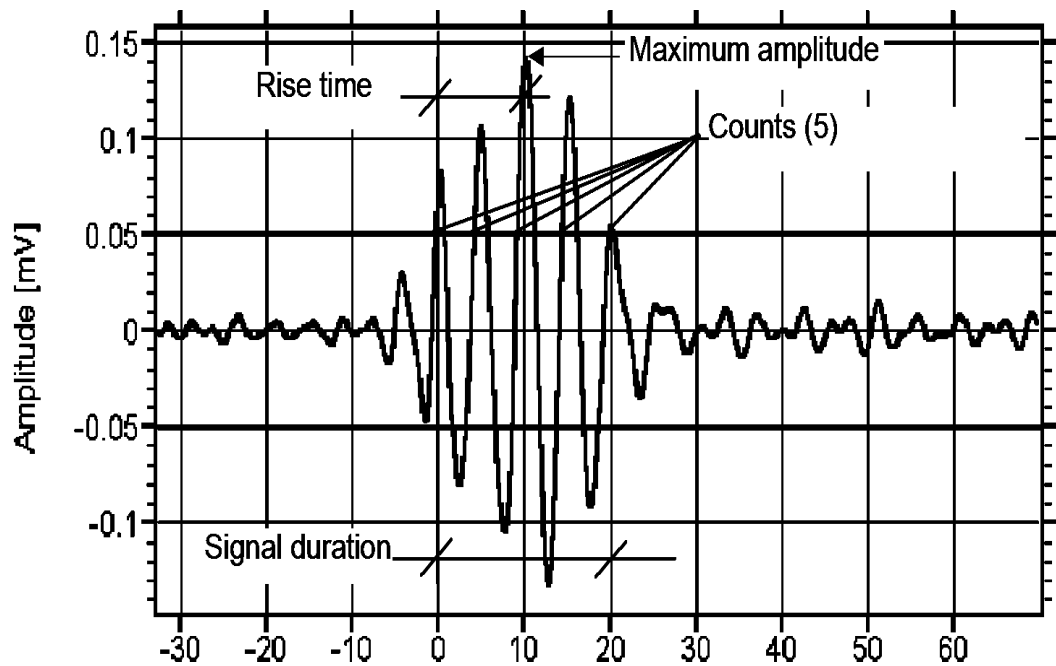


Figure 2.3: Features of transient signals; Adopted from Vallen 2005 [140]

2.3.3 AE Signal Parameters and Representation

The signal received after an event has taken place needs to be analysed. For this a number of signal parameters have been singled out as useful measurements to characterize the signal waveform. The most important and widely used AE parameters are amplitude, arrival time, rise-time, duration, energy, RMS, Decay time and counts. One has to determine these important parameters of the waveforms in order to compare the results of the structure or object under test with a database of defect-free and defect containing test objects. The information that is represented by these parameters is given in table 2.2 overleaf.

Table 2.2: AE Signal Parameters and Representations (Adopted from Vallen 2005, [140])

Parameters	Representation
Amplitude	Representation of emitted stress pulse a sinusoidal wave (used for source classification)
Arrival Time	Absolute time of first threshold crossing (used for location calculation)
Rise-time	Time interval between first threshold crossing and peak amplitude
Duration	Time interval between first and last threshold crossing
Energy	Integral of squared (or absolute) amplitude over time of signal duration (related to elastic energy released from the material)
RMS	Root Mean Square of the continuous background noise before the burst
Decay Time	Time taken to reach a level below the threshold from a maximum signal output level
Counts	Number of times the sensor signal exceeds the preset threshold voltage (it depends on the frequency of the sensor, the damping characteristics of the sensor, the damping characteristics of the material and the threshold level)
Hit	A burst detected by the AE system
AE – event	Physical event producing AE, e.g. crack Formation

As Vallen states that 'the simplest AE parameter to measure is counts. Terms such as total counts (adding up counts from all the bursts), count rate (counts per unit time or unit stress increase) are employed to process large number of bursts. A detected burst is a valid signal (above the threshold level) and is

termed as a 'hit'. Most of the bursts with low amplitude and long duration are friction noise". The peak amplitude is one of the vital burst features. The AE technique source classification in composite materials is based on peak amplitude. Table 2.3 illustrates the AE source classification for composites based on the peak amplitude [140].

Table 2.3: AE Source Classification for Composite Based Materials on Peak amplitude [141]

<u>Peak Amplitude (dB)</u>	<u>Classification</u>
Low Amplitude (40-60 dB)	Micro-cracks at the interface of paste and aggregate
Higher Amplitude (60-70 dB)	Increased Micro-cracking
High Amplitude (>70 dB)	Damage Zone

AE events are from both micro-cracks and macro-cracks. Nagaraja Rao et al. (1999) [142], based on parametric analysis, classified the AE events into micro-crack and macro-crack phases, and their classification is given in the table 2.4:

Table 2.4: Micro-crack and Macro-crack Phases [Adopted from 142]

<u>Phase</u>	<u>Peak Amplitude (dB)</u>
Micro-crack Initiation	44-60
Micro-crack Extension	61-70
Macro-crack Initiation	71-80
Macro-crack Extension	81-100

'The dB scale is a logarithmic expression for a factor or a ratio according to the equation $A[dB] = 20 \times \log (V_s / V_{ref})$ (2.4)

where V_s = source voltage and

V_{ref} = reference voltage [140]

The addition of dB values corresponds to the multiplication of their factors. Usually, the maximum amplitude of a burst is given in dB_{AE} , so the reference voltage is $1 \mu V$ ' [140] (V_{ref} in equation 2.4 above).

CHAPTER 3

MATERIALS AND METHODS

3.1 Components of Modern Concrete: Concrete, Cement, Mortar and Aggregates

Modern concrete consists of the following basic ingredients: concrete, cement mortar and aggregates. Concrete is a composite material which is consisted of a binding medium wherein there are embedded particles or fragments of aggregates. Aggregate is the granular material, such as sand, gravel, crushed stone or iron-blast furnace slag, used with a cementing medium to form hydraulic cement concrete or mortar. The term coarse aggregate refers to aggregate particles larger than 2 mm, and the term fine aggregate refers to aggregate particles smaller than 2 mm. Mortar is a combined mixture of sand, cement, and water, i.e. concrete with no coarse aggregate. Cement is a finely pulverised material which by itself is not a binder, but develops the binding property as a result of hydration [143].

3.2 Cement and Concrete: Ordinary Portland Cement

In terms of quantity the most extensively used man-made structural material is concrete, which is produced by mixing mineral lumps (usually stones), called aggregate, with water and cement. The aggregate, which consists of coarse and fine lumps, may comprise about three-quarters of the volume of the concrete. The rest of the volume is occupied by the cement paste, which is formed by the reaction of water with the cement, and air voids. In many ways concrete may be viewed as a composite material with the cement paste as the matrix and the aggregate as the filler material [144].

The composition of cement varies but the most commonly used formulation is that of Portland Cement. The composition of Portland Cement can be varied to give the appropriate properties for a specific application. There are four main types of Portland Cement commonly available:

- i) ordinary,
- ii) rapid hardening
- iii) low heat and
- iv) sulphate resisting.

Since this research is concentrating on the AE characteristics of normal concrete, for which Ordinary Portland Cement OPC is normally used, it is important to briefly look at the manufacturing processes of OPC and the fundamental properties of concrete [119].

Ordinary Portland Cement (OPC) is one of the most commonly used cement for a wide range of applications. Portland cement is a mixture of about 75% limestone, CaCO_3 , and 25% clay, mainly aluminium silicate with iron and alkali oxides. These are ground together and heated in a kiln at a temperature of between 1400 and 1500⁰C. A series of reactions occur until the mixture coalesces together into lumps of clinker about 5 to 10 mm in size. After cooling, this clinker is mixed with 3 to 5% by weight of gypsum, CaCO_4 , and ground to give cement powder. The function of the gypsum is to control the initial setting rate. Apart from the gypsum, the cement contains tricalcium silicate, di-calcium silicate, tri-calcium aluminate, tetracalcium aluminoferrite and alkali oxides [119].

When water is added to cement it turns into a paste which is workable and pourable. A series of reactions take place. In the first stage a considerable amount of heat is evolved by the reactions as the cement sets to a rigid material, which takes a few hours. After setting the next stage has the cement hardening and its compressive strength increasing. This takes many days. Figure 3.1 shows how the compressive strength varies with time.

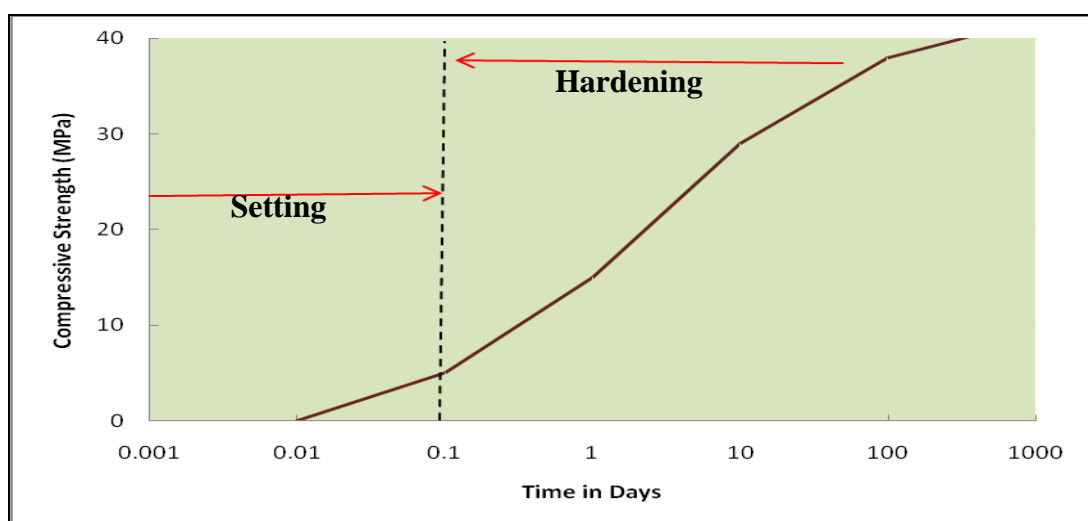


Figure 3.1: Hydration of cement; Adopted from [119].

In general terms the reaction that occurs when the water is added is that initially there is a high rate of heat evolution when the alite and aluminate hydrate.

The grains then become coated with gels, a gel being a swollen polymer network of high viscosity. It is this gel coating which gives hydrated cement its paste-like consistency. Fine needle-like crystals then begin to form and interlock. The cement is then set. During hardening, growth and interlocking of these needle-like crystals continue, along with the formation of plate-like hexagonal crystals known as portlandite. The resulting structure of hydrated and hardened cement is thus an interlocked mass of crystals and amorphous fibres consisting of partially dried-out silicate gel in the fibres and portlandite in the crystals [119].

The cement contains pores between fibres, between fibres and crystals and larger spaces where the gel did not grow as a result of air pockets or trapped water. A totally hydrated cement requires a water to cement ratio of about 33~40%. Below that value the cement will contain un-reacted grains while above it there will be excess water. The excess water will lead to greater porosity as a result of becoming trapped within the hardened cement. Figure 3.2 shows how the compressive strength of the hardened cement depends on the water/cement ratio after a hardening time of about of 28 days.

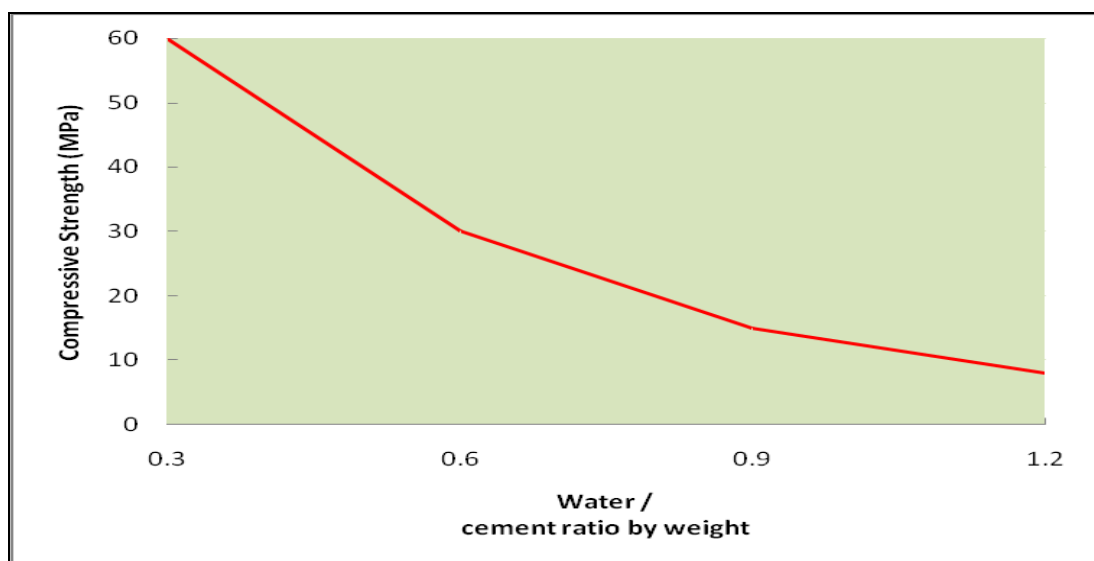


Figure 3.2: Relationship between compressive strength of the hardened cement and water/cement ratio; Adopted from [119].

Concrete is a composite structure with the cement being used to bind together particles of sand and aggregate. The properties of the concrete depend on the relative proportions of water, cement, sand and aggregate in the material, the average size of the aggregate particles, the type of aggregate used and its surface texture. Typically, concrete with a Portland cement/water ratio of 0.5 and using crushed aggregate will have a compressive strength after 28 days of about 50 MPa, its tensile strength being about one-tenth of the compressive strength. The modulus of elasticity is typically about 30 GPa [119].

3.2.1 Additives

Additives are commonly used in industry when producing concrete and are defined as *'...materials other than water, aggregate, or hydraulic cement which are used as ingredients of concrete and which are added to the batch immediately before or during mixing. Their function is to modify the properties of the concrete....'* [145]. Additives can be introduced into a concrete mix in order to enhance or obtain numerous characteristics. These characteristics can be used to classify and group additives into categories.

3.2.2 Accelerators: Needs and Types

Admixtures that are accelerators are added to concrete to increase the rate of early strength development in concrete to

- allow earlier removal of formwork;
- lower the required period of curing;
- advance the time that a structure can be played in service;
- partly compensate for the delaying (retarding) effect of low temperature during cold weather concreting;
- in emergency repair work [1].

Accelerators are designed to speed up the early strength development of concrete. They are usually based on calcium chloride, which increases the hydration rate of the calcium silicates and to a certain level the tri-calcium aluminate (C_3A) (a compound that is responsible for quick setting of strength) in the cement. Significant improvements can be achieved between the ages of one day and seven days, particularly in cold weather – for instance, the three day strength of concrete at ambient temperature may be doubled at a

temperature of 2°C. The use of calcium chloride does not affect the long term strength of concrete. Majority effects are the side-effects of the material – the susceptibility of steel in structural concrete to corrosion is significantly raised in the presence of chlorides, such that BS 8110 (standard of British Standard *structural use of concrete*) now restricts chlorides, measured as chloride ion content, to 0.1 per cent by weight of cement in pre-stressed concrete or steam-cured concrete, or 0.2 per cent when use of sulphate-resisting cement is made. The permissible limit of chloride ion content in other steel-containing concretes is 0.4 per cent. These chloride ion contents are equivalent to roughly 50 per cent greater percentages than that of anhydrous calcium chloride by weight. Any chlorides existing in the aggregates – for instance, from sea-dredged sources ought to be incorporated. The shrinkage of concrete also increases due to the existence of chlorides. Chloride-free accelerators are nowadays available but these are more expensive than chloride-based accelerators and it should be noted that more rapid strength development can be attained by other methods; for instance, use of water-reducing agents or increased cement content [146].

V.N. Ramachandran of Canadian Building Digest reported that, “the addition of small quantity of certain materials to concrete to promote desirable properties is almost same age as the use of cement itself. The Romans made use of blood, pig’s fat and milk as additives to pozzolanic cements to enhance their workability and durability. Currently, many hundreds of chemicals claim to possess one or more useful effects that have been recommended for incorporation into concrete. These are commonly known as admixtures and are added to water, aggregate and hydraulic cement just prior to or during mixing” [147].

Majority of admixtures are known according to the function they perform. Some of the examples are water-proofers, water reducers, retarders, water reducing accelerating agents, and accelerators [147].

A number of chemicals are known to act as accelerators for concrete e.g. sodium chloride, calcium chloride and potassium carbonate, (along with others) – but calcium chloride is most commonly used. It’s easy accessibility, low cost, foreseeable performance characteristic, and successful application over several decades made it a popular accelerator [147].

Concrete has to fulfil various performance needs. According to V.N. Ramachandran, adding calcium chloride promotes several desirable properties and affects others; but the performance of a concrete that contains calcium chloride admixture can sensibly be predicted only when both the short and long-range effects have been established. Such knowledge allows well-judged use of admixtures. Initially, the science of admixtures was the zone of an expert, but with highly developed building technology and growing new demands on builder, engineer and architect it is essential that all engaged in building have as much awareness of admixtures and the effects they have on cement, aggregate or the mixing water [147].

3.2.3 Chemical Effects on Concrete

Concrete may deteriorate under conditions where it is exposed to solutions of sulphates. The sulphates react with calcium and aluminium ions in the cement paste forming calcium sulphate and calcium sulphoaluminate hydrates, which provides explanation for concrete disruption. There is evidence that if calcium chloride is present, then resistance to sulphate attack is decreased. Therefore, for concrete exposed to sulphate attack, calcium chloride is not a recommended option. In certain cases, it may be used in a concrete member exposed to a sea water environment, but its usage should be determined by the severity of exposure and the function of the member (CSA A231-1973) [148].

3.2.4 Calcium Carbonate in Concrete

Throughout the ages, the benefit of make using of lime in mortar has been acknowledged by builders. Lime based mortars tend to crack in the form of a much reduced number of micro-cracks. Lime is popular for its capability to enhance the plasticity and workability of mortar [149].

Calcium carbonate has found a unique application in concrete and is being increasingly used as quality filler in concrete applications, such as concrete wares e.g. paving stones. It can improve the concrete density, pre-stability and durability [150].

3.2.5 Sodium Sulphate in Concrete

Sodium sulphate delays the hydration during the initial stage, i.e. at the mixing process stage; and accelerates the hydration during a later stage when the concrete has been cast. According to US Patent 4144086, "concrete products possessing a high strength after a short hardening period are manufactured by adding sodium sulphate to a normal concrete mixture in a quantity of 0.1–5 per cent by weight of the cement, preferably 0.5–1.5%, of the weight of the cement. The concrete mix is maintained at a temperature of 30°-90° C during the mixing process, and the cast concrete is held at a temperature of 30°-90° C for a period of at least two hours" [151]. When possible, the concrete mix should be cast in a mould in such a way that no noticeable decrease in temperature should take place during the casting process. The positive effect of the sodium sulphate appears to be attained because of the increase of the ion activity in the water phase; it causes a delay to the hydration of the cement component. If possible, the sodium sulphate should be added to the concrete mix towards the end of the mixing process, when the other components have been properly mixed [151].

3.2.6 Other Additives in Concrete

According to Jennifer Chrisman [150] of EUCD (Euclid chemical), the use of silicate solution as a curing compound puts the concrete at risk for low strength development and surface durability issues. Therefore, silicates should not be used as a suitable option for curing new concrete [152].

However, according to [153] Industrial Chemicals Division of PQ Corporation, sodium silicate and sodium meta-silicate are multi-functional and are used to:

- Reduction in slurry costs
- Reduction the price of cement
- Prevent solids from segregating
- Accelerate the times of setting
- Decrease free water in normal and heavy weight cements
- Promote earlier strength"

Apart from its use as an admixture for cement, sodium silicate can also be used pre and post cementing to improve the cement bond at the cement-formation and cement casting interface; and are also used in:

- Flushing the well-bore prior to cementing
- Remediating poor cementing [153].

According to Barbour, Ronald Lee, [154], Potassium Chloride can be used as an additive to improve high early strength, accelerate setting times, thus enabling the concrete structure to be put into service quicker, reducing labour cost, and allowing pre-cast concrete and concrete masonry manufacturers to attain rapid form and mould turnover. Marcantoni Paul [155] also reported the same regarding sodium chloride.

3.3 Expansive Cement (Modified Portland cement)

Expansive cement when mixed with water forms a paste similar to OPC, that during the early hydrating period occurring after setting volumetrically increases considerably more than does Portland cement paste. Therefore to minimise cracking caused by drying shrinkage in concrete slabs, pavements, and structures this type of cement is used; so this category of cement is termed as shrinkage-compensating concrete [156].

The development of compressive, tensile, and flexural strength in shrinkage-compensating concrete is generally influenced by the same factors as Portland cement concrete. Polivka and Wilson found that for a given water/cement ratio (in the range 0.4 to 0.65), the compressive strengths of type K cement concrete were significantly higher than that of type I Portland cement concrete. In the case of shrinkage compensating concrete, a denser cement paste matrix and a stronger transition zone between the cement paste and the coarse aggregate are the factors causing strengths higher than those of a Portland cement concrete made with an equivalent water/cement ratio [157].

3.4 Aggregates in Concrete

Aggregates are important components of concrete described as inert granular materials such as sand, gravel, or crushed stone. Aggregates generally occupy 70 to 80% of the volume of concrete and therefore have a significant effect on its properties. Although aggregates are looked upon as a filler material thus influence strength, durability, cost and micro-mechanisms in concrete [158].

Compared to cement, aggregates are much cheaper and greatest economic benefit is obtained by using as much aggregate as possible in concrete. Its use also significantly improves both the volume stability and the durability of the resulting concrete. Traditional concrete aggregate usually consists of sand (fine aggregate) and various sizes and shapes of gravel or stones. In general, aggregates are used in concrete because they:

- enormously reduce the cost
- reduce the heat during curing and hence reduce thermal stress
- minimize the drying shrinkage of the concrete
- help produce a concrete with satisfactory plastic properties.

Generally it has been believed that the strength of aggregate has little influence on the strength of normal strength concrete as opposed to paste strength and paste-aggregate bond. As early as 1960's, through 1000 tests, direct tensile bond strength between aggregate and cement paste or mortar was found to be much less than the tensile strength of the paste or mortar, and dependent on the type of rock, surface roughness of aggregate, and water to cement ratio [159]. The interface between aggregate and paste has an effect on the strength of the aggregate. The rough surface of the aggregate joined with the cement paste makes concrete tough.

However, it was recently demonstrated that based on the entire load-deflection response, concrete containing stronger coarse aggregate, such as glacial gravel, are a lot less brittle at early ages than are concretes containing weaker aggregate [160]. There is an increasing attention in replacing alternative aggregate materials, mainly as a potential use of recycled materials. Although there is considerable research on many different materials for aggregate substitutes such as wood products/wastes, sintered sludge

pellets and others, the only two that have been applied are glass cullet and crushed recycled concrete itself [161].

3.5 Waste Materials

Waste materials management is a challenging task for municipal authorities worldwide. There is a need worldwide for an environmentally friendly construction material because of the purpose of reducing carbon dioxide (CO₂) emissions, save non-renewable energy resources, provide aesthetically pleasing and healthy surroundings and at the same time reduce waste. Research carried out by Chandra, Cyr and their team [8] recommended two options of recycling waste: i) either a setting in a controlled landfill, generally following a solidification and stabilisation treatment, or ii) a reuse in building or road works (concrete, road foundations, embankments).

Such waste materials can partially be used, or processed, to produce materials appropriate for use as aggregates or fillers in concrete. They may also be processed into cementing systems or used as clinker raw materials. New grinding and mixing technology makes the use of these secondary materials simpler. Developments in chemical admixtures: superplasticisers, air entraining agents, etc, help in controlling production techniques and in attaining the desired properties in concrete [8]. The use of these products is not only a partial solution to environmental and ecological problems; it considerably improves the microstructure, and therefore the durability properties of concrete, which is not easy to achieve by the use of pure Portland cement [8].

The objective is not only to make the cements and concrete cheaper, but to offer a blend of tailored properties of waste materials and Portland cements that are appropriate for specified purpose. This requires better understanding of micro-mechanical properties (micro-crack mechanism and interfacial bonding), although other investigations are being carried out such as understanding the behaviour of chemistry of such products. There is a growing need for better awareness of material properties and better control of the microstructure developing in the construction materials to increase durability. A mixture of different binders and modifiers to produce cheaper and more durable building materials will solve to some degree the ecological and environmental problems [8].

There are a number of experimental studies [8] that are taking place to understand the mineralogical and physical characteristics of these waste materials, such as XRD (X-ray diffraction) and optical and electron microscopy. The reason for including waste materials in this investigation is to understand the interfacial bonding (*between waste aggregates and cement paste*) and crack bridging and arrest offered by the waste aggregates as compared to normal aggregates. This will also facilitate the impact of some of these waste materials (glass and rubber as aggregates) on the micro-mechanical properties of the final product, i.e. Portland cement based concrete, in terms of improvement or deterioration. The study is taken from the point of view of concrete engineers, materials technologists, who are concerned about the micro-behaviour of such materials, but due to the lack of appropriate techniques under in-situ conditions, are unable to understand the events taking place at the micro-mechanical level.

The experimental technique that is developed for this particular investigation is novel in the sense that this allows the investigation to take place on an on-line situation, where stress related emissions are related to the actual events. This will allow a better predictability and benefits that these materials will bring to monitor fracture behaviour of concrete on a micro-level basis. Thus it will enable us to identify the exact location of the cracks and the influence of admixtures on concrete. The performance of waste materials as aggregates and their bonding with concrete/cement matrix can be observed on an on-line basis with the technique developed for this investigation. This on-line basis examination makes this investigation novel.

3.5.1 Glass Aggregates as Waste Materials

The recycling of waste glass is a major problem for city corporations world-wide. Refuse glass in millions of tons of are generated every year. New York City for example, collects more than 100,000 tons per year and needs to pay Material Recycling Facilities (MRF's) up to \$45 per ton for the dumping of the glass, commingled with metals and plastics. Although MRF's does not have much difficulty with profitably dumping of the metals and plastics, markets for recycled glass are limited to nonexistent. It is cheaper to manufacture than recycle. Thus the environmental issue of disposing of glass safely remains a major concern [162].

Development of new building materials from waste glass has been made over the last few years. According to New Jersey Department of Transportation, there are large number of environmental reasons why sustained efforts should be made to reduce the amount of glass in the solid waste stream. Other forms of waste, such as paper and organic constituents of garbage decompose; but glass does not when dumped on the land and constitutes a high quantity of incinerator residue. Studies have indicated that cost savings will be seen in reduced expenses for glass transport to distant landfills [163].

According to Canadian Building Digest, [164], "the strength of concrete containing glass is lower than that with gravel aggregate and is particularly low when high alkali cement is used. Flexural strengths also show a similar trend. Replacement of cement with about 20 to 30% fly ash is effective in controlling the large retrogression of strength". Waste glass is prone to alkali-aggregate reaction. Considerable expansion takes place in the presence of high alkali cement, which accounts for the low strengths in glass-based concrete. For instance, compared to an expansion of 0.018 percentage at about 12 months for gravel-concrete, the glass-concrete may display an expansion of about 0.3 percentage [164].

As reported by Charles Camp, [165] "Alkali-aggregate reaction, which is an expansive reaction between certain reactive forms of silica with the aggregate and alkalis in the cement paste. The result of such a reaction/expansion is overall cracking in the structure, manifesting itself in mapping or pattern cracking at the surface". By using low-alkali cements this reaction can be controlled fairly easily, but because of the changes in manufacturing, low-alkali cements may not be feasible. A proper or better method is to avoid aggregate with the proven or potential record of activity. A low water/cement ratio is very impermeable and will slow down the reaction but not stop it. No adverse reaction will occur without external water [165].

Field-testing carried out by Toolbase Services [166] have shown that crushed and screened waste glass can be used as a sand replacement in concrete and almost all-waste glass could be used in concrete applications, including glass that is inappropriate for uses such as glass bottle recycling. According to their research [166], some of the specific glass waste materials that are of use as fine aggregate are non-recyclable clear window glass and fluorescent bulbs with tiny amounts of contaminants. The recommended applications for such

waste-glass concrete are bike paths, footpaths, gutters and similar non-structural type of constructions. Glass aggregates usually perform its role as a crack arrestor that promotes concrete durability, though this depends on the specific glass aggregate properties, the concrete and its final application. The acceptable size of the aggregate mainly determines the cost, which are in the region of \$15 to \$20 per cubic yard. Smaller aggregate for example, glass sand is the more expensive. Glass aggregate will permit a wider range of aesthetic/decorative choices for concrete [166].

The Waste and Resource Action Programme (WRAP), describes the phenomenon of glass aggregate in the following terms "Recycled crushed glass is a hard inert material with high compressive strength and has been used extensively in the USA as a substitute for natural aggregates. Significant quantities are now being used in a number of applications in the UK".

Meyers, C, Xi, Y and Jin, W, Meyers, C, Baxter, S [167], [170] investigated the partial replacement of natural aggregate by waste glass in Portland cement concrete. Their research has shown that several approaches can effectively control the expansion of ASR due to glass aggregate.

An extensive research was carried out at the University of Colorado by Yumping Xi, Yue Li, Zhaohui Xie and Jae S. Lee on utilising waste glass as aggregates in concrete. They carried out tests using various types of glass colours and sizes, and reported that types of glass were found to have a significant effect on the ASR expansion. Soda-lime glass, Pyrex and fused silica glass exhibited ASR expansion; but window glass, plate glass, and windshield glass were found to have caused insignificant ASR expansion in the ASTM C1260 test [168].

According to the reports published by Concrete Technology Unit, Dundee Concrete Technology Unit, Dundee University, their ASR testing programme has identified differences in the ASR expansion behaviour of different colours of glass cullet. The green glass displayed the largest expansion and flint glass the lowest, but the approach taken has been to consider all colours as being able to cause as much expansion as green glass. However, the same report states that concrete containing crushed glass as a filler aggregate has not shown harmfully expansive ASR behaviour, although it was decided to still

class the material as 'highly reactive', given the potential for expansive reactions of the coarser material [169].

Where the option of crushed glass is to be used in concrete, the BS EN 206-1 and BS 8500 [170] specifications should be conformed to and the following specifications should be followed:

- i) Crushed glass filler aggregate can be used to replace not more than 20% (by mass) of natural fine aggregate.
- ii) The maximum size of aggregate (including glass) (D_{max}) shall be 20 mm [170].

After considering the above, scientists at Commonwealth Scientific and Industrial Research Organisation (CSIRO), Australia have carried out extensive field and laboratory testing on the use of waste glass in concrete, (CSIRO, Australia). After all these studies, Australian scientists have approved the use of waste glass in concrete production, (Kwesi Sagoe-Crentsil of CSIRO [171]). Results of the investigations have shown that waste glass that is "crushed and screened is a strong, safe and economical alternative to using sand in concrete" [171].

Although a lot of ongoing and open-ended research is taking place and there is a number of pros and cons of using glass as aggregates in concrete, the following properties are certainly not to be ignored:

- With virtually zero water absorption it can contribute to the durability of the concrete;
- Its hardness is higher to most natural aggregates;
- By using glass, concrete flow properties can be improved and, therefore higher-strength lower water mixes can be employed;
- A contribution to the concrete strength can be obtained since very finely ground glass has pozzolanic properties.

After carefully considering all the investigations carried out by eminent researchers, it was decided for this particular research to use windscreen glass which causes (according to Yumping Xi, Yue Li, Zhaohui Xie and Jae S. Le) [168] almost negligible ASR expansion.

3.5.2 Rubber Aggregates

There have been a lot of concerns on disposing used tyres all over the world, especially in developed countries. The continuous amount of rubber waste in landfills from the disposal of waste tyres has caused a major environmental concern. Rubber is not easily biodegradable, nor can it be safely burnt, because this will deliver toxic gases and will lead to environmental pollution. Recent introduction of chipped and crumbed rubber tyre particles as a recycled aggregate in concrete production provides a cheap and effective solution to reuse large quantities of waste rubber tyres that creates a severe environmental problem [172].

According to the research carried out by M. Hossain et.al. [173]; it was reported that the use of chunk rubber from recycled tyres as a road construction material can minimise the scrap-tyre waste problems of rural communities.

As far as Portland Cement and Concrete is concerned, which is being utilised for this particular research, rubber from granulated tyres can be utilised as an elastic aggregate. This alters the brittle failure of concrete and enhances its capacity to absorb higher amounts of energy prior to failure. According to Goulias DG and Ali AH, "strength characteristics of concrete may significantly be compromised by the replacement of coarse aggregate with rubber particles due to the high compressibility of rubber particles, producing localised stresses and bonding problems between the rubber particles and the cement matrix" [174]. However, using fine graded rubber as partial substitute of fine aggregates may create a ductile behaviour with large deformations prior to complete disintegration of concrete and affect strength to a lesser extent [174].

A. Maher and F. Ansari reported that tyre rubber has been used in hot-mix asphalt and Portland cement concrete. The strength and toughness properties of concrete were examined, in which various quantities of rubber-tyre particles of several sizes were used as aggregate. The concrete mixtures showed lower compressive and splitting-tensile strength than exhibited by normal concrete. These mixtures did not however exhibit brittle failure, but a ductile and plastic

failure, and had the ability to absorb a large amount of energy under compressive and tensile load conditions [175].

Besides a few pieces of work carried out by a number of researchers on concrete with rubber as aggregates, which only reports the measurement of mechanical properties, one group of researchers carried out investigation and showed that the addition of 10% (by weight of mortar) of NaOH-treated tyre rubber particles in mortar reduced the sorptivity (a measure of the capacity of the medium to absorb a liquid by capillarity) considerably, and improved the resistance to acid attack, hence indicating the favourable effects of the rubber on the transport properties in spite of the decrease in flexural strength observed in the specimens. Their investigations also showed that 'small rubber particles can improve some mortar properties even when used in a high proportion' [176].

In any research involving any particle as concrete with aggregates the first and foremost implication is its effects on its mechanical properties and fracture toughness performance of concrete. In an extensive research carried out by M. M. Taha, A.S. El-Dieb and M.M. Abdel-Wahab, [172] as reported by CTU, [169] Dundee, they came to the conclusion that:

- i) 'it is possible to produce 15-20 MPa concrete incorporating chipped rubber tyre particles as a replacement of coarse aggregate in concrete;
- ii) rubber tyre particles can be used in normal strength concrete applications where a reduced compressive strength is not of major concern e.g. pavements;
- iii) the inclusion of rubber tyre particles in concrete results in a significant reduction in its compressive strength, and on the other hand a significant enhancement in its fracture toughness;
- iv) the optimal replacement level of the rubber tyre particles in normal concrete strength should be governed by a compromise between the compressive strength, and fracture performance of concrete dependent on the type of application;

- v) A 50% replacement level by volume of the coarse aggregates seems to be the optimum replacement level producing enhanced fracture toughness and reasonable compressive strength (15 MPa at 28 days);
- vi) The effect of the rubber tyre particle replacement level on the fracture toughness of concrete should be considered when a relatively high probability of concrete cracking is anticipated" [172].

3.6. Concrete Reinforcements

3.6.1 Fibres in Concrete

The tensile strength of concrete is typically only about one tenth of its compressive strength is relatively brittle, irrespective of whether it contains natural or waste glass aggregate. Therefore regular concrete is generally reinforced with steel reinforcing bars. It is turning out to be increasingly popular, for many applications to reinforce the concrete with small, randomly distributed fibres. Increasing the energy absorption capacity and toughness of the material is their main purpose, but also the increase in tensile and flexural strength is often the prime objective [177].

As a result of many desirable properties of concrete, it offers itself to a variety of innovative designs but two characteristics have made its use limited: it's brittleness and weakness in tension. Fibre-reinforced composites improvement in the plastics and aerospace sectors over the past few years has offered a technical basis to improve these deficiencies. The promise of thinner and stronger constituents reduced weight and controlled cracking by basically adding a small amount of fibres is a striking element of fibre-reinforced concrete [178].

M.S. Shetty states that "plain concrete possesses a very low tensile strength, limited ductility and little resistance to cracking. Internal micro-cracks are essentially present in the concrete and the poor tensile strength it has is due to the propagation of such micro-cracks, eventually leading to brittle fracture of the concrete". In the past, attempts have been made to impart improvement in tensile properties of concrete members by the method of using conventional reinforced steel bars and also by applying restraining techniques. Although both these methods provide tensile strength to the

concrete members, they however, do not increase the inherent tensile strength of concrete itself. In plain concrete and other similar materials that are brittle, cracks (micro-cracks) in structure develop even before loading, particularly due to drying shrinkage or other causes of volume change. The width of these initial cracks seldom exceeds a few microns, but their other two dimensions may be of higher magnitude. When loaded, the micro-cracks (spread) propagate and open up, and due to the effect of stress concentration, further cracks form in places of minor defects. The structural cracks progress gradually or by small jumps because they are retarded by various obstacles, changes of direction in bypassing the more resistant grains in matrix. The expansion of such micro-cracks is the main reason of the inelastic deformations in concrete. It has been recognised that the addition of small, closely spaced and uniformly dispersed fibres to concrete would act as crack arrester and would significantly improve its static and dynamic properties [1].

M.S. Shetty also states that this type of concrete is known as Fibre Reinforced Concrete. Fibre reinforced concrete can be described as a "composite material consisting of mixtures of cement, mortar or concrete and irregular (discontinuous), discrete, uniformly dispersed suitable fibres". Although every type of fibre has been tried out in cement and concrete, not all of them can be effectively and economically used. Each type of fibre has its characteristic properties and limitations. Some of the fibres that could be used are steel fibres, polypropylene, nylons, asbestos, coir, glass and carbon [1].

Cracks will propagate, sometimes rapidly, when the loads imposed on concrete approach that for failure; fibres in concrete provide a means of arresting the crack growth. The same beneficial effect is obtained with reinforcing steel bars in concrete because they act as long continuous fibres. Short continuous fibres have the advantage, however, of being uniformly mixed and dispersed throughout the concrete. The most common fibres are steel, glass, asbestos, polypropylene and carbon. Fibres are generally distributed at random in concrete as a rule, but, processing the concrete so that the fibres become aligned in the direction of applied stress results in even greater tensile or flexural strength [178].

Fibres improve the flexural strength, the toughness, or both, and are selected on the basis of their availability, cost and fibre properties. The basic difference

between the plain concrete and fibre reinforced concrete is found in their toughness performance.

As already mentioned in chapter 1, W. Jason Weiss, Byounggeon Kim, and Hulya Kayir [179] investigated fibre reinforced cement mortars restrained from volume changes to quantify damage using acoustic emission. They reported that fibre reinforced specimens demonstrated acoustic evidence of cracking at approximately the same time as un-reinforced mortars, but cracks in fibre reinforced mortars became visible at a later stage which is attributed to the crack bridging which used the fibres to transmit forces across the crack [179]. Their conclusion was that the apparent inconsistencies between researchers that indicate fibres do not significantly alter free shrinkage, creep, and residual stress development, yet they can markedly have an effect on the visibility of cracks [179].

In the mechanical behaviour of tension-weak concrete or mortar matrices, useful improvements can be attained by incorporating discrete fibres (glass, steel and carbon) in concrete. Such composites with their better mechanical properties could provide a long lasting material under sever loading on one hand, and environmental conditions [180].

3.6.2 Glass Fibre Reinforced Concrete

Glass fibres were originally found to be alkali reactive and products in which they were used deteriorated quickly. Alkali-resistant glass containing 16% zirconia was effectively developed in the 1960's and was in commercial production in the UK by 1971. During the 1970's and 1980's other sources of alkali-resistant glass were developed in other parts of the world, with higher zirconia contents. Alkali-resistant glass fibres are used in the manufacture of glass-reinforced cements (GRC) products, which have a wide range of applications. As the Cement and Concrete Institute of New Zealand reports that glass fibre is available in continuous or chopped lengths and "fibre lengths of up to 35 mm are used in spray applications and 25 mm lengths premix applications. Glass fibre possesses high tensile strength (2 - 4 GPa) and elastic modulus (70 - 80 GPa) but possess brittle stress-strain characteristics (2.5-4.8% elongation at break) and low creep at room temperature. Claims have been made that up to 5% glass fibre by volume has been used successfully in sand-cement mortar without balling". Glass fibre products exposed to outdoor

environment have shown a loss of strength and ductility. The reasons behind this are not clearly apparent and it is speculated that alkali attack or fibre embrittlement are possible causes. GRC has been confined to non-structural uses where it has wide applications. GRC products are used extensively in agriculture; for architectural cladding and components; and for small containers [181].

Glass fibres are effectively used to prevent cracking problems due to shrinkage stresses in the production of thin sheets. Alkali-resistant (AR) glass fibres have a density that is similar to that of concrete. This ensures uniform mixing in the matrix as well as low rebound losses, especially relevant in plastering applications. AR glass fibres are superior to the conventional synthetic fibres even in the plastic stage since they provide around 200 million reinforcing points thereby ensuring a better bond between the concrete matrix and the reinforcement. The fibres also have an elastic modulus which is significantly higher than concrete. This enables the fibres to provide an effective reinforcement during the hardened stage of concrete.

Independent studies conducted by Saint Gobain [182] have shown the following major benefits in concrete at small dosage additions of 600 g/m³ of Anti Crack HD (high dispersion) (engineered alkali-resistant (AR) glass fibre):

- 85 percent reduction in plastic shrinkage cracking;
- Reduction in bleeding (water rising to the surface) – 25 percent;
- Increase in compressive strength by 13 percent;
- Increase in flexural strength by 15 percent;
- Reduction in permeability by 50 percent;
- Reduction in freeze/thaw expansion by 66 percent [182].

3.6.3 Carbon Fibre-Reinforced Concrete

As mentioned above cement based materials are the most widely materials used in construction. Developing and enhancing the mechanical properties of cement concrete systems took the greatest interest for a long period of time and have witnessed numerous improvements. One of the new methods to enhance concrete systems is adding of short carbon fibres to the concrete mixtures [183].

Holger D. Basche et. al. reported that "the bond strength increases with the fibre thickness, if the fibres are embedded in epoxy resin matrices and also with the concrete strength". The construction of concrete structures reinforced with carbon fibre is more expensive than using commonly reinforced concrete. However, considering the service life of such structures, carbon fibres can be more economical because their usage can ensure the durability with a lower concrete cover and costs for monitoring and maintenance can also be reduced [184].

Carbon fibre is obtainable as individual chopped or as continuous strands fibres. Continuous strands are usually pre-placed and aligned to provide the optimum fibre orientation during manufacture. Chopped fibres are typically included during the mixing process and are therefore orientated at random right through the mix. An adequate mix of chopped carbon fibre, cement and water is hard to attain due to the large surface area of the fibre [181].

Victor Y. Garas and C. Vipulanandan [180] investigated destructive and non-destructive evaluation of carbon fibre reinforced cement mortar. They carried out impact resonance test and pulse (ultrasonic) velocity test to determine non-destructive properties and reported that increasing the fibre content decreased the Young's modulus of elasticity but increased the failure strain; fibre contents of more than 1% decreased compressive strength of the mortar [180].

3.7 Non-Destructive Characterisation of Concrete

3.7.1 Ultrasound Testing

As mentioned in chapter 2, compressive strength of concrete can be measured through the destructive testing of samples, but this is not always possible and can be time consuming as well as not economically feasible. Since concrete is a heterogeneous material and due to its various possible composition, it is rather a difficult material to monitor and characterise using non-destructive testing techniques [185].

Out of all the non-destructive testing techniques, ultrasound has been found to be most flexible and accurate, where a clear relationship has been developed between the ultrasonic pulse velocity and the compressive strength of concrete. According to the British Standards 8047 the method by which the

compressive strength of concrete can be determined using ultrasound is as described in chapter 2.

Figure 3.3 illustrates a correlation that has been drawn between the ultrasonic pulse velocity, rebound value and the compressive strength of concrete. The graph is specific to Portland Cement and is provided by the manufacturer of the ultrasonic testing equipment [186] (Proceq Testing Equipment, Canada). This graph was experimentally derived after research was carried out on over 700 concrete specimens. The procedure by which the compressive strength of the concrete specimens were determined using the ultrasonic pulse measurement and the rebound value is explained in chapter 4, section 4.1.1.1.

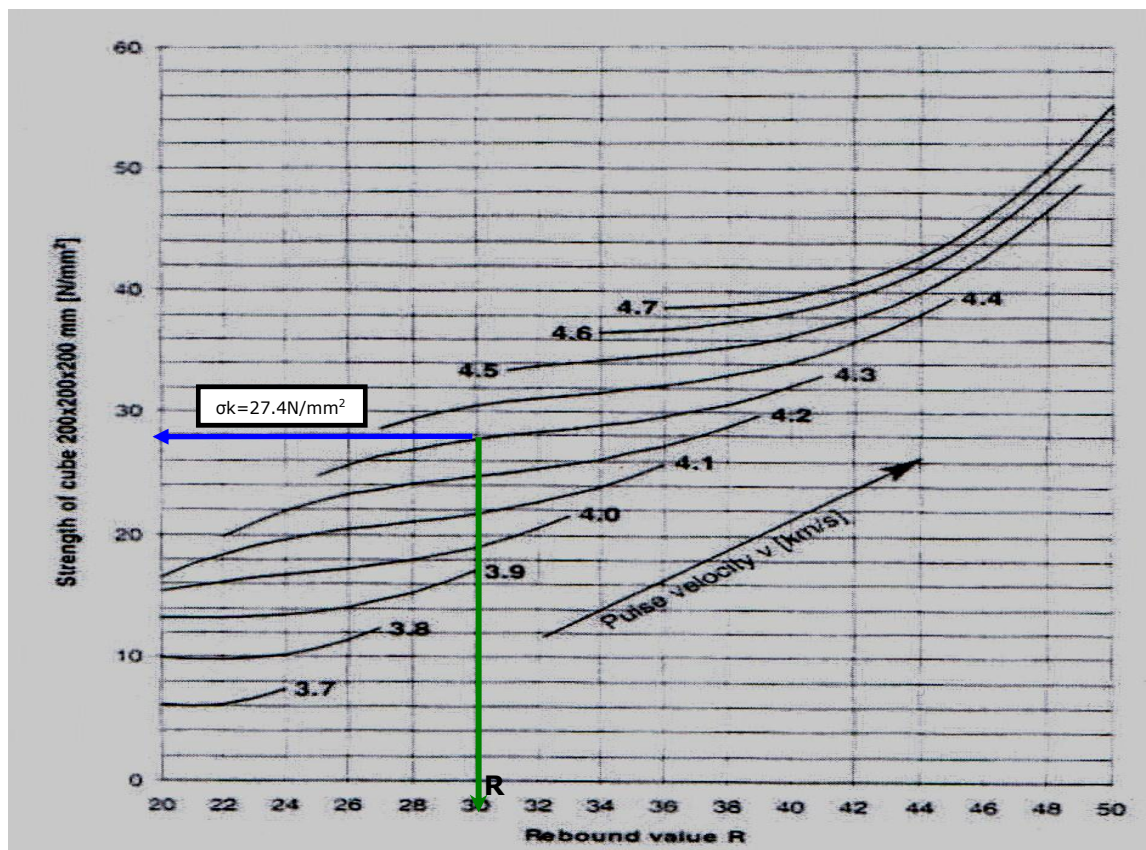


Figure 3.3: Rebound Value vs. Strength of cube [186] (Adopted from Proceq Testing Equipment, Canada)

3.8 Flexural Strength of Concrete

3.8.1 Bend Tests

With many brittle materials, such as ceramics or glass, the conventional tensile test cannot be used because of problems of preparing suitable test pieces and effectively holding them in the test machines. The presence of flaws at the surface, e.g. produced by the act of clamping them in the test machine, can also easily lead to failure. For such materials a bend test is used. The materials are in the forms of beams and bent by three-point bending as shown in figure 3.4.

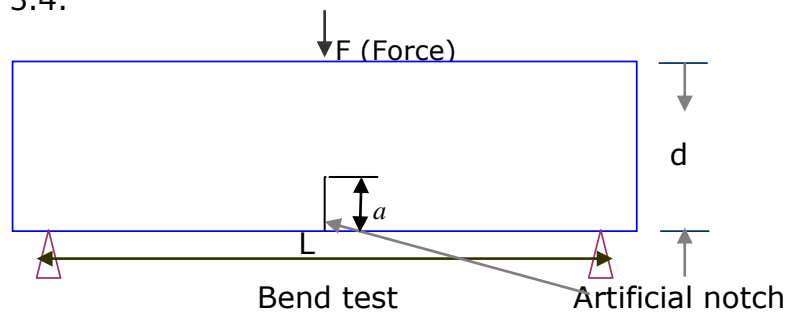


Figure 3.4: Arrangement for 3-point bend test

The term flexural strength or modulus of rupture is used for the surface stress in the beam when breaking occurs. For a beam, the stress σ at a distance y from the neutral axis is related to the bending moment M and the second moment of area I of the beam section by:

$$\frac{\sigma}{y} = \frac{M}{I}. \quad (3.1)$$

With three point loading, $M = \frac{FL}{4}$. (3.2)

For a rectangular cross-section beam, $I = \frac{bd^3}{12}$, (3.3)

where b is the breadth of the section and d its depth. The maximum stress will occur at the surface when $y = \frac{d}{2}$. (3.4)

Thus, for a rectangular cross-section beam:

$$\text{Flexural Strength (Modulus of Rupture)} = \frac{3FL}{2bd^2} \quad (3.5)$$

Flexural strength values for materials tend to be about twice their tensile strength values. Because cracks and flaws tend to close up in compression, brittle materials tend to be much stronger in compression than tension [186] Fracture toughness is evaluated using the following equation:

$$\text{Fracture Toughness } K_c = \frac{3FLYa^{0.5}}{2bd^2} \quad (3.6)$$

$$\text{i.e. } K_c = \text{Modulus of Rupture} \times Ya^{0.5} \quad (3.7)$$

(Taking the dimensionless value of $Y=1.12$; adopted from [187] and [188])

3.8.2 Flexural / Three Point Bend Test

Three-point bend tests were carried out on the Denison Avery 7150 loading frame. A rubber pad was employed on all rollers to minimise the frictional noise and any unwanted vibration pick-ups. The tests were done at a constant displacement rate of 0.25 mm/minute. The load cell amplifier output was connected to one of the parametric inputs of the AE system to record applied load to the block under test. The central roller was in an eccentric position with respect to the notch as shown in figure 3.5.

The position of centre load point is significant in three-point bending test arrangement. The bending point curvature is a maximum at the centre roller position and not at the tip of the notch. The centre load offset produces two unequal moments (Force x arm length) in the specimen causing more damage and AE activity in the longer arm compared to the shorter.

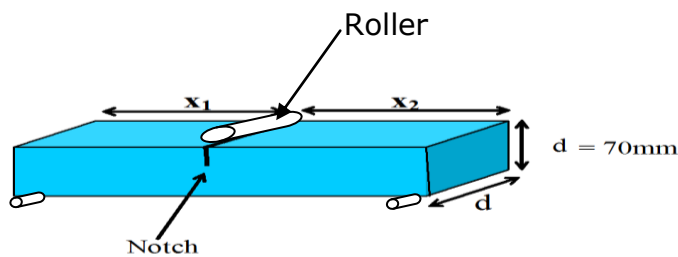


Figure 3.5: Central roller in an eccentric position with respect to the notch

The stress σ applied to the specimen;

$$\sigma = \frac{My}{I} \quad (3.8)$$

$$y = \frac{\text{notchdepth}}{2} = \frac{t}{2} \quad (3.9)$$

$$M = \frac{F}{2} \times \frac{x}{2} \quad (3.10)$$

$$y = \frac{10}{2} = 5 \text{ mm,}$$

Therefore due to centre offset of 10 mm, $x_1=115$ mm, $x_2=95$ mm.

$$M = \frac{Fx}{4} \quad (3.11)$$

I = Second moment of area m^4

$$= \frac{td^3}{4} \quad (3.12)$$

$$\sigma_1 = \frac{My}{I} = \frac{Fx}{4} \times \frac{t}{2} \times \frac{12}{td^3} \quad (3.13)$$

$$\sigma_1 = \frac{3Fx_1}{d^3} \quad (3.14)$$

$$\sigma_2 = \frac{3Fx_2}{d^3} \quad (3.15)$$

The centre roller was offset near to one sensor, approximately 10 mm. The offset of the central roller position changed the moment (force x distance) at the notch, causing more damage to the longer arm than the shorter. All tests were carried out under the eccentric load condition.

CHAPTER 4

EXPERIMENTAL METHOD

4.1 Ultrasonic Examination

One of the main objectives of this research was to use the ultrasound technique to understand the long term development of the microstructure of concrete. As previously established part of this experimentation was conducted using ultrasonic non-destructive testing methods; applying the relationship between different ultrasonic and mechanical parameters of concrete, discussed in chapter 2. Using the ultrasonic test system as shown in figure 4.1, the development of the relationship between compressive strength and velocity of concrete was monitored on a daily basis over a 28 day period.

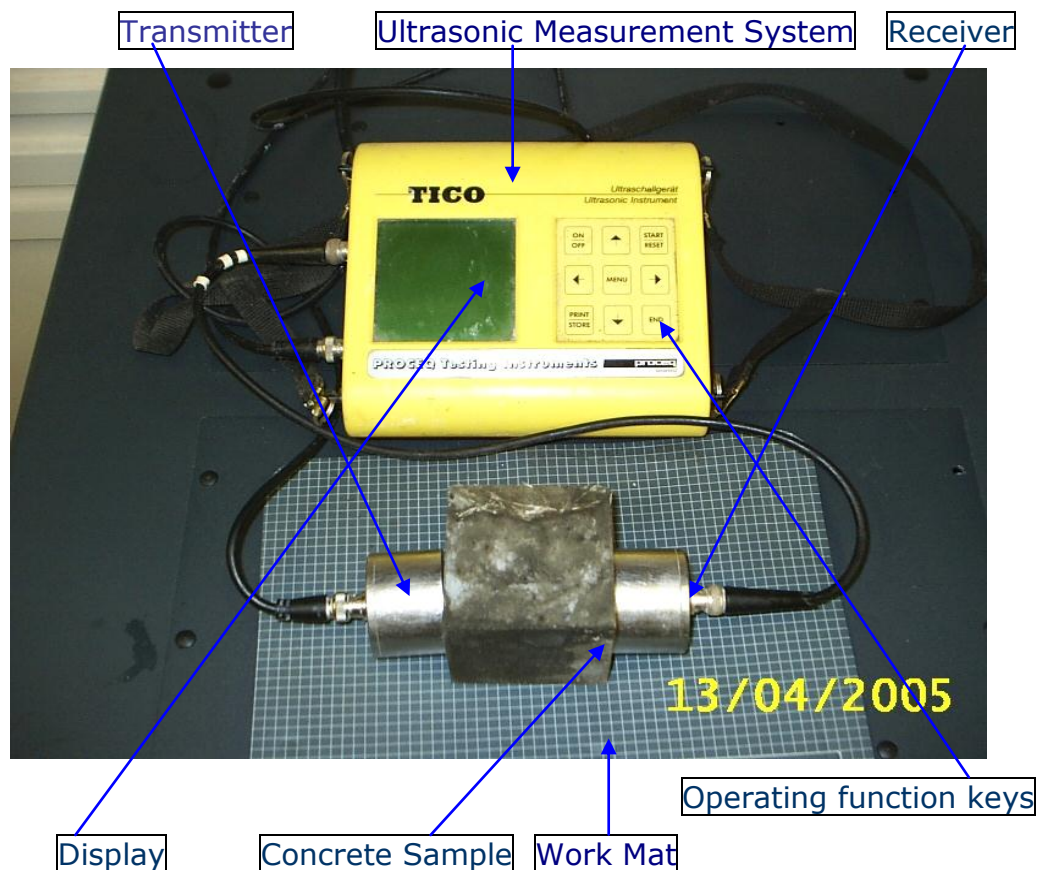


Figure 4.1: Ultrasound Measurement Experimental Set-up

4.1.1 Test Procedure

The procedure for operating the ultrasonic system in order to determine the compressive strength of the concrete test sample is as follows:

- a) Using the main menu function on the system, the width of the concrete test piece is entered. This is to enable the unit to calculate the ultrasonic pulse velocity from transmitter to receiver.
- b) Applying a generous amount of ultrasound couplant to opposite sides of sample block. This allows a good contact to be made between the transmitter/receiver transducers and test piece.
- c) Position transducers on either side of sample as shown in the figure 4.1.
- d) Whilst applying pressure to the transducers, press 'START'. The transmitter repeatedly transmits an ultrasonic pulse through the test piece until it arrives at a constant value, i.e. the meter measures the time taken for the ultrasonic pulse to travel through the sample several times to ensure the reading is correct (distance is input). The time required for the pulse to travel from transmitter to receiver and the pulse velocity is displayed on the meter. For automatic display of the pulse velocity in the measurement screen, the distance between the transmitters is input with an accuracy of 1% using the cursor keys. For the direct transmission the distance between the measurements points accurately to ± 1 of the length, maximum length at direct transmission 15 m.
- e) Employing the graph relating compressive strength, ultrasonic pulse velocity and the rebound value; described in chapter 3, the appropriate rebound value can be obtained from figure 3.3. Test report CUR 69 of the TNO (the Netherlands) describes the method with which the concrete strength can be calculated using a combination of the Rebound value of a Schmidt hammer type N and the pulse velocity. This mathematical relationship was derived from the test results of more than 700 samples. After the mean rebound value R has been input, the cement type (i.e. Portland in this case) is chosen. A calculation of the

concrete strength is displayed in the measurement image as $\sigma k=27.4$ (N/mm^2) as shown in figure 4.2. This value is obtained when the pulse velocity is in the range between 4300 m/s and 4400 m/s at a rebound value of 30 as represented by arrow R in figure 3.3 (page 93).

- f) This rebound value is now entered into the test meter using the main function as previously discussed.
- g) The transducers are positioned on the sample as before and the testing program on the meter is initiated again. The meter transmits the ultrasonic pulse repeatedly as before, verifying the measurements. The meter now displays values for time, velocity and compressive strength of the concrete sample. The measurement images are shown in figures 4.2 and 4.3.
- h) The procedure a-g can now be repeated again for verification of results. A typical example of ultrasonic measurement for a plain mortar result is shown in table 4.1.

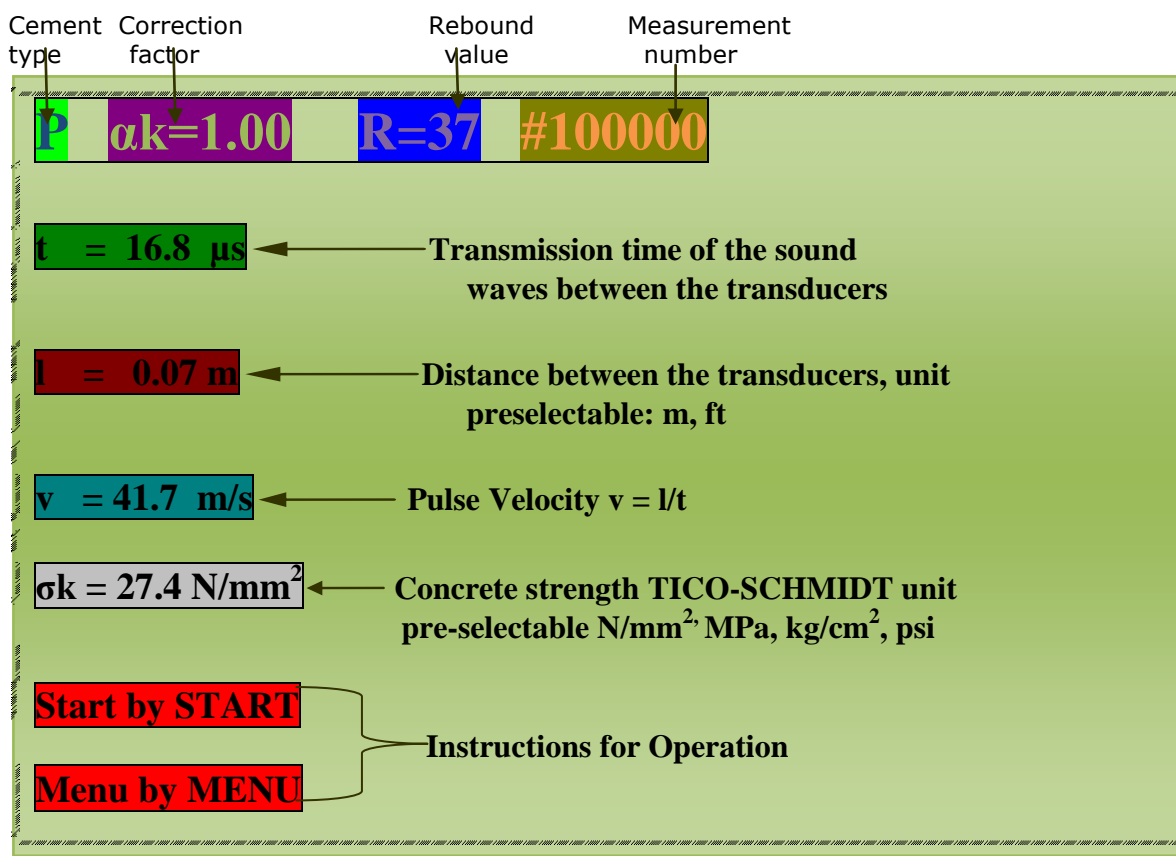
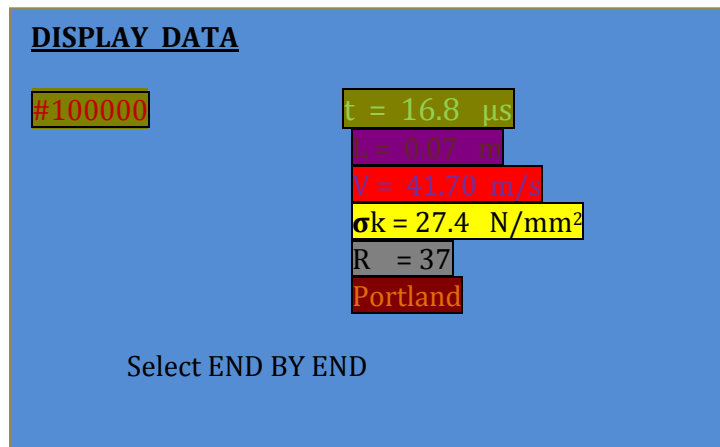


Figure 4.2: Ultrasonic measurement image of a plain mortar



The measured values can be called up from the memory by means of the cursor keys and can be shown on the display.

Figure 4.3: Ultrasonic display data of a standard mortar

Table 4.1: Ultrasonic measurement carried out on plain mortar over a 28 day period

No Additive (Plain Mortar) 70 mm ³				
	Time	Velocity	Rebound Value	Estimated Compressive Strength
Day	Micro Seconds ±0.5	(m/s) ±100	R±1	(N/mm ²) x 10±1.5
1	20.1	3480	-----	-----
2	18.7	3740	24	8.5
3	18.1	3870	27	13.8
4	17.8	3930	30	17.7
5	17.6	3980	33	21.4
6	17.6	3980	33	21.4
7	17.6	3980	33	21.4
8	17.5	4000	33	21.6
9	17.5	4000	33	21.6
10	17.5	4000	33	21.6
11	17.5	4000	33	21.6
12	17.4	4020	33	21.9
13	17.3	4050	33	22.2
14	17.3	4050	33	22.2
15	17.3	4050	33	22.2
16	17.3	4050	33	22.2
17	17.3	4050	33	22.2
18	17.2	4070	34	23.4
19	17.2	4070	34	23.4
20	17.2	4070	34	23.4
21	17.2	4070	34	23.4
22	17.2	4070	34	23.4
23	17	4120	36	25.9
24	16.8	4170	37	27.4
25	16.8	4170	37	27.4
26	16.8	4170	37	27.4
27	16.7	4190	37	27.4
28	16.8	4170	37	27.4

4.1.2 Compressive Testing

Compressive testing was conducted on a number of concrete test samples in order to verify the accuracy of results obtained from the ultrasonic testing method and in so doing, provide further evidence proving the relationship between ultrasonic pulse velocity and the compressive strength of concrete. The sample under compression shows deterioration in the forms of visible cracks before final fracture. In service a structure will be unsafe if it shows deterioration with visible cracks. Hence the strength should be recorded when the sample shows deterioration of visible cracks. Therefore it was not necessary to test all the test samples to destruction. A representative number of samples containing different additives in different quantities would provide an adequate verification. The compressive testing machine provides uniaxial loading, powered by hydraulic pump and the AE was monitored simultaneously as shown in schematic diagram, figure 4.4 and compressive test machine and the digital display meter is shown in figure 4.5 (a) and 4.5 (b).

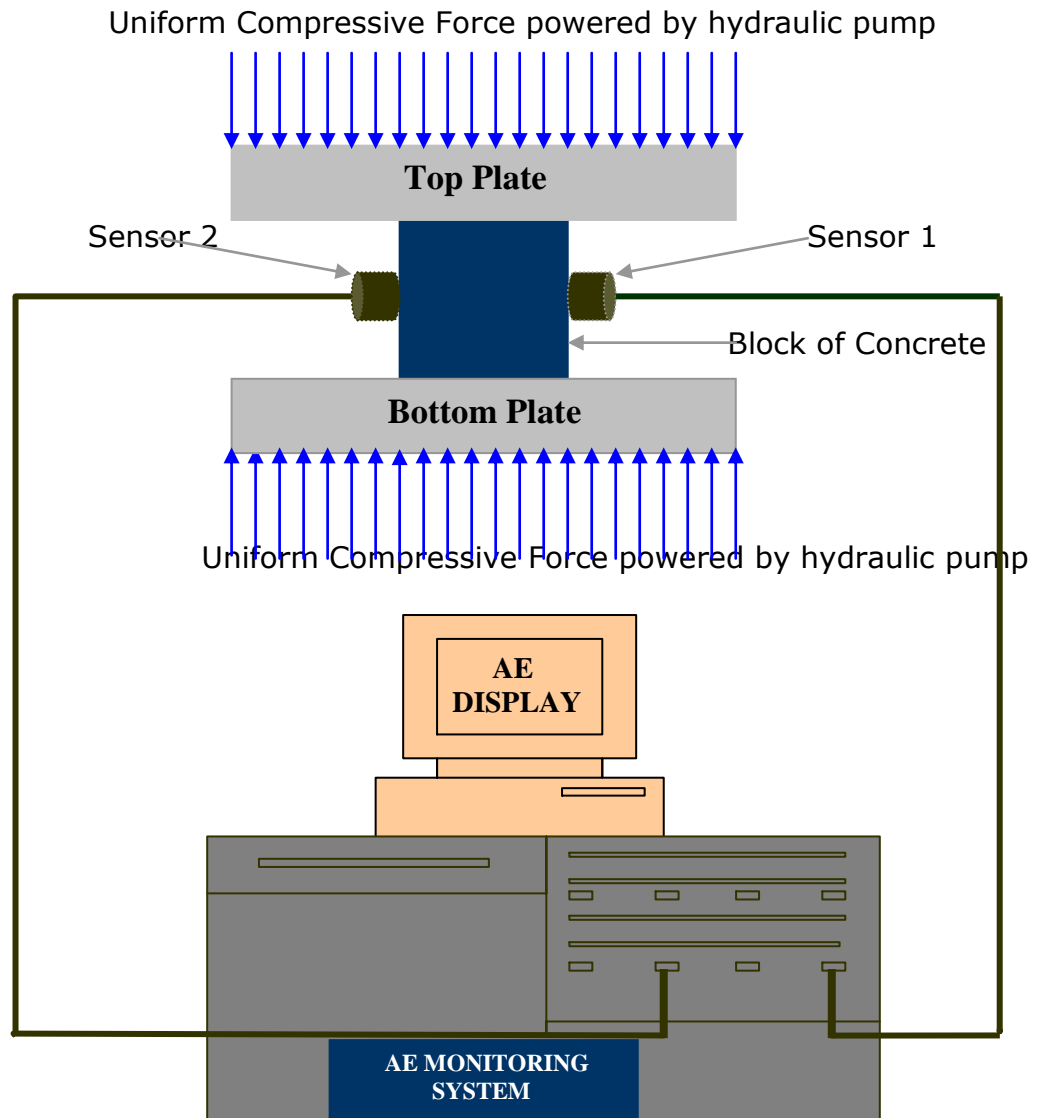


Figure 4.4: Schematic diagram of a compressive test set-up

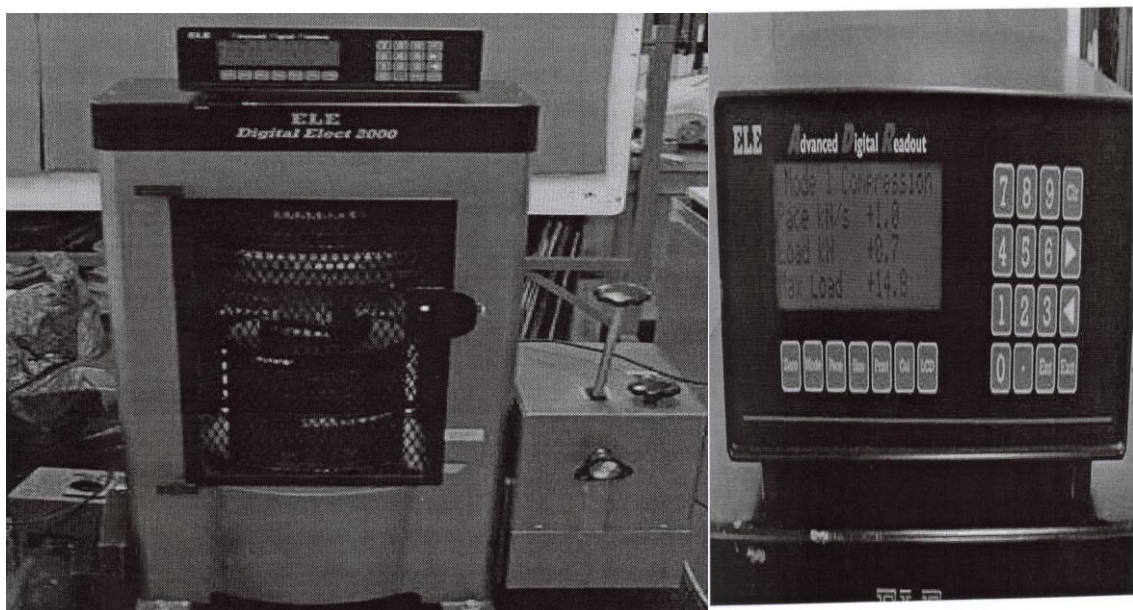


Figure 4.5: (a) Compressive test machine powered by hydraulic pump

(b) Digital display meter

The operation sequence for compression testing is as follows:

- a) The test sample is positioned on the test plate and the safety door is secured in place.
- b) The hydraulic testing unit is interfaced with the digital display meter of the computer, shown in figure 4.5 (b). Using the menu function on the display the dimensions of the test sample and the rate of load increase was selected. The rate of load increase is however only a guide as the actual operation of hydraulic compression is controlled manually, i.e. during compression the digital meter measures the rate at which the load is increasing and compares this with the desired value. A '+' or '-' indicating the deviation from this desired value is then depicted on the digital display. This therefore provides a certain level of guidance to the operator of the hydraulic pump.
- c) With the hydraulic pump in operation, load is gradually applied to the sample, controlled manually using a lever. Steadily the lever is drawn backward, slowly increasing the applied load. A measure of the applied load throughout is displayed on the monitor.
- d) The sample is tested to failure. The applied load at which the sample fails is then displayed on the monitor.
- e) The procedures in a to d was repeated for approximately 100 samples containing various additives.

4.2 Acoustic Emission Monitoring System

The Acoustic Emission (AET) AMSY4 AE Vallen System (shown in figure 4.6) was used for testing and monitoring/recording the AE events when the block and cubed specimens were subjected to applied load and compressive loads. The Vallen AE system is a microcomputer based system which makes full use



Figure 4.6: The Acoustic Emission (AET) AMSY4 AE Vallen System

of computer technology to allow in-situ data acquisition, processing and evaluation. It comprises a microprocessor, a number of channels of AE input (only two channels are used for this research) and the acoustic emission signals are recorded on each channel thus giving full computer automation. The system is able to give accurate results through its powerful real-time capabilities, measurement techniques, graphics display, source location, signal parameters (such as arrival time, peak amplitude, rise time, signal duration, energy, number of threshold crossings, etc) and the storage of data.

4.2.1 Sensors

AE resonant sensors made of piezoelectric ceramic PZT (lead-zirconate-titanate) were employed in the experiments reported in this thesis. They are converters of mechanical waves into an electrical signal. The piezoelectric sensors used in this project were DECI SE 150-M sensors which have a resonant frequency of 150 kHz. The sensors capture the energy which are usually un-damped or lightly damped. Thus the sensitivity of the recording signal is not lost. Piezo-electric sensors have been found to be most appropriate for AE testing and are commonly used for monitoring force, strain, temperature and acoustic emission [140] and [140a]. They are robust and more sensitive than other techniques, e.g. capacitive, electro-dynamic, or laser-optical sensors. They also have the advantage of being stable, highly reliable, and rugged and have an unlimited life.

4.2.2 Pre-Amplifiers

Since the AE signals are very weak, preamplifiers were connected right after the transducers to minimise the noise interference and prevent the signal loss. Sometimes the sensors and the preamplifiers are built as one unit, but for the particular experiments in this thesis, the preamplifiers are separate. The preamplifier provides a gain of 100 kHz (40 dB) and includes a band-pass filter of (150 kHz) to eliminate noise that prevails at low frequency. Then, the signals pass through a filter to eliminate the noise. The main amplifier amplifies the signals before being sent to the signal conditioner. The amplified AE signal is transmitted to the acoustic emission system via a signal cable. After that, the AE features are extracted and stored in the computer for further analysis.

4.2.3 Personal Computer and Software

The Vallen AE systems use computer that provides a menu-driven parameter input and system control. An online help system offers quick access to help texts explaining the use of the software. First the result of a data acquisition is simply a file containing the features of all the bursts of both the sensors along with the external parameters, such as force, load, and others. If the complete waveform is to be saved, an additional file is created. During the test the

measured data is online analysed and displayed, so the operator may immediately recognise the possible developments of defects within the test object. The operator than may halt the load increase in order to minimise possible danger to man, environment, and the tested object. The tasks of the PC are:

- Data acquisition and storage (all data are stored)
- Data analysis, online/offline
- Logical filtering (plausibility)
- Location calculation and clustering
- Statistics
- Display of the results (graphically and numerically)
- Self test of the system hardware
- Sensors coupling test, recording of the sensor frequency response

A summary of AMS4 System is given in section 4.10.

4.3 Acoustic Emission Parameter Set-up

AE bursts are not only produced by the defects that are looked for, but can also originate from small events such as peak values in the background noise, which sometimes exceed a low threshold. Hence it is essential to determine those characteristics that distinguish the wanted from the unwanted bursts. The peak amplitude is one of the most important and relevant burst features. Crack signals show medium to high amplitudes and have duration of some 10 micro-seconds, depending on the parameters of the test object.

4.3.1 Threshold Selection

Prior to the commencement of a test the threshold voltage is an important parameter that has to be set, so that the noise signals do not mask the AE signals. In the course of recording the data from the AE system other sources (e.g. electrical, mechanical etc) parasite the AE signals. It is possible to erase this noise by setting up a threshold level. There are two possibilities for the threshold level setting. The first is to use a fixed threshold (figure 4.7a) and the second to use an automatic threshold (figure 4.7b). The value of the automatic threshold changes with the changing noise pattern during the AE signal acquisition. An automatic threshold ensures that the threshold will rise and fall if the background noise varies.

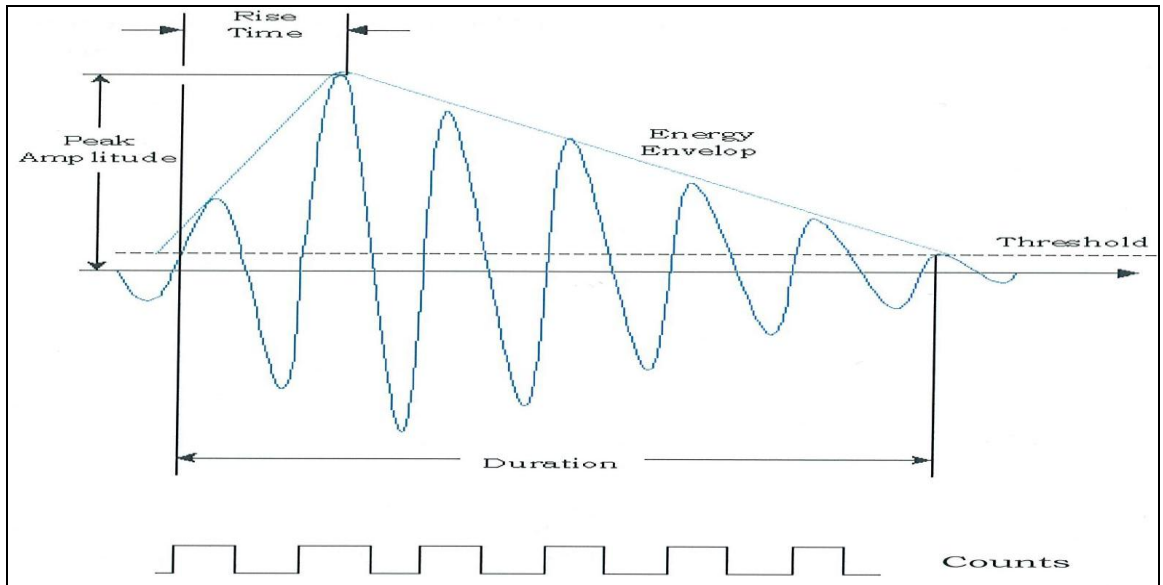


Figure 4.7a: The AE signal with the threshold setting

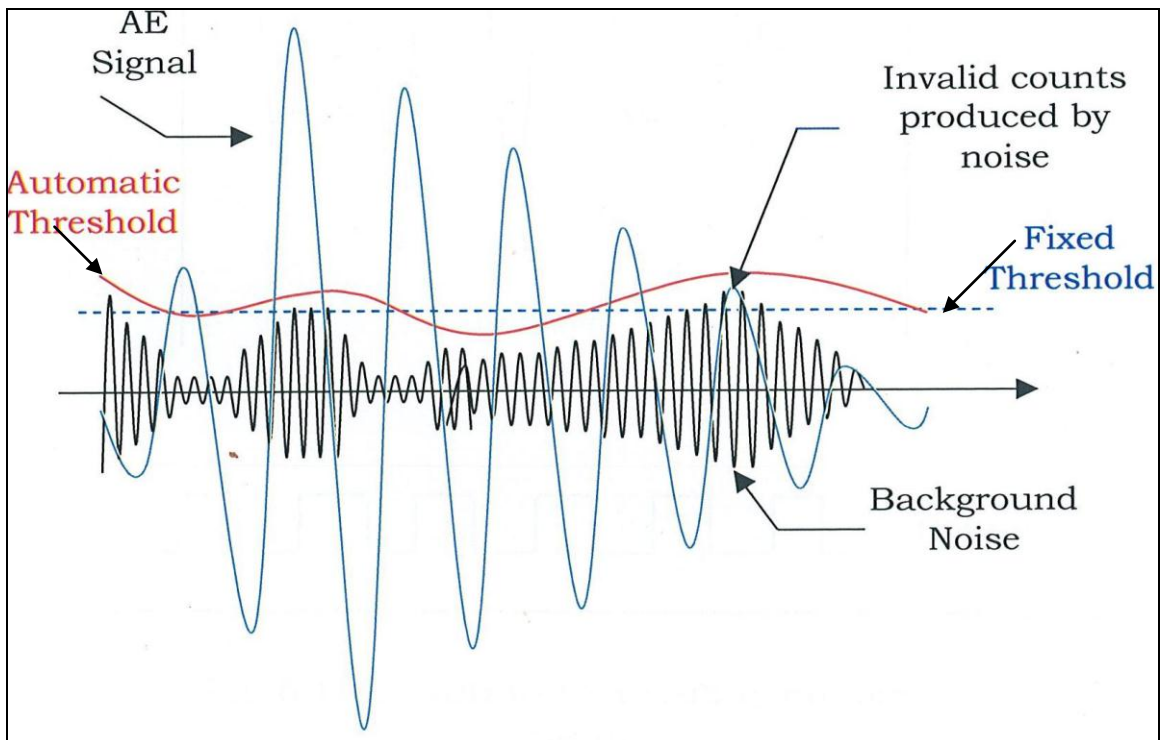


Figure 4.7b: The AE signal with the automatic threshold setting

With automatic selection the contamination of AE signals by noise was avoided completely. The purpose of the automatic threshold is to automate the process of setting the threshold on each channel to keep it acceptably above noise background variations, while still remaining as sensitive as possible to valid emission activity. This is accomplished mainly by electronic design of the threshold circuit. For the experiments reported in this thesis, the automatic selection process was used.

For the AMSY4 system the typical settings are:

Acquisition rate : 10 MHz

Threshold voltage : ± 0.05 mV

The gain : 40 dB

The system uses a continuous sampling rate of 10 MHz for feature extraction.

4.3.2 Test Method (Sensor Coupling Test (Auto-calibration))

Using this function (auto-calibration) the coupling of the sensors can be verified automatically. One channel transmits an electrical test pulse to the attached sensor. This sensor emits a mechanical wave, which is detected by the neighbouring sensors. The plausibility of the received amplitude allows the drawing of conclusions on the quality of the coupling. The automatic coupling test is carried out before and after the test in order to confirm a constant quality of the coupling during the whole test.

As part of the experimentation, it is very important to have a well defined measurement procedure and this must not vary between each test, so similar tests can be carried out under the same environmental condition and results compared directly. This eliminates the influence of external factors such as vibrations on the floor that may alter the results between samples. A typical result plot of an auto-calibration for a plain mortar sample is shown in figure 4.8.

Id	DSET	CHAN	A	R	D	CNTS	E	RMS	THR	PAO
			[dB]	[μ s]	[μ s]		[eu]	[μ W]	[dB]	[mV]
La Label 1: 13:14 Resume										
DT 25 February 2003, Host Time: 13:14										
Ht	6	2	44.5	15.2	45.4	7	610E-2	0.3	31.0	2.500
Ht	7	1	33.2	3.0	9.4	1	218E-2	0.3	31.0	2.500
Ht	10	2	32.9	13.6	17.6	3	300E-2	0.4	31.0	2.188
Ht	13	1	35.5	2.0	35.0	2	212E-2	1.0	31.0	1.875
La Label 2: 13:14 Start of Calibration										
Ht	17	2	38.9	5.4	40.4	4	268E-2	1.0	31.0	2.500
Ht	21	2	32.5	0.2	3.8	1	237E-2	5.6	31.0	2.813
Ht	24	1	71.2	19.0	111.2	15	517E-1	0.3	31.0	2.188
Ht	25	2	93.8	91.4	1809.6	238	830E01	4.5	31.0	2.188
Ht	28	1	71.2	19.0	111.2	15	517E-1	0.2	31.0	2.813
Ht	29	2	93.8	91.4	1809.6	237	831E01	2.7	31.0	2.813
Ht	31	2	41.9	56.2	259.8	32	108E-1	2.5	31.0	2.188
Ht	34	1	71.2	18.8	111.4	15	518E-1	0.1	31.0	2.500
Ht	35	2	93.8	91.4	1868.0	238	832E01	1.9	31.0	2.500
Ht	38	2	33.6	0.2	16.8	2	220E-2	1.7	31.0	2.188
Ht	41	1	71.2	19.0	111.2	15	518E-1	0.1	31.0	2.813
Ht	42	2	93.8	91.4	1809.6	237	832E01	1.5	31.0	2.813
Ht	46	2	71.2	18.8	96.2	13	508E-1	0.7	31.0	3.125
Ht	47	1	93.8	91.6	1829.6	241	866E01	8.6	31.0	3.125
Ht	50	1	32.1	2.0	2.6	1	108E-2	7.3	31.0	2.500
Ht	53	1	32.9	2.8	3.6	1	150E-2	5.6	31.0	2.813
Ht	56	2	71.2	18.8	96.2	13	508E-1	0.3	31.0	2.500
Ht	57	1	93.8	91.6	1809.6	241	866E01	4.8	31.0	2.500
Ht	60	1	34.0	17.8	32.0	5	219E-2	3.9	31.0	3.125
Ht	63	1	35.9	3.8	21.6	4	175E-2	3.4	31.0	3.125
Ht	66	2	71.2	18.8	96.0	13	508E-1	0.2	31.0	2.188
Ht	67	1	93.8	91.6	1806.4	239	866E01	3.0	31.0	2.188
Ht	70	2	71.2	18.8	96.2	13	509E-1	0.1	31.0	2.500
Ht	71	1	93.8	91.6	1829.6	241	866E01	2.2	31.0	2.500
La Label 3: 13:14 End of Calibration										

Ht: hit; *DSET*: dataset; *Id*: **D** (duration(μ s)), **A** (maximum amplitude (dB)), **E** (energy (eu)), **R** (rise-time (μ s)), **CNTS** (number of threshold crossings), **DSET**: Dataset, **CHAN**: Channel, **RMS**: Root Mean Square of the Continuous Background Noise (before burst); **THR**: Threshold (dB); **PAO**: Parametric input (mV)

Figure 4.8: A plot of calibration for a plain mortar sample

4.4 Equipment Used

The following items were utilised for the manufacture of concrete samples:

- Moulds, three sets, measuring 140x70x70, 210x70x70 and 70x70x70, all units in mm.
- Electronic Scales, to weigh ingredients, Large basin used as mixing bowl.
- Pestle and Mortar to grind the glass; 4 mm, 2mm and 1mm sieves.
- A builders trowel to mix ingredients; Egg brush to apply oil to the moulds.
- Protective Clothing, glasses and gloves; Tupperware Boxes for glass storage.
- A pair of scissors to cut the rubber into pieces.
- A spatula to stir the mixture.
- A metal blade of 2mm width to make the artificial crack (detonator of crack).

4.5 Sample Moulds

The moulds in which the samples of concrete were prepared are made of wood, as shown in figure 4.9 (a).



Figure 4.9 (a): A wooden mould sample

Two different sizes of moulds were used, one 21 cm length and the other with a length of 14 cm. Samples for compressive tests were prepared from mild steel moulds measuring 70mm x 70mm x 70mm. A typical un-notched sample specimen with its dimensions is shown in figure 4.9b.

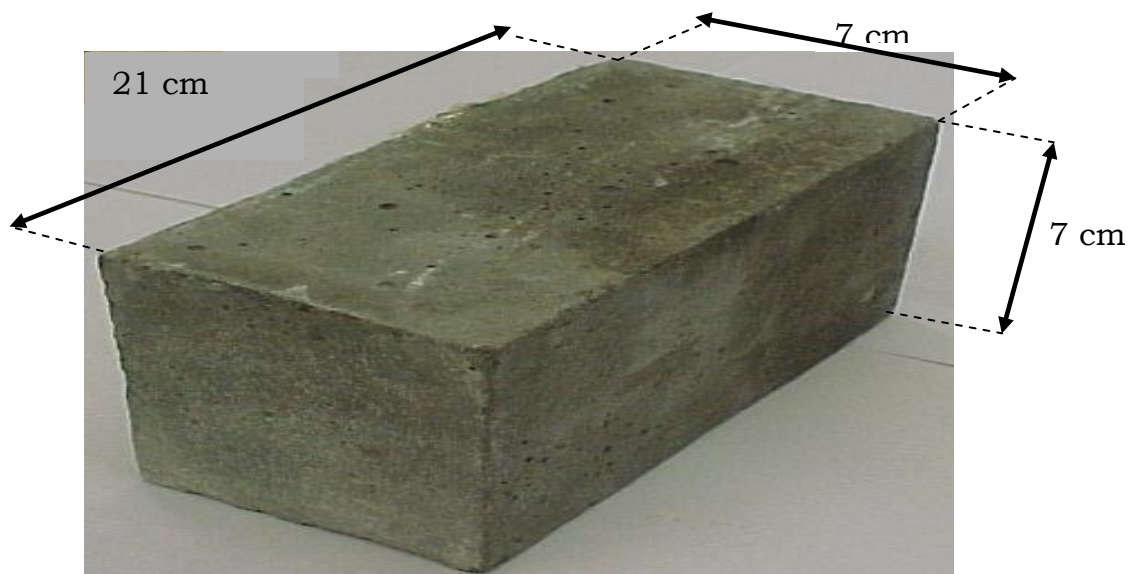


Figure 4.9 (b): An un-notched sample specimen

4.5.1 Sample Preparation

The mass of Cement-Sand-Water proportion (3:3:1) for the sample preparation for plain mortars of different dimensions are given in Table 4.2

Table 4.2: Cement-Sand-Water preparation for sample report

Mould Size (mm x mm x mm)	Cement (g)	Sand (g)	Water (g)
210 x 70 x 70	900	900	300
140 x 70 x 70	600	600	200
70 x 70 x 70	300	300	100

The aggregates and the additives were added with subsequent deduction of sand. A complete list of the samples produced, denoting the type and quantities of the additives and aggregates introduced into the concrete mix are given in appendix A.

4.6 Couplant in US and AE measurement

The coupling agent is imperative to the quality of sensor coupling. It provides a good acoustic contact between the sensor and the surface of the test object. The contact surfaces of the samples are prepared for the load test (compressive) and for mounting of the AE transducers on the samples. The contact surfaces were polished by using sand papers (coarse grit size 200 followed by fine grit size 100). This is to ensure good contact between the transducers and the samples in order that both the acoustic emission and ultrasonic waves are transmitted effectively. Appropriate couplants were selected for US and AE tests, i.e. industrial silica gel was used for US experiments, and silicone grease was used for AE tests.

4.7 Manufacturing of Specimens

Moulds were constructed using wood and treated with yacht varnish to avoid the water absorption by the wood from the cement mix. To obtain accurate results from the three point bend (flexural) tests it is important that the specimens are of the same dimensions, in particular the cross-sectional area. The moulds allow the manufacture of blocks that are 21×7×7 (cm) in the first set and 14×7×7 (cm) in the second set. The moulds allow the manufacture of five blocks at a time so that the specimens could be made in unison, thus ensuring as much similar conditions for the manufacturing of blocks. Several trials were carried out to ensure the manufacturing procedure were reliable. The sizes, surface conditions, and also vibration (manual) procedures were established to avoid porosity and damping conditions. This procedure eliminates the variations in size as much as possible.

The sand and cement were sieved in order to remove any small lumps, allowing a fine dust of cement and sand to be mixed in a bowl. The water was then added and the mixture was mixed thoroughly with the aid of a blender. The mixing process was carried out until there was no excess water in the bowl and an even consistency was achieved. A small amount of oil was applied to the moulds with an egg brush to avoid the blocks from sticking to the surfaces in the moulds. The mixture was then added to the mould, wiping away any excess. In the cases where an aggregate was used it was added at this point so that all the aggregates was used in the sample (the listing of which are given in appendix A). In this research, concrete mortars were manufactured with the following additives and put under destructive/US compression test:

- Plain Mortar
- Mortars with Sodium Sulphate/Calcium Chloride/Potassium Chloride/Sodium Chloride/Sodium Silicate/Sodium Silicate/Glass Powder

The following samples were manufactured with the following additives/aggregates:

- Mortars with Glass/Rubber Aggregates
- Mortars with Sodium Sulphate/Calcium Chloride/Sodium Silicate

and the AE behaviours were monitored during the mechanical compression test.

The following samples were manufactured, put under 3-point flexural test:

- Mortars with Sodium Sulphate/glass slide
- Mortars with calcium carbonate/glass slide
- Expansive Cement Mortar/glass beads/pebbles
- Mortars with Glass Aggregates/Glass Slide
- Mortars with Rubber Aggregates

and the acoustic emission behaviour was monitored during the test

At this stage the specimens were vibrated vigorously and knocked to allow any air bubbles that were present in the sample to be removed as the contents settled. The concrete was then allowed to set in the mould and rest for two days after which it was removed and submerged in water. The reason for placing the sample in water was to ensure that the sample was allowed to cure at a constant temperature and that the block is exposed to as much water as it is needed for the hydration process to take place. The container they were kept in allowed the blocking out of light so that no part of the sample was subjected to the effect of light. At this stage the blocks were allowed to cure for twenty-eight days in water to achieve the appropriate level of hardness.

4.8 Preparation of Waste Aggregate: Glass

The glass aggregate, shown in figure 4.10, was collected from broken car windows. These were crushed in a pestle and mortar by hand. Protective clothing was worn when handling the glass.

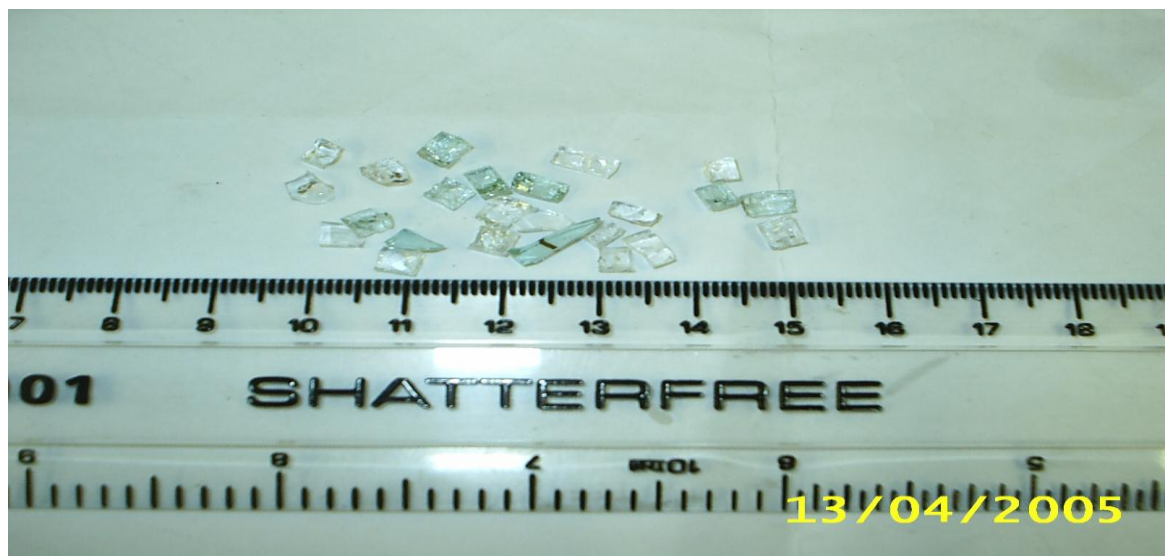


Figure 4.10: Broken glass from car windows

The glass was then sieved with various sizes of sieve mesh as illustrated in figure 4.11 (a). The largest mesh was 4mm and the next was 2mm and finally there was 1mm. One of the sieves is shown in 4.11 (b).

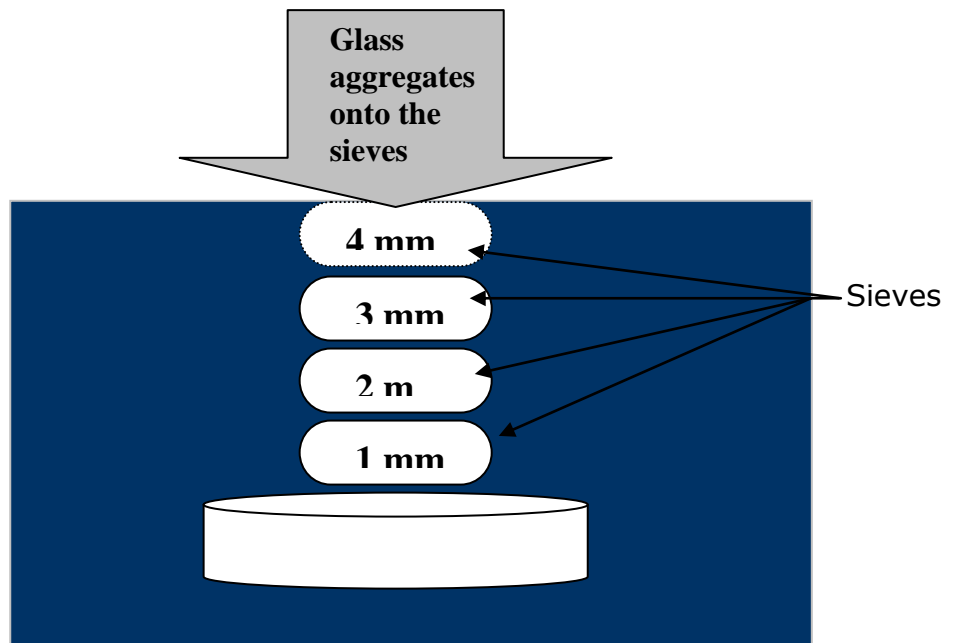


Figure 4.11 (a): Sieve set-up



Figure 4.11 (b): A Sieve sample

Glass enters the upper sieve and then shaking takes place allowing the smaller pieces to reach the bowl at the bottom. In this work therefore the glass, which was labelled 4-2 mm was small enough to pass the first sieve but too large to pass the second sieve. In exactly the same way the glass, which is referred to as 2-1 mm is caught between the two lower sieves. In the final bowl powder

collects 0-1 mm and this was also used. The mass of the glass was simply weighed on the scales before being added to the mould.

4.8.1 Rubber

Rubber was taken from an old tyre (Michelin MXT 165/70/R13). Firstly, large pieces of rubber were cut from the tyre with a knife. Then, little pieces of rubber were cut with scissors. These pieces have roughly a cubic shape, and were approximately 4 mm in size.

4.9 Flexural 3-point bend tests set-up: Instron flexural testing machine

The flexural tests were carried out on Denison Testing Machine, with a maximum load setting at 600 kN, to cause fracturing of the sample. The sample mounting and experimental set up is shown in figures 4.12 (a) for a notched specimen.

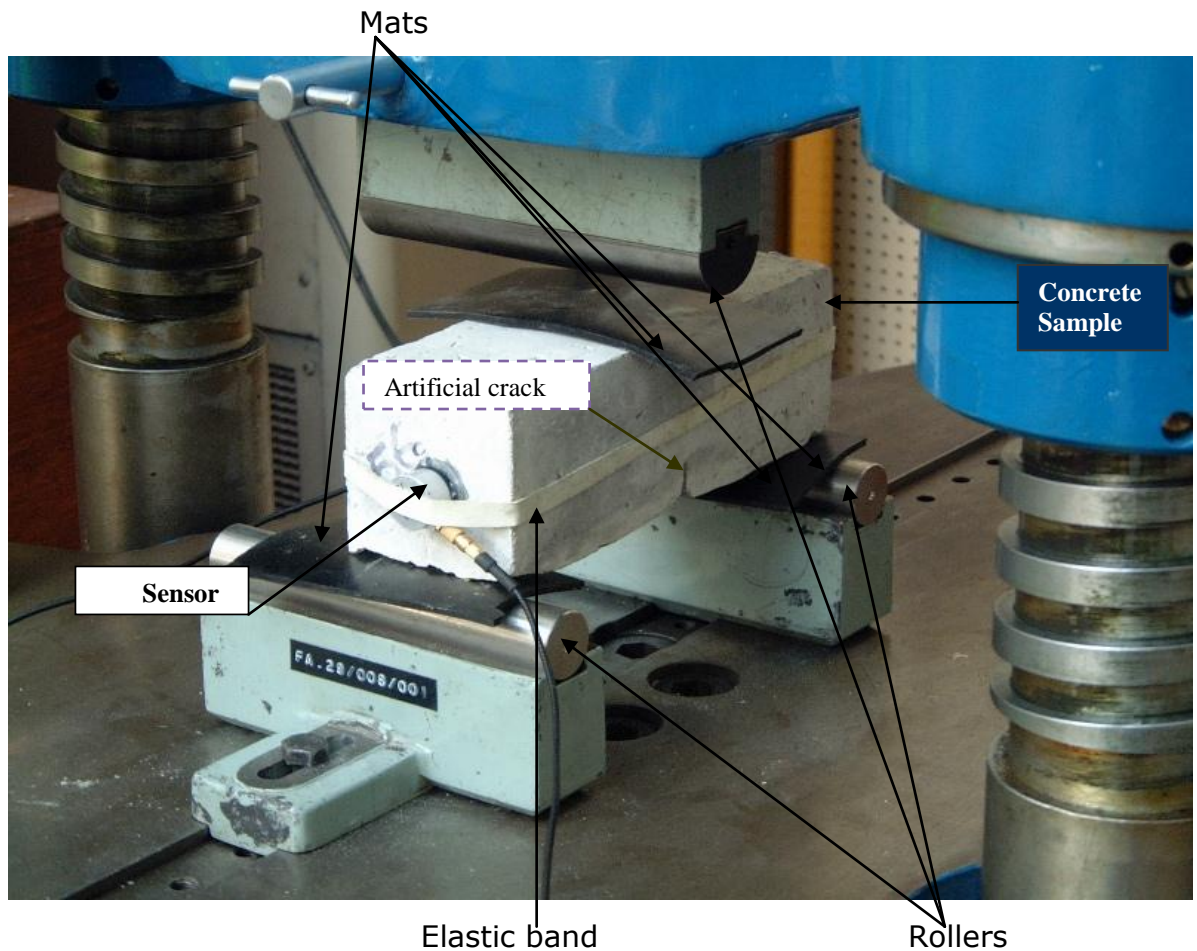


Figure 4.12 (a): Sample mounting on a Flexural Machine

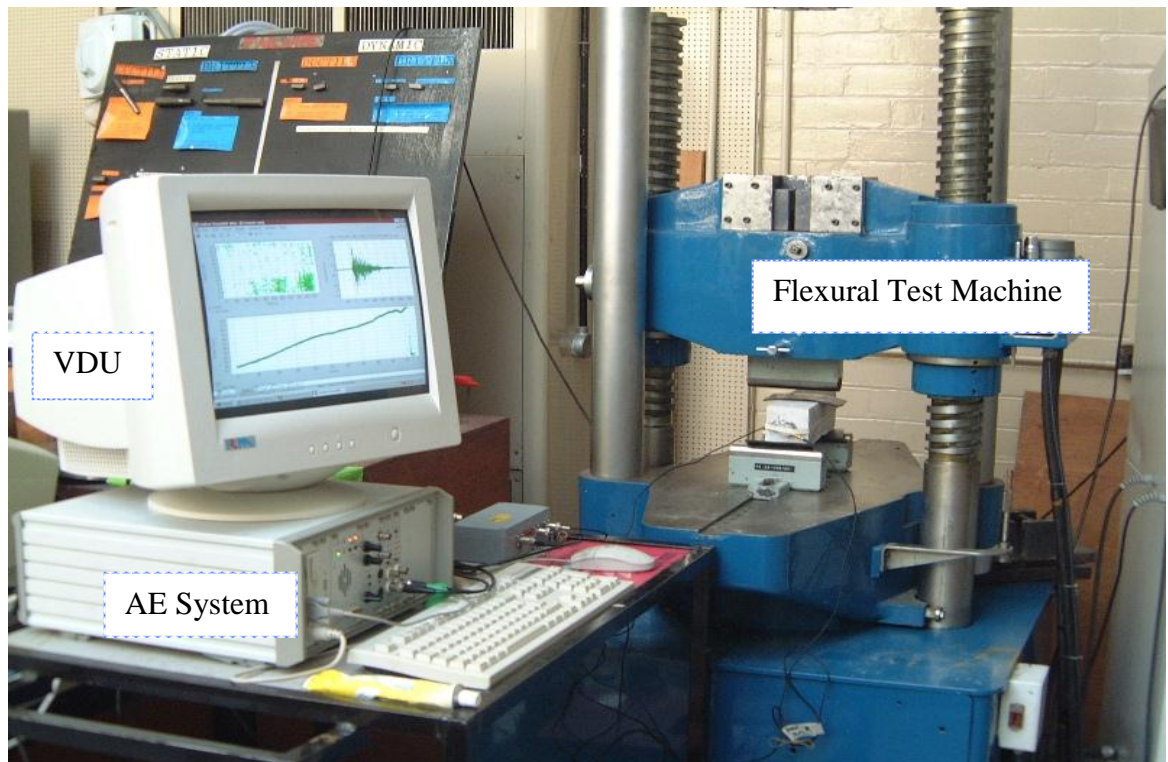


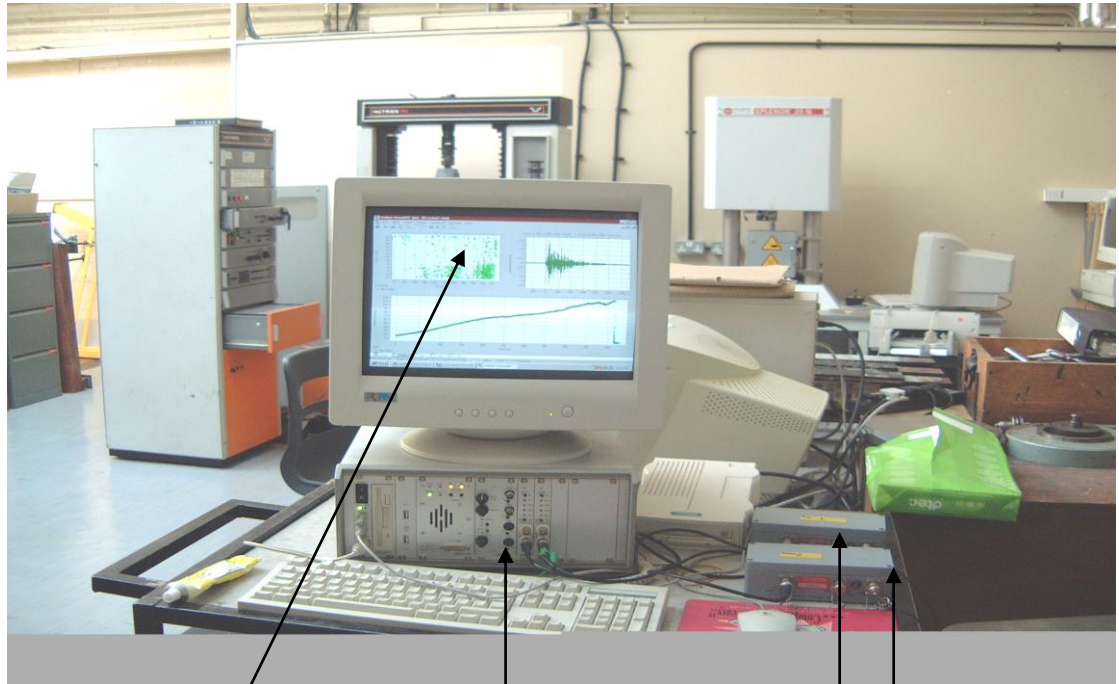
Figure 4.12 (b): Experimental set-up of 3-point flexural bend test

The sample was loaded at a rate of 0.25 mm/min. This was kept as the standard rate for all the samples. The experimental set-up of 3-point flexural bend test is shown in figure 4.12 (b).

4.10 Acoustic Emission Set-up

In order to record the acoustic emission the blocks must be prepared by cleaning the surface at either end. For clear signal transfer from the blocks to the transducer of the acoustic emission set up, a couplant was applied to the block in a generous manner. The transducers were then applied and rubbed into the block to ensure a close contact. They were finally secured in place with elastic bands, which secured the transducers, ready for the three point bend test. At this point it is important to calibrate the transducers. This is done by auto-calibration techniques (described above) in which one transducer in turn is excited by a pulse and emits a wave signal, which is detected by the other transducer at the other end of the sample.

This process ensures that the system is set up, coupling of transducers are adequate to detect the acoustic emission signals with same sensitivity. This also facilitates source location. Figure 4.13 shows the Vallen System.



Display of AE Signals AE Vallen hardware unit Pre-amplifiers

Figure 4.13: A.E. Vallen set up

The two preamplifiers used in order to amplify the small acoustic emission signal from the test piece, are shown in figure 4.13.

The Vallen acoustic emission system uses continuous sampling rate of 10 MHz. The system has special integrated circuits (ic's) (Fields programmable gate arrays) with thousand of processing elements that can be linked by software. The system also has data buffer which prevents data loss in case the CPU is engaged with other tasks and temporarily is not ready to accept other data. The system is capable of up-to 144 channels working in parallel. The research work described in this report uses 2 channel system with transient recorders. The transient recorder allows recording of complete waveform which extremely useful for frequency domain analysis of the acoustic emission signals.

The acoustic emission Vallen AMSY4 system allows the software to be used and tailored to analyse the acoustic emission data in a manner, which allows the interpretation of the results relating to specific events, time, exact location in the specimens where the events took place and the size of each event that occurred during the duration of the tests. For the purpose of this project a calibration step had to be carried out on every sample individually. The procedure for calibration involved opening the Vallen control panel and

selecting the auto-calibration mode. Once opened the parameters for the test were set up, these included the threshold (31-35 dB selected for this research), the gain (set at 40 dB) and the distance between transducers.

Once the recording facility was set in place, the following multi-plots parameters were selected:

- i) Amplitude (dB) vs. Time (s) vs. Load Parametric (mv)
- ii) X-Location (cm) vs. Time (s) vs. Load Parametric (mv)
- iii) Hits vs. Load Parametric (mv)
- iv) X-Location (cm) vs. Amplitude (dB) vs. Energy (energy unit-eu)
- v) Duration (μ s) vs. Time (s) vs. Load Parametric (mv)
- vi) Cascaded Energy vs. Time (s)

An example of the multi-plot is shown in figure 4.14.

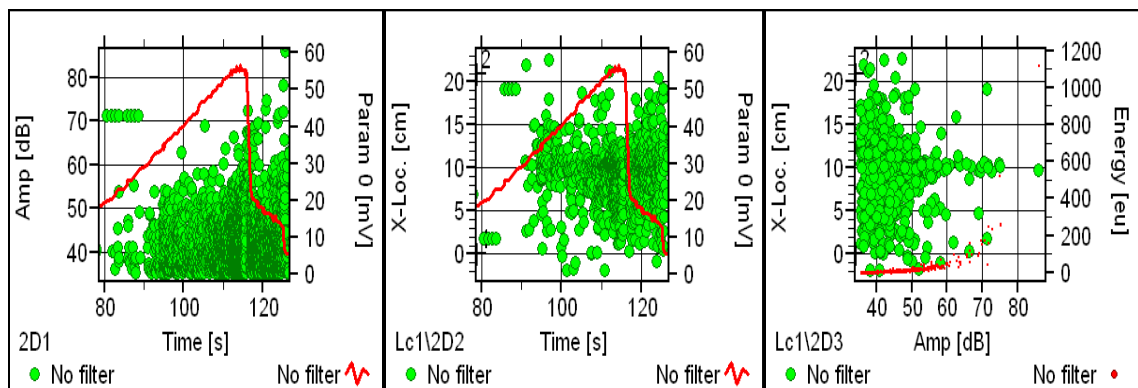


Figure 4.14: An example of a typical AE Multi-plots

The 3 dimensional multi-plots created allowed location to be drawn on the X-axis, against the number of hits on the Y-axis and finally the time on the Z-axis. An example of this is shown in figure 4.15. This gave an insight into the acoustic events emitted from a 3-dimensional point of view.

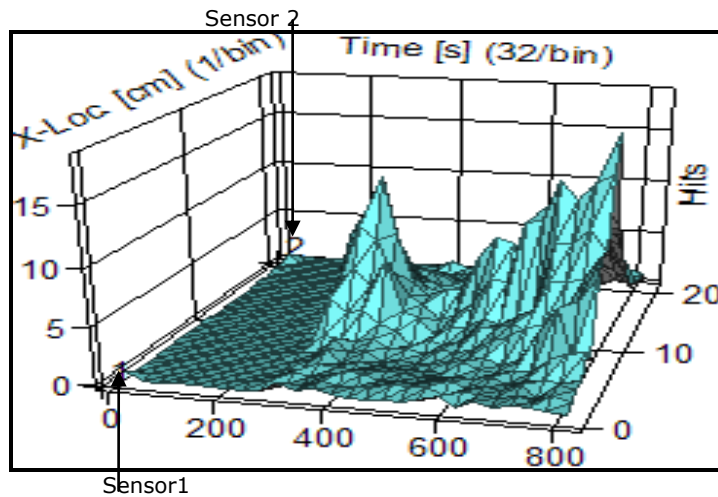


Figure 4.15: A 3-dimensional plot for sample BG1, a plain mortar

A listing and a waveform is also created by the software which showed the numerical values of each parameter as shown in figure 4.16.

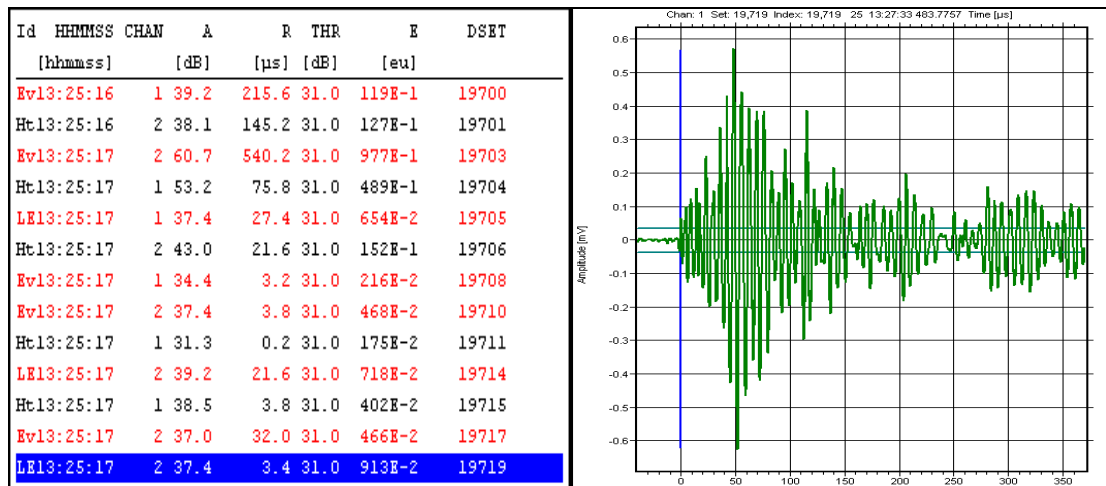


Figure 4.16: AE listing and Waveform for sample BG1, plain mortar

CHAPTER 5

5.0 RESULTS AND DISCUSSION

Results of this work based on Ultrasound, Microscopic and Acoustic Emission techniques are given in two sections.

(A) Ultrasonic and Microscopic Techniques

The results presented and discussed in this section are based on the following:

- Verification of ultrasonic compressive strength with the mechanical crush test results to develop a model for monitoring strength during curing;
- The effect of sample size on compressive strength;
- The effect of various additives on curing time and strength using Ultrasound;
- Evaluating compressive strength of concrete containing waste materials using ultrasound;
- Calculation of the modulus of elasticity of concrete containing waste materials;
- Examining the microstructure of concrete using microscopy;

(B) Acoustic Emission Techniques

The results presented and discussed in this section are based on the following:

- Toughness monitoring of concrete containing various additives;
- AE behaviour of concrete containing waste materials under compressive load;
- Interfacial bonding between glass aggregates and cement;
- Detecting crack growth mechanism using AE in concrete under flexural load;
- Monitoring toughening behaviour of concrete due to different mechanism under flexural load;
- Effect of crack bridging and expansive matrix on AE signal parameters;
- AE monitoring of cracks in concrete containing rubber aggregates;
- Comparison of AE signals parameters emitted from mortars containing admixtures and waste aggregates of mixed sizes;
- Verification of the contribution of admixtures towards toughening of concrete with the aid of AE;
- Comparative study of AE characteristics between compression and flexural condition.

5.1 The Development of Ultrasonic Model to Monitor the Compressive Strength in Mortar with additives and Concrete over 28 days Curing Period

The compressive strength of various samples was estimated using measured wave velocity (ultrasound) with rebound value. This estimated value is accurate to ± 1.5 MPa. The compressive strength of various samples was also measured using a mechanical crush test as described in chapter 4. The variance in the measured compressive strength was typically ± 3.5 MPa. The results of these two methods of ultrasound and mechanical crush test to determine the compressive strength of 5 replicate samples with each type of additive are presented in figure 5.1.

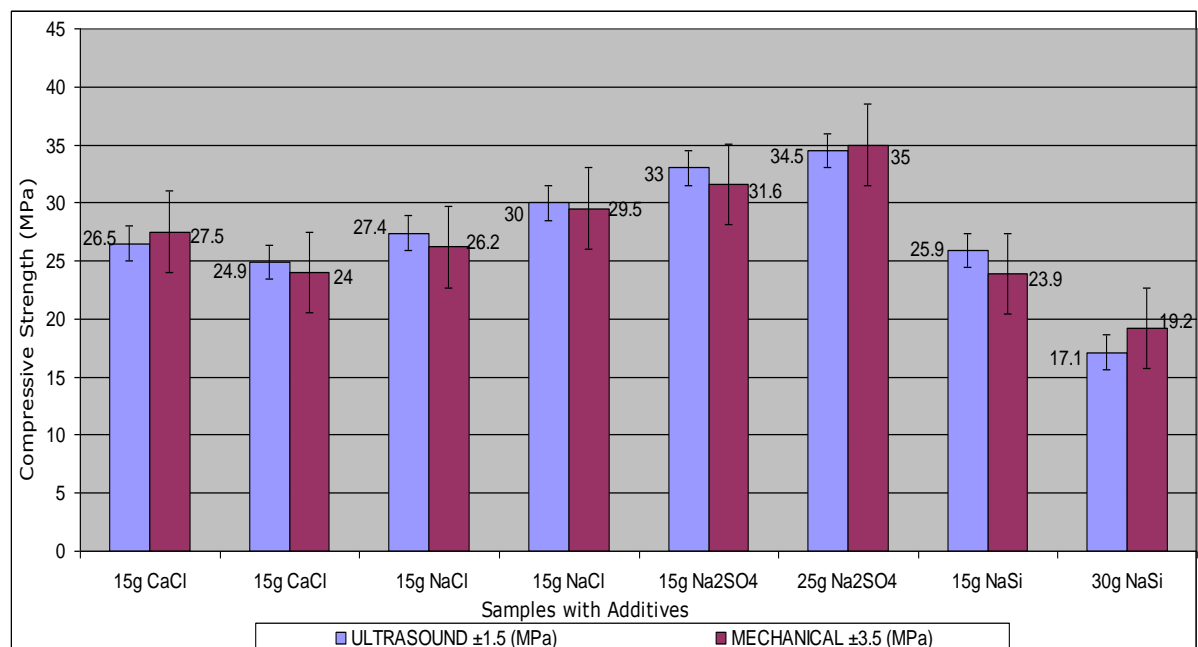


Figure 5.1: A comparison of compressive strength of mortars with various additives (CaCl: Calcium Chloride, NaCl: Sodium Chloride, Na₂SO₄: Sodium Sulphate, NaSi: Sodium Silicate) on strength of mortar obtained using mechanical and ultrasound tests.

It is obvious that the average compressive strength depends on the type and quantity of the additive. In some cases the average value is higher than the mechanical test results. The percentage difference in the results for both techniques of compressive strength measurements (Ultrasound and Mechanical) are shown in figure 5.2. It can be seen that six additive samples resulted in a percentage difference within 5%. Only one sample had a percentage difference of -11%. The average percentage difference for the tests carried out on all the

samples is 3.15%. The percentage difference in other studies reported elsewhere [130a] is within 20% between NDT and Destructive tests.

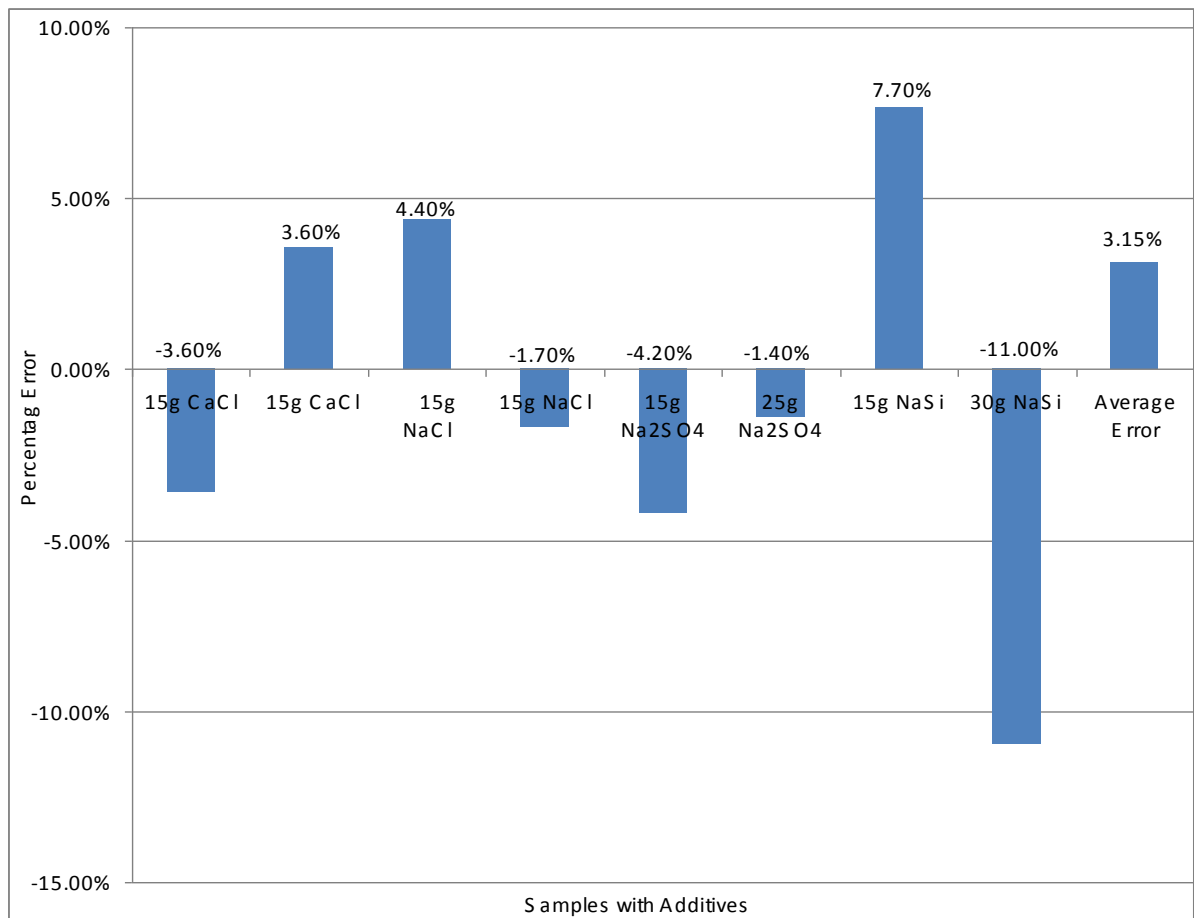


Figure 5.2: Percentage difference in compressive strength measurements of using two (US and crush test) techniques.

Hence it is apparent from figure 5.2 that a close correlation exist between the results obtained using the destructive and non-destructive testing methods. This therefore demonstrates that the ultrasonic technique is an accurate and reliable method of determining the compressive strength of concrete.

5.2 The Size Effect of Sample Geometry

The compressive strength analysis of concrete in this research has been based on small 70 mm³ samples. The construction industry uses blocks of dimensions such as 100×200×400 mm. In order to demonstrate the relationship between the development of the properties of concrete and geometrical size, samples of different dimensions were examined, therefore a series of three moulds, homologous in design, were manufactured to evaluate the effect of size and curing on the measured compressive strength. For the purpose of consistency, a single batch of concrete mixture was produced and distributed among the three moulds of dimensions: (i) 70×70×70 mm³, (ii) 140×70×70 mm³ and (iii) 210×70×70 mm³. These samples were then monitored using the ultrasound NDT method (described in chapter 4). The results of compressive strength during the setting and hardening time (curing) are given in table 5.1 (a-c). It is apparent from the tables that the compressive strength depends on the curing time but does not depend on the size of block. The ultrasound velocity is dependant on the type and kind of material and gives an average strength of the block. Since all the blocks are manufactured using the same components in exactly similar condition, hence the measured values of average strength (velocity) on various stages of curing is approximately similar. It is not possible to carry out a crush test on sample which is undergoing hardening. Therefore no comparison can be carried out between the two methods.

Thus the ultrasound technique is potentially superior to the mechanical crush test. It is faster, cheaper, more accurate and flexible on various sizes and shapes of samples and curing conditions.

Table 5.1 i) Small sample size 70×70×70 mm³ ±1 mm³

(a): Ultrasound parameters results for small sized samples

Days	Time (Micro Seconds) ±1	Velocity (m/s) ±100	Rebound Value ±1	Compressive Strength (MPa) ±1.5
1	19.5	3590	N/A	N/A
2	18.7	3740	24	8.5
4	17.9	3910	30	17.3
7	17.6	3980	33	21.4
21	17.2	4070	34	23.4

Table 5.1 ii) Medium sample size 140×70×70 mm³ ±1 mm³

(b): Ultrasound parameters results for medium sized samples

Days	Time (Micro Seconds) ±1	Velocity (m/s) ±100	Rebound Value ±1	Compressive Strength(MPa) ±1.5
1	39.5	3540	N/A	N/A
2	36.7	3810	24	8.2
4	35.5	3940	30	17.9
7	35.2	3980	33	21.4
21	34.3	4070	34	23.4

Table 5.1 iii) Large sample size 210×70×70 mm³ ±1 mm³

(c): Ultrasound parameters results for large sized samples

Days	Time (Micro Seconds) ±1	Velocity (m/s) ±1	Rebound Value ±1	Compressive Strength (MPa) ±1.5
1	59.7	3520	N/A	N/A
2	56.4	3720	24	7.9
4	53.2	3950	31	18.9
7	52	4040	33	22.1
21	51.6	4070	34	23.4

These readings in table 5.1 (a-c) demonstrate the consistency of results recorded throughout the period of analysis for different sizes of samples. A summary of the compressive strength in table 5.1 (a-c) is shown in figure 5.2a.

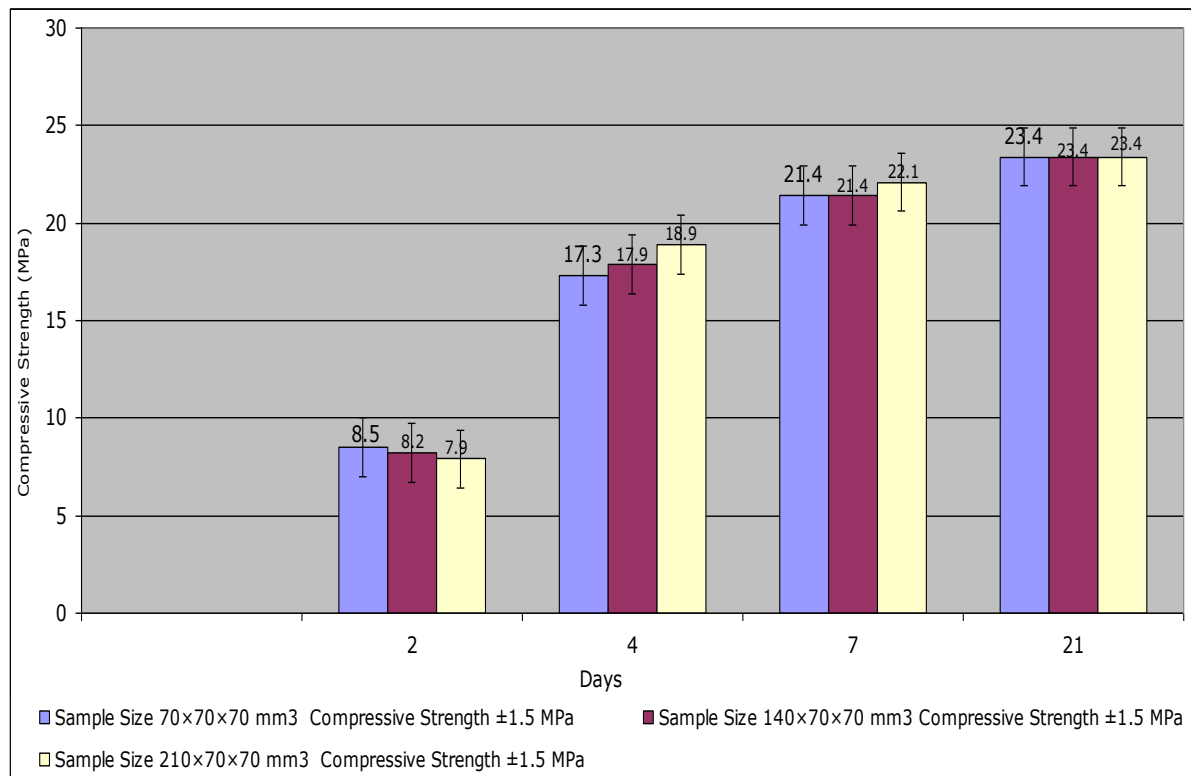


Figure 5.2a: Summary of the compressive strength over 21 day for different sizes of samples

The development of compressive strength of the homologous samples for each day, in all cases was found to be similar throughout the period of analysis. This therefore proves that the geometry of concrete has no significant bearing on the curing process.

The block of concrete with no additive is used as a standard measurement model from which the analysis of the effect of the introduction of additives in the concrete mixture is built around. Other plain blocks of concrete mortars (samples 2-5) with no additive were also manufactured and the measurements were recorded. All of them exhibit almost equal results with identical increase in compressive strength (see appendix A).

From figure 5.3 (Sample 1), it is apparent that the rate of increase of the compressive strength has two trends. The initial slope shows a high rate of hardening over the first few days, followed by the relatively slow growth in strength which is not linear over the remaining period of measurement.

The suitability of ultrasound technique is obvious from the apparent shape of the graph which indicates various hydrating chemical and physical reaction occurring during the curing time. After few days of manufacturing, the block apparently has settled on the surface crest but inside the core of the block is constrained affecting the chemical reaction and physical changing possibly development of residual stress, porosity etc. The non-linear region of the graph is a valid expectation of events occurring in the sample.

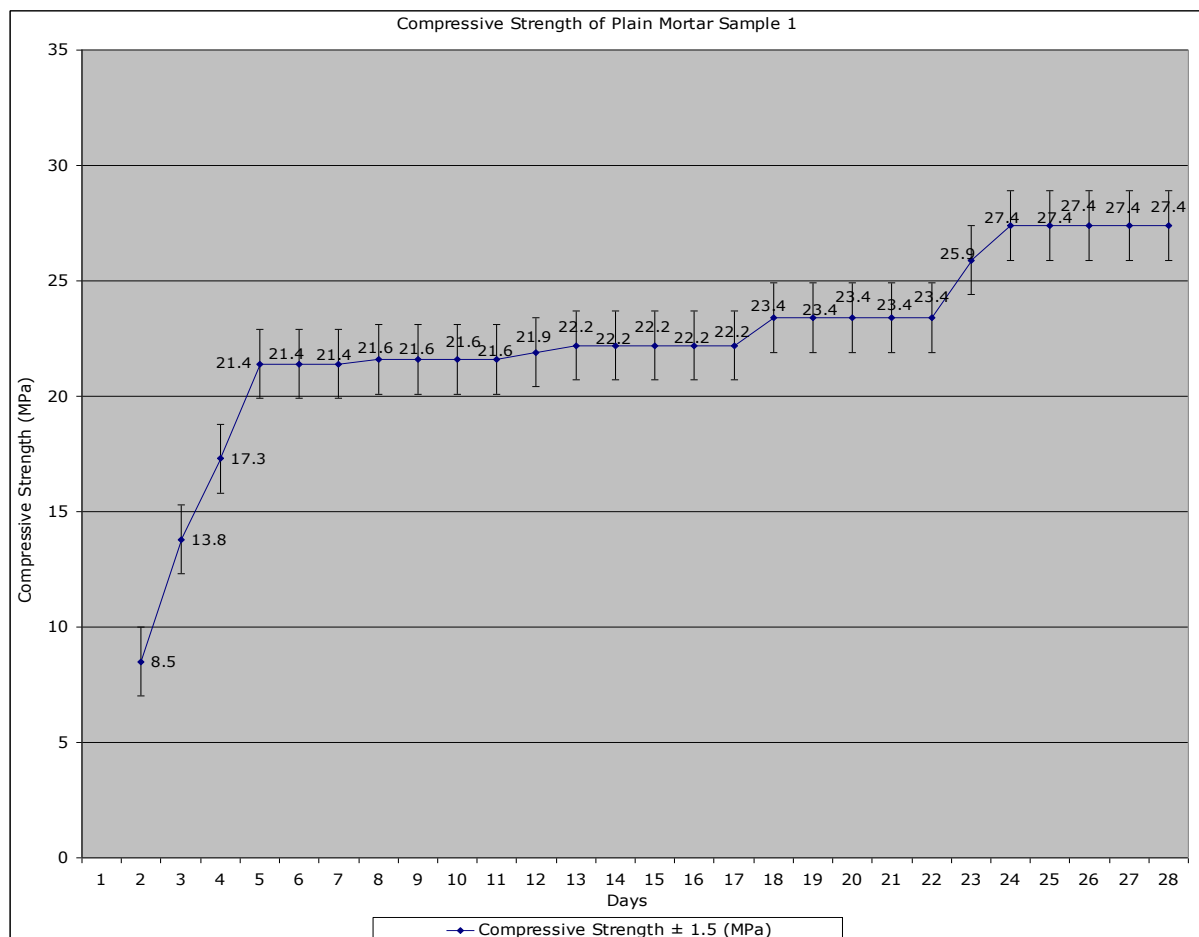


Figure 5.3 Sample 1: The change in compressive strength (measured using ultrasound) of a standard mortar (without additives) with respect to time.

One of the findings in this work is that after 23 days the compressive strength started to increase from 23.4 MPa to the final setting strength of 27.4 MPa as shown in figure 5.3. This is probably due to a chemical reaction that may have occurred towards the end of the curing period.

5.3 Effect of Various Additives in Mortar on 28 Day Initial Hydration Time and Strength

The introduction of additives changes both slopes of the rate of initial hydration and the curing rate. These changes are dependent on the type of aggregates and the additives. The analysis of the effect of additives can be calculated using the following formula:

$$R = \frac{d\sigma}{dt} \dots\dots\dots (5.1)$$

Where R is the average rate of curing (MPa/hr), $d\sigma$ is the compressive strength attained after the initial curing period (MPa) and dt is the time of the initial curing period (hr). Table 5.2 shows the calculated initial curing rates for the samples using various additives.

Table 5.2: Values of the hydration period, compressive strength and curing rate for various additives

Additive	Initial Hydration Period (days×24)	Compressive strength after initial hydration (MPa)	Curing Rate (MPa/hr)
Zero additive	5 × 24 = 120 hrs	21.4 ±1.5	0.18 ±0.0017
15g Potassium chloride	3 ×24 = 72 hrs	17.3 ±1.5	0.24 ±0.0025
25g Potassium chloride	4 × 24 = 96 hrs	17.7 ±1.5	0.18 ±0.0043
15g Sodium silicate	8 × 24 = 192 hrs	17.3 ±1.5	0.09 ±0.0015
30g Sodium silicate	7 × 24 = 178 hrs	7.9 ±1.5	0.04 ±0.0043
10g Sodium sulphate	4 × 24 = 96 hrs	25.9 ±1.5	0.27 ±0.005
15g Sodium sulphate	4 × 24 = 96 hrs	25.7 ±1.5	0.27 ±0.0024
25g Sodium sulphate	4 × 24 = 96 hrs	23.4 ±1.5	0.24 ±0.0036
5g Calcium chloride	5 × 24 = 120 hrs	22.6 ±1.5	0.19 ±0.0017
15g Calcium chloride	5 × 24 = 120 hrs	17.1 ±1.5	0.14 ±0.0025
25g Sodium chloride	5 × 24 = 120 hrs	17.0 ±1.5	0.14 ±0.0015
15g Sodium chloride	5 × 24 = 120 hrs	21.4 ±1.5	0.18 ±0.0017
10g Powdered glass	5 × 24 = 120 hrs	21.7 ±1.5	0.18 ±0.005
30g Powdered glass	5 × 24 = 120 hrs	21.9 ±1.5	0.18 ±0.0025
50g Powdered glass	5 × 24 = 120 hrs	21.9 ±1.5	0.18 ±0.0025

The introduction of additives into these mortars demonstrate that the correct quantity may stimulate an increase in both the rate of initial hardening and the magnitude of the compressive strength attained over the curing period. These additives have actively altered and enhanced the chemical process of curing from the start of hydration until the final setting period and probably beyond. The results of the monitoring changes in compressive strength of mortars due to the introduction of different chemical additives are as follows:

I. Mortar with Calcium Chloride

The effect of the addition of calcium chloride in different concentrations as compared to a standard model is shown in figure 5.4. A 5g addition of calcium chloride generates a positive effect on the rate of hardening and the final compressive strength attained. Increasing the concentration of calcium chloride in the mixture to 15g is however shown to reduce the initial rate of hardening and have little effect on the final compressive strength attained.

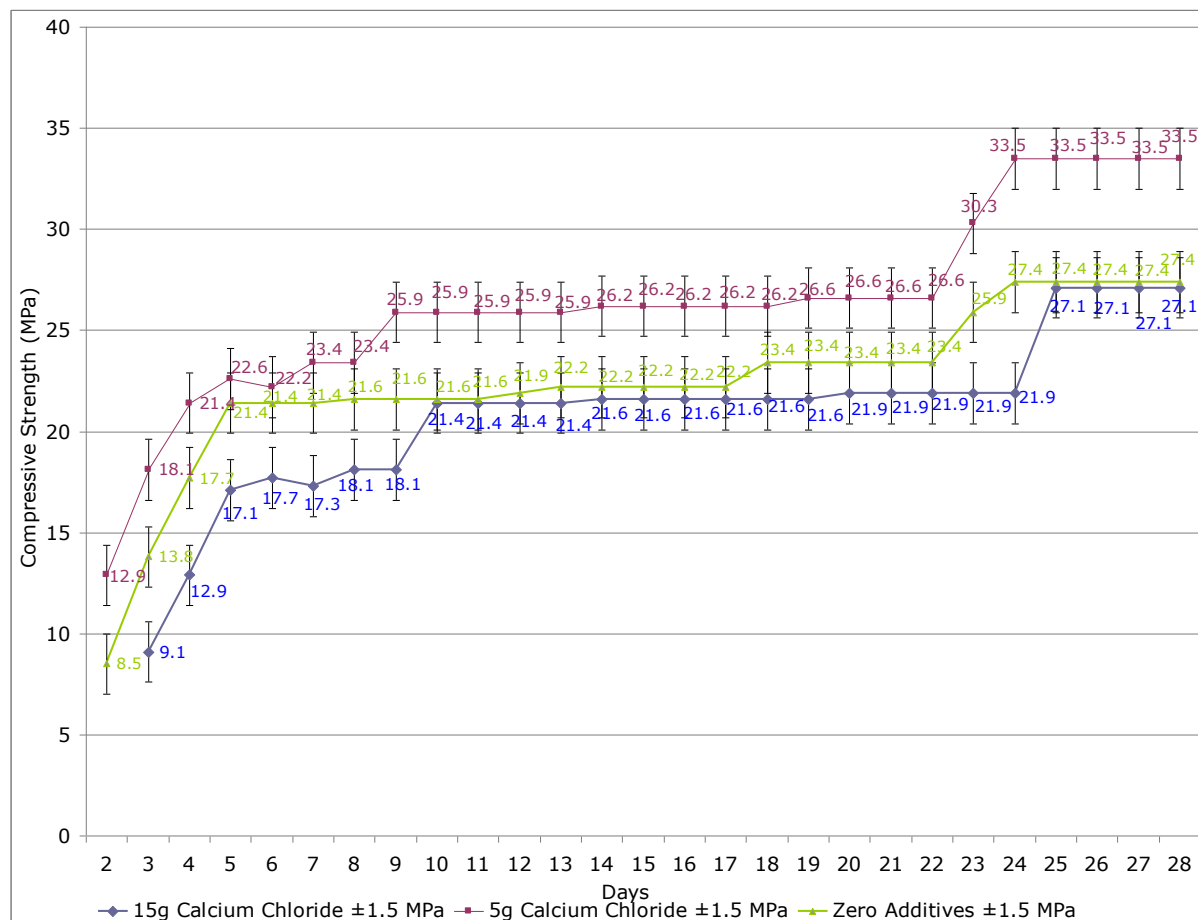


Figure 5.4: Typical changes in compressive strength of a mortar sample with addition of calcium chloride with respect to time.

The variation in the proportion of calcium chloride introduced into the mixture is showing a dramatically different effect on the compressive strength attained by the end of the 28 day as shown in figure 5.5. These results demonstrate that the addition of calcium chloride in the mortar will stimulate an increase in both the rate of initial hardening and the magnitude of the compressive strength attained over the curing period.

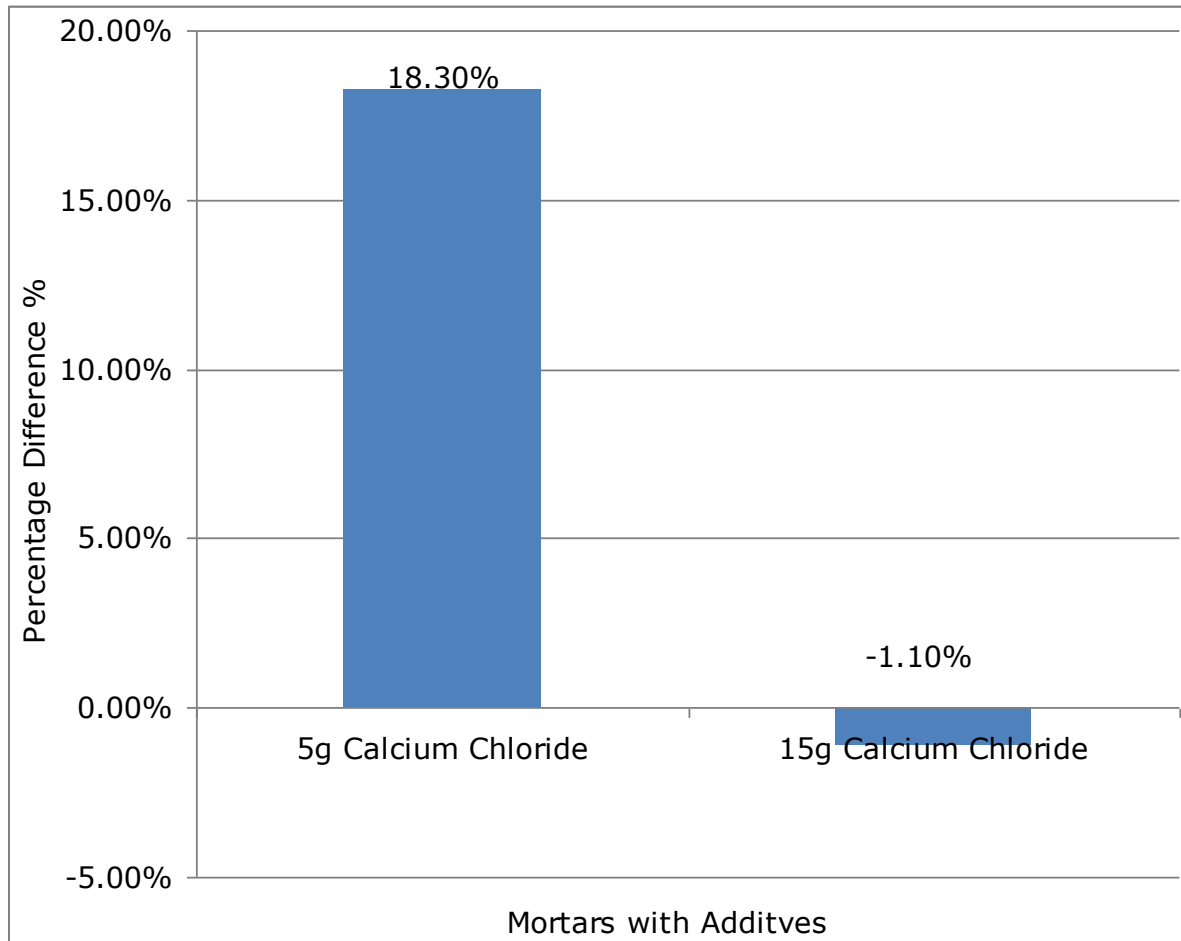


Figure 5.5: Percentage variation in compressive strength due to the addition of calcium chloride as compare to standard model.

II. Mortar with Potassium Chloride

Potassium chloride was found to generate an increase in the initial rate of curing. The positive effects of this additive were however short lived. At the end of the 28 day-period the compressive strength attained by the material was lower than the standard block. This is shown in figure 5.6 for additions of 15g and 25g of potassium chloride. A percentage based measure of this negative effect (reduction in strength) as compared to the standard model due to introduction of this additive is illustrated in figure 5.7. An explanation of the

addition of potassium chloride to concrete mix is a change in the cement water ratio resulting in the final strength of the block. Potassium chloride may also produce additional reaction which may be affecting curing rate and curing trend of the block samples. Potassium chloride is not seen to be causing any big deviation from the standard model, but at the 28-day period the final compressive strength attained by the concrete is reduced.

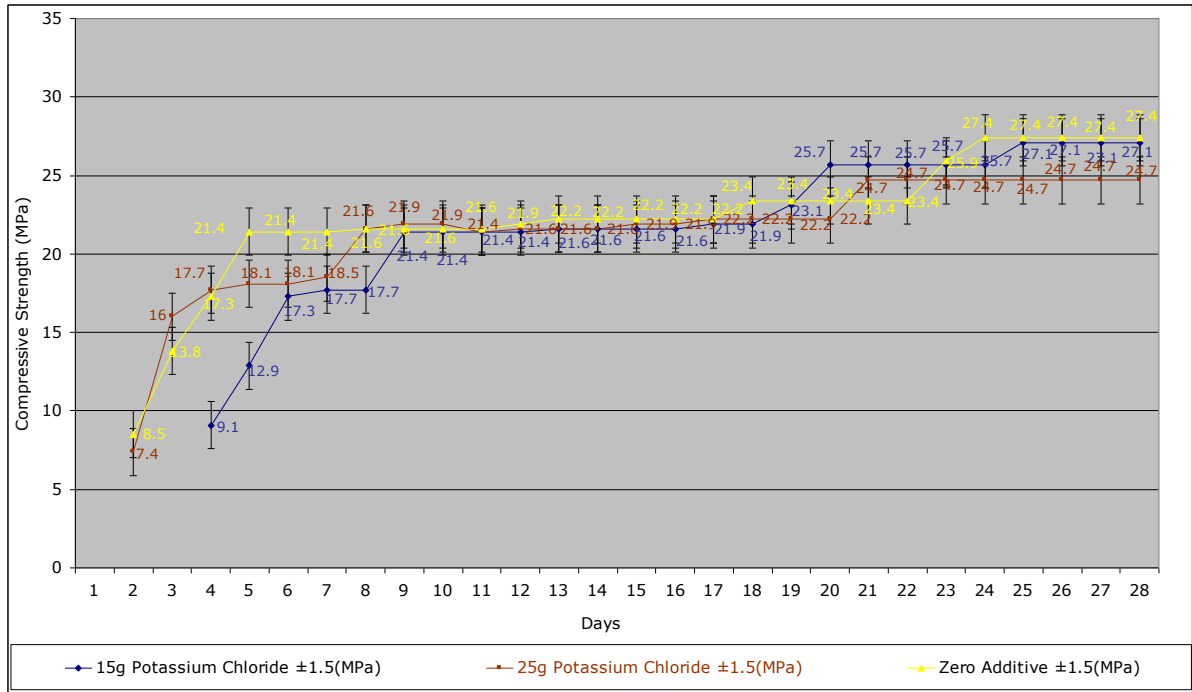


Figure 5.6: The change in compressive strength of a mortar with additions of potassium chloride with respect to time

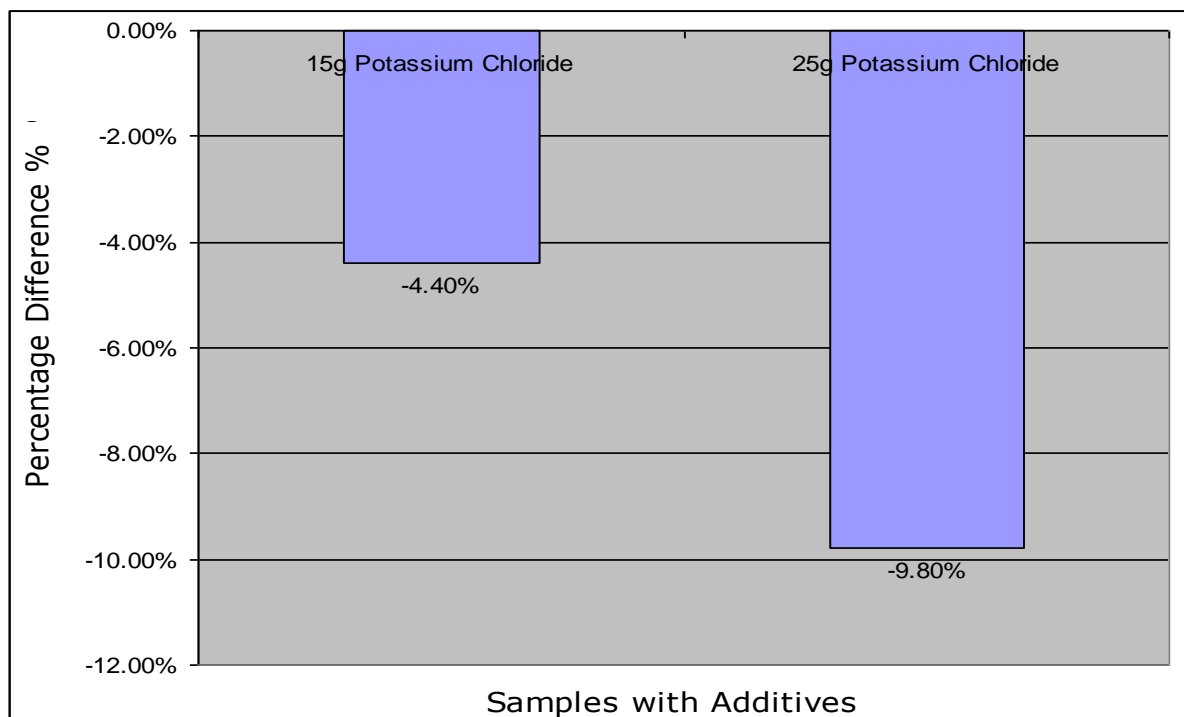


Figure 5.7: Percentage variation in final compressive strength due to the additions of potassium chloride as compared to standard model

III. Mortar with Sodium Silicate

The addition of sodium silicate was found to significantly retard the hydration process. This additive stimulated a major reduction in both the initial rate of curing and the compressive strength attained by the material. Figure 5.8 shows compressive strength with respect to time (days). The initial cure rate is slower with several jumps and reduction in the final compressive strength. One discovery of adding sodium silicate is that unlike other additives, there are several constant jumps in compressive strength before final setting. The finding of adding sodium silicate as additive is contrary to the report by Jenifer Chrisman [152], where it is reported that sodium silicate can be used as an accelerator. However, the reduction in compressive strength noticed from this specimen is in total agreement with Donald J. [151], where it is reported that adding silicate solution compound puts the concrete at risk of low strength development.

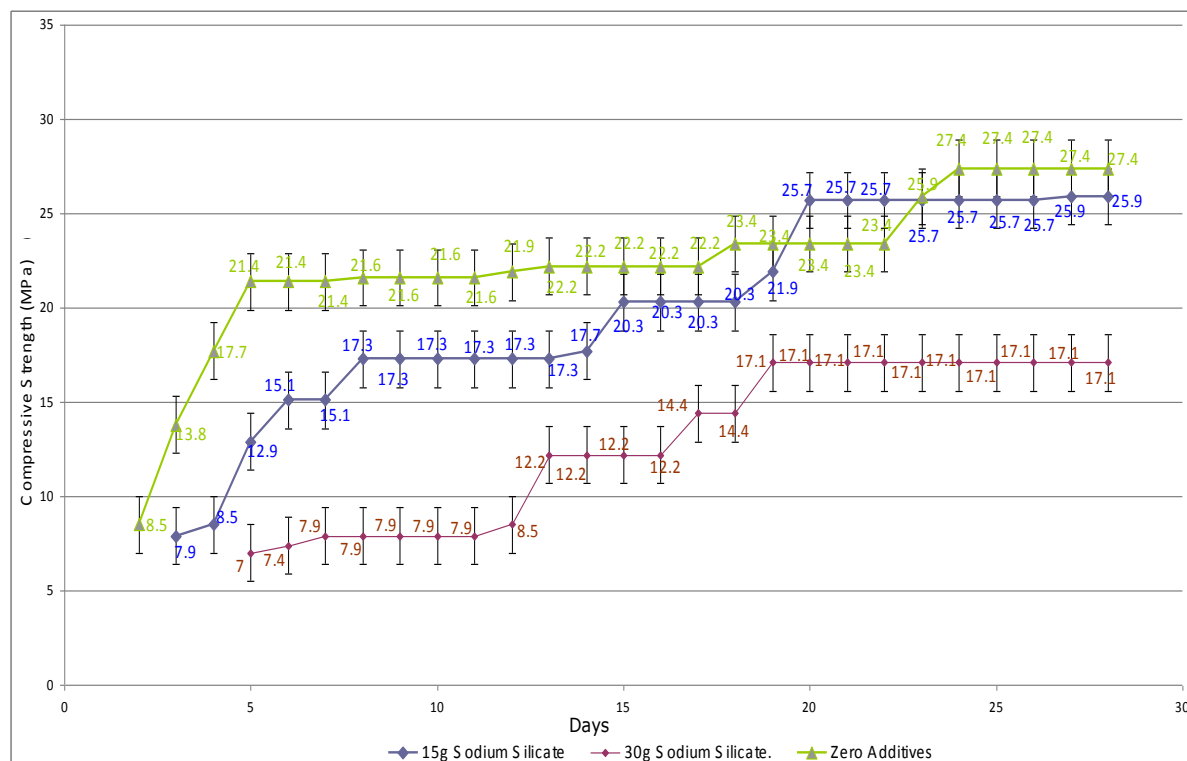


Figure 5.8: Typical change in compressive strength of a mortar sample with addition of sodium silicate with respect to time

The percentage variation in compressive strength as compared to the standard model due to the introduction of sodium silicate at the end of the 28 day period is shown in figure 5.9. The effect of 15g sodium silicate on compressive strength is almost equal (minor negative effect i.e. -5.5%) to that of plain concrete. The

effect of the 30g addition of sodium silicate contributed to detrimental effect (substantial reduction i.e. -37.6%) on final compressive strength.

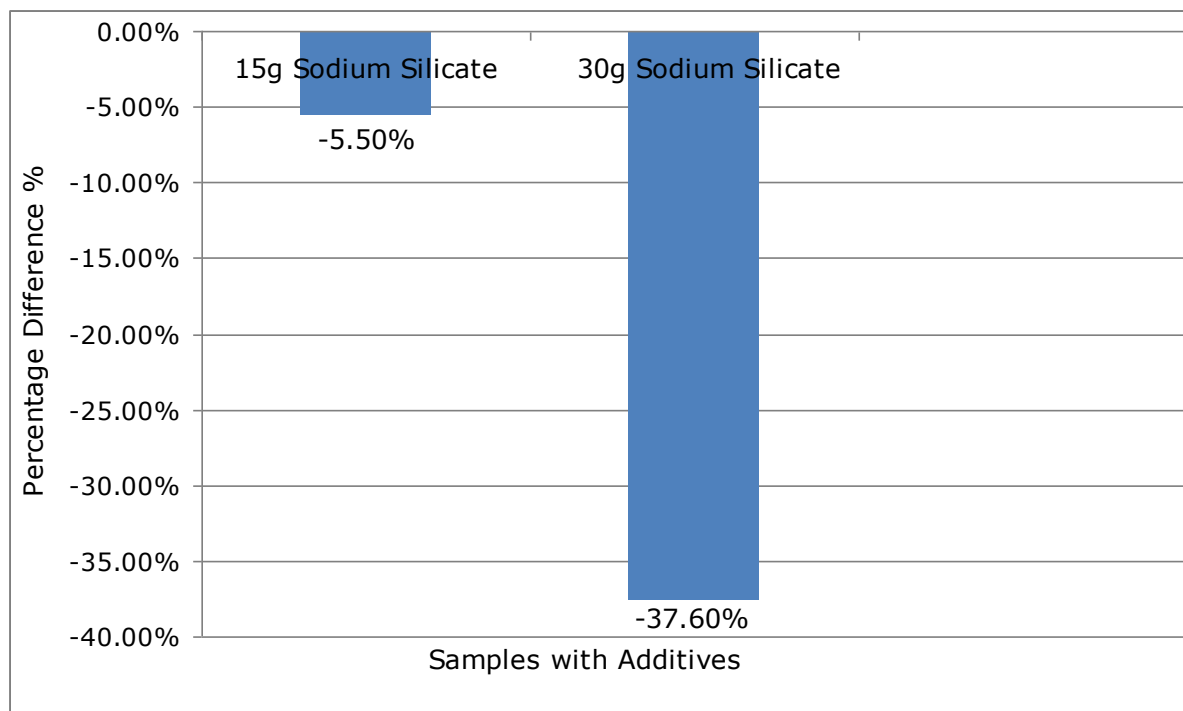


Figure 5.9: Percentage variation in final compressive strength due to addition of sodium silicate as compared to standard model.

IV. Mortar with Sodium Sulphate

Sodium sulphate in proportions of 1.3%, 2% and 3% were used as additives in concrete. Sodium sulphate was found to stimulate a major increase in both the rate of development of strength (0.18 to 0.27 MPa/hr), and the compressive strength (27.4 to 33 MPa) attained by the end of the measurement period. Figure 5.10 shows this effect. The findings in this specimen is in total agreement with the report published by Arnold Donald J., [150] and [151], where it is stated that concrete containing sodium sulphate in a quantity of up to 5% by weight of cement have a high strength after a short hardening time.

The highest compressive strength occurred with smaller addition of additive (i.e. 15g sodium sulphate). Figure 5.11 illustrates the percentage increase in compressive strength by final measuring period as compared to the standard mortar.

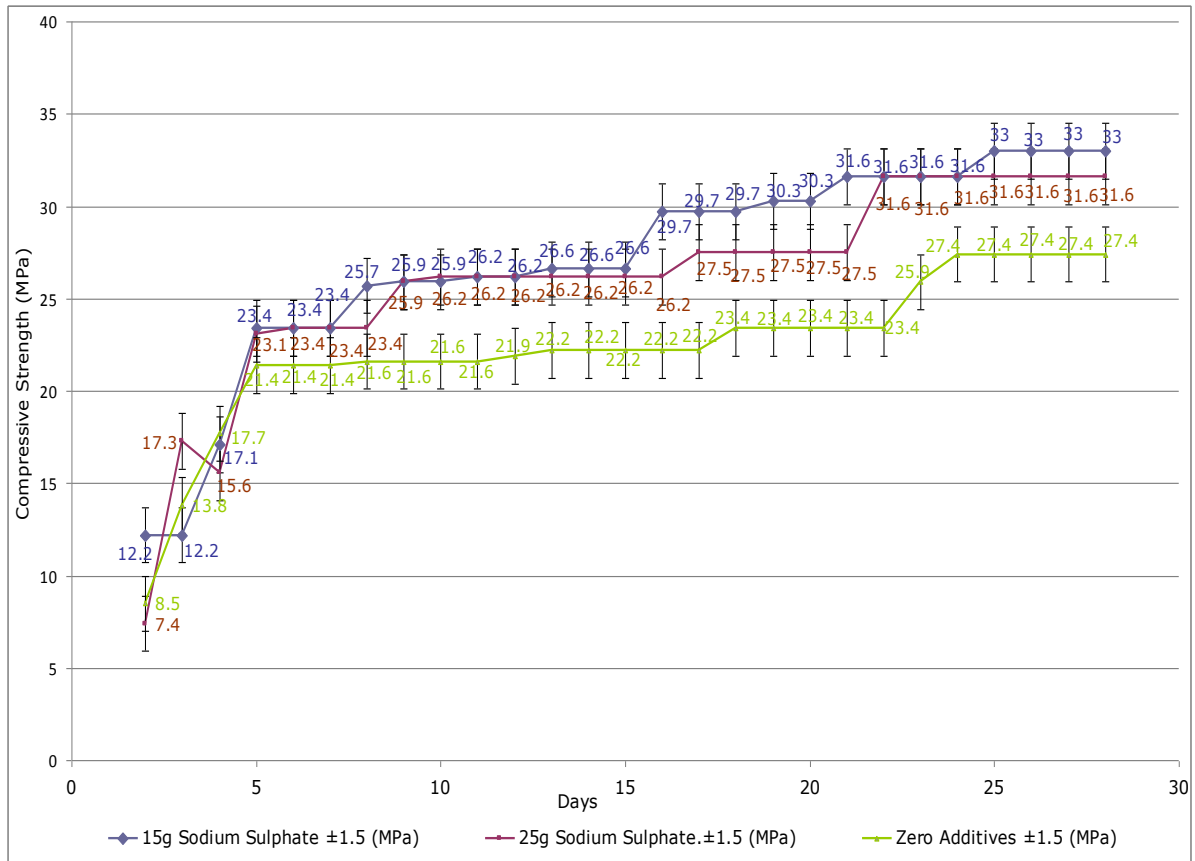


Figure 5.10: The change in compressive strength of a mortar with additions of sodium sulphate with respect to time

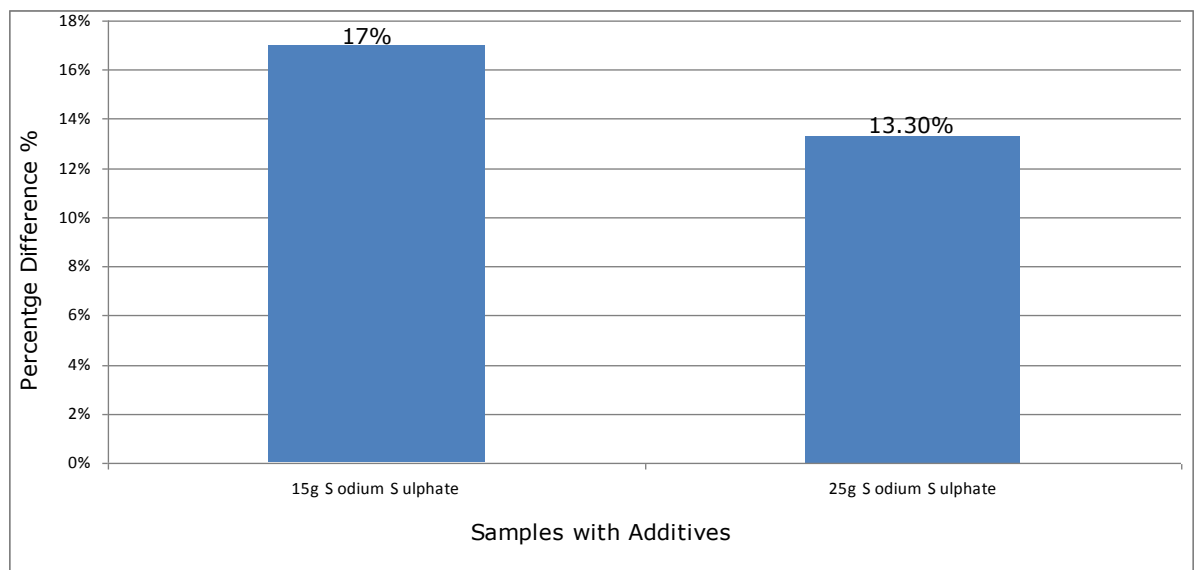


Figure 5.11: Percentage variation in final compressive strength due to addition of sodium sulphate as compared to standard model.

V. Mortar with Sodium Chloride

Measured quantity of sodium chloride was introduced into the concrete mixture to influence the curing rate. A 15 g addition of sodium chloride produces a small increase (from 0.18 to 0.182 MP/hr i.e. approximately 1%) in the initial rate of

curing, as shown in figure 5.12. This finding is in agreement with the report by Marcantoni Paul [155]. The addition of 25g of sodium chloride reduces (0.18 to 0.14 MP/hr i.e. approximately 22%) this initial curing rate. After the initial curing period, the development of compressive strength in the samples containing proportions of sodium chloride closely follows that of the plain concrete model. Towards the end of the 28-day period the compressive strength attained by the test samples closely correlate with that of the plain concrete as shown in figure 5.12. Figure 5.13 illustrates the percentage increase in compressive strength by the final measuring period as compared to the standard mortar.

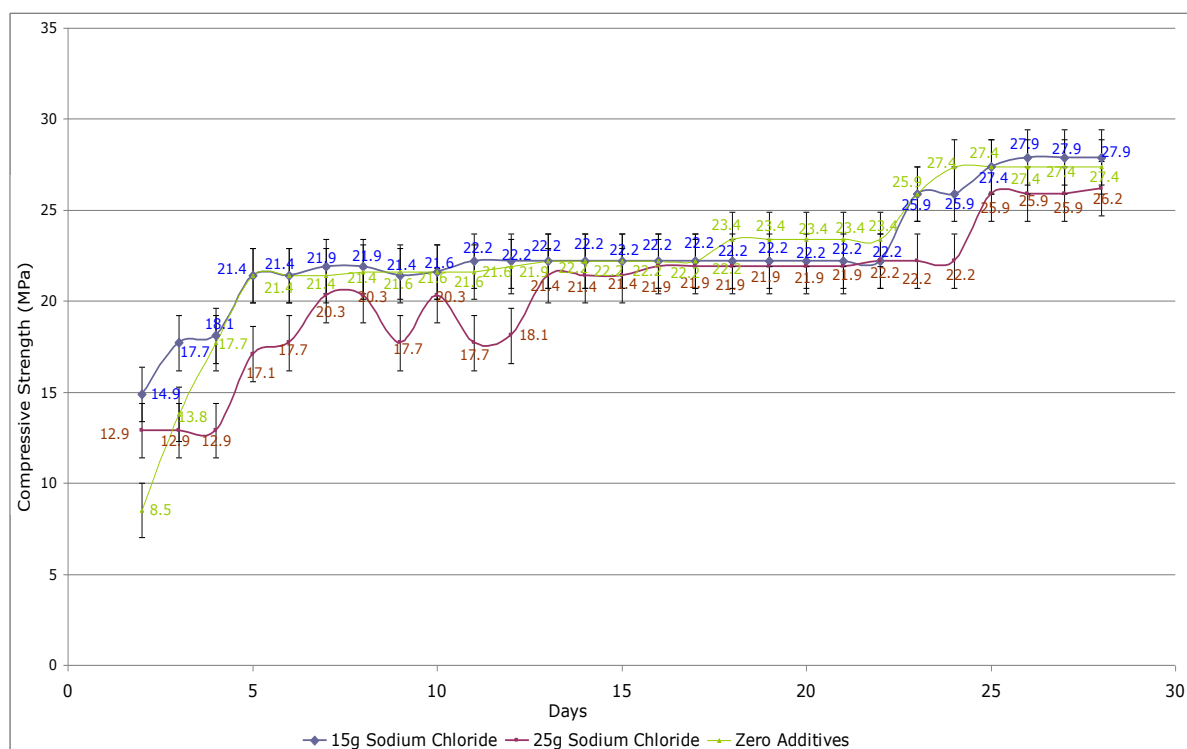


Figure 5.12: The change in compressive strength of a mortar with additions of sodium chloride with respect to time.

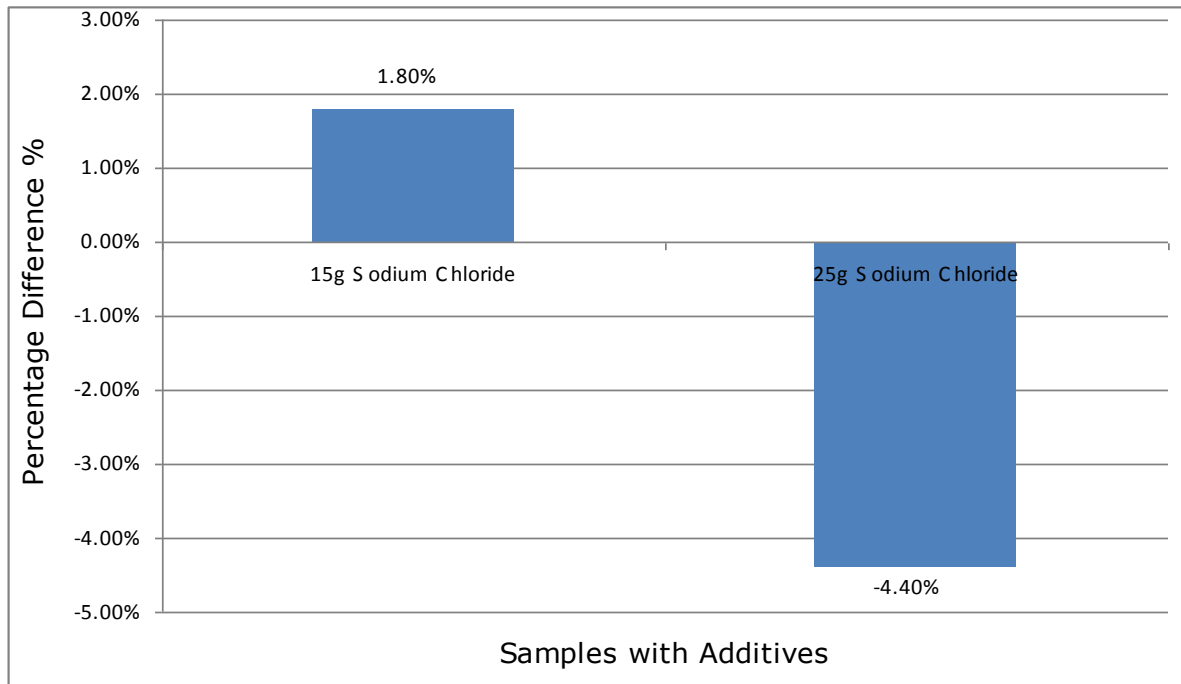


Figure 5.13: Percentage variation in final compressive strength due to addition of sodium chloride as compared to standard model.

5.4 The Effect of Additives on the Micro-structure of Concrete

It is well known that concrete is a complex material which consists mainly of cement, sand, water and aggregates. The compressive strength obtained by a certain concrete mixture is directly related to the bonding of these ingredients and the structure they form during hydration. The proportion and the type of additives which were introduced into the concrete mixture have demonstrated a significant effect on the hydration process and the resultant compressive strength. Examination of some typical samples was carried out using SEM (Scanning Electron Microscope) in order to observe the effects of additives on the structural bonding of concrete. This type of microscope functions using an electron beam rather than reflected light. An electron beam is scanned over the surface of the material. The beam is reflected back from the surface, is collected and then translated into the magnified image. The variations in colour in the magnified image describe the contours of the material surface. The results of SEM examination of these typical samples each containing calcium chloride (15 g); sodium sulphate (15 g) and sodium silicate (15 g) respectively were examined. The SEM photographs (figures 5.14 - 5.20) illustrate the composition and bonding of the three samples, and it can be seen that the microstructures of the three samples varied significantly, which were taken under similar condition at 500 and 2000 times magnifications for comparison. These three

samples were tested to failure, but it cannot be assumed that cracks present in these images are due to the mechanical testing, as these cracks may have occurred during the sectioning of the material for microscopic analysis. The sections were also chemically analysed using Energy Dispersive x-ray Analysis (EDXA). The examination and the operation of SEM and EDXA are added in appendix B.

5.4.1 Mortar with Sodium Sulphate

The structure of the concrete sample containing sodium sulphate at 500 times magnification is shown in figure 5.14. The image has a densely packed angular structure; the structure across the majority of this sample is shown to be somewhat consistent, with a relatively large pore space.

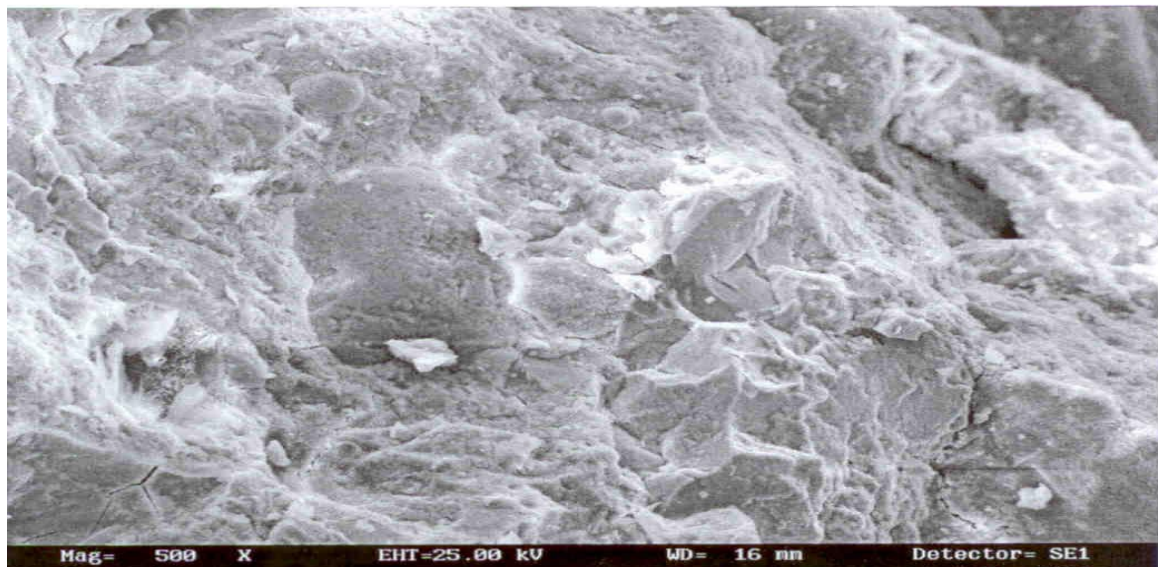


Figure 5.14: Microscopic Structure of Mortar Sample with Sodium Sulphate, 500 times magnification

The same sample is magnified 2000 times and is shown in figure 5.15. The formation of small needle like crystals is appearing to be uniformly distributed. EDXA analysis of this test sample is shown in figure 5.16. The Calcium content for this mortar was highest at 67.7%.



Figure 5.15: Microscopic Structure of Mortar Sample with Sodium Sulphate, 2000 times magnification

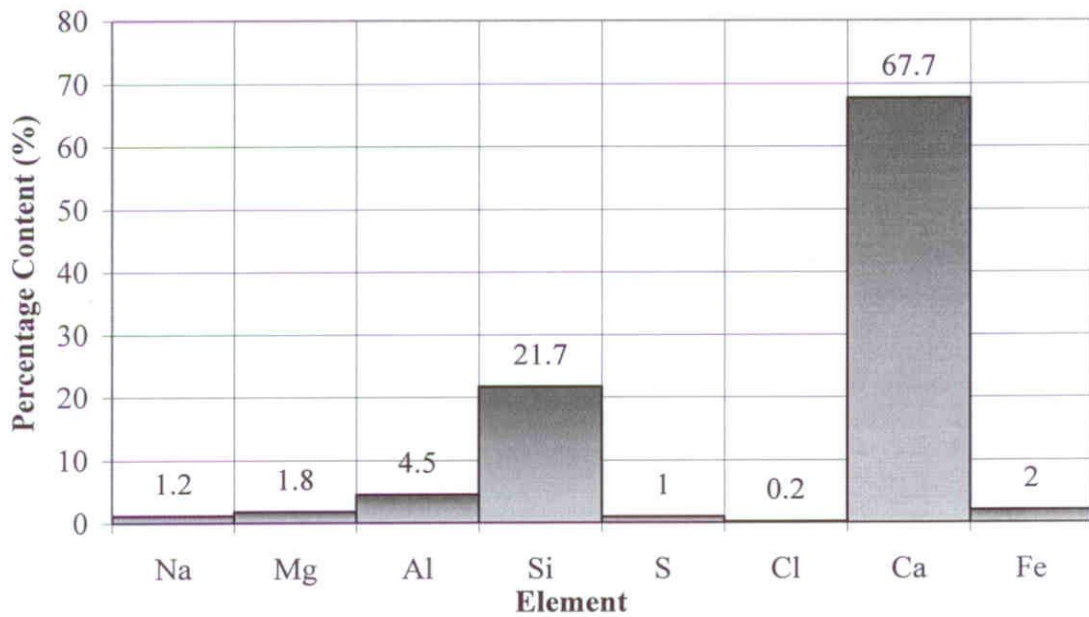


Figure 5.16: Elemental composition of mortar with sodium sulphate – percentage content by weight (Na: Sodium, Mg: Magnesium, Al: Aluminium, Si: Silicon, S: Sulphur, Cl: Chlorine, Ca: Calcium, Fe: Iron)

5.4.2 Mortar with Sodium Silicate

A sample containing sodium silicate is magnified 500 times using the SEM. At this magnification, there is already the appearance of large needle like crystals, as shown in figure 5.17. The analysis of these crystals revealed high concentrations of silicon. A view of the same sample at 2000 times magnification is shown in figure 5.18.

Large needle-like crystals

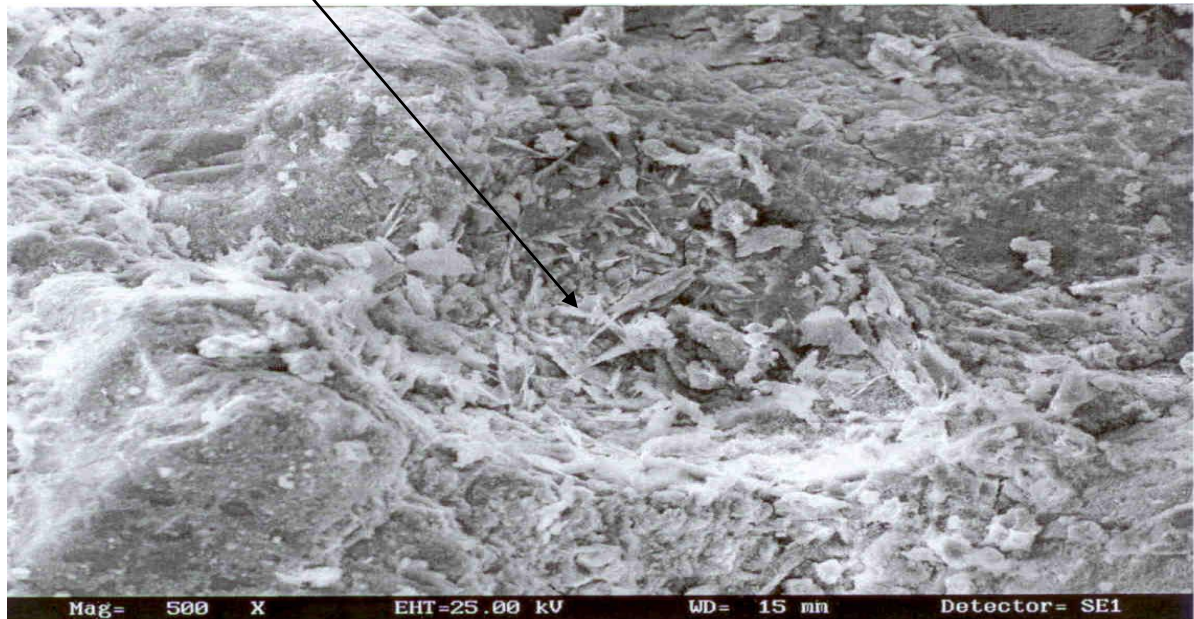


Figure 5.17: Microscopic Structure of Mortar Sample with Sodium silicate structure, 500 times magnification

Large needle-like crystals

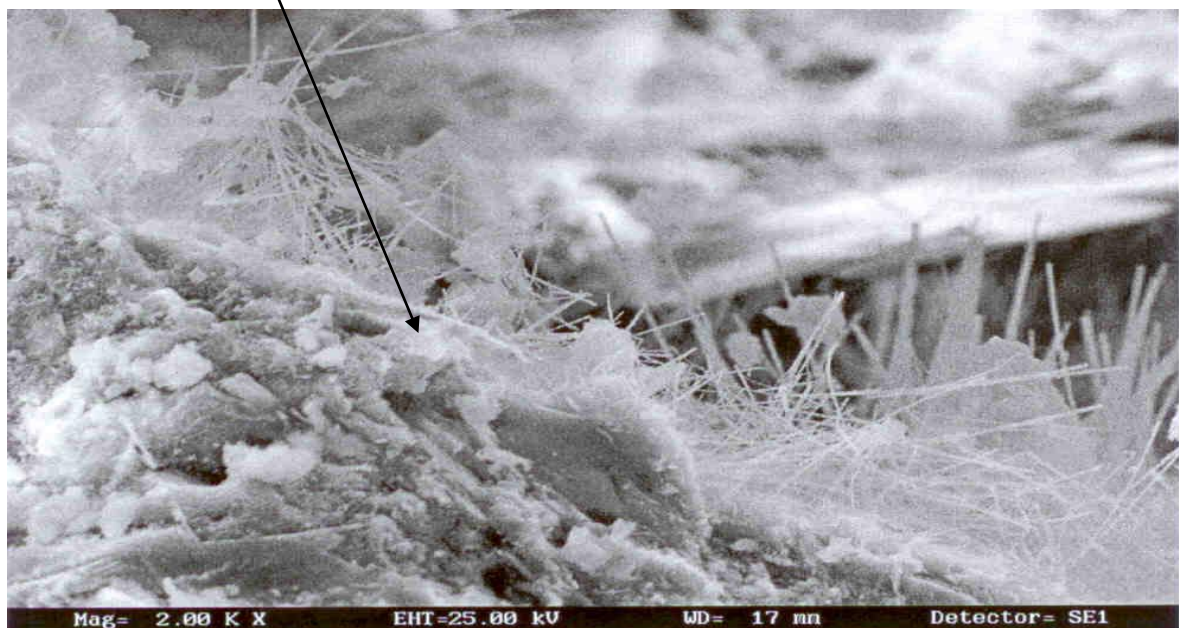


Figure 5.18: Microscopic Structure of Mortar Sample with Sodium silicate structure, 2000 times magnification

A comparison of micrographs reveals the microstructure has been modified as a result of the addition of additives. A similar trend can be seen in the elemental analysis of the samples using EDXA, see figure 5.19.

The image best illustrates the quantity and length of the needle like crystals. The bottom left hand corner of this image is also a quantity of granular type crystals. EDXA analysis of this test sample revealed the following elemental composition shown in figure 5.19.

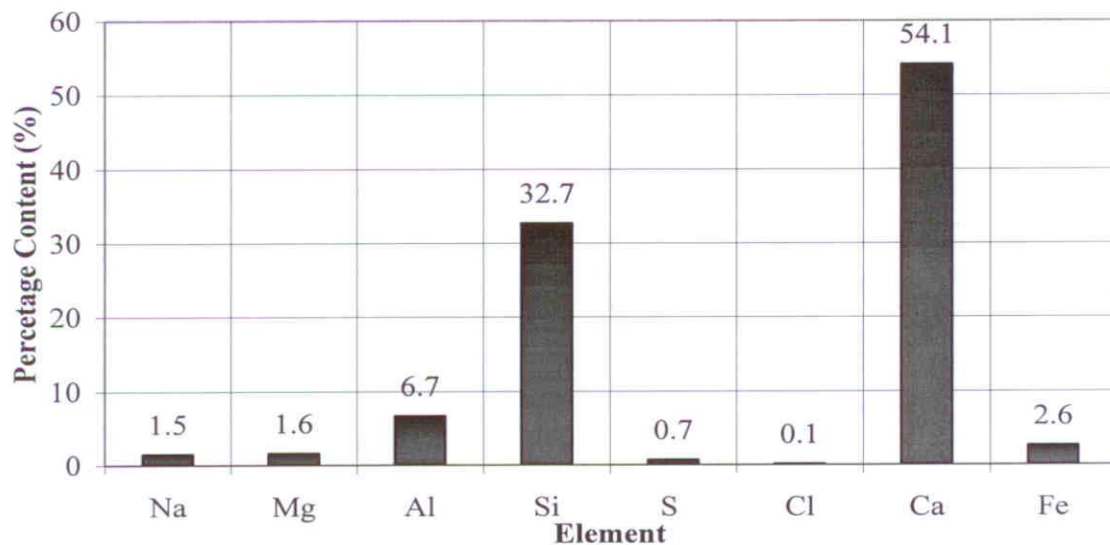


Figure 5.19: Elemental composition of mortar with sodium silicate – percentage content by weight (Na: Sodium, Mg: Magnesium, Al: Aluminium, Si: Silicon, S: Sulphur, Cl: Chlorine, Ca: Calcium, Fe: Iron)

5.4.3 Mortar with Calcium Chloride

Addition of calcium chloride in concrete mix had shown an increase in both the rate of initial hardening and the magnitude of the compressive strength attained over the curing period. Therefore the structure of the concrete sample containing calcium chloride with a 500 and 2000 times magnification was observed which is shown in figures 5.20 and 5.21 respectively.

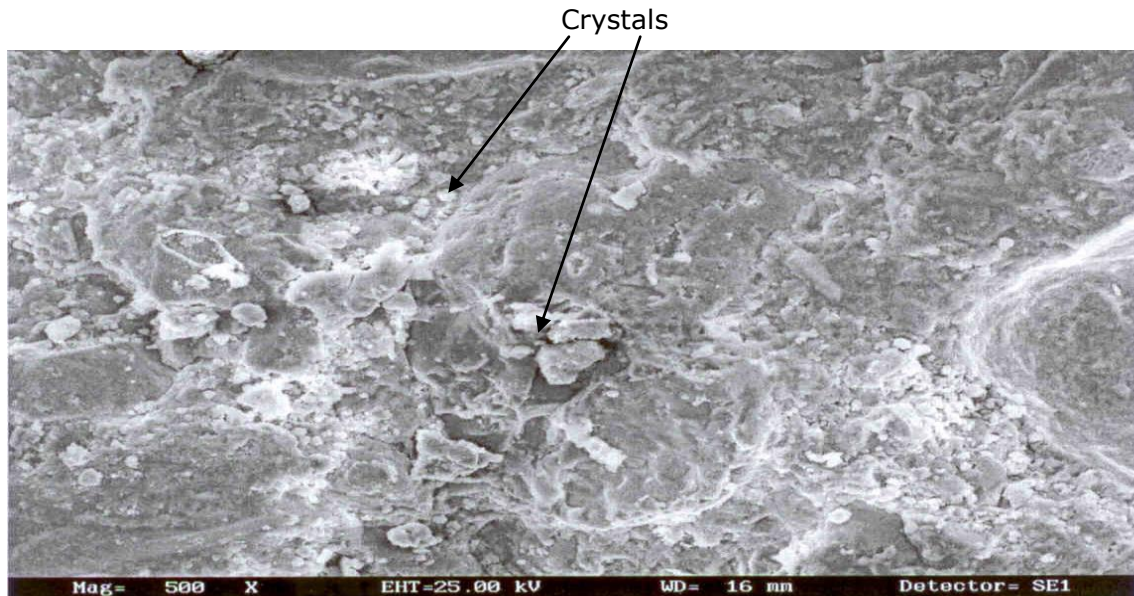


Figure 5.20: Microscopic Structure of Mortar Sample with Calcium chloride, 500 times magnification

The structure of this sample appears to be less angular than sodium sulphate with fewer contours, exhibiting a uniform regular structure throughout. There is also the appearance of numerous granular crystal scattered throughout the material. Figure 5.21 illustrates a view of this sample at 2000 times magnification.



Figure 5.21: Microscopic Structure of Mortar Sample with Calcium chloride-2000 times magnification

At this increased magnification the regularity of the structure is still apparent. The granular crystals, which were found to appear in the sample, are again shown to be dispersed throughout. The EDXA analysis of this concrete sample revealed the elemental composition shown in figure 5.22.

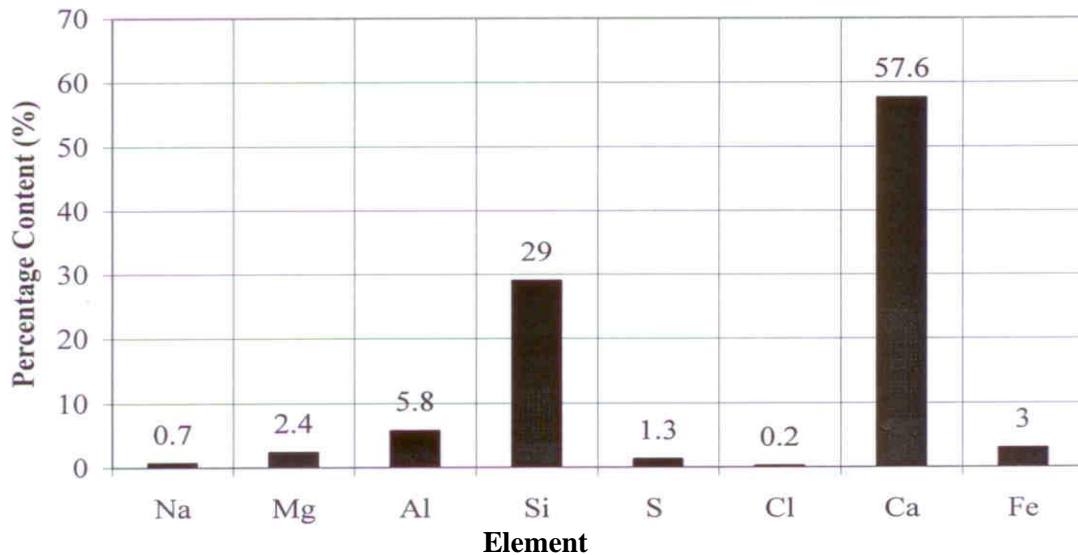


Figure 5.22: Elemental composition of mortar with calcium chloride – percentage content by weight (Na: Sodium, Mg: Magnesium, Al: Aluminium, Si: Silicon, S: Sulphur, Cl: Chlorine, Ca: Calcium, Fe: Iron)

The addition of calcium chloride has modified the elemental composition of the sample. A comparison with a sample containing calcium chloride and sodium sulphate indicate that a 10% increase and 7% drop in the elemental content of Ca and Si respectively.

The SEM analysis of concrete specimens clearly illustrates the great variations in the microstructure and composition of the material due to the introduction of additives.

The micro-structural variations between these three samples are:

- a) The sample with calcium chloride was found to structure somewhat similar to that of sodium sulphate, smaller in dimension. Throughout the sample, small granular crystals are distributed.
- b) The sample containing sodium sulphate exhibited a relatively large, chunky, angular structure, consistent all over the sample;
- c) The sample containing sodium silicate was found to have a random structure, showing crystals which are large needle shaped;

The aforementioned variations at micro-structural level led to the following mechanical changes:

1. Adding 5g Calcium Chloride to mortar makes a steep increase in the compressive strength during the first four days of curing and a substantial increase at the end of 28 day period as compared to a standard mortar. This indicates that introducing calcium chloride in small proportion in a mortar mixture increases the hydration reaction process.
2. Adding sodium sulphate to mortar increases the compressive strength during initial curing period (initial 4 days) and stimulates a major increase in compressive strength at the end of 28 day period as compared to a standard model. This indicates that introducing sodium sulphate in a mortar mixture stimulates an increase in hydration reaction.
3. Adding Sodium Silicate to mortar lowers the compressive strength throughout the curing period, thus resulting in lower compressive strength at the end of 28 day period as compared to a standard model. This indicates that introducing sodium silicate in a mortar mixture delays the hydration process.

The addition of sodium sulphate and calcium chloride in concrete has resulted in the significant increase of compressive strength of the material. The structures of these samples were found to be regular all across the material. The addition of sodium silicate in concrete results in a drop in the strength of the mortar. The comparison of these micrographs suggests that regularity in the micro-structure of concrete promotes increased strength and their elemental content results suggest that chemical reaction and other physical micro-structural changes have modified the strength of concrete blocks.

5.5 Compressive Strength of Concrete Containing Waste Materials as Aggregates

i) Concrete with Glass Aggregates

The introduction of chunk of broken glass aggregates was found to stimulate a substantial increase in the compressive strength of concrete mortars. The aggregate phase is stronger than the cement phase and has no direct influence on the strength of concrete except in the case of some highly porous and weak aggregates, such as pumice. The size and the shape of the coarse aggregate can, however, affect the strength of concrete in an indirect way [14]. The stiffness, shape, texture, maximum size, and grading of both coarse and fine aggregate (characteristics of concrete) are known to exercise significant influence on compressive strength of concrete [62, 119 and 159]. The results obtained from this research shows that the addition of glass aggregates increase the compressive strength as shown in figure 5.23. The compressive strength results obtained from ultrasound tests are lower than those obtained from the mechanical crush test, seen figure 5.23. An explanation for this difference may be the higher load bearing capacity of a chunk of glass. If the bonding between cement paste and glass aggregate is good, the mechanical result would indicate relatively higher strength value.

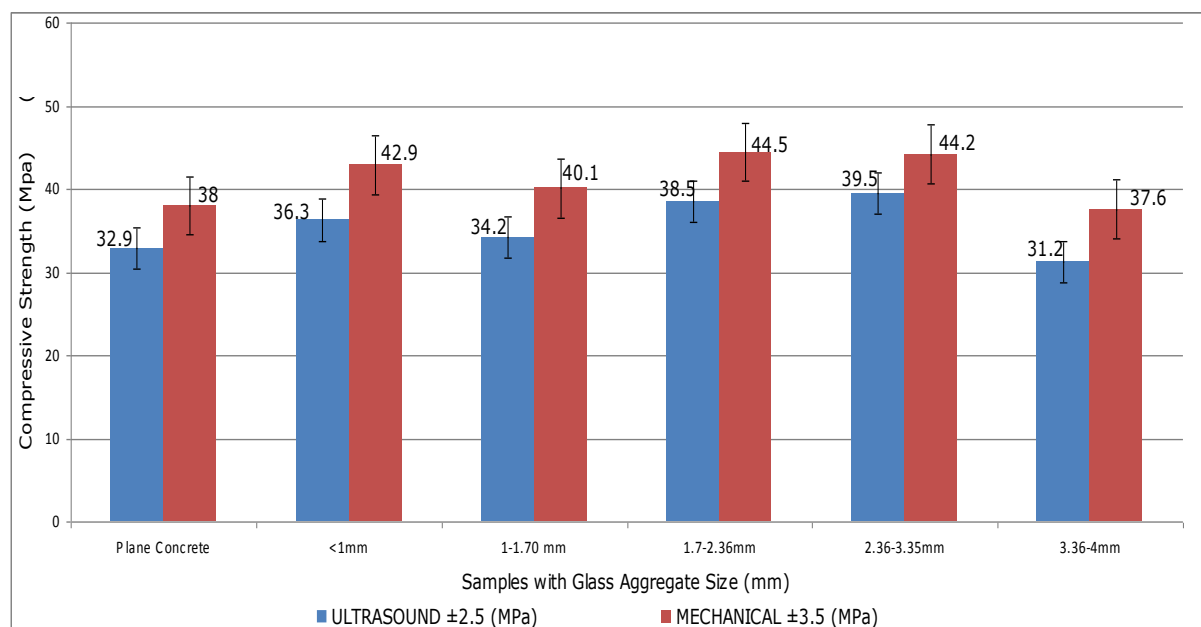


Figure 5.23: A comparison of compressive strength obtained between actual mechanical and ultrasound tests due to the introduction of different sized glass aggregates in concrete.

The results of compressive strength with glass aggregate increases with the size of the aggregate up to 3.35 mm, see figure 5.23. Aggregate in the range 3.36-4 mm shows no significant change in the strength compared to the plain concrete. The ultrasound technique however gives an overall average resistance of the material to ultrasound wave propagation. The difference in the compressive strength using the two techniques is shown in figure in 5.24.

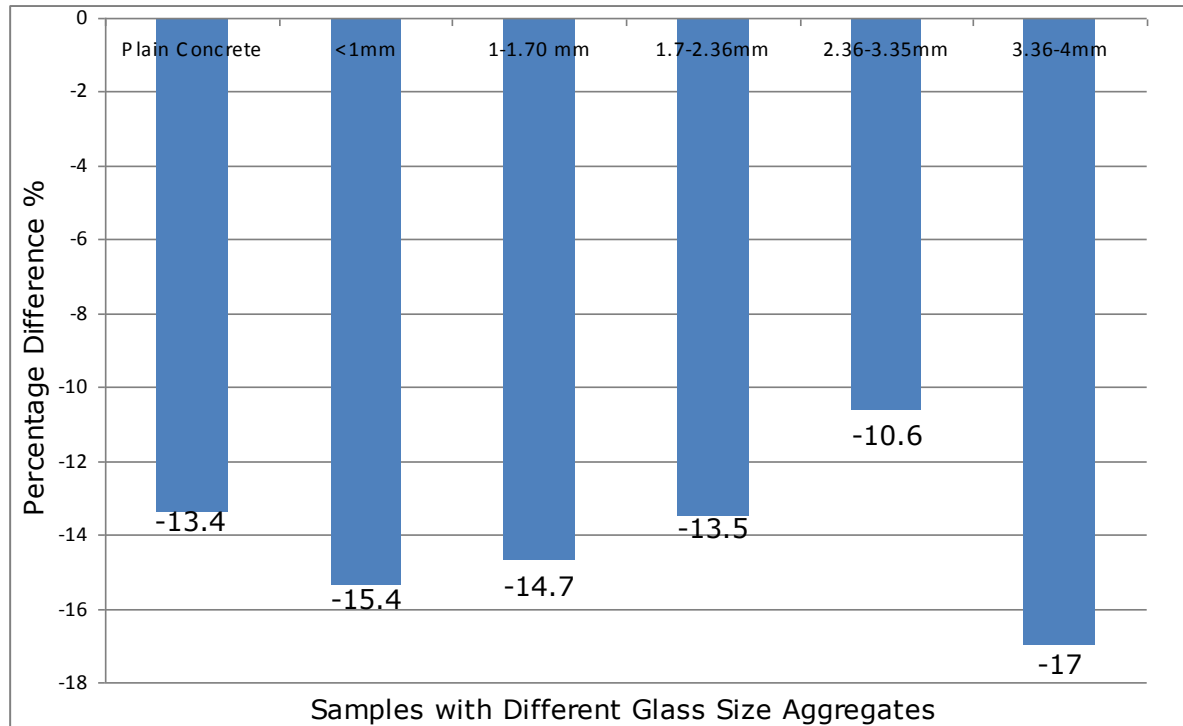


Figure 5.24: Percentage error variation between samples introduced from the mechanical and ultrasonic measurement techniques.

The strength values obtained for the mechanical and ultrasonic test results are shown in figure 5.25. The best fit line for ultrasound is $y = -0.18x + 40.587$ (with $R^2 = 0.0007$) and for mechanical test is $y = -0.04x + 34.627$ (with $R^2 = 0.012$). The comparative strength values for different sizes of glass aggregate obtained from ultrasound technique demonstrate lower coefficient of variation than the mechanical test results. There is no trend that can be seen between the compressive strength and the aggregate sizes since the sample with the largest aggregate size (3.36-4 mm) shows no significant changes in the strength compared to the plain concrete. Hence the relationship between the two variables can not be predicted.

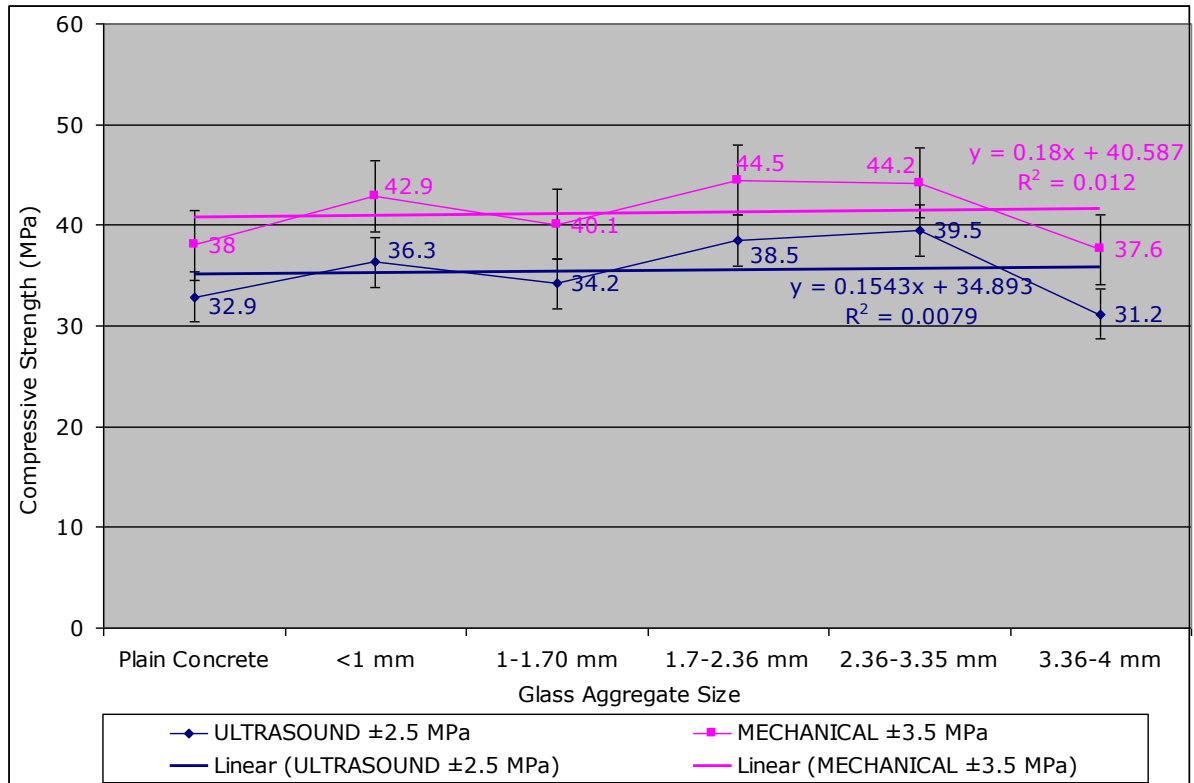


Figure 5.25: The best fit line of compressive strength obtained by ultrasound and mechanical methods for glass aggregates

ii) Concrete with Rubber Aggregates

The concrete samples with various amount of chopped rubber tyre as aggregates were manufactured with care under similar conditions. The results of strength measurement for these samples are shown in figure 5.26. It is apparent from the figure that an increase in the content of rubber decreases its compressive strength. An obvious explanation of this is that:

- i) Rubber is more elastic than the cement matrix;
- ii) Interfacial transition zone between rubber and cement paste is relatively weak.

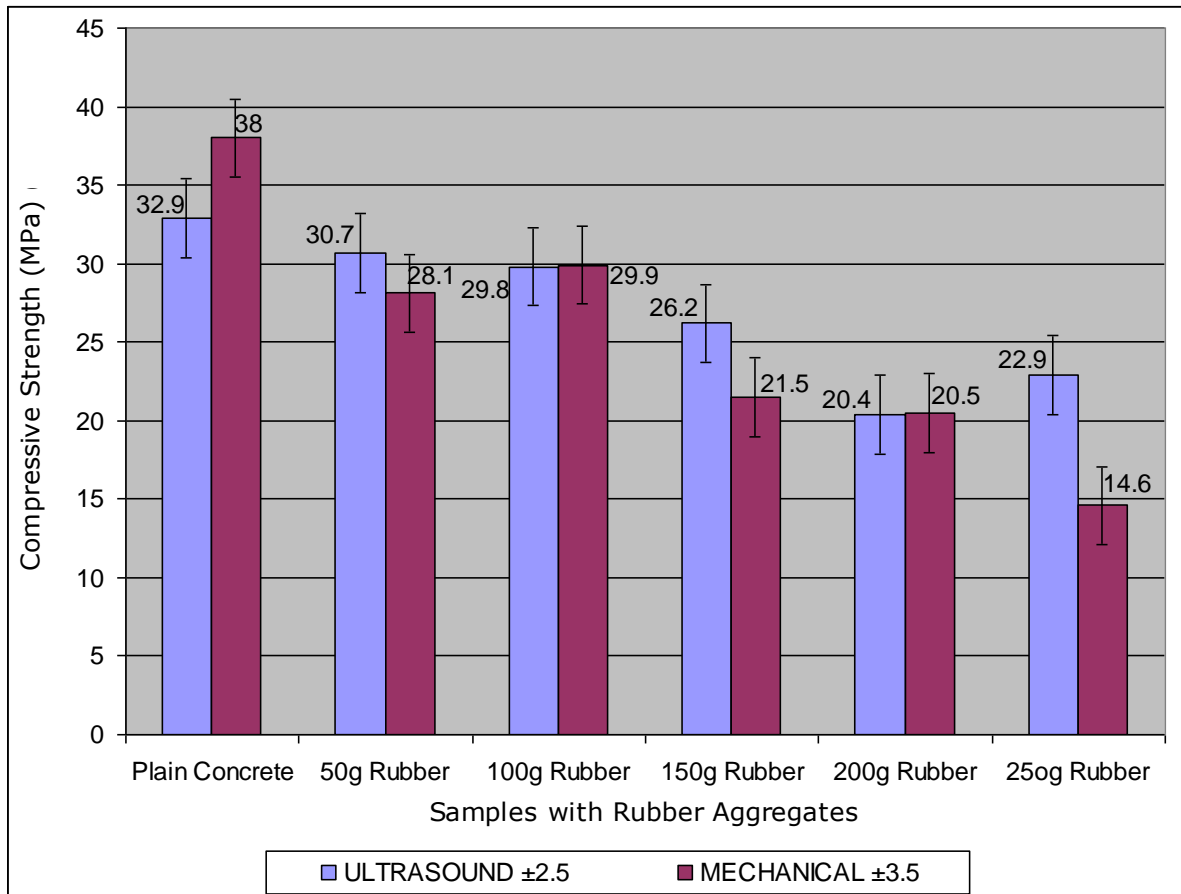


Figure 5.26: A comparison of compressive strength obtained between mechanical and ultrasound tests due to the introduction of rubber aggregates in concrete.

However the bonding between the cement paste and rubber aggregate is relatively poor due to lack of affinity of water to rubber which can be seen on the surface of the block. The difference between the mechanical and ultrasonic test results in the error variation of the measurement techniques is shown in figure 5.27.

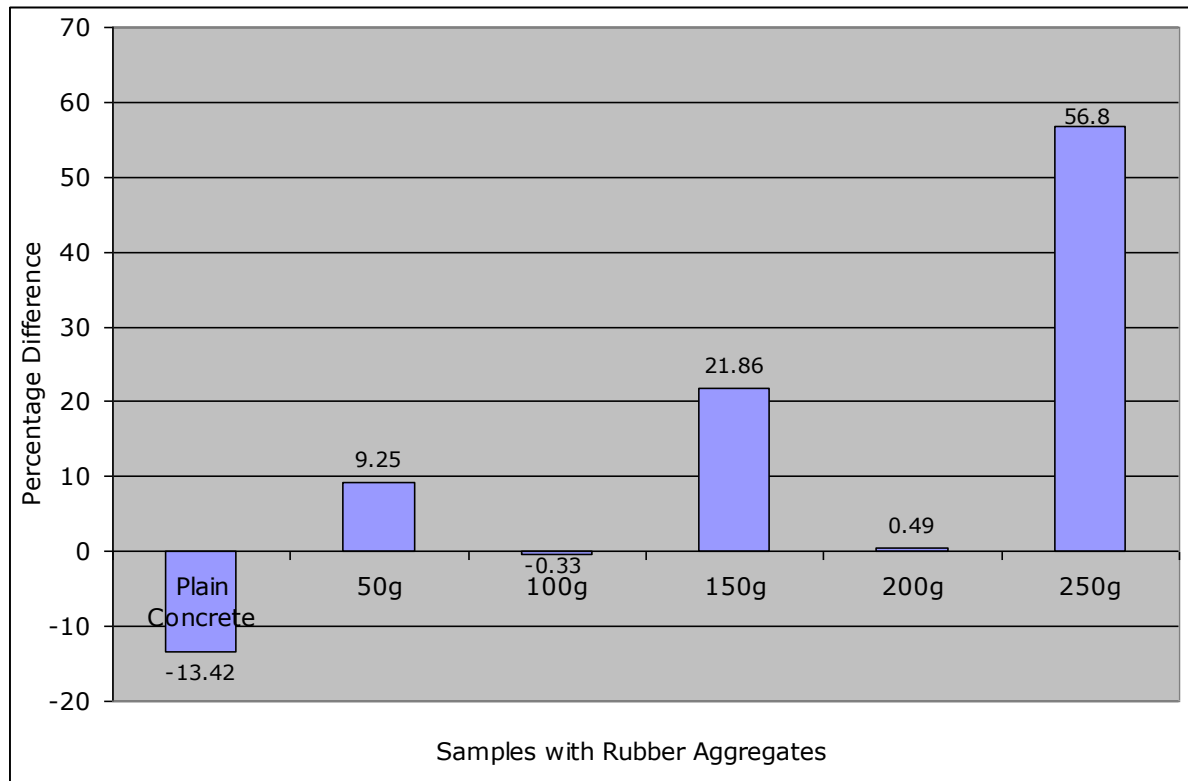


Figure 5.27: Percentage difference variation between samples introduced from the mechanical and ultrasonic measurement techniques for rubber aggregates.

The strength values obtained for the mechanical and ultrasonic test results are shown in figure 5.28. The best fit line for ultrasound is $y = -2.4143x + 35.6$ (with $R^2 = 0.8702$) and $y = -4.2343x + 40.253B$ (with $R^2 = 0.917$). The comparative strength values for different quantity of rubber aggregate obtained from ultrasound technique demonstrate less coefficient of variation than the mechanical test results. The reason for this could be the ultrasonic waves may have refracted due to the presence of rubber aggregates hence leading to scattering.

It is apparent from the results that under mechanical loading the elastic and non-elastic component of the sample behave differently making the concrete brittle. The ultrasound results however are dependant on the bonding of the concrete phases (e.g. cement phases, aggregate phases, transition zone) and their respective bonding properties (e.g. strong or weak bonding).

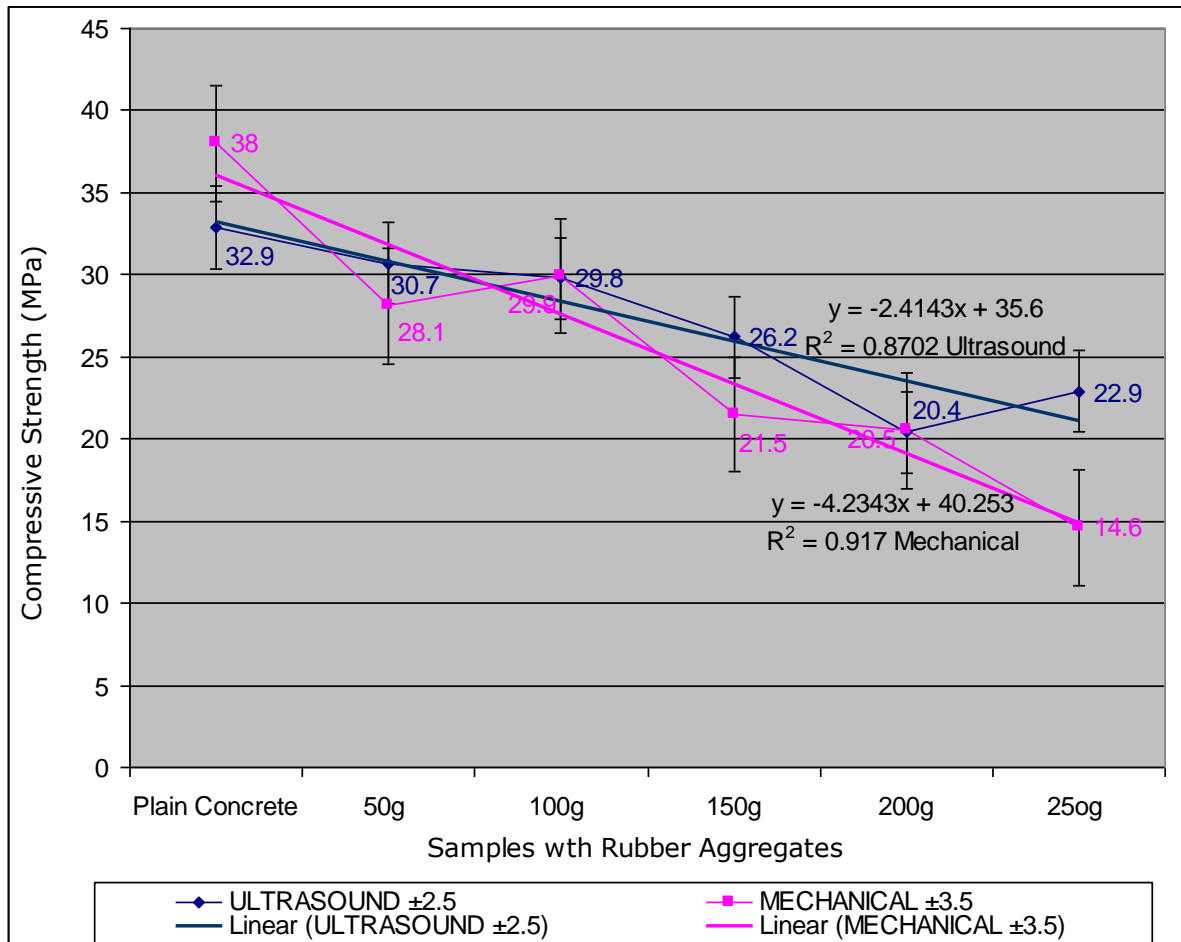


Figure 5.28: The best fit line of compressive strength obtained by ultrasound and mechanical methods for rubber aggregates

5.5.1 Calculation of the Modulus of Elasticity of Concrete Containing Waste Materials

A quantitative assessment of the modulus of elasticity (E) of concrete was carried out using the equation (2.1) specified in chapter 2. The results obtained are shown in table 5.3 and figure 5.29:

(a) Concrete Containing Glass Aggregates

Table 5.3: Modulus of Elasticity for samples with different sizes of glass aggregates

Glass Aggregates	Density kg/m^3	Mechanical Strength (MPa)	E (GPa)
Plain Concrete	2220.4	38.00	27.8
Less than 1mm	2214.1	42.90	28.8
1.00–1.70 mm	2162.3	40.10	26.9
1.70– 2.36 mm	2219.1	44.50	29.3
2.36– 3.35 mm	2190.4	44.20	28.5
3.35– 4.00 mm	2174.3	37.60	26.6

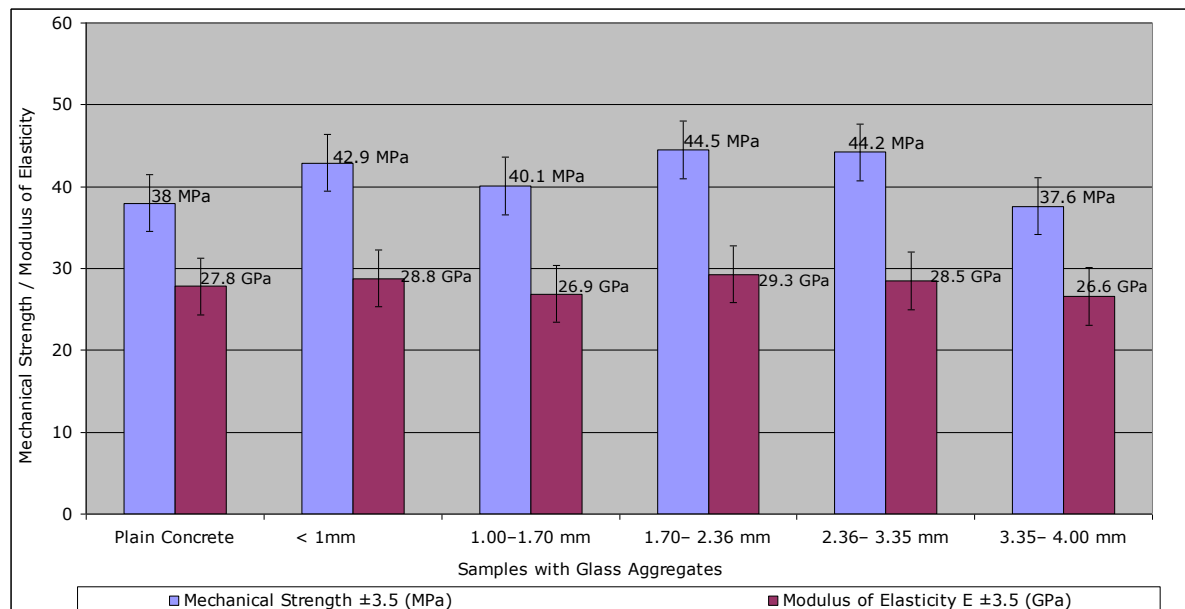


Figure 5.29: The modulus of elasticity to the aggregate size ratio in terms of compressive strength.

There is no significant variation in density, compressive strength, wave speed or Young's modulus for the glass aggregates particle sizes considered here as seen in figures 5.29 and 5.30.

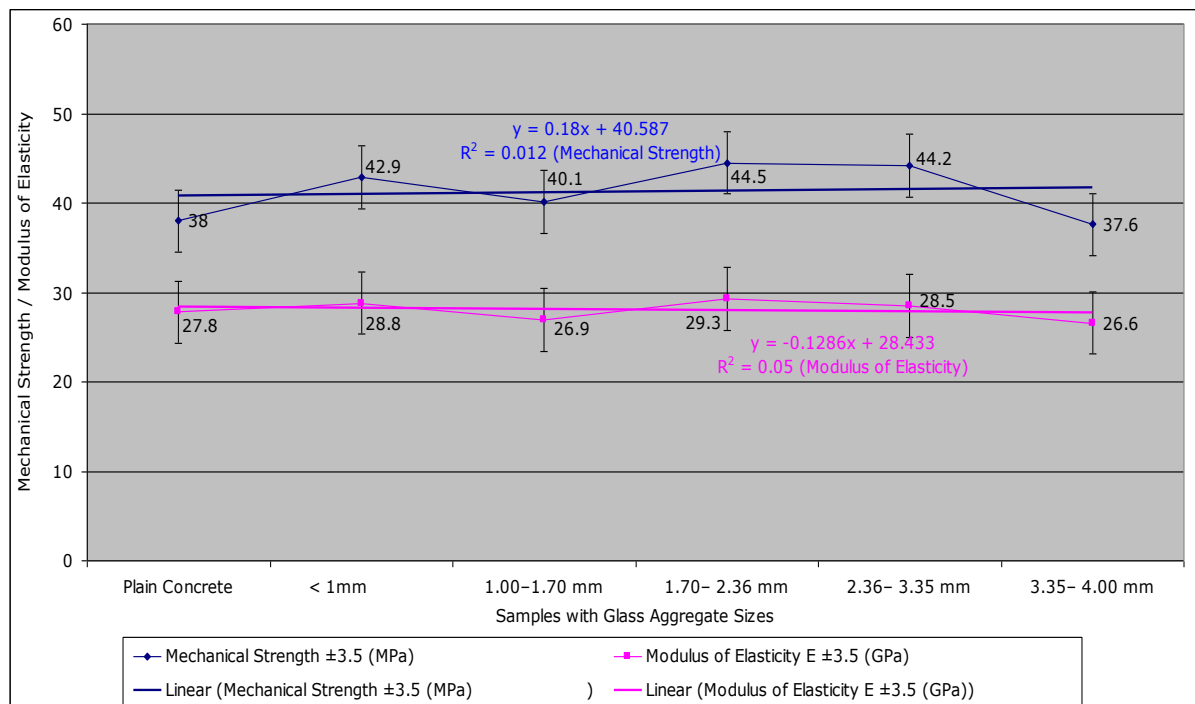


Figure 5.30: The best fit line of mechanical strength and modulus of Elasticity obtained by ultrasound and mechanical methods for glass aggregates

(b) Concrete Containing Rubber Aggregates

Using the same method as above, the modulus of elasticity was calculated using equation (2.1) specified in chapter 2 and is given in table 5.4 and figure 5.31:

Table 5.4: Modulus of Elasticity for samples with different quantities of rubber aggregates

Rubber Aggregates	Density (kg/m ³)	Mechanical Strength (MPa)	E (GPa)
Plain Concrete	2220.4	38.0	27.8
50g Rubber	2134.4	29.4	23.6
100g Rubber	2123.6	29.8	23.5
150g Rubber	2085.4	23.9	21.1
200g Rubber	2053.8	20.5	19.4
250g Rubber	1998.1	18.8	17.9

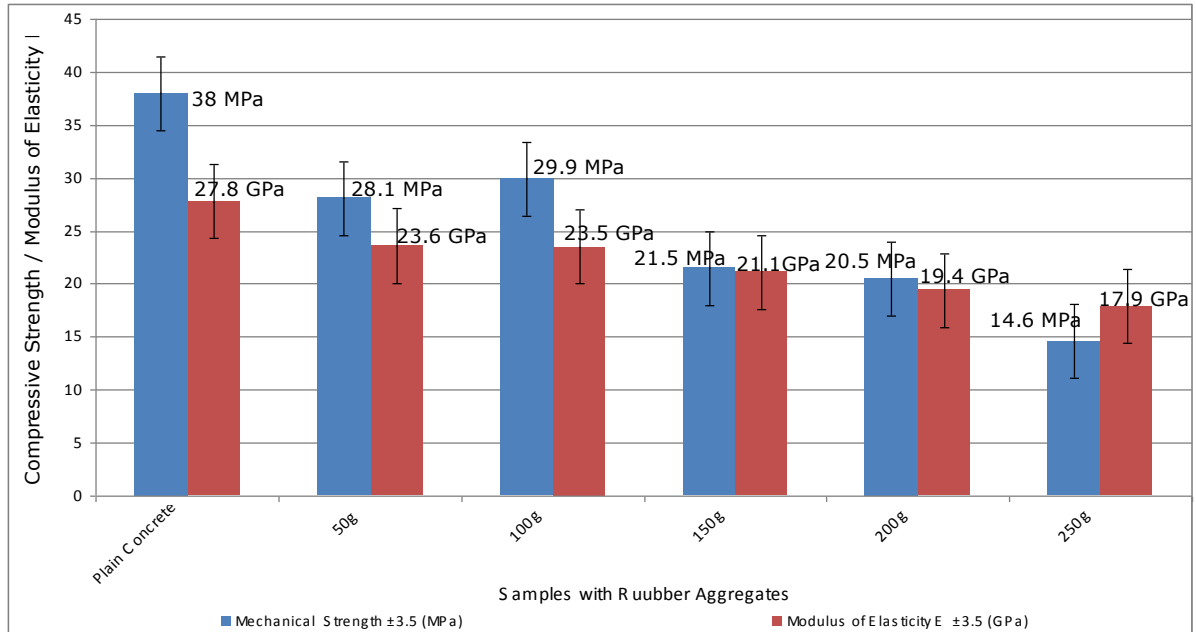


Figure 5.31: The modulus of elasticity of concrete with rubber aggregates to the ratio of rubber in terms of compressive strength.

Density, mechanical strength and young's modulus are inversely proportional to quantity of rubbers added to the mixture, i.e. Gradient of mechanical strength $M = -4.2343$ and modulus of elasticity $M = -1.8429$, with coefficients of variation $R^2 = 0.917$ and $R^2 = 0.9502$ respectively, as indicated in figure 5.32.

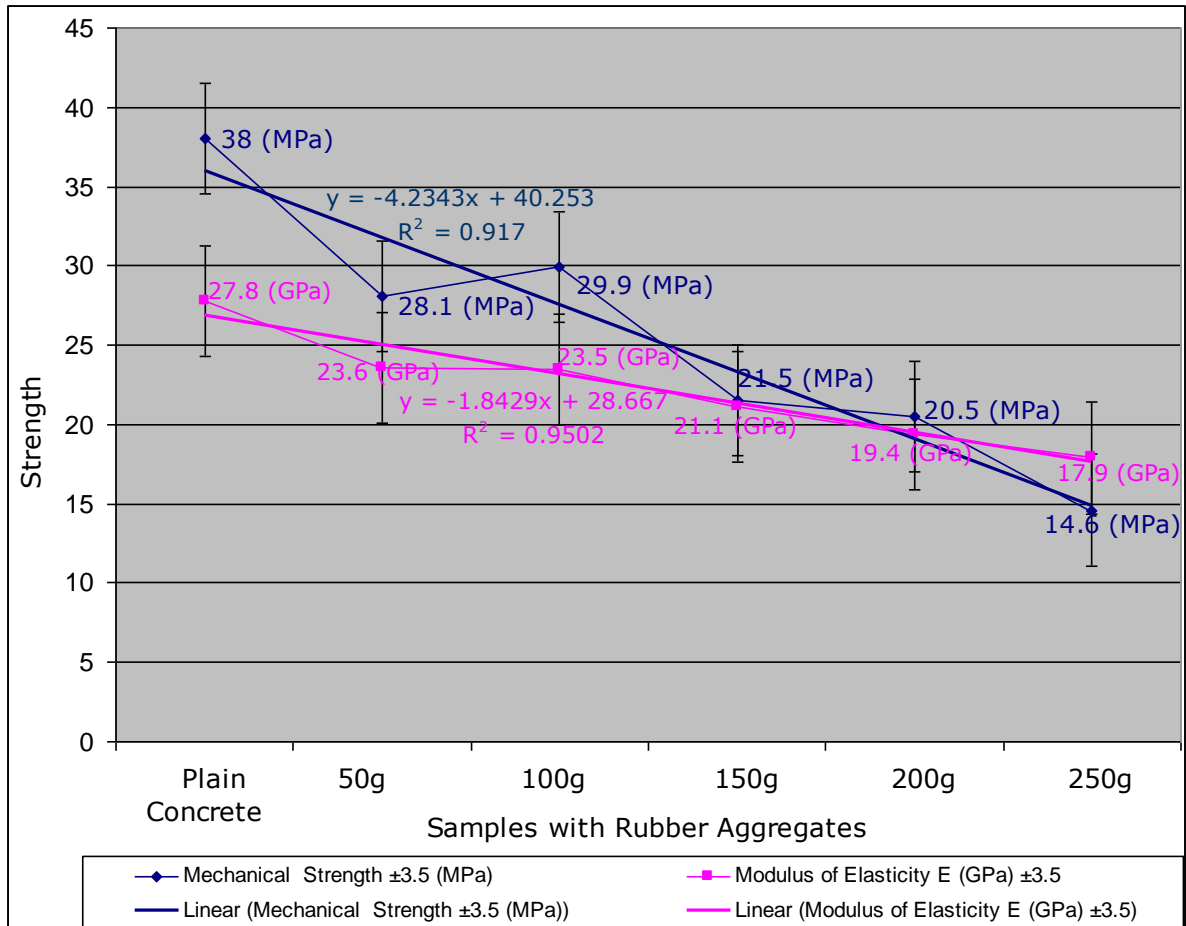


Figure 5.32: The best fit line of mechanical strength and modulus of elasticity for rubber aggregates

5.6 Brief Summary of Ultrasound and Microscopic Results

The work entailed the analysis of the development of compressive strength through the use of ultrasound. The use of ultrasound in this way to characterise the curing process is a relatively new approach acquired from by Schmidt hammer testing. This particular technique employed the use of both ultrasound velocity and the rebound value data developed from Schmidt hammer tests on concrete (described in chapter 2). Through the use of this method, a clear pattern was recognised describing the development of the compressive strength during curing period.

A comparison of compressive strength measured using ultrasound and *the* mechanical crush test on a number of test samples enhanced the accuracy and reliability of the results. By the comparative analysis of these two techniques, it was found that the measurements showed good correlation with the experiments on mortar specimens with admixtures. The use of the ultrasonic inspection method was convenient and non-destructive. The result obtained

from the ultrasonic test was more reliable than the mechanical test method. In the case of mechanical strength measurement, the results are dependant on the personal judgement and visibility of apparent damage in the specimen. A cracked specimen which is in service is likely to be rejected however it may still carry the applied load. On the contrary, ultrasound provides an average strength of the material based on the ability of ultrasound to propagate through it.

This therefore demonstrates that the use of ultrasound in this investigation under the condition described and for the materials under investigation is a useful, considerably cheap, faster and easier method of estimating the compressive strength of concrete at any stage of curing.

The introduction of additives in concrete demonstrated effective development of the properties of the material. The ultrasound technique has enabled to investigate the effect of additives in concrete and on the development of the strength. This investigation has shown that the use of additives in mortar have actively altered and enhanced the hydration and curing process producing the beneficial/detrimental affect on the strength of concrete.

It is observed that the rate of curing is dependant on the type and quantity of the additives, e.g. sodium sulphate accelerate the curing process whereas sodium silicate retards it.

The analysis of the effects of the addition of waste materials as aggregates in a concrete mixture demonstrated interesting results. The glass was introduced into a concrete mixture in both powdered form and in pieces up-to 4mm in size. It is also anticipated that glass; a chemical inert material has no effect on hydration reaction of concrete. It was determined that the introduction of glass into a concrete mixture would have a similar effect to increasing the proportion of aggregate. The addition of glass pieces was found to stimulate an increase in the compressive strength of the material. This increase in strength is due to strong interfacial bonding between the cement matrix and glass aggregates. This will be further discussed in the AE monitoring of concrete.

Rubber, introduced in concrete as part of aggregate is harmful for the strength properties of the concrete. But rubber brings to concrete other properties which might be useful in certain domains of application. Rubber acts as a damper of failure and it also makes concrete lighter. It will be useful in such circumstances where vibration must be mitigated. This decrease in strength is due to weak interfacial bonding between the cement matrix and rubber aggregates. This will also be further discussed in the AE monitoring of concrete.

The introduction of glass powder in concrete as part of an aggregate does not seem to have a positive effect on the properties of concrete. This can be explained by the fact that the powdered glass have about the same properties as sand thus increasing the sand to cement ratio leading to weaker strength.

The sodium sulphate and calcium chloride addition in concrete have exhibited to significantly increase the compressive strength of the mortar. The structures of these samples were established to be somewhat consistent throughout. Sodium silicate in concrete stimulates a significant decrease in the strength of the mortar. The comparisons of these results therefore suggest that consistency in the structure of concrete, promotes increased strength.

The results obtained from the ultrasound characterisation provide a clear illustration of the variation in the properties of mortars as a result of the introduction of various additives. It has been shown that admixtures can be effectively used to alter the properties of a curing mortar. The effects of the additives on the curing characteristics of these mortars (curing rate and compressive strength) may be related to their density, porosity and structure. These effects appear to be related to the admixture concentration. It has been shown that the changes are more apparent when the concentration of the additive is small. Increasing the proportion of an additive may have the effect of saturating the hydration reaction. The results obtained using ultrasonic technique in comparison with the mechanical test was within 3.16% percent error, this falls within the acceptable limit of 20% according to BS 4408 as reported by Olowofoyeku Adeoye M. and Olutoge Festus A. [130a]. From these results, it has also been demonstrated that ultrasound can be successfully used to determine the compressive strength of concrete from an early age. In the construction industry, the ability to pre-determine the strength of concrete

through modelling this way may reduce the time spent waiting for concrete to set to obtain certain strength. Thus a better streamlining of work and increased production can be achieved. Since ultrasound testing equipment is lightweight and easy to operate, it is appropriate for on site industrial applications.

The work has demonstrated that strength depicted in the curing curve for a sample is dependent on the composition and not on the size of the block. Thus each individual curve is a model characteristic of the concrete block. In mass production of blocks this model can be utilised efficiently, non-destructively, and safely to control the production.

CHAPTER 6

6.1 AE Monitoring of Concrete Blocks Containing waste materials as aggregates under Compressive Load

The fundamentals of the acoustic emission technique have been described in chapter 4. AE is a passive technique, unlike the ultrasound testing which require an input of external source of mechanical energy (ultrasound): for example in order to determine the compressive strength or micro-structure, a beam of ultrasound of desired frequency is utilised to interact with the material to provide the relevant information. In the case of AE, under stress (mechanical, thermal, chemical etc.) the material undergoes deformation producing wave energy. These waves are captured and analysed to characterise the deformation. The objective of this work described in this section is to investigate the micro-structural changes occurring during compressive loading.

Three sets of samples were tested and each set contained samples of plain mortar, mortars with glass aggregates and mortars with rubber aggregates. In total nine samples were tested, typical results of one set is shown in figures 6.1, 6.2 and 6.3. All samples were subjected to compressive loading. The samples were tested in the original condition as taken out of the mould. The Vallen AMSY4 AE system was employed to monitor the failure behaviour of the blocks under load.

For each test the AE system parameters were set up and auto-calibration was carried out to check that both sensors are receiving the signals with similar sensitivity.

The AE results monitored during compression tests for plain mortar, mortars containing glass and rubber aggregates respectively are shown in figures 6.1, 6.2 and 6.3, a (i and ii), b (i and ii) and c (i and ii).

The various recorded AE signal parameters shown in the figures 6.1, 6.2 and 6.3 respectively are: (a) (i) amplitude against time (green) versus load (red curve), (ii) x-location against time (blue dots) versus load (red curve); (b) (i) Location against amplitude (green dots) versus energy (yellow) and (ii) Energy against time (yellow dots) versus load (red curve); and (c) (i) Duration against time (light blue dots) versus load (red curve) and (ii) 3-D plot of X-location against time versus hits (red pyramids) recorded during the test.

i) Plain Mortar

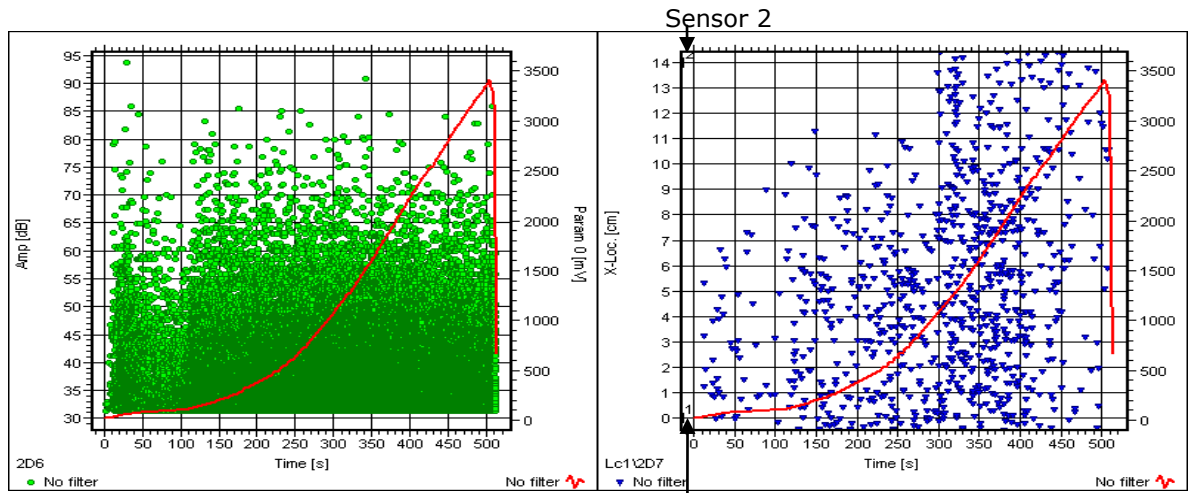
Figure 6.1 (a) (i) shows that the load on the specimen increases linearly from 150 seconds onwards reaching a maximum of 3400 mV at 520 seconds. During this period, random events with peak amplitude below 90 dB occurred. More prominent events were recorded at 250, 350 and 450 seconds. Before the load drops, an event occurred indicating the final fracture of the block.

Figure 6.1 a (ii) shows location of events with time. The located events are distributed throughout the block during the period 250 seconds and 350 seconds which are possibly related to material crumbling under compression generating cracks.

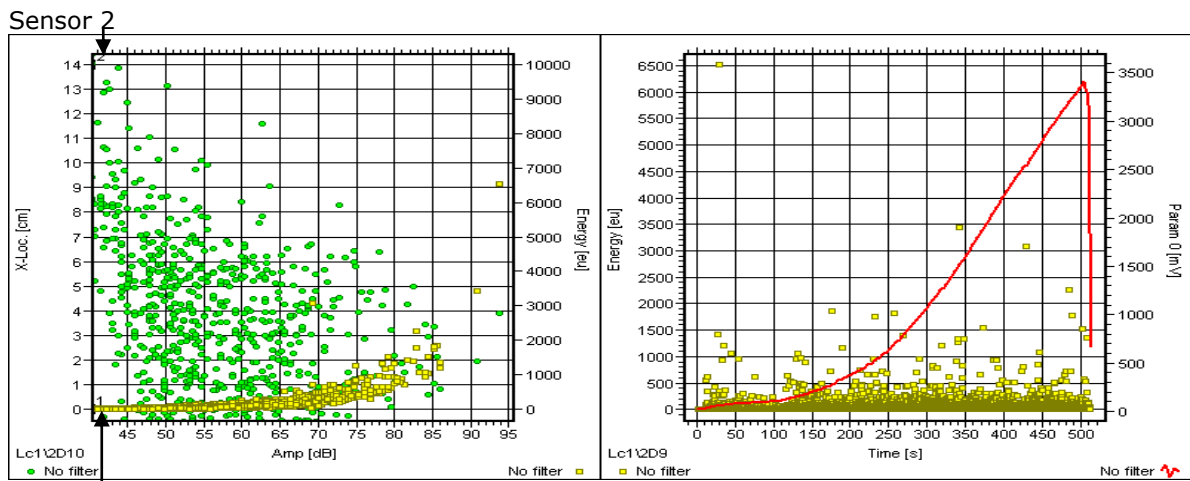
Figure 6.1 (b) (i) shows location versus amplitude versus energy. It is apparent that events with higher peak amplitudes (60 dB - 85 dB) possessing higher energy occurred mostly in the location 0-7 (close to sensor 1) of the specimen. The damage is confined to central and sensor 1 region.

The higher peak energy possessing higher event duration took place during 250-450 seconds (see figures 6.1 (b) (ii) and (c) (i)). This indicates that the block has suffered damage during this period but continued to carry the load reaching the maximum and then suddenly drops at 520 seconds.

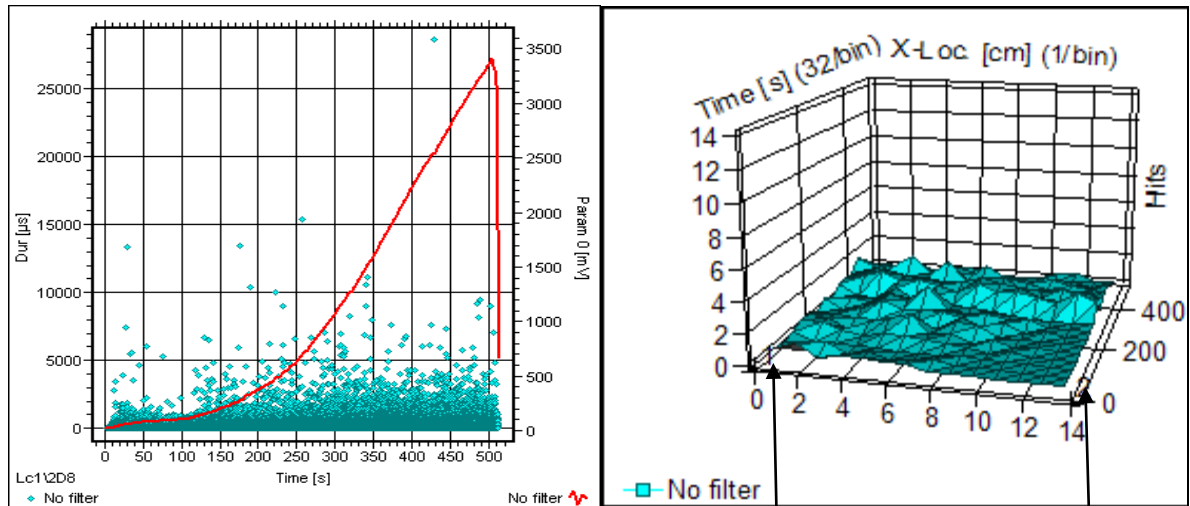
Figure 6.1 (c) (ii) depicts the localised events which are related to damage inside the block. As seen in figure 6.1 (b) (i), most of the hits were recorded towards sensor 1 i.e. 0-7 cm indicating deterioration of the region.



a) (i) Amplitude (dB) vs Time (s) vs Parametric load (mV) (ii) X-Location (cm) vs Time (s) vs Parametric load (mV)



b) (i) X-Location (cm) vs Amplitude (dB) vs Energy (μJ) (ii) Energy (μJ) vs Time (s) vs Parametric load (mV)



c) Duration vs Time (s) vs Parametric load (mV) (ii) 3-D plot of Time (s) vs X-Location (cm) vs Hits



 AE Amplitude
  AE Parametric Load
  AE Activities
  AE Energy
  AE Duration
  Hits

Figure 6.1: AE Plots for Plain Mortar under Compressive Load

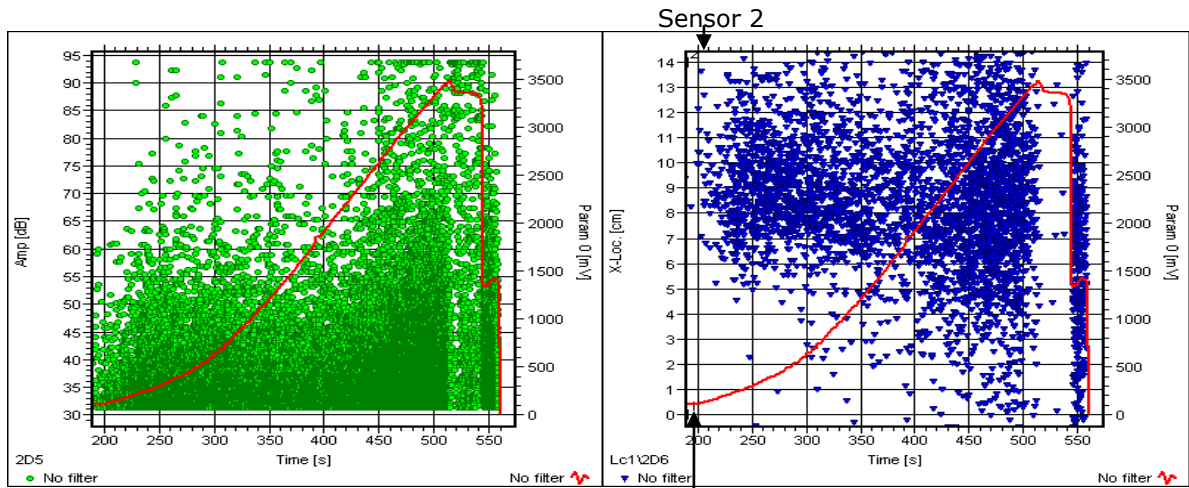
ii) Glass Aggregates

Figure 6.2 (a) (i) shows distribution of amplitude versus time against load. The load gradually increases reaching a maximum value of 3600 mV at 520 seconds. Then the load drops to 3470 mV and remains at this value for about 20 seconds and then sharply drops to 1400 mV. The load rises slightly before dropping to final failure. The recorded amplitude show several events occurring in the sample with the increase of load. The events taking place during 450 seconds and 518 seconds are of higher peak amplitude $>$ or $=$ 95 dB. The events during 518-548 seconds are less frequent but mostly of high peak amplitude. These load drops and events indicate that under stress, glass aggregates are offering resistance to extension/propagation of damage. This resistance is less, not noticeable in the plane concrete block.

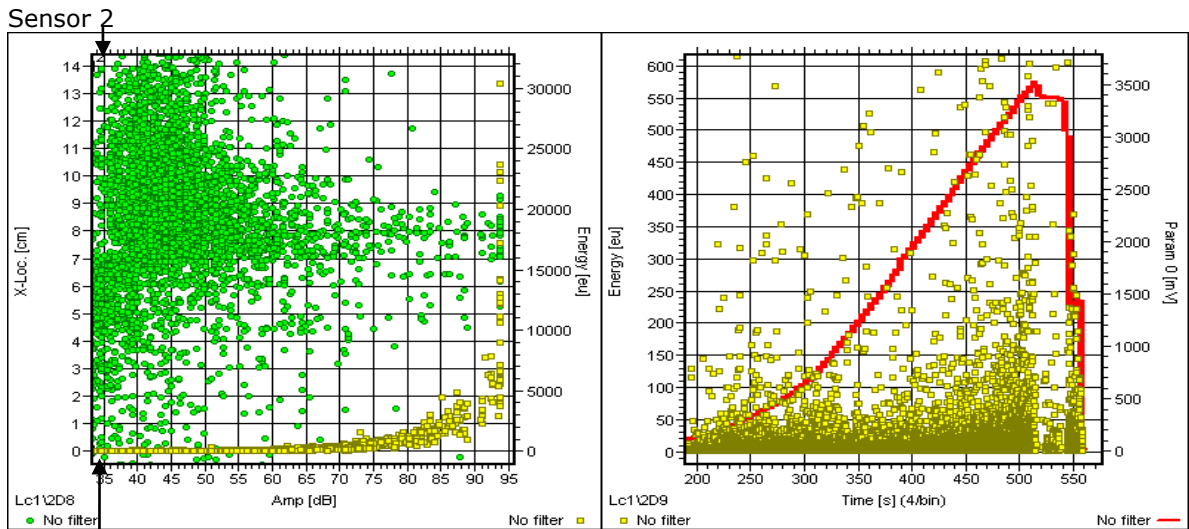
Localised events with time against load are shown in figure 6.2 (a) (ii). Most of the events are located in the central region and near sensor 2. Very few localised events were recorded during 518-548 seconds. It appears that the glass aggregates were blocking the cracks propagation. Once the resistance is overcome the block failed. From the location against amplitude versus energy plot in figure 6.2 (b) (i), it is apparent that the most events of low amplitudes ($<$ 55 dB) possessing lower energy occurred in the central region (7-10 cm) of the block.

The high energy possessing high duration events took place during 400 and 520 seconds. This indicates that the cracks had to overcome major obstacles (glass aggregates) during this period. The higher amplitude and energy events are related to higher duration level indicating crack jumps or resistance to crack propagation, see figure 6.2 (b) (ii) and (c) (i).

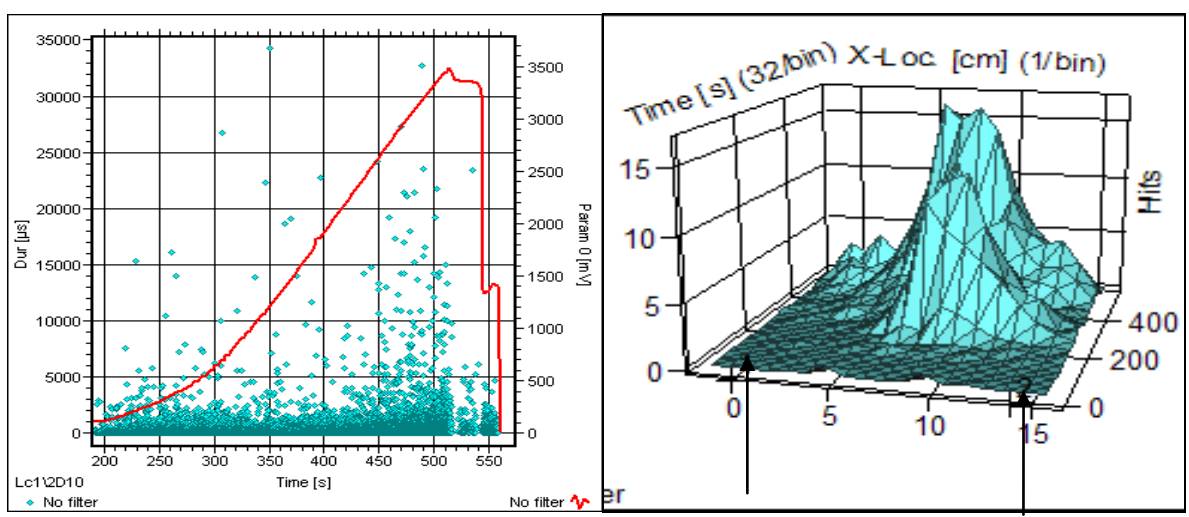
Figure 6.2 (c) (ii) depicts the localised events which are related to damage inside the block. Most of the higher number of hits occurred towards 6-14 cm region, i.e. sensor 2, indicating major damage in this zone.



a) (i) Amplitude (dB) vs Time (s) vs Parametric load (mV) (ii) X-Location (cm) vs Time (s) vs Parametric load (mV)



b) (i) X-Location (cm) vs Amplitude (dB) vs Energy (μeV) (ii) Energy (μeV) vs Time (s) vs Parametric load (mV)



c) (i) Duration vs Time (s) vs Parametric load (mV) (ii) 3-D plot of Time (s) vs X-Location (cm) vs Hits

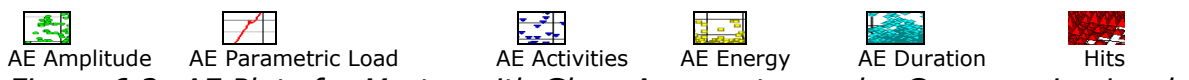


Figure 6.2: AE Plots for Mortar with Glass Aggregates under Compressive Load

iii) Rubber Aggregates

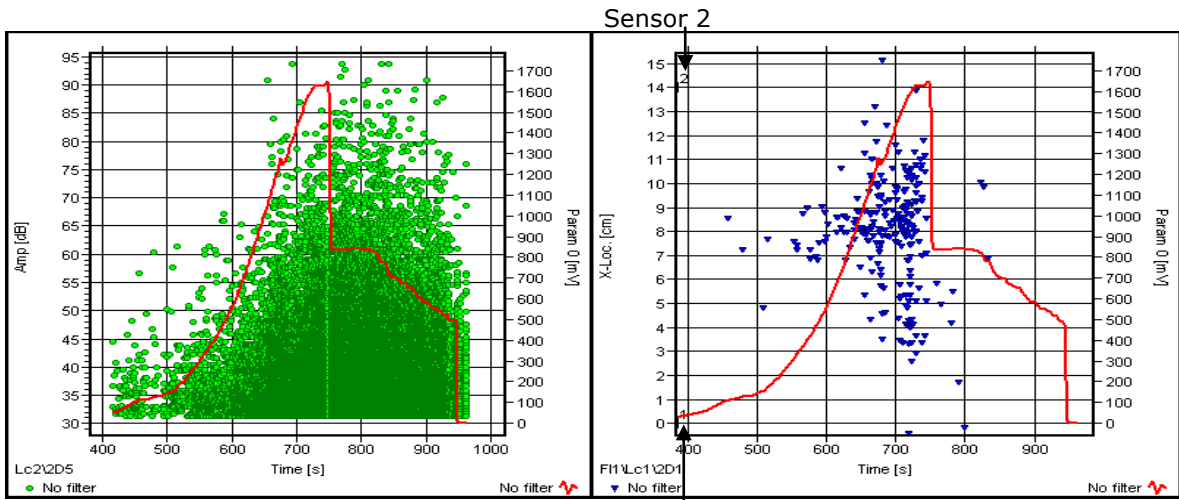
Figure 6.3 (a) (i) shows distribution of amplitude versus time against load. The load rises steeply starting at 550 seconds reaching a value of 1600 mV at 670 seconds. Very few events of amplitude (higher than 70 dB) events are recorded during this period. The load remains at this value for a duration of 30 seconds then sharply drops to 810 mV. It remains constant for about 60 seconds then gradually drops to a value of 480 mV and then sharply drops to a minimum at final failure of the block. The localised AE activities are shown in figure 6.3 (a) (ii) which are very few in number when compared with plain mortar and mortar containing glass aggregates. Most of the activities are seen in the central region, i.e. 5-10 cm.

The addition of rubber changed the AE behaviour of the sample and weakened the sample. This can be seen in figure 6.3 (b) (i) and (ii), where most of the high amplitude events possessing higher energy are mainly below 70 dB and 1000 e μ .

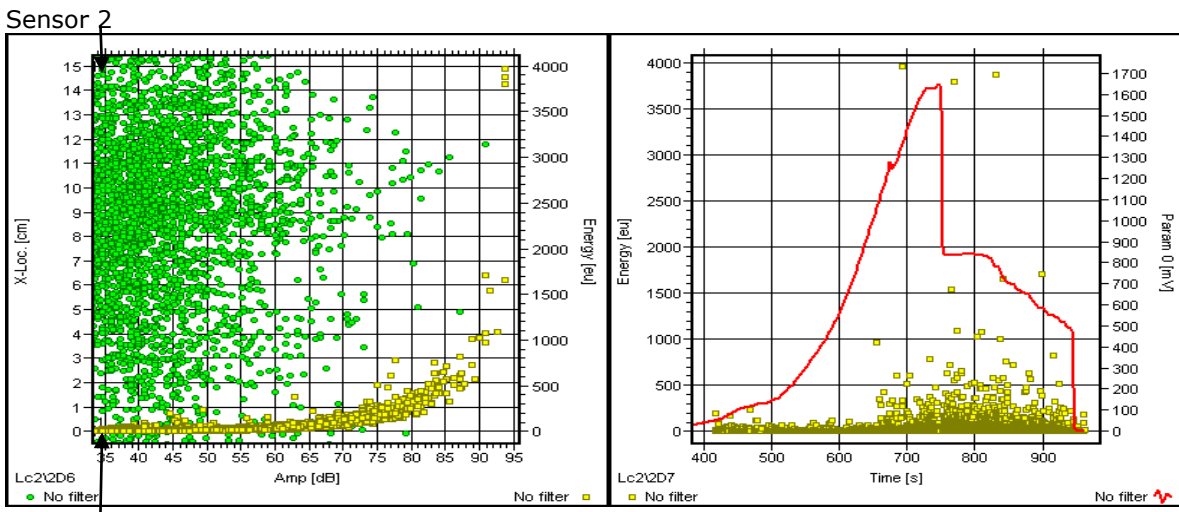
The biggest energetic event takes place at the time of failure with amplitude of 85.5 dB, and an event duration (348.2 μ s), figures 6.3 (b), (i), (ii) and 6.3 (c) (i). This is where a crack deflection may have taken place probably due to a rubber aggregate. The duration events are of short duration (highest being 5500 μ s) just before the first load drop as seen in figure 6.3 (c) (i). The type of failure was probably caused by the content of rubber. The failure load was half the glass aggregate sample, this also coincides with the lower number of AE activities, especially around the lower amplitude region.

Figure 6.3 (c) (ii) shows 3-D representation of hit activity with location and time showing relatively less activity and mostly confined to central region of the specimen. The AE activity picks up at around 600 seconds and number of hits then increases particularly around 740 seconds. From the behaviour of rubber based mortar under compressive load two observations can be made:

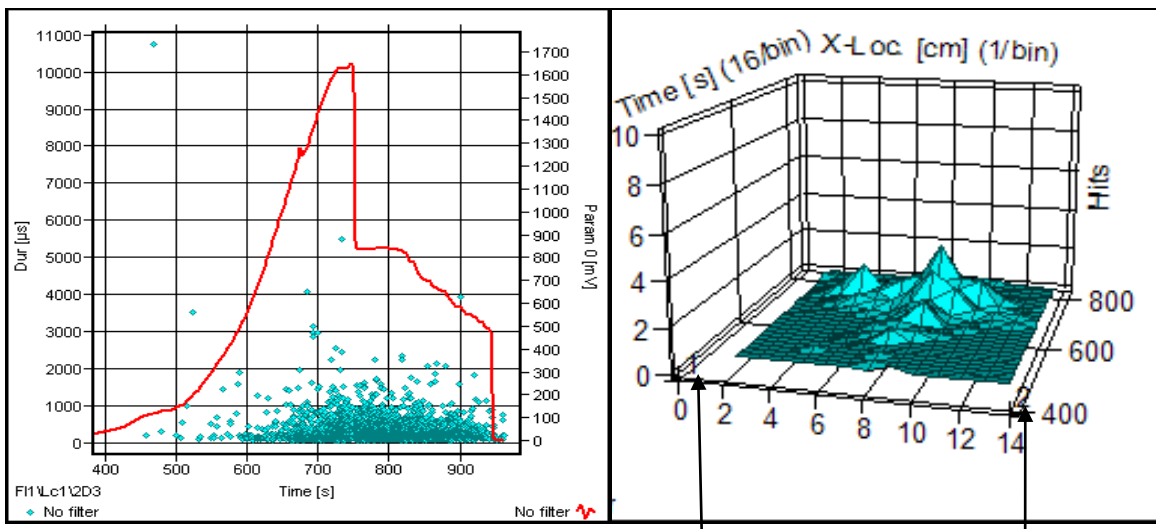
- a) Specimen is weaker in strength due to poor bonding between rubber and cement matrix;
- b) Rubber aggregates were relatively larger in size than glass aggregate and were more elastic, hence their resistance to propagation of cracks /jump is less effective.



Sensor 2
 a) (i) Amplitude (dB) vs Time (s) vs Parametric load (mV) (ii) X-Location (cm) vs Time (s) vs Parametric load (mV)



Sensor 1
 b) (i) X-Location (cm) vs Amplitude (dB) vs Energy (eJ) (ii) Energy (eJ) vs Time (s) vs Parametric load (mV)



Sensor 1
 c) (i) Duration vs Time (s) vs Parametric load (mV) (ii) 3-D plot of Time (s) vs X-Location (cm) vs Hits



AE Amplitude AE Parametric Load AE Activities AE Energy AE Duration Hits

Figure 6.3: AE Plots for Mortar with Rubber Aggregates under Compressive load

6.2 Summary

The results obtained clearly reflect the influence of aggregates on the behaviour of concrete under compressive load. A comparison of the 3-dimensional plots of AE activities of the samples shows clear differences of fracture nature. The variation of hits is seen to have a close correlation with the compressive strength for the sample containing glass aggregates. The highly toughened nature of the sample containing glass aggregates and the detrimental effect on the toughness due to the addition of rubber aggregates is visible from the higher amplitude and energy profile of the respective multi-plots. Therefore, the AE results obtained from this investigation indicate that the glass aggregates prevented the occurrence of micro-cracks with improved compressive strength and bonding.

The sample with glass aggregates appeared to prevent or arrest the crack growth evidenced by less activities of smaller amplitude recorded before failure compared to the plain sample. The events of larger amplitudes are more common in this specimen than the plain sample, this may be attributed to crack bridging, crack deflection, and de-bonding of glass aggregates.

Fewer AE activities were recorded in the samples with rubber content, but the elastic behaviour is higher than the sample with glass content, since the failure is not as abrupt as the other two. Observations made from the results indicate that the first and second failure events are due to propagation and joining of micro-cracks.

The elastic nature of rubber has arrested the propagation of micro-cracks and made it difficult to form bigger crack. This is evidenced by a few high amplitude events and shorter event duration.

It can be concluded that the glass aggregates provide better toughening than rubber aggregates under compressive load, but that rubber helps to avoid complete failure initially. This sample with glass aggregates demonstrate concentrated AE activity in the central region with improved strength and toughness of the material. The glass aggregates made a big contribution to the toughening of the sample, and the rough surfaces of glass aggregates provided good bonding with the cement matrix structure, this is indicated by high amplitude and energy events, in figures 6.2 (a) (i) and 6.2 (b) (i).

The results obtained from the AE experimentation showed that each sample exhibited its distinct behaviour when loaded under compression. The sample with glass content had more activity recorded as shown in table 6.1, with higher number of events having bigger amplitudes indicating strong resistances to cracks which either prevent or arrest the crack growth.

Table 6.1: Type of mechanism contribution made by aggregates under compressive load

<u>Samples</u>	<u>Number of amplitude events >75 dB</u>	<u>Number of energy events > 1000 eμ</u>	<u>Mode of changes in Properties</u>	<u>Contribution made by aggregates</u>
Plain Mortar	23	9	Normal	Normal Plain Mortar
With Glass Aggregates	80	> 50	Provided bonding with cement structure;	Increased toughening
With Rubber Aggregates	20	15	Arrested the propagation of micro-cracks;	Increased Elasticity

The sample with rubber content showed elastic behaviour where the failure under load is not as abrupt like other samples. The elastic nature of rubber arrested the propagation of micro-cracks and made it difficult to form bigger cracks. The capacity to hold the load to prevent sudden failure and arresting the propagation of micro-cracks makes samples of this type suitable to withstand cyclic stresses.

For all the specimens, AE activities dominate the characteristics to evaluate mechanical damage in concrete. Low amplitude, shorter duration events occurred at low load levels; higher amplitude and longer duration events occurred as load level increases.

AE monitoring of concrete under compressive load provide valuable insight into failure behaviour. The blocks showed no visual damage up to the failure point thereafter cracks appear with corresponding load drops leading to final failure. AE activity relates damage to the load and time of occurrence.

6.3 Interfacial Bonding between Glass Aggregates and Cement

The interest in quasi-brittle fracture stems from the ability of refractory technology to engineer micro-structures that allow stable growth of damage. This can give improved thermal shock resistance as well as non-linear stress-strain curves in tension. Originally, it was thought that this improvement was principally promoted by isolated bonding between the large material grains, but it became clear that micro-structural residual stresses were important, as were grain bridges knitting the crack together. The key to transferring this mechanism for fired ceramic to cement based materials is the development and control of residual stresses within the mortar [115-118].

Despite the importance of the interfacial zone on the overall short and long term performance of cement based composite materials, the nature of the interface and the interfacial bond is not fully understood. Moreover, the determination of the quality of the bond between aggregate and the matrix is rather difficult and no standardised method is available. Thus, there is a need to undertake research that aims to explore the properties and the behaviour of the interfacial zone between aggregate particles and matrices in concrete.

The purpose of this work is to investigate the interfacial bonding that exists between cement matrix and aggregate using flexural destructive tests. Acoustic Emission signals are monitored and related to the microscopic and macroscopic changes that are taking place in the material.

Loading causes damage in the matrix and interfacial bonding between the aggregates and the matrix (the strength or the weakness of bonding) which is broken causing the AE activities. The amount of aggregates and the size of aggregates have a direct relation to the interfacial strength / weakness, which in turn has an effect on the strength of AE signals / spread of AE activities while the sample or the structure is under tension. This means that AE signals have a direct relation with the damage occurring in the structure and at micro-structural level the bonding/de-bonding/pull-out events are linked to the intensity of AE signal parameters.

No standardised method is available to investigate the cracking mechanism, except visually inspection of the fractured surfaces after the test. With the aid of AE, the crack initiation and propagation events can be studied during the test. The bonding strength plays a significant role in toughening the specimen. This has been reported in earlier work by I. J. Merchant, et. al [118] which suggested that the bond between the aggregate and the matrix can control the crack path and consequently the toughness.

The three-point bend test enables the application of large forces, which can generate cracks in a material. If the load is sufficient then the test piece will fracture in failing to cope with the strain. The three-point bending test allows the scientist an insight into the types of forces, which are in action within the material and how it is bound together.

In total ten (two sets of five) samples were manufactured from two moulds of sizes $(140 \times 70 \times 70) \text{ mm}^3$ and $(210 \times 70 \times 70) \text{ mm}^3$ respectively. The glass aggregates were produced by breaking smooth glass slides. Pieces of glass in the range 1-2 mm and 2-4 mm were separated.

These samples were un-notched in order to monitor crack generation and propagation within the material and subjected to flexural load as described in section of 4.5 of chapter 4. AE monitoring was carried out using the AMS4 Vallen System.

The measured load at breaking point using the three-point bend test is given in table 6.2. It is observed that the flexural strength varies, because concrete is weak in tension compared to compression and the concentration of aggregates varies along the specimen blocks, whereas the compressive strength of concrete is consistent.

Table 6.2: Load results at breaking point of three point bend test

<u>Block Name</u>	<u>Load (kN) at Breaking Point</u>
Plain Concrete (BD1) Small Sample	25.40
40g Powdered Glass (BA2) Small Sample	15.5
40g 2-1mm Glass Aggregates (BC1) Small Sample	25.41
40g 4-2 mm Glass Aggregates (BE1) Small Sample	22.25
80g 4-2mm Glass Aggregates (BB2) Small Sample	22.84
Plain Concrete (BG1) Large Sample	12.54
60g Powdered Glass (BI1) Large Sample	11.48
60g 2-1mm Glass Aggregates (BF1) Large Sample	7.15
60g 4-2mm Glass Aggregates (BH1) Large Sample	8.48
120g 4-2mm Glass Aggregates (BJ1) Large Sample	9.97

6.4 Three-points Tests on Smaller Blocks

In order to investigate the fracture behaviour of concrete under flexural loading, AE monitoring was carried out. For each test the AE system parameters were set up and also auto calibration was carried out to that check both the sensors are responding to the signals with similar sensitivity. The flexural tests were carried out on Denison load frame. The rollers were arranged and test parameters were set up. Once the load on the specimen starts to rise, the AE

system is switched on to recording mode. Various AE parameters and signal waveforms were recorded. For the purpose of comparison, the results of the AE multi-plots of typical concrete samples with and without aggregate additives are shown in figures 6.4-6.13.

Each figure displays the following 6 parameters:

- a) AE event amplitude and load against time;
- b) AE location and load against time;
- c) AE event duration and load against time;
- d) AE location and duration events against amplitude;
- e) Energy and Duration against Load; and
- f) 3-D plot of Location and Time against Hits.

For example the AE plot of amplitude and load distribution with time for the plain concrete sample (figure 6.4a) indicates two distinct regions. Region I has non-linear characteristic which is apparent in all samples tested under similar loading condition. Region II is the linear loading region with increasing AE activity with load and time. There are unique changes in this region, which reflects the presence of and type of aggregates in the sample. These changes are discussed for each sample and a final comparison of the results is then carried out.

6.4.1 Sample BD1: Plain Concrete

The AE results obtained for a plain sample under bending tests are shown in figure 6.4 (a-e). In part a) the AE plot of Amplitude (dB) versus Time (s) versus Load Parameter (mV), (location load 25.4 kN), are shown. Relatively few AE events are observed during the first 60 seconds and these events are of low amplitude and short duration events. Larger crack events start to develop as a result of increased load when the load curve becomes linear and the AE activities occur with large amplitudes and longer duration. The sample fails at (135) seconds after the initiation of the test, at location 9.59 mm, producing a large amplitude event of 82.5 dB. A number of high amplitude and longer duration events were recorded as the sample approaches near failure as shown in figure (d) and (e).

During the time 60-110 seconds, low load level, 35-60 dB amplitude and 0-400 μ s duration events occurred. This is probably related to the load bars contact settling on the sample. As the load increases, the AE activities increase with amplitudes >70 dB and durations up-to 1000 μ s, and these events suggest larger cracking events in the sample. The energy and hits rate increase with time as the cracks approach to final failure as shown in figures (e) and (f).

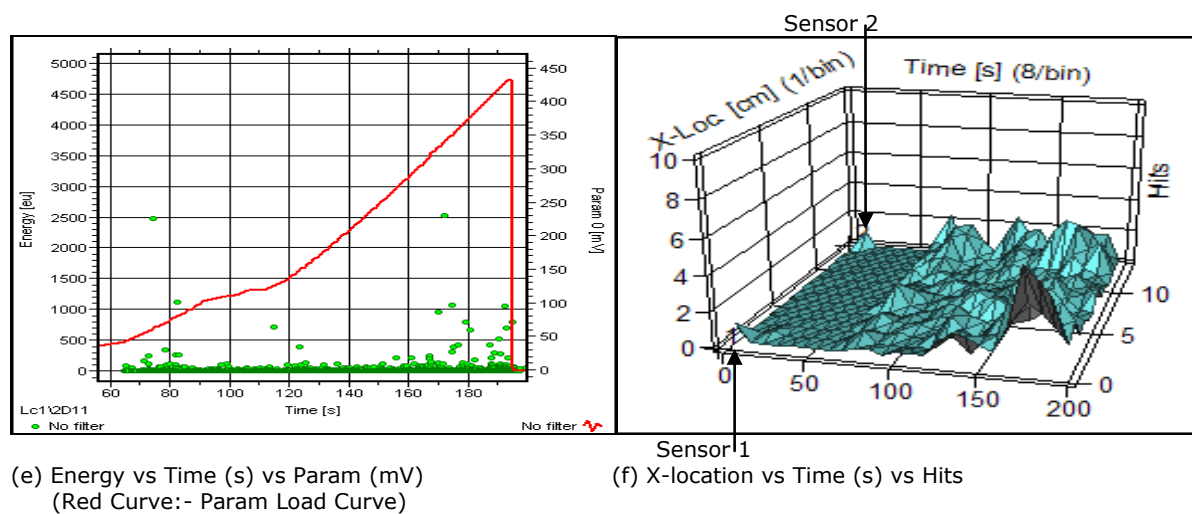
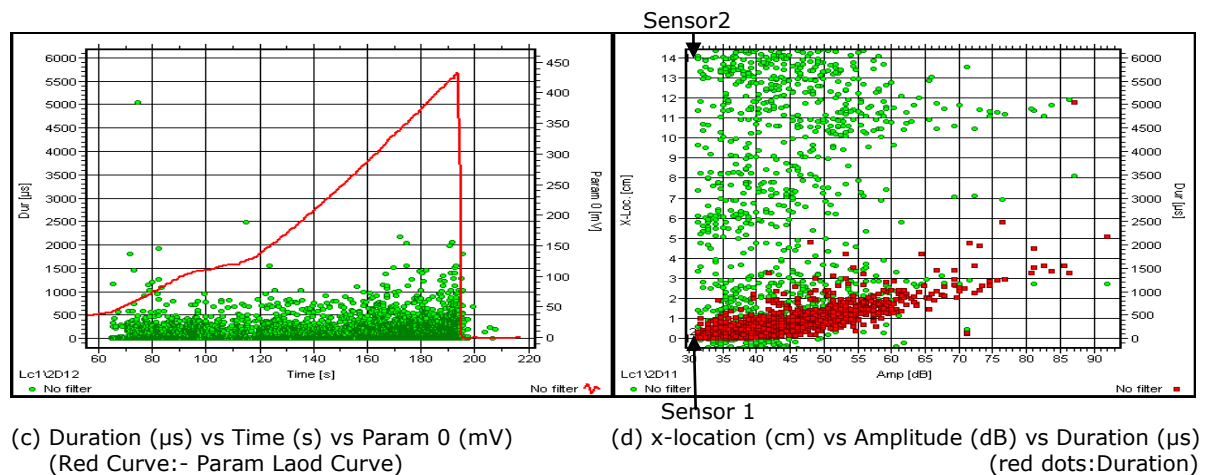
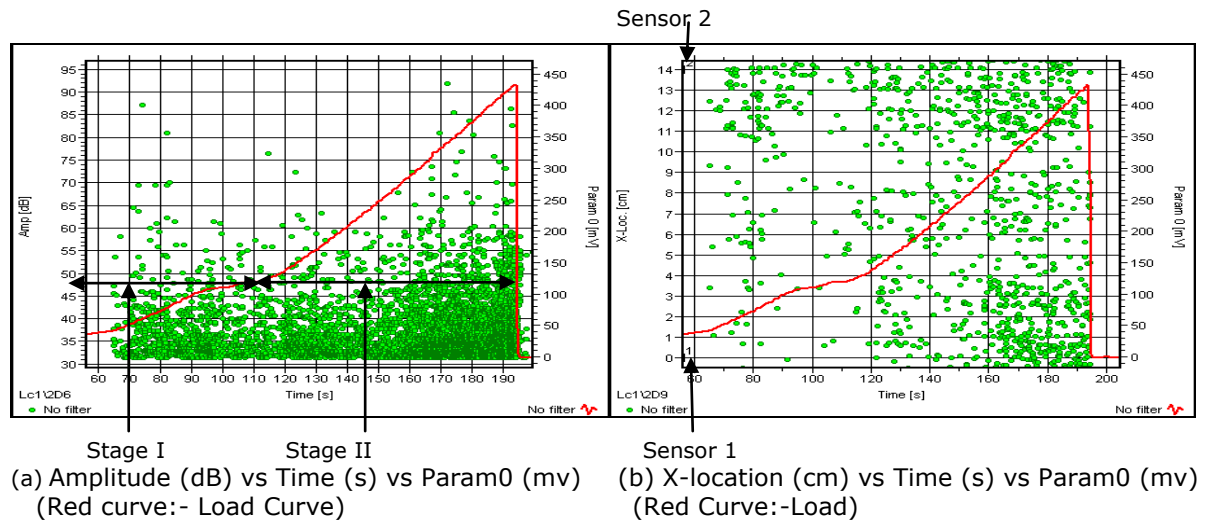


Figure 6.4:- AE plots for sample BD1 (plain concrete)

6.4.2 Sample BA2: Powdered Glass

Figure 6.5 shows the results for the flexural test on specimen containing powdered glass aggregate, 40g, <1mm which lasted for approximately 140 (i.e. 100-240) seconds. Initially activities were of low amplitudes, short duration, (< 60 dB and < 600 μ s), as shown in figure 6.5 (a-f). In the linear region of the load, curve between 180 and 235 seconds, the micro-cracks may be developing to form bigger cracks, leading to intermittent high amplitudes and long duration (>60 dB and >800 μ s). The sample eventually fails after 100 (235) seconds of the initiation of the test, with a 78 dB amplitude event with all energy events up-to failure (<600 e μ) as shown in figure (e). The low energy level events suggest that the cracks and the bonding between the cement matrix and aggregates are weak. The numbers of hits are mainly located near the sensor 2 region as shown in figure (f) indicating that the failure is not due to large number of micro-cracks but a few intermittent cracks.

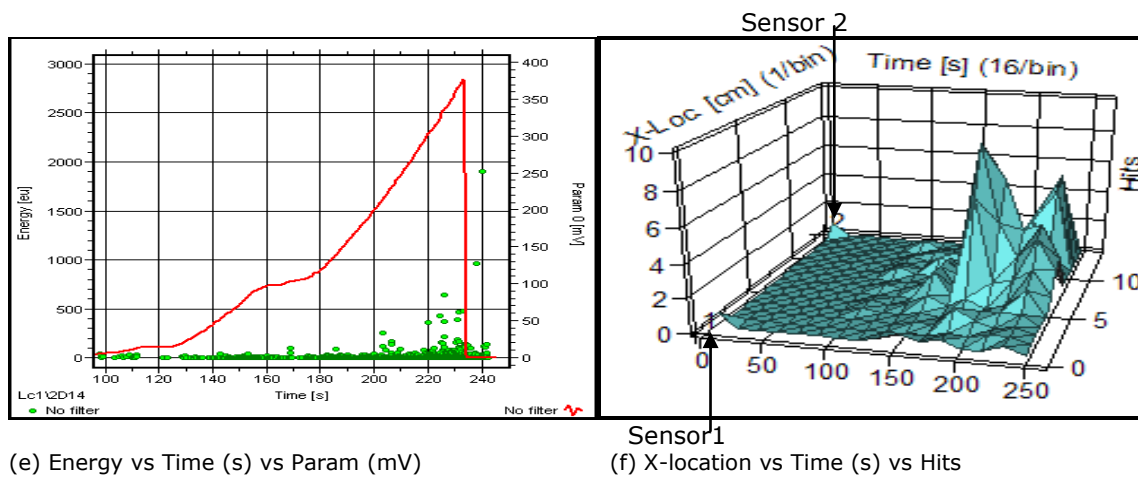
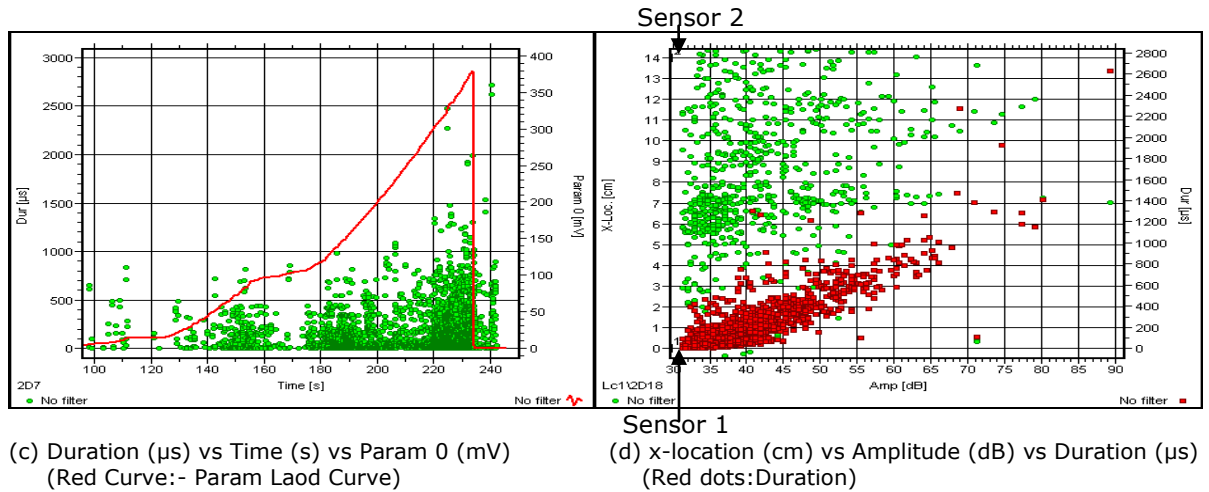
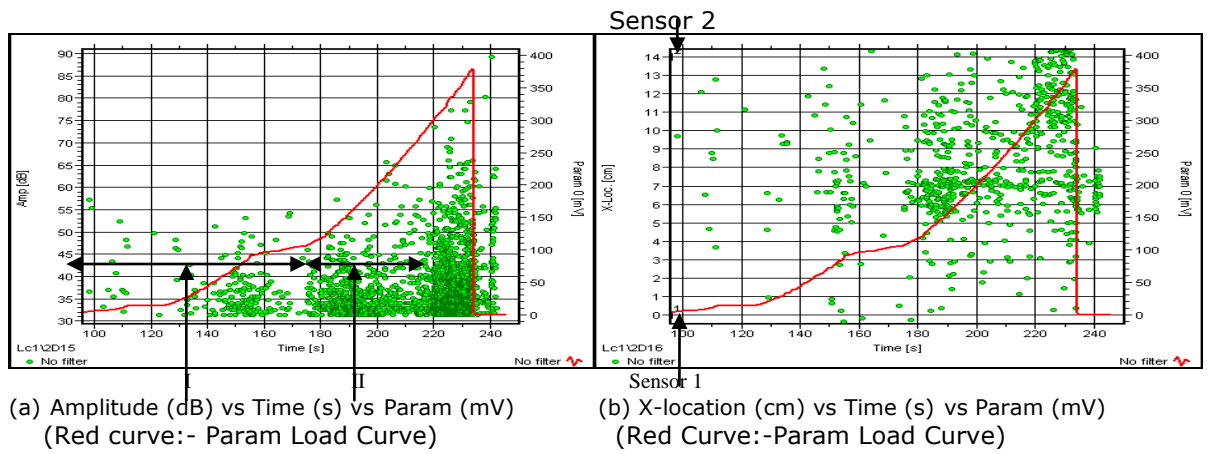


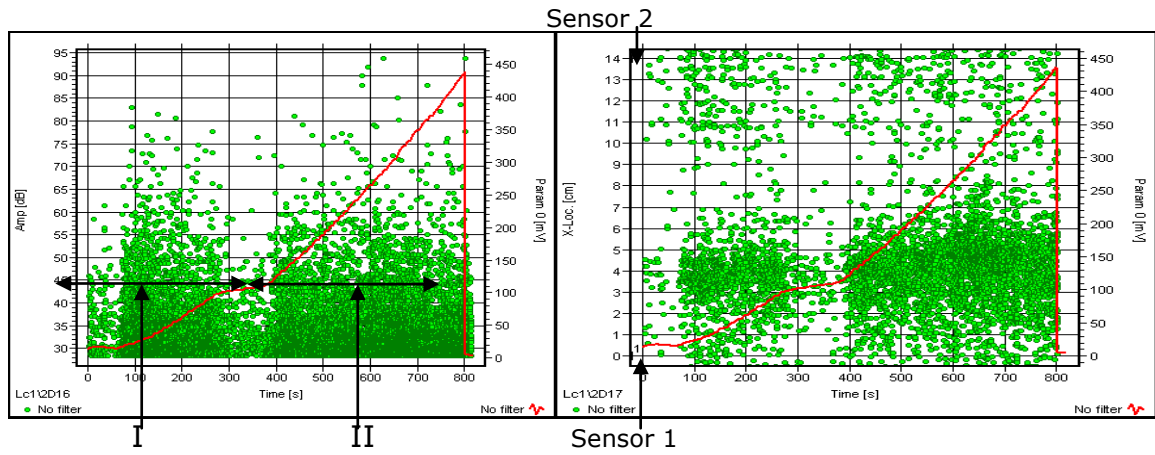
Figure 6.5:- AE plots for sample BA2 (containing powdered glass)

6.4.3 Sample BC1: 40 g 2-1 mm Glass Aggregates

This specimen exhibited AE activity during the test, which lasted for 800 seconds as shown in, figure 6.6 (a-f). It can be seen that the AE hits are very dense from the initiation of the test until the end. The activities are taking place with low and high amplitude; long and short duration events taking place throughout the test. This is an indication of crack arrests and de-bonding, micro-crack formation merging to form bigger cracks. Most of the de-bonding probably took place in the linear region of the load curve indicated by the activities of higher amplitudes and longer duration in this region. There is a reduction in AE reduction in AE intensity between 300 and 400 seconds.

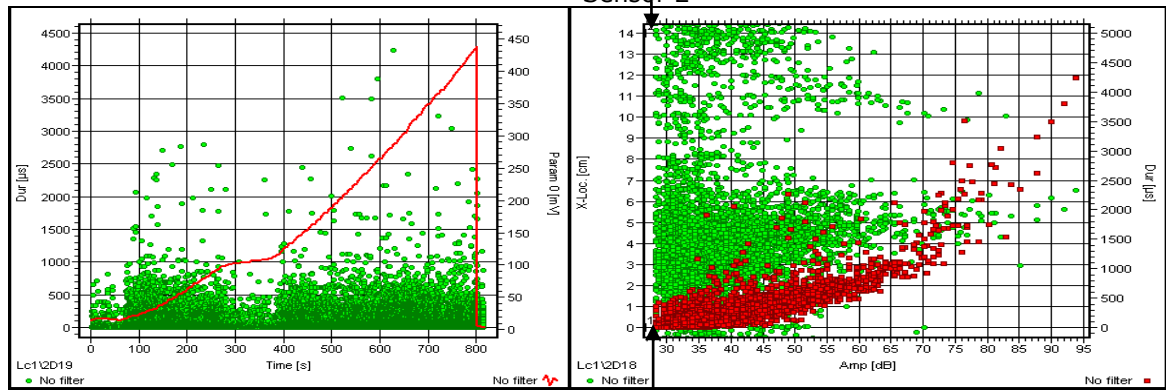
When compared with the plain concrete, the effect of glass bonding with the cement matrix can clearly be seen even from the beginning of the test, as a large number of events with high amplitudes (>60 dB) occurred. The amount of AE activities that took place also shows the high level of toughening exhibited by this specimen with a number of events with high duration (>1000 μ s) and high energy (> 1000 e μ) level (see figures 5.36 d and e).

As the specimen is a non-standard type (without notch) the AE events and hits are dominant in two regions of the specimen (see figure 6.6 d and f), mainly on the lower part of the graphs.



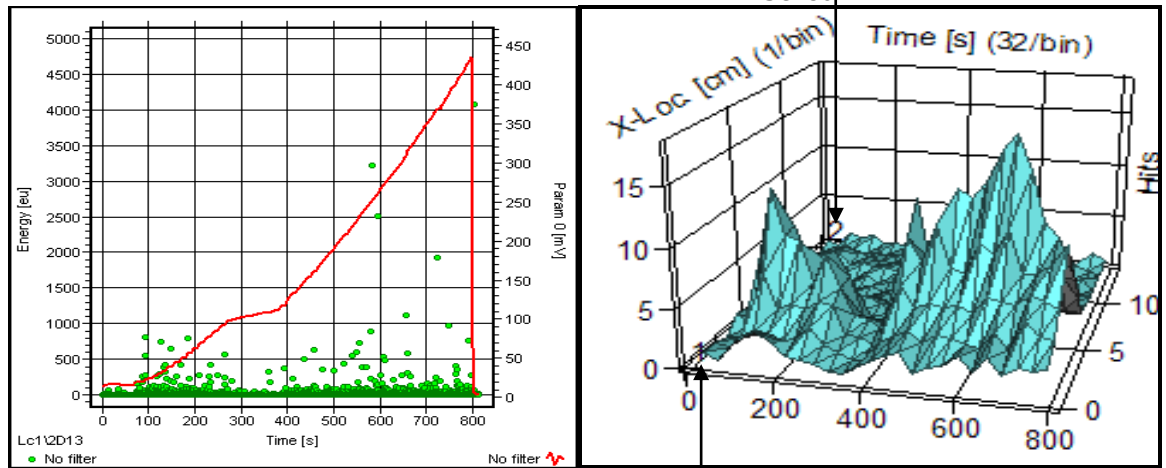
(a) Amplitude (dB) vs Time (s) vs Param (mV)
(Red curve:- Param Load Curve)

Sensor 1
(b) X-location (cm) vs Time (s) vs Param (mV)
(Red Curve:-Param Load Curve)



(c) Duration (μ s) vs Time (s) vs Param 0 (mV)
(Red Curve:- Param Load Curve)

Sensor 1
(d) x-location (cm) vs Amplitude (dB) vs Duration (μ s)
(Red dots:Duration)



(e) Energy vs Time (s) vs Param (mV)
(Red Curve:- Param Load Curve)

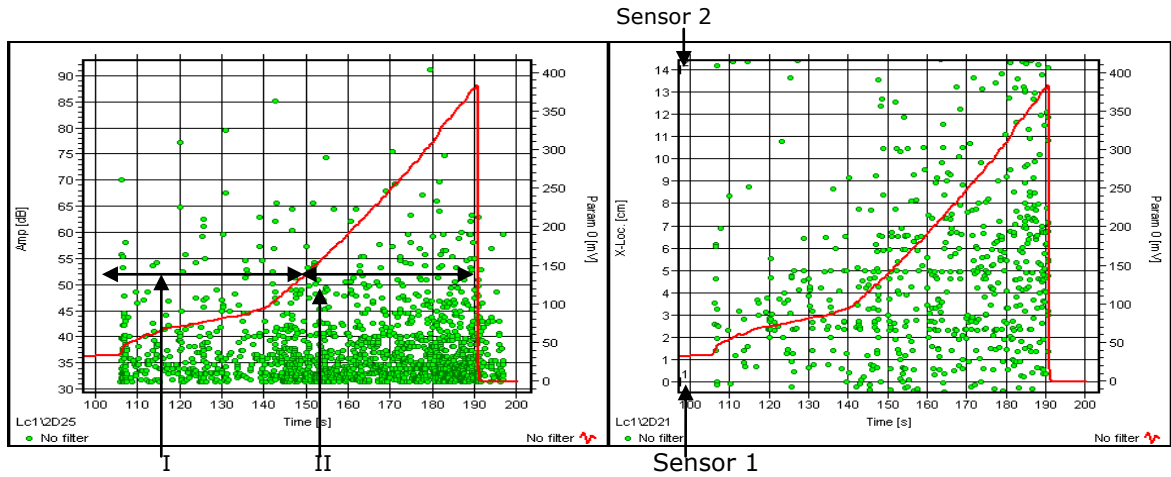
Sensor 1
(f) X-location vs Time (s) vs Hits

Figure 6.6:- AE plots for sample BC1 (with 40g 2-1mm aggregates)

6.4.4 Sample BE1: 40g 4-2 mm Glass Aggregates

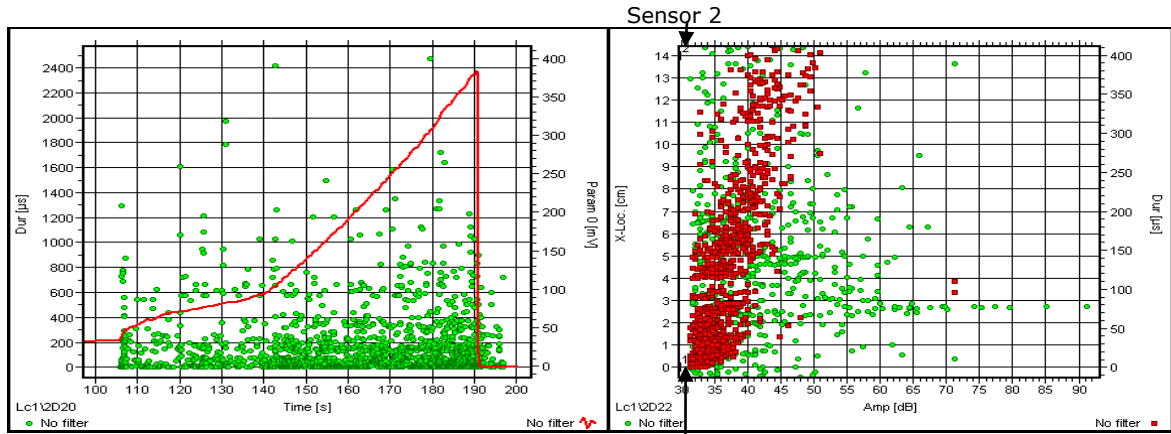
This specimen has the large glass particles with 40g 4-2mm glass aggregates which under load exhibited a lot of AE activities at low amplitudes (< 50 dB) and low event duration throughout the test as shown in figure 6.7 (a-f). From 140 seconds onwards, the parametric load on the sample was seen to increase linearly to 370 mV. As a result of de-bonding and micro-cracks development, bigger cracks formed and the sample failed. It is apparent that a comparison of 6.7 (d, e and f) with 6.6 (d, e and f) which shows the localised AE activities, energy events and hits in the sample, that the major damage is in two regions and that the number of events are fewer in the sample containing large size aggregates. The reason for this may be due to fewer numbers of inclusions in large aggregate sized sample.

A large smooth surface aggregate will offer less resistance to crack propagation than a small size aggregate. On a smooth surface the crack can easily move if the surface is rough than the crack movement will be restricted.



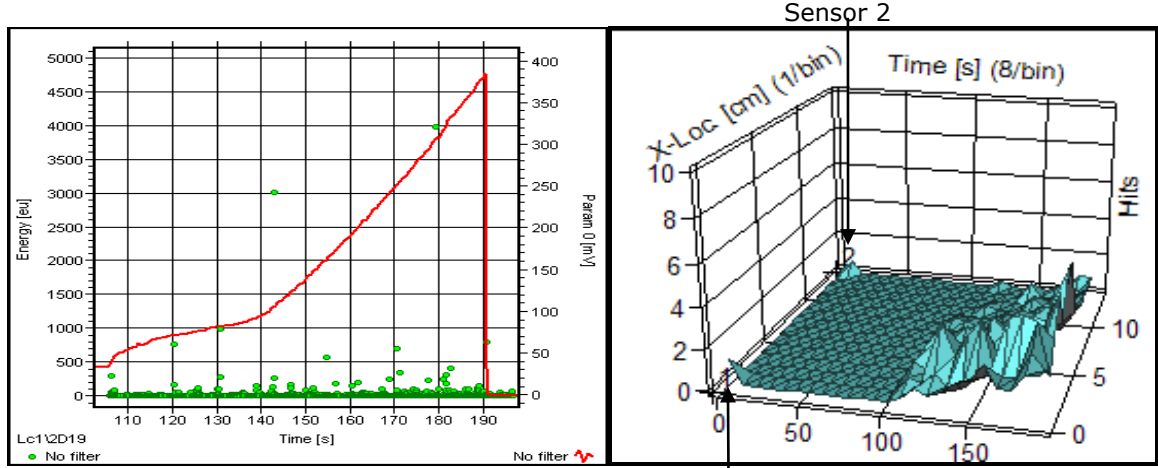
(a) Amplitude (dB) vs Time (s) vs Param (mV)
(Red curve:- Param Load Curve)

(b) X-location (cm) vs Time (s) vs Param (mV)
(Red Curve:-Param Load Curve)



(c) Duration (μ s) vs Time (s) vs Param 0 (mV)
(Red Curve:- Param Load Curve)

(d) x-location (cm) vs Amplitude (dB) vs Duration (μ s)
(Red dots:Duration)



(e) Energy vs Time (s) vs Param (mV)
(Red Curve:- Param Load Curve)

(f) X-location vs Time (s) vs Hits

Figure 6.7:- AE plots for sample BE1 (with 40g 4-2mm aggregates)

6.4.5 Sample BB2: 80 g 4-2 mm Glass Aggregates

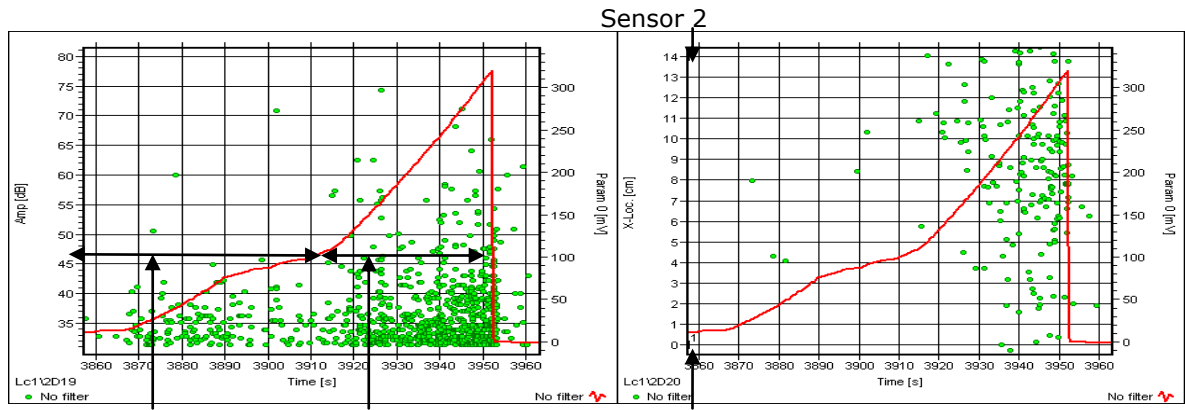
In this sample doubling the amount of glass aggregates added would increase the amount of inclusions. A comparison of plots 6.8 (a-f) with 6.6 (a-f), assuming equal number of inclusion indicates that the compactness of the two samples is different. This sample with larger size aggregate and more inclusions apparently has more un-bonded regions, hence demonstrating lesser toughening by fewer activities. This is supported by few small amplitude level and short duration events.

The AE activities of low amplitude and short duration during stage II (3910 seconds to 3952 seconds) is an indication of micro-cracks formation. In terms of toughening this sample is very weak, as indicated by fewer AE activities.

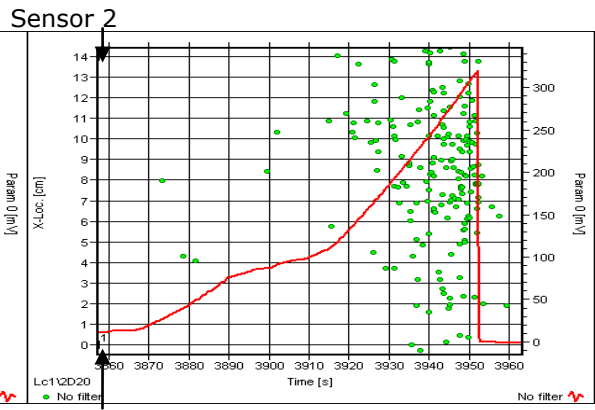
A number of possible reasons for this is:

- (a) Increasing the amount of aggregates from 40g to 80g has changed the cement-water ratio. If there is not enough water, hydration reaction will not be complete producing a weaker bonding.

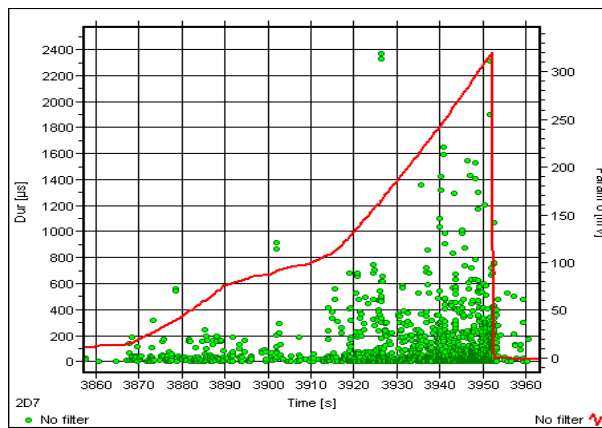
- (b) If weaker interfacial bonding leads free movement of cracks producing less energetic events.



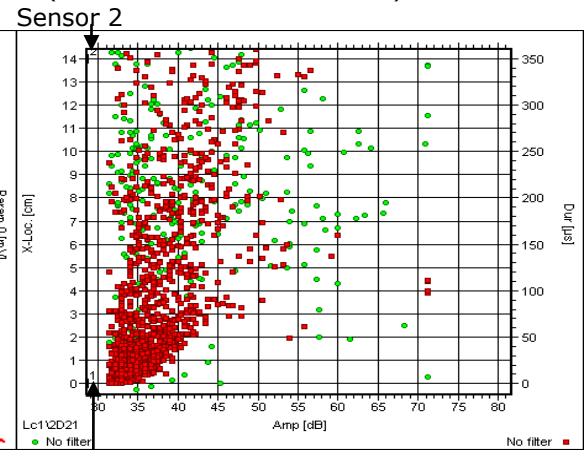
(a) Amplitude (dB) vs Time (s) vs Param (mV)
(Red Curve:- Param Laod Curve)



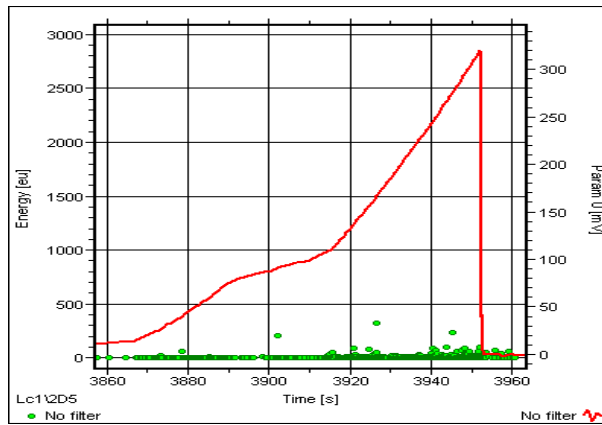
(b) X-location (cm) vs Time (s) vs Param (mV)
(Red Curve:- Param Laod Curve)



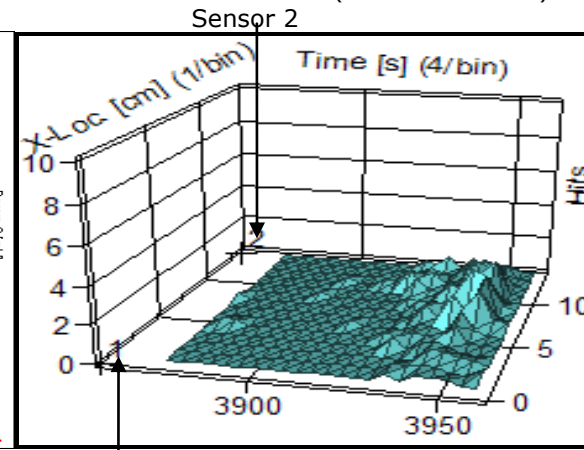
(c) Duration (μs) vs Time (s) vs Param 0 (mV)
(Red Curve:- Param Laod Curve)



(d) x-location (cm) vs Amplitude (dB) vs Duration (μs)
(Red dots:Duration)



(e) Energy vs Time (s) vs Param (mV)
(Red Curve:- Param Laod Curve)



(f) X-location vs Time (s) vs Hits

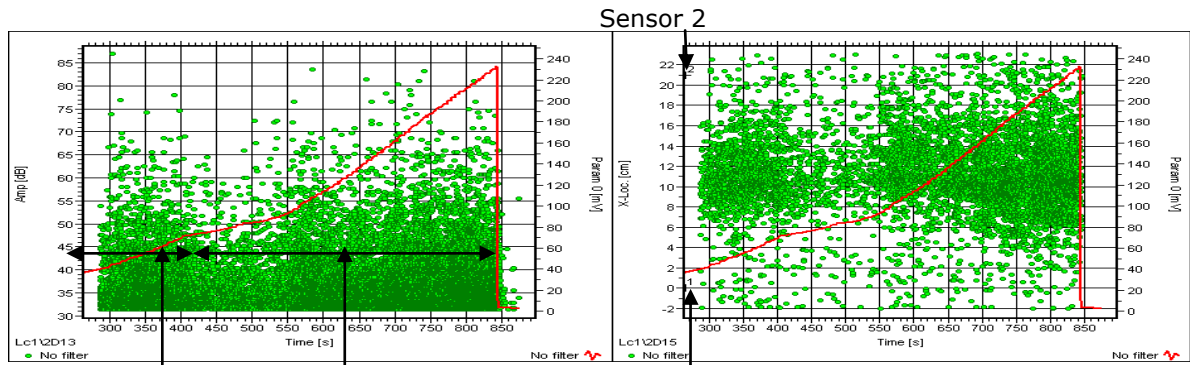
Figure 6.8:- AE plots for sample BB2 (with 80g 4-2mm aggregates)

6.5 Three-points Tests on Larger Blocks (210×70×70 mm)

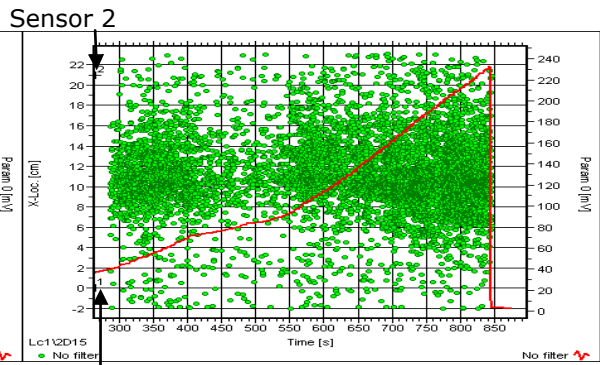
6.5.1 Sample BG1: Plain Concrete (BG1)

Figure 6.9 (a-f) shows recorded AE parameters for the plain concrete (non-standard sample block (larger size i.e. 210×70×70 (mm))). In the linear region (stage II) of the plot several intermittent high activity distribution are present indicating damage. These activities of peak amplitude >65 dB are of larger event duration and appear to be in the centre of the specimen. Figure 6.9 (b) and (d) show localised damage with an indication that sensor 2 picked up more events than sensor 1 (also shown with hits recorded in figure 6.9 (f)). It is apparent from figure 6.9 (a) that higher peak amplitude occurs in the central region. The crack initiates and propagates leading to fracture of the sample with events of longer duration and higher energy level (see figure 6.9 (c and e)). The nature of fracture sample and fracture surfaces are shown in figure 6.9 (g). The increased activities towards the final part of the test confirm that the critical crack growth occurs at this point.

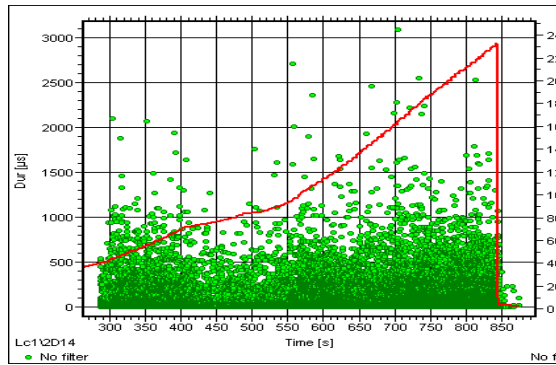
The plain concrete sample, has exhibited more AE activities than any other specimen, this may be due to the bars settling onto the specimen. The AE activities recorded during the loading condition of this sample follows a pattern similar to smaller plain mortar sample. The reason for increased activities may be due to the larger size of this specimen.



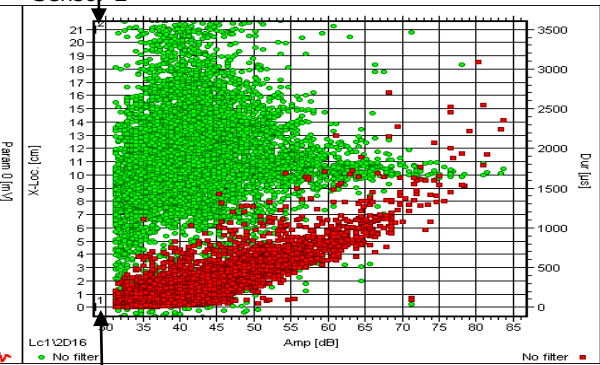
(a) Amplitude (dB) vs Time (s) vs Param (mV)
(Red Curve:- Param Load Curve)



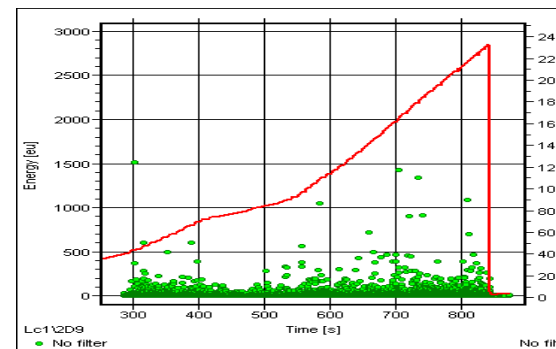
(b) X-location (cm) vs Time (s) vs Param (mV)
(Red Curve:- Param Load Curve)



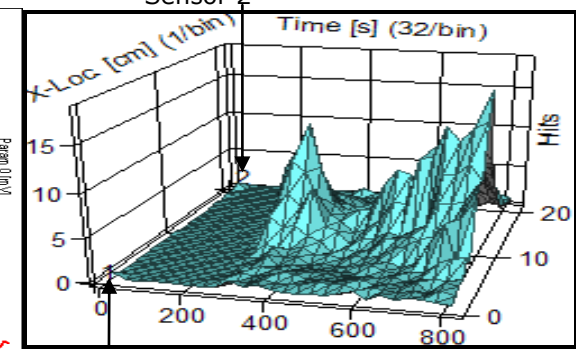
(c) Duration (μ s) vs Time (s) vs Param 0 (mV)
(Red Curve:- Param Load Curve)



(d) x-location (cm) vs Amplitude (dB) vs Duration (μ s)
(Red dots: Duration)



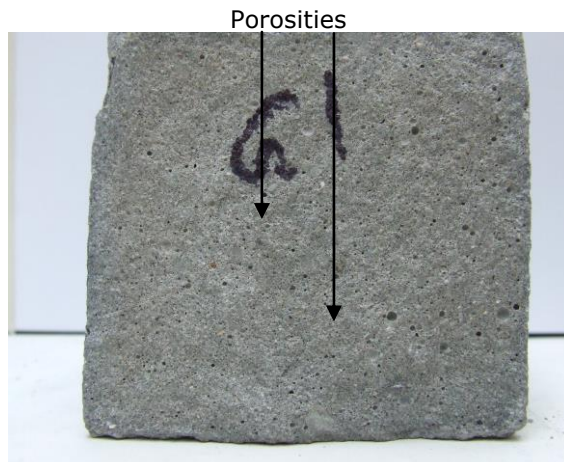
(e) Energy vs Time (s) vs Param (mV)
(Red Curve:- Param Load Curve)



(f) X-location vs Time (s) vs Hits



Fractured Sample
g) Plain Mortar



Fractured Surface

Figure 6.9:- AE plots for sample BG1 (plain concrete)

6.5.2 Sample BI1: 60g Powdered Glass

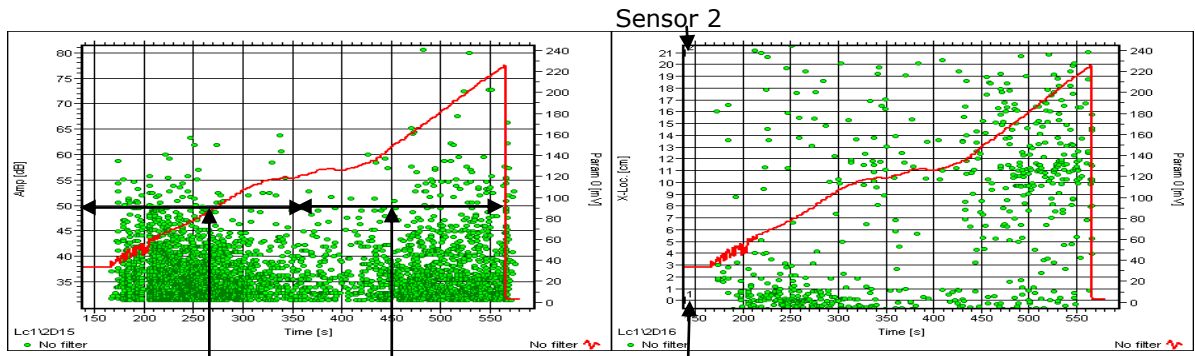
The effect of an addition of crushed glass powder to the concrete block is that the AE activity is reduced considerably as shown in figure 6.10 (a-g).

The number of higher peak amplitude events (> 60 dB) are only 8 with few localised events (figure 6.10 (a and b)). The maximum load carried by the sample is relatively low (220 mV) indicating brittleness or lack of toughness of the material.

The number of events with long duration (>1000 μ s) are only 8 and only 2 events with high energy level (>1000 eu) (see figure 6.10 c, d and e). The number of few localised events also reflect the number of low hits which are sparsely distributed throughout the sample (figure 6.10 (f)).

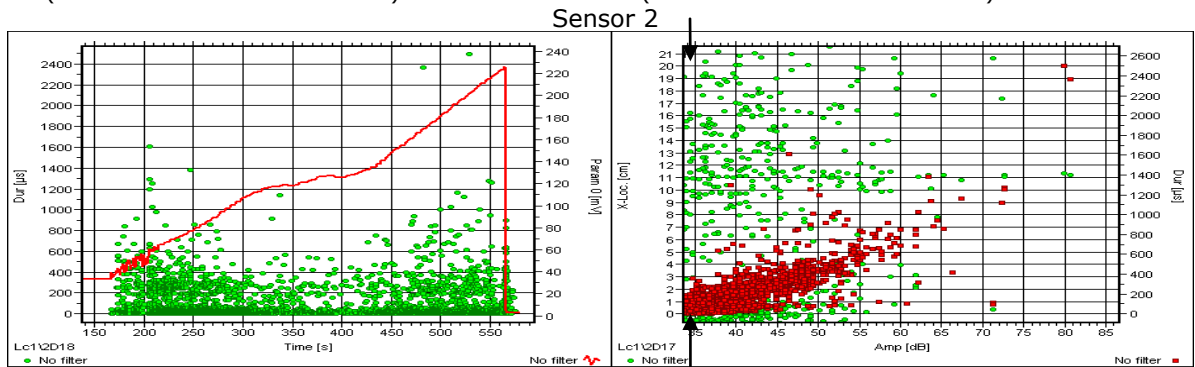
Compared to other specimens, this specimen has exhibited fewer activities than any other sample in this batch, since the ratio of sand to cement has changed leading to a porous sample because the glass powder aggregates act as sand. This is also the reason for very few activities at high amplitudes.

The fractured sample with crack path and fractured surface is shown in figure 6.10 (g). On the fractured surface glass powder can be seen (white particles sticking out).



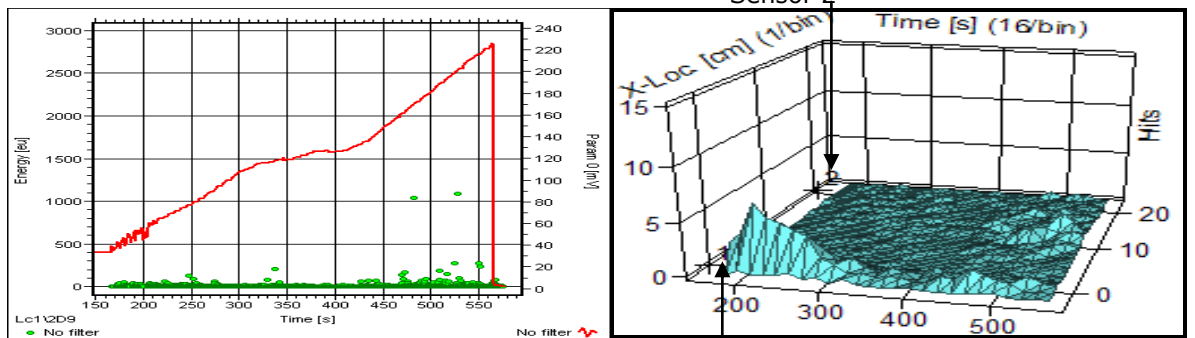
(a) Amplitude (dB) vs Time (s) vs Param (mV)
(Red Curve:- Param Load Curve)

(b) X-location (cm) vs Time (s) vs Param (mV)
(Red Curve:- Param Load Curve)



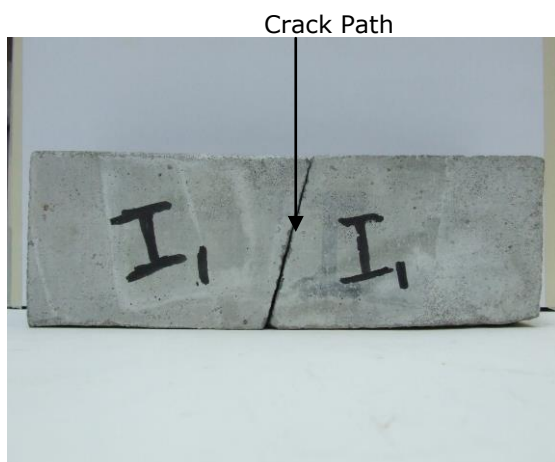
(c) Duration (μ s) vs Time (s) vs Param 0 (mV)
(Red Curve:- Param Load Curve)

(d) x-location (cm) vs Amplitude (dB) vs Duration (μ s)
(Red dots:Duration)

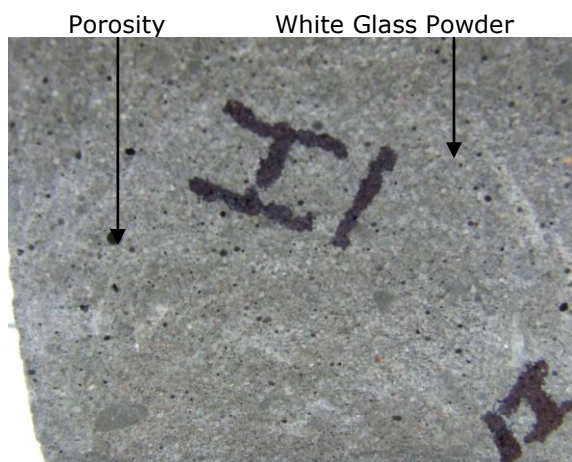


(e) Energy vs Time (s) vs Param (mV)
(Red Curve:- Param Load Curve)

(f) X-location vs Time (s) vs Hits



Fractured Sample
g) Powdered Glass Mortar



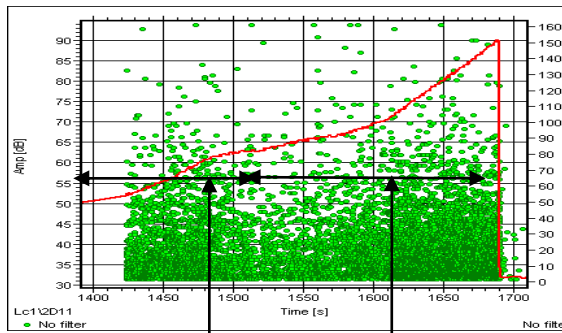
Fractured Surface

Figure 6.10:- AE plots for sample BI1 (with powdered glass)

6.5.3 Sample BF1: 60g 2-1mm Glass Aggregates

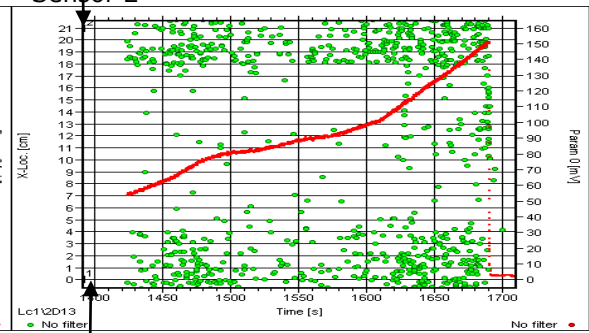
Figure 6.11 (a-g) shows AE plots of sample containing 60g of 2-1 mm glass plate aggregates. This specimen exhibited AE activities throughout the test duration. In the linear region, AE activities are high with peak amplitude and longer duration events and high energy events (see figures 6.11 a, c, d and e). Three major events occur at 1630, 1660 and 1690 seconds. These events take place at location 160 mm, 30 mm and in the central region of the specimen. Majority of the hit events recorded are located near the sensors 1 and 2 as shown in 6.11 (f).

From the AE activities, it is evident that a lot of micro-cracks and crack bridging took place in this sample, which is supported by the low amplitude and short duration activities. Bigger cracks developed as a result of micro-cracks and debonding during the final stage of the test until final fracture. This implies that the sample did show some toughening, although the flexural strength dropped sharply which is probably due to the existence of large porosities in the specimen. The specimen breaks in the central region and the fractured sample and surface are shown with the fracture section showing glass pullout in figure 6.11 (g).

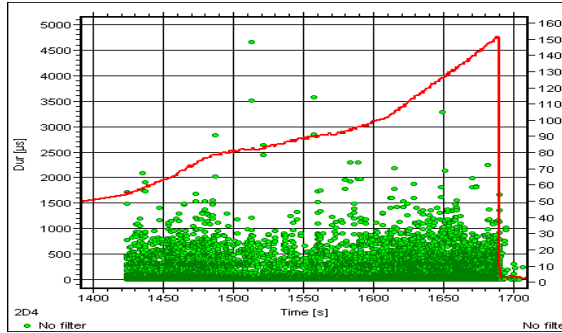


(a) Amplitude (dB) vs Time (s) vs Param (mV)
(Red Curve:- Param Load Curve)

Sensor 2

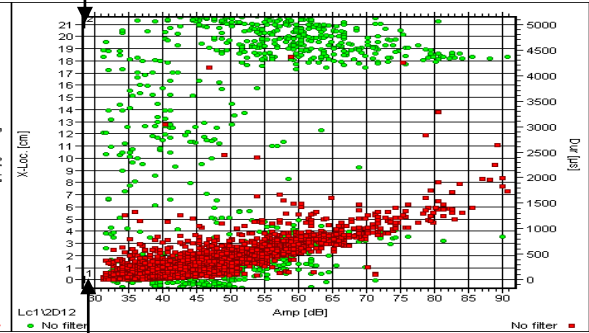


(b) X-location (cm) vs Time (s) vs Param (mV)
(Red Curve:- Param Load Curve)

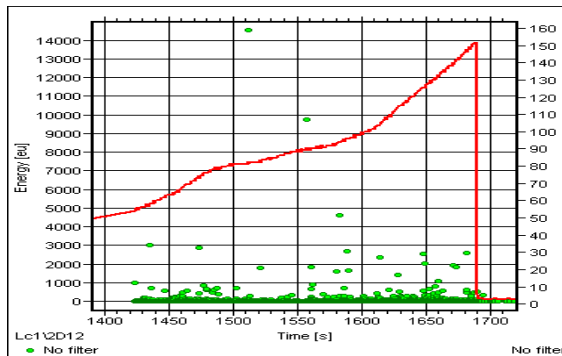


(c) Duration (μ s) vs Time (s) vs Param 0 (mV)
(Red Curve:- Param Load Curve)

Sensor 2

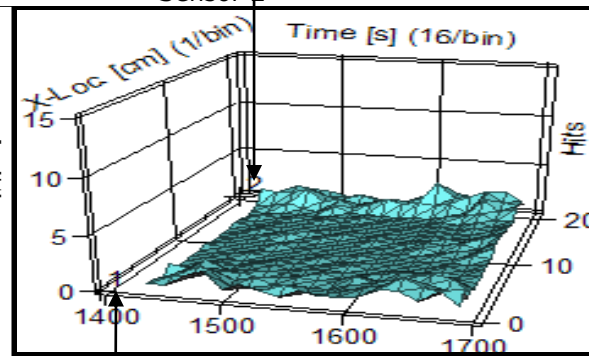


(d) X-location (cm) vs Amplitude (dB) vs Duration (μ s)
(Red dots:Duration)

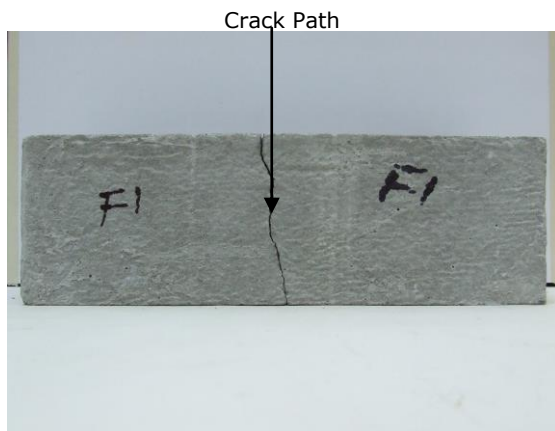


(e) Energy vs Time (s) vs Param (mV)
(Red Curve:- Param Load Curve)

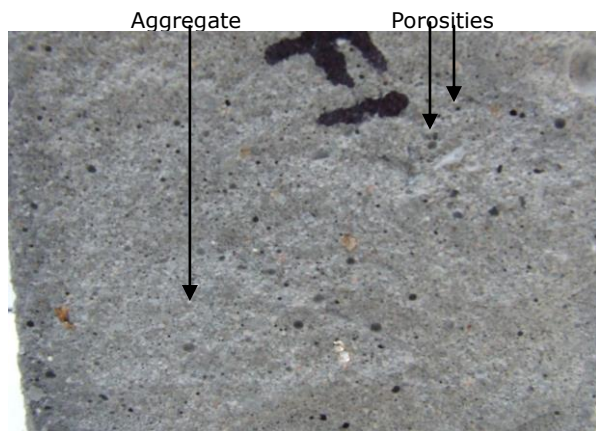
Sensor 2



(f) X-location vs Time (s) vs Hits



Fractured Sample
g) Mortar with 2-1mm glass aggregates



Fractured Surface

Figure 6.11:- AE plots for sample BF1 (with 60g 2-1mm aggregates)

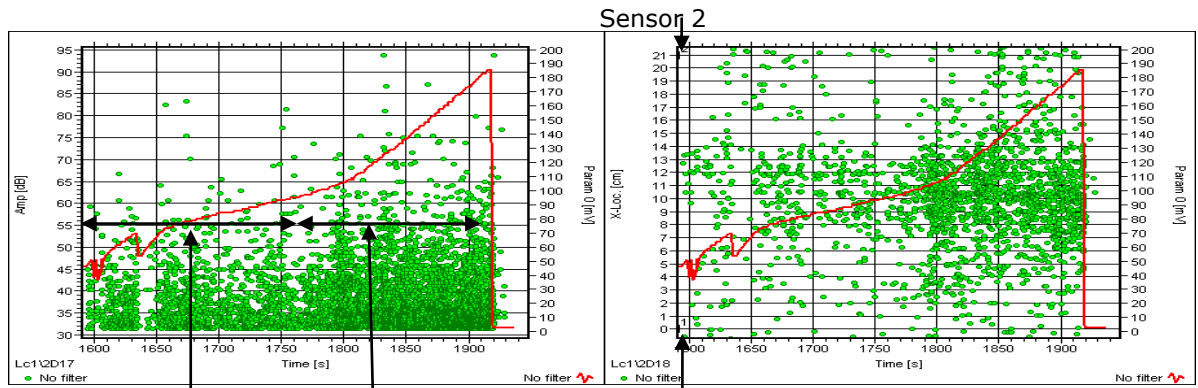
6.5.4 Sample BH1: 60g 4-2mm Glass Aggregates

Figure 6.12 (a-f) show AE plots of sample containing 60g 4-2mm glass aggregate. The AE hits activity is more than sample of size 140×70×70 mm. The obvious reason for this is the larger volume of the blocks.

The AE activity is prominent in the linear region of load plot between the time slot 1800-1900 seconds (figure 6.12 (b)). At least 6 major events can be seen in figure 6.12, plot (c) and (d). Some of these events are high peak amplitudes and longer event duration. The plot in figure 6.12 (b) shows localised events which are mostly in the central region of the sample. The events with peak amplitude >65 dB and higher duration are confined to narrow central band. Crack propagation and crack jump usually produce high energy and long duration events.

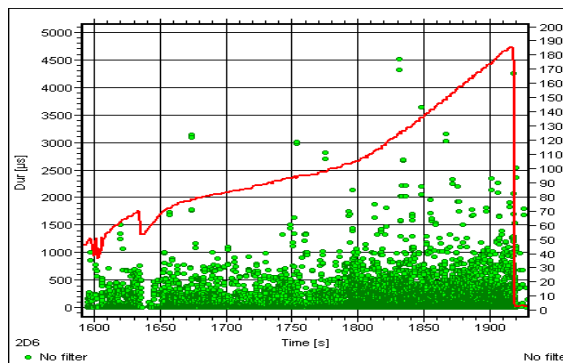
The events have higher peak amplitudes and longer duration. The pull-out events are more energetic as indicated by the longer duration events, figure 6.12 (c, d and e). These events also produce high energy and event duration events.

In the linear region, a large number of activities at low amplitude (60 dB) and short duration (<1000 μ s) are seen to be taking place, which is probably due to the micro-crack propagation and micro-cracks at the interface of glass aggregates and cement matrix. Most of the hits recorded are seen to be taking place towards the end of the test (figure 6.12 (f)). The fractured surfaces of the sample shown in figure 6.12 (g) are pull-out regions in glass aggregate.

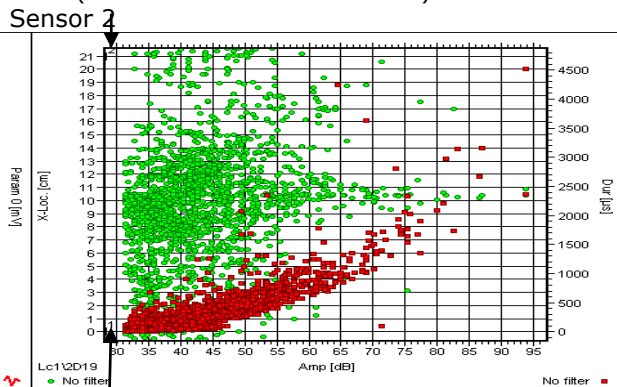


(a) Amplitude (dB) vs Time (s) vs Param (mV)
(Red Curve:- Param Load Curve)

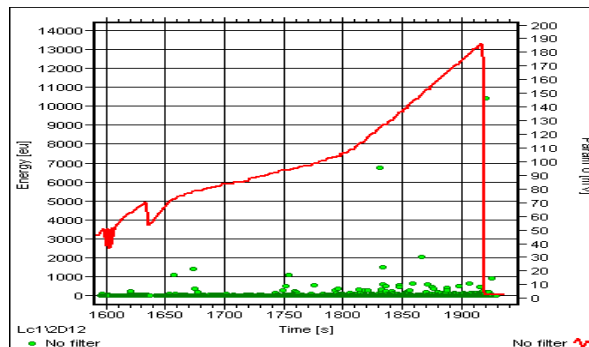
(b) X-location (cm) vs Time (s) vs Param (mV)
(Red Curve:- Param Load Curve)



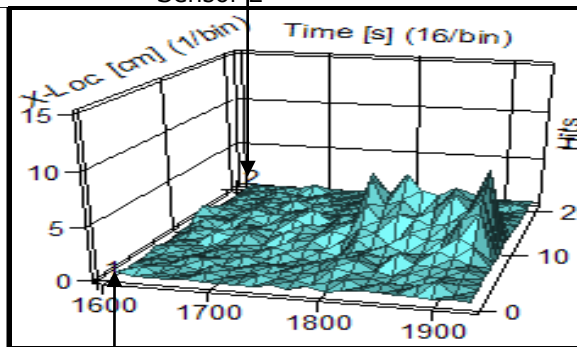
(c) Duration (μ s) vs Time (s) vs Param 0 (mV)
(Red Curve:- Param Load Curve)



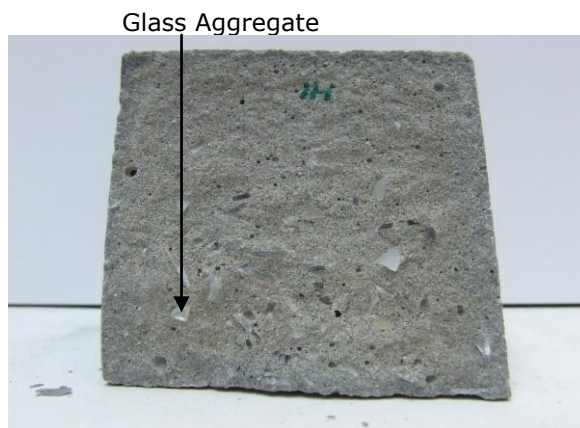
(d) x-location (cm) vs Amplitude (dB) vs Duration (μ s)
(Red dots: Duration)



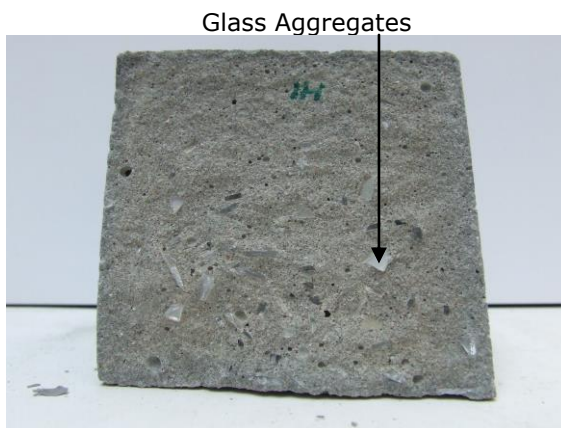
(e) Energy vs Time (s) vs Param (mV)
(Red Curve:- Param Load Curve)



(f) X-location vs Time (s) vs Hits



Fractured Surface
g) Mortar with 60g 4-2mm glass aggregate



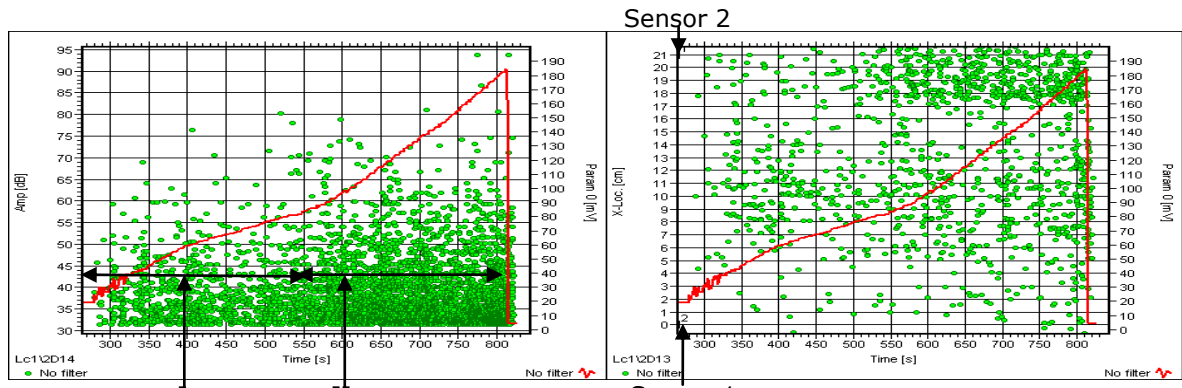
Fractured Surface

Figure 6.12:- AE plots for sample BH1 (with 60g 4-2mm aggregates)

6.5.5 Sample BJ1: 120g 4-2mm Glass Aggregates

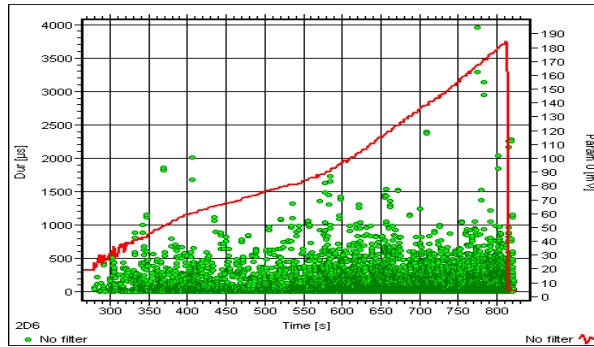
The test on this specimen lasted approximately for 500 seconds, with most of the activities taking place at low amplitudes with short event duration (<60 dB and <1500 μ s) as shown in figures 6.13 (a-f). It appears to behave like plain concrete mortar block. The addition of 120g of glass aggregates has affected the cement/water ratio leading to incomplete hydration reaction. A specimen with aggregate shows toughening which is apparently lower in this sample. The larger quantity of aggregates (large amount of glass fragments) have caused a number of crack arrests / bridging and de-bonding to occur during the test on this sample. In stage II, (the linear region) the AE activity has increased with higher amplitudes and longer event durations taking place, possibly caused by the micro-cracks and a few small pull-out events / de-bonding.

The fractured sample and surfaces are shown in figures 6.13 (g). The fractured surface exhibit glass breakage (bridging) of glass aggregate.

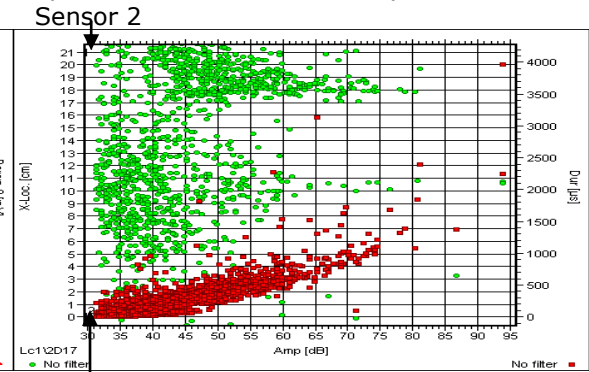


(a) Amplitude (dB) vs Time (s) vs Param (mV)
(Red Curve:- Param Load Curve)

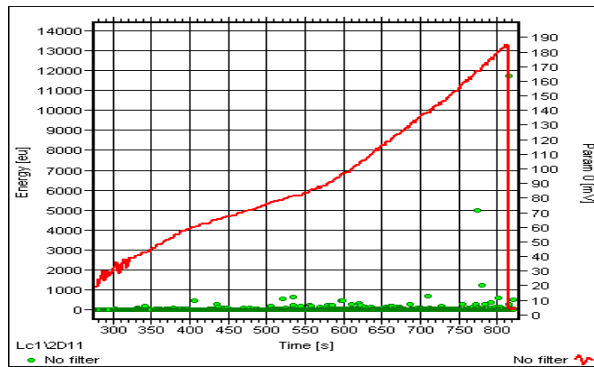
Sensor 2
(b) X-location (cm) vs Time (s) vs Param (mV)
(Red Curve:- Param Load Curve)



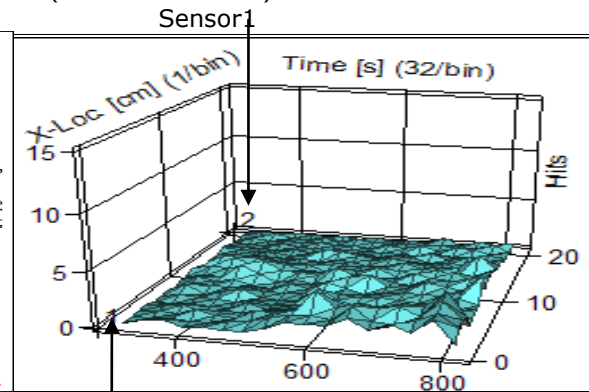
(c) Duration (μ s) vs Time (s) vs Param 0 (mV)
(Red Curve:- Param Load Curve)



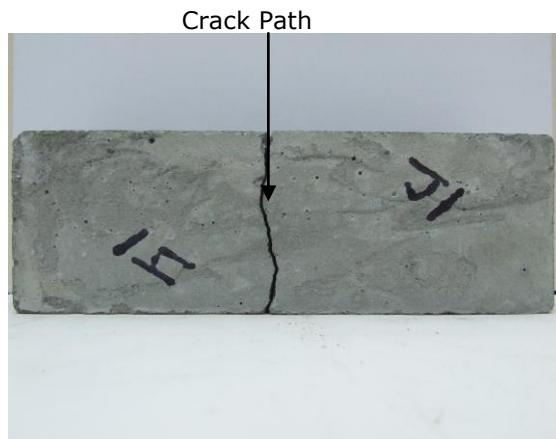
Sensor 1
(d) x-location (cm) vs Amplitude (dB) vs Duration (μ s)
(Red dots: Duration)



(e) Energy vs Time (s) vs Param (mV)
(Red Curve:- Param Load Curve)



Sensor 2
(f) X-location vs Time (s) vs Hits



(g) Fractured Sample



Fractured Surface

Figures 6.13: AE plots for sample BJ1 (with 120g 4-2mm aggregates)

6.5.6 Comparison and Discussion on the AE Test Results

The results from the AE monitoring show that specimens from both batches exhibit distinct and unique behaviour under flexural load until fracture. A summary of AE monitoring results obtained from un-notched mortars containing glass aggregates under flexural tests are shown in table 6.3.

Table 6.3: A.E. monitoring results summary of un-notched mortars containing glass aggregates

<u>SAMPLES</u>	<u>Region of localised events of high Activity</u>	<u>Number of AE Activity in Relation to Plain Sample</u>	<u>Number of events of peak amplitude > 60 dB</u>
Plain Mortar (<i>BD1</i>) <i>Small Sample</i>	50-60 mm	Normal	50
40g Powdered Glass (<i>BA2</i>) <i>S</i>	60-80 mm	Very Low	30
40g 2-1mm Glass (<i>BC1</i>) <i>S</i>	50-60 mm	Very High	99
40g 4-2mm Glass (<i>BE1</i>) <i>S</i>	60-70 mm	Medium	23
80g 4-2mm Glass (<i>BB2</i>) <i>Small Sample</i>	50-60 mm	Very low	9
Plain Concrete (<i>BG1</i>) <i>L</i>	90-110 mm	High	223
60g Powdered Glass Aggregates (<i>BI1</i>) <i>Large Sample</i>	90-200 mm	High	8
60g 2-1mm Glass Aggregates (<i>BF1</i>) <i>Large Sample</i>	150-220 mm	Low	235
60g 4-2 mm Glass Aggregates (<i>BH1</i>) <i>L</i>	60-160 mm	Very High	97
120g 4-2mm Glass (<i>BJ1</i>) <i>L</i>	80-140 mm	High	92

From the chart in figure 6.14, it can be seen that the samples BB2 and BE1 (with 40g 4-2 mm glass aggregates and 80g 4-2 mm glass aggregates respectively) produced the least number of hits compared to other samples. This relates to the fewer AE activities generated under load due to fewer number of aggregate inclusions. From the statistical results (in table 6.4 and figure 6.15), sample BC1 (40g 2-1 mm glass aggregates) recorded more than half the total percentage of hits out of all the small sized samples. This indicates that the glass aggregates in this sample were dislodged from the cement matrix resulting in large number of AE hits.

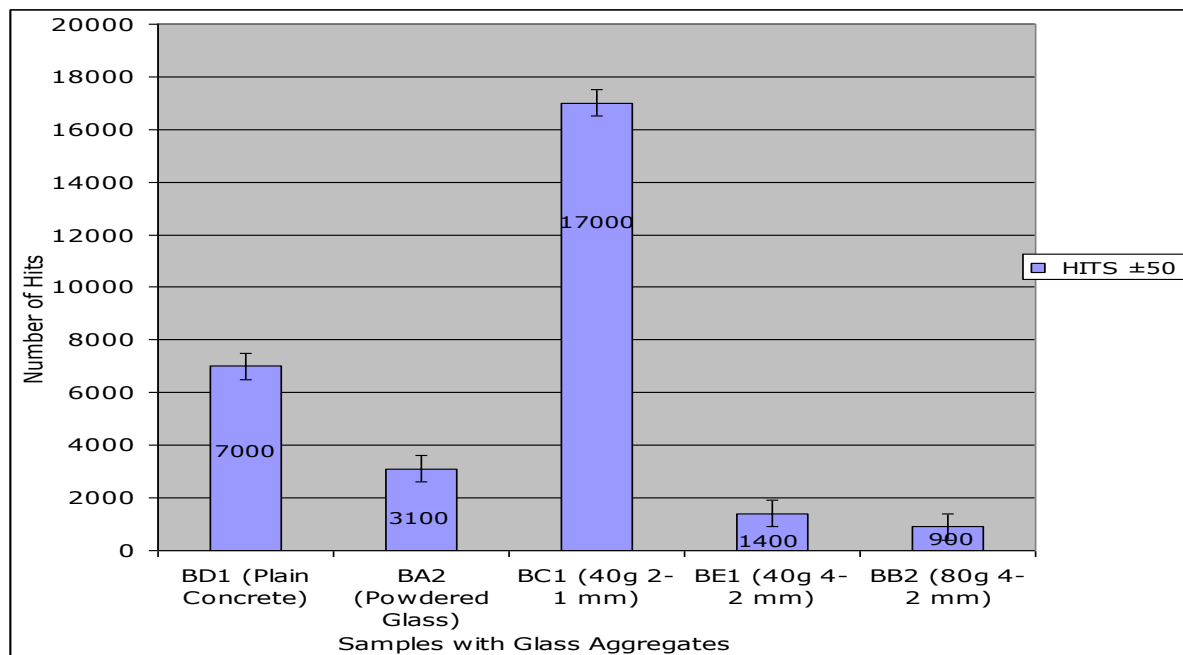


Figure 6.14: Variations of AE Hits captured by different smaller sized un-notched mortars under flexural load test

Table 6.4: Percentage of Hits in each Sample

SAMPLES	% OF HITS IN EACH SAMPLE
BD1 (Plain Concrete)	24
BA2 (Powdered Glass)	10
BC1 (40g 2-1 mm Glass Aggregates)	58
BE1 (40g 4-2 mm Glass Aggregates)	5
BB2 (80g 4-2 mm Glass Aggregates)	3

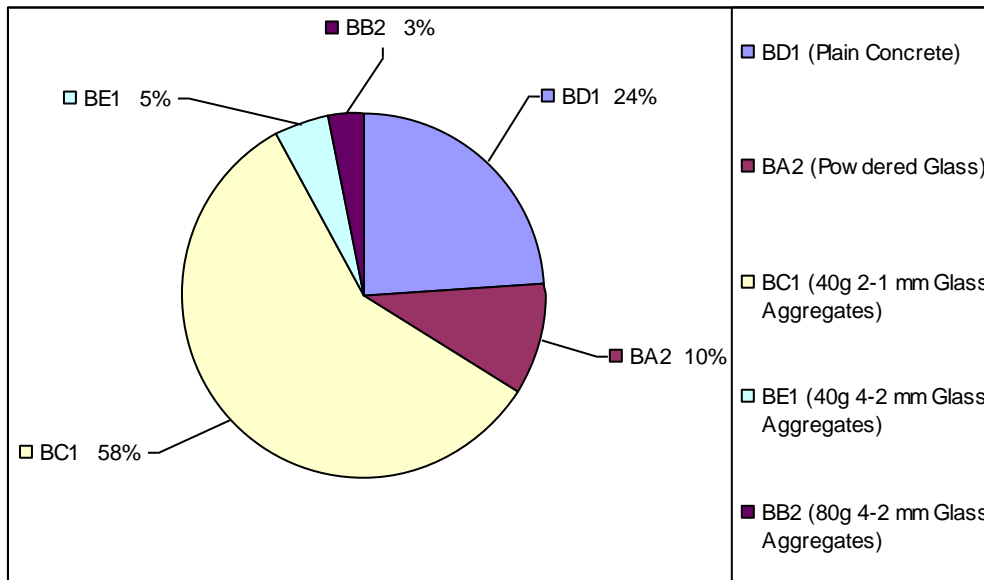


Figure 6.15: Percentage of Hits variation in each of the smaller sized un-notched mortars under flexural load test

It can be seen from the chart in figure 6.16, sample BG1 had the largest number of AE hits produced during the test, the probable reason for this is due to the three point bend test bars settling on the specimen. This is why the percentage hits are higher as can be seen in table 6.5 and figure 6.17. The least percentage of hits produced was by BI1 (sample with powdered glass), as the powdered glass had increased the sand cement ratio and thus weakening the sample in terms of toughness. The sample BF1 (60g 2-1 mm aggregates) recorded the highest percentage of hits, suggesting that the specimen faced strong resistance to cracks because of strong bonding of glass aggregates with cement matrix.

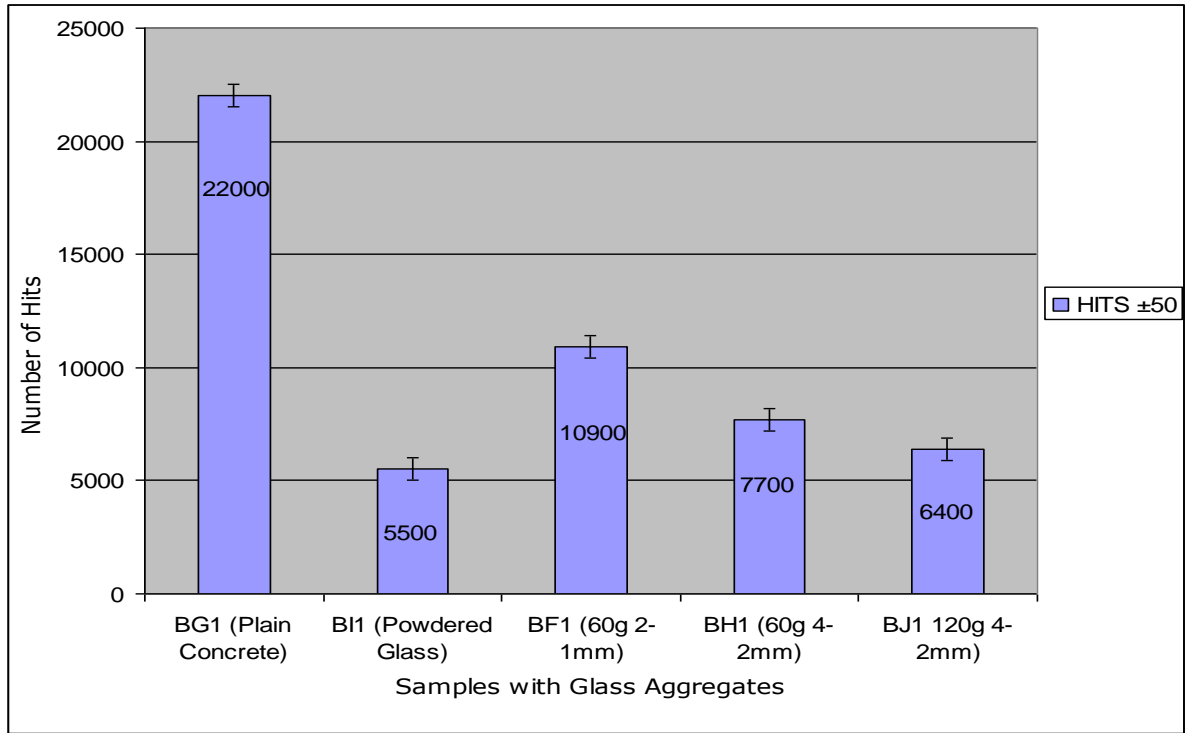


Figure 6.16: Variations of AE Hits captured by different larger sized un-notched mortars under flexural load test

Table 6.5: Percentage of AE hits in the bigger sized un-notched samples

SAMPLE	% OF HITS IN THE SAMPLE
BG1 (Plain Concrete)	42
BI1 (Powdered Glass)	10.5
BF1 (60g 2-1 mm Glass Aggregates)	20.5
BH1 (60g 4-2 mm Glass Aggregates)	15
BJ1 (120g 4-2 mm Glass Aggregates)	12

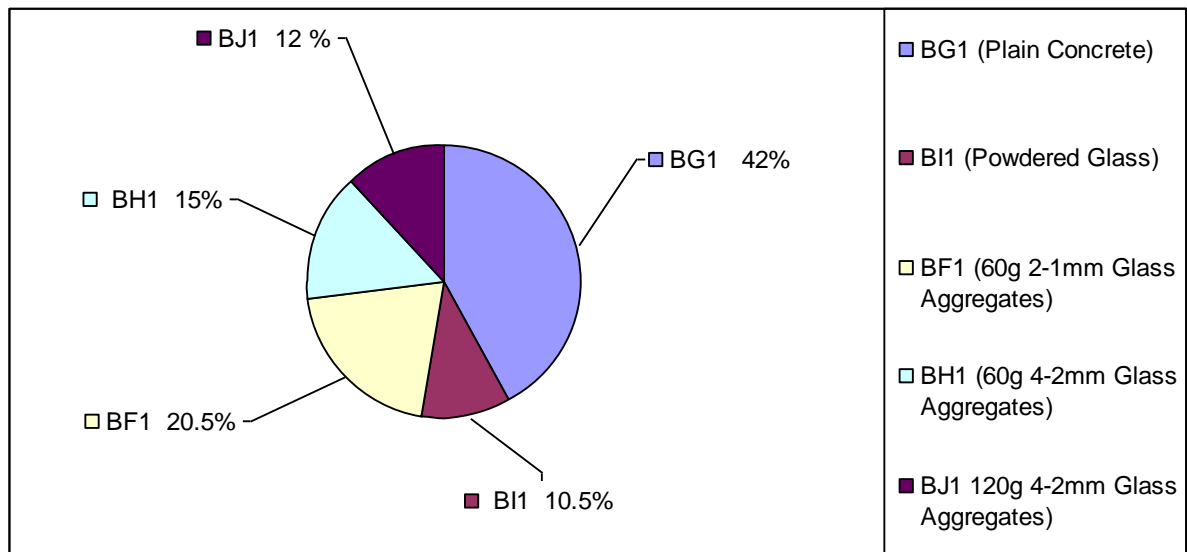


Figure 6.17: Percentage of Hits variation in each of the larger sized un-notched mortars under flexural load test

The glass aggregates used in samples BB2 (80g 4-2mm), BC1 (40g 2-1mm), and BE1 (40g 4-2mm) prevented or arrested the crack growth and the occurrence of micro-cracks. This is the reason for less activity recording in these samples compared to samples BA2 (powdered glass) and BD1 (plain mortar), (specimens with powdered glass and plain mortar respectively). This indicates that the glass aggregates used provided bonding structure with the cement structure, which is visible from the longer duration taken for these samples to reach peak failure.

There were similarities noticed between the AE activities recorded for samples BA2 (powdered glass) and BD1 (plain mortar), this is because the powdered glass acted in a similar manner to sand aggregates rather than coarse glass aggregates, i.e. for both specimens, the activities above 50 dB were mostly of low event duration (majority activities lie between 300 μ s–1200 μ s).

However, the addition of powdered glass has had no beneficial effect on the enhancement of the mechanical properties of the mortar (i.e. lowering the strength, the toughness, and no evidence of strong bonding being provided between the aggregates and cement structure).

Comparison between samples BB2 (80g 4-2 mm), BC1 (40g 2-1 mm) and BE1 (80g 4-2mm) showed that the use of 40 g 2-1 mm glass aggregates in specimen BC1 increased the load strength as well as the toughness, indicated by longer duration to reach failure as well as the high number of activities. This is because of the small sized (2-1 mm) glass used as aggregates, which provided crack bridging rather than strong bonding.

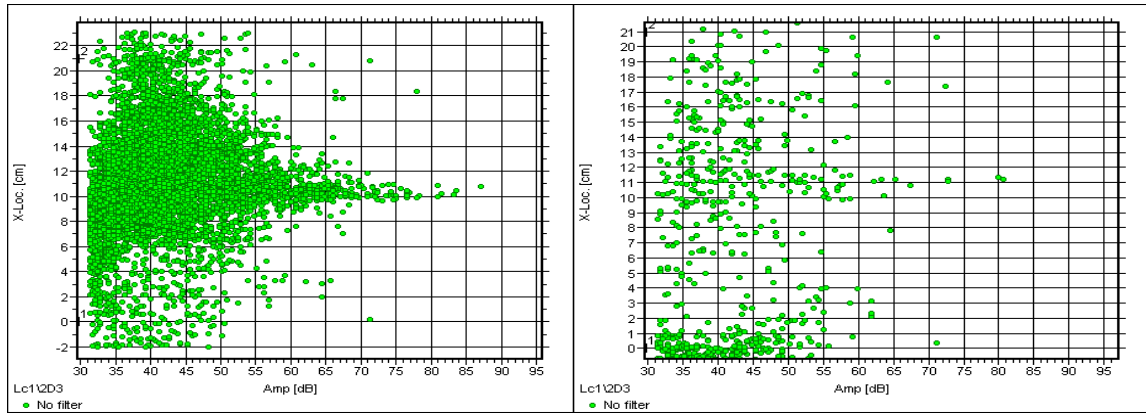
When comparing samples BF1, BG1, BH1, BI1 and BJ1 (large sized specimens), it can be seen that specimen BI1 (with powdered glass) shows that it has the least number of AE activities recorded. This shows that the powdered glass as aggregate is detrimental to the toughening of mortar, even though the load strength here is seen to be higher than samples containing rough glass aggregates. The few activities recorded above 50 dB are the formation of bigger cracks that have resulted from the micro-cracks that have accumulated as seen from the activities below 60 dB level. No evidence of crack arrest/bridging or de-bonding is visible from the activities. When compared with specimen BG1

(plain concrete sample), the detrimental effect of adding glass powder is clearly visible on the AE plots.

The AE plots based on amplitudes versus location shown in figures 6.18 (a-e) exhibit distinctive feature for each of the sample. The addition of glass aggregates of different mass and sizes in each batch altered the AE activity pattern indicating the changes in toughness level of each specimen.

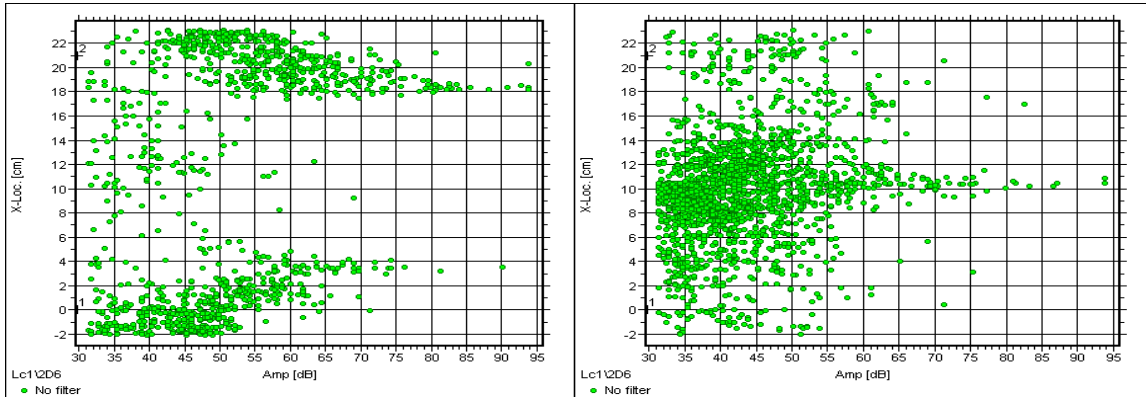
It can be seen that taking the plain sample as the base (figure 6.18 a), sample with powdered glass exhibited its own distinctive AE response under flexural load, i.e. acoustic activities decreased significantly as a result of adding powdered glass aggregate (figure 6.18 b). The reason for this is due to addition of powder which acted like sand and this weakened the sample (as explained in section 6.5.2). Increasing the size of aggregates caused AE activities with amplitudes in higher range (> 80 dB) to take place under load (figures 6.18 c, d and e); this is an indication of toughening of samples (i.e. better interfacial bonding of aggregates with cement paste).

Figures 6.18 c and 6.18 d, i.e. (BF1 and BH1 (samples with 60g 2-1mm and 60g 4-2mm glass aggregates)) show a number of very high amplitude (85 dB) events indicating that the glass aggregates are strongly bonded to the cement matrix, therefore it was made difficult for cracks to propagate. From the layout of these plots, (samples BF1, BH1 and BJ1), it can be said that aggregates do not contribute much in arresting micro-cracks or crack propagation, but may provide good bonding with the cement structure if used in appropriate amount.



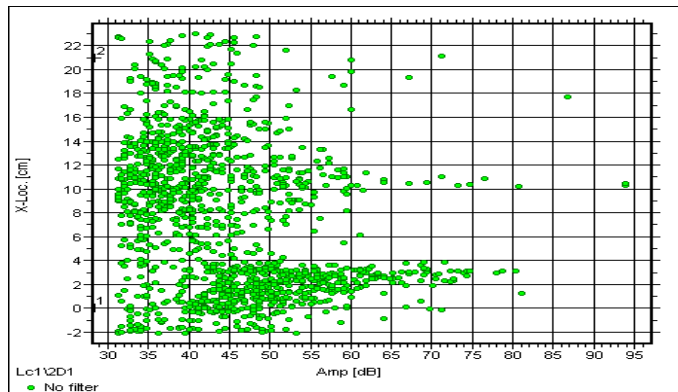
a) BG1 Plain concrete

b) BI1 Powdered glass



c) BF1 60g 2-1mm glass aggregates

d) BH1 60g 4-2mm glass aggregates

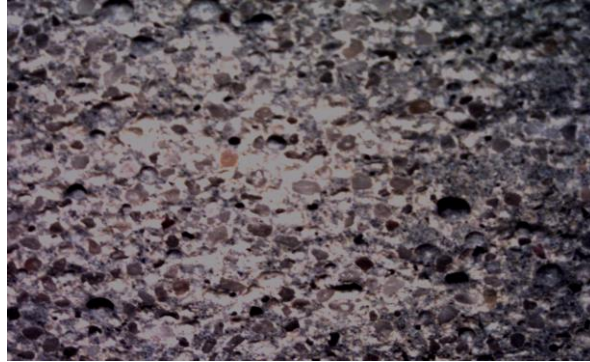


e) BJ1 120g 4-2mm glass aggregates

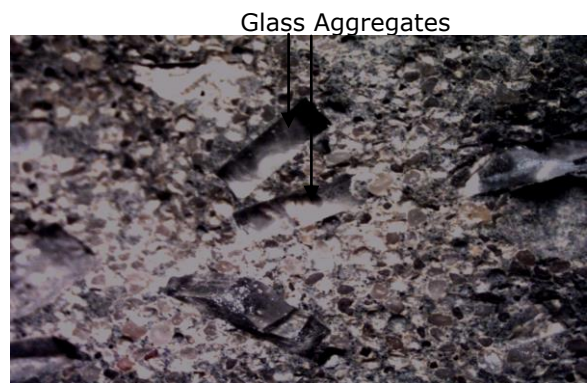
Figure 6.18 (a-e): Distribution of AE amplitude (dB) against Location for different size of glass aggregates

It can be deduced that aggregate in the form of waste glass can be used in manufacturing concrete mortar provided that the mixture is of appropriate amount and size. Mortar samples with higher sized aggregates, produced few AE activities with high amplitude regions (above 60 dB). This can be attributed to good link between cement matrix and aggregates. Therefore crack cannot easily propagate overcoming the interfacial bonds. This is supported by the optical photographs in figures 6.19 (b-d). The smaller sized aggregates are firmly bonded to the matrix (figure 6.19 (b)) and the larger aggregates are indicating

pull out event (figure 6.19 (c and d) to the adequate pinning manipulating the propagation of crack through the sample.



(a) BD1: Plain Concrete



(b) BC1: 40g 2-1mm Glass Aggregates (c) BE1: 40g 4-2 mm Glass Aggregates



(d) BB2: 80g 4-2 mm Glass Aggregates

Figure 6.19 (a-d): Optical Micro-graphs of the Fractured Surfaces of the concrete samples

The complex and brittle nature of the material make it difficult to evaluate tensile properties of concrete. The AE monitoring of flexural tests facilitated in depth study of the micro, macro mechanics-taking place under load in the specimen. The three-point test was used in this investigation to understand crush behaviour.

It is evident from the results that visual observation does not reveal material deformation. Just before fracture, crack/cracks become visible and specimen fracture. However AE data does reveal various events as they occur in the specimen relating to crack formation, crack arrest, pull out events, crack growth and propagation up to final fracture.

AE monitoring has also revealed differences in the fracture behaviour of small and large size blocks. Large sized specimens behave more like beams and fracture at relatively higher loads and provide more data relating to damage. Small sized specimens act more like cubes and the damage is related to lesser number of activities.

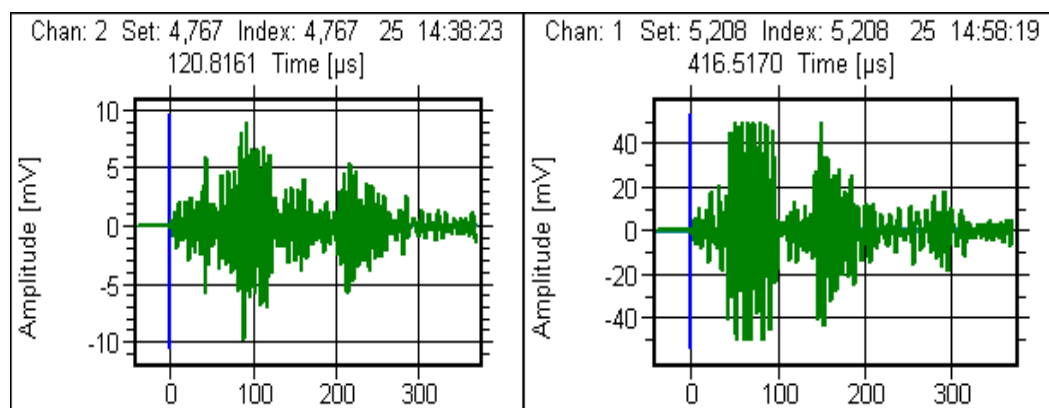
6.5.7 AE Waveforms: AE Frequency Domain Analysis

Although the T.D. (time domain) AE parameters namely peak amplitude, event duration etc and their analysis provide valuable information about the activities occurring in a sample under load, the analysis of AE waveforms provide additional information which are specific to damage and material characteristics. A material under stress produces acoustic waves containing wide range of frequencies. Some of the frequency component in the signal is modified during their propagation through the material. This modification depends on the nature of the material.

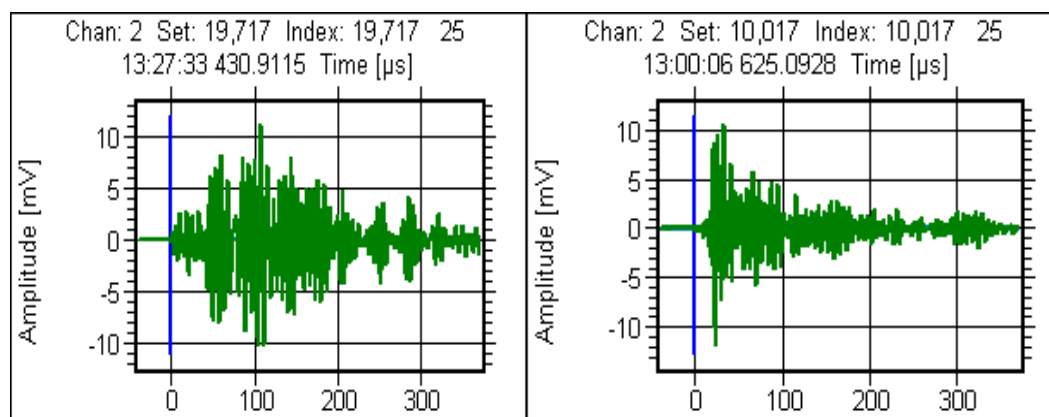
AE systems are capable of recording AE time domain parameters as well as waveforms with software to analyse and classify them. Few typical wave waveforms indicating pattern differences relating to the nature of the samples undergone flexural testing are given.

Although the three point plots provide a number of information about the acoustic activities, analysis of AE waveforms provide extra information for specific moments and hits. Waveforms are related to the specific sound which the sample produces during the test, thus using of source acoustic emission. An AE event may be friction of the rollers or a deformation (crack) that may produce sound amplitude signal but waveforms (frequency content) of the signal will be different. Thus waveform analysis is an additional tool for characterising the material.

The AE waveforms (shown in figures 6.20 (a-d)) for a few samples (BI1, BJ1, BG1, BF1) were captured from similar regions of the amplitude versus time plots. Using the calculation from equation (2.4) in chapter2, $A[\text{dB}] = 20 \times \log(V_s/V_{\text{ref}})$, it can be seen that they all have amplitude, above 70 dB and occur just before the final fracture. It is evident in figure 6.20 (b), BJ1, (sample containing 120g 4–2 mm aggregates), the signal recorded has very high energy.



a) AE Waveforms for mortar with 60g powdered glass (sample BI1) b) AE Waveforms for mortar with 120g 3.36-4 mm aggregates (sample BJ1)



c) AE Waveforms for Plain mortar (sample BG1) d) AE Waveforms for mortar with 60g 2-1mm aggregates (sample BF1)

Figures 6.20 (a), (b), (c), and (d): AE waveforms for different samples

The study of interfacial bonding between concrete and an aggregate with the aid of AE is informative. The addition of an aggregate significantly increased the amplitude of the waveforms, indicating that more energy is being released at specific points (e.g. glass pull-out) within the matrix. At certain specific locations the signal from certain defects (e.g. crack) is distinctively greater. Pattern recognition technique can provide valuable insight into the change in waveforms.

6.6 AE Monitoring of Cracks in Concrete with the Increment of Glass Aggregate Sizes under flexural condition

One of the objectives of the research is to investigate toughening mechanism (grain-bridging/micro-cracking) and fracture nature of concrete. Addition of glass and rubber as aggregates to concrete has facilitated good understanding of these mechanisms. Utilisation of waste materials to manufacture environmentally friendly concrete as discussed in chapter 1 has received numerous attentions from different quarters. Some encouraging results have been obtained with the addition of waste materials in enhancing the mechanical properties of concrete. From the compressive and flexural tests conducted in this investigation, it has been established that glass as aggregate (up to a certain size) has caused an increase in strength of mortar. These waste materials have proved to be useful in resisting the cracks (only visible at macroscopic level), but their response under flexural condition at micro-structural level needs to be investigated, so that micro-crack formation or grain bridging reliability can be determined from toughened and non-toughened mortars. Therefore, mortars were manufactured with glass aggregates of different sizes and put under flexural tests, so that the suitability of the aggregates and their appropriate sizes in terms of strength and toughness can be understood, using AE technique as a tool. All the samples were manufactured cured and were allowed to set under the same condition.

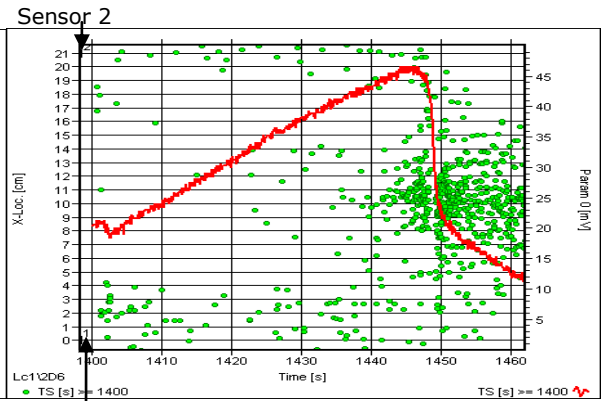
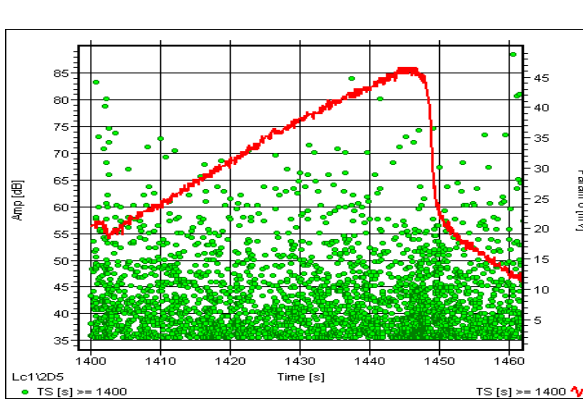
6.6.1 Plain Mortar: Sample KOLA0B

A plain concrete mortar without any glass aggregates was manufactured, cured and was left to set for the standard 28 days. At the end of the 28 day period, this mortar was put under flexural test and the AE activities were monitored on-line. The AE characteristics of this mortar sample can be used as a model to make a comparison with other mortars containing glass aggregates.

AE characteristic of the plain concrete mortar specimen is shown in figures 6.21 a-c. The load curve steadily rises from 1400 seconds, when the actual test was started (figures 6.21 (a) and (b)). The activities were recorded by both sensors at low amplitudes (<40 dB) throughout the specimen. The events with higher amplitudes (> 50 dB) mainly took place in the central notched portion of the specimen (8-13 cm); the failure of the specimen occurred with a high amplitude event of 73.1 dB at location 10.17 cm.

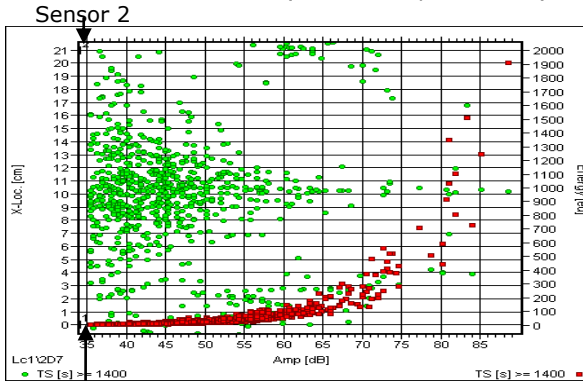
A large number of activities were recorded after the failure was recorded by both sensors, mainly of low amplitudes. Very few high amplitude events (> 55 dB) were also picked up by sensor 2 at location 15-21 cm as shown in figure 6.21 (c). Since most of the activities recorded are of low amplitudes with low energy level, it is an indication that these are probably due to the existence of porosities throughout the specimen. Therefore the main mode of failure in this specimen is micro-cracks that led to the final failure of the mortar. The values of AE parameters recorded at the event of failure are shown in the listing highlighted by blue shadings in figure 6.21 (d). The transient waveform captured at failure for this specimen is a small signal, captured just at the point of failure 6.21 (e). Compared to the failure event, the relatively long rise time of the waveform to reach the peak amplitude supports the low level failure of the sample. The number of AE hits cascaded (2250 hits) are shown in figure 6.21 (f).

The fractured surface of the sample and crack path can be seen in figure 6.21 (g). The structure appears to be homogeneous with random indentations due to fracture of pores.



a) Amplitude (dB) vs time (s) vs load param (mV)
(Red curve: param load)

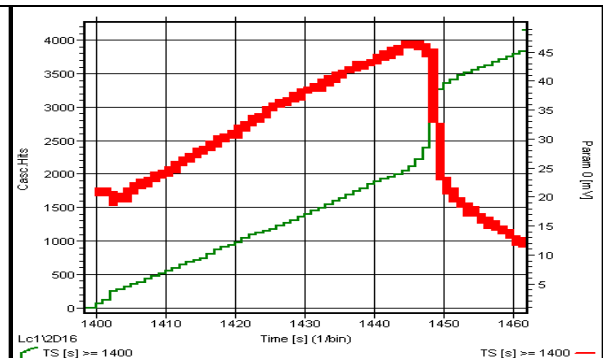
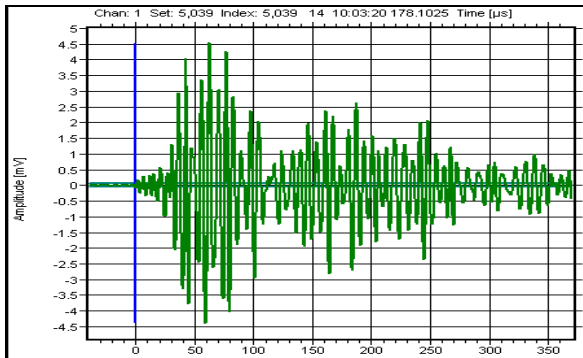
b) X-location (cm) vs time (s) vs load param (mV)
(Red curve: param load)



Id	DSET	A	R	E	D	X	TRAI
	[dB]	[μ s]	[eu]	[μ s]	[μ s]	[cm]	
Ev	8700	35.9	0.2	289E-2	0.8		5035
Ev	8701	35.9	0.2	280E-2	1.0		5036
Ev	8703	45.6	27.8	994E-2	175.6		5037
Ev	8704	36.6	3.4	560E-2	11.2		5038
LE	8707	73.1	63.2	462E00	1313.6	10.17	5039
Ht	8708	73.9	61.0	593E00	1360.0		5040
Ev	8710	39.2	6.8	715E-2	71.4		5041

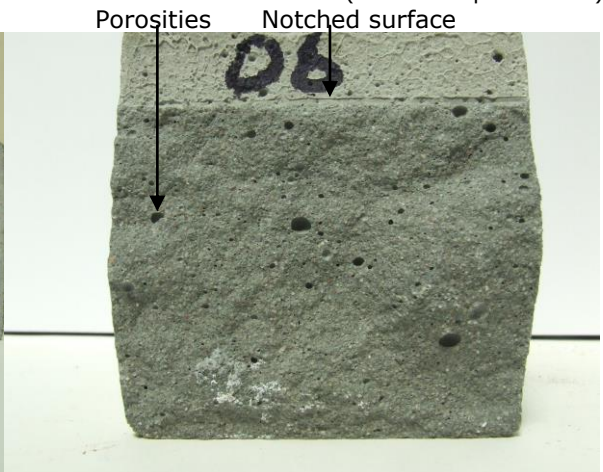
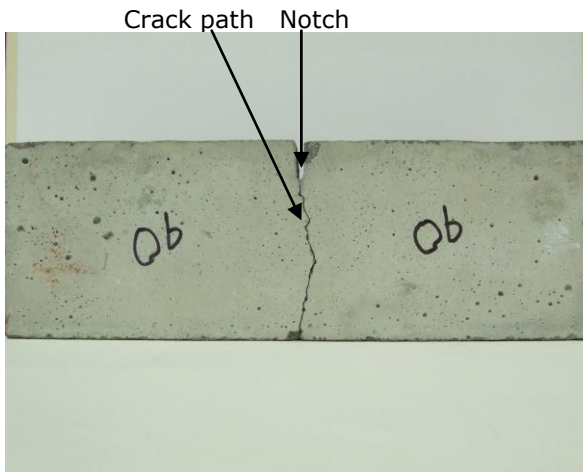
c) X-location (cm) vs amplitude (dB) vs energy (eu)

d) Located events listing



e) AE waveform

f) Cascaded Hits vs Time (s) vs Param load (mV)
(red curve: param load)



g) Fractured sample

Fractured surface

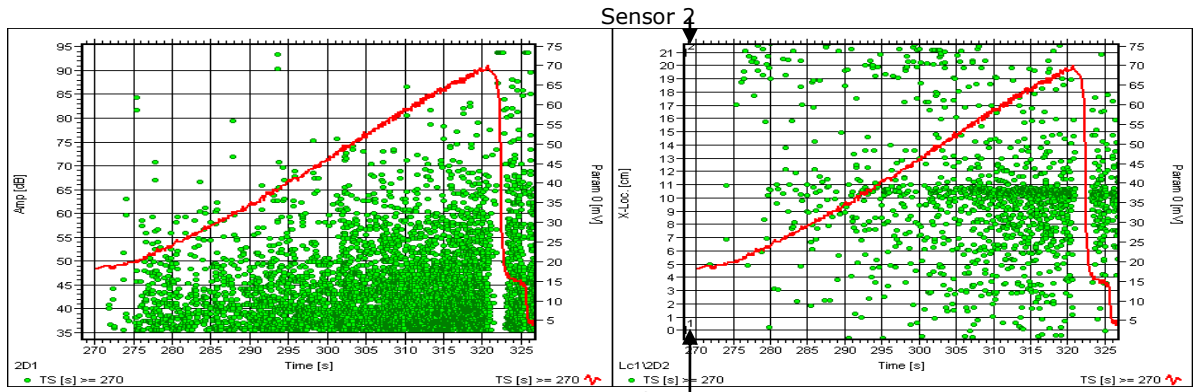
Figures 6.21: AE plots and fractured specimen for Plain Mortar

6.6.2 Mortar with < 1mm Glass aggregates: Sample KOLA2B

The addition of glass segments in this sample (< 1mm glass aggregates) has had a clear effect on this sample at micro-structural level during the flexural test. The load curve steadily started to rise from 275 seconds (when the test was initiated), to 322 seconds when the specimen failed in a semi-brittle manner (figures 6.22 (a) and (b)). The flexural test lasted longer than plain sample for this sample which is probably as a result of the addition of rough aggregates. Very small sizes of aggregates used in this specimen had facilitated the micro-cracks in this specimen to pass through the glass segments, which probably have taken over a lot of sites of porosities that exist in the plain mortar sample.

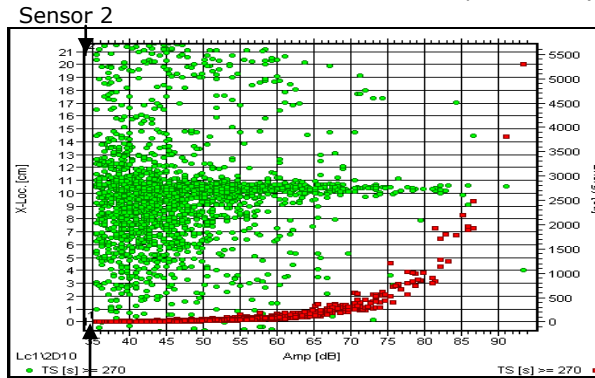
The number of micro-cracks in this sample also appears to be higher indicated by relatively high number of events at low amplitudes (< 55 dB), therefore the toughening is greater. Activities with very high amplitudes (> 70 dB) took place mainly in the central notch region (9 - 13 cm) of the specimen and this led to the final failure of the sample in this region, an indication of major events such as big fractures (figures 6.22 (a) and (b)). Unlike the plane mortar, the micro-cracks in this mortar appear in an even pattern, this is probably due to the large number of glass segments distributed throughout the mortar. As it is clearly visible from the AE plots, the final failure in this sample is the gradual increase of micro-cracks to form the bigger crack and finally to failure with most of the activities recorded by sensor 1 (see figure 6.22 (c)). The glass aggregates added in this specimen therefore mainly acted as obstacles to micro-cracks.

The values of AE parameters recorded at the event of failure are highlighted by blue shadings in figure 6.22 (d). The transient waveform shown in figure 5.48 (e) captured at the point of failure in this specimen clearly indicates the effect of the addition of glass aggregates, where the size of the signal is relatively larger than the waveform captured for plain mortar. The number of cascaded hits are 3000 as shown in figure 6.22 (f). Fracture surface and crack path of the specimen is shown in figure 6.22 (g). Glass aggregates can be seen strongly bonded to the cement matrix.



a) Amplitude (dB) vs time (s) vs load param (mV)
(Red curve: param load)

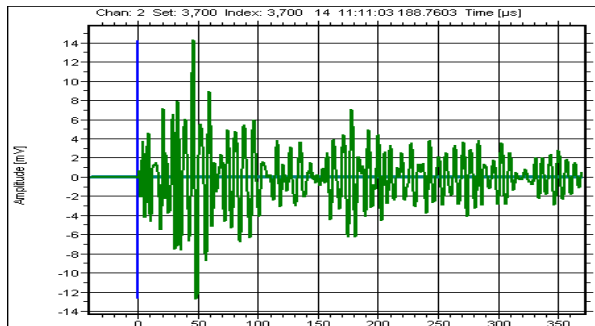
b) X-location (cm) vs time (s) vs load param (mV)
(Red curve: param load)



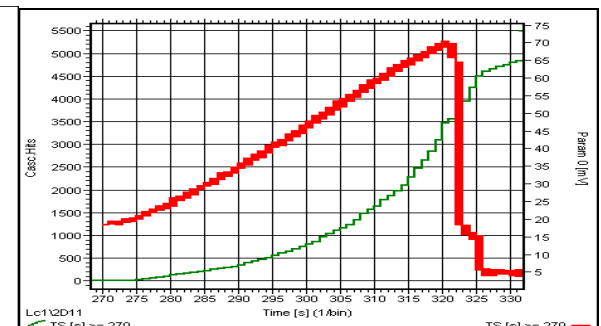
c) X-location (cm) vs amplitude (dB) vs energy (eu)

Id	DSET	A	R	E	D	X
		[dB]	[μ s]	[eu]	[μ s]	[cm]
Ht	5806	46.4	69.0	237E-1	410.8	
LE	5808	45.6	23.2	208E-1	383.2	10.25
Ht	5809	44.1	106.2	168E-1	300.6	
LE	5811	83.3	46.6	124E01	1560.8	10.63
Ht	5812	82.5	47.2	147E01	1563.2	

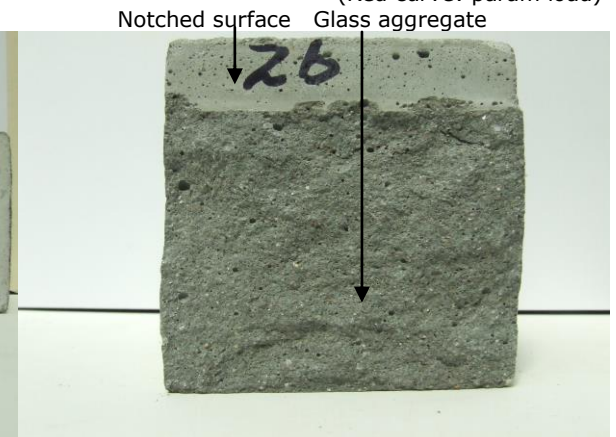
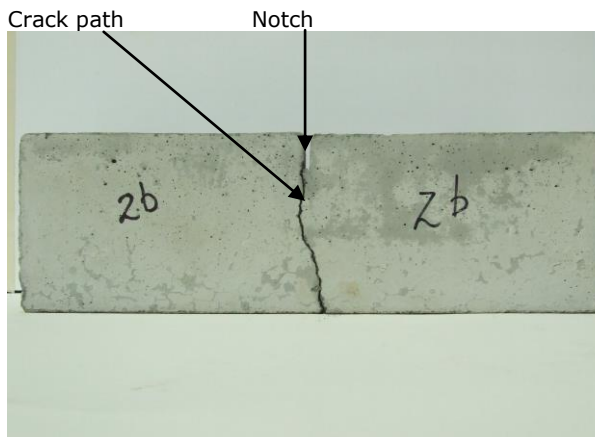
d) Located events listing



e) AE waveform



f) Hits vs Time (s) vs Param load (mV)
(Red curve: param load)



g) Fractured sample

Fractured surface

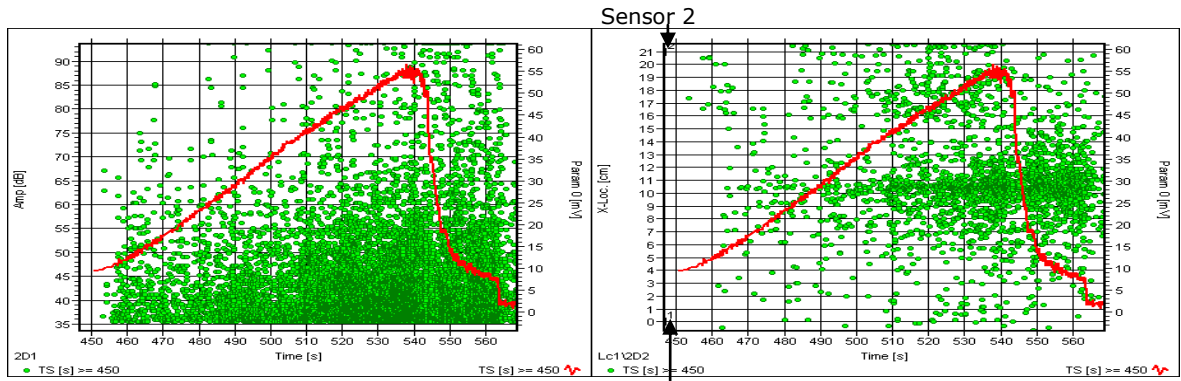
Figures 6.22: AE plots and photo of fractured sample of Mortar with <1mm glass aggregates

6.6.3 Mortar with 1 – 1.7 mm Glass aggregates: Sample KOLA 5B

The introduction of the same amount of glass aggregates with a range of 1-1.7 mm size exhibit differences in AE activities compared to standard specimen, see figures 6.23 (a and b). The load curve rises steadily from 455 seconds (when the actual test was started) and drops at 540 seconds, with the activities being recorded by both sensors, indicating micro-crack initiation and propagation are taking place throughout the sample, therefore a very high level of toughening in the specimen can be noticed.

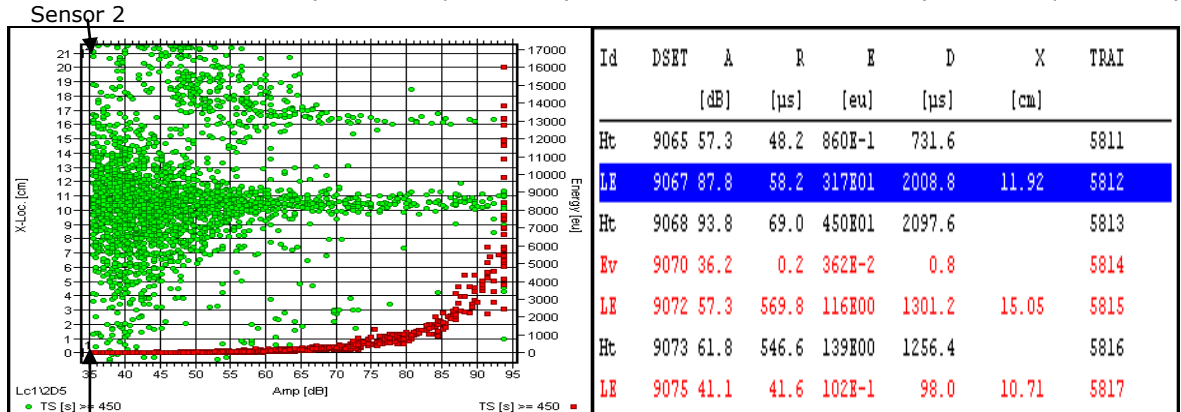
The specimen failed at the notch (weaker region and under tension), location 11.92 cm with very high amplitude of 87.8 dB and long event duration of 2008.8 μ s. The transient waveform captured at failure indicates a high signal level at this event indicating a strong bond between the cement pastes and aggregate, therefore the sample does not fail abruptly. A large number of events with long duration were recorded for this sample. The micro-crack propagation has resulted in the formation of larger cracks hence the higher number of events with high energy level (see figure 6.23 (c)). The crack in this sample appeared to be arrested with improvement in flexural strength. This sample has indicated an increase in toughness but no gain in strength under flexural condition compared to specimen KOLA2B (mortar with <1mm glass aggregates).

The values of AE parameters recorded at the event of failure are shown in blue shadings in figure 6.23 (d). The TR waveform is stronger and larger for this specimen which is indicated by the large amplitude and the time it takes to reach the peak is shown in figure 6.23 (e). The larger aggregate size has had an effect on the signals. The numbers of cascaded hits are far higher than plain mortar (KOLA 0B) and mortar with <1mm aggregates (KOLA 2B) (4700 hits) which is probably due to huge number of activities (both at low and at high level) as shown in figure 6.23 (f). Fracture surface and crack path of the specimen is shown in figure 6.23 (g). Glass aggregates are seen to be bonded with pull-outs throughout the surface.



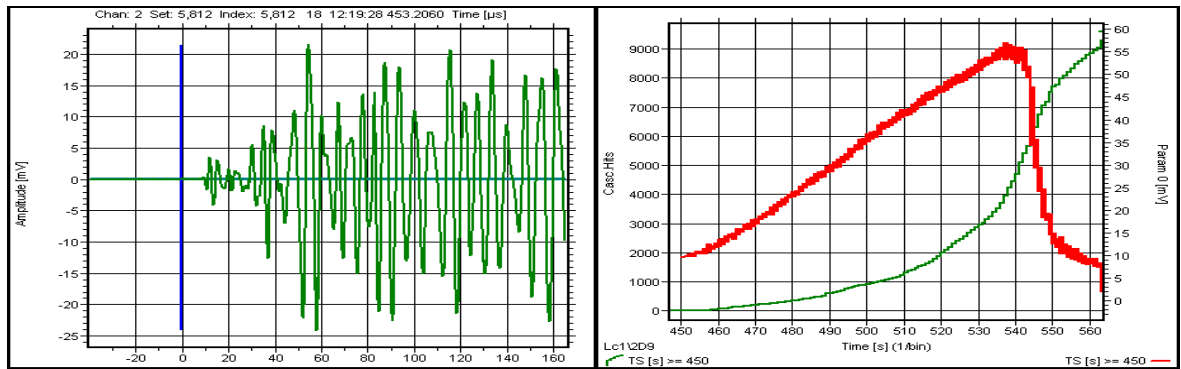
a) Amplitude (dB) vs time (s) vs load param (mV)
(Red curve: param load)

b) X-location (cm) vs time (s) vs load param (mV)
(Red curve: param load)



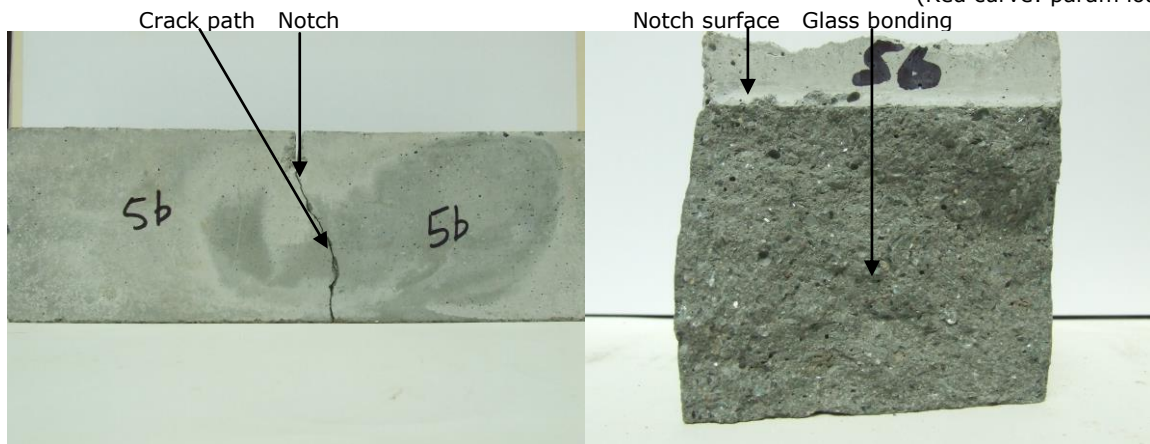
c) X-location (cm) vs amplitude (dB) vs energy (eu)

d) Located events listing



e) AE waveform

f) Hits vs Time (s) vs Param load (mV)
(Red curve: param load)



g) Fractured Sample

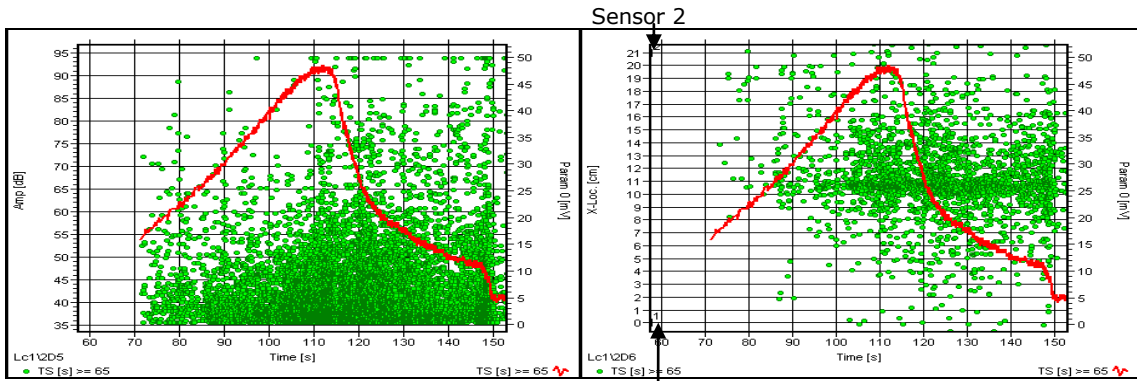
Fractured Surface

Figures 6.23: AE plots and photographs of fractured Mortar with 1-1.7mm glass aggregates

6.6.4 Mortar with 1.7 – 2.36 mm Glass aggregates: Sample KOLA4B

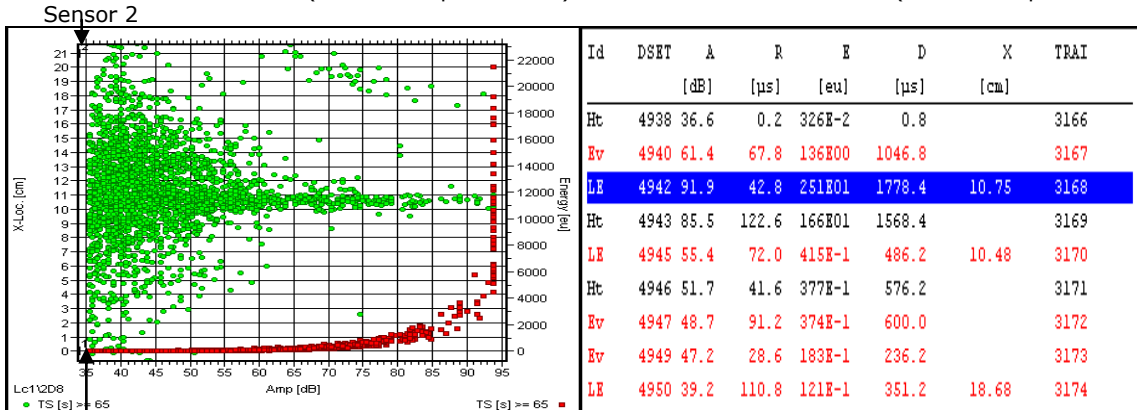
The introduction of glass aggregates with increased size has exhibited lower AE activities with high amplitudes occurring at the higher load. The recorded AE signal parameters are highly energetic indicating that aggregates of this size range offer stronger resistances to cracks. The distribution of activities from very low (above threshold level) amplitude to very high amplitude level indicates toughening due to micro-cracks as well as grain bridging, but as the pattern suggests, toughening is mainly due to micro-cracks, since most of the activities recorded are at very low amplitudes (<55 dB) shown in figures 6.24 (a) and (b). A large number of low AE events start taking place as soon as the test is commenced; the activities are picked up by both sensors. This indicates that a lot of micro-cracks exist at the interface of cement paste and aggregates, thus a high level of toughening in this specimen. These micro-cracks lead to further micro-cracking, brittle glass failure, indicated by a large number of activities occurring between amplitude ranges of 55 dB and 70 dB (see figure 6.24 (c)). Although very few activities can be seen above this level, the main damage zone starts appearing after 100 seconds (amplitude >70 dB). During the failure of the sample, there are also resistances offered by the aggregates, as indicated by the events of very high amplitude (>70 dB). Most of the activities that took place above 70 dB were mainly glass pull-out events, leading to final failure with a major pull out, as indicated by the very high amplitude event at 114 seconds.

The sample failed after very high amplitude, big energetic, long duration, and relatively short rise-time event takes place (91.9 dB, 251E01, 1778.4 μ s, and 42.8 μ s respectively) as shown in the listings in figures 6.24 (d). The failure has taken place when a higher volume pull-out event took place. This is evident in the energetic transient waveform (40 mV) shown in figure 6.24 (e). The numbers of cascaded hits (4000 hits) recorded have fallen as shown in figure 6.24 (f). This is probable due to lesser number of activities that took place under test. The fracture surface and crack paths are shown in figure 6.24 (g). Indentation and pull-out are seen on the fractured surface.



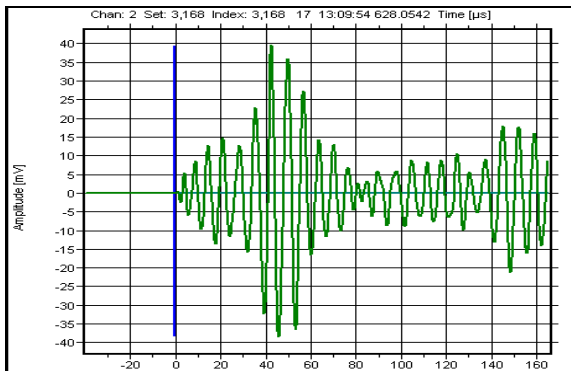
a) Amplitude (dB) vs time (s) vs load param (mV)
(Red curve: param load)

b) X-location (cm) vs time (s) vs load param (mV)
(Red curve: param load)

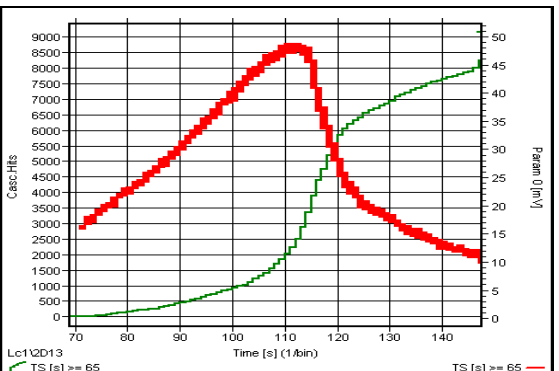


c) X-location (cm) vs amplitude (dB) vs energy (eu)

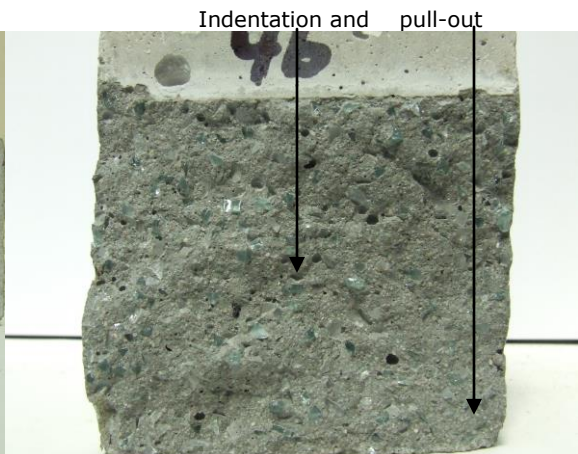
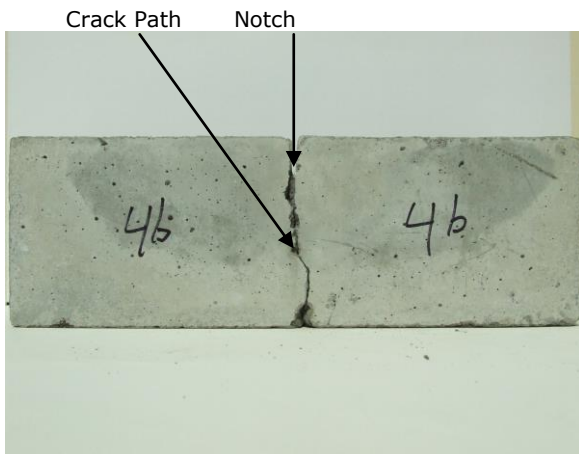
d) Located events listing



e) AE waveform



f) Hits vs Time (s) vs Param load (mV)
(Red curve: param load)



g) Fractured Sample

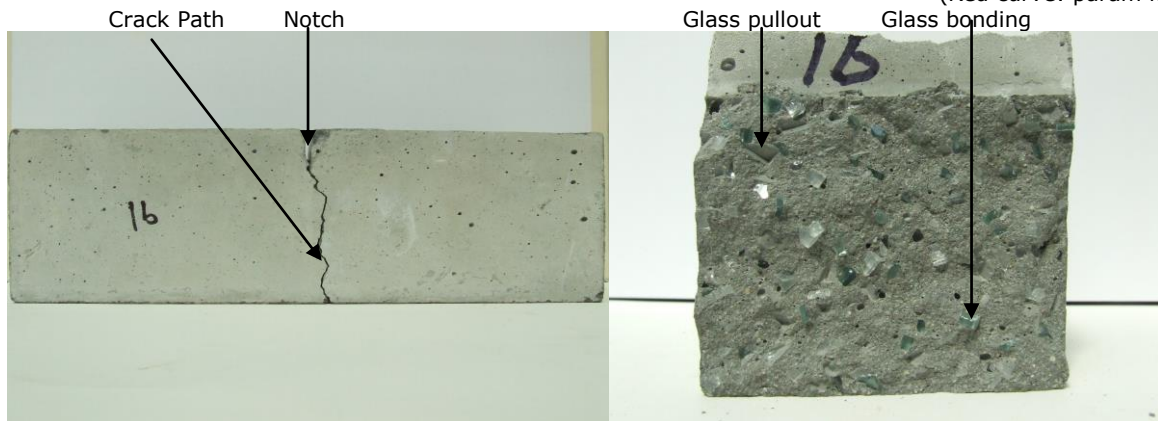
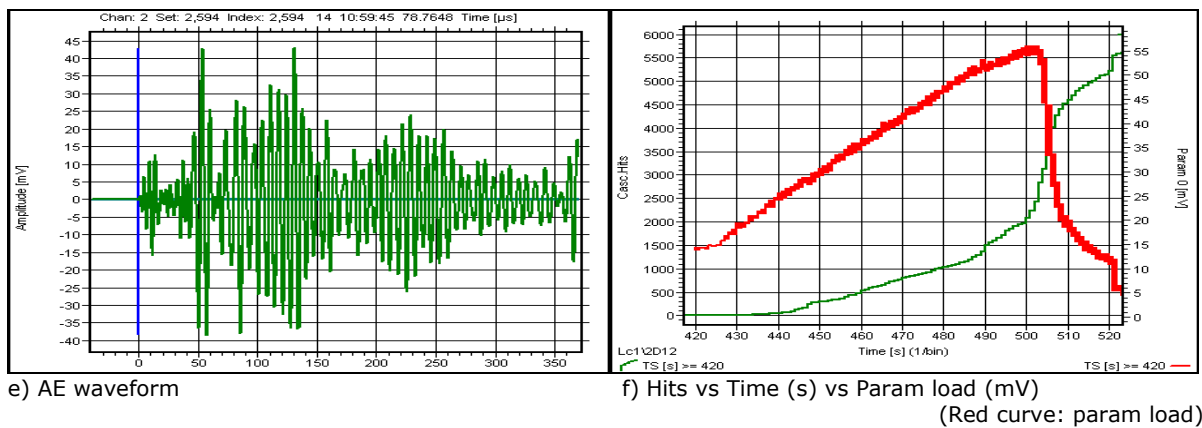
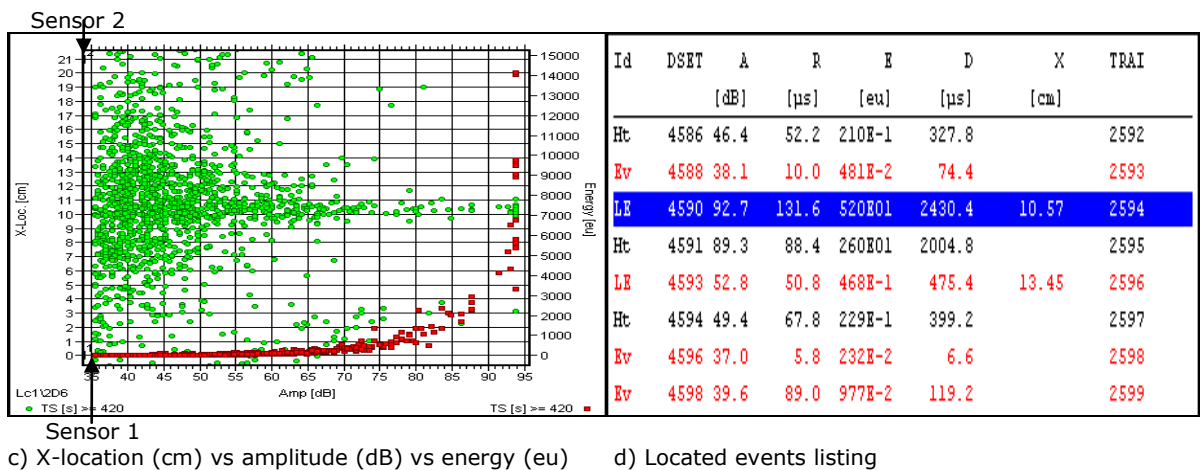
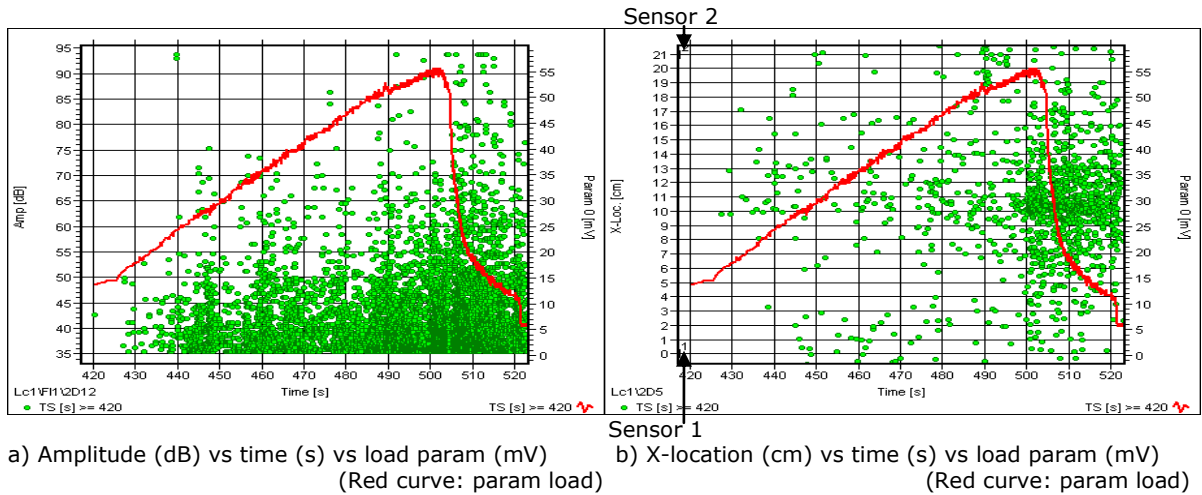
Fractured Surface

Figures 6.24: AE plots and photographs of fractured Mortar with 1.7-2.36mm aggregates

6.6.5 Mortar with 2.36 – 3.35 mm Glass Aggregates: KOLA1B

AE Monitoring of sample manufactured with Glass aggregate size range of 2.36-3.35 mm show a drop in activity during flexural test indicating less toughening occurring under test in the mortar. Both sensors were active in picking signals from the central portion of the specimen (9-13 cm). Compared to other specimens containing glass aggregates less than 2.36 – 3.35 mm size, there are fewer events at low amplitude, and of short duration. A large number of events were recorded at high amplitudes (> 55 dB) with increasing load, (see figure 6.25 (a) and (b)). This is an indication of large crack arrests/crack manipulation, as visible from the skewness of the load curve. The number of activities are almost equally recorded by both sensors with only 11 events of (amplitudes above 70 dB and energy events above 2000 eu) (shown in figure 6.25 (c)).

The specimen failed at 500 seconds (almost after 100 seconds of loading). The failure happened with a big pull out event as indicated by the sudden load drops, giving rise to high amplitude, long event duration, big energy and short rise time, (92.7 dB, 2430.4 μ s, 520E01 and 131.6 μ s) as shown in the listings 6.25 (d). The high value of transient waveform indicates the large crack that leads to final failure 6.25 (e). The failure location is estimated to be between 10 and 11 cm. A number of events (both major and minor) took place during the final failure as indicated during load drop. The numbers of recorded cascaded hits have fallen to 2800 (see figure 6.25 (f)). The crack track and fractured region shows very irregular structure with large pultrusions and indentations, (figure 6.25 (g)).



g) Fractured Sample Fractured Surface

Figures 6.25: AE plots and photographs of fractured Mortar with 2.36-3.35 mm glass aggregates

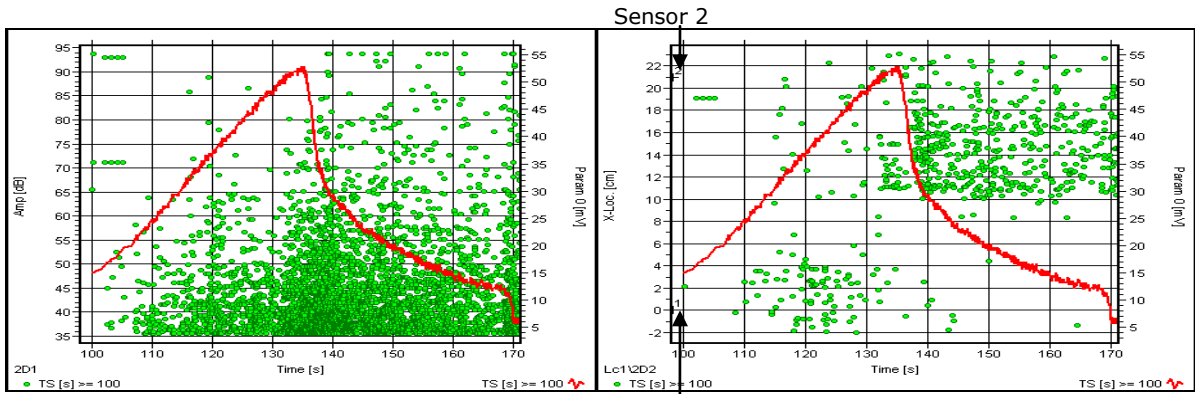
6.6.6 Mortar with 3.35 – 4 mm Glass Aggregates: Sample KOLA 3B

The addition of aggregates with this range of sizes in mortar has increased the load of the specimen compared to plain mortar. The AE characteristics have changed significantly in comparison to other specimens. Most of the events took place between location 10-21 cm (which were picked up by sensor 2) as shown in figures (6.26 (a and b)). This is probably due to most of the aggregates settling at this end of the specimen as seen in figure 6.26 (C). The toughening in this specimen is significantly lower in this mortar this is due to the lesser number of glass segments (but of same weight, i.e. 530 g).

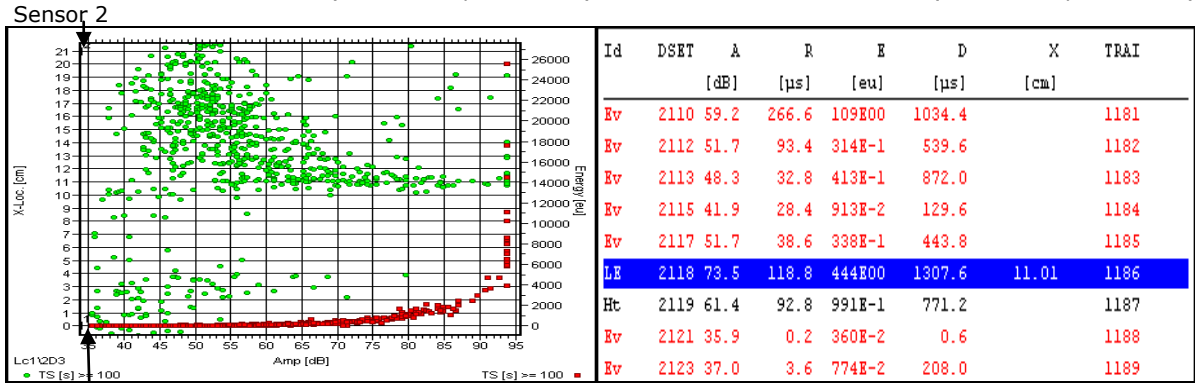
The load curve steadily rises (few micro-cracks initiated and propagating), facing few obstacles such as pull out events, until obstructed by a large pull out event, when the load drops at 134 seconds (or 34 seconds after the proper test was started). This pull out event at failure was a large activity in this mortar with high amplitude (73.5 dB at a failure location of 11.01 cm shown in figure 6.26 (c and d).

The transient waveform captured at failure is larger and stronger than any other waveforms captured from failure point of other specimens as shown in figure 6.26 (e). The least number of recorded hits (2500) are in this sample (figure 6.26 (f)). This is probably due to fewer micro-cracks that took place during the test.

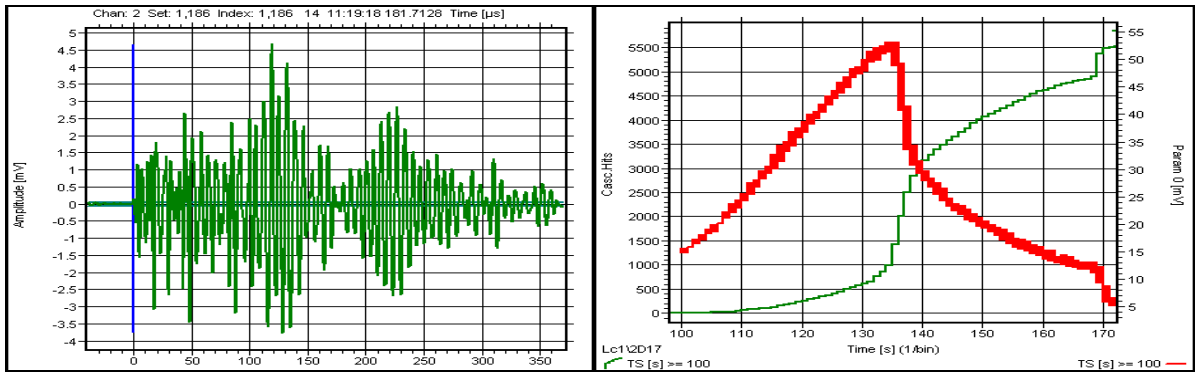
The aggregate sizes used in this specimen have made a big contribution to the resistances of the crack paths offered by the aggregates. This is also clearly reflected in the size, shape, and the value of the waveform, which is indicated by the peak amplitude value and the duration of the signal as in the listing of 6.26 (d). The crack fractured region and fractured surface shows large pultrusions and indentations as shown in figure 6.26 (g).



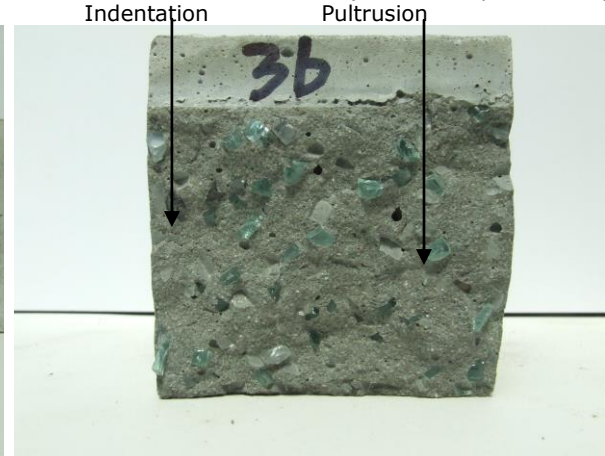
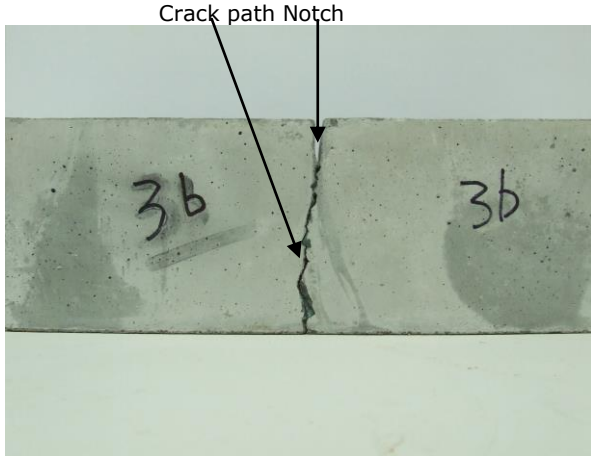
a) Amplitude (dB) vs time (s) vs load param (mV) (Red curve: param load) b) X-location (cm) vs time (s) vs load param (mV) (Red curve: param load)



c) X-location (cm) vs amplitude (dB) vs energy (eu) (Red curve: param load) d) Located events listing



e) AE waveform f) Hits vs Time (s) vs Param0 (mV) (Red curve: param load)



g) Fractured sample Fractured surface

Figures 6.26: AE plots and photographs of fractured Mortar with 3.35 mm-4 mm Glass Aggregates

6.6.7 Discussion

For all the specimens, at the initiation of the test, a large number of AE hits were recorded very rapidly within a very short span of time. The reason for such quick recording is probably due to the roller head touching the rubber pad resting on mortar. From this point, micro-cracks were initiated and grew in large numbers rapidly between the weak boundaries. Therefore, many AE signals were emitted and recorded under flexural condition, so AE hits increased rapidly. As the flexural load proceeded, the cracks propagated, facing resistances from the aggregates resulting in crack arrests (minor and major) and strong bonding between cement paste and glass, AE hits also increased steadily.

Prior to failure, the cracks faced bigger resistances from glass, major pull-out event occurred with long durations, therefore a rise in AE hits were noticed during this period. The AE hits increase rapidly in plane concrete and the least increase is in specimens with 2.36-3.35 mm aggregates and in specimen with 3.35-4mm aggregates. This is an indication of the stronger resistance offered by the glass aggregates. In all the specimens, it can be observed that there exists a significant trend in the variation of total AE hits during the entire testing period.

The AE cascaded hits pattern is varied for all the specimens. In the case of plain mortar, the rate of AE hit increase is steady and rises in a linear manner; while all other samples show a mixture of exponential and semi-exponential behaviour. This is due to the glass aggregates blocking the crack paths during the tests.

The bar chart in (figure 6.27) shows a comparison of AE hits between different samples. The number of AE hits cascade captured by different samples is tabulated.

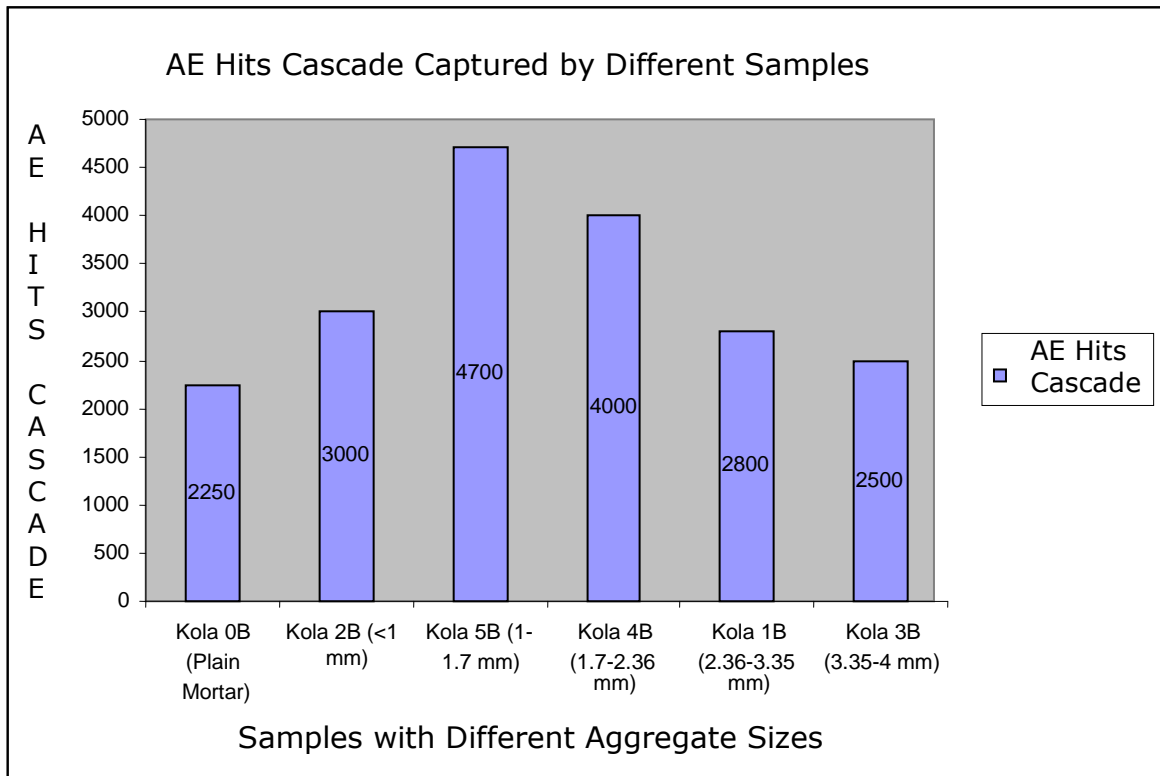


Figure 6.27: Variation of AE hits cascade captured by different samples

The number of AE hits for each sample shows a difference in variation. The number of AE hits is significantly increased in mortar with <1mm glass aggregates (i.e. KOLA2B) compared to plain concrete mortar (KOLA0B) once glass aggregates (<1 mm) are introduced. However, once the other specimens are put under test with increased size of aggregates (2.36-3.35 mm and 3.35-4 mm aggregates), the AE hits exhibit a decrease in number. As the aggregate size is increased, the AE hits start decreasing. This correlates with the amount of toughening for each specimen. The mortar containing <1 mm aggregates (KOLA2B), for example, had indicated excessive amount of AE activities (as shown in the AE plots), this was an evidence of high level of toughening in the specimen. The sensors recorded highest number of AE hits for this mortar under flexural test.

The mortar (sample KOLA3B) containing 3.35-4 mm aggregates had exhibited the least number of AE activities (as was shown in the AE plots); therefore less toughening had occurred during the test. The AE hits are also seen to be lowest for this specimen. Therefore, it can be deduced that more toughening in a specimen results in more AE hits picked up by the sensors.

6.6.8 Flexural Strength Measurements

The flexural strength (Modulus of Rupture) and fracture toughness for each sample were calculated using the equations (3.5) and (3.6) described in chapter 3. The results for each sample containing incremental aggregate sizes are shown in table 6.6.

$$\text{Modulus of Rupture } (\sigma) = \frac{3FL}{2bd^2} \text{ and the}$$

$$\text{Fracture Toughness } (K_C) = \frac{3FLYa^{0.5}}{2bd^2} \text{ (i.e. } K_C = \text{Modulus of Rupture} \times Ya^{0.5}\text{)}$$

(Taking the dimensionless value of $Y=1.12$; adopted from William D. Callister, Materials Science and Engineering: An introduction, 7th Edition, 2006, [187].

Table 6.6: Flexural strength and Fracture Toughness for each sample containing incremental aggregate sizes

<u>SAMPLES</u>	<u>MODULUS OF RUPTURE (MPa)</u>	<u>FRACRURE TOUGHNESS (K_c) MPa.m^{1/2}</u>	<u>NUMBER of AE HITS</u>
KOLAOB (Plain concrete)	1.9	0.213	2250
KOLA 2B (< 1mm)	3.1	0.34	3000
KOLA5B (1.0 -1.7mm)	2.79	0.31	4700
KOLA 4B (1.7-2.36 mm)	1.64	0.18	4000
KOLA1B (2.36-3.35mm)	2.20	0.24	2800
KOLA3B (3.35 – 4 mm)	2.08	0.23	2500

The relation between the Modulus of Rupture, fracture toughness and the AE hits are shown in figure 6.28. The addition of glass aggregates have resulted an increase in the breaking load of the mortars in comparison to the plain concrete. Only the sample containing 1.7-2.36 mm aggregates (KOLA4B) had shown an adverse effect on the maximum load, this was probably due to the bad preparation and quality of the mortar. All the other samples had indicated an increase in the breaking load, and thus in the flexural strength.

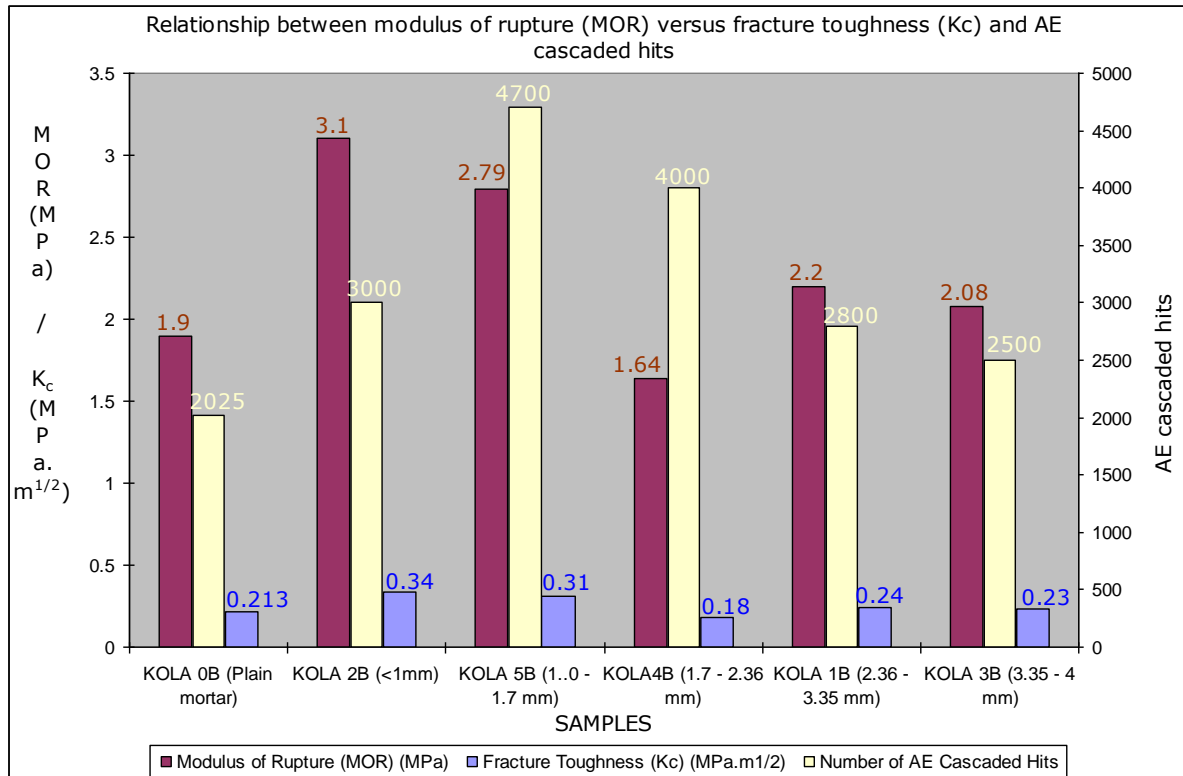


Figure 6.28: Relationship between modulus of rupture (MOR) versus fracture toughness (Kc) and AE hits.

Addition of glass aggregates had an effect on the Modulus of Rupture and the fracture toughness of concrete; this also resulted in intense AE hits recorded under the flexural condition. The excessive amount of AE hits recorded during testing of sample KOLA2B (containing <1 mm glass aggregates) corresponds to the high Modulus of Rupture, this is probably due to the large number of glass segments. Although the maximum load and the flexural strength have increased due to the addition of glass aggregates up-to a certain size, which is also reflected on the AE hits, but no evident link can be established between the strength of concrete and the size of glass used.

However, the hits versus time plots show that specimens with 2.36-3.35 mm and 3.36-4 mm glass aggregates (samples KOLA1B and KOLA3B) offer stronger resistance to the cracks resulting in high energy, high event duration pull out events (sudden load drop). The time taken from the maximum load to final fracture depends on the number of these pull out events and degree of porosity in the tested block.

The larger sized aggregates have prevented or arrested the crack growth and the occurrences of a high number of micro-cracks and this is the reason for less

activity recording in samples with 2.36-3.35 mm aggregates (KOLA1B) and 3.35-4 mm (KOLA3B) shown in figures 6.25 (b) and 6.26 (b). The results of samples KOLA2B (with < 1mm glass aggregates) and KOLA5B (with 1 - 1.7 mm glass aggregates) as shown in figures 6.22 (a, c) and 6.23 (a, c) which have majority activities with low amplitude activities recorded compared to any other samples. This confirms that these two specimens had more micro cracks and crack propagations than any other samples. Therefore it can be deduced that the sample with <1mm glass aggregates (KOLA2B) is the best amongst all the specimens in this batch in terms of toughening.

The toughening in sample with the largest aggregate size, i.e. 3.36 to 4 mm (KOLA3B) is controlled by crack bridging; the strong bonding between the cement paste and the aggregates as was shown in pictures (figures 6.21 (g) - 6.26(g)) where the crack faced resistance.

In the sample with the smallest aggregate size (<1 mm glass aggregates), the toughening is a contribution due to micro-crack formation. All the other samples show toughening which are due to both micro-crack formation and crack bridging.

6.6.9 Summary

The failure mechanisms of concrete containing different sizes of glass aggregates under flexural condition have exhibited different AE characteristics. With the addition of glass aggregates, the toughening of concrete mortar is increased. This toughness is only valid if the use of glass aggregates used is confined up to 1 mm, as indicated by excessive amount of AE activities. The toughness however does not increase with the size of glass aggregates, nor does the flexural strength, but no adverse effect on its strength is observed. The AE behaviour for different samples under flexural load has their own distinctive and unique characteristics. This is indicated by the number of AE hits and the pattern of activities for each block. The sizes of aggregates have exhibited their own distinctive features.

From the analysis above it can be concluded that the usage of glass aggregates do not have an adverse effect on the strength, toughness of mortar under flexural condition. However, the sizes of glass aggregates do make an impact on both the strength and the toughness of the concrete mortars.

6.7 Monitoring Toughening Behaviour due to Addition of Various Additives and Aggregates

A comparison is made between different toughening modes that are obtained due to the addition of various methods and ingredients (i.e. additives, aggregates and slide). A suggestion can therefore be made regarding the effective method that can be used as a toughening enhancer.

The followings are investigated:

- i) Mechanism (Grain Bridging / Micro-cracking);
- ii) Interfacial Mechanism;

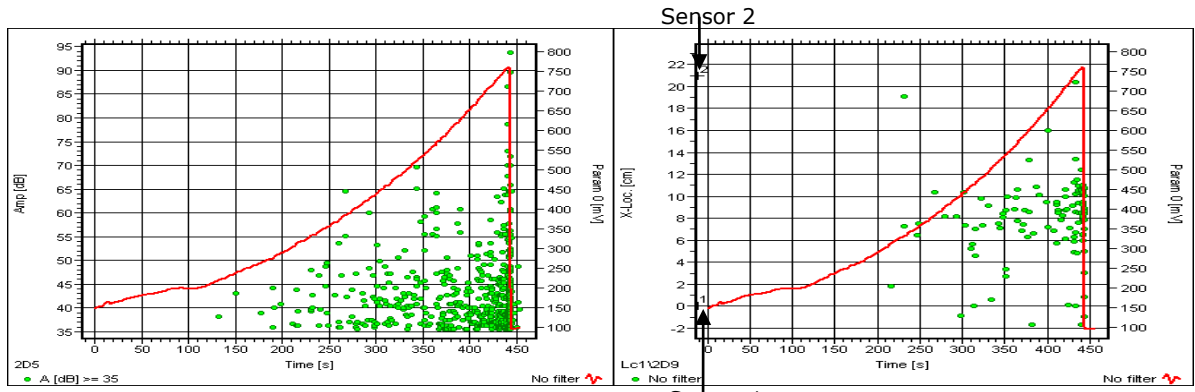
6.7.1 Crack Bridging and Grain Bridging: Plain Mortar, Mortar with Glass Plate, Mortar with Glass Aggregates and Glass Plate

Three mortar samples were manufactured with the following compositions (i) plain mortar, (ii) mortar containing glass plate, and (iii) mortar with glass plate and glass aggregates. The purpose of putting these mortars under flexural test was to see the effect of crack bridging on toughness of concrete.

6.7.2 Plain Mortar

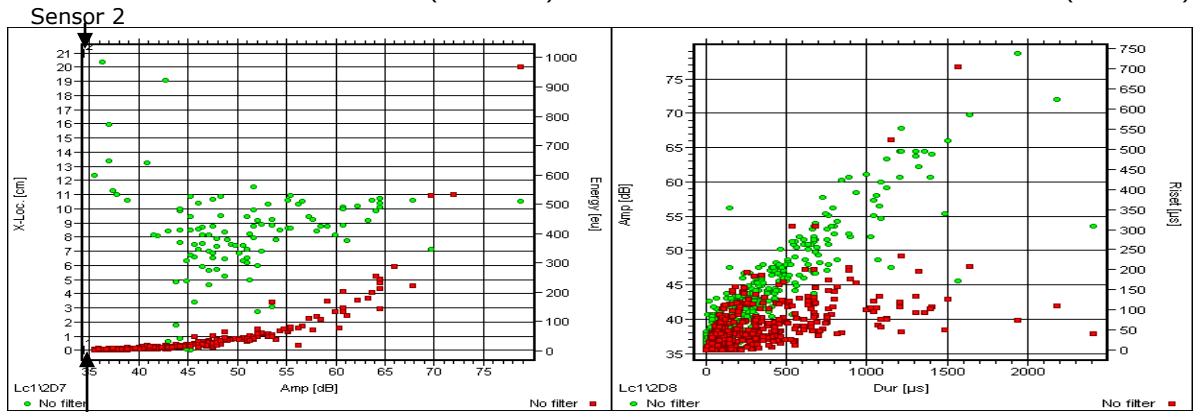
The AE activities and load versus time plot for plain mortar under flexural condition is shown in figures 6.29 (a)-(c). In plain mortar, initially few activities were noted at very low amplitudes (<45 dB) which may be due to the rollers settling on the rubber pads. Once settled, the AE activities increased as the load progressively rises. Most of the activities are at low amplitudes (<60dB), this indicates that voids existed while causing these events in the specimen. Very few (<12) AE activities were recorded at higher amplitudes (>60 dB). The number of events with high energy at high level (> 500 eu) is only 3 and the number of high level rise-time events are 2 (> μ s), (see figure 6.29 (b) (i) and (ii)). The numbers of hits increase with mid-high amplitudes (> 60 dB) as the sample approaches failure as shown in figure 6.29 (c) i) and ii). The sample fails with few high amplitude events indicating a formation of major crack as a result of coalescent of micro-crack leading to fracture.

Optical photographs of fracture samples and surfaces are shown in figure 6.29 (d) i) and ii). Porosities can be seen on the fractured surface.



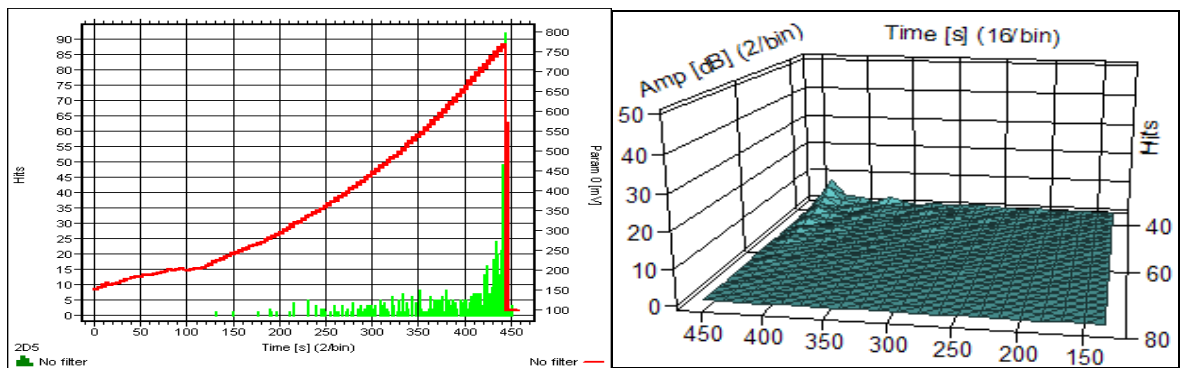
a) i) Amplitude (dB) vs time (s) vs parametric load (mV) (Red curve)

ii) X-location (cm) vs time (s) vs parametric load (mV) (Red curve)



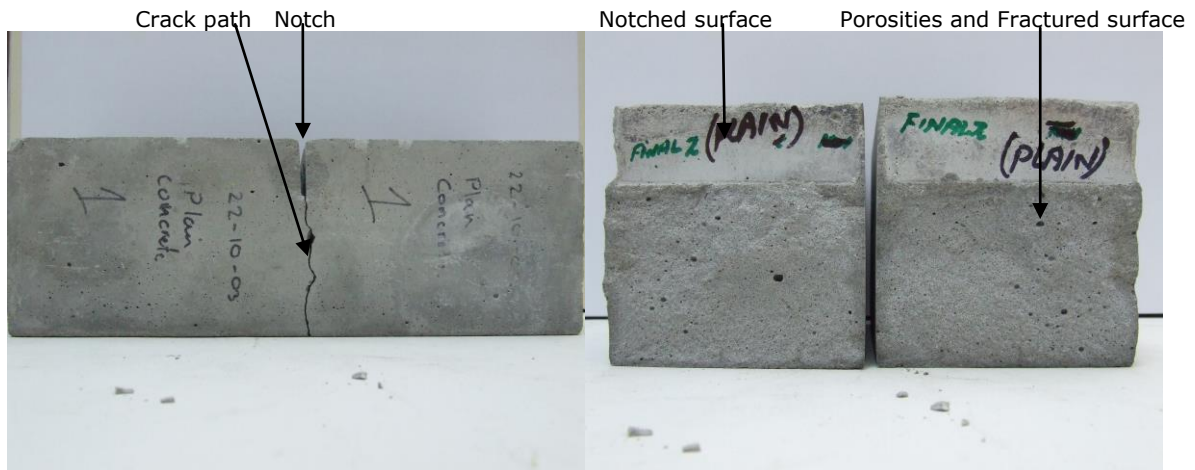
b) i) X-location (cm) vs Amplitude (dB) vs Energy (eu) (Red dots)

ii) Amplitude (dB) vs Duration (μs) vs Risetime (μs) (Red dots)



c) i) Hits vs time (s) vs param load (mV) (red curve)

ii) 3D Plot of Hits vs time (s) vs Amplitude (dB)



d) i) Plain Mortar

ii) Fractured surface

Figure 6.29: AE Plots and Optical photographs of fractured sample and surface for plain mortar

6.7.3 Mortar with Glass Plate

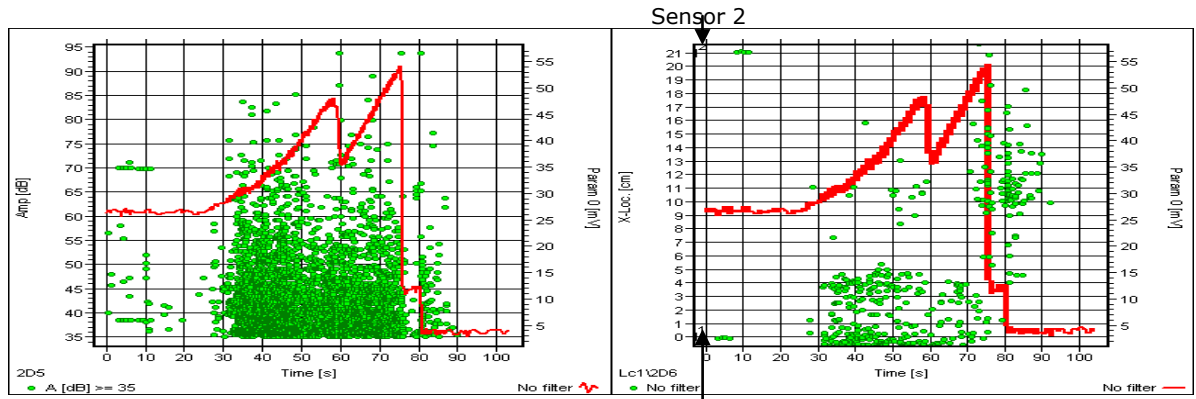
At the start of the flexural test very few AE activities were recorded for about 30 seconds; (figure 6.30 (a) i) and ii). This is due to the roller settling on the rubber pad placed on the sample to dampen the friction. With increasing load on the sample AE activities were recorded at low amplitudes (<60 dB), this is attributed to the formation of micro-cracks that lead to macro-crack (since some activities are visible at higher amplitudes (>70 dB)). The number of events with high energy level (> 500 eu) is 6 (see figure 6.30 (i)).

After about 55 seconds, the crack possibly reached the glass slide and the load dropped, therefore no AE activities in the higher amplitude region (>70 dB) were observed between 55 and 60 seconds. The AE activities during this period were of low amplitudes, this is due to the events occurring in the matrix and glass boundary region.

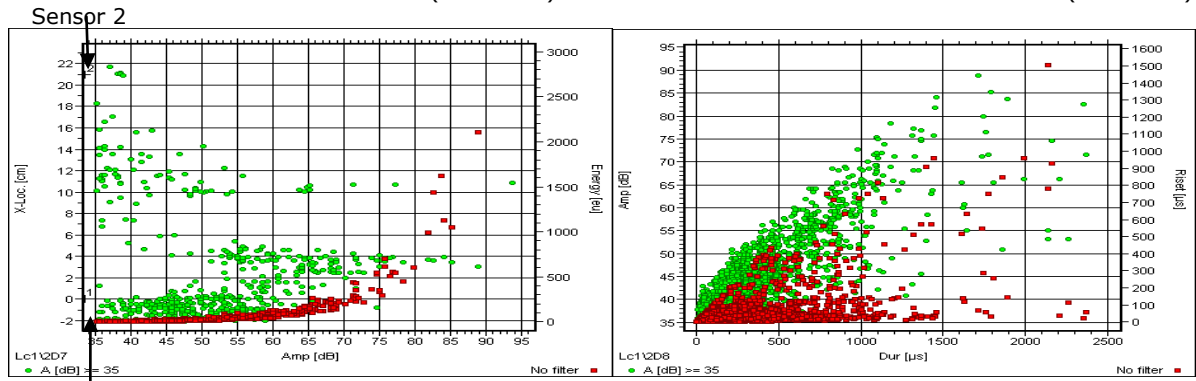
Finally, the load is taken over by the glass plate, which eventually fails with a sharp load drop (as indicated by a few high amplitude events), at location 10-11 cm. At this point the AE events were high amplitude, longer duration and short rise time intervals (>70 dB, $1000 \mu\text{s}$, and $< 200 \mu\text{s}$) as shown in figure 6.30 (b) i) and ii).

The number of hits also dropped with the load drop which is also attributed to the crack obstacle by glass plate (as shown in figure 6.30 (c) (i)). This is also seen in 3-D the plot where the drop in numbers of hits is visible at 55 seconds.

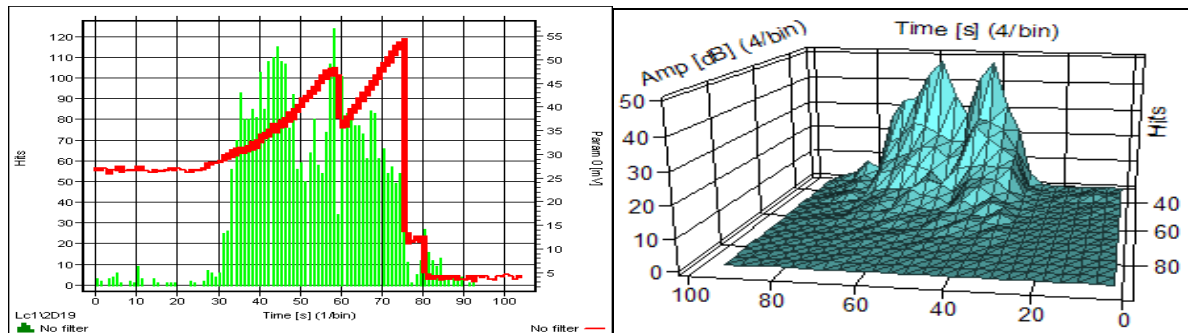
Optical photographs of fractured sample and surface are seen in figure 6.30 (d). The crack path follows a straight path, which is probably the reason for a number of high peak amplitude in the central region (as seen in figure 6.30 (b) i). The glass slide is seen to be settled towards the lower part of the specimen because of the vibration of the mould during sample preparation as seen on the fractured surface. This is linked to the load curve rising at 60 seconds and dropping at 74 seconds which is probably linked to crack propagation after the glass slide is overcome.



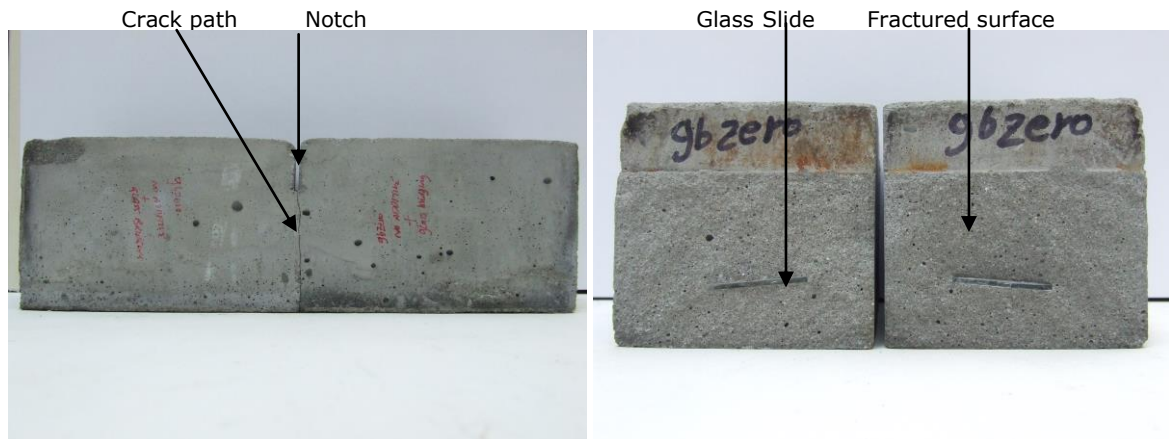
a) i) Amplitude (dB) vs time (s) vs parametric load (mV) (Red curve) ii) X-location (cm) vs time (s) vs parametric load (mV) (Red curve)



b) i) X-location (cm) vs Amplitude (dB) vs Energy (eu) (Red dots) ii) Amplitude (dB) vs Duration (μ s) vs Risetime (μ s) (Red dots)



c) i) Hits vs time (s) vs param load (mV) (red curve) ii) 3D Plot of Hits vs time (s) vs Amplitude (dB)



d) Mortar with Glass Slide Fractured surface

Figure 6.30: AE Plots and Optical photographs of fractured sample and surface for mortar with glass slide

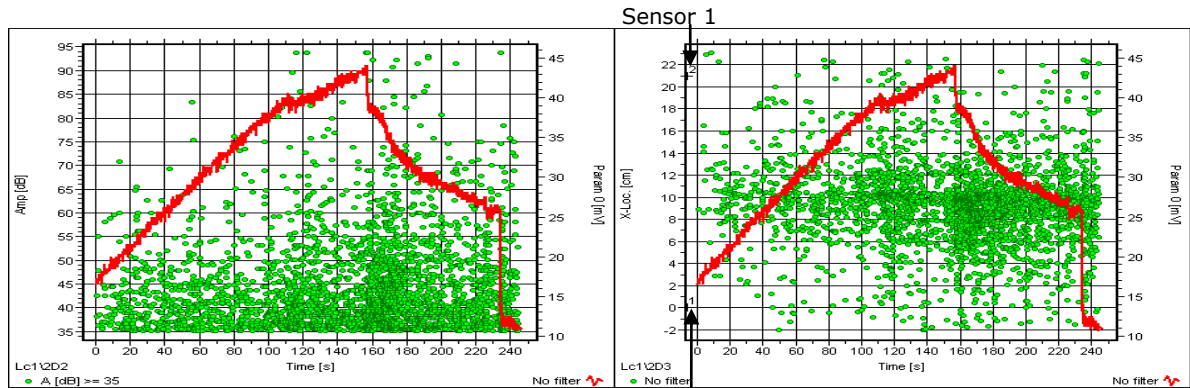
6.7.4 Mortar with Glass Plate and Glass Aggregates

In the case of sample containing both glass aggregates and glass plate it is evident in figures 6.31 (a) i)-ii) that after a period of 111 seconds, the load is transferred to the glass plate (changed slope) and the crack after propagating from the notch is completely bridged by the plate. The crack overcomes this obstacle with a sharp load drop after 156.25 seconds, producing high energy, long duration and short rise-time events. The glass aggregates then becomes active by deflecting the crack causing a number of major pullout events before final fracture of the block.

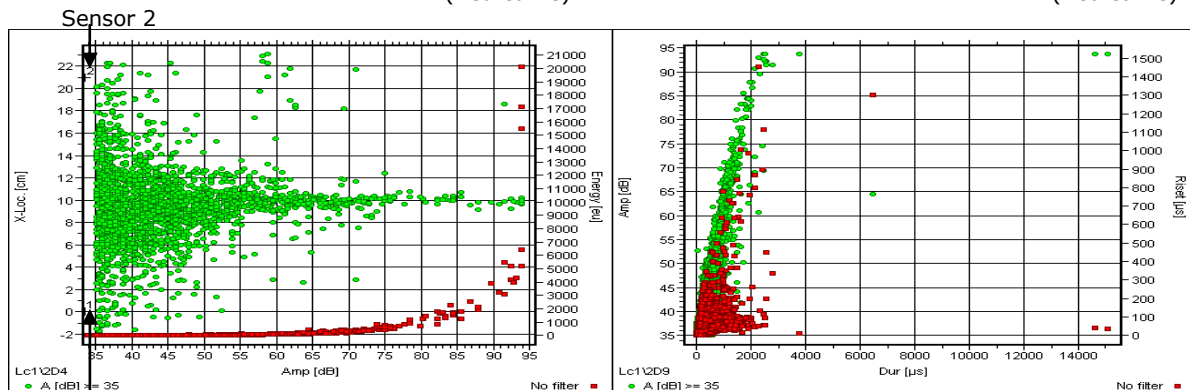
It is apparent from the AE plots shown in figures 6.31 (a) i) and ii), (b) i) and ii) (c) i) and ii); that the extra AE activity is the result of addition of glass aggregates to the concrete block. It is conspicuous from the flexural test results of these blocks that the additional sources of AE are due to deflection of crack, arrest of crack, pullout events at glass aggregates and major pullout events at porous regions.

The energy emitted from this sample containing glass aggregates is of higher magnitude compared to plain mortar block and the mortar with glass plate only with events of very short rise time and longer duration. The change of crack path due to glass plate is apparent and distinguishable in both specimens as can be seen in AE plots and optical micrographs as shown in figure 6.31 (a)-(d).

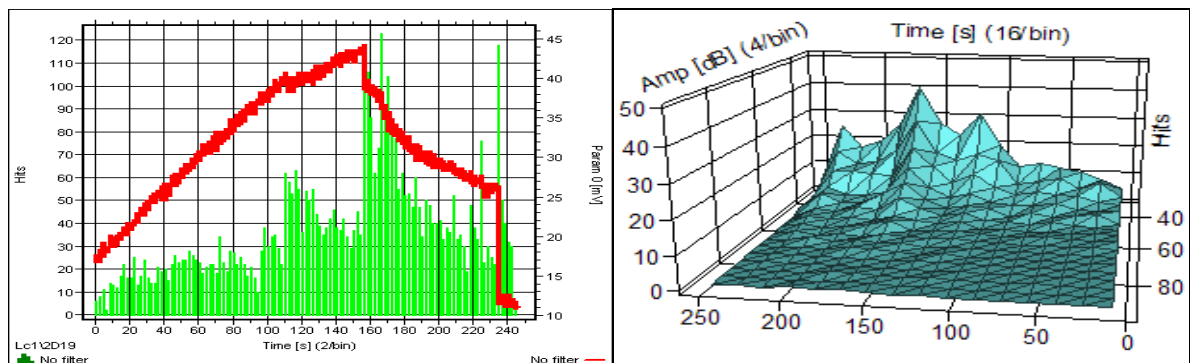
The load-time history plot for both samples containing glass plate shows distinct deviation from the linear behaviour at various times and exhibits three slopes representing the initial strength of the mortar, the strength of the glass plate and the final strength of the mortar containing glass aggregates. The effect of the introduction of glass aggregates can clearly be seen from the 3-d plots in figures 6.31 (c) (ii).



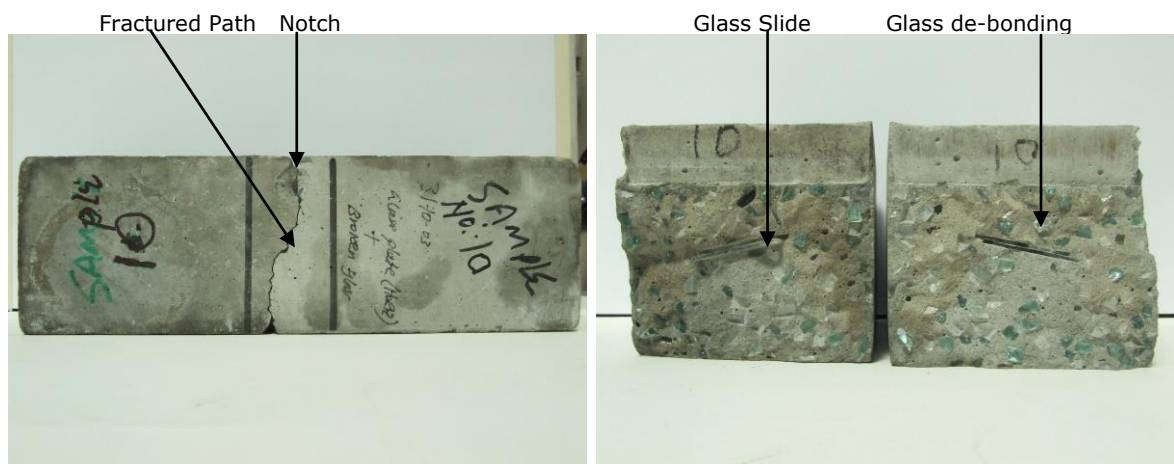
a) i) Amplitude (dB) vs time (s) vs parametric load (mV) (Red curve)
 ii) X-location (cm) vs time (s) vs parametric load (mV) (Red curve)



b) i) X-location (cm) vs Amplitude (dB) vs Energy (eu) (Red dots)
 ii) Amplitude (dB) vs Duration (μs) vs Rise (μs) (Red dots)



c) i) Hits vs time (s) vs param load (mV) (red curve)
 ii) 3D Plot of Hits vs time (s) vs Amplitude (dB)



d) Mortar with Glass Slide and Glass Aggregates

Figure 6.31: AE Plots and Optical photographs of fractured sample and surface for plain mortar with glass aggregates and glass plate

From the number of AE hits produced by each of the sample under applied load, it can be established that the inclusion of each component had contributed to its own share in generating AE hits. By looking at figures 6.32, 6.33 and table 6.7, it can be deduced that in any typical mortar sample containing glass slide (sample gbzero), the number of AE hits increase by almost 6 times more the plain mortar (table 6.7 and figure 6.33). Increasing the content (sample 10 which contains glass plate and glass aggregates), additional hits are produced indicating further toughening of this type of sample. This is an implication that another similar type of specimen tested by the same apparatus and tested under the same conditions would also demonstrate identical level of toughening.

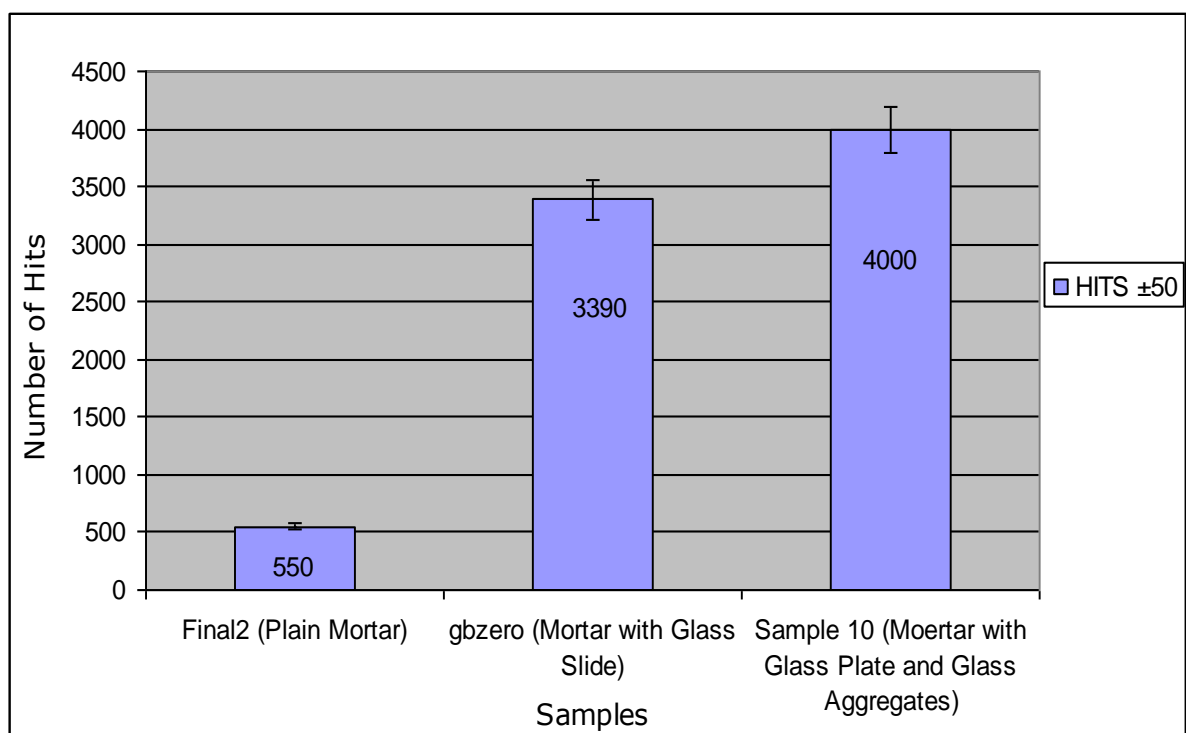


Figure 6.32: Number of AE hits captured by different samples under applied flexural load

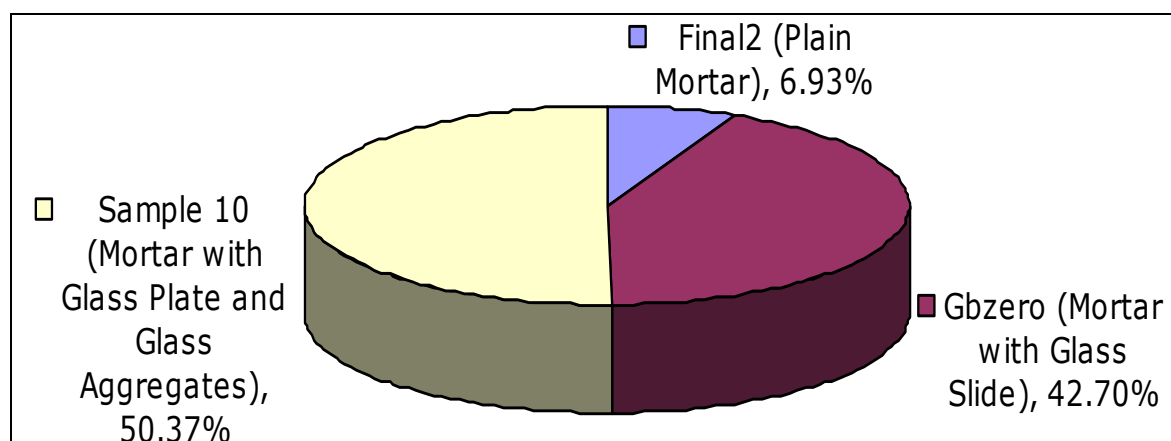


Figure 6.33: Pie chart showing percentage of AE Hits for each sample

6.7.5 Summary

The mortar sample with glass plate failed abruptly which is an indication of the brittleness mortar as there are no obstacles to arrest, deviate or modify the crack propagation path. The crack follows a flatter path (see figure 6.30 (d)). The fracture nature of sample with glass plate and glass aggregates demonstrate control on the crack path due to the interfacial bonding between the glass inclusions and matrix, which is an indication of toughening.

From the AE plots obtained, the glass plate region is very clearly visible by:

- i) the lesser number of AE activities generated;
- ii) the deviation of the crack paths;
- iii) the location of glass plate below the notch in the two samples are approximately 44 mm and 29 mm respectively. Hence the time taken to failure for the two samples is different.
- iv) a minor resistance to crack propagation.

This investigation has demonstrated an obvious advantage of AE monitoring technique in the control of toughening behaviour in a complex material like concrete.

Crack growth occurs in three different ways (figure 6.34):

- i) Crack growth takes place when the two sides of the crack are subjected to a tensile force. The two sides of the crack move away from one another in the opposite directions perpendicular to the tip of the crack.
- ii) Crack growth occurs when the two sides of the crack move away from one another parallel to the tip of the crack.
- iii) Final crack growth takes place when one side of the crack moves into the void and the other side move towards the tip of the crack.

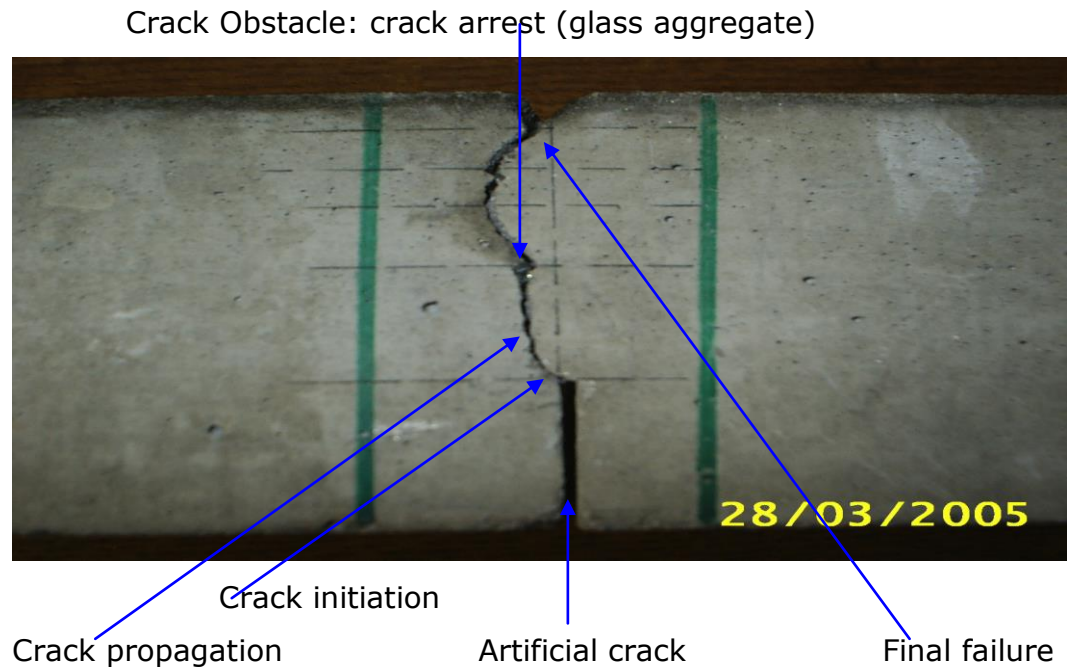


Figure 6.34: Crack growth paths of mortars

The crack growth is usually linked to the applied load but it propagates through the path of least obstacles resistance, e.g. it will travel through voids, which allow a path of lesser resistance. Therefore, crack growth manipulation can be carried out by the introduction of obstacles (aggregate) or modification of the material resistance by the introduction of admixtures. In real life situations, the monitoring of structures may be able to detect the initiation of crack growth from the defective points.

Cracks begin from regions which are essentially free from flaws, and can also occur at the point of defects which are already present. In the three point flexural test, the crack is instigated by the intense load applied, that breaks the sample block into two different pieces. The initial loading of the blocks resulted in acoustic emission activity throughout. The larger force is applied on the central portion of the sample, compared to the outer portion, therefore the sample brakes in the central portion causing the crack to propagate in this region rather than other parts of the specimen. The development of crack growth has been observed with the introduction of aggregates in concrete mortar, i.e. the cracks avoid the aggregate region. As it can be seen from figure 6.35, the crack propagates through the specimen; when it is arrested by an aggregate, it has to find way around or through the aggregate. The crack then finds the path around the aggregate and continues to develop through the sample, as can be clearly seen in figure 6.35.

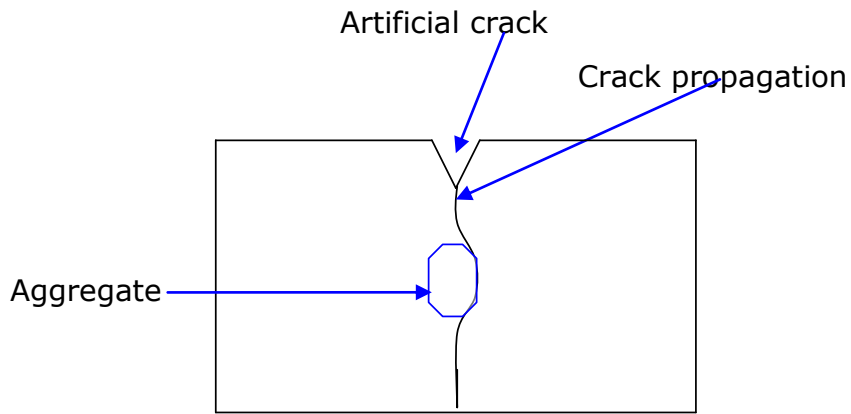


Figure 6.35: Crack propagation in a mortar

Crack bridging (the phenomenon of arresting of the crack occurring in the sample and its effect on the crack) has a direct link on the acoustic events taking place during the test, which means that the cracking mechanism has a direct relationship with the AE signals being emitted. No current work existed connecting AE directly to the type of cracking mechanism in concrete mortar with an aggregate, therefore from this research it has been established that the AE signals are directly related to this kind of grain bridging/micro-mechanism and interfacial technology.

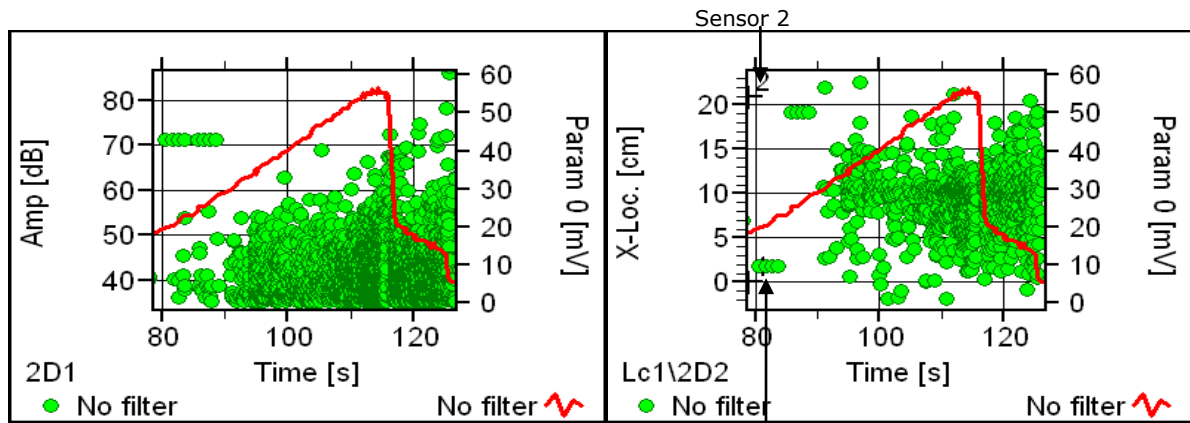
6.8 AE Monitoring of Cracks in Concrete Containing Rubber Aggregates under flexural load condition

As mentioned in chapter 1, waste rubber has recently found some space in concrete industry for applications as aggregates, due to their wide availability and places where strength of concrete is not a major factor to be considered such as pavements, decorative slabs. However, some potential may be discovered if AE characteristics are examined to investigate whether any improvement in toughness of mortars containing rubber chunks as aggregates, and resistances to cracks under flexural tests can be obtained.

Therefore, an attempt is made to see the effect of rubber at micro-structural level with the aid of AE, when used as an aggregate in mortar. The rubber aggregates added in these specimens were of random sizes with increased mass. All the samples were manufactured, cured, and allowed to set under similar condition for 28 days. Emphasis was put on weight proportion of aggregates (although they were randomly distributed and the size did not exceed 6 mm) rather than the sizes. This was because the AE effect of rubber aggregate sizes was not to be observed, but to see the effect of proportion of rubber chunks on the AE parameters. So, an appropriate recommendation can be made regarding the proportion of rubber that can be safely put in use during manufacturing of mortar blocks. In this investigation, four specimens were tested each containing 100g, 150g, and 200g of rubber aggregates.

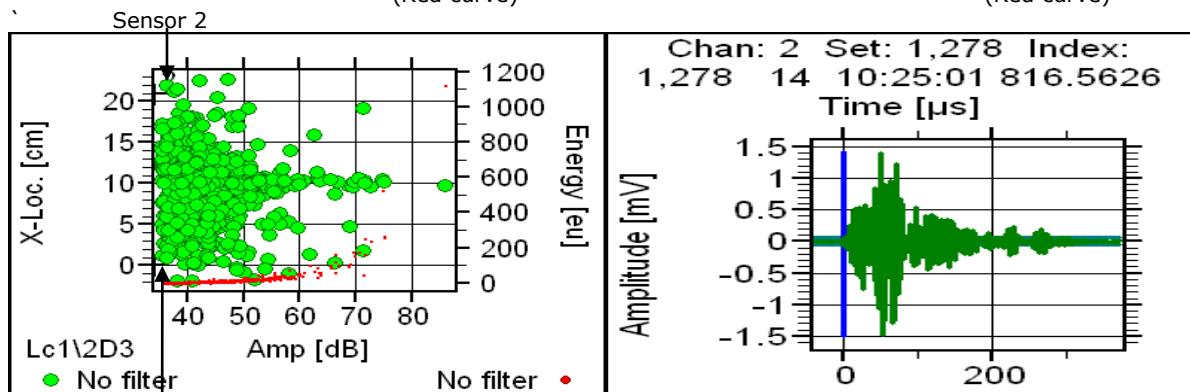
6.8.1 Mortar with 100 g rubber aggregates: Sample Kolar 2b

A sample containing 100g waste tyre rubber was subjected to flexural test. At the start of the test AE activity was low (<55 dB) as seen in figure 6.36 (a). With increasing load localised events (both sensors picking up the signals) with amplitude >55 dB were recorded (see figure 6.36 (b)). When the load reached the peak value, events with large amplitude were observed. A sudden drop of load to 30% the peak value occurred. Few events of higher peak amplitude and lower duration continued until the fracture. Only a few activities were recorded at high amplitude level (above 70 dB), this is probably an indication of very few resistances offered by the rubber chunks to big cracks (see figure 6.36 (c)), and resistance that was offered was easily overcome by the crack.



(a) Amplitude (dB) vs Time (s) vs Param load (mV) (Red curve)

(b) X-location (cm) Time (s) Param load (mV) (Red curve)



(c) X-location (cm) vs Amplitude (dB) Energy (eu) (Red dots)

(d) AE Waveform

Id	DSET	A [dB]	R [μs]	E [eu]	TRAI	X [cm]	D [μs]
LE	2044	54.7	46.8	264E-1	1271	10.27	267.0
Ht	2045	53.9	52.2	241E-1	1272		211.4
LE	2047	47.9	127.4	175E-1	1273	10.60	263.6
Ht	2048	49.4	94.0	233E-1	1274		246.0
LE	2051	40.8	69.6	539E-2	1275	8.06	75.0
Ht	2052	37.0	26.0	364E-2	1276		27.0
Ev	2053	45.3	34.2	131E-1	1277		254.0
LE	2055	63.3	53.8	640E-1	1278	10.68	302.8

(e) AE Listing

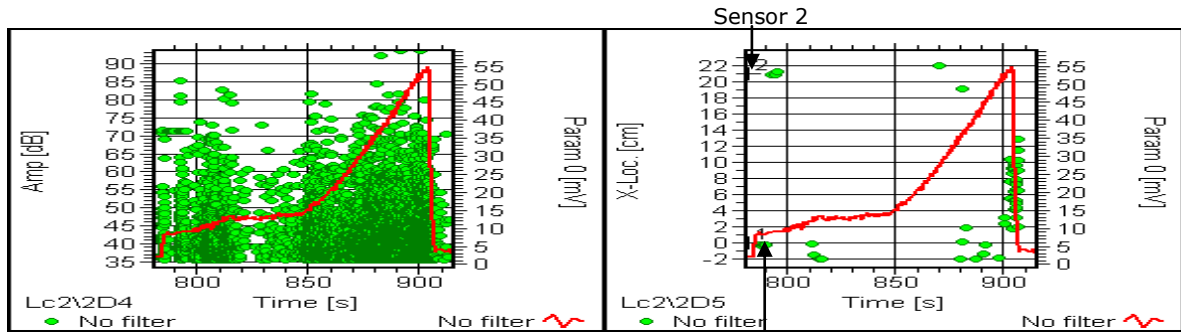
Figure 6.36: AE plots and AE listing for Sample Kolar2b (with 100g rubber)

The transient waveform recorded at failure (as seen in figure 6.36 (d)) shows a small event failure. The sample fails at location 10.68 cm with an event of relatively high amplitude, long duration, and short rise time and of medium energy level (63.3 dB, 302.8 μs, 53.8 μs, and 640E-1 eu respectively) as shown in the listing (see figure 6.36 (e)). This happens after the crack overcomes the resistance offered by rubber aggregates. However, the failure indicate a relatively large resistance and the failure path deviates from straight path due to some deflection caused by rubber chunks, therefore some high energy events with larger amplitudes were recorded.

6.8.2 Mortar with 150 g rubber aggregates; Sample Kolar 3b

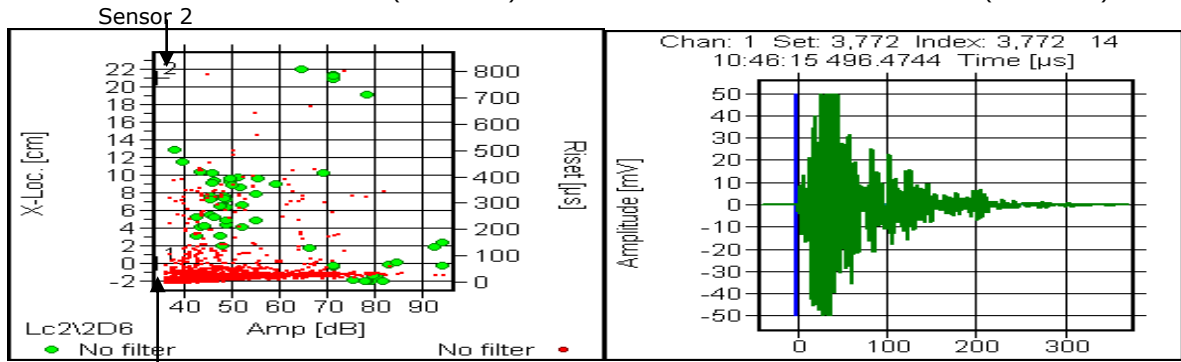
The increment of rubber aggregates to 150g made very little contribution to toughening of the specimen. From figure 6.37 (a) it can be seen that from 950 seconds the load curve rises with events of low amplitude. The AE characteristics of this specimen exhibits very little recorded activities by both sensors, as the load curve rises steadily until failure point. The plot X-location vs. Time vs. Param (as seen in figure 6.37 (b)) shows that both sensors did not pick up all the activities that were taking place in the sample. This is because the stress waves emitted are not strong enough for both the sensors to pick up simultaneously. However, there were some activities recorded in this graph mostly near to sensor 1 where small visible cracks were seen after the test.

From the plot of location vs amplitude (dB) vs Energy (eu) (as seen in figure 6.37 (c)), it can be seen that the resistances to cracks are fewer than sample containing 100g rubber, (indicated by a couple of activities above 70 dB) and a few high energy events (eu), which is probably due to either the absence of aggregates or the presence of easier path for the crack to follow.



(a) Amplitude (dB) vs Time (s) vs Param load (mV)
(Red curve)

(b) X-location (cm) Time (s) Param load (mV)
(Red curve)



(c) X-location (cm) vs Amplitude (dB) Energy (eu)
(Red dots)

(d) AE Waveform

Ev	6899	72.4	22.8	142E00	3637	280.0	
Ev	6944	60.3	34.6	355E-1	3663	206.4	
Ev	6956	71.6	28.6	123E00	3669	290.0	
Ev	6958	69.4	36.4	999E-1	3671	783.2	
Ev	6963	61.8	29.0	278E-1	3673	191.2	
Ev	7054	62.2	32.4	573E-1	3722	564.2	
Ev	7059	70.9	36.4	126E00	3725	276.8	
Ev	7099	60.7	27.2	389E-1	3748	372.2	
LE	7141	93.8	29.0	242E01	3772	1164.8	2.81
Ht	7142	63.3	139.2	106E00	3773	340.8	

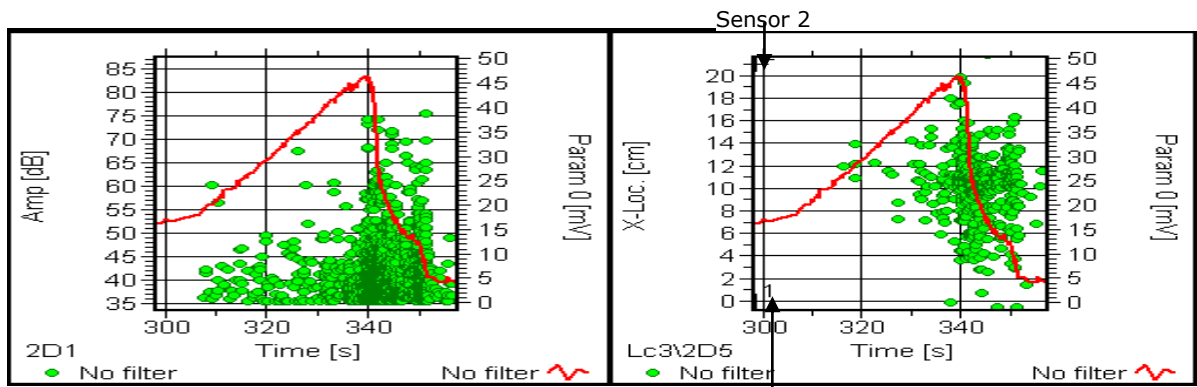
(e) AE Listing

Figure 6.37: AE plots and AE listing for sample Kolar3b: (Mortar containing 150g rubber)

The TR waveform shown in figure 6.37 (d) indicates a big event. The numbers of captured waveforms are very few, but the one identified at the failure region is a big waveform. The specimen fails at location 2.81 cm following a big fracture when the crack overcomes a large and reasonably strong bonded piece of rubber, which is a large event of high amplitude, low rise time, very long duration and high energy level (93.8 dB, 29 μ s, 1164 μ s, and 242E01 eu respectively) as seen in figure 6.37 (e). The peak load on the specimen suddenly drops producing a brittle failure, unlike the sample with 100g of rubber there was no resistance after the failure occurred. This is a drop in strength compared to the previous specimen (sample with 100g rubber). This is an indication of weak specimen and poor bonding between the cement paste and the rubber chunks, which have resulted in very few AE activities being recorded.

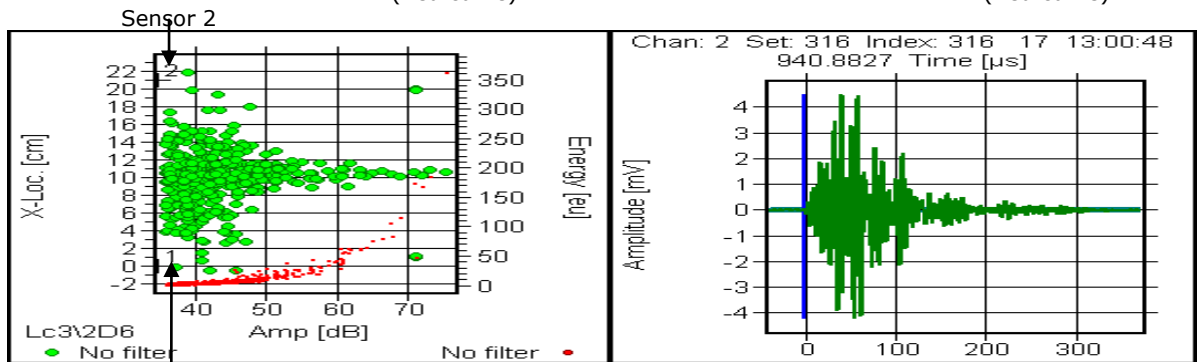
6.8.3 Mortar with 200g rubber aggregates: Sample Kolar4b

In this specimen, addition of 200g of rubber provided some toughening but a drop in strength (seen from the red load curve of figure 6.38 (a)). At the beginning of the test, all the activities recorded were of low amplitude (<55 dB) as can be seen in figure 6.38 (a). As the test proceeded, activities were mainly picked by sensor 1 with majority of them being at low amplitudes (< 55 dB) and low energy events as seen in figure 6.38 (b) and (c) and (d). This is an indication of micro-crack propagation and other modes of failure such as rubber chunks being detached from the cement paste very easily. The load curve steadily rises and the failure occurs after a small deflection takes place.



(a) Amplitude (dB) vs Time (s) vs Param load (mV) (Red curve)

(b) X-location (cm) Time (s) Param load (mV) (Red curve)



(c) X-location (cm) vs Amplitude (dB) Energy (eu) (Red dots)

(d) AE Waveform

Id	DSET	A	R	E	TRAI	D	X
		[dB]	[μs]	[eu]		[μs]	[cm]
Ht	689	37.0	4.0	291E-2	315	62.8	
LE	691	73.1	39.6	185E00	316	315.0	10.91
Ht	692	74.2	42.4	171E00	317	316.2	
LE	693	43.0	42.6	683E-2	318	75.4	10.96
Ht	694	40.8	63.6	521E-2	319	71.4	
LE	696	67.8	48.6	843E-1	320	253.4	10.42
Ht	697	68.2	44.8	125E00	321	257.6	
LE	698	41.9	35.6	448E-2	322	64.2	7.99

(e) AE Listing

Figure 6.38: AE plots and AE listing for sample Kolar4b (Mortar with 200g rubber)

The TR waveform captured at fracture point (as seen in figure 6.38 (d)) is a relatively large waveform though more attenuated than the specimen sample with 100g rubber aggregates since the failure here is not as big as the former. The attenuation of the signal is due to rubber and poor bonding.

The sample failed at location 10.91 cm with high amplitude of 73.1 dB, short rise time 39.6 μ s, a relatively long duration of 315 μ s and high energy level of 185E00 (see the listing in figure 6.38 (e)). The failure was less brittle in nature, as rubber offered some resistance.

The failure in this sample was a very gradual one and not as abrupt as the specimens with lower content of rubber. This was probably due to high content of rubber in the sample which were trying to resist the failure but these resistances were not strong enough, hence the number of low amplitude and low event duration activity being recorded.

The activities recorded at high amplitudes (above 70 dB) are more than any other samples, indicating few resistances offered by rubber chunks, but not very strong, which is reflected by the activities not exceeding the amplitude value of more than 75 dB.

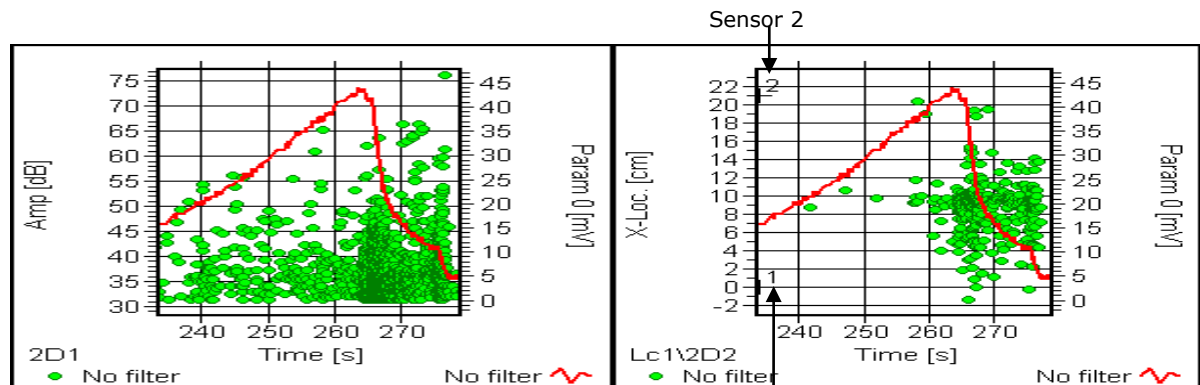
6.8.4 Mortar with 250g rubber aggregates; Sample Kolar 5b

Increasing the amount of rubber aggregates has caused changes in AE characteristics under tension. At the beginning of the test (from 23 seconds to 255 seconds) all the activities recorded were of low amplitude (<55 dB), see figure 6.39 (a)). Few activities were recorded throughout the duration of the test. Most of the events were recorded by sensor 1 at low amplitudes (< 55 dB), as shown in figure 6.39 (a and b). This meant a number of crack initiation and propagation activities took place.

Although a few minor obstacles caused by rubber aggregates must have been overcome, but no such events are evident from the AE characteristics, as it is visible from figure 6.39 (c) with all the activities below 70 dB and energy level below 100 eu. This is probably because no strong resistance is offered by rubber aggregates therefore cracks find it easier to bypass the rubber and proceed.

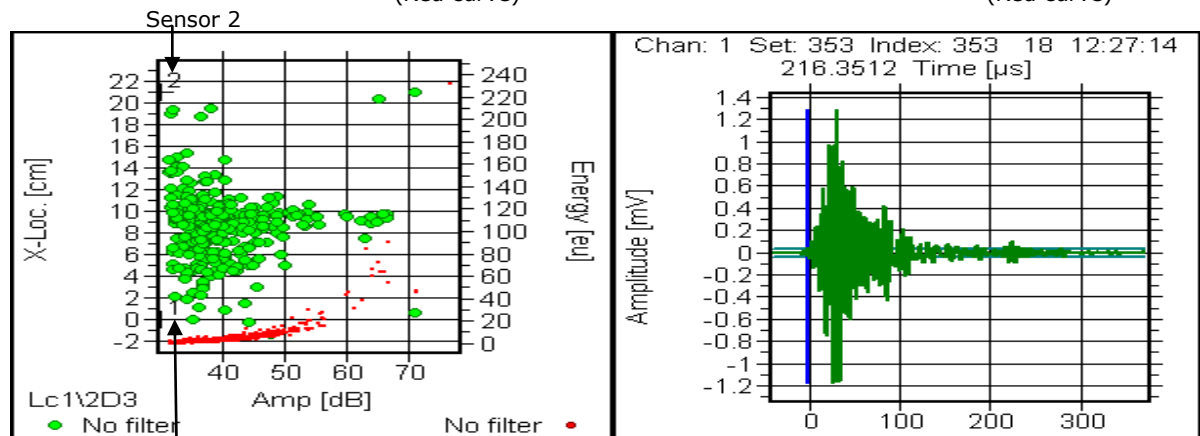
This in turn is due to poor interfacial bonding between the cement matrix and the rubber aggregates.

The TR waveform captured at failure point (figure 6.39 (d)) is a small waveform. This is a clear illustration that the AE energy released at this point was small, the event was weak hence the crack found it easier to proceed compared to other specimens. The failure occurred at location 9.18 cm with an event of high amplitude of 62.2 dB, low rise time 30.2 μs , relatively long duration of 281.4 μs but not much high energy level which was only 388E-1 eu (see figure 6.39 (e)).



(a) Amplitude (dB) vs Time (s) vs Param load (mV) (Red curve)

(b) X-location (cm) Time (s) Param load (mV) (Red curve)



(c) X-location (cm) vs Amplitude (dB) Energy (eu) (Red dots)

(d) AE Waveform

Id	DSET	A	R	E	TRAI	D	X
		[dB]	[μs]	[eu]		[μs]	[cm]
Ev	760	31.3	0.2	105E-2	350	0.4	
LE	761	47.9	28.6	110E-1	351	124.0	9.79
Ht	762	41.5	22.8	465E-2	352	118.8	
LE	764	62.2	30.2	388E-1	353	281.4	9.18
Ht	765	56.2	49.8	238E-1	354	245.6	
Ev	767	40.4	21.0	336E-2	355	55.6	

(e) AE Listing

Figure 6.39: AE plots and AE listing for sample Kolar5b (Mortar containing 250g rubber)

The number of AE hits produced by various specimens containing rubber aggregates in different quantities is shown in figures 6.40 and 6.41. As the rubber content increased, the AE hits started dropping indicating a decrease in toughness level, with the exception of sample KOLAR 4B (containing 200g rubber aggregates). The reason for this may be due to a few resistances faced by cracks from rubber chunks that increased the hit numbers. The specimens with rubber aggregates generated the least number of hits in total when compared with samples in other experiments indicating the weakening effect of these samples when put under flexural condition.

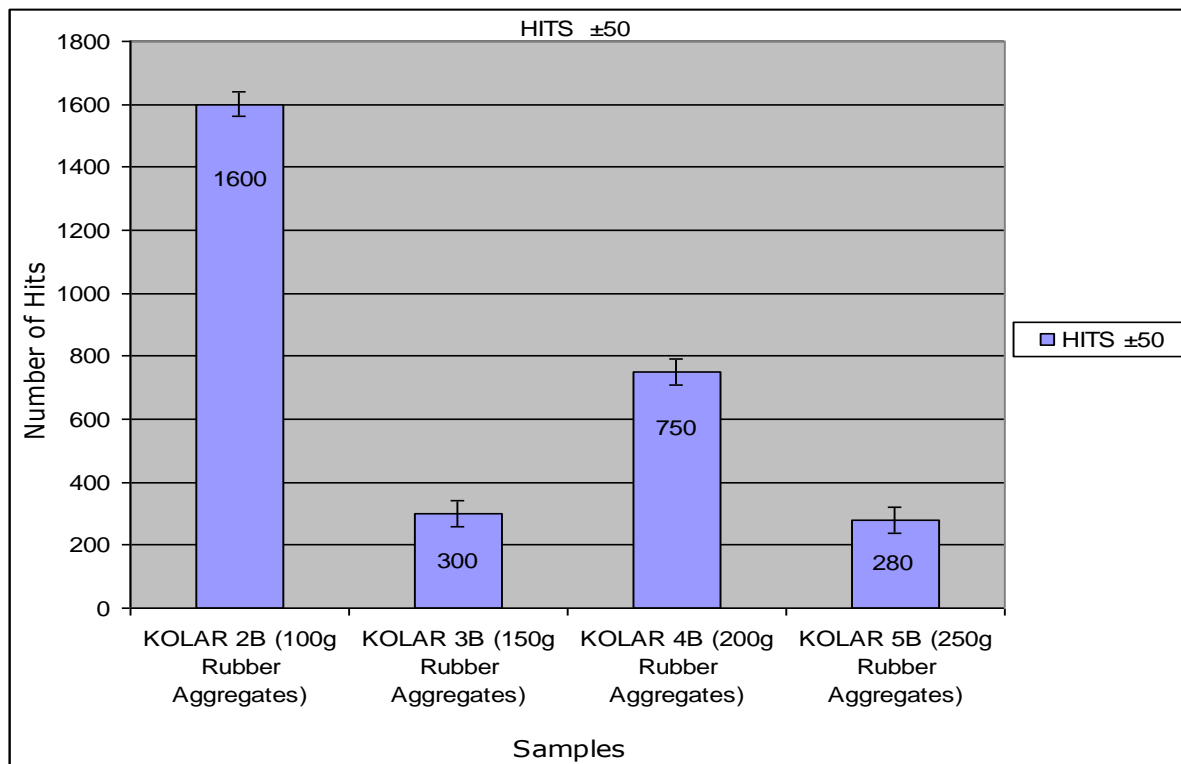


Figure 6.40: Number of AE hits captured by samples with different quantities of rubber aggregates under applied flexural load

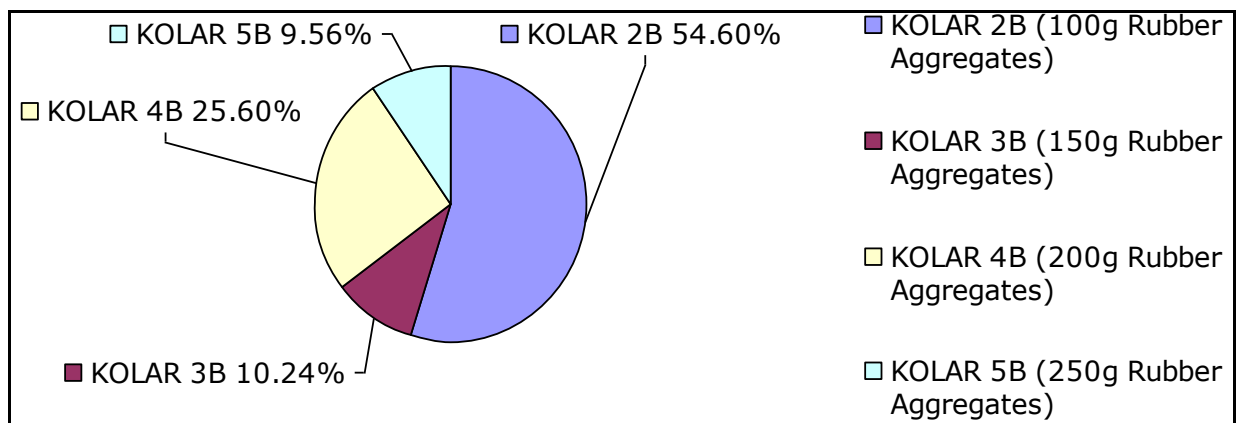


Figure 6.41: Pie chart showing percentage of AE Hits under applied flexural load

6.8.5 Summary

The main observations in the above investigation are:

- i. Poor bonding between the cement matrix and the rubber;
- ii. Weak pull-out events;
- iii. Damping and alteration of AE signal in the material;
- iv. Brittle fracture nature.
- v. Cracking leading to macro-fracture.

The two major effects that have been observed due to the addition of waste rubber to the concrete blocks are when compared with a plain mortar or concrete with glass aggregates as mentioned in sections 6.3-6.6 are:

- (i) Change in AE characteristics, i.e. fewer AE activities at amplitude, duration and energy level;
- (ii) Increase in attenuation of AE signals.

This may be due to change in water cement aggregates ratio, increased porosity and poor interfacial bonding between cement paste and the rubber, as seen in the figure 6.42.

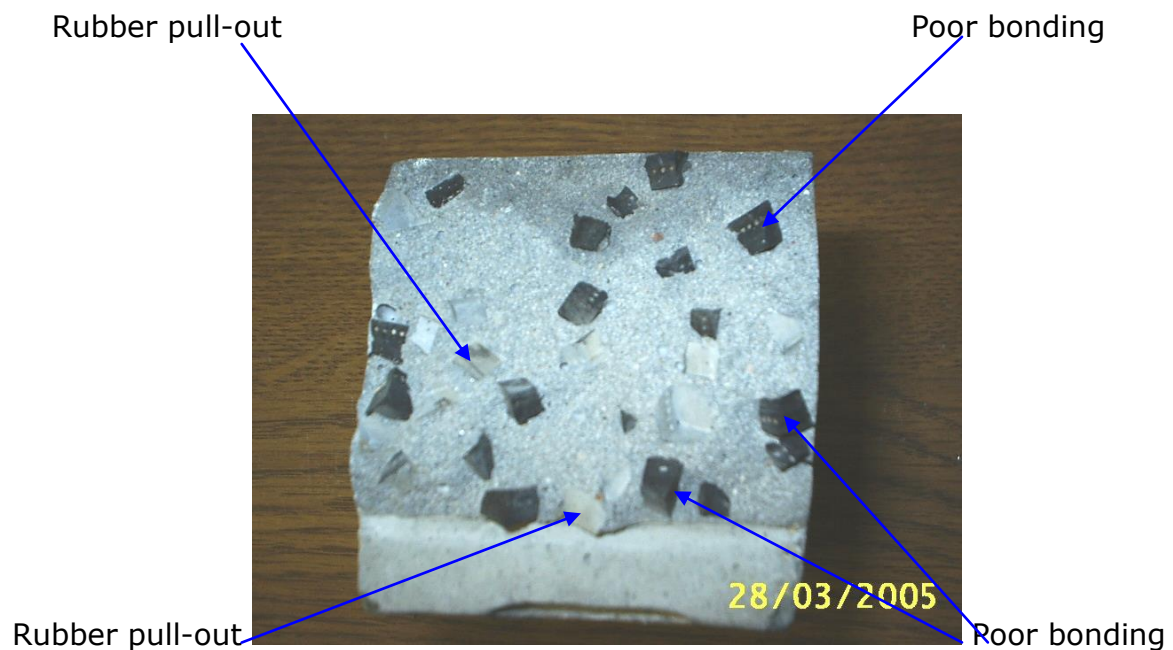


Figure 6.42: interfacial bonding of rubber with mortar

Addition of rubber in concrete alters the sound propagation characteristic, causing more scattering and absorption of the energy at rubber mortar interface. This attenuation resulted in heavily damped AE signals, highest recorded peak amplitude was in the range of 66 dB to 86 dB (except for sample kolar3b i.e. mortar with 150g rubber) and most of these high-energy signals had event duration within 1200 μ s. AE waveforms recorded contained only 2 or 3 modes and were heavily damped.

From the results of AE characteristics obtained above, rubber as an aggregate can be used in concrete mortar, under condition where a situation similar to flexural condition can prevail, but only a limited amount can be used for reason of safety and durability. Therefore, compared to glass aggregates, rubber can be used more as inert filler rather than as a toughening material, or strength improvement ingredient.

Nevertheless, the use of rubber chunks may provide enhanced toughness, mechanical properties, flexural strength and good interfacial bonding if the surfaces of the rubber chunks are treated with coupling agents, which will make the surface rougher and hence better bonding with cement paste and stronger resistance to cracks can be achieved.

CHAPTER 7

7.1 Toughness Monitoring of Concrete with Altered Properties Under Compression

Since the use of certain additives in mortars exhibited significant changes in the setting, curing and final compressive behaviour of the concrete mortars, and also the SEM analysis has shown variations in the microstructures, it has become necessary to gain an insight into the toughening mechanisms of these cubes. If the modified properties of the concrete system can be observed by studying at the toughening mechanism on-line, then the long term requirement of the cement systems can be improved; this will make a significant contribution to the field, because long term stability of the toughening mechanism and development of the microstructure can be identified. There is reported technique available to observe these effects, AE is used for this purpose, i.e. to monitor and determine the crack initiation, failure modes and behaviour of the samples when subjected to compressive loads. Therefore, some of the samples that were put under compressive crush test were monitored using AE, thus developing a comparative understanding of failure mechanism of concrete with enhanced mechanical properties in compression. The idea here is to look at the emission profile of the specimens containing different admixtures rather than to look at the load strength.

Online monitoring of toughening mechanism of concrete is not available. In order to understand the fracture behaviour of concrete with various additives under compressive load, AE monitoring was carried out. AE technique provides a tool for monitoring micro-cracks, crack initiation, crack propagation and failure modes irrespective of the composition of concrete. This is a very sensitive technique as emission profile of a sample is highly dependant on the composition and the nature of the concrete mortars.

7.1.2 Plain Concrete Mortar (No additive)

This plain mortar under compression exhibited some AE activities randomly spread throughout the location of this sample. During the test there were intervals of quiet periods without any activities being recorded, although the sample was under compressive load. This must have been due to the presence of pores in the sample. Most of the AE activities had taken place during the initial stage of the test, i.e. between 0 – 40 seconds as shown in figure 7.1 (a) with hits against time.

Majority of these activities were of high amplitudes (> 60 dB) and took place mainly near sensor 1. Low amplitude (< 55 dB) activities took place near sensor 2, figure 7.1 (b). The highest energetic event (730E01), had long event duration of $48345.6 \mu\text{s}$, short rise-time of $1274.8 \mu\text{s}$ and high amplitude of 90.8 dB, figure 7.1 (c). The sample cracked at this point. It was observed from this multi-plot that, after the crack a quiet period prevailed and then a large number of activities started taking place mostly at low amplitude (< 55 dB) and low event duration ($< 1000 \mu\text{s}$), figure 7.1 (b) and (c). These plots also indicate that the crack that occurred was not due to propagation and joining of micro-cracks but a sudden drop of material strength after a few micro-cracks propagated to form a bigger crack. Number of activities recorded above the amplitude value of 70 dB are 34 . This indicates the crack level accumulated due to a few micro-cracks that have been generated during the compressive load. The cascaded energy recorded with time rose to $24\text{E}5$ (figure 7.1 (d)) which reveals that there are few constants (i.e. no increase in energy) over the duration of the test; this is probably due to quiet period that prevailed during the test when no hits were recorded.

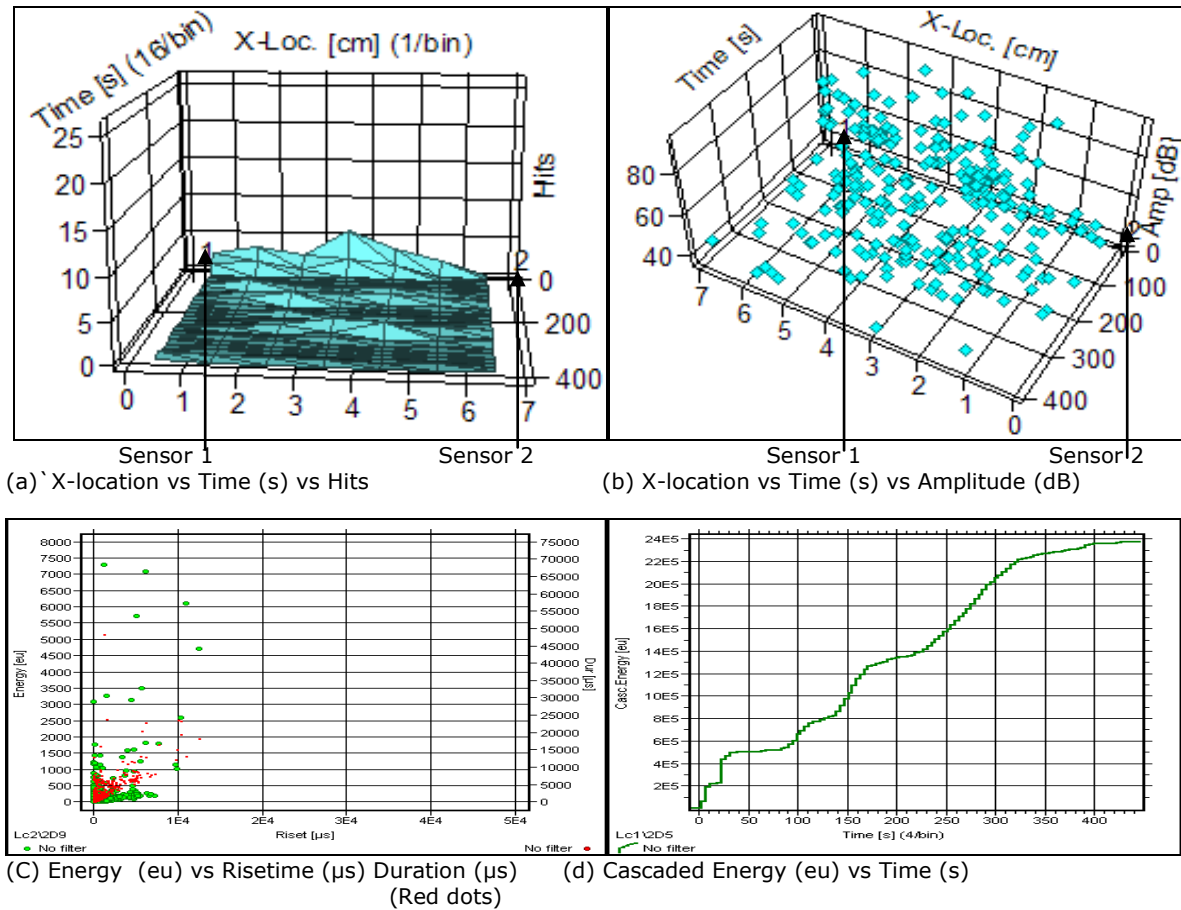


Figure 7.1: AE plots of plain mortar under compression

7.1.3 Mortar with Calcium Chloride

The sample was put under compression and the number of hits recorded are shown in figure 7.2 (a) with hits against time. The AE activities recorded under compression test of this sample are huge which may be due to the presence of calcium chloride. Throughout this sample, small granular crystals are distributed, as was seen in the SEM micrographs, figures 5.20 and 5.21. The AE events occurring at low amplitudes are attributed to the toughening of concrete due to the distributions of small granular crystals.

From the SEM micrographs (in figures 5.20 and 5.21), it was seen that the internal structure was consistent throughout the sample and this was confirmed by AE behaviour that is consistent throughout the block. The density of AE activities occurred at very small amplitudes (30 – 50 dB) throughout the location of the cube, as shown in figure 7.2 (b). The distribution of AE activities is characterised by low amplitude duration events, this confirms that the micro-cracks accumulating due to the presence of calcium chloride lead to the final

failure of the sample, rather than an abrupt failure at high amplitude (figure 7.2 (b)), or high energy and high duration event as shown in figure 7.2 (c).

The high toughening mode is represented by a large number of low amplitude (< 55 dB) events, shorter event duration (< 10,000), and a large number of rise-time events of <1000 μ s (see figure 7.2 (c). This is also evident from the number of cascaded energy which rose to 35E5 (see figure 7.2 (d)). The numbers of activities recorded above the amplitude value of 70 dB are over 250. This indicates that the ultimate crack resulted due to the high number of micro-cracks that have been generated during the compressive load.

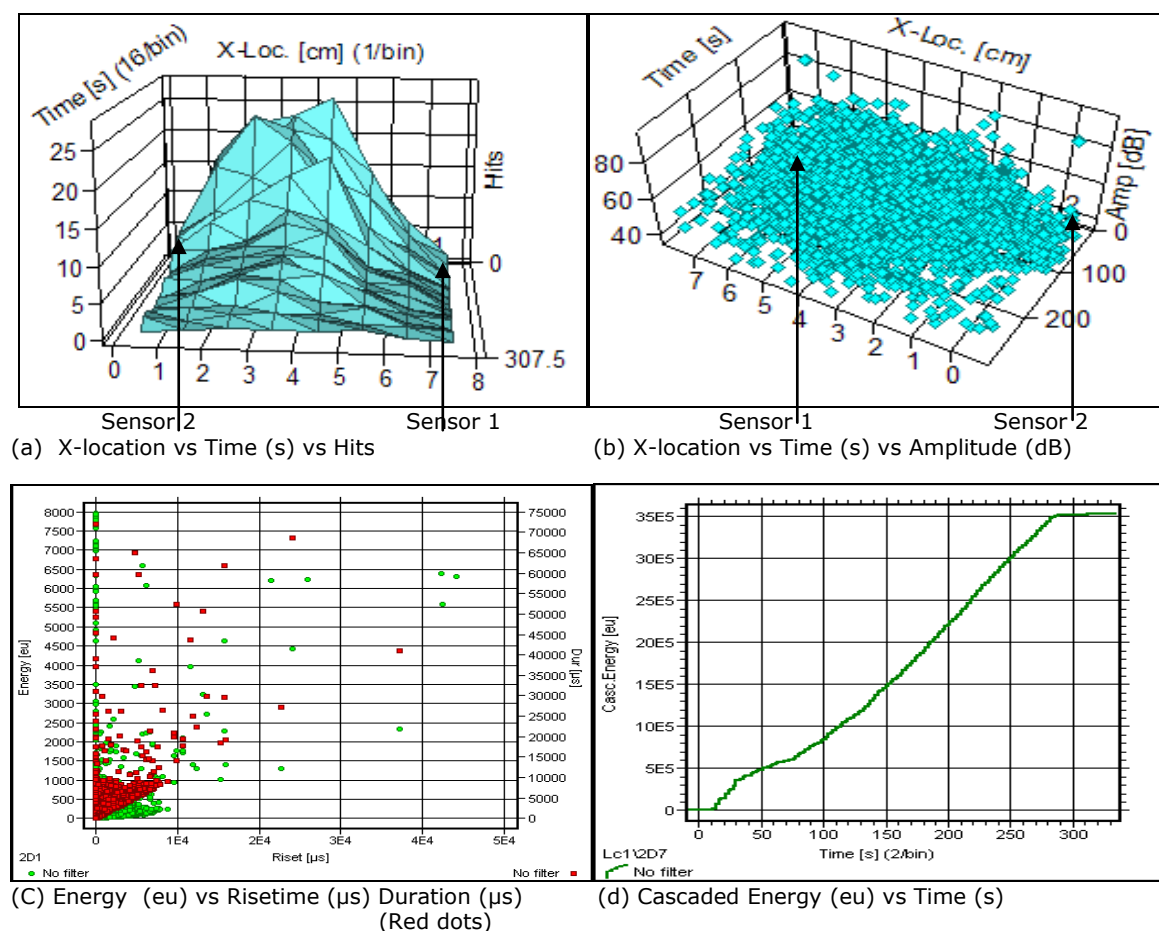


Figure 7.2: AE plots of mortar (15g Calcium Chloride) under compression

7.1.4 Mortar with Sodium Sulphate (10 g, 15 g and 25 g)

The AE behaviour of this sample (mortar with 10g sodium sulphate) under compression generates most of the activities at low amplitudes, with short duration and of low energy. The numbers of hits recorded are between 100-200 seconds which are denser than the plain mortar specimen. After this a quiet period prevailed until final failure where a few hits were recorded as seen in

figure 7.3 (a). This indicates that micro-cracks initiated in this sample at the beginning of the test lead to crack propagation of events with high amplitudes (> 55 dB) as shown in figure 7.3 (b). The activities are quiet between 0 -20 seconds and also between 120 – 160 seconds near sensor 2. This can be attributed to the large pore space in the micro-structure of the sample as is visible in the SEM photographs, figures 5.14 and 5.15. From the figures 7.3 (c) and (d), the AE energy, rise-time, duration activities and AE cascaded energy are weaker when compared with figures 7.1 (c) and (d) (plain mortar sample). This is an indication of weak micro-cracks that took place which resulted in failure of the concrete.

Since the addition of sodium sulphate was seen to be making an increase in the compressive strength of the mortar as compared to the normal concrete, as was seen in section 5.3, therefore the content of this additive was increased to 15g and 25g respectively to examine its effect on the toughening mechanism. This technique exhibited significant increase in the AE activities, thus altering the level of toughening. The micro-cracks (spread of AE activities with low amplitudes, short duration and low energy level) are scattered all throughout the cube, with almost no quiet period, figures 7.4 (a) and 7.5 (a). The number of activities recorded above the amplitude value of 70 dB is over 80, figures 7.4 (b) and 7.5 (b). Figure 7.4 (c and d) indicates that the AE activities and cascaded energy are of weaker level with 15g sodium sulphate; while figure 7.5 (c and d) gives an indication of further weakening of AE activities and AE cascaded energy. This indicates that the crack failure resulted due to the high number of micro-cracks that have been generated during the compressive load. This is evident that the level of toughening was found to be greater than the plain mortar but less than the sample with calcium chloride.

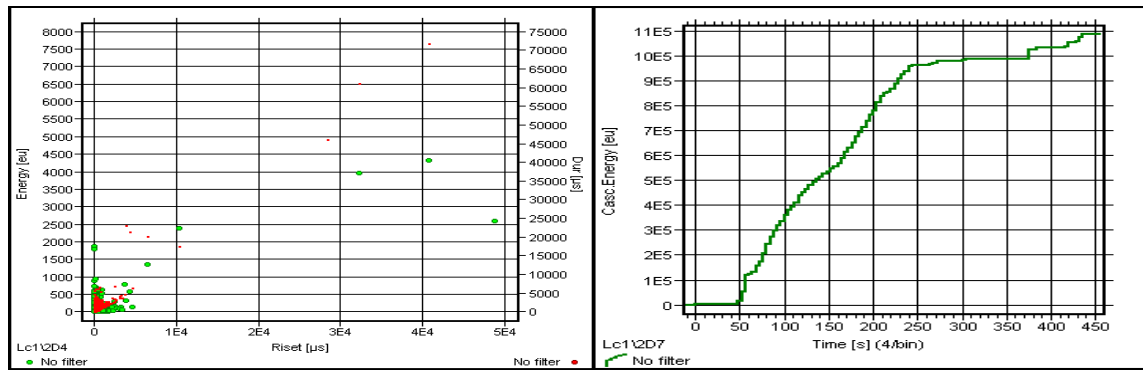
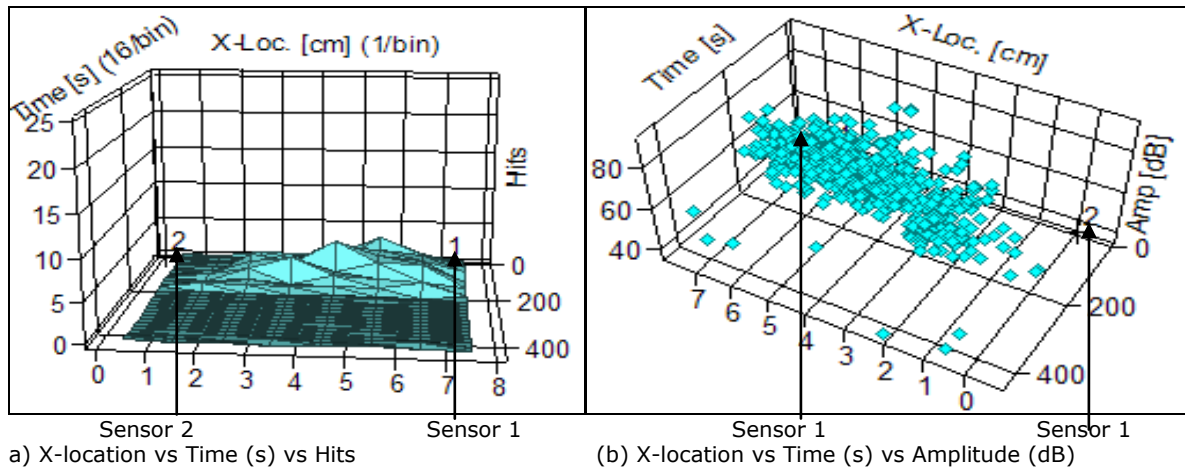


Figure 7.3: AE plots of mortar (10g Sodium Sulphate) under compression

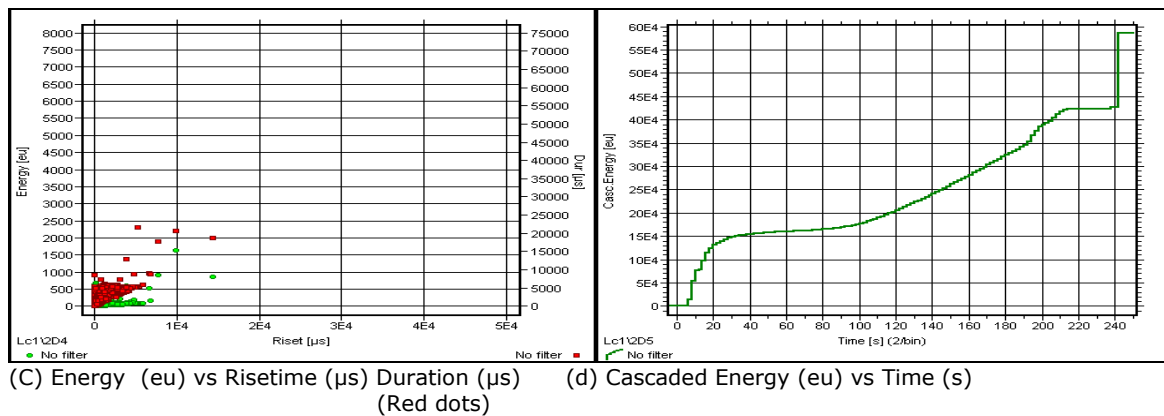
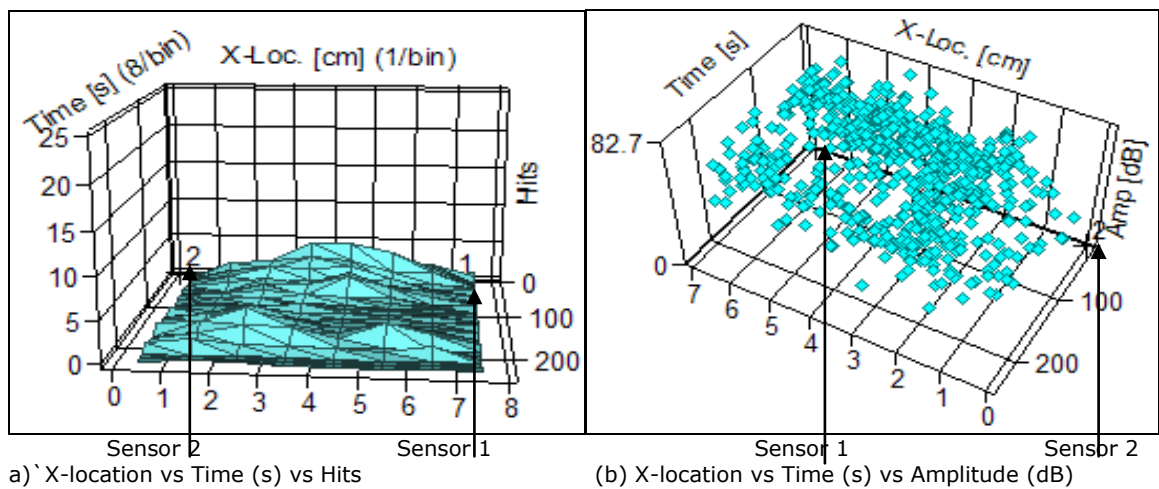
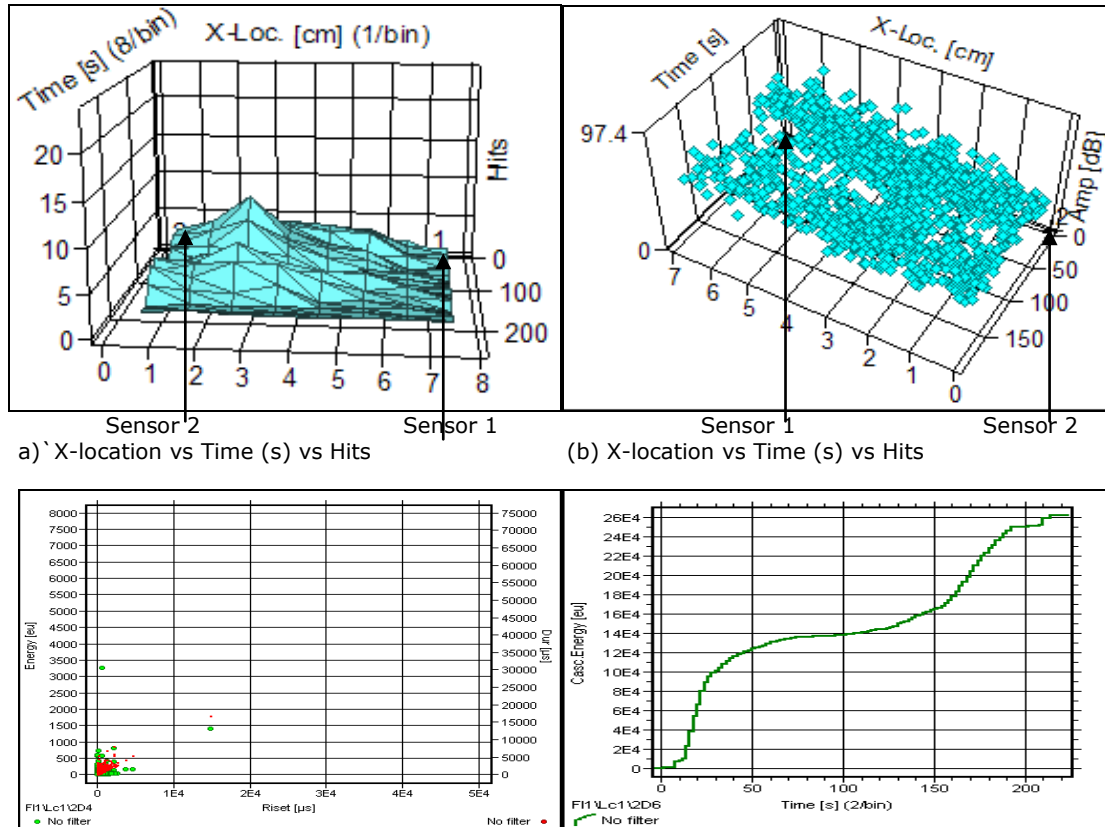


Figure 7.4: AE plots of mortar (15g Sodium Sulphate) under compression



(C) Energy (eu) vs Riset (μs) Duration (μs) (Red dots) (d) Cascaded Energy (eu) vs Time (s)
 Figure 7.5: AE plots of mortar (25g Sodium Sulphate) under compression

7.1.5 Mortar with Sodium Silicate

The sample failed with very few AE activities taking place with only a few hits recorded during the test period as seen in in figure 7.6 (a). Most of the activities occur at relatively high amplitudes (> 55 dB), low energy, low duration and low rise-time events; this indicates that only a few micro-cracks are present, figure 7.6 (b and c). This is probably due to the presence of a random structure, showing crystals, which are of large, needle shaped, shown in figures 5.17 and 5.18. Very few events at both low and high amplitude were recorded. However, events with high amplitude were lesser in number than the low amplitude events compared to the activities to the sample with no additives. The cascaded energy recorded rose to only 17E4, (see figure 7.6 (d)), which is far lower than any other specimen in this investigation. This indicates the detrimental effect of this additive in terms of and toughening.

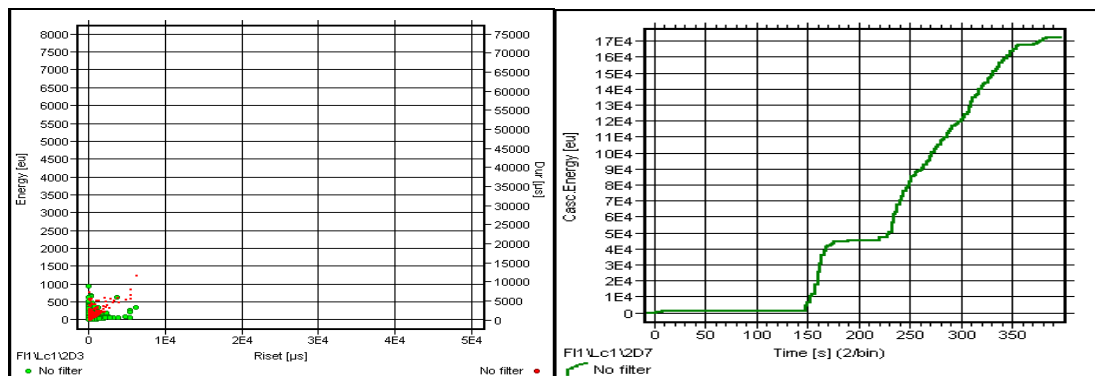
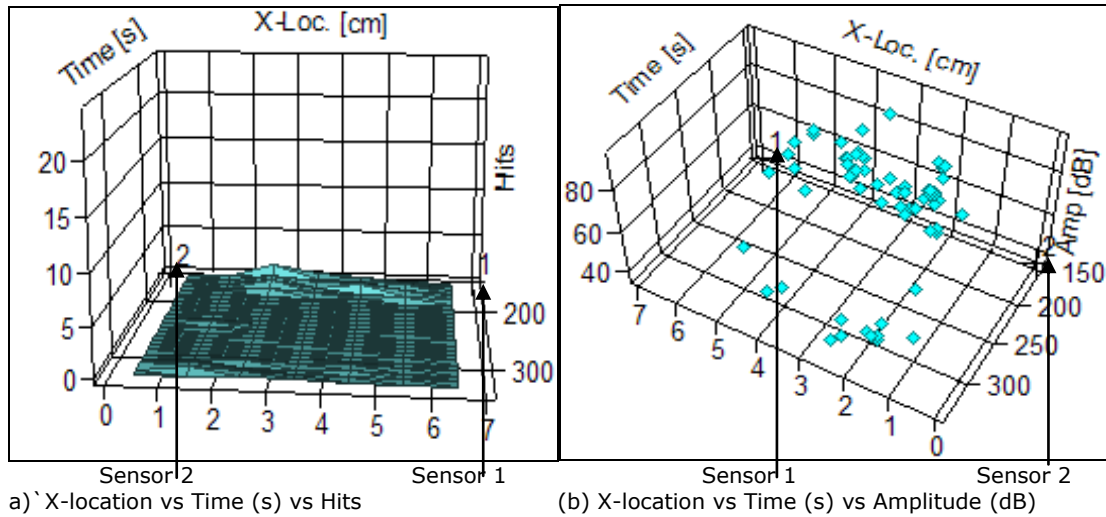


Figure 7.6: AE plots of mortar (15g Sodium Silicate) under compression

7.1.6 Summary

The 3-dimensional AE plots shown in figures 7.1 (a) to 7.6 (a) show the hits variation of different samples containing admixtures. The addition of calcium chloride shown in figure 7.2 (a) has the largest number of hits variation, and sodium silicate has the least (in figure 7.6 (a)). Addition of sodium sulphate (in figures 7.3-7.5 (a)) also exhibit a large number of hits, but less than the sample with calcium chloride (figure 7.2 (a)). These changes in hits variation reflect the behaviour of mortars containing various additives when put under compressive load.

The stress waves (AE) released during the monitoring of the compressive testing carried additional information relating to the source of failure and the strength and micro-structural property of the material. Analysis of the AE signal parameters such as amplitude and duration provide valuable graphical representation (figures 7.1 to 7.6 (b and c)) of the failure mechanism of the sample. The AE signal parameters recorded for the samples showed distinct

variations. The signal peak amplitude, which relates to the stress applied on the individual sample showed huge variations in their distribution, which indicates the effect of the introduction of additives. It is evident that the most activities had occurred in the sample containing calcium chloride, which means that the majority of the micro-cracks took place in this specimen. The detrimental effect of the introduction of sodium silicate is clearly visible from the AE characteristics while the observed AE activity obtained by the addition of calcium chloride and sodium sulphate is very high as seen in figures 7.1 (b) to 7.6 (b). This is an indication of the higher level of toughening under compression with the introduction of two additives. It can be seen that all the samples failed between 3-4 cm, however the mode of failures is different for each sample as can be in figures 7.1-7.6 (b), (c) and (d). While the sample with sodium sulphate increased the compressive strength as was seen in section 5.3 (IV), the toughening was highest with calcium chloride. The acoustic energy emitted from different samples during the test can be correlated to toughening modes. The sample with calcium chloride exhibited the largest number of acoustic energy emission at higher level than any other sample, while the sodium silicate emitted the least at very low level. The use of calcium chloride does not solve all the problems in concrete practice, and there may be some detrimental effect of its use on some type of concrete, corrosive effect for example on pre-stressed reinforced concrete steel. Nevertheless, calcium chloride plays an important role in toughening of plain concrete and increases its toughness provided, that it is used in an appropriate amount as established in this research.

Hence, the addition of additives have altered the properties of concrete and changed its strength and microstructure, thereby altering the AE characteristics which indicates the toughening as well as weakening provided by different additives. This is further consolidated by the cascaded energy recorded by the Vallen System during the AE monitoring when the samples were under compression. The plots of cascaded energy accumulated are shown in figure 7.1 (d) – 7.6 (d).

The plot for sodium chloride (sample NaCl) indicates the correlation of highest value (3,500,000 eu) cascaded energy with the highest number of hits for this same sample (rising to 25), and the recorded lowest cascaded energy for sodium silicate sample, (170,000 eu) is linked to the number of hits (rising to 2 hits) for sample with sodium silicate. The same pattern is followed in the case of

other samples. In another word, higher and lower level of toughening is related to higher and lower level of recorded cascaded energy respectively.

The use of sodium sulphate (an appropriate amount) has enhanced the mechanical property leading to better toughening and thus altered acoustic behaviour (less than calcium chloride). The use of sodium silicate has shown no enhanced effect on the mechanical properties, rather it has had a detrimental effect, and this is also confirmed by the acoustic emission results. Therefore, by appropriate mixture, concrete blocks with enhanced toughness can be manufactured, which is quite relevant to high strength concrete where low toughness is highly visible. It can be concluded from the above analysis that the admixtures that are discussed in this thesis may increase the compressive behaviour (if a suitable amount is used) but not necessarily the toughness of the concrete and vice versa.

The experimentations observed have proved that with the addition of admixtures the only toughening method that can be obtained is in the form of micro-cracks. No other toughening mode could be observed or exist as expected. The activities that were seen to be taking place at higher amplitudes are not due to crack arrest, crack deflection or crack bridging, but only because of the accumulation and propagation of micro-cracks that have led to cracks which resulted in final failure. Comparisons of the results extracted by the addition of additives in mortars are given in table 7.1.

Table 7.1: AE response of concrete with different additives under compressive loading

<u>SAMPLES</u>	<u>AE Activities Generated</u>	<u>Toughening Level</u>	<u>Energy (eu) Above 1000</u>
Plain mortar; (figure 7.1)	Few activities	None	23 emissions;
Calcium Chloride; (figure 7.2)	Numerous and continuous activities	Very High;	32 emissions;
Sodium Sulphate; (figures 7.3, 7.4 and 7.5)	Large number; high amplitude	High;	Mostly below 1000; above 1000 only 8 emissions; up-to 10000
Sodium Silicate; (figure 7.6)	Very few events	None;	Mostly below 100;

From the chart shown in figures 7.7 and 7.8, the number of hits produced by samples with calcium chloride is the highest followed by the sample with 10g sodium sulphate. This demonstrates the degree of toughness of these specimens under compression load as a result of the introduction of admixtures. The introduction of sodium silicate in the mortar drastically reduced the number of hits under compression load (i.e. brought down the hit level to nearly 2 percent), hence indicating a significant reduction in the toughness level of the sample. The random micro-structure of the specimens with this additive (as was seen in section 5.4.2, chapter 5) shows the detrimental effect sodium silicate have on mortars. This is also linked to the lowering of the compressive strength over the initial curing period and the final 28 day period.

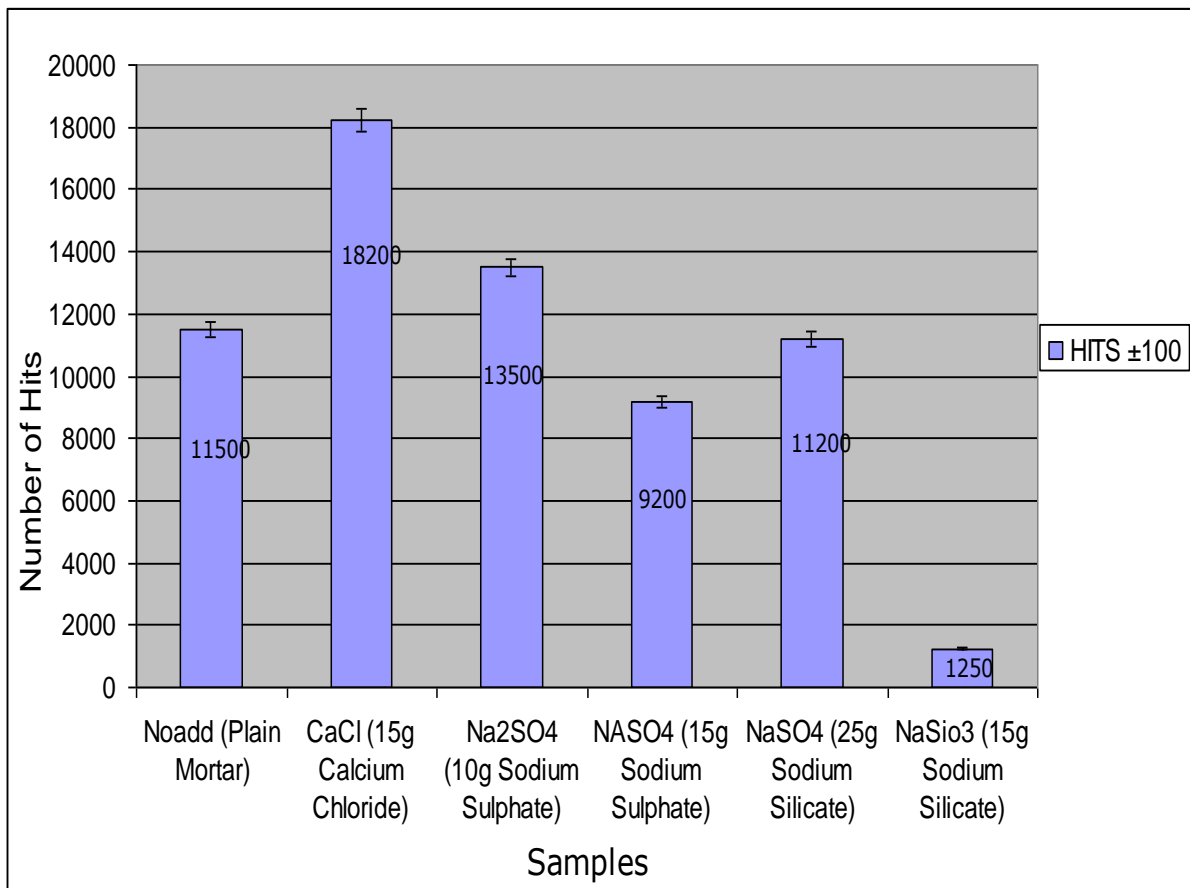


Figure 7.7: AE hits produced in samples with admixtures under compressive load

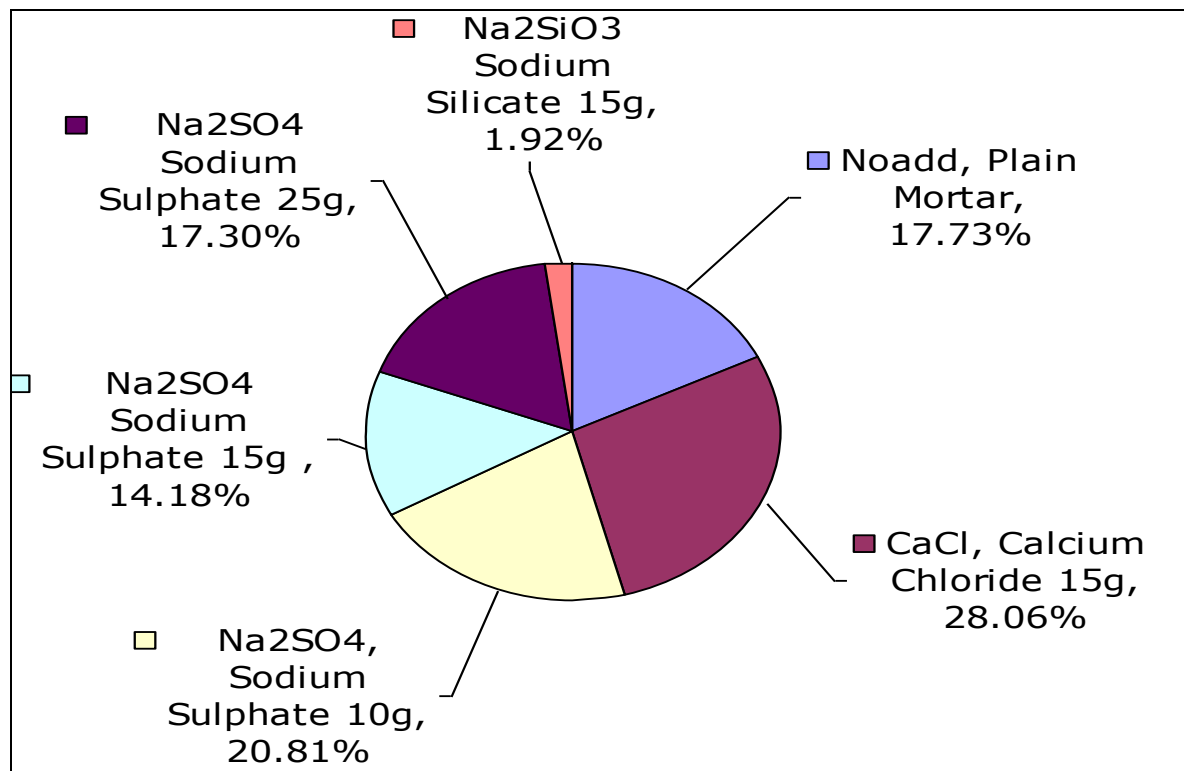


Figure 7.8: Percentage AE hits produced by mortars with admixtures under compressive load

It has become evident from the above analysis that a distinct difference is observed in the emission profiles, particularly in the samples with calcium chloride and sodium sulphate. The energy emitted from each sample show distinct characteristics of the admixtures in the sample and its reaction when load is applied.

As mentioned above, the specimen with sodium silicate is seen to be the most detrimental mortar in terms of toughening; therefore this particular additive must be avoided. Sodium sulphate and calcium chloride are shown to be the promising admixtures that can be given good attention to obtain enhanced properties of concrete.

7.2. AE Monitoring of Expansive Cement Concrete Blocks Containing Smooth and Rough aggregates under Flexural Load

As reported in chapter 3, expansive cement is used to minimise cracking caused by drying shrinkage in concrete slabs, pavements, and structures; therefore this category of cement is termed as shrinkage-compensating concrete. In the case of shrinkage compensating concrete, a denser cement paste matrix and a stronger transition zone between the cement paste and the coarse aggregate are the factors causing strengths higher than those of a Portland cement concrete made with an equivalent water/cement ratio. Therefore, Concrete mortars manufactured with expansive cement containing various glass beads, pebbles and rough glass aggregates (all of mixed sizes 3 mm) were prepared, cured for 28 days in the established manufacturing condition for this work. The flexural tests were carried out under AE monitoring to determine the behaviour of these aggregates under such a condition. So that it could be identified whether the glass beads or pebbles are more effective than coarse glass aggregates in terms of interfacial bonding with the cement paste.

7.2.1 Expansive cement with 3 mm Glass Beads; Sample Exglbds3: Glass Beads

The AE monitoring of flexural test results (for a block containing mixed size 3 mm diameter beads) are shown in figure 7.9 (a) to (e). At the initiation of the test, majority of the AE events recorded were of low amplitude level (< 55 dB) (see figure 7.9 (a)). The load curve steadily rose with AE activities mainly being picked up by sensor 2 as seen in figure 7.9 (b).

With increasing load, the AE activities were picked up by both sensors and were steadily increasing in number, but not rising above 55 dB level. This indicates that a large number of micro-cracks were forming and the glass beads with smooth surfaces were making micro-cracks to move easily over the surface of the aggregates through the mortar. Prior to final failure, a large number of activity took place with few major events such as development and deflection of cracks that may have taken place as indicated by a few events above 60 dB.

The 3-D plot (figure 7.9 (c) gives a clear illustration of the event distribution at the appropriate location with high energetic events appearing in the region 9-12 cm. The smooth surface of glass bead facilitates easier crack movement leading to adverse effect on flexural strength. Therefore only few activities above 55 dB, duration and rise-time > 1000 μ s are visible in figure 7.9 (d), indicating that no major obstacle existed on the crack path. This was also confirmed in figure 7.9 (a) where the load versus time plot is smooth indicating progressive crack development and a final brittle fracture, with less resistance. The highest energetic recorded events from pull out and large size crack growth had peak amplitude within 70.5 dB (figure 7.9 (d)). The events with amplitude >55 dB (from figure 7.9 (e)) are only 7 indicating the easier movement of crack with no major obstacle. The fractured surface can be seen in figure 7.9 (f), with glass beads bonded to the matrix.

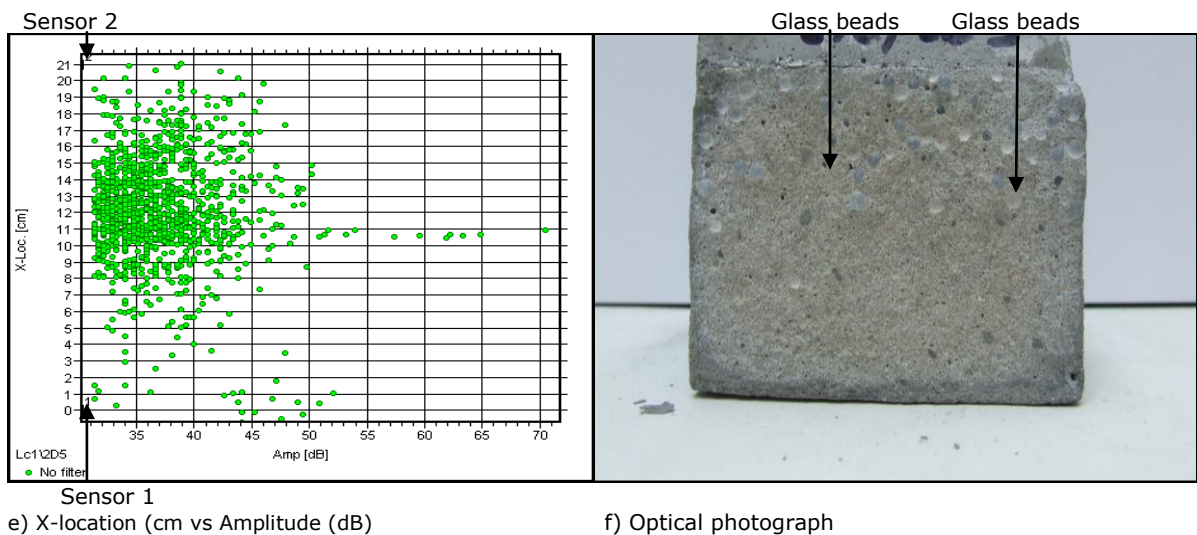
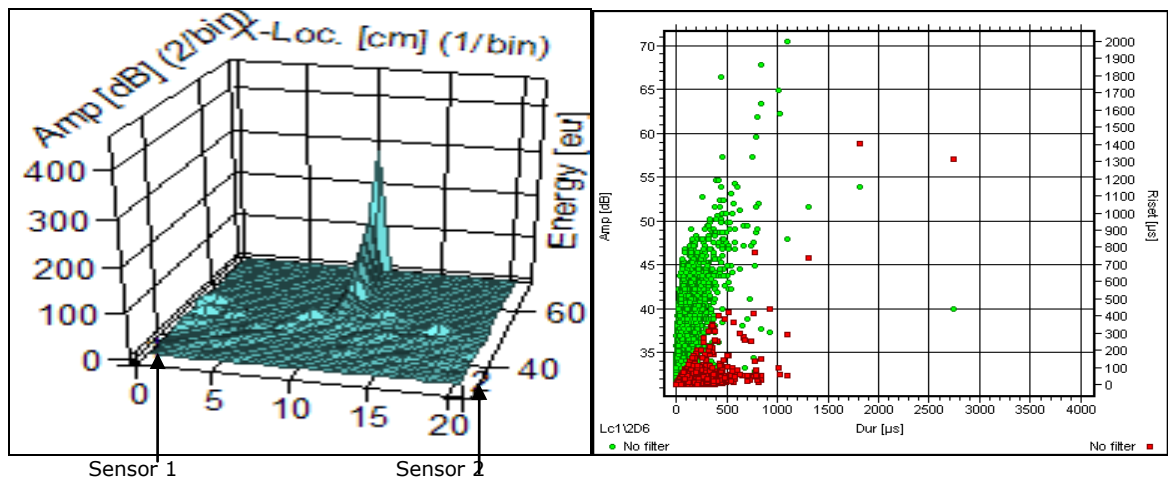
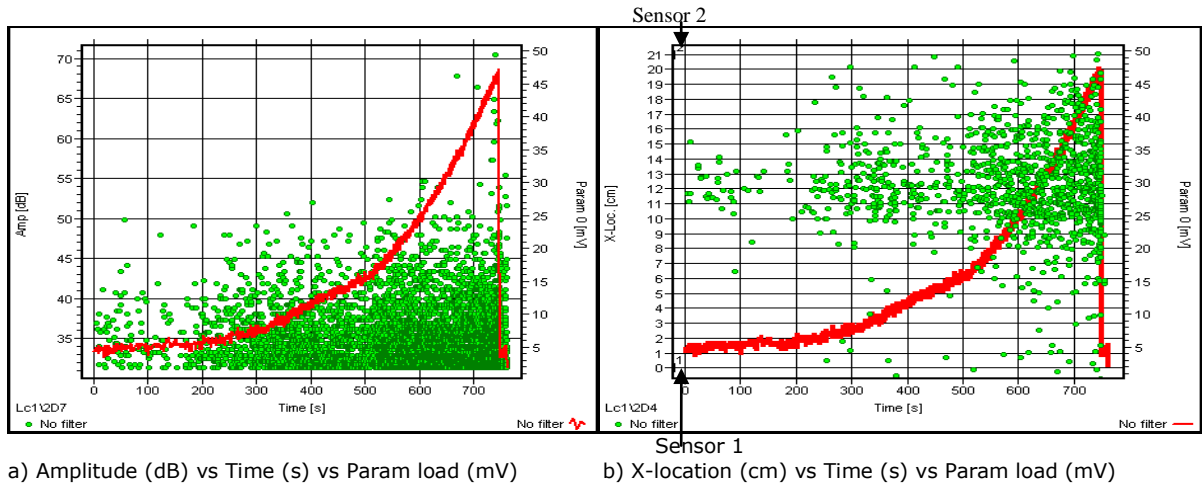


Figure 7.9: AE Plots and fractured surface for Expansive cement mortars with glass beads (3mm)

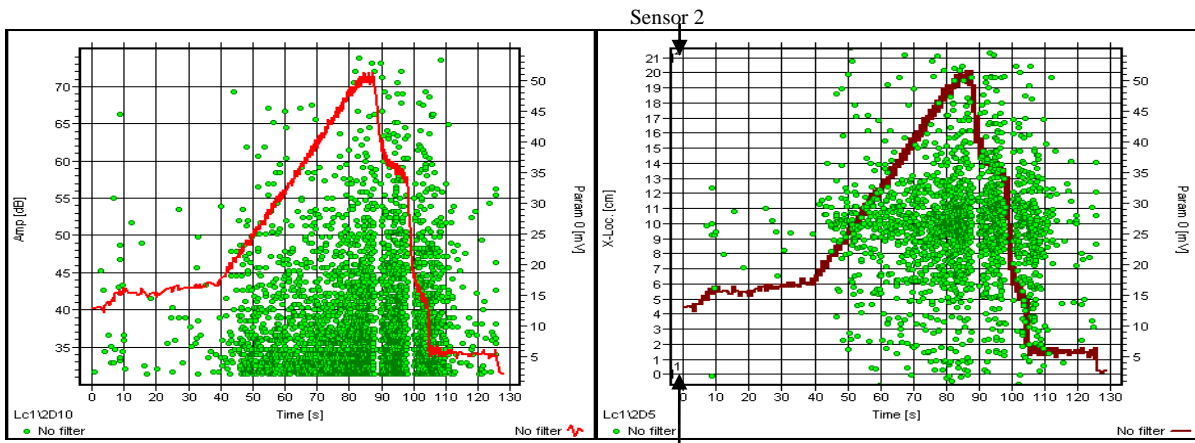
7.2.2 Expansive cement with 3 mm Pebbles Sample: Expeb3

The introduction of pebbles as aggregates in mortars has contributed to the changes in AE behaviour of the mortar during flexural test. Both the AE activity and load history are shown in figures 7.10 (a) and (b). Majority of the activities recorded under flexural condition are at low amplitudes (< 55 dB) as seen in figure 7.10 (a). As it can be seen from the AE plot 7.10 (b) (X-Location vs. Time vs. Param curve), very few activities were picked up by both sensors at very low amplitudes (<40 dB) at the initiation of the test. This is probably due to roller friction and the movement of rubber pads when the rollers were settling on the pads, which were resting on the specimen. After 50 seconds, the high amplitude activities started appearing in large numbers giving rise to major events such as large cracks, pull out events and crack deflection (figures 7.10 (a), (b) and optical graph (f)).

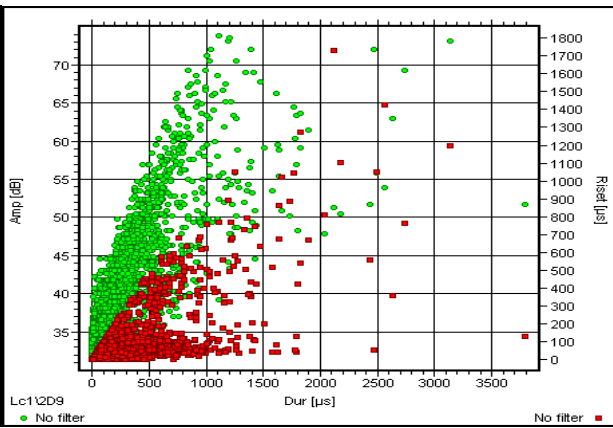
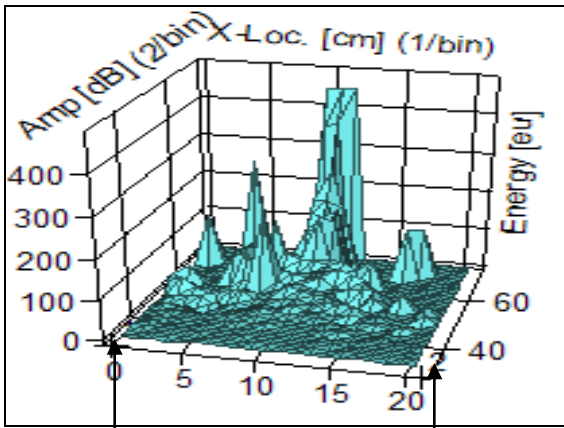
The 3-D plot (figure 7.10 (c) provides a clear illustration of event distribution that gives an indication of micro-cracks, crack arrests and pull out events gradually that led to eventual failure. The amount of energy being emitted in each event is much higher than the expansive cement sample with mixed size 3 mm Glass Beads (figure 7.10 (c)). The sample failed at location 10.20 cm with high amplitude of 73.9 dB, short rise-time of 48.2 μ s, very long duration of 1113.2 μ s, and high energy level of 406E00 (figure 7.10 (c) and (d)). This is an indication of major crack arrest after which the failure occurred at 87 seconds.

The pebbles appear to provide more resistance to cracks than the glass beads due to better interfacial bonding. Therefore the sample is more toughened compared to the specimen containing glass beads, as indicated by large number of low amplitude (<55 dB) AE activities in figure 7.10 (e).

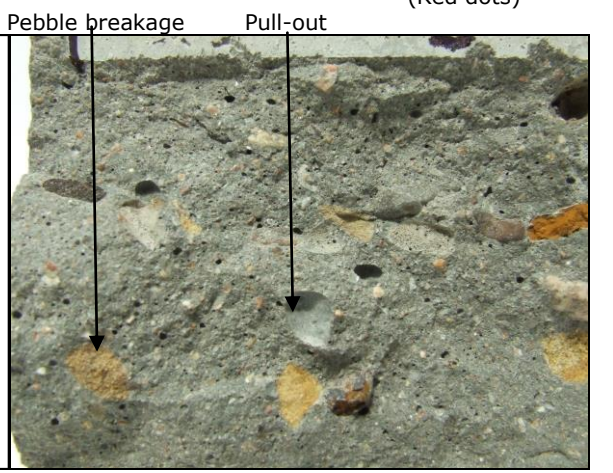
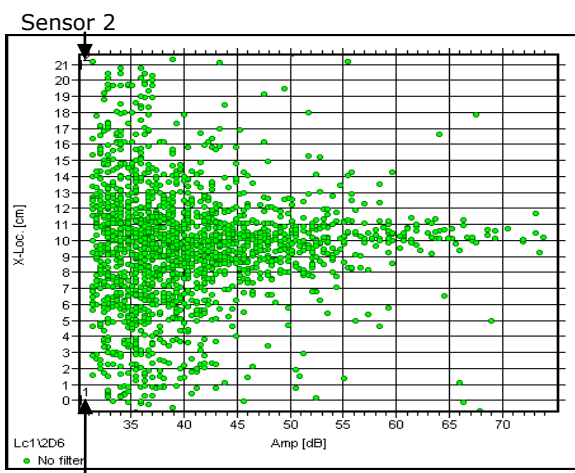
Up-to maximum load, the curve was linear and then showed several load drops indicating crack movement and arrest by the pebble aggregates and fracture of weak pebbles (see figure 7.10 (f) i.e. fracture surface with yellow region of pebble surface).



a) Amplitude (dB) vs Time (s) vs Param load (mV); b) X-location (cm) vs Time (s) vs Param load (mV)



c) 3-d: Amplitude (dB) vs X-location (cm) vs Energy (eu); d) Amplitude (dB) vs duration (μ s) vs Risetime (μ s) (Red dots)



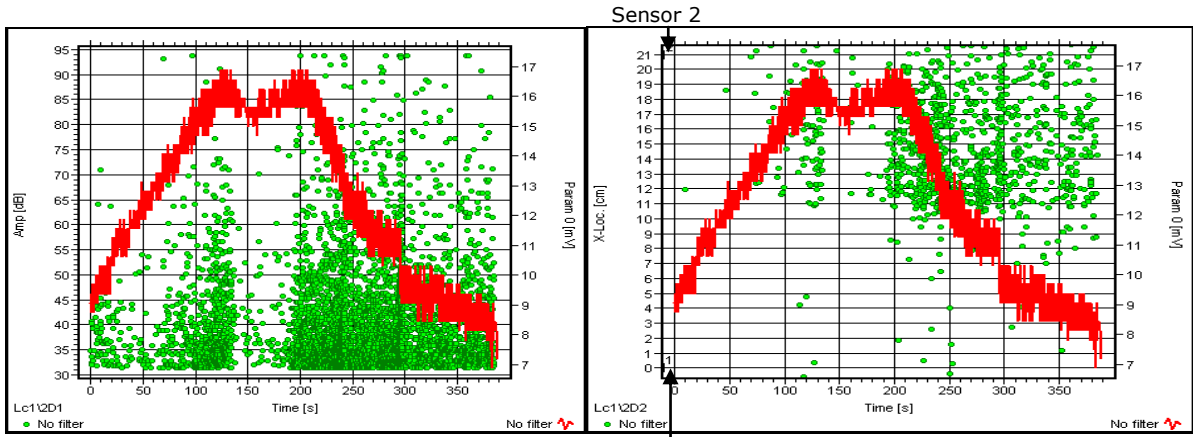
e) X-location (cm) vs. Amplitude (dB); f) Optical graph of mortar with pebbles

Figures 7.10: AE plots and optical graph for Expansive cement mortars with pebbles (3mm).

7.2.3 Expansive Cement Mortars with Rough Glass Aggregates (3mm) (Sample a2e)

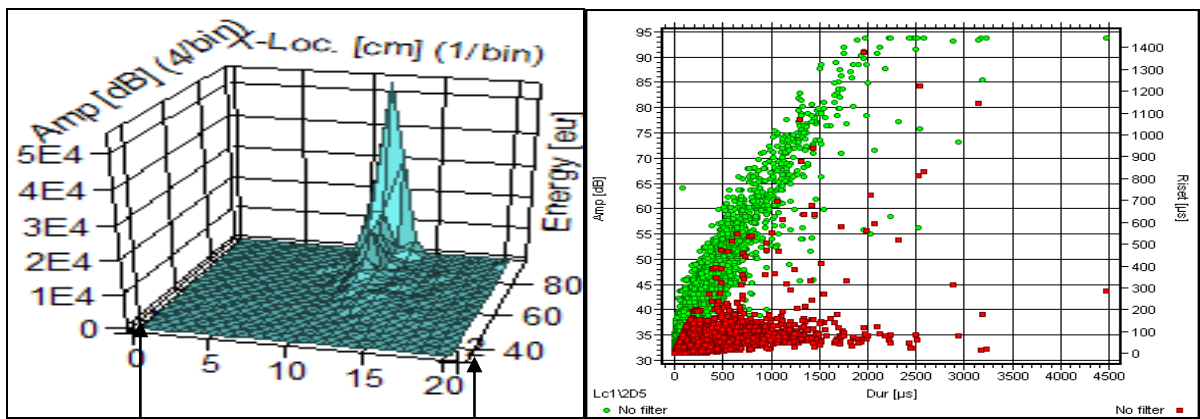
The introduction of rough glass aggregates changed the load pattern as well as the AE activity pattern of the specimen under test. The load curve is more skewed, and the AE activities are far fewer (especially at lower amplitudes) than the other two samples (specimens with glass beads and pebbles) as seen figure 7.11 (a); the reason for this is that sensor 1 picked up very few signals as shown in figure 7.11 (b). This is also visible in figure 7.11 (c) where the 3-D plot shows few activities are picked up by sensor 1. The other reason for less activities being recorded at low amplitude region is that the rough surface aggregates resisted the crack development and a large number of pull-out events occurred, therefore AE activities of higher amplitudes, longer duration and shorter rise-time can be seen (>70 dB, >1000 μ s, 200 μ s) as shown in figure 7.11 (d). At 120 seconds, the load drops possibly due to a major event and picks up again. During this period an almost quiet period existed, this is attributed to a large chunk of glass arresting the crack. At this point the glass chunk de-bonds from the cement matrix (the load is resting on the glass chunk) and the crack proceeds until failure. The major events such as strong pull-out, de-bonding of glass chunks is attributed to the activities of higher energy >500 e μ , amplitude >70 dB (see figure 7.11 (c) and (e)). The sample finally fails after 200 seconds. The fractured surface is shown in figure 5.73 (f), where strong pullout and de-bonding can be seen which are attributed to the high amplitude, high energy, longer duration, long rise-time (as seen in figure 7.11 (c), (d) and (e)).

The mortar sample with glass beads had the propagation of cracks increased rather than arresting cracks due to the smooth glass bead surfaces. Even though both the glass beads and glass aggregates are of same size (3 mm) and have smooth surfaces, but the glass beads assisted the crack development by providing easier path unlike the rough aggregates.



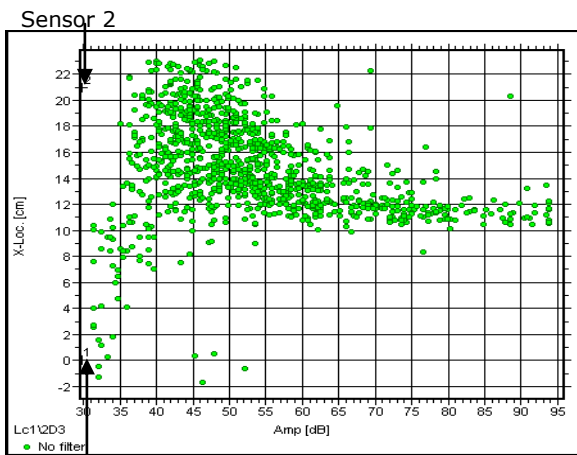
a) Amplitude (dB) vs Time (s) vs Param load (mV);

b) X-Location (cm) vs Time (s) vs Param load (mV);

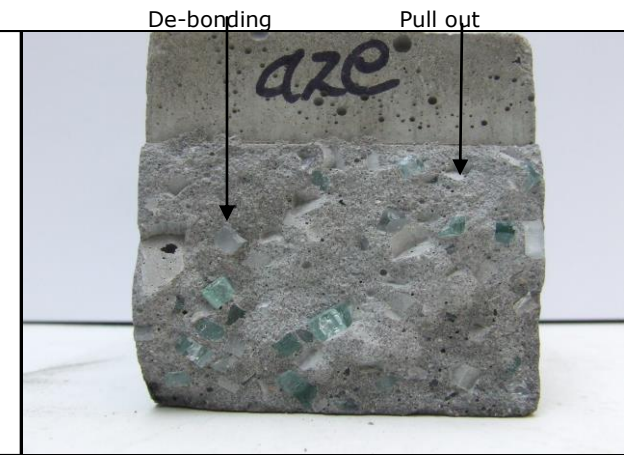


c) 3-D: Amplitude (dB) vs X-location (cm) vs Energy (eu);

d) Amplitude (dB) vs duration (μ s) vs Rise-time (μ s); (Red dots)



e) X-location (cm) vs Amplitude (dB);



f) Optical graph of mortar with 3 mm aggregates;

Figures 7.11: AE plots and optical graph for Expansive cement mortars with rough glass aggregates (3mm)

7.2.4 Summary

The AE characteristics show that the rate of AE activity increases with the load almost simultaneously and at failure the events are at highest peak in (sample with 3mm glass beads). This implies that the changes at micro-structural level are consistent throughout the test. The AE activity in sample with pebbles (specimen with expeb3) is non-linear and the micro-structural changes are varied throughout the duration of the test. The main reason for this is that the glass beads are all of the same structure (smooth rounded), while the pebbles (although same size 3 mm) are mostly of varied structure.

Therefore it can be deduced that sample with pebbles offer stronger resistance to cracks compared to glass beads. Interfacial bonding between cement and pebbles are better than the cement-bead bonding and cracks can easily move around the beads, but the cracks pass through the pebbles causing the fracture of aggregates. From the AE characteristics, it can be observed that cracks find it easier to proceed over the smooth surfaces of glass beads than to pass through the pebbles, therefore far fewer activities are seen to be recorded at high amplitudes. The interfacial bonding between the pebbles and the cement paste is also stronger than glass beads. Therefore pebbles are better for use as aggregates in concrete mortar compared to glass beads, since more toughening, better interfacial bonding hence higher flexural strength is achievable with pebbles.

From the 3-D AE plots, (as shown in figures 7.9-7.11 (c)), the AE energy profile is least in the expansive cement mortar with glass beads and the most is in the expansive specimen mortar with rough glass aggregates. This means that the glass beads provided the least resistance to crack therefore less energy released to confront the crack while in the specimen with the rough glass aggregates provided the most resistance and therefore the energy released is highest.

Figures 7.12 and 7.13 illustrate the number of hits produced by samples with 3 mm aggregates. The specimen with glass beads generated highest number of percentage of hits compared to the others. The possible reasons behind this hits generation may be:

a) the smooth surface of glass beads assisted the cracks to progress easily, therefore a large number of activities took place;

b) a large number micro-cracks took place under load that generated extra percentage of hits.

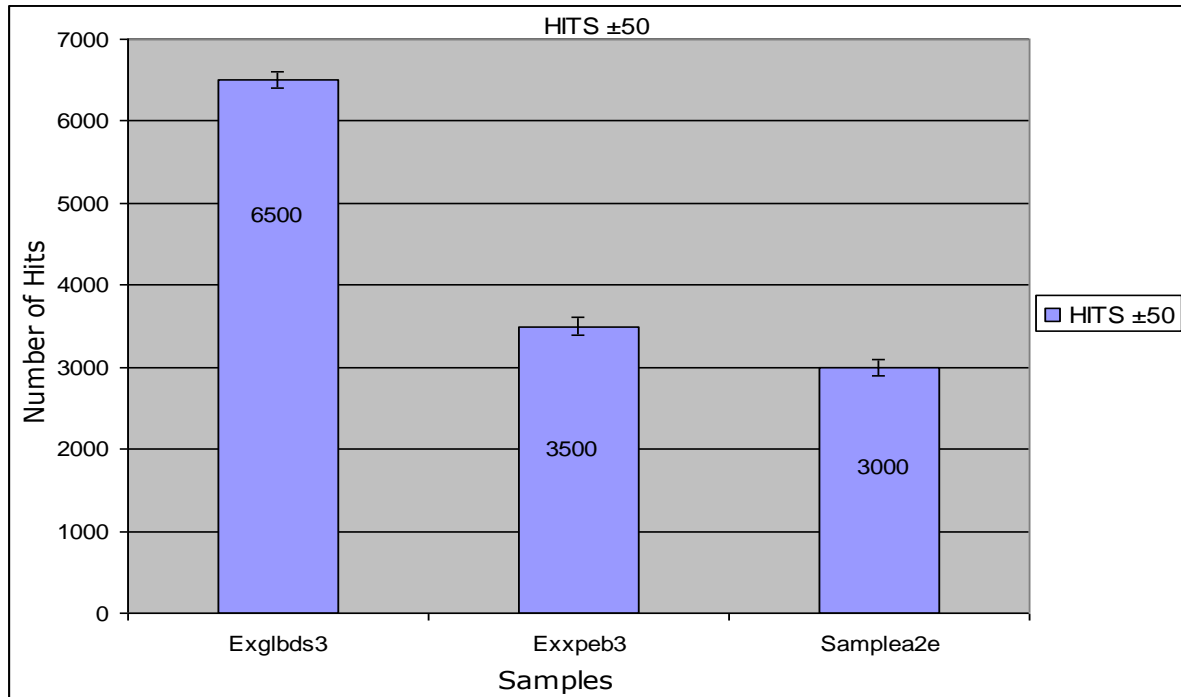


Figure 7.12: AE hits produced by expansive cement based mortars with aggregates under flexural load

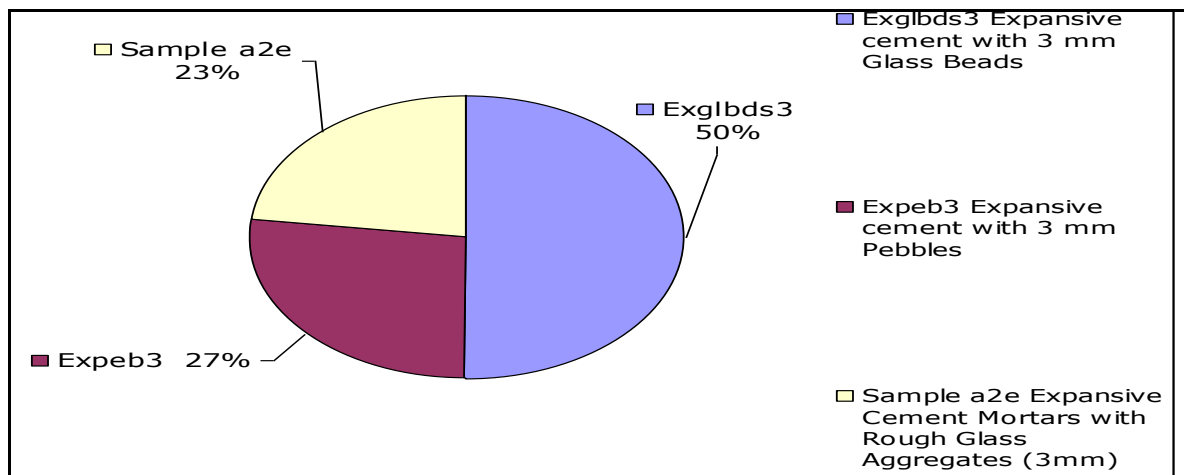


Figure 7.13: Percentage of AE hits produced by expansive cement based mortars with aggregates under flexural load

However, in the other two samples their respective aggregates contributed to AE hits with high magnitude. Although the hits are small in number, but (as discussed above and also seen from the photographs of the fractured surfaces) the sample tests resulted in high energy units.

7.3 AE Monitoring of Ordinary Portland Cement Matrix with Admixtures and Glass Plate

Batches of concrete blocks were manufactured using Portland cement containing glass plate, glass aggregate and calcium carbonate (CaCO_3) added to mixture. Flexural tests were carried out to study the effect of composition and aggregates on the study of the grain-bridging/micro-cracking mechanism and the interfacial technology simultaneously. This work will enable a comparative understanding and merits of these techniques that can be developed and a recommendation can be made regarding the enhancement of the mechanical properties regarding the strength and toughness of concrete mortars at micro-structural level during the flexural load condition.

The AE plots shown in figures 7.14 (a-c) (i) and (ii) depicts the behaviour of each mortar sample containing (a) glass slide; (b) calcium carbonate and glass slide; and (c) glass slide, calcium carbonate and glass aggregates. Comparisons of fracture load (strength) of plain concrete samples indicate that addition of CaCO_3 to OPC enhances toughness of the block by relaxation of residual stress (micro cracking) under load.

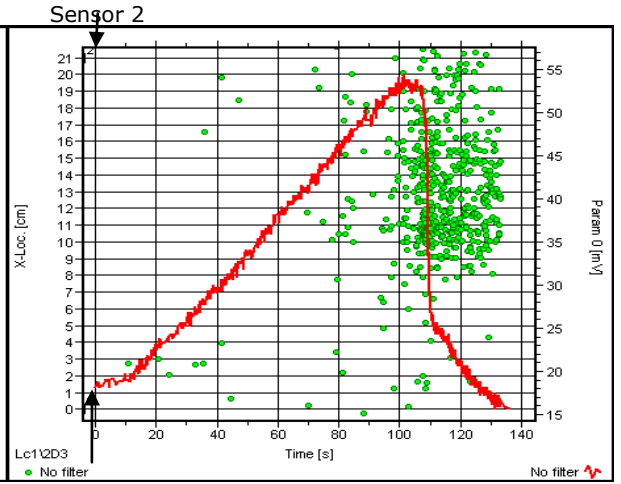
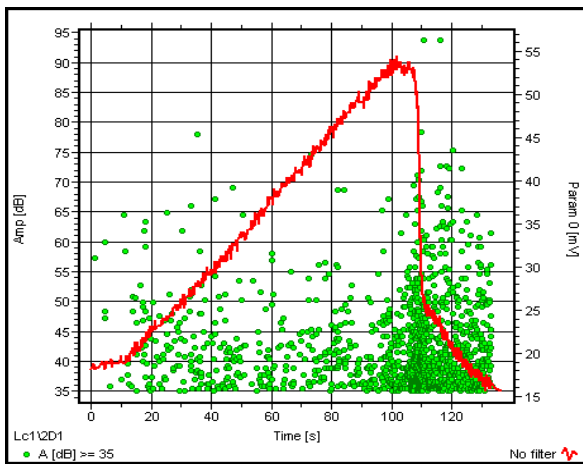
Sample containing CaCO_3 showed an increase of 60% strength over OPC block. Similar results were obtained with blocks containing glass aggregates and a glass plate. These obstacles offer resistances by deflecting cracks and arresting crack propagation through the block respectively.

The results of the block containing a glass plate are shown in figure 7.14 (a) (i) amplitude (dB) vs time (s) and (ii) X-location (cm) vs time (s), with load/location curve (ordinary Portland cement + glass plate). The glass slide is probably taken by the crack at 70 seconds, where the load curve shows slight deflection. From figure 7.14 (a) (ii), it is visible that most of the localised activities are recorded towards the end of the test.

The strength of the block containing CaCO_3 is higher than the OPC block, as seen in figure 7.14 (b) (i) amplitude (dB) vs time (s) and (ii) X-location (cm) vs time (s), with load/location curve (calcium carbonate + glass plate). It can be seen that the load versus time plot is less skewed and become smooth when the load is transferred to the glass plate (linear region). When the crack arrested by

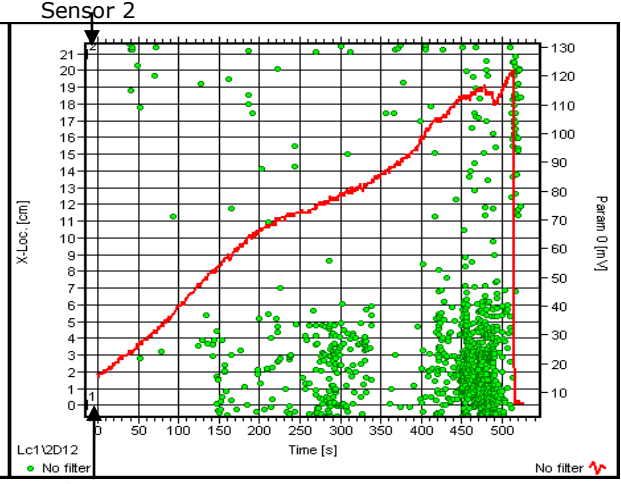
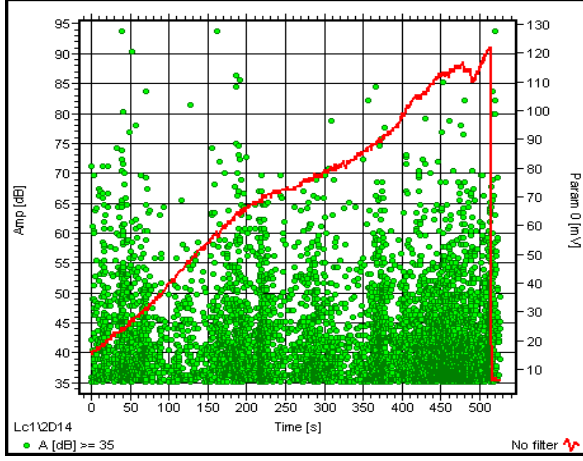
the plate overcomes the obstacle, an energetic event occurs and the block fractures. The localised events are taking place throughout the test (from beginning to end) may be an indication of the effect of the addition of calcium carbonate, (see figure 7.14 (b) (ii)). The large density of events gives an indication of the effect of the introduction of calcium carbonate and glass slide (see figure 7.14 (b) (ii)).

The test results of the blocks containing a glass plate, calcium carbonate and glass aggregates are shown in figure 7.14 (c) (i) amplitude (dB) vs time (s) and (ii) X-location (cm) vs time (s), with load / location curve (calcium carbonate + glass plate + glass aggregate). This indicates the addition of glass aggregates have made additional contribution to toughening, with activities at low and high amplitudes. The AE activities (at low and high amplitudes) give an indication of the resistances to micro-cracks as well as resistances to major cracks. Numerous localised events (more than the other samples) are recorded throughout the test mainly picked up by sensor 1, which may be due to the fact that most of the glass aggregates may have settled at in the vicinity of sensor 1.



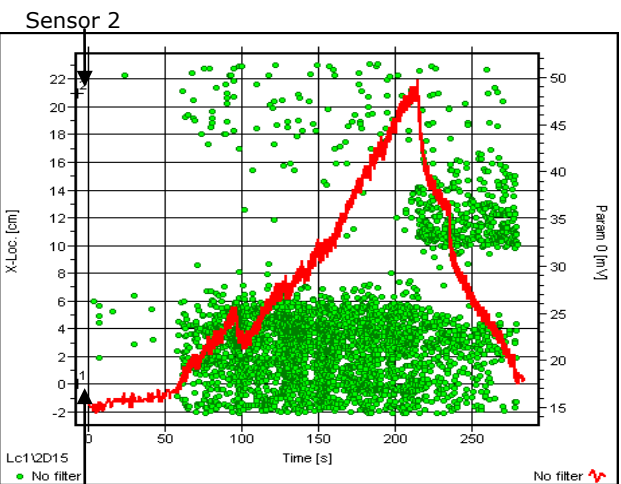
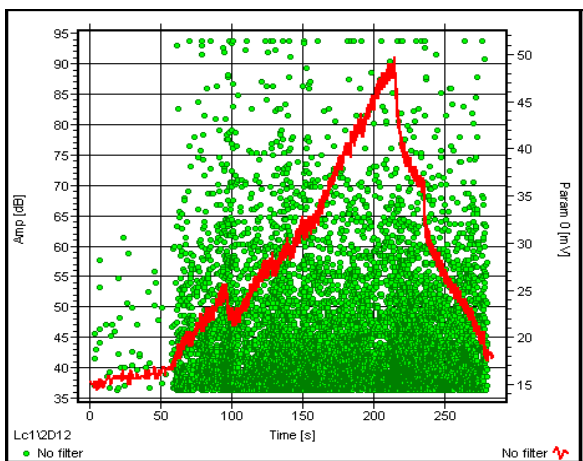
(i) Amplitude vs Time (s) vs Param (mV)
a) Mortar with glass slide

(ii) X-Location (cm) vs Time (s) vs Param (mV)



(i) Amplitude (dB) vs Time (s) vs Param (mV)
b) Mortar with calcium carbonate and glass slide

(ii) X-Location (cm) vs Time (s) vs Param (mV)



(i) Amplitude (dB) vs Time (s) vs Param (mV)
C) Mortar with calcium carbonate, glass slide and glass aggregates

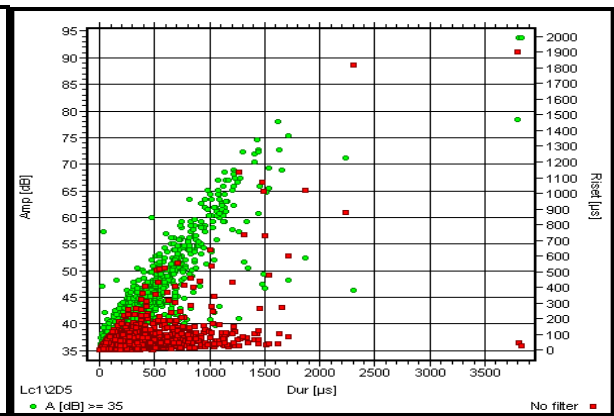
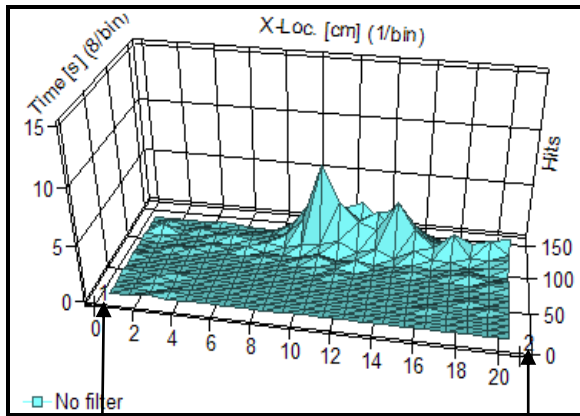
(ii) X-Location (cm) vs Time (s) vs Param (mV)

Figure 7.14: AE plots of different motors

The 3-dimensional AE plots (figure 7.15 (a-c) (i's)) show clear distinction between the specimens; the effect of the addition of calcium carbonate and glass aggregates along with the glass slide is clearly distinguishable, the number of hits in these plots have increased. The glass slide region is also clearly visible in these plots. In figure 7.15 (a) (i), the sample that is plain mortar with the glass slide, the slide is indicated by increase in hits level between 80 and 90 seconds. In specimen which is Mortar with calcium carbonate and glass slide, rise in hits level between 450 and 500 seconds signals the crack reaching the glass slide (see figure 7.15 (b) (i)). In the specimen with calcium carbonate, glass slide and glass aggregates, increased hits level between 90 and 110 seconds probably point towards the glass plate that obstructs the crack movement as seen in figure 7.15 (c) (i). Hence from the 3-d plots it can be seen that the effect of the addition of glass plate in all specimens reflect on the rise in the level of hits. The addition of calcium carbonate is seen to make an increase in the number of hits (figure 7.15 (b) (i)); introduction of glass aggregates make further increase in hits number as seen in figure 7.15 (c) (i).

As soon as the crack is arrested by the glass slide, the volume of acoustic activities emitted from this region drops to almost zero. From figure 7.15 (a) (ii), it can be seen that the plain mortar with glass slide exhibits most of the activities are of low amplitudes (< 55 dB) and short rise-time (eu). The number of AE activities with both higher and lower amplitudes; long and short duration; low and high rise time becomes dominant with the addition of calcium carbonate and glass aggregates (figure 7.15 (b) and (c) (ii's)). The activities with highest amplitudes are the most dominant in specimen with the calcium carbonate and glass aggregates. This is also reflected on the rise-time activities on different samples. This means that both toughening and the strength are enhanced using this method of manufacturing mortar blocks.

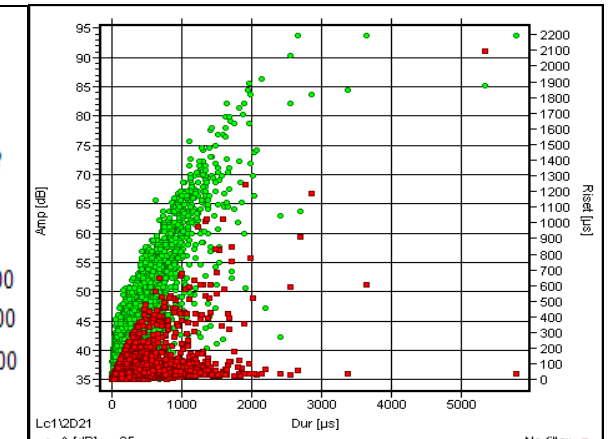
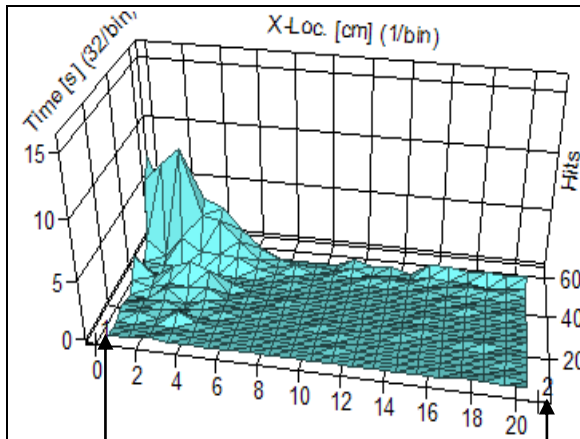
From both the load and hits versus time history multi-plots, it is apparent that the glass aggregates display inhomogeneous nature of the block. The path of cracks is more skewed as result of resistance offered by the glass aggregates. When the crack reaches the glass slide the load is transferred to the slide, the slope in the load versus time plot changes, until the crack overcomes this obstacle. The number of hits and load is higher for the blocks containing CaCO_3 and manufactured using the expansive cement.



Sensor 1 Sensor 2

(i) 3D Plot of X-location (cm) vs Time (s) vs Hits
a) Plain Mortar with glass slide

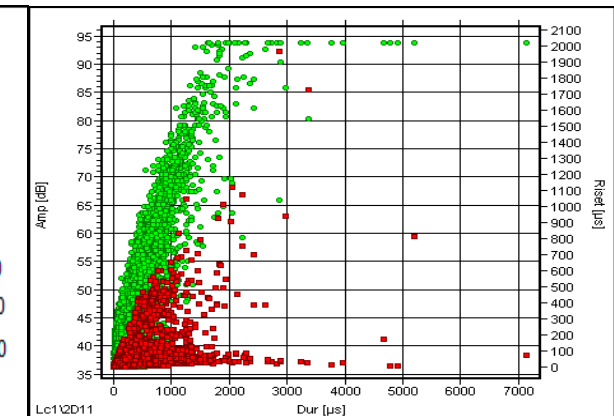
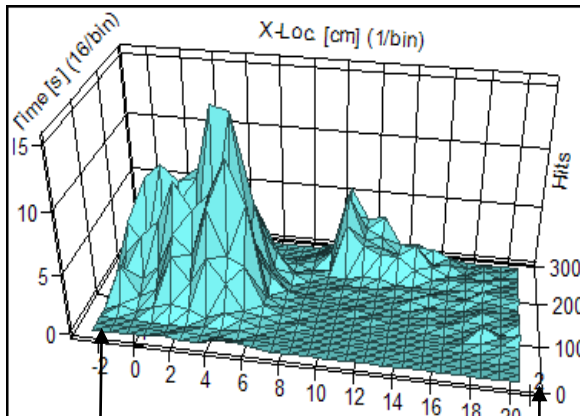
(ii) Amplitude (dB) vs Duration (μ s) vs Risetime (μ s)
(Red dots)



Sensor 1 Sensor 2

(i) 3D Plot of X-location (cm) vs Time (s) vs Hits
b) Mortar with calcium carbonate and glass slide

(ii) Amplitude (dB) vs Duration (μ s) vs Risetime (μ s)
(Red dots)



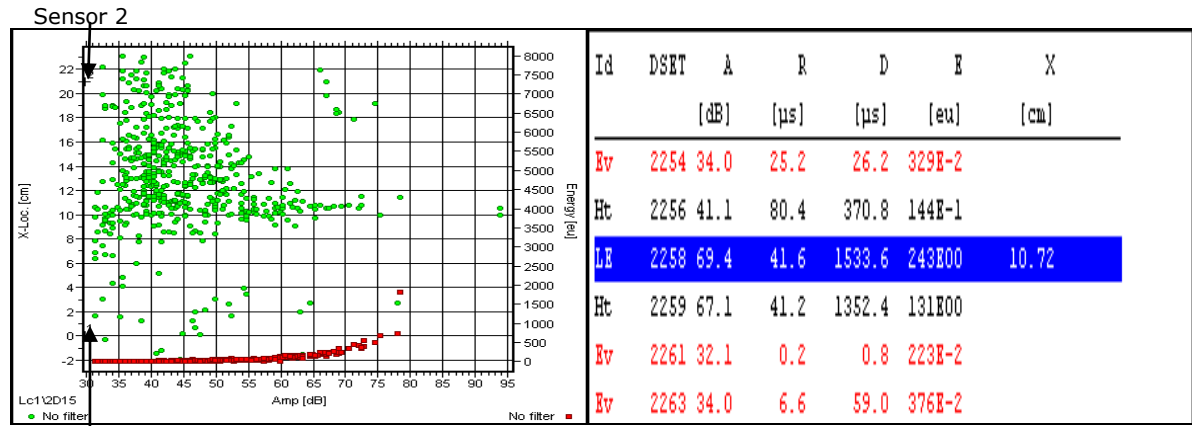
Sensor 1 Sensor 2

(i) 3D Plot of X-location (cm) vs Time (s) vs Hits
c) Mortar with calcium carbonate, glass slide + glass aggregates (Red dots)

(ii) Amplitude (dB) vs Duration (μ s) vs Risetime (μ s)

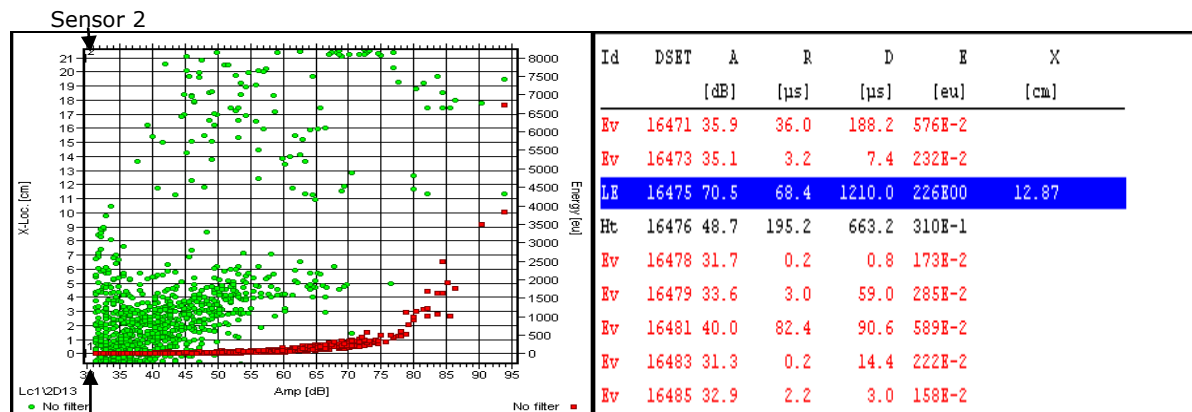
Figure 7.15: AE Plots of different samples

The AE response under flexural load exhibit the toughening behaviour of calcium carbonate and glass aggregates, (figures (7.16 (a-c) (i's))). The amplitude and the energy pattern changes to higher profiles with the introduction of calcium carbonate and glass aggregates. Events of higher amplitude (>70 dB) and high energy (> 500 eu) is a result of the introduction of calcium carbonate and aggregates, with huge increase in the AE activity variations, indicating a rise in toughness. The values of AE parameters at the location of final failure are given in the listings, with blue shadings (figures (7.16 (a-c) (ii's))).



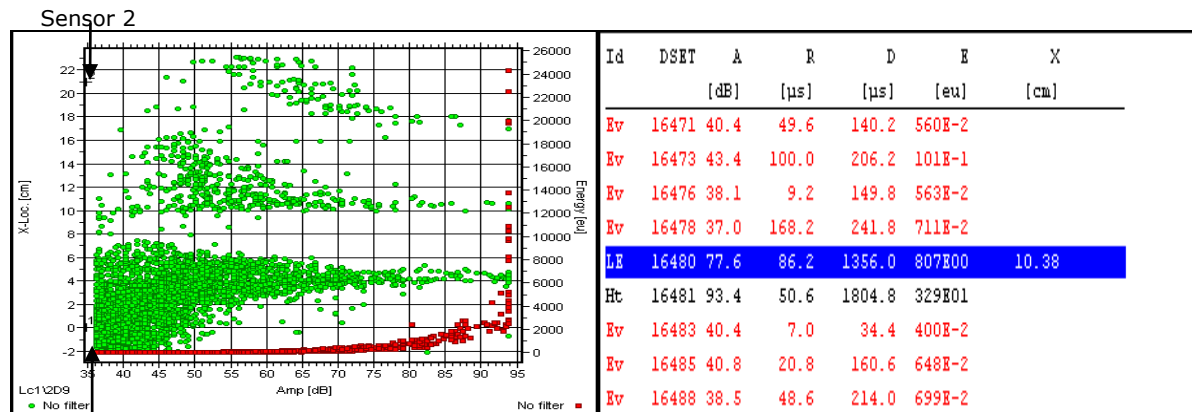
(i) X-location (cm) vs Amplitude (dB) vs Energy (eu); (ii) AE listing (Red dots)

a) Mortar with Glass Slide



(i) X-location (cm) vs Amplitude (dB) vs Energy (eu); (ii) AE listing (Red dots)

b) Mortar with calcium carbonate and glass slide



(i) X-location (cm) vs Amplitude (dB) vs Energy (eu); (ii) AE listing (Red dots)

c) Mortar with calcium carbonate, glass slide and glass aggregates

Figure 7.16: AE Plots and listing of different samples

Inclusions of glass slide, calcium carbonate as admixture and glass aggregate played their role in these mortars when subjected to flexural load. These roles can be reflected on the number of hits generated by each specimen as shown in figures 7.17 and 7.18. Addition of calcium carbonate as admixtures seems to have contributed to the accumulation of hits in sample CARA1. This is probably due to the accumulation of micro-cracks on an extensive scale.

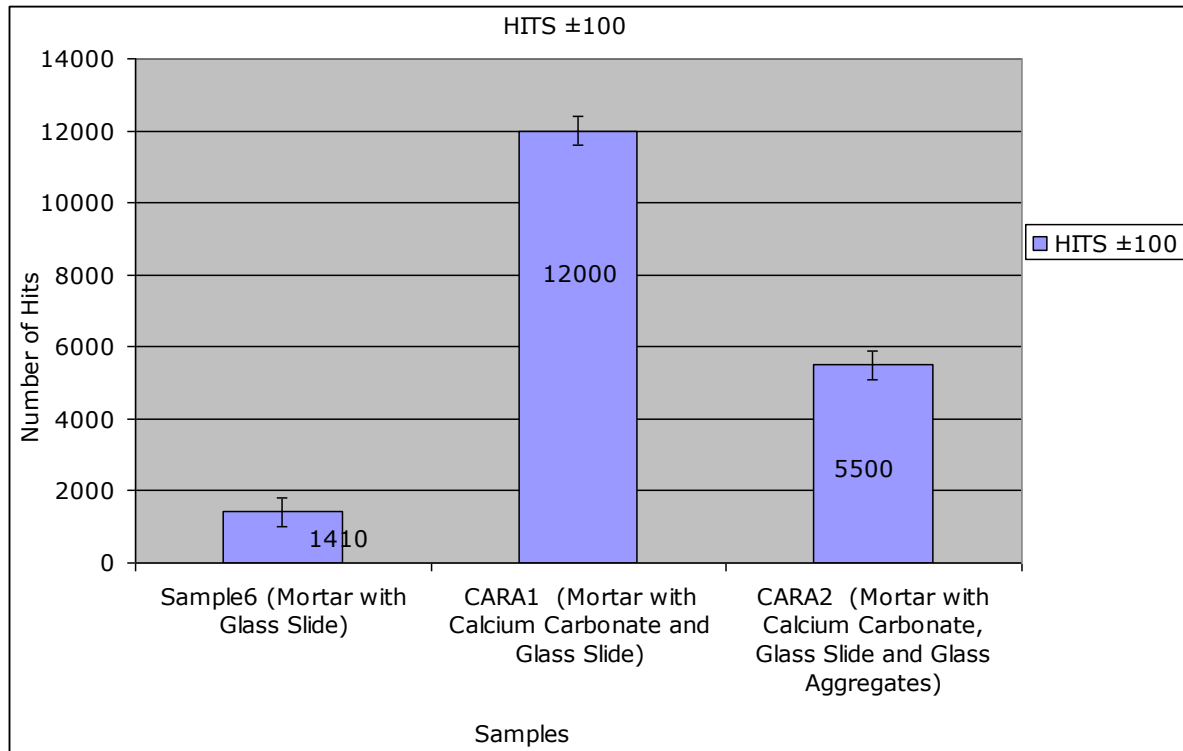


Figure 7.17: AE hits produced by different mortars with glass slide, glass aggregates and admixture under flexural load

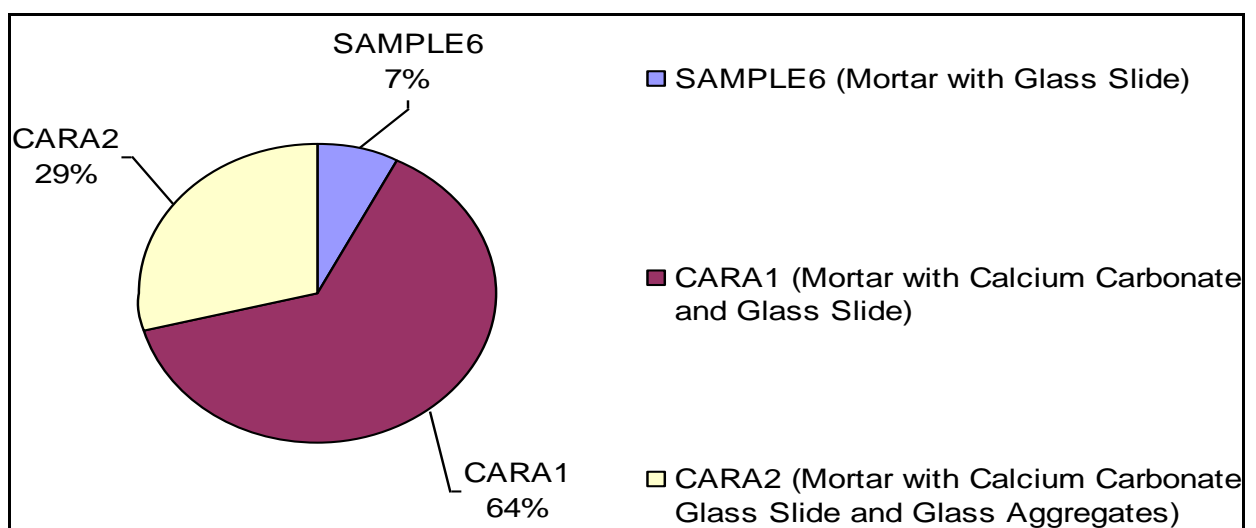


Figure 7.18: Percentage of AE hits produced by different mortars with glass slide, glass aggregates and admixture under flexural load

7.3.1 Summary

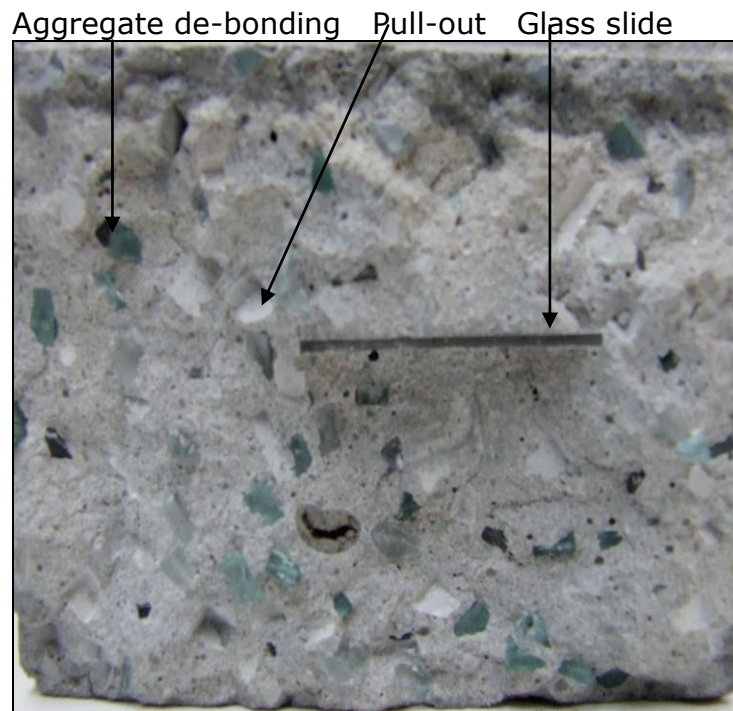
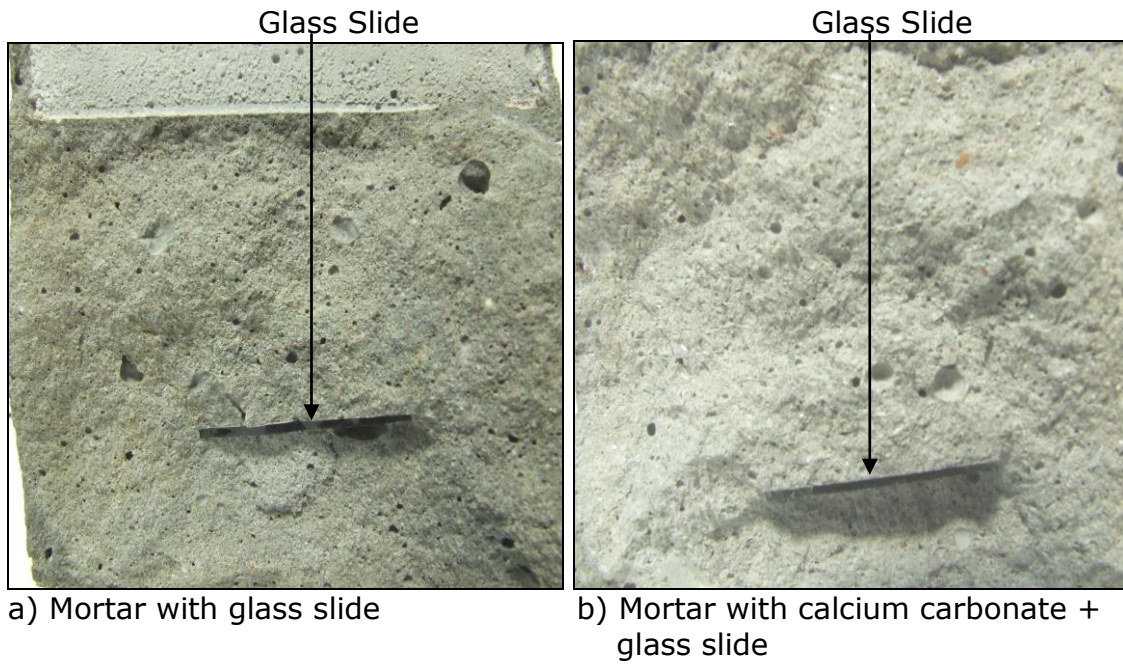
From the AE response, it is observed that in these mortar blocks, the contribution of glass slides during the flexural loading condition is mainly arresting the cracks and prolonging the time of failure rather than making a large contribution to the toughening of mortar. Therefore the use of carbonate and glass aggregates are recommended for use to obtain higher toughness and higher strength.

However, the use of carbonate, glass aggregates, and bridging technique (glass slide or a long reinforcing aggregate) simultaneously is a highly recommended technique to achieve the enhanced mechanical properties.

A summary of the AE monitoring during flexural tests are as follows:

1. In specimen containing glass slide: crack bridging/arrest occurs;
2. In specimen containing glass slide and CaCO₃: crack bridging occurs, micro-cracks are prominent, therefore toughening is dominant;
3. In specimen containing glass slide, CaCO₃ and glass aggregates: crack bridging occurs, micro-cracks are intense, toughening is dominant; strong resistances to major cracks are present therefore crack arrest, crack deflection and pull-out events are also dominant.

The fractured surfaces of concrete samples with glass slides, glass aggregates and calcium carbonate are shown in figure 7.19 (a-c). The topography of fracture surfaces are in close agreement with the AE observation. The effects of aggregate bonding, pull-out events, de-bonding that are visible from the fractured surfaces clearly support the recordings on the AE plots. A variety of major events that took place during the test resulted in strong AE signals with events of high amplitude, longer duration, and high energy. The effect of the addition of admixture (calcium carbonate) is visible on the fractured surfaces (changes in surface appearance) which resulted in the changes at micro-structural level and thus to the enhancement of toughening behaviour of specimens.



c) Mortar with calcium carbonate + glass slide and glass aggregates

Figure 7.19: Fractured Surfaces of specimens containing glass slide, admixtures and glass aggregates

CHAPTER 8

8.0 Comparison of AE Signal Parameters Emitted from Mortars

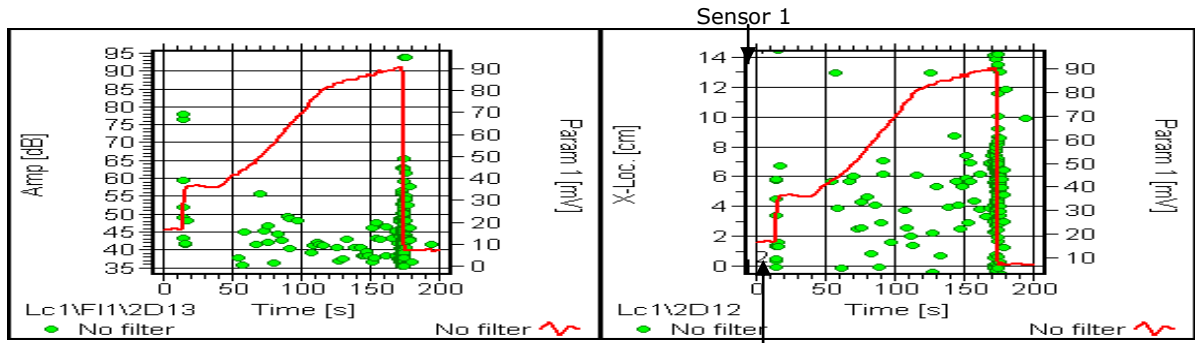
Containing Admixtures and Waste Aggregates of Mixed Sizes

8.1 AE Monitoring of Mortars samples (14 days curing) under Flexural Load

8.1.1 Sample Brglcam: Mortar with Glass Plate

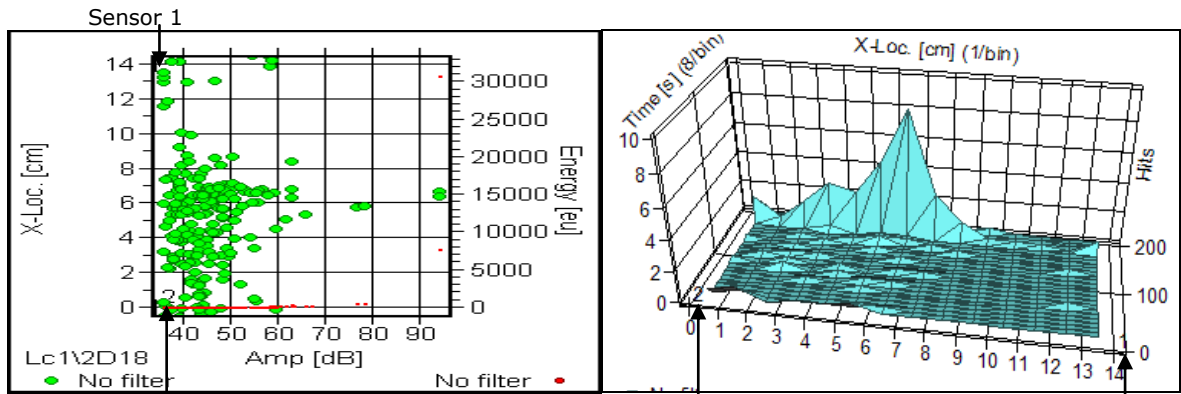
An attempt is made here to study the behaviour of mortars containing various admixtures under applied load and characterise the damage mechanisms such as micro-crack formation, and crack evolution during flexure tests. The results of the flexure tests of two mortar samples containing a glass plate and the other containing broken glass aggregates (14 days of curing) are shown in figures 8.1 and 8.2. The load vs. time plot for the sample with glass plate (see figure 8.1) exhibit two slopes representing the strength of mortar and glass plate.

The transition from one slope to the next in the plot indicates a sharp load transfer from the mortar to the glass plate. It is apparent from the AE source location vs. time plot that in samples crack initiates at approximately 30 mm and reaches the glass plate reinforcement at a location of 60-70 mm. The load is then transferred onto the glass plate and the crack is arrested. The AE activity now is mostly due to the manipulation of crack close to glass slide. When the load bearing capacity of the glass slide is reached it snaps leading to sudden fracture of the sample. From figure 8.1 (a), the number of AE activities are almost all <55 dB, only a few activities at high amplitude level that take place when the load drop. The AE amplitude versus Time and Load shows high energy events (exceeding 95 dB) at 150 seconds and sudden drop of load (final fracture). The AE activities are sparsely distributed across the specimen as seen in figure 8.1 (b). This is also reflected in the activities with the number of low amplitudes (< 55 dB), low energy (< 500 eu) and the number of hits as seen in figures (c) and (d). The specimen failure is shown in the AE listing (in figure 8.1 e) where it is shown that the located event (failure) is shown in the blue shading.



(a) Amplitude (dB) vs Time (s) vs Param (mV)

(b) X-location (cm) vs Time (s) vs Param (mV)



(c) X-location (cm) vs Amplitude (dB) vs Energy (eu); (d) 3-D plot of Time (s) vs X-location (cm) vs Hits

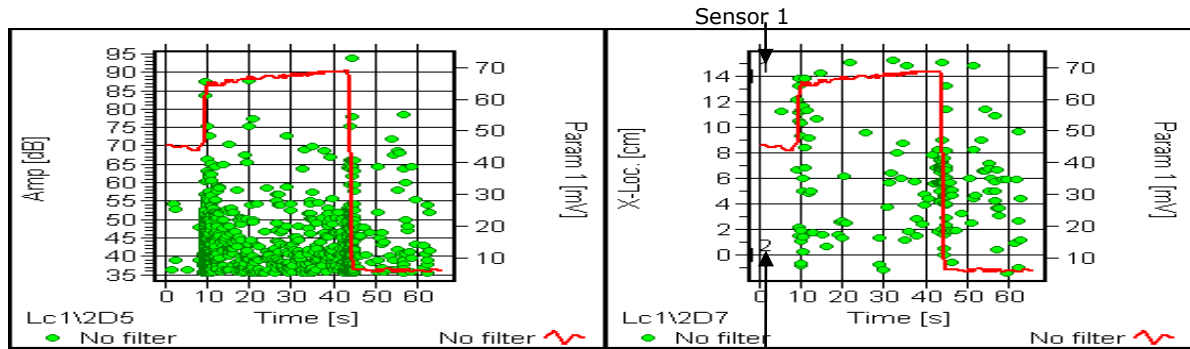
Id	DSET	A [dB]	R [μs]	E [eu]	TRAI	D [μs]	X [cm]
LE	1075	50.5	65.2	438E-1	508	982.0	6.27
Ht	1076	51.7	61.0	406E-1	509	950.4	
LE	1078	52.0	35.6	323E-1	510	624.6	6.95
Ht	1079	48.3	73.6	296E-1	511	645.8	
Ev	1081	36.2	0.2	277E-2	512	0.8	
Ht	1082	53.9	57.4	418E-1	513	446.2	
Ev	1084	40.0	29.2	686E-2	514	100.2	

e) AE Listing

Figure 8.1: AE plots and listing of sample Brglcam (mortar with glass plate)

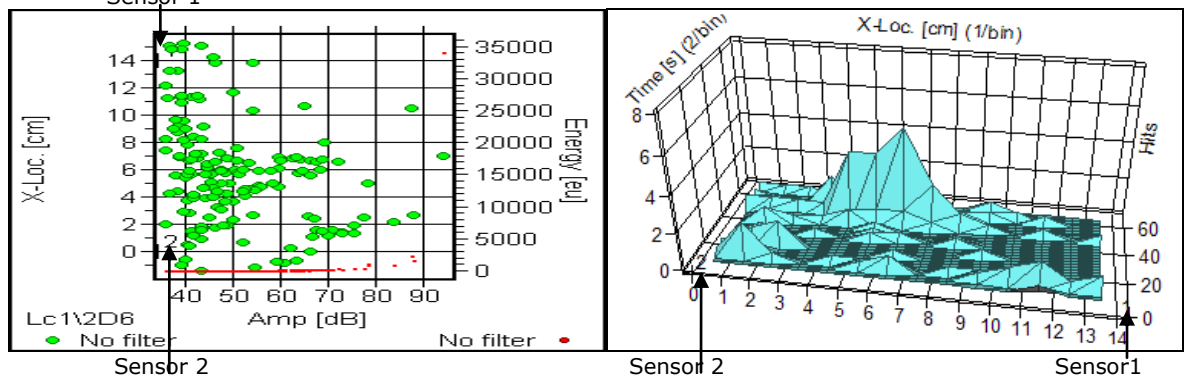
8.1.2 Sample Brglcam1: Mortar with Glass Aggregates

Results of the sample containing glass aggregates is shown in figure 8.2 (a) to (e). It is apparent from the results that due to insufficient curing time (14 days), the sample is very brittle (see figures 8.2 (a) and (b)). There are regions of high activity indicating easy crack propagation as the interfacial bonding between cement paste and glass aggregates is weak as seen in figure 8.2 (c). The 3-dimensional plots (figure 8.2 (d)) exhibit the distinctive behaviour between the effects of introducing glass aggregates and the normal mortar. Addition of glass aggregates have resulted in recording of higher densities of hits. The density of hits is greater with glass segments, spread out throughout the specimen. This means that the toughening is far greater in this specimen than sample brglacam (mortar with glass slide).



(a) Amplitude (dB) vs Time (s) vs Param (mV)

(b) X-location (cm) vs Time (s) vs Param (mV)



(c) X-location (cm) vs Amplitude (dB) vs Energy (eu); (Red dots)

(d) 3-D plot of Time (s) vs X-location (cm) vs Hits

Id	DSET	A [dB]	R [μs]	E [eu]	TRAI	D [μs]	X [cm]
Ev	1475	40.4	10.8	533E-2	865	37.4	
LE	1477	93.8	29.4	341E02	866	24595.2	6.98
Ht	1478	93.8	28.6	281E02	867	14208.0	
Ev	1480	64.5	27.4	112E00	868	700.4	
Ev	1482	61.8	215.4	107E00	869	725.0	
Ev	1484	78.0	228.6	109E01	870	1153.6	
Ev	1486	48.7	88.8	242E-1	871	382.8	
Ht	1487	46.0	63.6	151E-1	872	257.2	

e) AE Listing

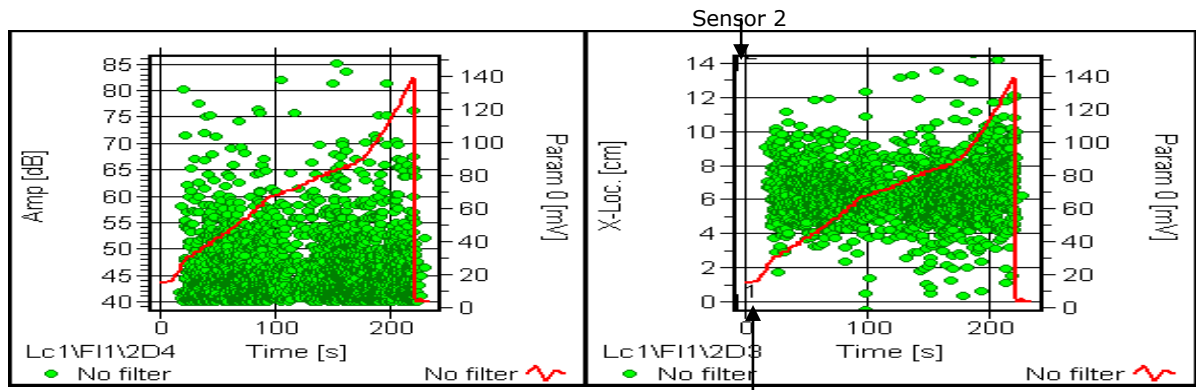
Figure 8.2: AE plots and listing of sample Brglcam1 (mortar with glass aggregates)

The specimen failure is shown in the AE listing (in figure e) where it is shown that the located event (failure) is shown in the blue shading. Cured samples for 14 days and putting them under flexural load test have had an effect on the AE characteristics. The number of AE activities are far lower than any other samples (all of which were cured under standard 28 days). The main reason for this is that the specimens are not set or cured properly, therefore the bonding between the cement paste and the aggregates are poor.

8.1.3 Mortar with Sodium Sulphate and Glass Plate (14 days curing)

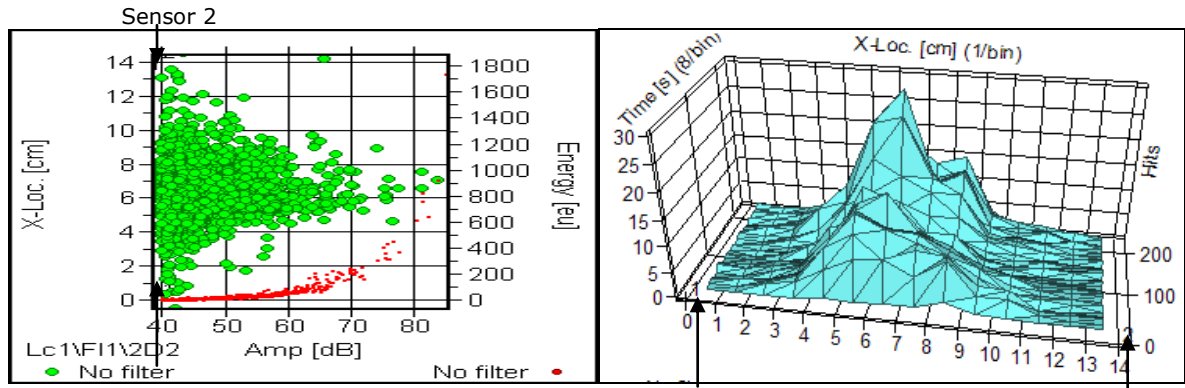
Sodium sulphate was seen to make an impact on the AE characteristic of mortar, i.e. positive effect on the toughening behaviour of concrete under compression (as seen in 7.7.3). The effect of the addition of sodium sulphate as additive into mortar can be examined in terms of AE characteristic under flexural condition. This therefore can give an indication of the suitability of this admixture on either the improvement or detrimental effect on concrete.

A comparison of samples containing glass plate (see figures 8.1 and 8.3) in mortar and mortar with sodium sulphate exhibit somewhat similar behaviour under flexural load. In both samples, the behaviour exhibited due to the presence of glass slides is very similar. When the crack is overtaken by the glass slide, for example, the numbers of activities being recorded are far less than the region before the plate takes over. All these activities are of very low amplitudes (<50 dB), which means that some toughening is present as a result of the inclusion of glass plates in the mortar. The energy being emitted from these events are of same level. The effect of the addition of sodium sulphate is clearly seen in figure 8.3, which is very different from figure 8.1 and 8.2 (plain mortars with (i) glass plates and (ii) glass plates and aggregates). The amount of AE response in this case is far greater (see figure 8.3 (a-d). The specimen failure is shown in the AE listing (in figure e) where it is shown that the located event (failure) is shown in the blue shading.



(a) Amplitude (dB) vs Time (s) vs Param (mV)

(b) X-location (cm) vs Time (s) vs Param (mV)



(c) X-location (cm) vs Amplitude (dB) vs Energy (eu); (d) 3-D plot of Time (s) vs X-location (cm) vs Hits (Red dots)

Id	DSET	A [dB]	R [μ s]	E [eu]	TRAI	D [μ s]	X [cm]
Ev	29784	28.8	0.2	107E-2		13.0	
Ev	29786	27.2	0.2	887E-3		21.2	
Ev	29788	26.1	0.2	617E-3		0.4	
LE	29790	38.5	25.8	571E-2		270.4	6.20
Ht	29791	34.7	19.0	438E-2		185.2	
Ev	29793	28.0	6.2	101E-2		7.0	
Ev	29795	26.1	0.2	882E-3		0.4	
Ht	29796	27.2	3.0	123E-2		28.6	
LE	29798	76.1	45.8	324E00		1814.4	7.17

e) AE Listing

Figure 8.3: AE plots and listing for sample NAS (Mortar with Sodium Sulphate + Glass Slide)

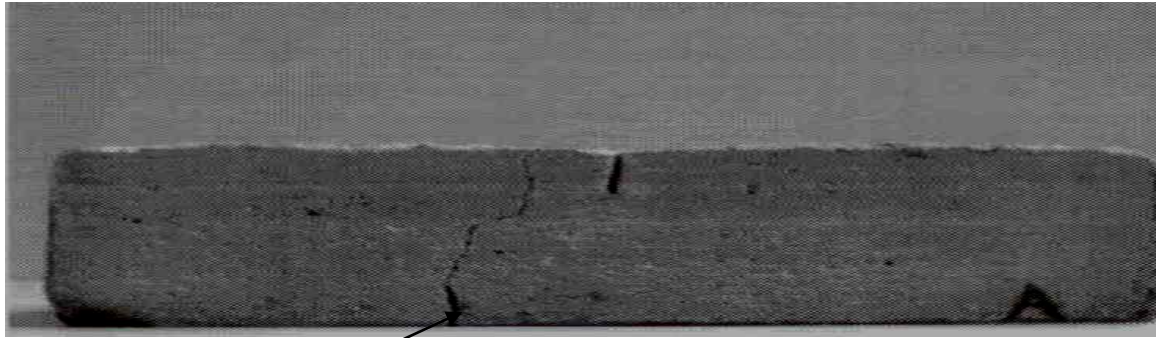
The AE activity of samples containing various admixtures is very different from the standard concrete samples indicating that the additives modify the mechanical properties and fracture nature of the mortars. The standard samples have failed at lower loads and shorter loading times. The signal waveforms at the onset of cracking and failure are quite different from the roller friction and micro-cracking events in all samples.

8.1.4 AE Monitoring of Glass Plate and Glass Aggregates (28 Days Curing) Under Flexural Load

The optical micrographs of the fracture surfaces of the mortar specimen containing glass additives are given in figures 8.4a and 8.4b, (Crack path through a notched concrete specimen with the inclusion of a reinforcing glass plate and glass aggregates into the matrix). Only a few pull out event can be seen, this is because only 15g glass aggregate was added to the mixture during preparation of the specimen.

The load versus time history plot for this sample shows distinct deviation from the linear behaviour at various times and exhibits three slopes representing the initial strength of the mortar, the strength of the glass plate and the final strength of the mortar containing glass aggregates.

The results of AE source location are shown in figure 8.5. It is clearly visible from the AE plots the change of crack path due to the insertion of glass slide. With increasing load on the sample an increase in AE activity occurs (indicating initiation and propagation of crack). When the crack reaches the glass plate it propagates in a new easy direction. However, soon after the obstacles (glass plate and glass aggregate) are overcome the recording of the activities in large density are again in progress until final fracture (see figure 8.5 (a) and (b)).



Crack propagation

Figure 8.4 a: Crack path through a notched concrete specimen with the inclusion of a reinforcing glass plate and glass aggregate in to the matrix.

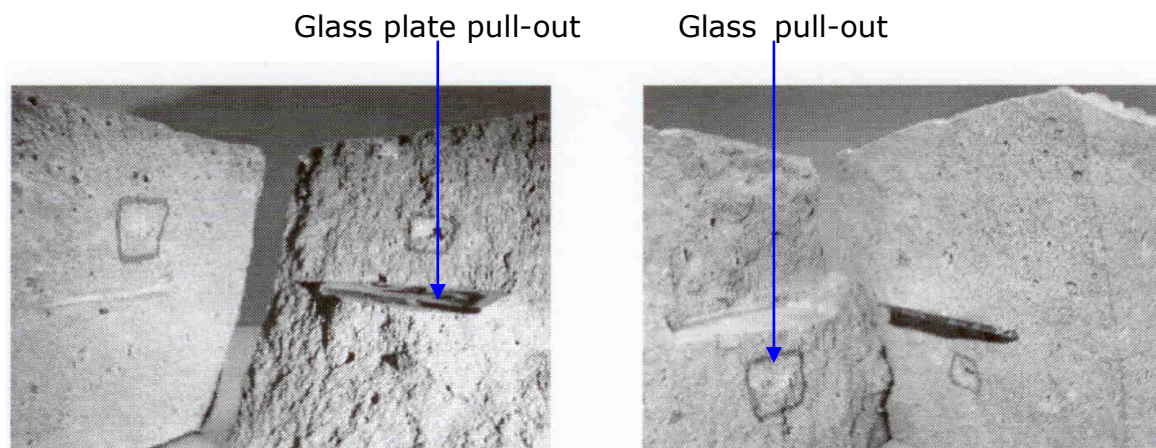
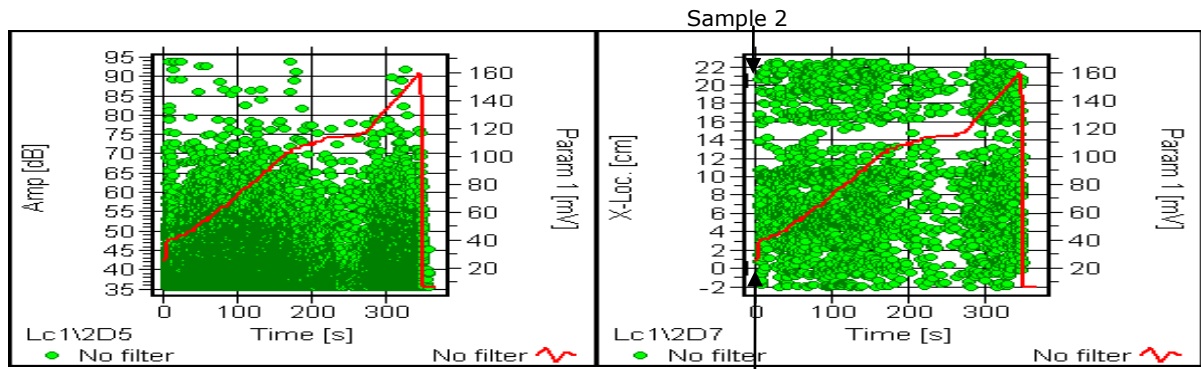


Figure 8.4 b: Fracture surface of the concrete specimen. Note the change of crack path due to glass plate and glass aggregate acting as a bridging grain (highlighted by the squared box).

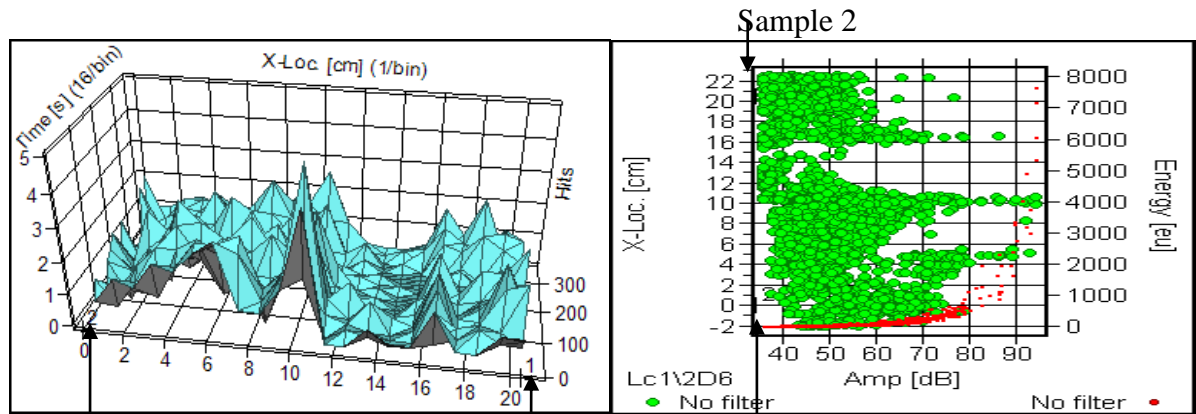
The small porosities visible in figure 8.4 b correspond to the numerous number of AE hits that were recorded at very low amplitudes (above threshold level of 35 dB to 50 dB) as shown in the AE plot (figure 8.5a).

The numbers of AE activities emitted are far denser than the mortars containing glass plate, glass aggregates or sodium sulphate as seen in the case of three specimens in this section.



(a) Amplitude (dB) vs Time (s) vs Param (mV)

(b) X-location (cm) vs Time (s) vs Param (mV)



(c) 3-D Plot: Time (s) vs X-location (cm) vs Hits

(d) X-location (cm) vs Amplitude (dB) vs Energy (eu) (Red dots)

Id	DSET	CHAN	A [dB]	R [μs]	E [eu]	X [cm]	D [μs]
Ev	23724	2	44.5	45.6	114E-1		247.0
Ev	23725	2	40.8	23.6	106E-1		290.2
Ev	23726	1	51.3	65.4	311E-1		491.8
Ev	23728	2	37.0	2.4	397E-2		29.6
LE	23730	2	75.4	28.8	633E00	9.15	1339.2
Ht	23731	1	70.1	46.4	219E00		948.0
Ev	23732	2	37.4	0.2	388E-2		4.4

(e) AE Listing

Figure 8.5: AE plots of Brgl2 (broken glass of mixed sizes and glass plate)

A comparison of figures 8.4 and 8.5 demonstrate that the locations of damage in the specimen namely crack arrest, crack propagation under the glass plate, fracture of glass plate, pull out of coarse glass aggregates and final mortar fracture corresponds to the area covered by the AE location events. Thus it is obvious that the AE source location provide a good estimate of the nature of the damage in the mortar under flexural loads. Other AE signal parameters e.g. Peak amplitude, which relates to signal energy released in the event and event duration versus location plots show damage in three regions and 70-100 mm region being the most prominent (see figure 8.5 (b), (c) and (d)). The failure of the specimen is seen in the AE listing with blue shading in figure 8.5 (e).

8.1.5 Discussion and Summary

Mortar containing sodium sulphate (28 days curing) breaks at a load of 7.59 kN after about 220s. This specimen exhibits excessive AE activity throughout the test period, (see figure 8.3). The time duration between 115-160 s is relatively quiet during which the crack appears to have reached the glass plate and arrested. The applied load is effectively on the glass plate which appear to behave linearly (elastic characteristics) until the maximum load at which it breaks. Amplitude versus event duration plot show high peak amplitude signals producing longer duration events. Location plots indicate crack propagation and final fracture in the 80-40 mm region. The excessive AE activity in the specimen can be related to toughening of mortar.

It is reported in [53] and [115] that addition of sodium sulphate result in the formation of ettringite, $\text{Ca}_6 \text{Al}_2 (\text{SO}_4)_3 (\text{OH})_{12} \cdot 26\text{H}_2 \text{O}$. This observation is very important step in understanding the toughening mechanism of mortar containing additives like sodium sulphate.

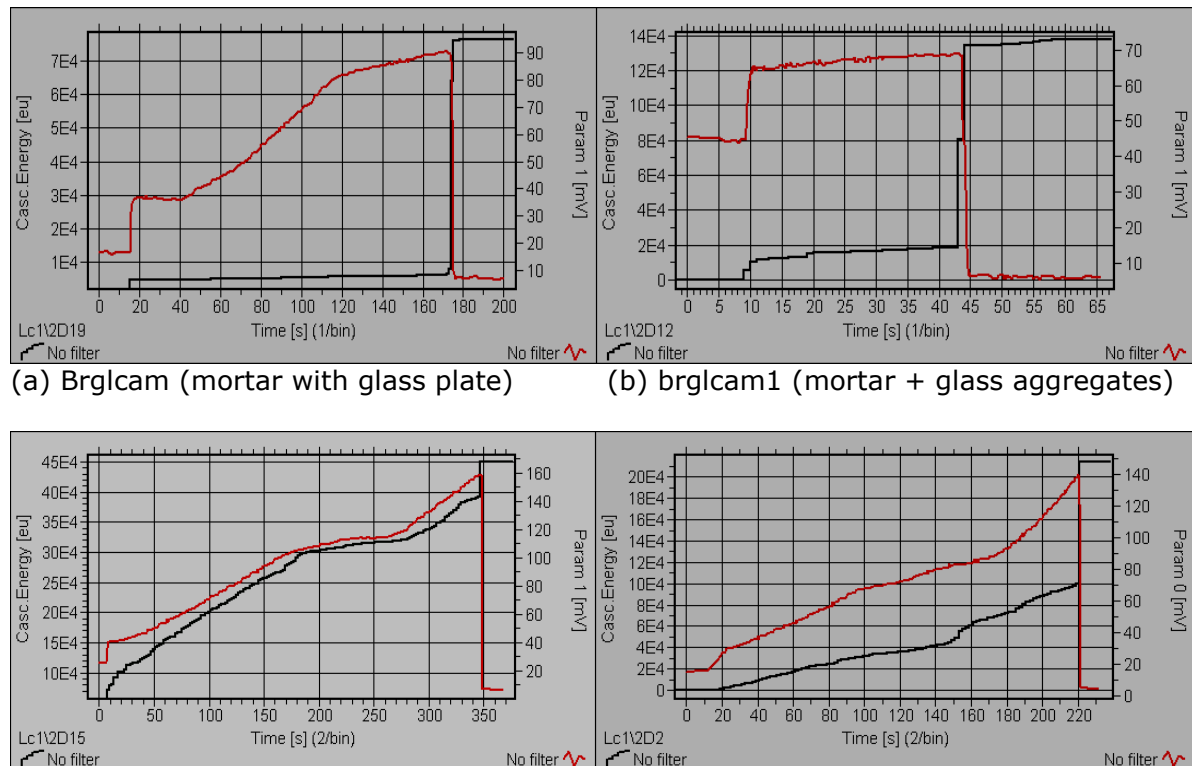
From the analysis of these AE plots it can be deduced that a good amount of toughening is obtainable by using sodium sulphate as admixtures in concrete mortar, but unlike the specimen containing broken glass, no major events such as cracks, fracture appear to be taking place. The highest energetic event takes place at location 7.17 cm with high amplitude of 76.1 dB and long duration of 1614.4 μs , when the sample fails.

Most of the activities in this sample are originated at the crack tip giving rise to micro-cracks that lead to crack propagation until taken over by the glass plate. This is indicated by the activities generated in the central region (6-9 cm) of the sample. The number of hits in 3-d plot also confirms this. The biggest event in this sample occurs when the brittle glass slide failure takes place, but no linear relationship can be observed between the increasing load and the different regions of the sample such as cement paste/mortar area or the glass plate regions.

From the AE characteristics exhibited from this particular sample, one prediction that can be made about this sample is that without the existence of the glass

slide, the activities would have been evenly distributed, though not of same strength (same amplitudes). This means the sample would have failed as a result of micro-cracks, without any major fracture being taking place.

The plots given in figure 8.6 show the cascaded energy for samples containing bridging and the effect of different aggregates and admixtures.



(a) Brglcam (mortar with glass plate) (b) brglcam1 (mortar + glass aggregates)
(c) Brgl2 (glass aggregates + glass plate) (d) Nas (Sodium Sulphate + glass plate)
Red curve: Load param; Green curve: cascaded energy

Figure 8.6: A comparison of cascaded energy of different samples under load with aggregates and additive

As it is clearly visible from the AE plots in figure 8.6, that although the inclusion of glass slides does increase the cascaded energy during the flexural test but at a slower rate, the addition of admixtures however cause a higher level of AE to be generated. The main reason behind this is that as it was noticed from the AE plots that when the crack reached the glass slide region only a few activities were recorded and almost a quiet period was prevalent, hence less energy emitted.

The highest energy is emitted from the specimen Brgl2, which contains glass aggregates of mixed sizes (1mm to 4mm). The reason for this here is clear; because of the difficulties the cracks and micro-cracks had to face to overcome the rough aggregate surface structures. The effect of admixtures such as

sodium sulphate and calcium carbonate do alter the micro-structural properties of mortar which was supported by the huge amount of micro-cracks, thus indicating high level of toughness (as was seen in the AE multi-plots of location versus time, location versus amplitude and amplitude versus time plots) and this is visible from the cascaded AE energy emission during flexural tests as shown in the plots, figure 8.6.

The flexural strength (Modulus of Rupture) and fracture toughness for each sample were calculated using the equations (3.5) and (3.6). The values for each sample are shown in the table 8.1 and the relationship is shown in figure 8.7.

Applying the equations from chapter 3,

$$\text{Modulus of Rupture } (\sigma) = \frac{3FL}{2bd^2} \quad (3.5) \quad \text{and the}$$

$$\text{Fracture Toughness } (K_C) = \frac{3FLYa^{0.5}}{2bd^2} \quad (3.6),$$

(i.e. $K_C = \text{Modulus of Rupture} \times Ya^{0.5}$)

(Taking the dimensionless value of $Y=1.12$; adopted from *Materials Science and Engineering: An Introduction, 3rd Edition, John Wiley & Sons, Inc. New York* [188].

Table 8.1: Tabulated results of flexural strength, fracture toughness, and A.E. energy of different specimens

<u>SAMPLES</u>	<u>FLEXURAL STRENGTH (MPa) (σ)</u>	<u>FRACTURE TOUGHNESS (Kc) (MPa.m^{1/2})</u>	<u>AE ENERGY (eu)</u>
Brglcam (plain mortar with glass slide)	7.37	0.82	78000
Brglcam1 (plain mortar with glass aggregates)	6.95	0.77	135000
Brgl2 (glass aggregates + Glass plate)	5.3	0.59	450000
NAS (sodium sulphate and glass slide)	9.36	1.04	210000

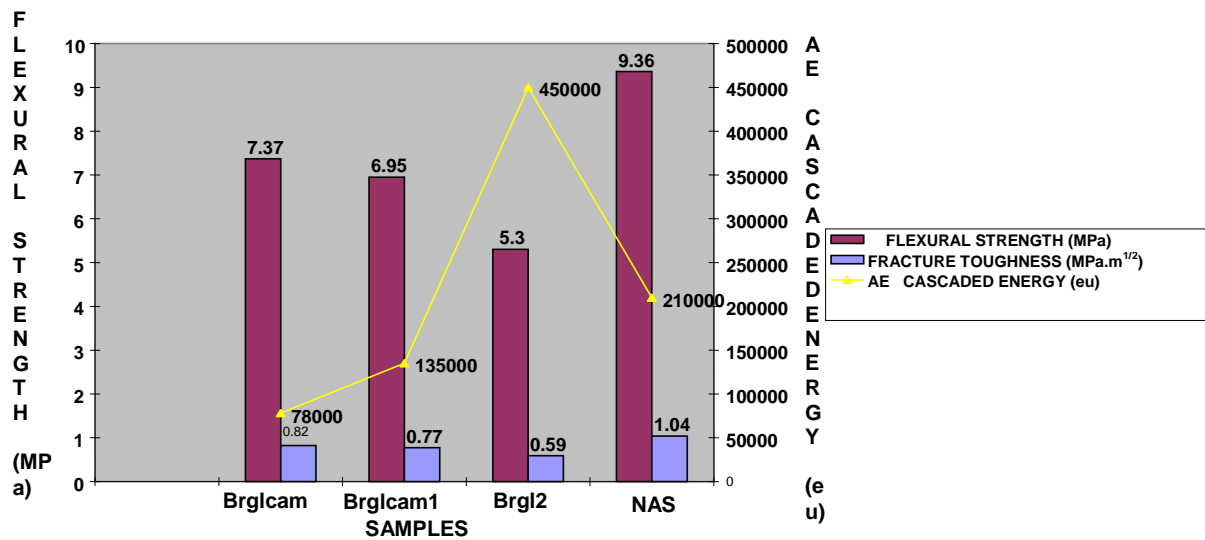


Figure 8.7: Relationship between flexural strength/fracture toughness and AE energy of different samples

The graph (in figure 8.7) exhibits the relationship between the AE energy and fracture toughness/flexural strength. Although the specimen containing sodium sulphate is the strongest in terms of flexural strength and fracture toughness, specimen brgl2 (containing glass aggregates and glass plate) exhibits the highest cascaded energy. This is due to higher number of hits taking place during the test since the cracks face obstacles with larger volume of glass chunks. Since a very high level of toughening has taken place in specimen containing sodium sulphate as indicated by large amount of micro-cracks, hence a higher number of hits, therefore significant level of cascaded energy was recorded during the flexural test.

A mortar can be toughened by the use of additives like sodium sulphate which produces micro-cracking and also by the manipulating of the crack propagation/growth. It is evident from the AE results shown in figure 8.3 that both the modes of toughening are present. These tests were carried out under identical similar condition. The time to reach the peak load can be related to strain; a toughened material has a higher strain and strength.

To summarise, the use of sodium sulphate has made a significant contribution towards the toughening of this specimen hence enhancing the mechanical properties (further verification of this is also be seen in plots shown in figures 8.6 and 8.7), while the glass slide has acted as a crack bridge to the crack path that may have formed due to the propagation of micro-cracks.

8.2 Further AE Monitoring of Mortars with Admixtures under Flexural Load

For further verification of the AE in relation to the expansive matrix (the role of sodium sulphate and calcium carbonate towards toughening mechanism), samples of plain mortar, and mortars containing sodium sulphate, calcium carbonate were prepared, cured and tested under similar condition and put under flexural test. The AE activity recorded during the test for these mortars are shown in figures 8.8, 8.9 and 8.10.

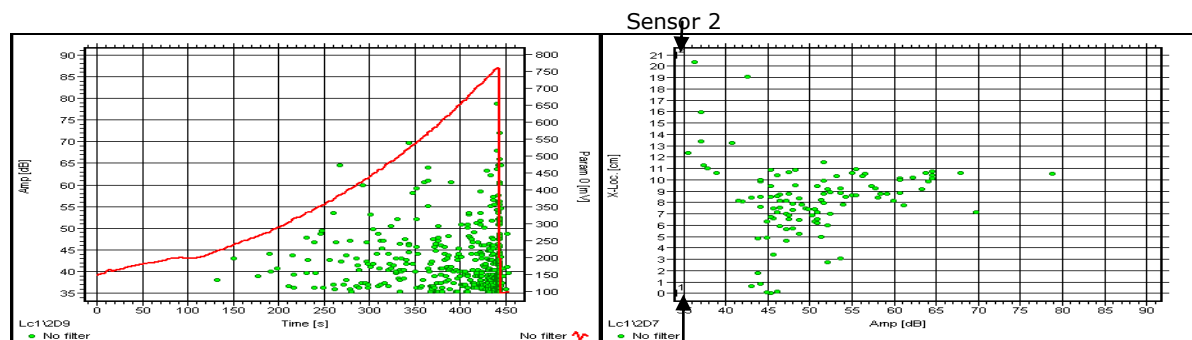
The AE activity under compression in specimens containing admixtures (sodium sulphate and calcium chloride) was far greater than a plain mortar, (as seen in section 7.1). The samples containing admixtures have the similar composition except the addition of sodium sulphate and calcium chloride. An obvious explanation of their extraordinary AE activity is the result of micro-mechanical damage in the material i.e. toughening mechanism. To observe the toughening behaviour of admixture under flexural condition, the AE response recorded provides further evidence that the addition of admixture contributes towards the enhancement of the mortars.

When looking at the AE plots of the plain mortar, it can be seen that very few activities were recorded; the amplitudes of almost all activities are between 40 70 dB and the duration not exceeding 2500 μ s (figure 8.8). Most of the activities in this specimen took place near the sensor 1 region (6-10 cm) of the specimen with the final fracture taking place in the central region (10-12 cm). A comparison of AE plots of the samples containing sulphate and a standard (plain mortar) indicate additional AE activity as a result of admixture sodium sulphate. The numerous AE activities recorded at low amplitudes (< 55 dB) present throughout the sample may be the results of micro-cracks which are related to the toughening of the mortar. There are a few activities of higher amplitudes (<70 dB), longer duration (>1000 μ s) and shorter rise-time (200 μ s) that lead the final fracture of the sample (figure 8.9).

The number of AE hits in specimen with sodium sulphate is higher than the plain mortar. The number of hits is higher in the central region of this sample, which is a further indication of major failure in this region. The distribution of AE

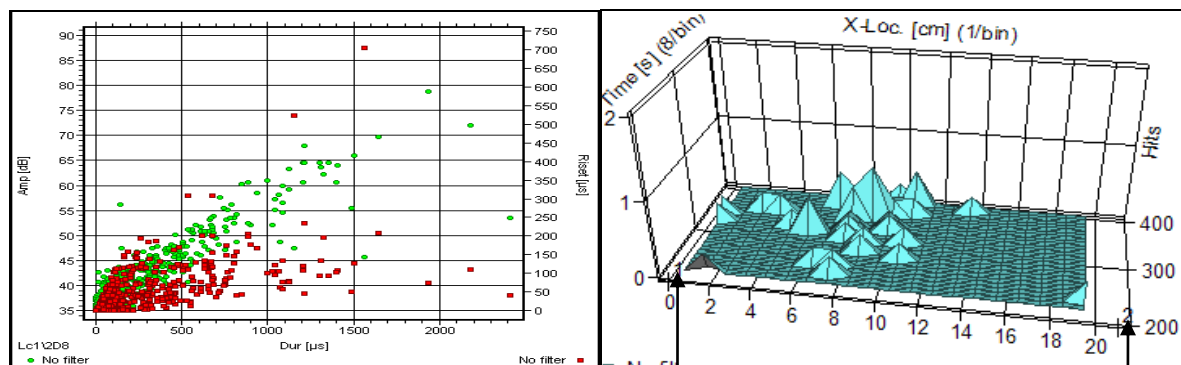
activities and hits throughout the sample indicates the activeness of sodium sulphate uniformly over the specimen, however, too excessive amount of activities are also partly due to the external noise picked up by the sensors, such as unavoidable friction or mounting methods.

The specimen with calcium carbonate as admixture have made some minor toughening in the sample, but no significant activities at higher amplitudes are taking place as seen in figure 8.10. The load curve gradually rises almost in a linear manner and the failure takes place suddenly (sharp drop of load to zero). The specimen breaks in a brittle manner at 142/143 seconds with a relatively small major event, giving rise to amplitude of 59.9 dB, and long duration of 828.4 μ s. The addition of calcium chloride has given minor improvement in strength and toughness, but no major resistance to cracks are visible from the AE plots. The activities above 60 dB indicate that the micro-cracks are being taken over by the formation and propagation of major cracks and are also indicated by the slight changes in the shape of the load curve at 60 seconds. The activities in the form of micro-cracks are propagating to form the bigger crack which propagates to cause the final fracture of the sample. Once the sample failed or lost its strength, it could not hold its strength any more and the failure was immediate.



(a) Amplitude (dB) vs Time (s) vs Param (mV);

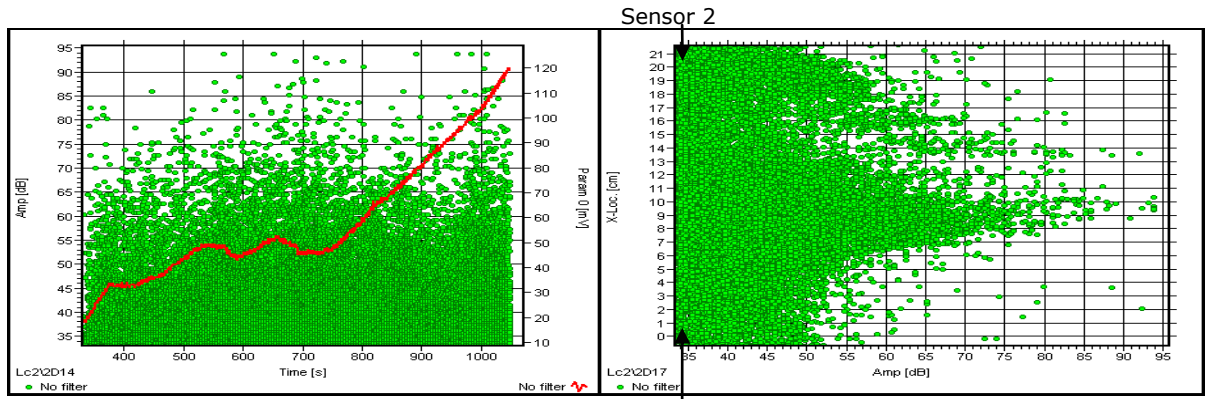
(b) X-location (cm) vs Amplitude (dB)



(c) Amplitude (dB) vs Duration (μ s) vs Risetime (μ s); (Red dots)

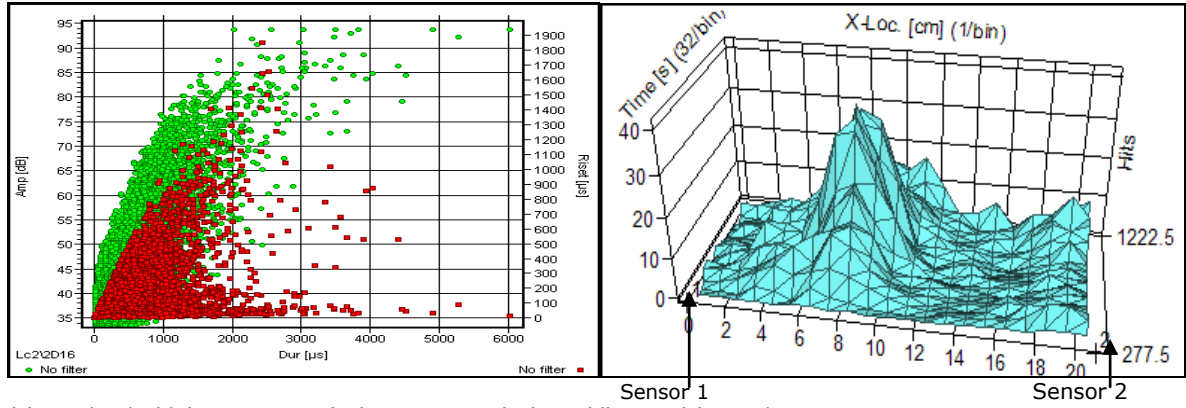
(d) Time (s) vs X-location vs Hits

Figure 8.8: AE plots for sample Final2: Plain Mortar



(a) Amplitude (dB) vs Time (s) vs Param (mV);

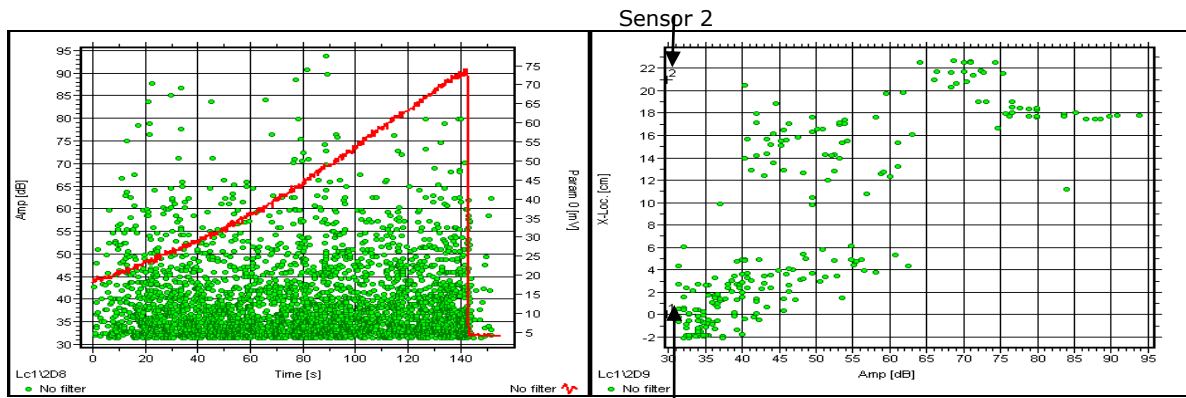
(b) X-location (cm) vs Amplitude (dB)



(c) Amplitude (dB) vs Duration (μ s) vs Risetime (μ s);
(Red dots)

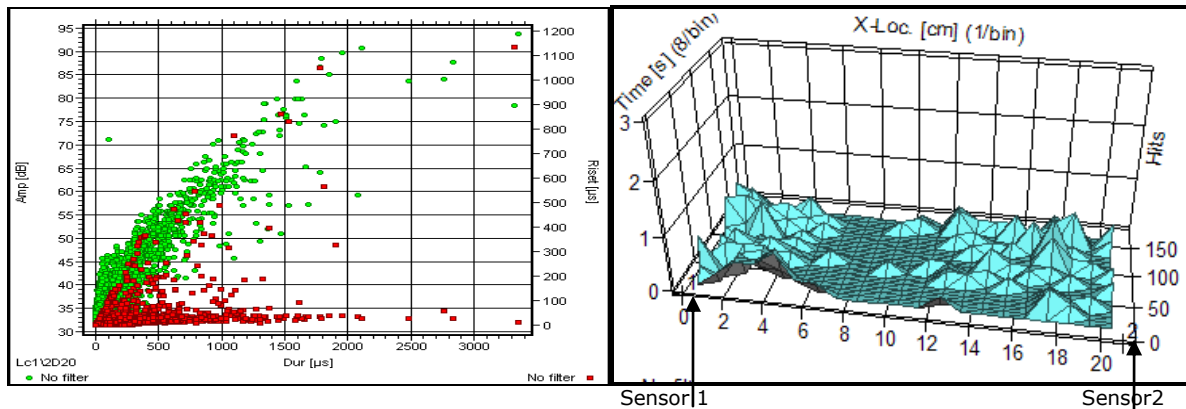
(d) Time (s) vs X-location vs Hits

Figure 8.9: AE plots for sample Conflex: Mortar containing sodium sulphate



(a) Amplitude (dB) vs Time (s) vs Param (mV);

(b) X-location (cm) vs Amplitude (dB)



(c) Amplitude (dB) vs Duration (μ s) vs Risetime (μ s);
(Red dots)

(d) Time (s) vs X-location vs Hits

Figure 8.10: AE plots for sample Cara4: Mortar containing calcium carbonate

8.2.1 Summary

The contribution of admixtures (both sodium sulphate and calcium carbonate) towards the changes in AE characteristics, i.e. increase in A.E. activity profile, can be seen in figure 8.11. Hence an indication of enhancement of toughening under flexural condition with the addition of sodium sulphate and calcium carbonate in mortars is observable with the increase (94%) in number of hits as seen in figure 8.12. The excessive amount of A.E. activities in mortar containing admixtures (especially sodium sulphate) under stress indicates the residual stresses at micro-structural level. Therefore the circumstantial evidence of the release of the residual stress that existed before (micro-crack formation leading to permanent deformation in flexural tests) now has been observed with the mechanism in action.

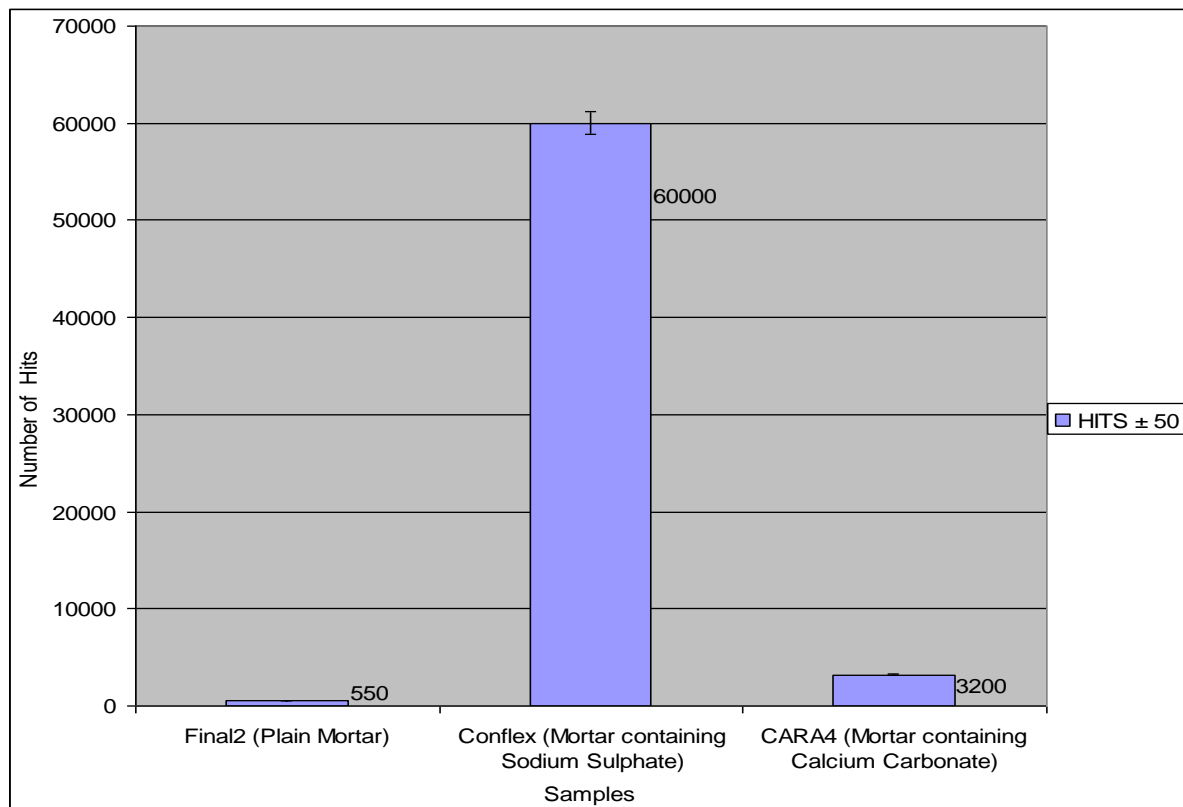


Figure 8.11: Comparison of AE hits produced by typical mortar and mortars containing admixture under flexural load

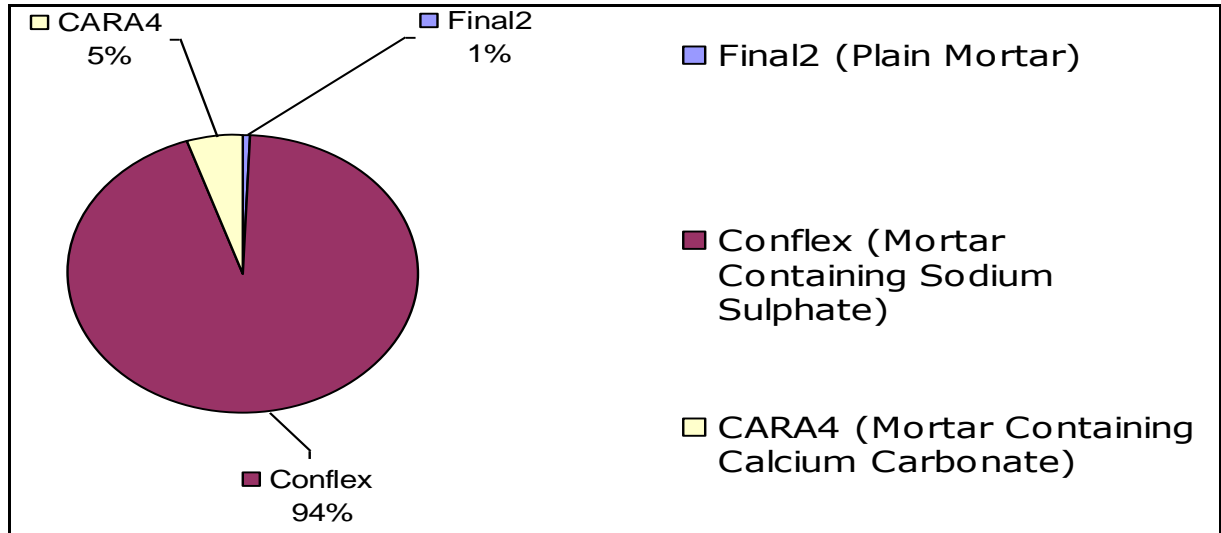


Figure 8.12: Percentage of AE hits produced by typical mortar and mortars containing admixture under flexural load

8.3 Comparative study of AE Characteristics between Compression and Flexural Condition

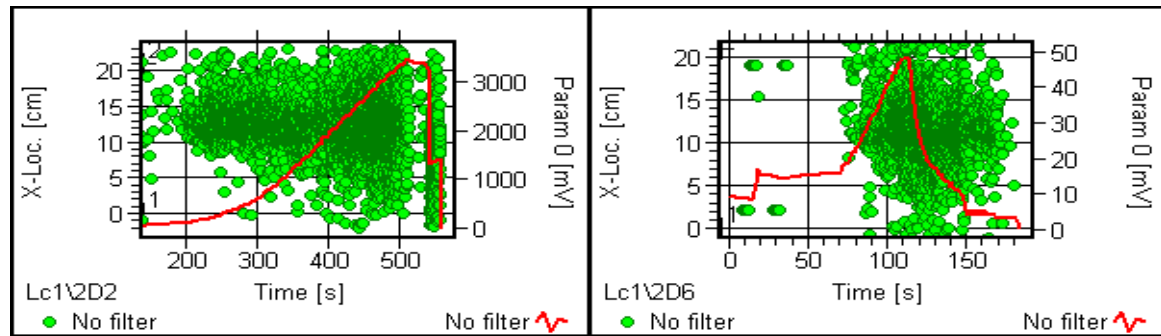
Concrete is stronger in compression, but weaker in tension. Two specimens were put under compression and flexural tests in a similar condition, i.e. both at room temperature and at same load speed. An attempt is made here to establish a link between these two mortars of same dimensions, (both of which were cured under same condition containing identical proportions of ingredients) in terms of AE characteristics. This will make a contribution to the field of concrete, where AE characteristics can be employed as a tool to differentiate between the compressive and flexural behaviour at micro-structural level. From the tests conducted and the results extracted for both samples the very first feature that can be observed is the behaviour of the load curve and the AE parameters as shown in table 8.2.

Table 8.2: AE Parameters under compression and flexural condition

<u>SAMPLES</u>	<u>LOAD</u> (mv)	<u>AE</u> <u>ACTIVITY</u>	<u>A</u> (dB)	<u>R</u> (μ s)	<u>E</u> (eu)	<u>D</u> (μ s)
KOLA 4A	3500	HIGH	93.8	18	130E02	17312
KOLA 4B	48	MEDIUM	83.7	48.2	182E01	1815.2

A: Amplitude, R: Rise-time, D: Duration and E: Energy at failure point
 Sample 4A: Compression load, Sample 4B: Flexural load

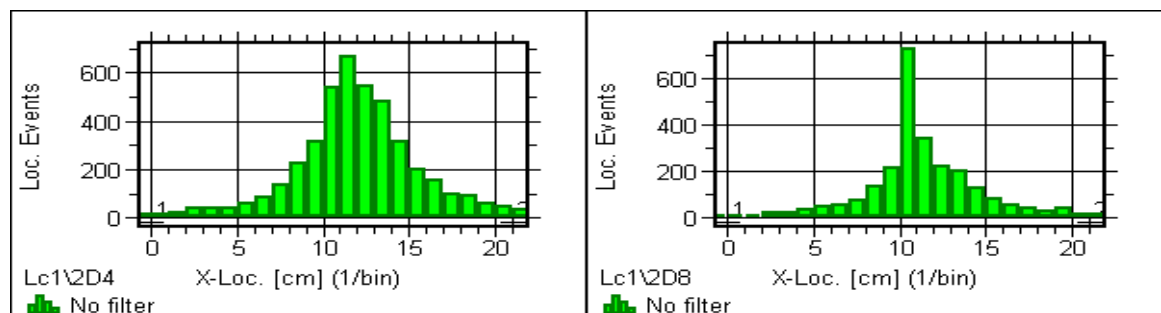
It took longer for the load curve (almost 6 times) to reach failure point under compression than flexural test, as shown in figure 8.13. It can be observed that more toughening took place during compression, but majority of these toughening are taking place before the peak load as in figure 8.13. This was due to the larger number of micro-cracks initiation and propagation during compression load.



Location (cm) vs Time (s) vs Param (mv) Location (cm) vs Time (s) vs Param (mv)
 KOLA4A:AE Activities recorded (Compression) KOLA4B: AE Activities recorded (Flexural)

Figure 8.13: Differences in AE activities under compression and flexural conditions

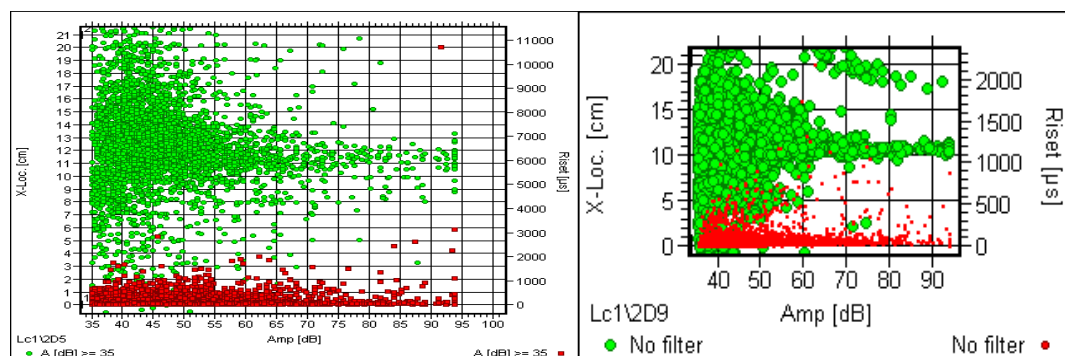
The distinctive difference between AE features under compression and flexural condition can be observed from the AE parameter 'located event' pattern, throughout the sample location shown in figure 8.14. The number of located events captured under compression (specimen kola4a) is at least three times higher than the sample under flexural test. In sample kola4a (compression), the located events are far more dominant than the sample kola4b (flexural). Although events are happening in both samples, but since kola4a is under uniaxial load, the event distributions are denser in this sample with a different distribution, this is because cracks propagate in a direction parallel to the applied load during compression, but perpendicularly during three-point bend situation.



Located Events vs x-location (cm) Located Events vs x-location (cm)
 KOLA 4 (Compression) KOLA 4B (Flexural)

Figure 8.14: Distribution of 'located events' under compression and flexural condition

Beside all the differences in strength and AE characteristics under these two conditions, one of the striking similar feature present in both samples is that the amplitude versus location signal patterns are indifferent, as shown in figure 8.15. The events with higher amplitudes are only visible in the central location of the specimens, e.g. most of the signals above 65 dB are recorded between location 8 and 12 cm. This indicates that the strength of the events/signals under both conditions is almost same, i.e. the predominant failure in terms of severity is in this particular location. The signals in the lower region (amplitudes < 50 dB) have the longer rise-time, which means that the events are weak and large number of micro-cracks are present.



X-location (cm) vs Amplitude (dB) vs Risetime (μ s)
(Red dots)

X-location (cm) vs Amplitude vs Risetime (dB) (μ s)
(Red dots)

KOLA 4A (Compression)

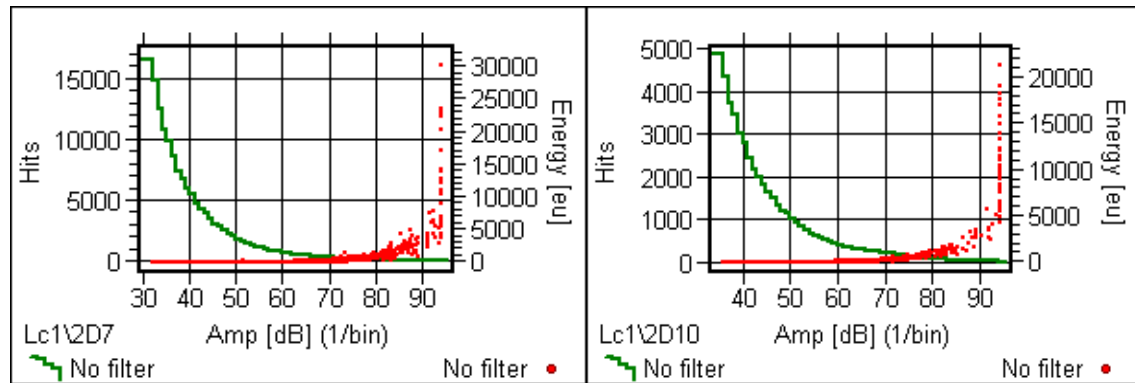
KOLA 4B (Flexural)

Figure 8.15: Amplitude signal pattern under compression and flexural condition

Both sensors recorded the activities during micro-crack initiation, propagation throughout the location of the specimens, as is observed from figure 8.15. A larger number of activities recorded within 50 - 70 dB in specimen kola 4A indicates that the cracks can propagate more easily under compression than under flexure.

Figure 8.16 shows plots of amplitude distributions in relation to the number of hits. The cumulative plots show how many hits have reached or exceeded the amplitude as specified on the horizontal axis. The curve for compressive behaviour indicates that there are a little more than 2000 (1950) hits with a maximum amplitude of 50 dB or more, while there are a little more than 1000 (1050) hits with a maximum amplitude of 50 dB or more in flexural condition. This huge difference indicates that the specimen under compression has to be rated more critical. The higher number of hits below 50 dB and low energy level indicates the amount of micro-cracks are initiated at the cement paste matrix, gradually leading to aggregate cement interface. The higher level of energy (in a

lesser number) being emitted with few hits at higher amplitude indicates fewer number of big events such as pull out events, crack arrests, crack deflection taking place in this region before final failure. This pattern is common under both conditions.



Hits vs Amplitude (dB) vs Energy (eu)

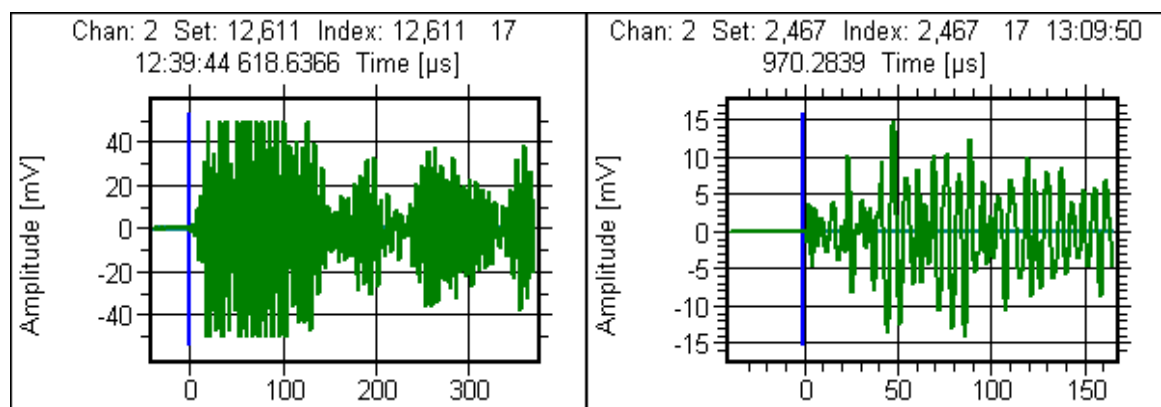
Hits vs Amplitude (dB) vs Energy (eu)

KOLA4A (Compression)

KOLA4B (Flexural)

Figure 8.16: Amplitude Distribution against number of hits under compression and flexural conditions.

The TR waveform for both samples (figure 8.17) indicates that signal waveform captured during compression is larger than the one during flexural condition. Both waveforms were captured from the region of final failure and they have large amplitude (above 70 dB), but the specimen Koal4a has very large amplitude, this is linked to the higher strength of mortar under compression.



KOLA4A (Compression)

KOLAR4B (Flexural)

Figure 8.17: TR Waveforms at failure point under compression and flexural load

AE characteristics under both conditions (compression and flexural) indicate that there are differences at micro-structural level, especially there is more toughening in the former. However, one similarity is that the major events are more dominant in the central region of both specimens, i.e. events with higher amplitudes are concentrated in the central portion of the specimens, while the micro-cracking activities (low amplitude events) are spread throughout the locations of the specimen, and these eventually lead to the final failure. However, the density of AE activities is higher under compression, and the AE signal parameters are also higher. The micro-cracks at the interface of paste and aggregate are present under both conditions, but more dominant under compression. This is indicated by the larger amount of activities with low amplitudes (< 50 dB) and short duration (< 200 μ s).

The study above proves the phenomenon that concrete is stronger in compression and weaker in tension (under flexural condition), which have been observed from a micro-structural point of view. At macroscopic level, the extent of damage is clearly visible under compression; the AE profiles also support this rituality. However it has not been possible to confirm linkage of the AE parameters with the practical load strength in terms of magnitude. Compressive strength for example, is ten times higher than flexural strength, but AE parameters are only three times higher, as observed from this analysis. Failure modes are different in the two tests hence their AE activities are widely different.

8.4 Optical Micrographs of the Fractured Sections

Some typical optical micrographs of the fractured sections are shown in figure 8.18. The glass pull-out and glass bonding behaviour is clearly visible, while the poor interfacial bonding between the cement paste and rubber supports the A.E. results, i.e. decrease in flexural strength and increased attenuation which lead to heavily damped A.E. signals. The glass pull-out micrograph clearly illustrates that the glass aggregates are active so the cracks are deflected, thus causing a number of major pullout events before the final fracture.



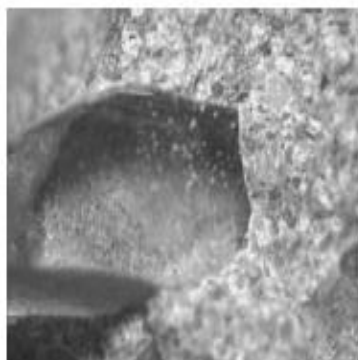
Glass slide + glass aggregate (top view)



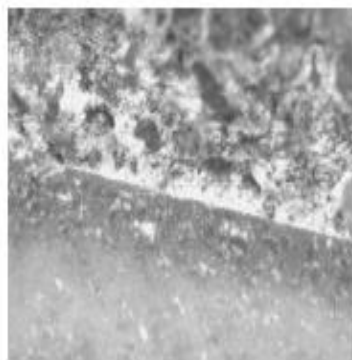
Rubber aggregate



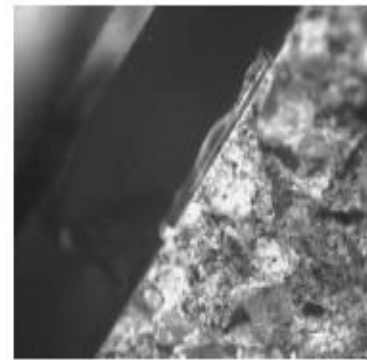
Glass slide (side view)



Glass aggregate aggregate (pull-out effect)



Glass slide bonding



Glass slide + rubber

Figure 8.18 Optical Figures: Optical micrographs of bonding between the cement paste and the aggregates.

The glass slide resting on the cement paste is seen to be well settled and though the bonding is not as good as the rough glass aggregates, but certainly better than the rubber chunk. However, the bonding between the plate and the paste is not so important in the enhancement of the mechanical properties or the toughness of the mortar, since the crack is overtaken by the slide.

8.5 Summary of Fracture Toughening Mechanism due to Different Inclusions

A summary of the admixtures, aggregates, and slides at micro-structural level that lead to different toughening mechanism and hence the resultant AE characteristics during the flexural tests are given in table 8.3.

Table 8.3: Role of admixtures and aggregates towards toughening and AE signals

<u>ADDITIVES</u>	<u>FRACTURE TOUGHENING MODE</u>	<u>ACOUSTIC EMISSION CHARACTERISTICS</u>
Sodium Sulphate	Micro-cracks	Low amplitude, short duration and low energy activities
Calcium Carbonate	Micro-cracks	Low amplitude, short duration and low energy activities
Glass Aggregates	By-pass of chunks pull-off event	High amplitude, long duration, short rise time and high energy level activities
Rubber Aggregates	Minor deflection; disintegration from cement paste	Activities with low amplitudes, short duration and high rise time; damped AE TR waveforms
Glass Plate/Slide	Crack bridging / Change of crack path	Relatively quiet period, few AE activities but of higher amplitudes

From the summarised table 8.3, it can be seen that the samples containing rubber aggregates are the poorest type of mortars both in terms of flexural strength and in toughening. The specimens with glass aggregates provide a high level of toughening; those with admixtures also provide high toughness but with an increased amount and different mode i.e. micro-cracks. The glass plate acts more as a bridge and changer of crack paths rather than as micro-cracks or a toughener. The differences in AE characteristics have clearly demonstrated these toughening and failure modes. Crack bridging is one of the numbers of toughening mechanism that have been engineered into ceramic-based

materials. However, the effect of such toughening is not an easy task to observe, especially on an in-situ basis. Acoustic Emission technique is an option to observe such mechanism at the slide matrix interface.

As it has been observed, using the AE characteristics obtained during the tests, the role of each reinforcing technique, bridging technique, or toughening technique, can clearly be distinguished at micro-structural level. Whether all these techniques are employed individually, or in conjunction with each other, their role during the flexural test can readily be identified.

In addition to this, the appropriate location, the size, the type and the exact source of the events/micro-events taking place due to these techniques used in a complex material such as concrete can also be identified with the greatest possible accuracy which no other physical technique can provide.

8.6 Summary of Research Investigations

The work carried out at in collaboration with Aberdeen University had shown that:-

- The presence of isolated holes in hardened cement paste gives as flat a fracture surface as dense cement.
- Making the particles un-bonded gives a flatter fracture path compared with bonded particles.
- Using spherical particles give rise to no increase in toughness with crack growth event if there is a flat fracture through the cement.
- Using non-spherical particles gives an increase in toughness with crack growth as long as the crack follows a flat path.

Therefore, it has become evident from their investigation that the incorporation of non-spherical particles into a brittle matrix, that are bonded to the matrix, gives rise to a flat-fracture path that promotes crack-pinning and leads to a rising toughness curve. The theoretical model developed was validated and extended in this research work through experimentation using the NDT techniques.

The ultrasound techniques used in this research enabled the findings of a clear pattern that illustrates the curing process and the development of the compressive strength of concrete mortars containing various additives and aggregates during that period. With the aid of ultrasound results obtained in this research, it has been possible to investigate the effect of additives in concrete and on the development of strength, e.g. sodium sulphate, calcium chloride had accelerated the curing process and compressive strength of concrete and sodium silicate retarded the processes. An effective improvement in the properties of the material has been established with the introduction of additives.

The ultrasound results have shown the addition of waste materials (glass) in concrete as aggregates stimulated an increase in the compressive strength of the material; while rubber was found to harmful to the strength of concrete. This alteration of strength is due to the strength of interfacial bonding between the cement matrix and aggregates.

The use of ultrasound technique for estimating the compressive strength of concrete with altered micro-structural properties at an early stage of curing has provided useful mechanical properties information on the changes occurring in the systems.

The AE results obtained validated the findings of the initial model with online observation and advanced the work further. Hence the work undertaken in this research contributed further to the understanding of toughening of the cement based materials.

The results of AE have shown that:

i) The addition of non-spherical (angular) inclusions in the form of glass aggregates acting as an interfacial bonding between the inclusions and the cement matrix. This controlled the crack path through the composite, the inclusions acted as bridge thus providing toughening. This is indicated by the strong AE events emitted when the crack is at the interface. The smooth spherical glass beads used as aggregates lowers the strength and toughness, i.e. bridging is not effective with glass beads, proof is given by the weak AE events taking place during the test.

ii) Additions of sodium sulphate, calcium carbonate to concrete mortar influenced the toughness behaviour (increased the toughness). Expansive cement (obtained from Lafarge Cement Limited) has also shown increase in toughening behaviour.

The excessive amount of AE activities has demonstrated that the introduction of sodium sulphate do play an important role in increasing the toughness of mortar as shown in figure 8.19, i.e.

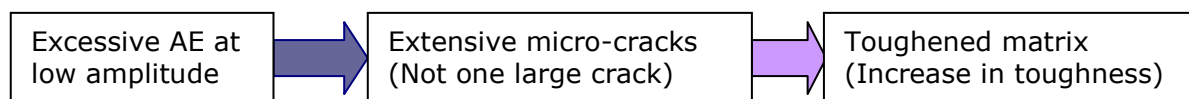


Figure 8.19: AE and micro-cracks related toughened matrix

This is clearly linked to the fact that circumstantial evidence of the release of residual stresses existence (micro-crack propagation/formation) leading to

permanent deformation in flexural test, but very difficult to observe the mechanism in action.

The AE activities of samples containing sodium sulphate/calcium carbonate (admixtures) is very different from the standard concrete mortars indicating that the additives modify the mechanical properties and fracture nature of the mortars. This in turn supports the theory that OPC plain mortar (without additives) exhibits some non-linear behaviour but is significantly enhanced by the addition of sulphate. When the peak load is applied, the samples remained intact, and on retarding, were capable of withstanding 50% of the initial maximum stress. This indicated extensive micro-cracking rather than the propagation of one large crack and consequently a toughened matrix.

With the addition of calcium carbonate, it was discovered that comparisons of fracture load (strength) of concrete mortar samples exhibited an enhancement in toughness of mortar samples by relaxation of residual stress (micro-cracking) under load. The same is the case with the samples made of expansive cement. This is visible from the AE emissions profiles where the number of AE events and hits are higher for the blocks containing CaCO_3 and expansive cements.

With the aid of AE, it has been possible to show that:

- i) With the introduction of sodium sulphate, calcium carbonate and expansive cement, the toughening of concrete mortars can be increased. This means that residual stresses are created by internal expansion of the matrix phase, this leads to toughening by the release of residual stresses as the micro-crack propagates. This is distinctive from the plain mortar which exhibits brittle behaviour. Such distinction has been grasped by the use of AE, which otherwise would have been impossible. The AE profiles monitored enables the observation of micro-cracks directly during the tests thus allowing seeing the toughening enhancement using admixtures.
- ii) The application of AE to improve, develop, and increase the understanding of manufacturing process of concrete, has

demonstrated that toughening of concrete can be enhanced by closure of macro-cracks obtainable by grain bridging.

- iii) With the aid of AE, it has been possible to observe micro-cracks, crack initiation, crack propagation, crack arrests, and crack bridging, crack deflections (that caused pull-out events) which were all due to the inclusions of glass plates and glass aggregates. This provided an opportunity to distinguish the difference between the brittle matrix (normal concrete mortar) and a toughened mortar. The effect of crack bridging and inclusions on AE signal parameters is different from those obtained from plain mortar samples.

A summary of the different toughening modes is given table 8.4.

Table 8.4: Establishing of toughening modes through research at RGU with the aid of AE

<u>Mortar Compositions</u>	<u>Toughening Mode (AE Confirmation)</u>
Plain Mortar with Sodium Sulphate	Relaxation of residual stress (micro-cracking)
Plain Mortar with CaCO ₃	Relaxation of residual stress (micro-cracking)
Plain Mortar with CaCO ₃ and Glass Aggregates	Relaxation of residual stress (micro-cracking) and crack deflection/interfacial bonding
Plain Mortar with Glass Slide	Crack propagation/arrests
Plain Mortar with Glass Aggregates	Crack deflection/crack bridging/interfacial bonding
Plain Mortar with Glass Aggregates and Slide	Crack deflection/pull-outs crack bridging/ crack arrests
Expansive Cement Mortar	No toughening/easier crack movement
Plain Mortar with Rubber Aggregates	Lowered toughening, easier crack movement, very weak bonding with cement paste

CHAPTER 9

9.0 SUMMARY OF DISCUSSIONS AND CONCLUSIONS

This research has demonstrated that for the materials and conditions employed in the non-destructive evaluation of concrete, ultrasound can be successfully used to determine the compressive strength of concrete samples during curing and setting. In the construction industry, and oil and gas industry (well casing) the ability to determine the strength of concrete in this way, will allow for the better streamlining of construction work and help to increase productivity.

This investigation provides a method of studying the characteristics of concrete due to the introduction of additives. It has shown that additives can be effectively used to manipulate the curing rate, compressive strength and micro-structure of concrete.

It is established that a close correlation exists between the results obtained using the destructive and non-destructive testing methods. This therefore demonstrates that the ultrasonic technique is an accurate and reliable method of determining the compressive strength of concrete. The development of compressive strength over the curing period was found not to be affected by the size of the block. This demonstrated that the geometry of concrete has no significant bearing on the curing process.

It was found that sodium sulphate as an additive in mortar increases both the initial curing rate and the final compressive strength attained by modified hydration reaction during the end of the 28 day curing period. Calcium chloride as an additive in the appropriate proportion caused an increase in both the rate of initial hardening and the magnitude of the compressive strength attained over the curing period. Sodium chloride however had no effect on the curing rate or the compressive strength and results obtained were similar to plain mortar. Addition of potassium chloride and sodium silicate were found to be detrimental both to the curing rate and compressive strength of concrete. The addition of sodium silicate as additives in concrete resulted in a drop in the strength of the mortar.

The structures of the samples containing sodium sulphate and calcium chloride were found to be regular throughout the material. The comparison of

micrographs suggests that regularity in the micro-structure of concrete promotes increased strength and their elemental content results suggest that chemical reaction and other physical micro-structural changes have modified the strength of the concrete blocks.

This investigation has demonstrated interesting results when a waste material such as glass was used as aggregates in a concrete mixture. The addition of glass pieces was found to stimulate an increase in the compressive strength of the material. This increase in strength is due to strong interfacial bonding between the cement matrix and glass aggregates. It was found that rubber, introduced in concrete as part of aggregate is harmful for the strength properties of the concrete. An obvious explanation is the poor interfacial bonding between cement matrix and rubber aggregates. However, rubber brings to concrete other properties which might be useful in certain domains of application. Rubber acts as a damper of failure and it also makes concrete lighter. It will be useful in such circumstances where vibration must be mitigated.

Toughening of mortars by the production of residual stresses through the alteration of internal micro-structures was observed. Certain admixtures when added to cement based systems produce residual stresses by internal expansion due to the formation of ettringite. This method provides toughening by the release of residual stresses as the micro-cracks propagate through the concrete. The contribution of other admixture to the enhancement of toughening behaviour has also been established.

From this research, it has been determined that regardless of the type of additives/admixtures/aggregates when used in mortars; it is possible to determine their role in toughening (fracture) mechanism.

One of the unique findings of this research is that a multiple mode of fracture (i.e. micro-cracks/residual stresses, crack deflection/crack bridging, crack arrest, pull-out events, interfacial bonding (strong or weak) can all be established at the same time on a single specimen. Each mode of toughening/failure can be discerned from the data obtained from a single test. For example, a specimen that contains admixtures, aggregates (rough or

smooth), plate, will give distinctive behaviour such as depicting its own fracture mode during the duration of the test. This distinction was captured from the tests and analysed successfully. Therefore the novel characteristics of each specimen (created by altering the micro-structure) can be confirmed and thus its altered micro-behaviour under an applied stress can be observed in real time using acoustic emission as a valuable tool.

One novel finding of this research is that glass in the form of coarse aggregates in mortar is a good toughener. However, powdered glass in a mortar does not play any role in bonding, toughening of mortar or increasing flexural strength. It is rather detrimental to the mechanical properties of concrete. The reason for this effect is that inert glass powder is similar to the chemical characteristic of sand. When glass powder is added the ratio of sand to cement is increased and changing the water cement/aggregate ratio thus leading to accelerated failure during flexural test.

In this investigation the Acoustic Emission technique has been successfully utilised to observe toughening mechanism and to study the behaviour of mortars with different admixtures. The damage mechanisms such as micro-crack formation, and crack evolution during flexural tests were characterised producing unique information in real time. Interfacial bonding and crack bridging/grain bridging have also been linked with the acoustic events during the test. It has been found that the differences in AE activity between the mechanism of toughened and non-toughened mortars rely on either micro-crack formation or on crack bridging. It totally depends on the type of admixtures, type of aggregates and their shapes, and their role in the toughening process.

To investigate toughening produced by crack manipulation, glass plates were implanted during the manufacturing of some mortar blocks. The glass plate was a real obstacle which the cracks had to overcome leading to fracture. It was shown that this mechanism could only be investigated using AE. The interfacial bonding between the matrix and glass aggregates dictates the strength of the mortar. This observation was also confirmed by the use of AE method.

Based on the characteristics of the AE signal in the time and frequency domain, it has been demonstrated that AE monitoring of mortar can provide a sensitive

technique for detecting events relating to crack initiation, propagation and crack arrest as well as micro-cracking due to the toughening mechanism. In summary the application of AE has enabled to study the novel cement based materials in the following ways:

- Identification of accurate location of cracks;
- Good tool for monitoring the influence of admixtures;
- Demonstration of toughening mechanism;
- Sensitive technique for monitoring crack evolution.

In conclusion it can be deduced from the work carried out in this research that the AE technique was found to be an excellent technique to characterise the structure, strength and defect of a complex composite material such as concrete in terms of mechanical and micro-structural properties, in real time. The outcome of this investigation led to the advancement of the model developed by the research group at Aberdeen University, i.e. the theoretical work carried out there is related and confirmed by the NDT results obtained from this research and extended further to various types of cements, additives and aggregates including waste materials.

Numerous research has been carried out elsewhere to alter the mechanical properties of concrete at micro-structural level, but no work has so far been conducted to modify the micro-structural properties with admixtures and waste materials and observe their response under compressive and flexural loading condition in a real-time situation. This research has accomplished this task.

CHAPTER 10

Recommendations and Suggestions for Future Research

This research provides an introduction into the study of concrete development and the influence of additives and waste materials as aggregates. This is a very broad and interesting subject area, involving the application of many different research methods and techniques. Although concrete has been used as a construction material for numerous years, there is still the opportunity for further research and development. Following on from this work, the possible area for further research using ultrasound technique and destructive methods may include:

1. An investigation to determine the peak concentration or proportion of chemical additives.
2. Research into the effects of combinations of additives.
3. The analysis of the effects of additives on the tensile strength of concrete.
4. Further investigation into the use of other waste materials and a combined use of waste materials.

Using the acoustic emission method the following recommendations are forwarded:

1. Optical and microscopic scanning evaluation to be used to evaluate the fractured surfaces (structural and micro-structural) of the cement samples and co-relate them with the AE results.
2. Train the AE AMSY4 system for source classification for better understanding of the modified cements behaviour under both compressive and flexural load.
3. Discover other potential techniques, thermal imaging technique, for example, to identify the regions of well set and cured portions within

the specimen and co-relate those regions with the AE activities taking place in those particular regions.

There is a large scope for future research in terms of materials by altering the properties of aggregates and admixtures themselves, e.g by giving treatment to aggregates. This will open the path to do further research with the aid of AE, since this will make alteration to the mechanical as well as physical properties of aggregate and hence the behaviour of concrete under tests thus leading to changes in AE characteristics.

Further studies about the quantities of glass aggregates to be introduced would be suitable to know how high the sand / glass ratio could be. In this research broken glass from car wind screen was used, further research could be carried out using different types of glass, for example from broken bottle, drinking glass, etc and their effects on the toughening behaviour could be observed using AE technique.

As it was developed and observed from this research that the glass aggregate size had an effect on the strength as well as AE behaviour of concrete, and it was discovered that the aggregate size does aid the bulk properties of the specimens, hence enhances the mechanical properties. Therefore further ideas could be developed to decide whether or not the specimen shape has an effect as well. The orientation of the inserted glass could also be controlled and studied.

Although rubber was seen to have an adverse effect on the flexural strength of concrete, but rubber brings some benefits to concrete, for example it lightens the concrete, and acts as a damper of failure. Therefore concrete may be put into use where vibration needs to be mitigated. Therefore further research about the effect on the mechanical properties in conjunction with AE monitoring of the size of rubber chunks introduced into concrete would be useful to conduct. The AE monitoring of the damping properties of concrete subjected to different types of vibration would also be useful.

The sheer volume of data is a major problem and perhaps the introduction of artificial intelligence to the analysing process would certainly be very beneficial. This would allow the waveforms to be categorised by an intelligent system, which could allow more accurate observations to be made with respect to all events.

As a summary, it can be said that a few suggestions are made here, but there is a lot of potential to make further research by modifying the materials as well as the techniques.

REFERENCES

1. M.S. Shetty, 2004, *Concrete Technology: Theory and Practice*, S. Chand and Company Limited, New Delhi.
2. N. Jackson and Ravindra K. Dhir, 1996, *Civil Engineering Materials*, Palgrave, New York.
3. Christian Meyer, *Concrete for the New Century*, Concretus, Association of New York City Concrete Producers, Spring/Summer 2002.
4. B. L. Karihaloo and A.D. Jefferson, April 2001, Magazine of Concrete Research, Number 2, 135-147.
5. The History and Importance of Concrete, 1996
<http://ciks.cbt.nist.gov/~garbo cz/appendix1/nodo4.html>
6. CSIRO, April 2002, *Recycled Glass as Concrete Aggregate*, Number 24, Built Environment and Construction Technology, Australia.
7. C. Meyer, 2002, *Concrete and Sustainable Development*, ACI 206
8. Satish Chandra, 1996, *Waste Materials Used in Concrete Manufacturing*, William Andrew Publishing.
9. Zbigniew D. Jastrzebski, 1987, *The Nature and Properties of Engineering Materials*, 3rd Edition, John Wiley and Sons.
10. N. Jackson and R. K. Dhir, 1996, *Civil Engineering Materials*, 5th Edition, Palgrave, New York.
11. F.A.A Crane, J.A Charles, 1997, *Selection for Mechanical Properties of Cement and Concrete*, Selection and Use of Engineering Materials, 3rd Edition, Butterworth-Heinemann, Sevenoaks.
12. J. M. Illston and P.L.J. Domone, 2001, *Construction Materials: Their Nature and Behaviour*, 3rd Edition, Spon Press, London.

13. Newman J. and Choo B.S., 2003, *Advanced Concrete Technology: Concrete Properties*, Butterworth Heinemann, Oxford.
14. Paul Mont, *Concrete as a Structural Material*, Available from: www.ce.berkeley.edu/~Paulmont/ce60New.chapter1.pdf, 2006.
15. Cement Association of Canada - Compressive Strength, 2005.
16. Pavement Interactive, Compressive strength, 2007, available from: <http://www.pavementinteractive.org/article/Compressive-Strength/>
17. National Ready Mixed Concrete Association, *Quality in Practice*, CEMSTONE Solutions, 2000, Maryland, USA
18. Don W. Pashley and Rees D. Rawlings, 2001, *Brittleness: A Tough Problem*, *Imperial College Inaugural Lectures in Materials Science and Engineering*, Department of Materials, Imperial College of Science, Technology and Medicine.
19. Jan G.M. Van Mier, 1997, *Fracture Processes of Concrete*, CRC Process: pp.17, 57- 65, pp. 88-93.
20. *Materials Research: Residual Stresses* Advanced Materials Measurement Techniques, 2005, National Physical Laboratory, Teddington, Middlesex.
21. Eric N. Landis, *Micro-Macro Fracture Relationships and Acoustic Emissions in Concrete*, *Construction and Building Materials*, Volume 13, 1999, No.1-2, pp. 65-72.
22. Ohtsu M., 1996, *The History and Development of Acoustic Emission in Concrete Engineering*, *Magazine Concrete Research*, 48,: pp. 321-330.
23. Maji A.K. Shah S.P, *Acoustic Emission Process Zone in Concrete*, *Experimental Concrete*, Volume 28, pp: 27-33, 1988.

24. Nomura N., Mihashi H., Izumi M., 1991, *Properties of Fracture Process Zone and Tension Softening Behaviour of Concrete*; In: Van Mier JGM, Rots JG, Bakker A., Editors, *Fracture Processes in Concrete, Rock and Ceramics*, London, Chapman and Hall: pp. 51-60.
25. Berthaud Y. Ringot E, Schmitt N., 1991: pp. 41-50, *Experimental Measurements of Localisation for Tensile Tests on Concrete*, In: Van Mier JGM, Rots JG, Bakker A., *Fracture Processes in Concrete, Rock and Ceramics*, London, Chapman and Hall.
26. Li Z, Shah S.P., 1994, *Micro-cracking in Concrete Under Uni-axial Tension*, *ACI Materials Journal* 91:pp. 372-381.
27. Ohtsu M, 1987, pp.:1-28, *Mathematical Theory of Acoustic Emission and its Application*, *Mem Fac Eng*, 32, Kumamoto University.
28. Surais W., Van Miler JGM, 1995, *Acoustic Emission Source Characterisation in Concrete Under Biaxial Loading*, *Material Structure*, 28.
29. Ohtsu M., Okamoto T., Yuyama S., 1998, *Moment Tensor Analysis of Acoustic Emission for Cracking Mechanisms in Concrete*, *ACI Struct*, 95.
30. M.S. Shetty, 2003, *Concrete Technology: Theory and Practice*, 15th Edition, New Delhi.
31. P. Kumar Mehta, Paulo J.M. Monterio, October, 2001, *Concrete Micro-structure, Properties and Materials*, Chapters 2 and 12, pp. 29-32 and 220-224, *Advances in Concrete Mechanics*.
32. Paul Monterio, *Micro-Structure of Concrete*, www.ce.berkley.edu/~paulmont/ce60new/chapter2.pdf, 2006.
33. Hans Henrik Basche, 1985, *Durability of Concrete Fracture Mechanical Aspects*, The Nordic Concrete Federation's Research Committee.

34. Shah S.P., Swarz S.E., Ouyang C., 1995: pp. 88-97, *Fracture Mechanic of Concrete*, John Wiley and Sons.
35. Li Vc, Maleej M., 1996, *Toughening in Cement Based Composites*, 18: (4) pp. 223-237.
36. Strubble I.J., Lange D., December 1997, *ASM International Volume 19*, Issue 22.
37. C.D. Pomeroy, 1980, *Physics in Cement and Concrete Technology*, Physics of Materials, No 30, pp. 171-175, The Institute of Physics, London.
38. Brown J.H. and Pomeroy C.D., 1973, *Fracture Toughness of Cement Pastes and Mortars*, *Cement and Concrete Research* 3, pp. 475-480.
39. Spooner D.C. and Dougill J.W., 1975, *A Quantitative Assessment of Damage Sustained in Concrete during Compressive Loading*, *Magazine of Concrete Research*, 27, pp. 151-160.
40. V. B. John, *Engineering Materials*, 1990, Macmillan Educational Limited, Basingstoke, pp. 180-195.
41. Mindes, S. and Young, J.F., 1981, *Concrete*, Prentice Hall, New Jersey.
42. John Newman, *Strength and Failure of Concrete under Short-term, Cyclic and Sustained Loading*, *Advanced Concrete Technology*, Concrete Properties, Elsevier, Butterworh Heinmann, 2003, pp. 6/3-6/35.
43. Mehta and Monterio, 1993, Larbi, 1993 and Scrivener 1989; Mehta P. K. and Monterio, 1993, Mehta P.K. and Monterio, 1993, *Concrete Structure, Properties and Materials*, 2nd Edition, Prentice Hall Inc., New Jersey.
44. Kotsovos M.D., 1983, *Effect of Testing Techniques on the Post-ultimate Behaviour of Concrete in Compression*, *Materials and Structures*, Volume 16, Number 91 pp 3-12.

45. Hsu T.C., Fioyd, O.S., Gerald, M.S., and Winter, G., 1963, '*Micro-cracking of Plain Concrete and the Shape of the Stress-Strain Curve*, ACI Materials Journal Volume 60, No. 2.
46. Shrive N.G. and El- Rahman M., 1983, '*Understanding the Cause of Cracking in Concrete*, Journal of the Engineering Mechanics Division, ASCE, Volume 97.
47. Wang E.Z., Shrieve N.G., 1995, '*Brittle Fracture in Compression: Mechanisms, Models and Criteria*, Engineering Fracture Mechanics, Volume 52, Number 6, pp. 1107-1126.
48. Mindess S. and Diamond S., 1982, '*The Cracking and Fracture of Mortar*, *Materials et Construction*, Volume 15, Number 86, pp 107-113.
49. Coz B.N. and Marshall D.B., '*Concepts for Bridged Cracks in Fracture and Fatigue*', 1994, *ACTA Metallurgy*, Volume 42, Number 2.
50. Balaguru N.P. and Shah S.P., 1992, '*Fibre-Reinforced Cement Composites*, pp. 500, M^cGraw-Hill, Inc., NY, USA.
51. Beaudion J.J., 1990, '*Handbook of Fibre-Reinforced Concrete, Principles, Properties, Developments Applications*', Noyes Applications, pp332;
Bentur A. and Mindess S., 1990, '*Fibre Reinforced Cementitious Composites*', Elsevier Applied Science, NY, USA, pp 620.
52. J.C. Anderson, K.D. Leaver, R.D. Rawlings, J.M. Alexander, 1986, '*Materials Science*, 3rd Edition, Van Nostrad (UK) Ltd, Berkshire, UK.
53. Antoine Naaman, '*Toughening Mechanisms*, 2001, ACBM, Centre for Advanced Cement Based Materials, University of Michigan.
54. Yu-Cheng Kan, K.C. Pei and Chien-Lung Chang, '*Strength and Fracture Toughness of Heavy Concrete with Various Iron Aggregate Inclusions*, Transactions, SMiRT16, August 2001, Washington DC.

55. John, P. and Shah, S.P, 'Fracture Mechanics Analysis of High Strength Concrete', ASCE Journal of Materials, Vol 1, No. 4, 1989, pp. 185-198.
56. Howard W. Chandler, Ian J. Merchant Robin J. Henderson, Donald E Macphee, Ali M. Siddiqui, Kevin Fraser, *Enhancing the Toughness of Cement Based Materials*; University of Aberdeen and Robert Gordon University, Aberdeen, Presented at Brittle Matrix Composites 6 Conference, October 2000.
57. Ansari F. October 1985, *Analysis of Micro-Cracked Zone in Concrete, Fracture Toughness and Fracture Energy*, Concrete Proceedings International Conference, Lausanne.-Amsterdam e.a.-1986.- pp.229 - 240.
58. Hubbard F.H. and Dhir K. 1984, 'Aggregate and Concrete Micro-fracture', Bulletin of Engineering Geology and the Environment, Volume 2, Number 1, pp. 245 -248.
59. Detriche Ch.H. and Ramoda S.A., October, 1985, *Effect of the Composition of Mortars and Testing Procedures on Fracture Toughness and Fracture Energy*, Concrete Proceedings International Conference, Lausanne, Amsterdam e.a.-1986. pp. 291-298.
60. Pontazopoulo S. J., *Role of Expansion on Mechanical Behaviour of Concrete*, December 1995, Journal of Structural Engineering, Volume 121, Number 12, pp. 1795-1805.
61. Mohammed E. Haque and Farhad Ansari, October 1996, Composite Beam Analogy Fracture Model for Concrete, *Journal of Engineering Mechanics*, Volume 122, Issue Number 10, pp. 957-965.
62. Nemati K.M., Monteiro P.J.M., and Cook N.G.W., August 1998, *A New method for Studying Stress-induced Micro-cracks in Concrete*, Journal of Materials in Civil Engineering Volume 10, Number 3, pp. 128-134.

63. Denarie E., Saouma V.E., Locco A., and Varelas D., *Concrete Fracture Process Zone Characterisation with Fibre Optics*, May 2001, Journal of Engineering Mechanics, Volume 127, Number 5, pp. 494-502.
64. Berthelot J.M. and Robert J.L., March 1990, *Damage Evaluation of Concrete Test Specimens Related to Failure Analysis*, Journal of Engineering Mechanics, ASCE, Volume 116, Number 3, pp. 587-604.
65. Andrew Starkey, Ana Ivanovic, Albert A. Rodger, Richard D. Neilson, The influence of load on the frequency response of rock bolt anchorage, *Advances in Engineering Software* 34 (2003), pp. 697-705.
66. J A Steele, R L Reuben, M Hamlin, E R Brown, *Acoustic emission from the tension fatigue of glass fibre reinforced plastics*, Proceedings Institute of Mechanical Engineers, 2004, Volume 218 Part I: Journals of Materials: Design and Applications.
67. Shah SP, Chois S, *Non-destructive techniques for studying the fracture Processes in concrete*, 1999, International Journal of Fracture, Volume 98, Issue 3-4, pp. 351-359.
68. Eric Landis, Michael Peterson, Scott Selleck, Surendra Shah, Zongjin Li, Alan Zdunek, and David Prine, *Developments in NDE of Concrete*, BIRL Industrial Research Laboratory, North Western University, June 1994.
69. *Study of the influence of the aggregate size distribution on mechanical properties of concrete by acoustic emission technique*, 2001, Cement and Concrete Research 31.
- 69a. Soulioti, D.; Barkoula, N.M.; Paipetis, A.; Matikas T. E.; Shiontani, T.; Aggelis D.G. Acoustic Emission Behaviour of Steel Fibre Reinforced Concrete Under Bending. *Construction and Building Materials*, 2009, 23, pp. 3532-3536.

70. Lysak, M.V., *Development of the theory of acoustic emission by propagating cracks in terms of fracture mechanics*, 1996, Engineering Fracture Mechanics Volume 55, pp. 443-452.
- 70a. Dimitrios G. Aggelis, Dimitra Soulioti, Nektaria M. Barkoula, Alkiviadis S. Paipetis, Theodore E. Matikas and Tomoki Shiotani, *Acoustic Emission monitoring of steel-fibre reinforced concrete beams under bending*, 2010, *J. Acoustic Emission*, 28.
71. Tasong. W. A., Lynsdale C.J. and J.C., *Aggregate-cement paste interface. Li: influence of aggregate physical properties*, Cement and Concrete Research, 1998, Volume 28, pp. 1453-1465.
72. Labuz J.F. Cattaneo S and Chen, 2001, Acoustic Emission at Failure in Quasi- Brittle Materials, *Construction and Building Materials*, Volume 15 pp. 225-233.
73. Eric N. Landis and D. B. Whittaker, *Acoustic Emission as a Measure of Fracture Energy*, 2002 Department of Civil Engineering, University of Maine.
74. H. Hadjab, J.-Fr.Thimus and M. Chabbat, *Fracture Process Zone in Notched Concrete Beams Treated by Using Acoustic Emission*, December 2000, NDT.net, Volume 12, Number 12.
75. Eric N. Landis and Lucie Baillon, Experiments to Relate Acoustic Emission Energy to Fracture Energy of Concrete, *Journal of Engineering Mechanics*, June 2002, Volume 128, Issue 6, pp. 698-702.
76. Yuyama, S., Okamoto, T., Shigeishi, M. and Ohtsu, M. 1995, Quantitative Evaluation and Visualisation of Cracking process in Reinforced by a Moment Tensor Analysis of Acoustic Emission, *Materials Evaluation*, Volume 53, No.6, pp. 751-756.

77. Li, Z. W., Yuyama S., Osawa I., Kimpara I., Kageyama K., and Yamaguchi K. 1998, Fracture Mechanics Study of Concrete Beams Reinforced with FRP Sheets by a Moment Tensor Analysis of Acoustic Emission, *Fracture Mechanics of Concrete Structure, Proc. FRAMCOS-3*, October 12-16, Gifu, Japan, AEDIFICATIO Publisher, pp. 1863-1872.
78. Yuyama S., Okamoto, T. and Ngataki, S. 1994, Acoustic Emission Evaluation of Structural Integrity in Repaired Reinforced Concrete Beams, *Materials Evaluation*, Volume 52, No 1, pp. 86-90.
79. Murakami, Y. and Yuyama, S., November 27-30, 1996, Acoustic Emission Evaluation of Structural Integrity in Reinforced Concrete Beams Deteriorated due to Corrosion of Reinforcement, *Progress in AE VIII (JSNDI), Proc. 13th Inter. AE Symposium.*, Nara, Japan, pp. 217-224.
80. Yuyama, S., Okamoto, T., Shigeishi, M. and Ohtsu, M., 1995, Acoustic Emission Generated in Corners of Reinforced Concrete Rigid Frame Under Cyclic Loading, *Materials Evaluation*, Volume 53, No 3 pp. 409-412.
81. Yuyama S., Li. Z.W., Yoshizawa. M., Tomokiyo. T., and Uomoto, T. 2000, Evaluation of Fatigue Damage in Reiforced Concrete Slab by Acoustic Emission, *Non-Destructive Testing in Civil Engineering-2000*, Uomoto T. ed., Elsevier, 25-27 April 2000, Tokyo, Japan, pp. 283-292.
82. Yuyama, S., Kishi, T., and Hisamatsu, Y., *Fundamental Aspects of AE Monitoring on Corrosion Fatigue Process in Austenitic Stainless Steel*, 1984, J. Mater. Ener. Syst., Am. Soc. Met., Volume 5, Number 4, pp. 212 - 221.
83. Shigenori Yuyama and Masayasu Ohtsu, Acoustic Emission Evaluation in Concrete, September 2000, Adopted from T. Kishi, M. Ohtsu, S. Yuyama, *Acoustic Emission – Beyond the Millennium*, Tokyo, Japan.

- 83a. Dunja MIKULIC, Bojan MILOVANOVIC, Ivan GABRIJEL, *Testing of compressive and Bending Strength of Concrete and Monitoring of Acoustic Emission Parameters NDTCE'09 Non-Destructive Testing in Civil Engineering, Nantes, France, June 30th – July 3rd, 2009.*
84. Chengsheng Ouyang, Eric Landis, Surendra Shah, November 1991, Damage Assessment in Concrete Using Quantitative Acoustic Emission, *Journal of Engineering Mechanics*, Volume 117, No 11, pp. 2681-2698.
85. Landis EN and Shah SP, *The Influence of Micro-cracking on the Mechanical Behaviour of Cement Based Materials*, 1995, Volume 2, Issue 3, pp. 105-118.
86. Bernd Weiler, Shilang Xu, Utz Mayer, *Acoustic Emission analysis applied to Concrete under different loading conditions*, 1997 Otto-Graf-Journal, Volume 8, pp. 255-269.
- 86a. Shohoei Momoki, Hwakian Chai, Dimitrios G. Aggelis, Akinobu Hiramama and Tomoki Shiotani, *Acoustic Emission for Characterisation Behaviour of Composite Concrete Elements Under Flexure*, *J. Acoustic Emission*, 27 (2009)
87. Beck P., Bradshaw T.P., Lark R.J., Holdford K.M., *A quantitative study of the relationship between concrete crack parameters and acoustic emission energy released during failure*, *Engineering Materials*, Volume: 245-246, pp. 698-702, (2002).
88. Keru Wu, Bing Chen and Wu Yao, *A study on the AE characteristics of fracture process of mortar, concrete and steel-fibre reinforced concrete beams*, *Cement and Concrete Research*, 30 (2000), pp. 1495-1500.
- 88a. Stahli P., van Mier JGM. Manufacturing, fibre anisotropy and fracture of hybrid fibre concrete. *Eng Fract Mech*, 2007, 74, pp. 223-42.

- 88b. Sivakuram, A.; Sathanam, M. *Mechanical properties of high strength concrete reinforced with metallic and non-metallic fibres*. *Cem. Concr Compos.* 2007, 29, pp. 603-8.
- 88c. RILEM TC212-ACD. *Acoustic Emission and related NDE techniques for crack detection and damage evaluation in concrete. Recommendation, 3; 2008.*
- 88d. Vogel, T., and Kocur, G.K., Classification of the damage condition of preloaded reinforced concrete slabs using parameter based acoustic emission analysis, *Construction and Building Materials*, Volume 24, pp 2332-2338, 2010.
89. Ohtsu, M., 1996, The History and Development of Acoustic Emission in Concrete Engineering, *Magazine of Concrete Research*, Volume 48, Number 177, pp 321-330.
90. McCabe, W.M., Koerner, R.M., Lord, A.E., 1976, Acoustic Emission behaviour of concrete laboratory specimens, *ACI Journal*, pp 367-371.
91. Ohtsu, M, Kaminaga, Y, and Munwam, 1999, M.C., Experimental and Numerical Crack analysis of mixed-mode failure in concrete by acoustic emission and boundary element method, *Construction and Building Materials*, Volume 13, pp 57-64.
92. L.S. Chang T.H. Chuang, *Ultrasonic Testing of Artificial Defects in Alumina Ceramic*, *Ceramic International* 23 (1997), pp. 367-373.
93. *Ultrasound Technique for Quality Control of Cementitious Materials*, Institute of Construction Materials, 1999, University of Stuttgart, Germany.
94. *Propagation of Ultrasound in Concrete- Spatial Distribution of the Young's Modulus*. Darmstadt Concrete17 (2002), available from: www.darmstadt-concrete.de/2002/propagation.html.

95. Christian U. Grosse, Hans-Wolf Reinhardt, *Fresh Concrete Monitored by Ultrasound Methods*, Otto-Graf-Journal Volume 12, pp. 157-168, 2001.
96. Thomas Voigt, Yilmaz Akkaya and Surendra Shah, *Determination of Early Age Mortar and Concrete Strength by Ultrasonic Wave Reflections*, May/June 2003, Journal of Materials in Civil Engineering, Volume 15, Issue 3, pp. 247-254.
97. Popovics S., *Strength and Related Properties of Concrete: a quantitative approach*, New York: John Wiley Sons Inc., 1998.
98. De Belie N, Grosse C.U., Kurz J., and Reinhardt H.W., *Ultrasound Monitoring of the influence of different accelerating admixtures and cement types for shotcrete on setting and hardening behaviour*, 2005, Magnel Laboratory for Concrete research, Ghent University, Belgium and Department of Construction Materials, Stuttgart University, Germany.
99. H.W. Reinhardt and C.U. Grosse, *Setting and Hardening of Concrete continuously monitored by Elastic Waves*, NDTnet July, 1996, Volume 1, Number 07.
100. I.N. Prassianakis and P. Giokas, *Mechanical properties of old concrete using destructive and ultrasonic non-destructive testing methods*, Magazine of Concrete Research, April, 2003, 55, No 2, pp. 171-176.
101. Yiching Lin, Chao-Peng Lai, and Tsong Yen, *Prediction of Ultrasonic Pulse Velocity (UPV) in Concrete*, Materials Journal: Concrete International, Volume 1, Issue 1, January, 2003.
102. Hisham Y. Qasrawi, *Concrete Strength by Combined Non-destructive Methods Simply and Reliably Predicted*, Cement and Concrete Research, Volume 30, Issue 5, May 30, Issue 5, 2000, pp. 739-746.
103. S. Popovics, K. Komlos, J. Popovics, *Comparison of DIN/ISO 8047 (Entwurf) to several standards on determination of ultrasonic pulse velocity in concrete*, NDTnet-April 1997, Volume 2, Number 04.

104. A. Van Hauwert, J. F. Thimus and F. Delannay, *Use of Ultrasonic to follow Crack Growth*, *Ultrasonics* 36 (1998), pp. 209-217.
105. Mary J. Sansalone and William B. Streett, *The Impact-Echo Method*, *NDTnet* 1998, February, Volume 3 No. 2. Available from:
<http://www.ndt.net/article/0298/streett/streett.htm>
106. M. Krause, C. Maierhofer, H. Wiggenger, O. Barmann, K. Langenberg, R. Frielinghaus, J. Neisecke, F. Wollbold, M. Schickert, *Comparison of Pulse-Echo-Methods for Testing Concrete*, *NDTnet*-October 1996, Volume 1 No. 10.
107. Thomas Voigt, Yilmaz Akkaya, Surendra Shah, *Non-Destructive Testing of Concrete Using Ultrasound*, 2001 Centre for Advanced Cement-Based Materials, North-western University, USA.
108. E. Grosse, *Ultrasound Technique for Quality Control of Cementitious Materials*, Institution of Construction Materials (IWB), 2000, University of Stuttgart, Germany.
- 108a. Abid A. Shah, *Concrete Damage Assessment with Innovative Non-Destructive Testin Techniques*, *International Journal of Geology*, Issue 3, Volume 5, 2011.
- 108b. H.K.Chai, S. Momoki, Y. Kobayashi. D. G. Aggelis, T. Shiotani. Tomographic reconstruction for concrete using attenuation of ultrasound. *NDT & E International*, 44(2), pp. 206-215, 2011.
109. A. Rosch, B. Hillemeier, E. Porzig, M. Krause, C. Maierhofer, *Air Voids, Poor Compaction and Areas of Low Concrete Strength Detection by Pulse Velocity Measurement*, 1995, Technical University of Berlin, Germany.
110. Ferreira Almir P., *Assessing Concrete Strength by In-situ Tests*, Roma 2000, 15th WCNDT, available from: www.ndt.net/article/

- 110a. B.Hobbs and K. Tchoketch, *Non-destructive Testing Techniques for the Forensic Engineering Investigation of Reinforced Concrete Buildings*, Forensic Science International, Vol. 167, No. 2-3, 2007, pp. 167-172.
- 110b. D. Breyse, *Combining Information, Reliability and Maintenance*, Diagnosis of NEC Works, 2008.
- 110c. Vasconcelos, G., Lourenco. P. B., Alves, C.A., Pamplona, J., *Ultrasonic evolution of the physical properties of granites*, *Ultrasonic*, 48, (2008): pp.453-466
- 110d. Raman, S.N., Safiuddin, M.D., Zain, M.F.M., *Non-destructive evaluation of flowing concretes in cooperating quarry waste*, *Asian journal of civil engineering (Building and Housing)*, 8(6), (2007), pp:597-614.
- 110e. Lourenco, P.B., Feio, A., Machado, J.S., Chestnut wood in compression perpendicular to the grain: non-destructive correlation for news and old wood, *Construction and Building Materials* 21(8): 1617-1627 (2007).
111. Garnier Vincent and Corneloup Gilles, *Non-Destructive Evaluation of Concrete Damage by Ultrasounds*, Roma 2000, 15th WCNDT, Available from: www.ndt.net/article/
112. Surendra P. Shah and Kolluru V. Subramaniam, *Use of Non-destructive Ultrasonic Technique for Material Assessment and in-Service Monitoring of Concrete Structures*, NDT.net – February, 2000, Volume 5, No. 02.
113. P. Smolarkiewicz, Carnot L. N Nogueira, and Kaspar J. Willam, *Ultrasonic Evaluation of Damage in Heterogeneous Concrete Materials*, European Congress on Computational Methods in Science and Engineering, Barcelona, September, 2000.
114. Christian U. Grosse, Bernd Weiler, Alexander T. Herb, Gunther Schmidt, Kai Hofler, *Advances in Ultrasonic Testing of Cementitious Materials*, 2000, Institute of Construction Materials, University of Stuttgart.

- 114a. *D. Breysse, Quality of NDT Measurements and Accuracy of Physical properties, Concrete NDTCE09, Nantes, July, 2009.*
- 114b. *Mitsuhiro Shigeishi, Kumamoto University, Japan Japanese Society for Non-Destructive Inspection (JSNDE), Concrete Research letters, Vol. 2(3) –Sep. 2011.*
115. Henderson R.J. and Chandler H.W., *The Fracture Behaviour of Dual Phase Composite Refractories, Engineering with Ceramics*, W.E. Lee and B. Derby Eds, British Ceramic Processing 59, The Institute of Materials, 1999, 225-231.
116. H.W. Chandler, D.E., Macphee. J. Atkinson and R. Henderson, *Enhancing The Fracture Toughness of Cement Based Materials*, Department of Engineering/Chemistry, University of Aberdeen, Journal of European Ceramic Society, 2000.
117. H.W. Chandler, D.E., Macphee. J. Atkinson, R. Henderson and I.J. Merchant, 1999, *Enhancing the Mechanical Properties of Materials*, Department of Engineering/Chemistry, University of Aberdeen.
118. H.W. Chandler, D.E., Macphee. J. Atkinson and R. Henderson, I. J. Merchant, 2002, *'Enhanced crack-bridging by un-bonded inclusions in a brittle matrix'*, Journal of the European Ceramic Society, 22, pp.129 - 134.
119. M. Philip, W. Bolton, 2002, *Technology of Engineering Materials*, The Institutions of Incorporated Engineers, pp. 289-290, Butterworth-Heinemann, Oxford.
120. The National Materials Laboratory Advisory Board (NMAB), Ad Hoc Committee on Non-destructive Evaluation, The American Society for Non-destructive Testing, 2005 (ASNT).

121. *Guidebook on non-destructive testing of concrete structures*, International Atomic Energy Agency, Series No 17., Vienna, 2002, Pages 1-3.
122. Deidrichs R. and Ginzel E., 2005. The e-Journal of Non-Destructive Testing. NDTnet. www.ndt.net/article/az/utidx.html
123. Moore P.O., McIntire P., Ness S. and Sherlock C.N., 2nd ed. 1996. *Non-Destructive Testing Handbook*.
124. F. L. Matthews and R.D. Rawlings, 1999, *Composite Materials: Engineering and Science*, Woodhead Publishing, Cambridge.
125. Nelligan Thomas J., 2005. *An Introduction to Ultrasonic Material Analysis*, Panametrics Inc. www.Panametrics-ndt.com/ndt/ndttechnology/materialanalysis.html.
126. Popovics S. *Analysis of Concrete Strength versus Ultrasonic Pulse Relationship* 2001, American Society For Non-Destructive Testing www.asnt.org/publications/materialseval/basics/feb01basics/feb01basics.htm
127. BS8047 Entwurf (8047), *Determination of Ultrasonic Pulse Velocity in Concrete*, 1995.
128. Jastrzebski Z. D., 1987- *The Nature and properties of Engineering Material*, 3rd Edition, Chapman & Hall, Cambridge.
129. Kong F.K. & Evans R. H.- *Reinforced and Pre-stressed Concrete*, 3rd Edition – Cambridge – Chapman & Hall – 1987.
130. BS EN 12504-2: 2001, *Testing in Concrete Structures Determination of the Rebound Number*;

- 130a. Olowofoyeku Adeoye M., Olutoge Festus A. Domestication Of Pundit Non-Destructive Test Chart in Measuring Compressive Strength Of Normal Strength Concrete Subjected To Elevated Temperature Australian Journal of Basic and Applied Sciences, 7(1):1-6, 2013. BS 4408: BS EN 12504-2:2012.
131. Green, A.T. *Stress Wave Emission and Fracture of Pre-Stressed Concrete Reactor Vessel Materials*. Second Inter-American Conference on Materials Technology, ASME, volume 1, August 1970.
- 131a. CAPGO PLY LTD, *Fatigue detection by acoustic emissions*, <http://www.capgo.com>, 1998-2013.
- 131b. Trevor J. Holroyd, *The Application of AE in Condition Monitoring*, BINDT CM2005 Conference, Cambridge, July 2005.
132. Dungeon, H.L. and Harris, D.O. *Acoustic Emission – A New Non-destructive Testing Tool*, Ultrasonic, volume 7, Number 3, 1969.
133. Morton, H. L. and Harrington, R.M. and Bjeletich, J.G. *Acoustic Emission of Fatigue Crack Growth*, Engineering Fracture Mechanics, volume 5, Number 3, 1973.
134. Nogin, S.I., Nesvijski, E.G. *The Parametrical Points of the Cracking Process in Concrete under Compression*, 1980, Journal of Concrete and Reinforced Concrete, Number 3, Moscow, Russia.
135. Landis, E.N. and Shah S.P. *Recovery of Micro-crack Parameters in Mortar Using Quantitative Acoustic Emission*, Journal of Non-destructive Evaluation, 12 (1993), Number 4;
136. Shah, S., Ouyang, C., Marikute, S., Yang, W., and Becq-Giradon, E., (1998). *A Method to Predict Shrinkage Cracking of Concrete*, ACI Journal, Volume 95, Number 4.

137. Edouard G. Nesvijski, Paulo J. Sarkis, *Acoustic Emission and Failure Predictions of Composites*, NDT.net, March 2000, Volume 5, Number 03.
138. Miinshiou Huang, Liang Jiang, Peter K. Liaw, Charlie R. Brooks, Rodger Seeley, and Dwaine L. Klarstrom, *Using Acoustic Emission in Fatigue and Fracture Materials Research*, November, 1998, Volume 50, Number 11, Journal of Materials.
139. Cole P.T., *Acoustic Emission, Part 7*. Northampton: The British Institute of Non-Destructive Testing pp. 1-18, July, 1988.
140. Vallen Systeme GMBH, Munich, Germany, 2005, available from: www.vallen.de
- 140a. Marschall K. and Gautschi GH. 1994 In-Process Monitoring with Piezoelectric Sensors, *Journal Materials Processing Technology*, 44, 345-352.
141. Zhifu Yang, Jason Weiss, and Jan Olek, *Using Acoustic Emission for Detecting Tensile Loading Damage and Assessing its Impact on the Freeze-Thaw Resistance of Concrete*, August, 2005, School of Civil Engineering, Purdue University, Indiana, Presented at CONMAT -05 3rd International Conference on Construction Materials, Vancouver, BC, Canada.
142. Nagaraja Rao et al. (1999) G.M. Murthy, C.R.L., and Raju, N.M. (1999), Characterisation of micro and macro cracks in rocks by acoustic emission. *Acoustic Emission Standards and Technology Update*. Edited by S.J. Vahaviolos, American Society for Testing and Materials, Special Publications, STP. 1353.
143. BS EN 13139:2002 – Guidance on the Use *Aggregate size for mortar*.
144. J.C. Anderson, K.D. Leaver, P. Leever, R.D. Rawlings, 2003, *Materials Science for Engineers*, 5th Edition, Nelson Thornes.

145. Nawy E.G., 1985, *Reinforced Concrete, A fundamental Approach*, Prentice Hall Inc., New Jersey, pp. 15.
146. G.D. Taylor, 1994, *Materials in Construction*, 2nd Edition, pp. 59.
147. Canadian Building Digest (CBD) 165, V.S. Ramachandran, Calcium Chloride in Concrete, 1974.
148. Canadian Building Digest, (CBD) 165, CSA A231-1973, Chemical Effects on Concrete.
149. The use of lime in mortar, May 2004, Data Sheet 18, Issue 1, Mortar Industry Association, Available at: www.mortar.org.U.K.
150. Calcium Carbonate, *2010*, The European Calcium Carbonate Association, IMA-Europe, Brussels, Belgium. Available from: www.ima-eu.org/cca.html.
151. Arnold Donald J., *Additives for Concrete*, March, 1979, Arnold US Patent 4144086.
152. The Use of Silicate Solution to cure Concrete, Jenifer Chrisman, Euro-chemical, Cleveland, 2007.
153. Sodium Silicates for Oilwell Cement, Bulletin 35-01, 2006, Industrial Chemical Divisions, PQ Corporation, Valley Forge, PA, USA.
154. Paul Marcantoni, US Patent 6, 656.264 B2, Settable Composition Containing Potassium Chloride, Ronald Lee Barbour, December, 2003.
155. Settable Composition Containing Sodium Chloride, US Patent 6780236, Marcantoni Paul, August 2004.
156. Portland Cement, Infrastructure, Materials Group, Federal Highway Administration, US Department of Transportation, 2011.

157. Polivka M. and Wilson C., Properties of Shrinkage Compensating Concrete, In: Kelvin Symposium on Expansive Cement, ACI SP-38, 1973.
158. A. Siddiqui, A. Choudhury, Ian Merchant, 2004, *Acoustic Emission Monitoring of the Fracture Behaviour of Concrete containing various size and shape of Glass Aggregates*, EWGAE, Berlin.
159. Thomas, T.C. HSU, and Floyd, O. Slate, 1963, *Tensile Bond Strength Between Aggregate and Cement Paste or Mortar*, Journal Proceedings, ACI, Volume 60.
160. Jensen, EA. and Hansen, W., 2000, *Fracture Energy Test for Highway Concrete: Determining the Effect of Coarse Aggregate on Crack Propagation Resistance*, Transportation Research Record, Number 1730.
161. Toolbase Services, PATH Technology Inventory, *Concrete Aggregate Substitutes*, Alternative Aggregate Materials, Home Innovation Research Labs, 2001.
162. *Concrete Materials Research*, pp. 3-5, Department of Civil Engineering and Engineering Mechanics, Columbia University, New York, August 2000.
163. *Recycled Materials in Portland cement Concrete*, New Jersey Department of Transportation, June 2000.
164. V.S. Ramachandran, Canadian Building Digest, *Waste and By-Product as Concrete Aggregates*, CBD-215, April 1981.
165. Charles Camp, CIVL 1101, 2005, Department of Civil Engineering, University of Memphis.
166. Toolbase Services, PATH Technology Inventory, *Concrete Aggregate Substitutes*, 2001, NAHB Research Centre, Upper Marlboro, USA.
167. Meyers C., Jin, W., and Baxter, S. "Glasscrete: Concrete with Glass Aggregate" ACI Materials Journal 97 (2), March-April 2000, 208-213.

168. Yunping Xi, Yue Li, Zhaohui Xie and Jae S. Lee, *Utilisation of Solid Wastes (Waste Glass and Rubber Particles) as aggregates in Concrete*, International Workshop on Sustainable Development and Concrete Technology, 2004, University of Colorado, Boulder, CO, USA.
169. Concrete Technology Unit, *Realising a High-Value Sustainable Recycling Solution to the Glass Cullet Surplus*, DTI Research Contract No.GW-12.10-108, 2003, Dundee Concrete Technology Unit, Dundee University.
170. BS EN 206-1:2002, Specification for Constituents Materials and Concrete and BS 8500-2:2002, Complimentary British Standards to BS EN 206-1.
171. Kwesi Sagoe-Crentsil of Commonwealth Scientific and Industrial Research Organisation (CSIRO), Waste glass used in concrete, Australia, available from: www.dbce.csiro.au, 2000.
172. M.M. Reda , A.S. El-Dieb, M.M. Abdel-Whab, *Fracture Toughness of Concrete Incorporating Rubber Tyre Particles*, ICPCM – A New Era of Building, Cairo, Egypt, Feb.18-20, 2003.
173. M. Hossain, M. Sadeq, L. Funk and R. Maag, *A Study of Chunk Rubber from Recycled Tyres as a Road Construction Material*, Proceedings of the 10th Annual Conference on Hazardous Waste Conference, pp. 188-197, 2000, Department of Civil Engineering, Kansas State University, USA.
174. Goulias DG and Ali AH, *Evaluation of Rubber-Filled Concrete and Correlation Between Destructive and Non-destructive Testing*, Cement, Concrete and Aggregates, pp 140-144, Volume 20, issue 1, 1998.
175. A. Maher and F. Ansari, *Recycled Materials in Portland Cement Concrete*, New Jersey Department of Transportation, Report Number FHWA 2000-3, June 2000.

176. Nadia Segre, A. Galves, J. Rodrigues, P. Monterio and I. Joekes *Use of Tyre Rubber Particles in Slag-Modified Cement Mortars*, 11th International Congress on the Chemistry of Cement, 2003, Cement and Concrete Institute of South Africa.
177. Professor Christian Meyer, *Concrete Materials Research*, pp. 11-14, Columbia University, New York, August, 2000.
178. J.J. Beaudoin, CBD-223, *Fibre-Reinforced Concrete*, Canadian Building Digest, National Research Council, Canada, April 1982.
179. W. Jason Weiss, Byounggeon Kim, and Hulya Kayir, *Using Acoustic Emission to Quantify Damage in Fibre Reinforced Cement Mortars Restrained From Volume Changes*, SYMPOSIUM KK, Design, Characteristics and Properties of Cementitious Materials, November, 26-28, 2001.
180. Victor Y. Garas and C. Vipulanandan, *Destructive and Non-destructive Evaluation of CFRC*, Proceedings, CIGMAT -2004 Conference and Exhibition. Department of Civil and Environment Engineering, University of Houston, Texas.
181. Fibre Reinforced Concrete, IB 39, 2009, Cement and Concrete Institute, New Zealand, available from: www.ccanz.org.nz.
182. Saint Gobain Vetrotex: *CEM-FIL alkali-resistant glass fibres*, Fibres in Concrete, March 2003, The Indian Concrete Journal.
183. Chung D.D.L. and Pu-Woei Chen, 'Carbon fibre reinforced concrete for smart structures capable of non-destructive flaw detection' *Smart Materials and Structures*, Volume 2, 1993.
184. Holger D. Basche, Nancy Freitag, Karsten Jauck, Gunter Schenck, Balthasar Novak, 'Carbon Fibre as an Alternative Reinforcing Element; Bond Behaviour of Carbon Fibres in Concrete' , Institut fur Massivbau und Baustofftechnologie, Unversitat Leipzig, Konsig und Heunisch, Bera tende Ingenieure, Leipzig, pp. 197-209, Lacer No. 5. 2000.

185. Popovivcs S. *Analysis of Concrete Strength versus Ultrasonic Relationship - 2001*. www.asnt.org/publications/materialseval/basics/feb01basics/feb01basics.htm
186. Proceq Testing Equipment, Bedienungsanleitung, 98 12 487 D/E/F, Ultrasonic Instruments, Switzerland. www.proceq.com✓
187. [William D. Callister, Jr.](#) *Materials Science and Engineering: An Introduction*, 7th Edition, 2006.
188. [William D. Callister, Jr.](#) *Materials Science and Engineering: An Introduction*, 3rd Edition, 2004, John Wiley & Sons, Inc. New York.

Appendix A
List of cubes and mortars with sizes and contents
No additive, Cube Size: (70×70×70) mm

Table A1: Ultrasound parameters results for a plain mortar cube

<i>Day</i>	<i>Time (Micro-second) ±1</i>	<i>Velocity (m/s) ±100</i>	<i>Rebound Value R ±1</i>	<i>Compressive Strength (MPa) ± 1.5</i>
1	20.1	3590	N/A	N/A
2	18.7	3740	24	8.5
3	18.1	3870	27	13.8
4	17.9	3910	31	17.7
5	17.6	3980	33	21.4
6	17.6	3980	33	21.4
7	17.6	3980	33	21.4
8	17.6	4000	33	21.6
9	17.5	4000	33	21.6
10	17.5	4000	33	21.6
11	17.5	4000	33	21.6
12	17.4	4020	33	21.9
13	17.3	4050	33	22.2
14	17.3	4050	33	22.2
15	17.3	4050	33	22.2
16	17.3	4050	33	22.2
17	17.3	4050	33	22.2
18	17.2	4070	34	23.4
19	17.2	4070	34	23.4
20	17.2	4070	34	23.4
21	17.2	4070	34	23.4
22	17.2	4070	34	23.4
23	17	4120	36	25.9
24	16.8	4170	37	27.4
25	16.8	4170	37	27.4
26	16.8	4170	37	27.4
27	16.8	4170	37	27.4
28	16.8	4170	37	27.4

5g Calcium Chloride, Cube Size: (70×70×70) mm

Table A2: Ultrasound parameter results for a mortar cube with 5g calcium chloride

<i>Day</i>	<i>Time (Micro-second) ±1</i>	<i>Velocity (m/s) ±100</i>	<i>Rebound Value R ±1</i>	<i>Compressive Strength (MPa) ± 1.5</i>
1	19.8	3540	-----	-----
2	18.3	3830	27	12.9
3	17.7	3960	30	18.1
4	17.6	3980	33	21.4
5	17.2	4070	33	22.6
6	17.3	4050	33	22.2
7	17.2	4070	33	23.4
8	17.2	4070	34	23.4
9	17	4120	34	25.9
10	17	4120	36	25.9
11	17	4120	36	25.9
12	17	4120	36	25.9
13	17	4120	36	25.9
14	16.9	4140	36	26.2
15	16.9	4140	36	26.2
16	16.9	4140	36	26.2
17	16.9	4140	36	26.2
18	16.9	4140	36	26.2
19	16.8	4170	36	26.6
20	16.8	4170	36	26.6
21	16.8	4170	36	26.6
22	16.8	4170	36	26.6
23	16.5	4240	39	30.3
24	16.2	4320	41	33.5
25	16.2	4320	41	33.5
26	16.2	4320	41	33.5
27	16.2	4320	41	33.5
28	16.2	4320	41	33.5

15g Calcium Chloride, Cube Size: (70×70×70) mm

Table A3:Ultrasound parameter results for a mortar cube with 15g calcium chloride

<i>Day</i>	<i>Time (Micro-second) ±1</i>	<i>Velocity (m/s) ±100</i>	<i>Rebound Value R ±1</i>	<i>Compressive Strength (MPa) ± 1.5</i>
1	21.5	3260	-----	-----
2	19.9	3520	-----	-----
3	19.4	3610	-----	-----
4	18.6	3760	24	9.1
5	18.3	3830	27	12.9
6	17.9	3910	30	17.3
7	17.8	3930	30	17.7
8	17.8	3930	30	17.7
9	17.6	3980	33	21.4
10	17.6	3980	33	21.4
11	17.6	3980	33	21.4
12	17.6	3980	33	21.4
13	17.5	4000	33	21.6
14	17.5	4000	33	21.6
15	17.5	4000	33	21.6
16	17.5	4000	33	21.6
17	17.4	4020	33	21.9
18	17.4	4020	33	21.9
19	17.3	4050	34	23.1
20	17.1	4090	36	25.7
21	17.1	4090	36	25.7
22	17.1	4090	36	25.7
23	17.1	4090	36	25.7
24	17.1	4090	36	25.7
25	16.9	4140	37	27.1
26	16.9	4140	37	27.1
27	16.9	4140	37	27.1
28	16.9	4140	37	27.1

15g Potassium Chloride, Cube Size: (70×70×70) mm

Table A4: Ultrasound parameter results for a mortar cube with 15g potassium chloride

<i>Day</i>	<i>Time (Microsecosnd) ±1</i>	<i>Velocity (m/s) ±100</i>	<i>Rebound Value R ±1</i>	<i>Compressive Strength (MPa) ± 1.5</i>
1	21.5	3260	-----	-----
2	19.9	3520	-----	-----
3	19.4	3610	-----	-----
4	18.6	3760	24	9.1
5	18.3	3830	27	12.9
6	17.9	3910	30	17.3
7	17.8	3930	30	17.7
8	17.8	3930	30	17.7
9	17.6	3980	33	21.4
10	17.6	3980	33	21.4
11	17.6	3980	33	21.4
12	17.6	3980	33	21.4
13	17.5	4000	33	21.6
14	17.5	4000	33	21.6
15	17.5	4000	33	21.6
16	17.5	4000	33	21.6
17	17.4	4020	33	21.9
18	17.4	4020	33	21.9
19	17.3	4050	34	23.1
20	17.1	4090	36	25.7
21	17.1	4090	36	25.7
22	17.1	4090	36	25.7
23	17.1	4090	36	25.7
24	17.1	4090	36	25.7
25	16.9	4140	37	27.1
26	16.9	4140	37	27.1
27	16.9	4140	37	27.1
28	16.9	4140	37	27.1

25g Potassium Chloride, Cube Size: (70×70×70) mm

Table A5: Ultrasound parameters results for a mortar cube with 25g potassium chloride

<i>Day</i>	<i>Time (Micro-secosnd) ±1</i>	<i>Velocity (m/s) ±100</i>	<i>Rebound Value R ±1</i>	<i>Compressive Strength (MPa) ± 1.5</i>
1	19.8	3540	-----	-----
2	18.9	3700	24	7.4
3	18	3890	29	16
4	17.8	3930	30	17.7
5	17.7	3960	30	18.1
6	17.7	3960	30	18.1
7	17.6	3980	30	18.5
8	17.5	4000	33	21.6
9	17.4	4000	33	21.9
10	17.4	4020	33	21.9
11	17.6	3980	33	21.4
12	17.5	4000	33	21.6
13	17.5	4000	33	21.6
14	17.5	4020	33	21.6
15	17.4	4020	33	21.9
16	17.4	4020	33	21.9
17	17.3	4020	33	22.2
18	17.3	4050	33	22.2
19	17.3	4050	33	22.2
20	17.3	4050	33	22.2
21	17.3	4090	36	24.7
22	17.1	4090	36	24.7
23	17.1	4090	36	24.7
24	17.1	4090	36	24.7
25	17.1	4090	36	24.7
26	17.1	4090	36	24.7
27	17.1	4090	36	24.7
28	17.1	4090	36	24.7

15g Sodium Silicate, Cube Size: (70×70×70) mm

Table A6: Ultrasound parameters results for a mortar cube with 15g sodium silicate

<i>Day</i>	<i>Time (Micro- secosnd) ±1</i>	<i>Velocity (m/s) ±100</i>	<i>Rebound Value R ±1</i>	<i>Compressive Strength (MPa) ± 1.5</i>
1	20.8	3370	-----	-----
2	19.4	3610	-----	-----
3	18.8	3720	24	7.9
4	18.7	3740	24	8.5
5	18.3	3830	27	12.9
6	18	3890	28	15.1
7	18	3890	28	15.1
8	17.9	3910	30	17.3
9	17.9	3910	30	17.3
10	17.9	3910	30	17.3
11	17.9	3910	30	17.3
12	17.9	3910	30	17.3
13	17.9	3910	30	17.3
14	17.8	3930	30	17.7
15	17.6	3980	32	20.3
16	17.6	3980	32	20.3
17	17.6	3980	32	20.3
18	17.6	3980	32	20.3
19	17.4	4020	33	21.9
20	17.1	4090	36	25.7
21	17.1	4090	36	25.7
22	17.1	4090	36	25.7
23	17.1	4090	36	25.7
24	17.1	4090	36	25.7
25	17.1	4090	36	25.7
26	17.1	4090	36	25.7
27	17	4120	36	25.9
28	17	4120	36	25.9

30g Sodium Silicate, Cube Size: (70×70×70) mm

Table A7: Ultrasound parameters results for a mortar cube with 30g sodium silicate

<i>Day</i>	<i>Time (Micro- secosnd) ±1</i>	<i>Velocity (m/s) ±100</i>	<i>Rebound Value R ±1</i>	<i>Compressive Strength (MPa) ± 1.5</i>
1	23.3	3000	-----	-----
2	21.1	3320	-----	-----
3	19.7	3550	-----	-----
4	19.4	3610	-----	-----
5	19.2	3650	-----	-----
6	19	3680	24	7
7	18.9	3700	24	7.4
8	18.8	3720	24	7.9
9	18.8	3720	24	7.9
10	18.8	3720	24	7.9
11	18.8	3720	24	7.9
12	18.8	3720	24	7.9
13	18.7	3740	24	8.5
14	18.5	3780	27	12.2
15	18.5	3780	27	12.2
16	18.5	3780	27	12.2
17	18.5	3780	27	12.2
18	18	3890	27	14.4
19	17.1	3890	30	17.1
20	17.1	3890	30	17.1
21	17.1	3890	30	17.1
22	17.1	3890	30	17.1
23	17.1	3890	30	17.1
24	17.1	3890	30	17.1
25	17.1	3890	30	17.1
26	17.1	3890	30	17.1
27	17.1	3890	30	17.1
28	17.1	3890	30	17.1

15g Sodium Sulphate, Cube Size: (70×70×70) mm

Table A8: Ultrasound parameters results for a mortar cube with 15g sodium sulphate

<i>Day</i>	<i>Time (Micro- secosnd) ±1</i>	<i>Velocity (m/s) ±100</i>	<i>Rebound Value R ±1</i>	<i>Compressive Strength (MPa) ± 1.5</i>
1	18.5	3780	27	12.2
2	17.7	3960	30	18.1
3	17.3	4050	33	22.2
4	17.1	4090	36	25.7
5	17.3	4050	33	22.2
6	17.1	4090	36	25.7
7	17.1	4090	36	25.7
8	16.9	4140	36	26.2
9	16.9	4140	36	26.2
10	16.9	4140	36	26.2
11	16.9	4140	36	26.2
12	16.8	4170	36	26.6
13	16.8	4170	36	26.6
14	16.8	4170	36	26.6
15	16.8	4170	36	26.6
16	16.8	4170	36	26.6
17	16.7	4190	39	29.7
18	16.7	4190	39	29.7
19	16.7	4190	39	29.7
20	16.7	4190	39	29.7
21	16.7	4190	39	29.7
22	16.4	4270	40	31.6
23	16.4	4270	40	31.6
24	16.3	4290	41	33
25	16.3	4290	41	33
26	16.3	4290	41	33
27	16.3	4290	41	33
28	16.3	4290	41	33

25g Sodium Sulphate, Cube Size: (70×70×70) mm

Table A9: Ultrasound parameters results for a mortar cube with 25g sodium sulphate

<i>Day</i>	<i>Time (Micro- secosnd) ±1</i>	<i>Velocity (m/s) ±100</i>	<i>Rebound Value R ±1</i>	<i>Compressive Strength (MPa) ± 1.5</i>
1	18.9	3700	24	7.4
2	17.9	3910	30	17.3
3	18.1	3870	29	15.6
4	17.3	4050	34	23.1
5	17.2	4070	34	23.4
6	17.2	4070	34	23.4
7	17.2	4070	34	23.4
8	17	4120	36	25.9
9	16.9	4140	36	26.2
10	16.9	4140	36	26.2
11	16.9	4140	36	26.2
12	16.9	4140	36	26.2
13	16.9	4140	36	26.2
14	16.9	4140	36	26.2
15	16.9	4140	36	26.2
16	16.9	4140	36	26.2
17	16.9	4140	36	26.2
18	16.8	4170	37	27.5
19	16.8	4170	37	27.5
20	16.8	4170	37	27.5
21	16.8	4170	37	27.5
22	16.8	4170	37	27.5
23	16.4	4270	40	31.6
24	16.4	4270	40	31.6
25	16.4	4270	40	31.6
26	16.4	4270	40	31.6
27	16.4	4270	40	31.6
28	16.4	4270	40	31.6

15g Sodium Chloride, Cube Size: (70×70×70) mm

Table A10: Ultrasound parameters results for a mortar cube with 15g sodium chloride

<i>Day</i>	<i>Time (Micro- second) ±1</i>	<i>Velocity (m/s) ±100</i>	<i>Rebound Value R ±1</i>	<i>Compressive Strength (MPa) ± 1.5</i>
1	19.3	3630	-----	-----
2	17.9	3910	27	14.9
3	17.8	3930	30	17.7
4	17.7	3960	30	18.1
5	17.6	3980	33	21.4
6	17.6	3980	33	21.4
7	17.4	4020	33	21.9
8	17.4	4020	33	21.9
9	17.6	3980	33	21.4
10	17.5	4000	33	21.6
11	17.3	4050	33	22.2
12	17.3	4050	33	22.2
13	17.3	4050	33	22.2
14	17.3	4050	33	22.2
15	17.3	4050	33	22.2
16	17.3	4050	33	22.2
17	17.3	4050	33	22.2
18	17.3	4050	33	22.2
19	17.3	4050	33	22.2
20	17.3	4050	33	22.2
21	17.3	4050	33	22.2
22	17.3	4050	33	22.2
23	17	4120	36	25.9
24	17	4120	36	25.9
25	16.8	4120	37	27.4
26	16.8	4120	37	27.4
27	16.8	4120	37	27.4
28	16.8	4120	37	27.4

25g Sodium Chloride, Cube Size, (70×70×70) mm

Table A11: Ultrasound parameters results for a mortar cube with 25g sodium chloride

Day	Time (Micro-secosnd) ±1	Velocity (m/s) ±100	Rebound Value R ±1	Compressive Strength (MPa)±1.5
1	20	3500	-----	-----
2	18.3	3830	27	12.9
3	18.3	3830	27	12.9
4	18.3	3830	27	12.9
5	18	3890	30	17.1
6	17.8	3890	30	17.7
7	17.6	3980	32	20.3
8	17.6	3980	32	20.3
9	17.8	3930	30	17.7
10	17.6	3980	32	20.3
11	17.8	3930	30	17.7
12	17.7	3960	30	18.1
13	17.6	3980	33	21.4
14	17.6	3980	33	21.4
15	17.6	3980	33	21.4
16	17.4	4020	33	21.9
17	17.4	4020	33	21.9
18	17.4	4020	33	21.9
19	17.4	4020	33	21.9
20	17.4	4020	33	21.9
21	17.4	4020	33	21.9
22	17.3	4050	33	22.2
23	17.3	4050	33	22.2
24	17.3	4050	33	22.2
25	17	4120	36	25.9
26	17	4120	36	25.9
27	17	4120	36	25.9
28	16.9	4140	36	26.2

Specimens put under compressive test

Table A12: Compositions of specimens containing glass aggregates put under mechanical and ultrasonic tests

Sample Name (All notched)	Aggregates (Glass aggregates)	Cement (g)	Sand (g)	Water (g)	Size
KOLA0B	Plain Mortar	1590	1590	530	210×70×70 mm
KOLA2B < 1mm Aggregates	530 (g)	1590	1060	530	210×70×70 mm
KOLA 5B 1-1.7 mm Aggregates	530 (g)	1590	1060	530	210×70×70 mm
KOLA 4B 1.7-2.36 mm Aggregates	530 (g)	1590	1060	530	210×70×70 mm
KOLA 1B 2.36-3.35 mm aggregates	530 (g)	1590	1060	530	210×70×70 mm
KOLA 3B 3.35 - 4 mm aggregates	530 (g)	1590	1060	530	210×70×70 mm

Specimens put under compression test

Table A13: Compositions of specimens containing rubber aggregates put under mechanical and ultrasonic tests

Sample Name (All notched)	Size	Cement (g)	Sand (g)	Aggregates	Water (g)
Plain Mortar	210×70×70 mm	1590	1590	Plain Concrete	530
Kolar 1b	210×70×70 mm	1590	1540	50 g rubber	530
Kolar 2b	210×70×70 mm	1590	1490	100 g rubber	530
Kolar 3b	210×70×70 mm	1590	1440	150 g rubber	530
Kolar 4b	210×70×70 mm	1590	1390	200 g rubber	530
Kolar 5b	210×70×70 mm	1590	1340	250 g rubber	530

Concrete specimens put under compression

Table A14: Compositions of specimens AE monitored while under compression

Sample	Size	Cement (g)	Sand (g)	Aggregates (g)	Water (g)
Plain Mortar	140×70×70 mm	600	600	Zero	200
Mortar with glass aggregates	140×70×70 mm	600	300	300	200
Mortar with rubber aggregates	140×70×70 mm	600	300	300	200

Specimens put under flexural test

Table A15: Compositions of un-notched specimens AE monitored while under flexural test

<i>Sample Name (All un-notched)</i>	<i>Additive</i>	<i>Cement (g)</i>	<i>Sand (g)</i>	<i>Water (g)</i>	<i>Size</i>
BA2	40g Powdered glass	600	560	200	140×70×70 mm
BB2	80g 4-2 mm glass Aggregates	600	520	200	140×70×70 mm
BC1	40g 2-1 mm glass Aggregates	600	560	200	140×70×70 mm
BD1	Plain Concrete	600	600	200	140×70×70 mm
BE1	40g 4-2 mm glass Aggregates	600	560	200	140×70×70 mm
BF1	60g 2-1 mm glass Aggregates	900	840	300	210×70×70 mm
BG1	Plain Concrete	900	900	300	210×70×70 mm
BH1	60g 4-2 mm glass Aggregates	900	840	300	210×70×70 mm
BI1	60g Powdered glass	900	840	300	210×70×70 mm
BJ1	120g 4-2 mm glass aggregates	900	780	300	210×70×70 mm

Specimens put under flexural test

Table A16: Compositions of notched specimens (containing glass aggregates) AE monitored while under flexural test

<i>Sample Name (All notched)</i>	<i>Aggregates (Glass Aggregates)</i>	<i>Cement (g)</i>	<i>Sand (g)</i>	<i>Water (g)</i>	<i>Size</i>
KOLA0B	Plain Mortar	1590	1590	530	210×70×70 mm
KOLA2B < 1mm glass aggregates	530 (g)	1590	1060	530	210×70×70 mm
KOLA5B 1–1.7 mm glass aggregates	530 (g)	1590	1060	530	210×70×70 mm
KOLA4B 1.7–2.36 mm glass aggregates	530 (g)	1590	1060	530	210×70×70 mm
KOLA1B 2.36–3.35 mm glass aggregates	530 (g)	1590	1060	530	210×70×70 mm
KOLA 3B 3.35–4 mm glass aggregates	530 (g)	1590	1060	530	210×70×70 mm

Specimens put under flexural test

Table A17: Compositions of notched specimens (containing aggregates and additives) AE monitored while under flexural test

<i>Sample Name (All notched)</i>	<i>Size</i>	<i>Cement (g)</i>	<i>Sand (g)</i>	<i>Water (g)</i>	<i>Aggregates</i>
Final2: Plain mortar	210×70×70 mm	1060	1060	353	Zero
gbzero: Mortar with Glass Plate	210×70×70 mm	1060	1060	353	Glass slide
Sample 10: Mortar with Glass Plate and Glass Aggregates (4 mm)	210×70×70 mm	1060	530	353	Glass slide and 530g rough glass
Exglbds3: Expansive cement with mixed size 3 mm Glass Beads	210×70×70 mm	1060	530	353	530g glass beads
Expeb3: Expansive cement with 3 mm Pebbles	210×70×70 mm	1060	530	353	530g pebbles
a2e: Expansive Cement Mortars with Rough Glass Aggregates (3mm)	210×70×70 mm	1060	530	353	530g rough glass aggregates
Mortar with glass slide	210×70×70 mm	1060	1060	353	Glass slide
Mortar with calcium carbonate and glass slide	210×70×70 mm	1060	1035	353	Glass slide and 25g calcium carbonate
Mortar with calcium carbonate, glass slide and glass aggregates	210×70×70 mm	1060	530	353	Glass slide, 25g calcium carbonate and 530g rough glass

Specimens put under flexural test

Table A18: Compositions of notched specimens containing rubber aggregates, AE monitored while under flexural test

Sample Name (All notched)	Size	Cement (g)	Sand (g)	Aggregates	Water (g)
Kolar 2b	210×70×70 mm	1590	1490	100 g rubber	530
Kolar 3b	210×70×70 mm	1590	1440	150 g rubber	530
Kolar 4b	210×70×70 mm	1590	1390	200 g rubber	530
Kolar 5b	210×70×70 mm	1590	1340	250 g rubber	530

Samples put under compression for AE monitoring

Table A19: Compositions of notched specimens containing additives, AE monitored while under flexural test

<i>Sample</i>	<i>Size</i>	<i>Cement (g)</i>	<i>Sand (g)</i>	<i>Additives</i>	<i>Water (g)</i>
Plain Mortar	70×70×70 mm	300	300	Zero	100
Mortar with Calcium Chloride	70×70×70 mm	300	295	5g Calcium Chloride	100
Mortar with Sodium Sulphate	70×70×70 mm	300	290	10g Sodium Sulphate	100
Mortar with Sodium Sulphate	70×70×70 mm	300	285	15g Sodium Sulphate	100
Mortar with Sodium Sulphate	70×70×70 mm	300	275	25g Sodium Sulphate	100
Mortar with Sodium Silicate	70×70×70 mm	300	285	15g Sodium Silicate	100

Specimens put under flexural test

Table A20: Compositions of notched specimens (containing additives, aggregates and glass plate insertion) AE monitored while under flexural test

Sample Name (All notched)	Size	Cement (g)	Sand (g)	Additives	Water (g)
Brglcam: Mortar with Glass Plate (14 Days Cured)	140×70×70 mm	600	600	Glass slide	200
Brglcam1: Mortar with Glass Aggregates (14 Days Cured)	140×70×70 Mm	600	585	15g Glass aggregates	200
NAS: Mortar with Sodium Sulphate and Glass Plate (14 Days Cured)	140×70×70 mm	600	590	10g Sodium sulphate and glass plate	200
BRGL2: Broken Glass of mixed glass size and glass plate (28 Days Cured)	210×70×70 mm	1060	1045	15g Rough glass and glass plate	353

Specimens put under flexural test

Table A21: Compositions of notched specimens (containing additives) AE monitored while under flexural test

Samples	Size	Cement (g)	Sand (g)	Additives (g)	Water (g)
Final2: Plain mortar	210×70×70 mm	1060	1060	Zero	353
Conflex: Mortar containing sodium sulphate	210×70×70 mm	1060	1035	25g Sodium sulphate	353
Cara4: Mortar containing calcium carbonate	210×70×70 mm	1060	1035	25g Calcium carbonate	353

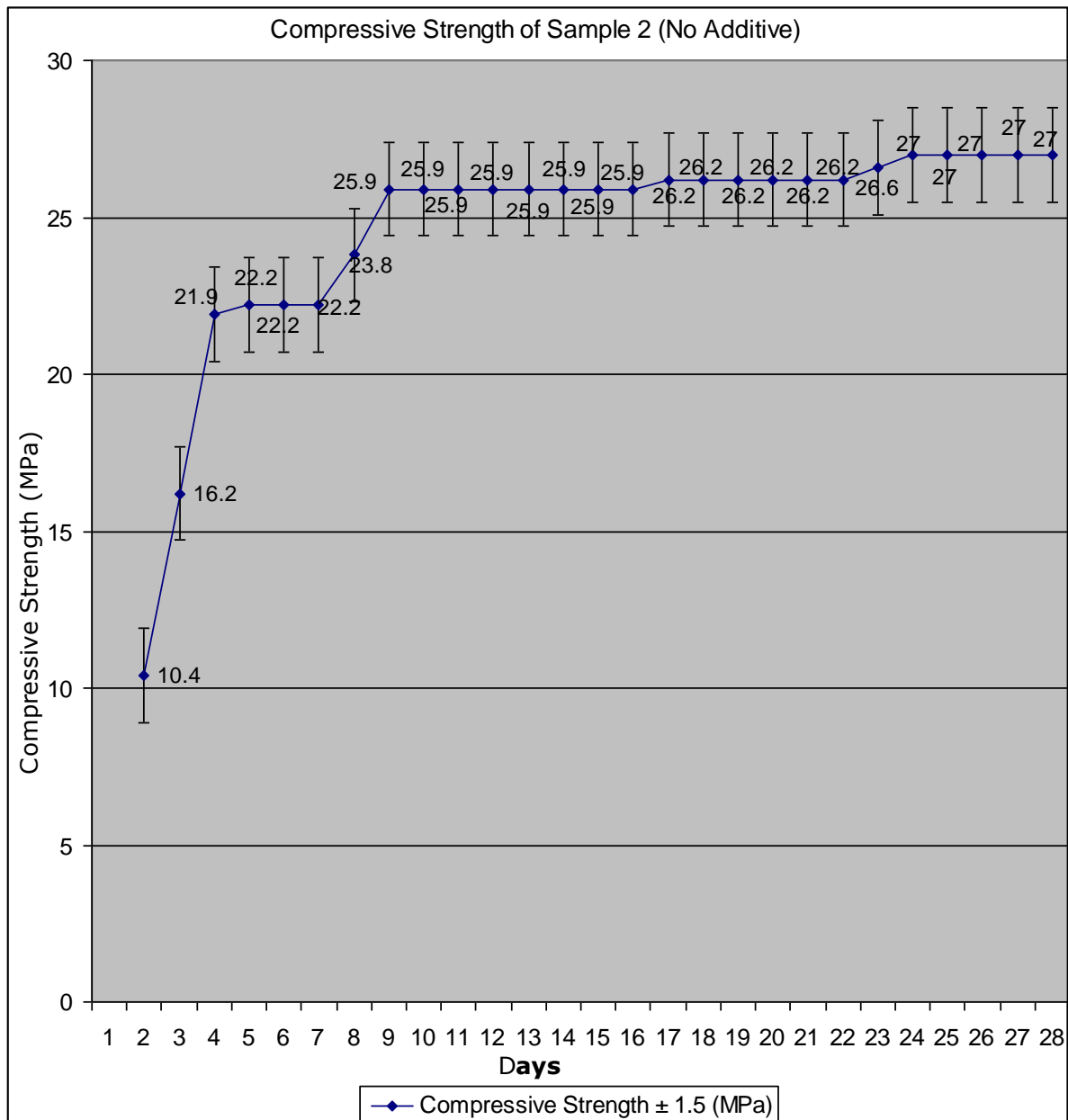


Figure A1: Sample 2:- The change in compressive strength (measured using ultrasound) of a standard mortar (without additives) with respect to time.

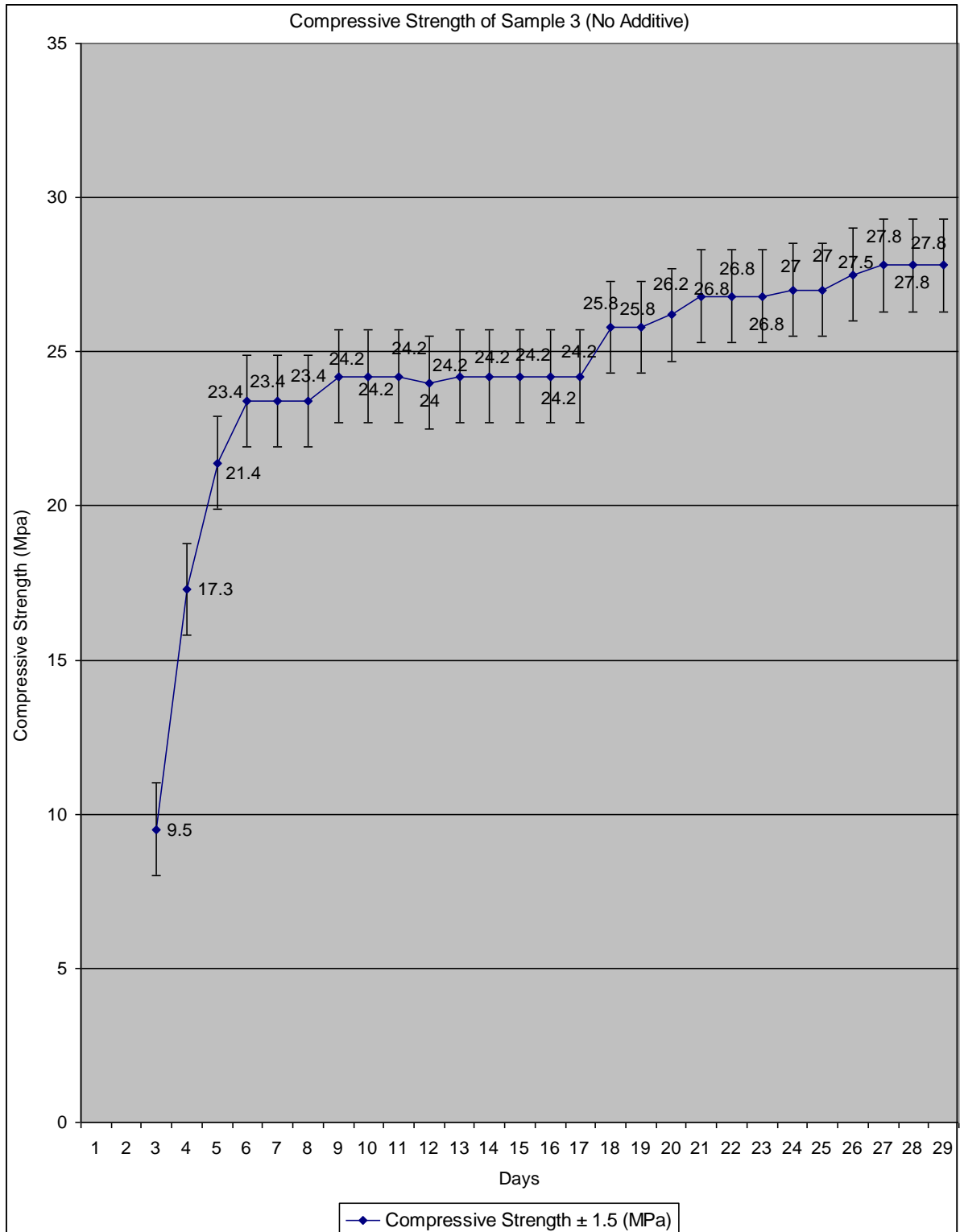


Figure A1: Sample 3:- The change in compressive strength (measured using ultrasound) of a standard mortar (without additives) with respect to time.

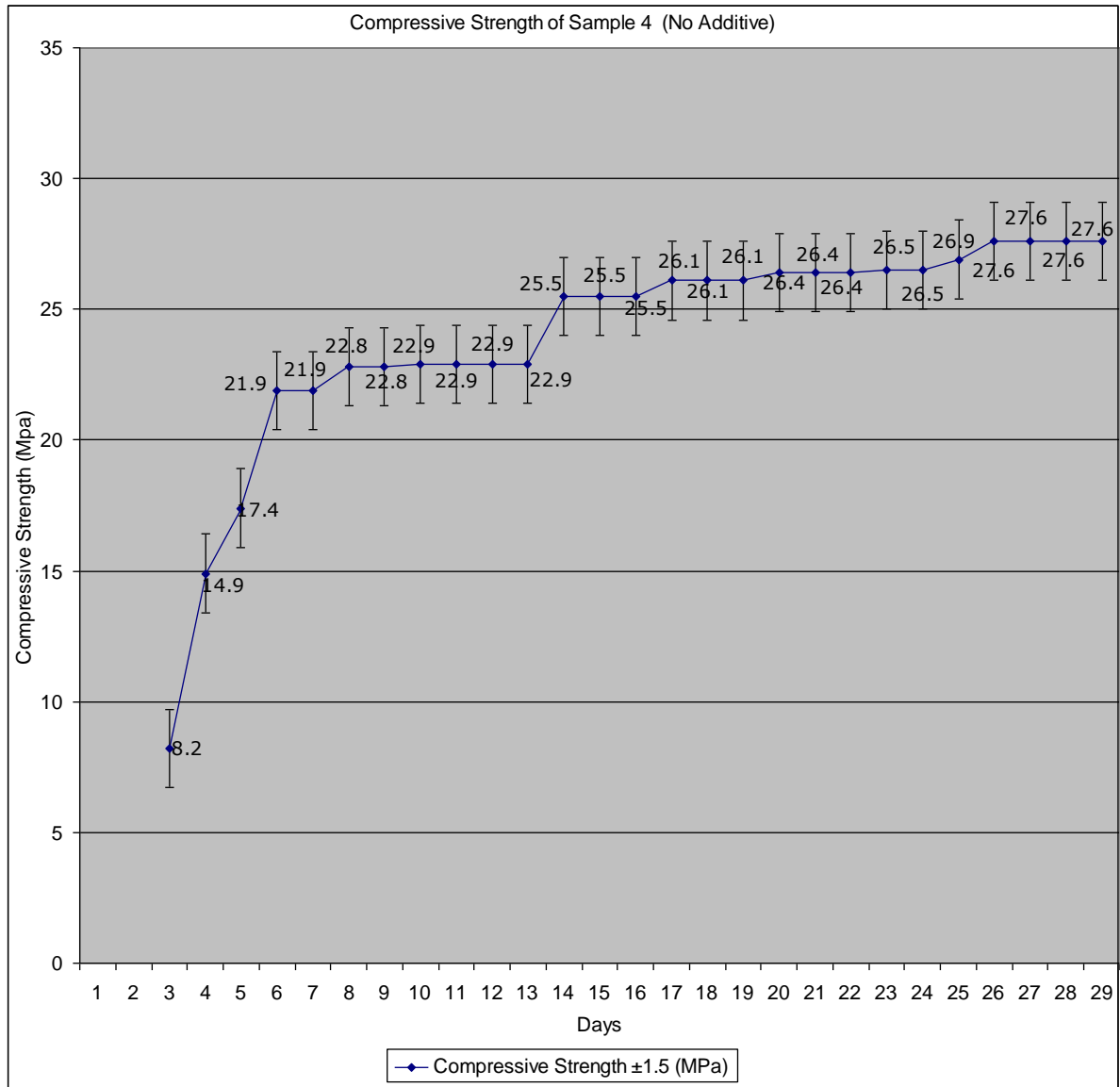


Figure A1: Sample 4:- The change in compressive strength (measured using ultrasound) of a standard mortar (without additives) with respect to time.

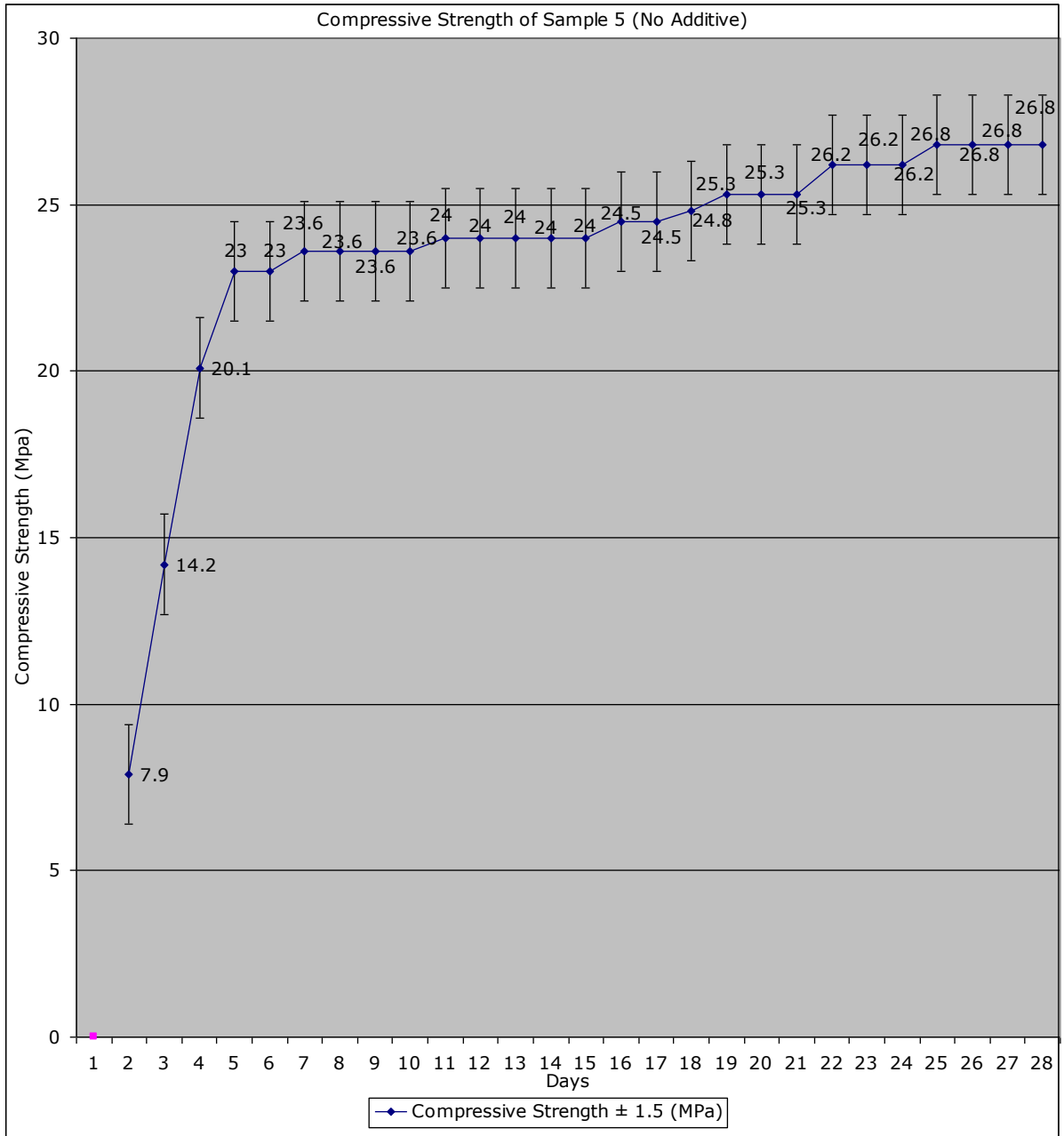


Figure A1: Sample 5:- The change in compressive strength (measured using ultrasound) of a standard mortar (without additives) with respect to time.

APPENDIX B 1

Scanning Electron Microscope (SEM)

As the diffraction of light ultimately sets a natural limit to the detail that can be resolved by a microscope, it was realised that if the wave nature of the electron could be exploited a significant advance in microscope performance would be achieved. In practice a light microscope has a resolution limit of approximately 0.001mm where as with the development of electron microscopes this limit has been pushed to around 0.00001mm. The scanning electron microscope (SEM) was developed between 1929 and the early 1960s as a tool for imaging surfaces at this higher resolution.

As well as producing high-resolution images, the SEM can be used as analytical tool by examining the large variety of signals stimulated by the interaction of the electron beam and the specimen. The scanning electron microscope can be a useful tool over a wide variety of scientific disciplines.

Principle of Operation

The SEM generates a finely focused beam of electrons which is made to scan across the sample under inspection (see figure B1.1). The beam originates from the heating from a tungsten wire filament (Thermionic emission) housed in an electron gun at the top of the microscope column. The beam electrons are accelerated towards the specimen by means of an applied accelerating voltage between the filament assembly and an anode plate. The SEM column sample chamber are maintained under a high vacuum to allow the electrons forming the beam an unhindered path from the filament to the sample surface.

As the beam travels down the column, it undergoes electron optical demagnification as it passes through two electromagnetic lenses (condenser lenses). Just above the specimen the beam comes under the influence of a set of scan coils which deflect the beam in a raster pattern across the sample surface. This scanning action is synchronised with the display monitor where an image is generated line by line. The smaller the area covered by the raster on the sample surface, the higher the magnification obtained.

$$\text{MAGNIFICATION} = \frac{\text{Length of line scan on monitor}}{\text{Length of line scan on sample}}$$

Available magnification may exceed 300 000x with a resolution of 3-4nm. This compares a resolution capability of a light microscope of approximately 250nm.

With the courtesy of the School of Life Sciences, Robert Gordon University, Aberdeen.

Another advantage the SEM has over optical microscopy is the far greater depth of focus when viewing a sample. This allows rough surfaces to be imaged in sharp focus even at high magnification.

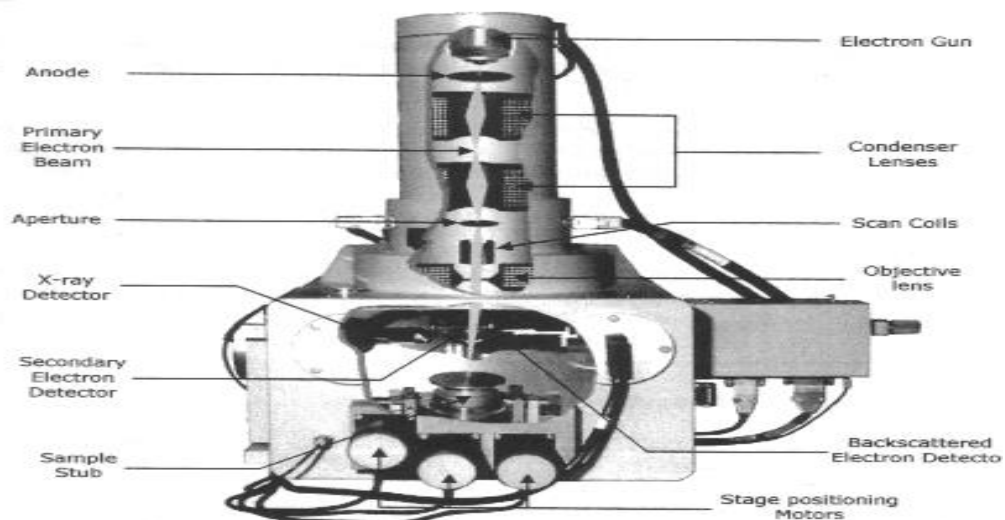


Figure B1.1: Scanning electron microscope electron optical column

Beam / Specimen Interaction

As the electron beam traverses the sample a number of different interactions occur resulting in a variety of signals being emitted from the surface (see figure B1.2). All of these signals can provide information about the specimen under investigation. SEM design can be tailored to accommodate a wide range of detecting instrumentation depending on the information required. The SEM is generally fitted with two imaging detectors, a **secondary electron detector** and a **backscattered electron detector**.

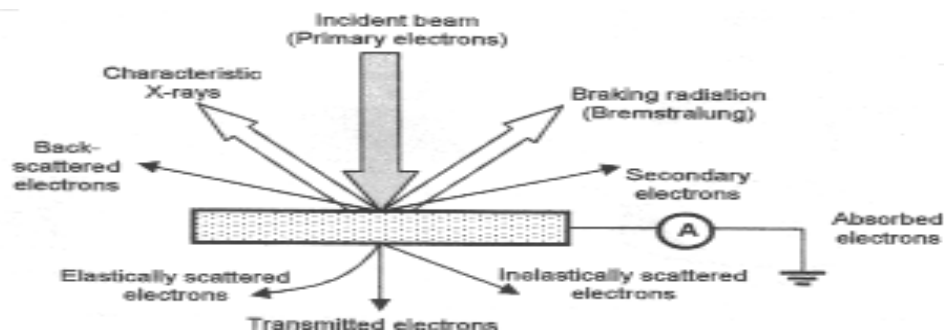


Figure B1.2: Beam – Specimen Interaction

Secondary electrons are low energy electrons (<50eV) emitted as a result of inelastic collisions between primary beam electrons and outer electrons of specimen atoms. Secondary electrons are emitted at random angles about the point of beam impact.

With the courtesy of the School of Life Sciences, Robert Gordon University, Aberdeen.

Backscattered electrons are primary beam electrons which escape the sample surface (elastically scattered) without losing much of their original energy. These electrons are very directional due to their high energy. Backscattered electron yield is related to the atomic number of the specimen atoms gives an image which is set to have "atomic number contrast". This type of image is useful for imaging material boundaries.

A third common type of detector fitted to the SEM is the Energy Dispersive X-ray Spectrometer. This allows the analysis of the characteristic x-rays emitted from the specimen due to x-ray fluorescence. Such systems allow the identification of the elements present in the sample.

Secondary Electron Detector

Secondary electrons are only detected from the top surface layers of the specimen at an approximate depth of 10 – 500 Å, depending on the specimen material and the accelerating voltage of the primary beam. Secondary electrons radiate out from the surface of the sample and are collected by a positively biased detector mounted at the back of the sample chamber. The energy of these electrons is converted via scintillation, light guide and photomultiplier tube into an electrical signal which is then displayed as a point of light on a cathode ray tube (CRT). As the primary electron beam scans a surface of light intensity map of the secondary electrons is built up line by line on the microscope display (See figure B1.3).

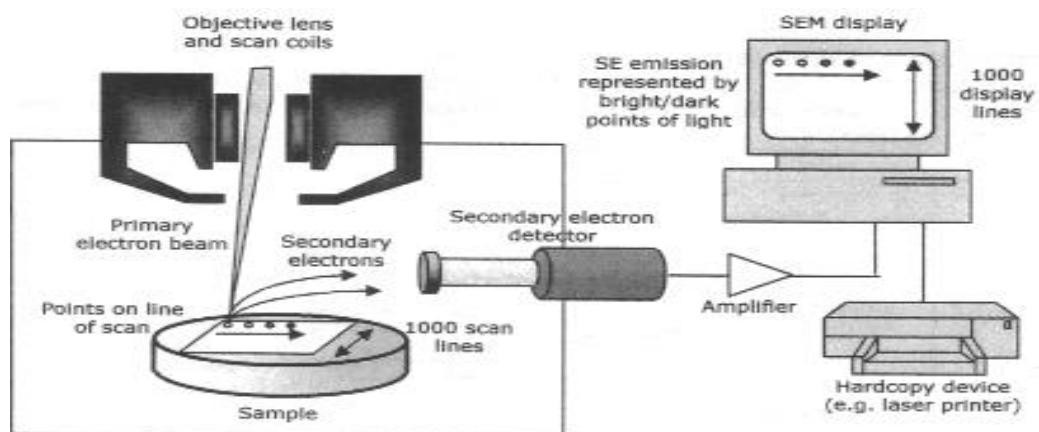


Figure B1.3: Generation of the secondary electron image

The brightness of a dot on a SEM monitor is modulated by the magnitude of the secondary electron signal from the corresponding point on the surface of the sample. The strength of the secondary electron signal is related to the physical shape of the surface therefore an image with topological contrast of the area is created. Surface inspection is mainly performed using secondary electron images because of the high magnification capability and large depth of focus.

With the courtesy of the School of Life Sciences, Robert Gordon University, Aberdeen.

Image Resolution

The SEM image resolution is governed by four basic factors; accelerating potential, probe diameter (current), scan rate and working distance. The amount of play available with these parameters depends greatly on the charge sensitivity of the specimen under investigation.

Accelerating Potential

This is the electron gun voltage that governs the energy of the primary beam electrons. The greater the potential the higher the resolution. High accelerating potentials increase the amount specimen charging by thermal or radiation damage.

Beam Diameter

In order to detect a change in the SE signal as the beam scans across a specimen, the beam diameter must be smaller than any surface feature of interest. Unfortunately reducing the beam diameter also reduces the area of beam-specimen interaction and therefore reduces the signal to noise ratio.

Scan Rate

In order to generate as strong a signal as possible it is important that the beam interacts with each point on the surface for as long as possible. This means that a slow scan rate gives the best resolution. However the main limiting step in composing an image is the operator's judgement of focus. Focusing can only be successfully carried out if fine adjustments are seen in real time (i.e. at fast scan rates).

Working Distance

The working distance is defined as the distance between the sample and the final lens of the electron optical column. By reducing the electron path from lens to sample the beam is concentrated more precisely on the sample surface (i.e. less chance of any beam divergence). The best resolution achieved at as short a working distance as possible.

With the courtesy of the School of Life Sciences, Robert Gordon University, Aberdeen.

Specimen Preparation

As the SEM is primarily used as a tool for the examination of surfaces, care must be taken so as not to damage any physical features. The specimen is normally fixed to an aluminium stub using a suitable adhesive. Such adhesives can be graphite suspension, silver paint, self-adhesive graphite pads or double-sided adhesive tape. The specimen must be clean, dry and free from any trapped liquid or gas before being placed on minimal amounts of sample preparation are required. Cleaning may be carried out in an ultrasonic bath using a suitable solvent. Any surface debris may be removed by blowing the sample using an air-duster.

One drawback using secondary electrons to form images is that specimen surfaces must be electrical conductors. If the specimen does not conduct electricity then electrons tend to build up on the surface (the specimen charges up) causing inconsistent emissions of secondary electrons. This has the effect of distorting the image or causing areas of very high contrasts.

To successfully image specimen that does not conduct electricity; the surface must be coated with a suitable conducting material (e.g. graphite, gold, platinum etc.). Ideally the particles of coating materials should be beyond the resolving power of the microscope to ensure that they do not hide any of the detail which the microscope is capable of resolving.

With the courtesy of the School of Life Sciences, Robert Gordon University, Aberdeen

APPENDIX B 2

Energy Dispersive X-ray Analysis

Introduction

X-ray Production

As the scanning electron microscope employs a high energy electron beam to illuminate a specimen, one of the by-products is the generation of x-rays as primary beam electrons interact with specimen electrons. The production of the x-rays occurs in two basic ways (see figure B2.1). As an electron in the primary beam enters the volume of the specimen atoms, it can be scattered elastically or inelastically.

Elastic scattering has the effect of causing primary electrons to slow down but in order for this to occur the electrons must give up energy and this can be accomplished by the emission of x-ray radiation. This type of radiation is known as bremsstrahlung and is observed as a continuous spectrum. This continuous spectrum is regarded as background radiation for EDXA spectrometers.

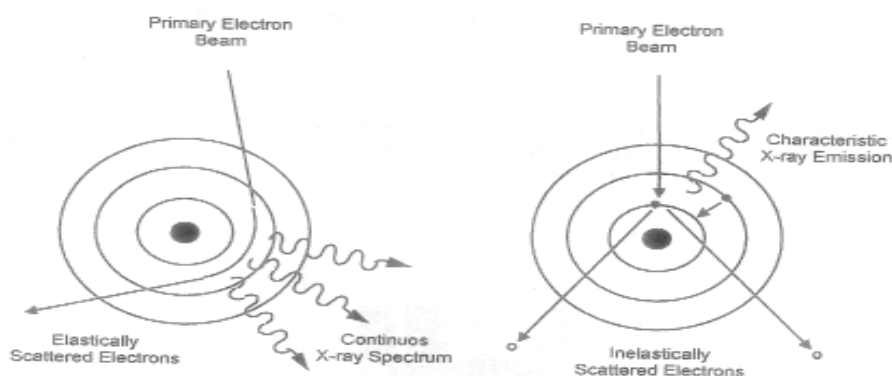


Figure B2.1: X-ray Production

Inelastic scattering occurs due to collisions between primary electrons and electrons within specimen atoms. The consequent rearrangement of electrons within electron shells, as atoms strive to reach their lowest energy states, results in the release of energy in the forms of x-ray photons. As the energy of these photons is related to the energy difference between electron shells, the x-ray photons are characteristic of the elements present in the specimen. By collecting and analysing these x-rays, qualitative and quantitative information about the component elements of a specimen may be obtained.

With the courtesy of the School of Life Sciences, Robert Gordon University, Aberdeen.

The additional hardware required to detect and measure the energy of the characteristic x-rays is shown in figure B2.2. Energy dispersive x-ray analysis (EDXA) is a very widespread technique which is regularly applied to biological or chemical as well as physical problems in materials science. Normal electron microscope imaging is usually performed during the course of the analytical procedure.

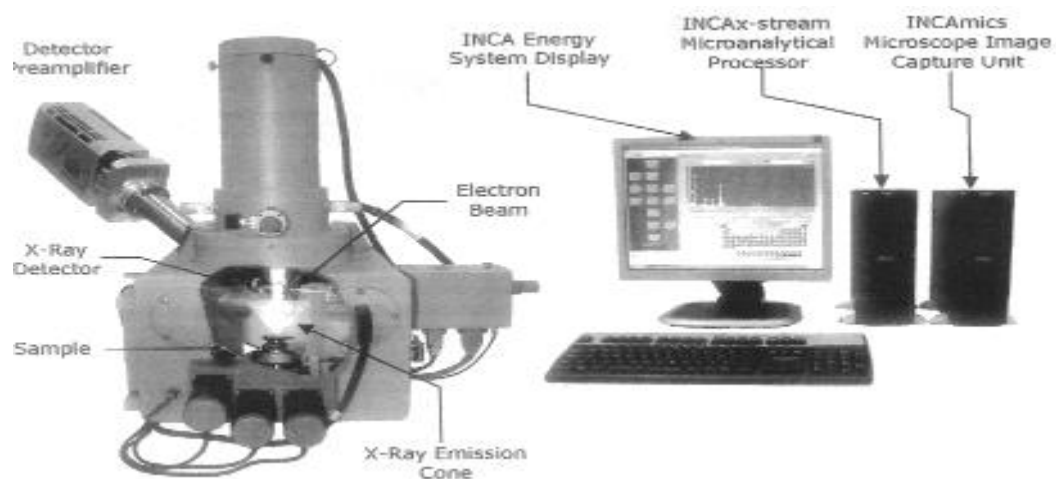


Figure B2.2: Energy dispersive X-ray Analysis System

Lithium Drifted [Si(Li)] Crystal Detector

Energy Dispersive spectrometers employ a solid-state detector usually involving a single crystal of silicon. The function of the detecting crystal is to convert the energy of an x-ray photon into an electrical signal of proportional magnitude. When an x-ray photon collides with a crystal, electrons are excited up to a high energy state and termed the conduction band. This leaves holes in the valence band. An applied bias voltage has an effect of sweeping the resulting charge to the electrodes on the opposing faces of the crystal. The more energetic the incident x-ray, the greater the charge difference generated across the crystal.

An ultra thin, opaque window protects the detector crystal from the SEM vacuum system (10^{-5} Torr). The window also protects any condensations (due to the very low temperature) of contaminants from the sample chamber forming on the crystal surface. The window also helps minimise the generation of spurious signals arising from incident secondary electrons, visible light or infrared radiation. Modern detector technology can allow the detection of beryllium ($Z=4$). Modern detectors are also fitted with electron traps that apply a positive potential near detector window to deflect any stray electrons away from the crystal (see figure B2.3).

With the courtesy of the School of Life Sciences, Robert Gordon University, Aberdeen.

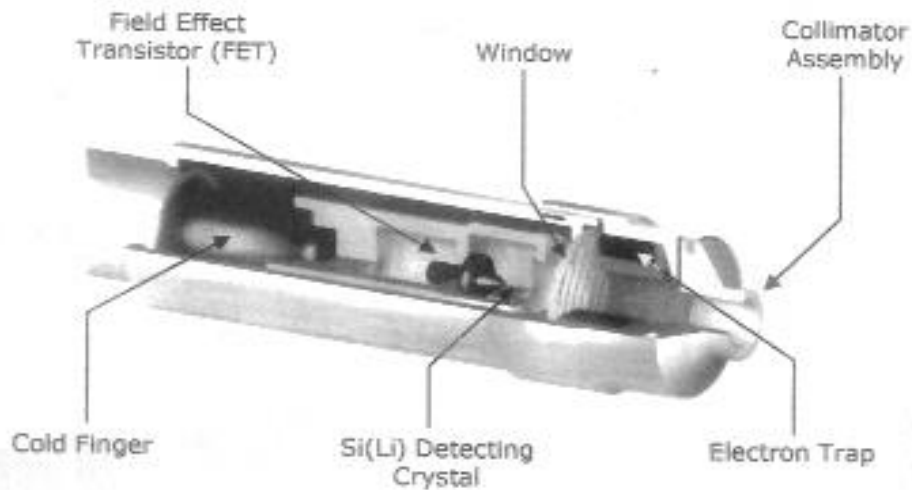


Figure B2.3: The Si(Li) detector assembly

When the primary electrons impact with a material, cone of x-rays is generated about the point of beam impact. This means in order to collect an x-ray signal efficiently the sample detector – detector geometry must be correct. Normally the sample is mounted flat in the sample chamber and the detector is oriented in such way away as to match the angle of x-ray take off. This means that a critical working distance is required of efficient collection of x-rays (see figure B2.4).

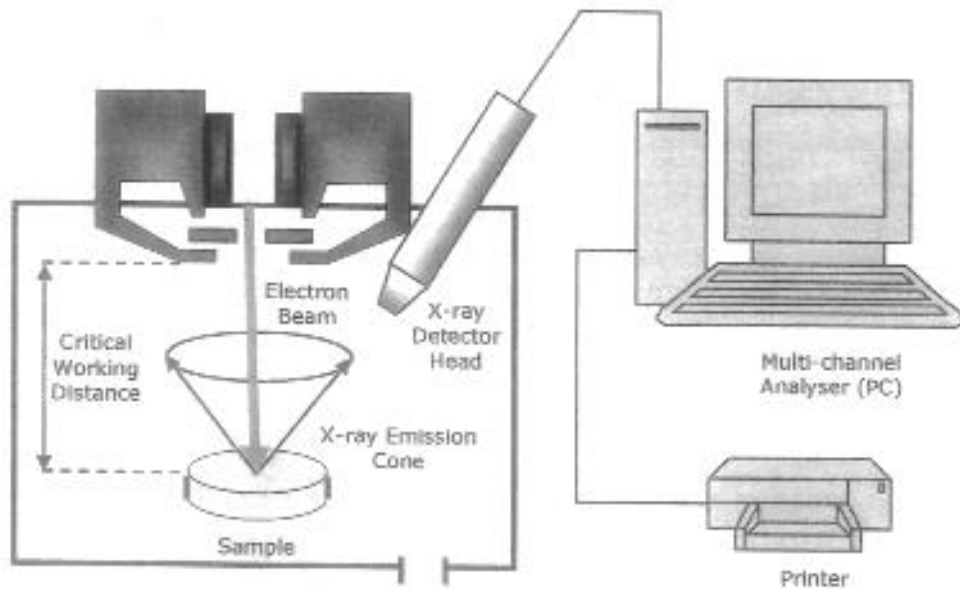


Figure B2.4: Sample- Detector Geometry

With the courtesy of the School of Life Sciences, Robert Gordon University, Aberdeen.